Novel Metal-Containing Enzymes: Missing Link in the Marine Phosphorus Cycle?

by

Linda Maria Westermann

A thesis submitted for the degree of Doctor of Philosophy

THE UNIVERSITY OF WARWICK

School of Life Sciences

October 2021

TABLE OF CONTENTS

LIST OF FIGURES

LIST OF TABLES

LIST OF APPENDICES

10th October 2021

ACKNOWLEDGEMENTS

Ten years ago today, I started my journey of becoming a marine biologist. So many people have been with me since day one of this journey and many more became a part of my life during this time, and all of them deserve my recognition.

I would first like to express my deep gratitude to my supervisor Prof Dave Scanlan, who has been an amazing mentor over the last four years. Thank you, Dave, for always supporting me, for trusting me, for continuously motivating me, for checking up on me during the lockdown, for challenging me, and for teaching me. A warm thank you to my co-supervisor Prof Yin Chen, for introducing me to the world of lipids, for helping me analyse tons of data, and for sharing his knowledge with me. I also thank my co-supervisor Prof Claudia Blindauer, who always helped with her expertise in Chemistry, especially all things protein-related.

I thank the members of my advisory panel, Prof David Roper, Dr Joseph Christie-Oleza, and Dr Elizabeth Fullam, for their help and suggestions throughout my PhD.

Credit is due to all former and present members of the Scanlan group, Chen group, and Christie-Oleza group for welcoming me, for making me a part of the community, and for making it difficult to leave.
A big thank you to my dear Audam, for being the best bench neighbour and an awesome friend. I am thankful for our laughs, hugs, talks, game and dinner nights, and karaoke parties. I am forever grateful that we did go the distance, together. Thank you, Branko, for being a wonderful friend and the best rant-buddy, for all your help and support inside and outside the lab, for all the hugs, and for the best IKEA trip ever. Thank you, Ian, for understanding my obsession with phosphorus and for the endless talks about my project and climbing. I want to thank Mar, for brightening up every day in the lab, for spending hours with me in the proteomics lab, for all the fun we had together, and for all your help. Thank you, Mussa, for teaching me everything I know about proteins, for your endless support and all the talks. Thank you, Rich, for all the discussions about my project, for sharing new ideas, for teaching me

new methods, for all the laughter and a shoulder to cry on, and for being an amazing friend. I couldn't have done this without you.
I also thank Alberto, Alevtina, Alexia, Andrew, Aurelija, Betty, Eleanor, Fabrizio, Fran, Gabriel, Holly, Izzy, Letizia, Madhav, Michi, Nello, Rebecca, Rhiannon, Richard, Rob, Rui and Severine, for all the talks and discussions during lunch and coffee breaks, for the fun times we had together inside and outside the labs, for all the cakes on Fridays, for all the hugs, for all the 'virtual' movie nights, coffee breaks, and game nights during the lockdown, and for making me feel home.

I am forever grateful to my two amazing friends and flatmates, Ele and Siree, more than I can put into words. Thank you both, for making living together such a blast and for creating a feeling of family. I will forever cherish our time together. My time in Coventry would have never been the same without you. I also thank Raffaele and Laurie, who have become wonderful friends. Thank you, my Victoria Court family, for keeping me sane during the lockdown. Hercules, you will never be forgotten. 'Ohana means family. Family means nobody gets left behind or forgotten' *Lilo & Stitch*.

I thank my dear friend, Isabel, for giving me the final push to follow my dream of becoming a marine biologist. Thank you, Chrissy and Chris, Michi and Chris, Natascha and Christoph, Kristina and Sascha, Felix and Kristin, Jan, and Stephan for continuously supporting me wherever I go. A warm thank you to my girls Anna, Jana, Lia, Mele, and Nadja, for being amazing friends since day one of my studies. And of course, I thank my best friend Jan, for always being my rock (no more words needed).

Last but not least, möchte ich meiner Familie danken, die mir immer mit viel Liebe, Verständnis und Rat zur Seite steht. Ich danke meiner Nichte Cora und meinen Neffen Nico, Mika, und Jona dafür, dass jeder Tag ein "Tante-Linda-Tag" sein kann, vor allem wenn ich eine Umarmung brauche. Ihr seid die Besten! Ich danke meiner Schwester Julia dafür, dass sie immer für mich da ist. Mein großer Dank gebührt meinen Eltern, die mich seit Tag eins immer unterstützt haben, die immer ein offenes Ohr für meine Sorgen haben, die immer an mich glauben, und auf die ich mich immer verlassen kann.

10th October 2021

DEDICATION

To my family.

‘Families are the compass that guide us.
They are the inspiration to reach great heights,
and our comfort when we occasionally falter.’
Brad Henry

DECLARATION

This thesis is submitted to the University of Warwick in support of my application for the degree of Doctor of Philosophy. It has been composed by me and has not been submitted in any previous application for any degree.

The work presented (including data generated and data analysis) was carried out by the author except in the cases outlined below:

- Chapter 3 and 5
  - The *Phaeobacter* sp. MED193 *phoB* knockout mutant was generated by Dr Ian D.E.A. Lidbury, a former research fellow in Prof Yin Chen's group.
- Chapter 3, 4, and 5
  - Proteomics samples were run by senior technician Dr Cleidiane Zampronio and lab manager Dr Andrew R. Bottrill at the Proteomics Research Technology Platform (University of Warwick). Sample preparation and data analysis were performed by me.
- Chapter 4 and 5
  - MicroScale Thermophoresis assays were performed by Chun-Yang Li at the College of Marine Life Sciences, Ocean University of China, Qingdao, China.
- Chapter 3
  - A list of putative Pho boxes in *Phaeobacter* sp. MED193 was generated and provided by Dr Marta Sebastián at the Department of Biology and Oceanography, Instituto de Ciencias del Mar, Barcelona, Spain.
- Chapter 4
  - Electron paramagnetic resonance spectroscopy and data analysis was performed by Dr Muralidharan Shanmugam at the National EPR facility at the University of Manchester. Samples preparation was done by me.
  - The hmm file was created by Alberto Torcello, a fellow PhD student in Prof Dave Scanlan's group.

SUMMARY

Phosphorus (P) is considered one of the most essential elements for living organisms. Due to its natural reactivity P only exists chemically bonded either as organic or inorganic phosphate (P_i), the preferred source of P for organisms. Ocean surface waters are often P_i limited and depend on exogenic fluxes to fuel marine ecosystems with this much-needed nutrient. Upon entering ocean waters, all sources of P enter the marine P cycle, a huge network that describes the various transformations and removal of P in the marine ecosystem. Oceans regulate the climate and represent an important sink for greenhouse gases. Therefore, climate change is no longer considered a danger for mankind alone, but there is increasing evidence that it will also dramatically impact our most important ecosystem. Because of this, it is necessary to fully understand marine nutrient cycles to allow more precise predictions for the future. My PhD project aimed to develop a better understanding of enzymes that are involved in P_i acquisition from organic P compounds in the marine environment and particularly, to understand how bacterial and archaeal membrane phospholipid headgroups are used as a source of P. I utilised a proteomic approach to identify key enzymes that are involved in the degradation and transport of these phospholipid headgroups. In addition, protein overexpression, enzyme activity assays, and substrate specificity evaluations were performed to characterise some of these prominent proteins found in the proteomics data. This thesis describes the identification and characterisation of two novel substrate-binding proteins (SBP) in the marine *Roseobacter Phaeobacter* sp. MED193 (MED193) that are essential for the transport of the phospholipid headgroups phosphoryl-ethanolamine (PE), glycerol-1-phosphate (G1P), and glycerol-3-phosphate (G3P). The SBP MED193_10041 component of a TRAP-transporter is required for the uptake of ethanolamine, a degradation product of PE. Not only does this SBP form a new cluster within the TRAP-transporter family, but the corresponding gene was found highly expressed in the Tara Oceans metatranscriptomics database. The SBP MED193_19449 component of an ABC-transporter can bind dihydroxyacetone phosphate, an oxidation product of G1P and G3P. Furthermore, I describe the degradation pathway of phosphocholine (PC) in MED193. However, the SBP of PC or choline remains unknown. In addition, this work focused on phosphatases from MED193 and the marine phototroph *Synechococcus* sp. WH8102 that are required for the hydrolysis of organic P compounds. I used biochemical methods to describe these proteins and bioinformatics was deployed to identify key metals that are required for enzyme activity, confirming the requirement of an iron-calcium cluster for the activity of PhoX-type phosphatases. The combination of these methods allowed us to discover new enzymes and describe new pathways within the marine P cycle.

ABBREVIATIONS

2-AEP	2-aminoethyl-phosphonic acid
ASW	Artificial seawater
ATP	Adenosine triphosphate
Ca^{2+}	Calcium
DGTS	Diacylglyceryl-trimethylhomoserine
DHAP	Dihydroxyacetone phosphate
DP	Dissolved phosphorus
DIP	Dissolved inorganic phosphorus
DOP	Dissolved organic phosphorus
EDTA	Ethylenediaminetetraacetic acid
EPR	Electron paramagnetic resonance spectroscopy
Fe/Fe^{3+}	Iron
GAPDH	Glyceraldehyde-3-phosphate dehydrogenase
GP	Glycerol-phosphate
G1P	Glycerol-1-phosphate
G3P	Glycerol-3-phosphate
G3PDH	Glycerol-3-phosphate dehydrogenase
G6P	Glucose-6-phosphate
Hmm	Hidden Markov model
LB	Lysogeny broth
LC-MS	Liquid chromatography-mass spectrometry
LC-MS/MS	Liquid chromatography with tandem mass spectrometry
LogFC	Minimal log_2 fold change
MB	Marine broth
MSA	Multiple sequence alignment
MST	MicroScale thermophoresis
P	Phosphorus
P_i	Inorganic phosphate
PC	Phosphocholine
PE	Phosphoryl-ethanolamine
PP	Particulate phosphorus
PIP	Particulate inorganic phosphorus
POP	Particulate organic phosphorus
PlcP	Phospholipase C
*p*NP	*para*-nitrophenol

*p*NPP	*para*-nitrophenyl-phosphate
*p*NPPC	*para*-nitrophenyl-phosphorylcholine
PtdCho	Phosphatidylcholine
PtdEtn	Phosphatidylethanolamine
PtdGro	Phosphatidylglycerol
Seq.ID	Protein sequence identity
SPE	Sphingosyl-PE d17:1/12:0
TRAP-T	Tripartite ATP-independent periplasmic transporter
v/v	Volume per volume
w/v	Weight by volume
Zn^{2+}	Zinc

CHAPTER 1 INTRODUCTION

"Life can multiply until all phosphorus is gone, and then there is an inexorable halt which nothing can prevent."
Isaac Asimov (1919-1992)

1.1 Importance of phosphorus for living organisms

It was the chemist Isaac Asimov who recognised the significance of phosphorus (P) for living organisms. P is one of the most common elements in the Earth's crust (Benitez-Nelson, 2000; Paytan & McLaughlin, 2007). However, P-availability is limited (Benitez-Nelson, 2000; Lougheed, 2011). Due to its high reactivity, P naturally only occurs in chemically bonded form, either as organic or inorganic phosphate (P_i) (Pasek, 2008; Pandey & Parveen, 2011).

P_i is essential for DNA and RNA, where it forms the backbone of both molecules in connection with a quintuple sugar (Benitez-Nelson, 2000; Koolman & Röhm, 2019). It also provides energy to cells as adenosine triphosphate (ATP) (Gajewski et al., 1986; Paytan & McLaughlin, 2007; Koolman & Röhm, 2019). ATP is the most important form of chemical energy and the input molecule of P_i into cellular metabolism. The incorporation of P_i into organic molecules and energy production occurs through hydrolysis of ATP, leading to the dissociation of one of the three P_i groups (Gajewski et al., 1986). This group can further bind to another substrate and transfer it to a higher energy level (Paytan & McLaughlin, 2007; Karl, 2014), a process known as phosphorylation (Lin et al., 2016). For example, kinases transfer P_i from ATP onto other molecules, converting ATP into adenosine diphosphate (ADP). ADP can be converted back to ATP by phosphorylation, thereby closing the cycle (Kornberg, 1957; Gajewski et al., 1986). Additionally, P_i is an important element of cell membranes. Phospholipids form a lipid bilayer, enabling membrane proteins to move in the fluid mosaic model (Paytan & McLaughlin, 2007; Koolman & Röhm, 2019). Although P_i is essential for intracellular processes, high concentrations can be harmful to the organism (Kulaev et al., 2005). For example, excess cytosolic P_i disrupts Mg^{2+}-dependent processes in *Salmonella enterica* serovar Typhimurium, leading to an overproduction of

ATP and ribosomal RNA, sequentially inhibiting bacterial growth and viability (Bruna et al., 2021). If the intracellular P_i concentration rises above a certain threshold, bacteria can either restrict P_i uptake (Bruna et al., 2021) or accumulate P_i as polyphosphates (Kulaev et al., 2005; Achbergerová & Nahálka, 2011). Polyphosphates are linear and unbranched chains of two up to 10^6 P_i groups and chemically linked by energy-rich phosphoanhydride bonds. The cleavage of P_i groups from polyphosphates releases the chemical energy stored in these phosphoanhydride bonds, which can sequentially be used for phosphorylation reactions, as described above (Kulaev et al., 2005; Achbergerová & Nahálka, 2011). In addition, polyphosphates are a common form of P_i storage, that can be used when P-availability declines (Achbergerová & Nahálka, 2011; Martin et al., 2014).

1.2 The marine phosphorus cycle

The marine P cycle has been studied extensively (Figure 1.1) (Föllmi, 1996; Benitez-Nelson, 2000; Baturin, 2003; Paytan, 2007; Sebastián & Ammerman, 2009; Moore, 2013; Karl, 2014; Van Mooy et al., 2015; Ruttenberg, 2019). Methods to estimate fluxes of various forms of P within the global oceans have been established over many years, summarised by Karl and Björkman (2001). Rivers transporting P from continental weathering events and P generated through human activities account for the highest influxes of P into the global oceans, around 60-100 x 10^{10} mol P per year (Föllmi, 1996; Carpenter et al., 1998; Delaney, 1998; Compton et al., 2000; Bennett et al., 2001; Migon et al., 2001). P from continental weathering processes and anthropogenic sources consist primarily of particulate inorganic P (PIP) and particulate organic P (POP), along with smaller fractions of dissolved P (Paytan & McLaughlin, 2007). Although high amounts of P enter the oceans, a large proportion of particulate P is deposited in coastal areas and is no longer available to the marine biota (Wollast, 1983). Higher salinity is required to desorb P from particles, thereby returning P to the marine P cycle (Froelich, 1988; Sundareshwar & Morris, 1999). While riverine and anthropogenic P influxes play a crucial role in retaining and altering the marine P cycle, atmospheric influxes account for 20 times less P input (Duce et al., 1991; Prospero et al., 1996).

Atmospheric P influxes from dust and volcanic ashes contain inorganic and organic P varieties (Yamagata et al., 1991; Bergametti et al., 1992; Resing & Sanson, 1999; Ridame & Guieu, 2002). Although atmospheric inputs are considered to alter P concentrations only locally, they are believed to be a relevant short-term input of P and adhered metal ions to nutrient-depleted open ocean regions as well (Yamagata et al., 1991; Resing & Sanson, 1999; Benitez-Nelson, 2000; Ridame & Guieu, 2002).

Upon entering the water column, P passes through a wide range of transformations. These include inorganic and organic variations of particulate or dissolved P (Paytan & McLaughlin, 2007). Particulate P (PP) can be separated from dissolved P (DP) by filtering (0.2 or 0.45 µm) and is composed of dead and living plankton and P that either precipitated as minerals or adsorbed to particles (Paytan & McLaughlin, 2007). Contrary to this, DP passes through a filter. displays known inorganic and organic forms of the DP pool. For example, orthophosphate (P_i) is the most common form of inorganic P in the DIP pool (~87%) and is bioavailable to organisms (Benitez-Nelson, 2000; Mahaffey et al., 2014). However, specific uptake systems and enzymes are necessary to utilise inorganic P compounds like phosphite and hypophosphite (e.g., Polyviou et al., 2015; Van Mooy, 2015; Bisson et al., 2017; Frischkorn et al., 2018). In addition, organic compounds that contain a C-P (phosphonates) or C-O-P (phosphate monoesters or phosphate diesters) bond and inorganic substrates that consist of more than one P_i group (polyphosphates or pyrophosphates) require hydrolysis before uptake (e.g., Ahn & Kornberg, 1990; Kulaev, 2005; Quinn et al., 2007; McGrath et al., 2013; Seweryn et al., 2015; Tian-Tian et al., 2019; Stosiek et al., 2020). All these variations and transformations of P are part of the marine P cycle.

Briefly described, P_i enters the marine P cycle through assimilation by phytoplankton, followed by transformation steps converting P_i to organic P compounds (Cotner & Wetzel, 1992). Phytoplankton is ingested by zooplankton or detritivores, and P is subsequently excreted as DIP or DOP (Cotner & Biddanda, 2002) or released through cell lysis of phytoplankton (Anderson & Zeutschel, 1970).

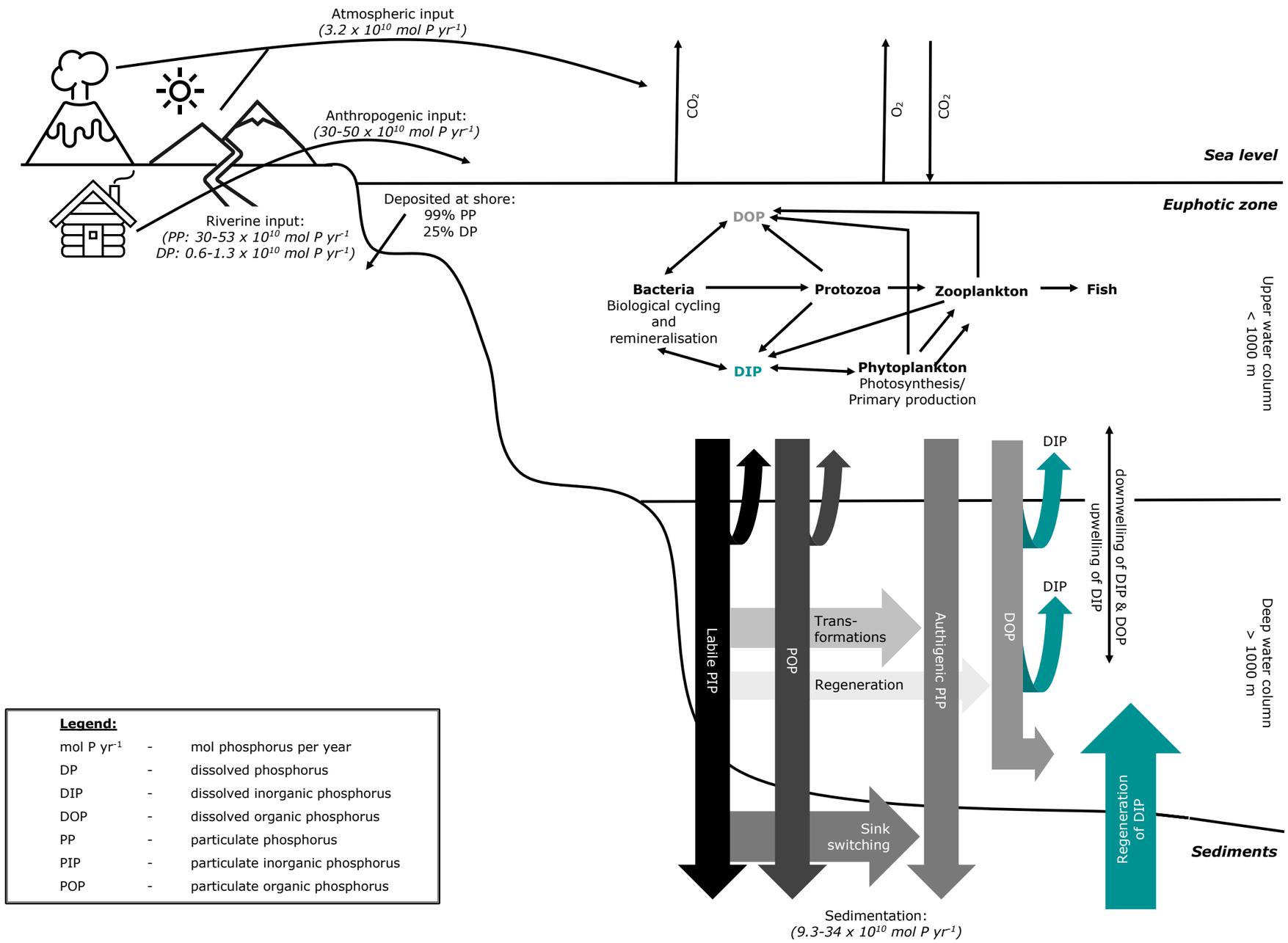

Legend:		
mol P yr^{-1}	-	mol phosphorus per year
DP	-	dissolved phosphorus
DIP	-	dissolved inorganic phosphorus
DOP	-	dissolved organic phosphorus
PP	-	particulate phosphorus
PIP	-	particulate inorganic phosphorus
POP	-	particulate organic phosphorus

Figure 1.1: ***The marine phosphorus cycle.***
Fluxes are given in italics and marine P cycle is described in the text. Adapted from Föllmi, 1996, Benitez-Nelson, 2000, and Paytan, 2007.

While DIP is instantly assimilated by phytoplankton again, some DOP is hydrolysed by specific enzymes of heterotrophic bacteria or phytoplankton, thereby releasing more DIP (Azam et al., 1983; Cotner & Biddanda, 2002). DIP and DOP can adsorb to particles to form PP, sequentially desorbs again, or sinks in the water column. PP is either remineralised in the sinking process or reaches the ocean floor (Delaney, 1998; Faul et al., 2005). Consequently, P that arrives at the ocean floor is buried as labile PIP, POP, or authigenic P (Figure 1.1, Faul, 2005; Paytan, 2007). Here, labile PIP represents the fraction of PP subjected to transformations into DOP, making it bioavailable to microorganisms again. The opposite of the labile fraction is the refractory fraction subjected to permanent burial (James et al., 2002). Some PIP is converted into authigenic P, specifically remineralised organic P that reprecipitates as calcium fluorapatite (Faul et al., 2005). Finally, around 9.3-34 x 10^{10} mol P per year is deposited in sediments (Berner & Berner, 1996; Filippelli & Delaney, 1996; Benitez-Nelson, 2000). Burial and remineralisation processes of P in marine deep-sea sediments are quite complex. For example, the transformation of labile PIP into authigenic P, as described above, is known as sink switching (Delaney, 1998). Recent studies estimate the residence time of P in the marine P cycle to be around 10,000-20,000 years (Ruttenberg, 2019). Given this, an "average" P atom is believed to cycle the global oceans ten times before it is ultimately removed (Karl, 2014).

1.2.1 Varieties of inorganic and organic phosphorus

A wide variety of inorganic and organic P exists in the global oceans, as listed in . The P-atom in all these variations occurs in different oxidation states (Paytan & McLaughlin, 2007; Pasek, 2008; Walsh, 2020). The P-atom of the most common form of P_i, orthophosphate, is in the fully oxidized P^{5+} state (Pasek, 2008; Van Mooy et al., 2015; Walsh, 2020). Noteworthy, a small fraction of the DIP pool contains hypophosphites and phosphites, which possess a P^{1+} and P^{3+} atom, respectively (Pasek, 2008; Van Mooy et al., 2015; Bisson et al., 2017; Walsh, 2020). Recent studies have described novel hypophosphite and phosphite transporters (Bisson et al., 2017), facilitating a new P pathway in the marine environment.

However, not many marine bacteria that use phosphite as a sole source of P have been described (Poehlein et al., 2013; Bisson et al., 2017). High energy events like radioactive decay or photolysis can reduce orthophosphate to phosphite. These events frequently occurred in the reducing environment of the early Earth. It seems likely that the ability to exploit these reduced P compounds is a remainder of the ancient planet Earth, shaping a small but prolific niche of P (Pasek, 2008).

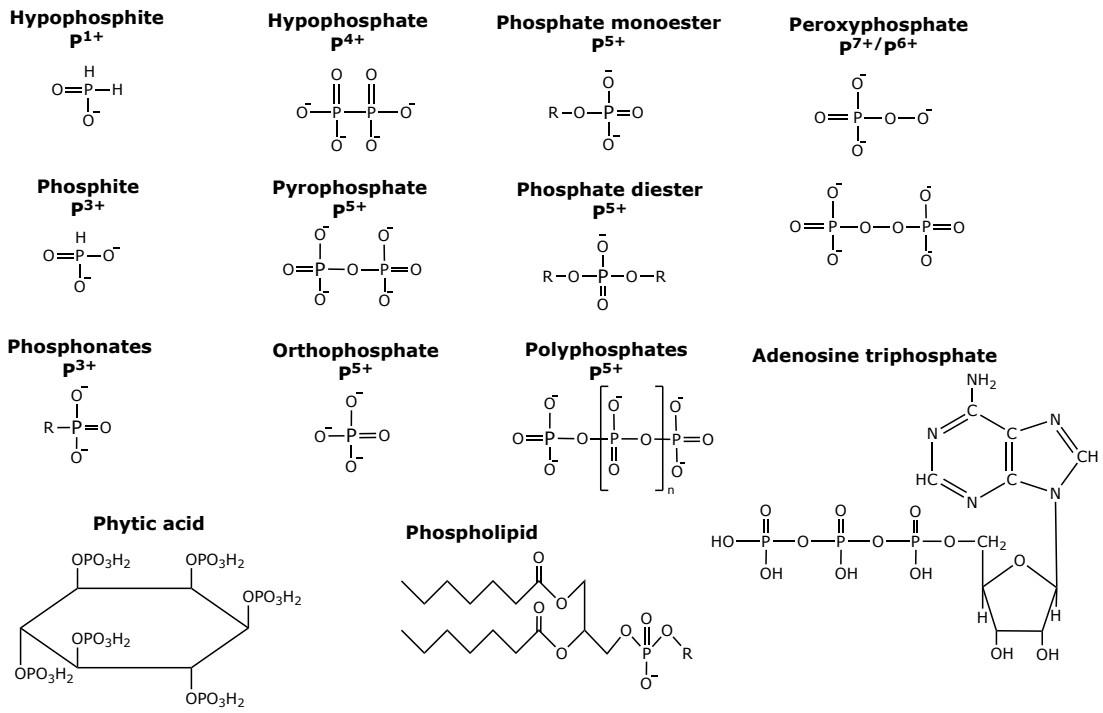

Figure 1.2: ***Variety of inorganic and organic phosphorus, including oxidation state of the P-atom.***
Organic phosphates have a C-P or C-O-P bond; R, residues containing at least one C-atom. Adapted from (Paytan & McLaughlin, 2007; Pasek, 2008).

In surface waters, the total DP pool is dominated by DOP (Björkman et al., 2000). The majority of this DOP pool occurs as phosphate monoesters and phosphate diesters, with both forms having a fully oxidised P^{5+} atom (Paytan & McLaughlin, 2007; Van Mooy et al., 2015). Monoester and diester bonds are a common feature of phospholipids, ATP, nucleic acids, and nucleotides (Van Mooy et al., 2015; Koolman & Röhm, 2019). These substrates are fairly easily hydrolysed by phosphatases, releasing bioavailable P_i in the process (e.g., Wanner, 1996). Upon cell death and cell lysis, these organic substrates are available to the wider microbial community. For example, phospholipases and transferases play a crucial role in phospholipid degradation and turnover. Lysophospholipids

are formed in the turnover process and sequentially reconverted into fully functional phospholipids or further degraded (Sahonero-Canavesi et al., 2019). In marine bacteria, around 10-20% of the cellular P content is integrated into phospholipids (Van Mooy et al., 2008), a lucrative source of P upon cell lysis. In addition, phosphonates (C-P), with a P^{3+} atom, account for around 5-10% of the DOP pool (Young & Ingall, 2010). Unlike the straightforward hydrolysis of monoester and diester bonds, a so-called C-P lyase machinery is indispensable to degrade phosphonates (e.g., Wanner & Metcalf, 1992; Quinn, 2007; Villarreal-Chiu et al., 2012; Sosa et al., 2017; Stosiek, 2020). A study conducted by Sosa et al. (2017) revealed that around 20% of analysed isolates from surface water samples of the North Pacific Subtropical Gyre possess complete C-P lyase pathway operons. The phosphonate degradation pathway in *Escherichia coli* (*E. coli*) involves a one-step mechanism that includes a redox reaction at the P centre, including a phosphite intermediate (Wanner & Metcalf, 1992).

While different forms of inorganic and organic P are essential to maintain a functional marine P cycle, the global P redox cycle also contributes majorly to the biogeochemical cycling of P (Van Mooy et al., 2015). The marine biogeochemical P cycle forced the development of adaptation mechanisms to the various forms of inorganic and organic P in living organisms. Since P_i is the preferred bioavailable form of P a regulatory system had to evolve to allow for P_i concentration measurements, P_i uptake control, P recycling, and the degradation of different P compounds.

1.2.2 Phosphate limitation in the marine environment

As mentioned above, P_i plays a crucial role in living organisms. For a long time, other nutrients such as nitrogen and iron (Fe) were considered the sole limiting nutrients in the marine environment (Björkman & Karl, 2003; Karl et al., 2001; Suzumura et al., 2012). However, regular inputs of trace metals through winds can supply enough Fe to temporarily support photosynthesis of phototrophs and thereby primary production in some regions (Kremling & Streu, 1993; Wu et al., 2000; Morel & Price, 2003). Contrary to this, areas like the Equatorial Pacific are considered high nutrients-low chlorophyll (HNLC) environments (Behrenfeld et al., 1996).

Although macronutrients like nitrate are never significantly depleted in HNLC environments, spring phytoplankton blooms rarely occur (Martin et al., 1994). Here, the lack of Fe inhibits photosynthesis, thereby reducing primary production, keeping the biomass at a relatively constant level (Pitchford & Brindley, 1999). In addition, nitrogen fixation by bacterial diazotrophs is a key process to introduce new nitrogen into ocean surface waters (Sellner, 1986; Ammerman et al., 2003; Moore et al., 2013), a process that requires high amounts of Fe (Benitez-Nelson, 2000; Morel & Price, 2003). Recent studies showed that P_i contributes majorly to the control of bacterial growth and primary production in the global oceans (Karl et al., 2001; Ammerman et al., 2003; Paytan & McLaughlin, 2007). Because of this, the focus shifted towards the availability of this essential nutrient.

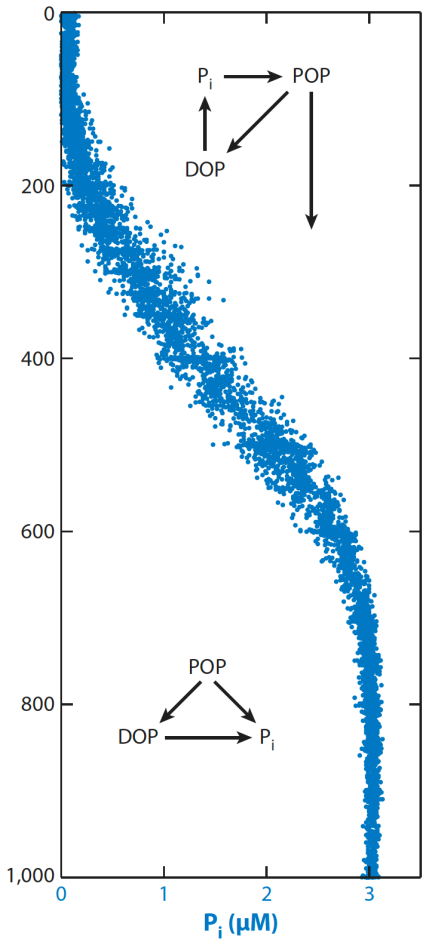

Figure 1.3: ***Changes in the P_i concentration (µM) in the water column to a depth of 1,000 m.*** *The upper fraction (0-150 m) represents the production of particulate matter, which sinks to the ocean floor. The lower fraction (> 150 m) represents the remineralisation of P_i from particulate matter. From Karl, 2014.*

Giant and anticyclonic subtropical gyres, which dominate global oceans, are critical for marine bacterial diversity and primary production

contributions. These gyres are chronically P_i deplete (Ammerman et al., 2003; Paytan & McLaughlin, 2007; Mahaffey et al., 2014; Karl, 2014). Whereas the concentration of bioavailable DIP is chronically low (Karl, Bidigare, et al., 2001; Zubkov et al., 2007; Browning et al., 2017), the DOP pool dominates the total dissolved P reservoir in surface waters (Björkman et al., 2000). The vertical profile of the water column shows that bioavailable P_i (DIP) decreases drastically in surface waters (Figure 1.3, Karl, 2014). Here, bacteria transform DIP into DOP that then sinks to the ocean floor as DOP or POP, as described in section 1.2. During the sinking process, both DOP and POP are remineralised by bacteria and archaea. In doing so, bioavailable DIP is generated. The vertical profile above represents only a minor fraction of the marine P cycle (Figure 1.1). However, it clarifies the importance of adaptations of marine bacteria to P_i limitation. The adaptation to limited P_i concentrations required the development of a sensitive stress response system which has been discovered and studied first in *E. coli*.

1.3 The *Escherichia coli* phosphate stress response

E. coli has a two-component regulatory system to gauge cellular P_i concentration and react to changes in external P_i (Figure 1.4) (Wanner, 1996; Baek et al., 2007; Karl, 2014). This two-component system consists of a transmembrane sensor histidine kinase (PhoR) and a transcriptional activator (PhoB). Together, PhoB and PhoR regulate the transcription of the Pho regulon. Genes of the Pho regulon include *phoA*, which encodes an alkaline phosphatase, *pstS*, encoding the P_i binding protein of the high-affinity Pst transporter and *pitA* and *pitB*, both genes encoding low-affinity P_i transporters (Wanner, 1996). During growth or P_i-limitation, the expression of Pho regulon genes can increase by a hundredfold (Wanner, 1996; Tetu et al., 2009). Conversely, an extracellular excess of P_i inhibits the expression of the Pho regulon (Wanner, 1996). When P_i becomes limiting, PhoR senses a decrease in the P_i concentration (Figure 1.4). PhoR autophosphorylates on a conserved histidine residue. The subsequent transfer of this phosphate group to an aspartate residue on PhoB leads to the activation of the latter. Activated PhoB facilitates transcriptional

activation by enabling the protein to bind to Pho boxes within the Pho regulon (Peterson et al., 2005; Baek & Lee, 2006). These so-called Pho boxes are specific regions on the *E. coli* genome that either activate or repress the transcription of genes (Santos-Beneit, 2015). Pho boxes comprises two 7-nucleotide direct repeat units that are separated by four non-conserved nucleotides, forming a 18-nucleotide sequence (Makino et al., 1988; Monds et al., 2006; Santos-Beneit, 2015).

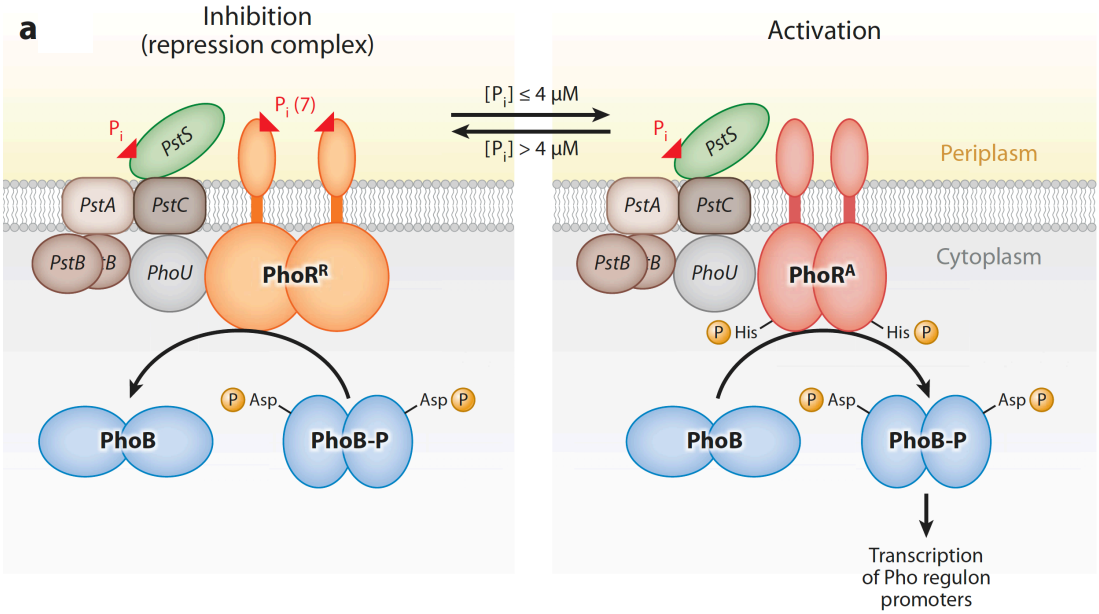

Figure 1.4: ***Schematic representation of the Pho regulon in Escherichia coli.*** *The system gets activated when the P_i concentration in the periplasm is below 4 µM. PhoR: transmembrane sensor histidine kinase, PhoB: transcriptional regulator factor, PstS: periplasmatic phosphate-binding protein, PstA: permease, PstC: permease, PstB: ATPase, PhoU: negative regulator. From Karl, 2014.*

As stated above, several genes involved in cellular P_i metabolism are activated during the P_i-stress response. Noteworthy, *pitB* is a constitutively expressed transporter and is not sensitive to P_i-concentrations like the high-affinity Pst transporter (Wanner, 1996; Baek & Lee, 2007). The Pst system belongs to the superfamily of ABC transporters, which, as a mutual feature, all share an ATP-binding cassette. The binding and hydrolysis of ATP allows the transport of ions up to macromolecules through the membrane (Wanner, 1996; Rees et al., 2009). The Pst system of *E. coli* consists of a periplasmic P_i binding protein (PstS), two permeases (PstA and PstC) and a cytoplasmic ATPase (PstB). PstS activity is closely monitored by the PhoBR system, informing the cell

about the current P_i concentration (Peterson et al., 2005). In addition, the protein encoded by the gene *phoU* represses the autophosphorylation of PhoR if P_i is in excess (Wanner, 1996). The high-affinity and low-affinity P_i transport systems allow *E. coli* to acquire P_i across a wide range of P_i concentrations. Marine bacteria, especially species that inhabit low P_i environments, have a very similar P_i-stress response. These phototrophic and heterotrophic bacteria are irreplaceable for the marine food web and ecosystem maintenance.

1.3.1 General strategies to overcome phosphate limitation

Low P_i conditions in the global oceans have forced marine bacteria to develop strategies for survival. There are two main strategies microbes elicit in nutrient-limited environments:

1) increase the acquisition of P_i from organic sources for example organic phosphates or phospholipids

   AND/OR

2) reduce their P_i requirements by altering cell physiology, e.g., decrease cell growth or adjust protein/DNA/macromolecule composition.

To facilitate these alterations the advancement of specific P_i acquisition systems (Scanlan et al., 1993; Hirani et al., 2001; Pitt et al., 2010; Cox & Saito, 2013), the ability to utilise alternative organic P-sources (Tetu et al., 2009; Cox & Saito, 2013; Lin et al., 2018), or the development of mechanisms to reduce P-requirements, e.g., lipid remodelling (Van Mooy et al., 2006, 2009; Sebastián et al., 2016), was required.

1.4 Significance of marine bacteria for the global ocean biogeochemistry

Microorganisms catalyse the vast majority of biogeochemical transformations of energy and matter on Earth (Chróst, 1990; Falkowski et al., 2008; Strom, 2008). These marine microbes account for 90% of the aquatic biomass (Biddanda et al., 2021). In ocean surface waters, marine food webs are fuelled by photosynthesis. Here, single-celled cyanobacteria

and algae provide virtually all energy and carbon (Carr & Wyman, 1994; Legendre et al., 2015). How this energy and carbon are then shared between a consortium of archaea, heterotrophic bacteria, fungi, protists, and higher organisms is still not fully understood. The microbial loop, which comprises more than 95% of all processes involved in aquatic metabolism, is the main route by which surface ocean bacteria and archaea acquire dissolved organic carbon (DOC) and DOP (Li, 1998; Karl et al., 2001; Buchan et al., 2014; Biddanda et al., 2021). Furthermore, the microbial loop resembles the activities that occur in the upper water column of the marine P cycle (Figure 1.1) and summarises the interactions between phytoplankton, bacteria, protozoa, archaea, viruses, and zooplankton in the euphotic zone. Marine microbes significantly influence the biogeochemistry of the ocean and the atmosphere by controlling the microbial loop, including the fluxes of carbon, P, and other important elements (Falkowski et al., 2008).

Marine cyanobacteria form the most diverse and widespread group of photosynthetic prokaryotes and possess a photosynthetic apparatus that is similar to eukaryotic chloroplasts (Carr & Wyman, 1994). The two genera *Synechococcus* and *Prochlorococcus* dominate the global oceans. They contribute around 25% to the oceanic net primary production and are responsible for roughly half of the overall oxygen production (Morel & Price, 2003; Thomson et al., 2003; Flombaum et al., 2013). Cyanobacteria produce dissolved organic matter (DOM) as a 'waste' product. DOM serves as a nutrient source for heterotrophic bacteria that cannot fix carbon. More DOM is released through cell lysis induced by viruses, and during sloppy feeding of zooplankton (Scanlan & Wilson, 1999; van den Meersche et al., 2004; Diaz et al., 2019). Heterotrophic bacteria can recycle DOM through respiration (Cotner & Biddanda, 2002; Biddanda et al., 2021), thereby releasing CO_2 that re-enters the atmosphere and is re-used by phytoplankton for sequential primary production (Carr & Wyman, 1994). However, this sensible and well-organised system of 'giving and taking' is endangered by climate change. Models suggest that climate change will most likely reduce the solubility of nutrients, slow down the biological pump, and lead to increased ocean stratification (Falkowski et al., 2008;

Deppeler & Davidson, 2017). The reduced availability of nutrients in surface waters will bring about lower productivity and smaller cell sizes (Peter & Sommer, 2015). Oceans are predicted to experience tropicalisation, with extensions of gyres towards the polar regions, reduced ice extent, higher sea levels, higher acidity, and lower oxygen levels than at present (Duarte, 2014). In addition, marine organisms will be impacted by temperature changes with many species approaching their thermal capacity (Burrows et al., 2014).

As demonstrated in this section, marine microorganisms are crucial for conserving our global oceans and the climate. Human-induced climate change will potentially change the biogeochemistry of the oceans over an incredibly short period. Because of this, it is essential to fully understand the current nutrient cycles in marine ecosystems to allow for the prediction of future changes.

1.5 The genus *Synechococcus*

As stated above, cyanobacteria play an important role in marine primary production (Field et al., 1998; Flombaum et al., 2013; Grob et al., 2013). The two major primary producers in the global oceans are members of the phototrophic genera *Synechococcus* and *Prochlorococcus* (Waterbury et al., 1986; Coleman & Chisholm, 2007; Scanlan et al., 2009). Even though *Synechococcus* is wider distributed, its abundance is about one order of magnitude lower than *Prochlorococcus* (Li, 1995; Ahlgren & Rocap, 2012; Flombaum et al., 2013). Species of the genera *Synechococcus* are characterised as small, unicellular, and ovoid to cylindrical cyanobacteria (Waterbury et al., 1986). In marine systems, habitats range from tropical waters to the polar circle. Their wide distribution required an adaptation to various environmental conditions, resulting in a rich diversity of strains and ecological niche adaptation (Scanlan et al., 2009; Palenik, 2012). Furthermore, the development of specialists and generalists has formed genomic variants within the genus. Based on 16S rRNA gene sequences, the *Synechococcus* lineage can be divided into three sub-clusters, with the major sub-cluster 5.1 being further subdivided into at least 10 genetically distinct clades (Figure 1.5,

Scanlan et al., 2009). Recent metagenomic studies suggest that all *Synechococcus* strains compromise a shared 'core' genome, a potential clade-specific genome and a strain-specific genome, that is variable and dominated by gene transfer (Dufresne et al., 2008; Palenik, 2012).

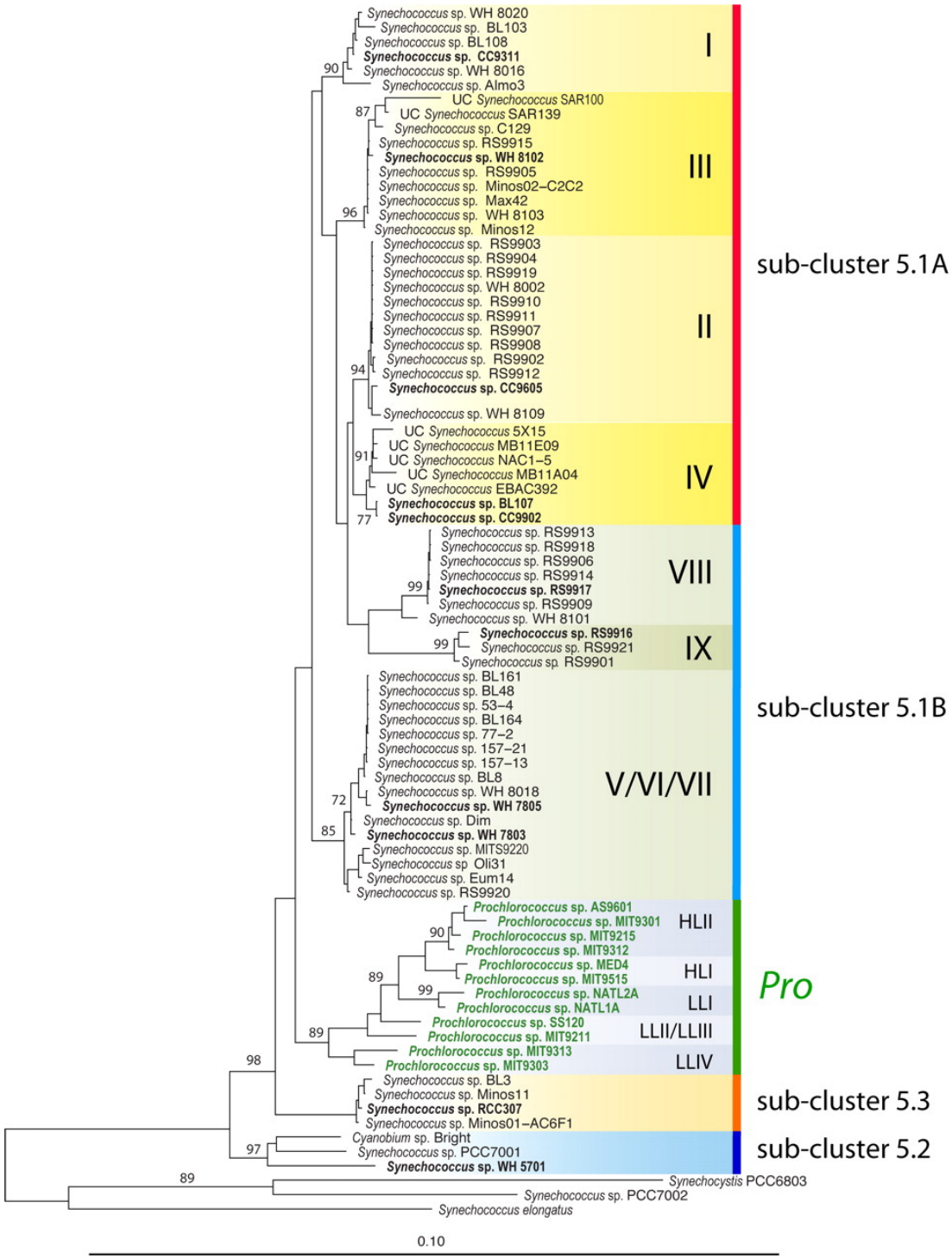

Figure 1.5: ***Phylogenetic relationships among marine members of the genera Synechococcus and Prochlorococcus.***
Neighbor-joining tree which is based on 16S sequences, bootstrap values >70% are shown. Sub-cluster 5.1 represents the largest cluster and is further subdivided into various clades. From Scanlan et al., 2009.

1.5.1 Phosphate stress regulation in *Synechococcus* sp. WH8102

Synechococcus sp. WH8102 (*Syn*. WH8102) is a model organism of *Synechococcus* clade III (Figure 1.6). Isolated from the North Atlantic Gyre, this lineage appears restricted to low nutrient conditions (Palenik et al., 2003; Scanlan et al., 2009). The development of a high-affinity P_i uptake mechanism was required for survival in these oligotrophic environments. *Syn*. WH8102 doesn't have the low-affinity *pitAB* system, like some other cyanobacterial species (Moore et al., 2005), which is consistent with the oligotrophic environment it inhabits. Furthermore, a homologous sequence to PhoU, a repressor of the PhoBR system at high P_i conditions, wasn't found (Morohoshi et al., 2002; Moore, 2005). Tetu et al. (2009) examined the Pho regulon in *Syn*. WH8102 and revealed several genes which have counterparts in *E. coli*. These genes include multiple putative alkaline phosphatase genes (SYNW0120, SYNW0196, SYNW2391, SYNW2390) and multiple, non-identical copies of *pstS* genes (SYNW1018, SYNW1815, SYNW2507). *PstS* encodes the periplasmic high-affinity P_i binding protein component of the Pst transporter system (Palenik, 2003; Moore, 2005; Tetu, 2009). The expression of genes encoding for alkaline phosphatases and PstS is upregulated during P_i starvation in *Syn*. WH8102 and other cyanobacterial genera (Aiba & Mizuno, 1994; Hirani et al., 2001; Suzuki et al., 2004; Moore, 2005; Tetu, 2009) and rapidly repressed after reintroducing P_i (Zeng & Chisholm, 2012).

Ostrowski et al. (2010) suggested a two-tiered response to P_i limitation in *Syn*. WH8102. First, the expression of the Pst system, including *pstS* genes, via the PhoBR regulatory system is activated (Figure 1.4). Subsequently, and potentially when P_i-concentrations reduce further, another transcriptional activator PtrA is induced by PhoBR. PtrA regulates and enhances the expression of various putative alkaline phosphatase genes, specifically SYNW0196 and SYNW2390 (Moore, 2005; Ostrowski et al., 2010). Even though Su et al., 2007, predicted SYNW2390 and SYNW2391 to be one transcriptional unit with two tandem Pho boxes (Su et al., 2007), the putative phosphatase SYNW2391 is directly induced by PhoB (Ostrowski et al., 2010). In addition to genes that are directly involved in P_i metabolism, genes that are linked to several cellular

processes, including metal ion transportation, are impacted by PtrA. One of these genes is SYNW2477, encoding a putative Zn^{2+} ABC transport system (Ostrowski et al., 2010). Previous work has shown that Zn^{2+} is required for the activity of phosphatases in *E. coli* (Coleman, 1992) and other model organisms (Shaked et al., 2006; Cox & Saito, 2013). The requirement of Zn^{2+} could explain the upregulation of gene SYNW2477, as more Zn^{2+} is needed to saturate some of the phosphatases (Ostrowski et al., 2010). Additionally, Cox and Saito (2013) showed that the relative abundance of SYNW2391 increased during P_i starvation when Zn^{2+} was added to P_i depleted cells. Whilst it is believed that Zn^{2+} appears to play a crucial part in the P_i-metabolism of marine cyanobacteria (Shaked et al., 2006; Cox & Saito, 2013), there is little or no information on the metal cofactors required for phosphatase activity in *Syn*. WH8102.

Given that no genes for the transport of organic phosphates have been identified so far, it is likely that *Syn*. WH8102 acquires P_i from alternative organic P sources through hydrolysis via 'alkaline' phosphatases (Grossman et al., 1994; Moore, 2005). In summary, zinc is believed to be a metal cofactor for most 'alkaline' phosphatases. As zinc concentrations in the oceans can drop dramatically (Jakuba et al., 2008), marine bacteria require zinc-independent phosphatases to secure their P_i-demands. A recently discovered alkaline phosphatase PhoX (Majumdar et al., 2005; Zaheer et al., 2009; Kathuria & Martiny, 2011; Yong et al., 2014), which shows no homology to the PhoA-type phosphatases, requires calcium and iron for activity. Studies suggested that alkaline phosphatases of the PhoX-type have a wider distribution in marine bacteria than PhoA-type phosphatases (Sebastián & Ammerman, 2009).

Understanding the metal requirements of these phosphatases will aid in identifying whether key metal micronutrients are also important in regulating the abundance of these organisms in situ. This feature is well known for iron (Kolber et al., 1994) which is a major requirement for many proteins of the photosynthetic machinery (Morrissey & Bowler, 2012).

1.6 *Phaeobacter* sp. MED193

The *Roseobacter* group belongs to the family *Rhodobacteraceae* and accounts for around 20-30% of marine bacterial communities (Brinkhoff et al., 2008; Luo & Moran, 2014; Simon et al., 2017). Until recently, the *Roseobacter* group was referred to as a clade. However, the latest phylogenetic studies demonstrated that this group is not monophyletic (Simon et al., 2017). Members of the *Roseobacter* group primarily inhabit marine environments but also found in less common habitats like sea ice and soil/sediments, or attached to surfaces (Buchan et al., 2005; Brinkhoff et al., 2008; Luo & Moran, 2014; Simon et al., 2017). Most *Roseobacters* follow a heterotrophic lifestyle, but a few members are also capable of phototrophy (Luo & Moran, 2014; Simon et al., 2017). In addition, *Roseobacters* can utilise various forms of organic and inorganic compounds and play a crucial role in the degradation of dimethylsulfoniopropionate (DMSP) (Chen & Schäfer, 2019), sulphur oxidation (Wang et al., 2021), and the synthesis of secondary metabolites (Brinkhoff et al., 2008; Daniel et al., 2018). To date more than 50 *Roseobacter* genomes have been fully sequenced, with most of these strains readily cultured (Luo & Moran, 2014). Recently, single-cell genomics allowed to (partially) sequence genomes of uncultivated *Roseobacter* strains (Feng et al., 2021). Studies have shown that members of the *Roseobacter* group closely interact with phytoplankton (Buchan et al., 2014), making them optimal candidates for microbial interaction studies (e.g., Christie-Oleza et al., 2015, 2017; Kaur et al., 2017).

In recent years, members of the *Roseobacter* group were used to investigate membrane lipids and lipid alterations as an adaptation mechanism to nutrient limitations (Sebastián et al., 2016; Smith et al., 2019, 2021). For example, *Ruegeria pomeroyi* DSS-3 compensates for the lack of phospholipids under P-limiting conditions by synthesising glutamine and ornithine lipids instead (Smith et al., 2019). A novel sulphur-containing amino lipid was recently described in *R. pomeroyi* DSS-3 (Smith et al., 2021). Lipid remodelling was discovered not long ago in *Phaeobacter* sp. MED193 (MED193) (Sebastián et al., 2016), but was previously described in phytoplankton and members of the SAR11 clade (Van Mooy

et al., 2006, 2009; Carini et al., 2015; Shemi et al., 2016). Thus, the capacity for lipid remodelling is widely distributed in the marine environment though not present in all marine *Roseobacter*. The replacement of phospholipids in MED193 requires a manganese-containing phospholipase C (Wei et al., 2018). It is noteworthy that strains of the genus *Phaeobacter* are widespread in marine environments, are easily cultivated, and can grow at high substrate concentrations (Brinkhoff et al., 2008). In addition, *Phaeobacter* strains are associated with biofilm-formation, adherence to surfaces, formation of aggregates, and fast cell growth making them optimal candidates for laboratory studies (Brinkhoff et al., 2008; Buchan et al., 2014).

1.6.1 Membrane lipids of marine *Roseobacter*

The *E. coli* lipid bilayer is primarily composed of two glycerophospholipids, phosphatidylethanolamine (PtdEtn) and phosphatidylglycerol (PtdGro), and small amounts of cardiolipin (Zhang & Rock, 2008). Phospholipids consist of two fatty acid chains linked to an *sn*-glycerol-3-phosphate backbone via an ester bond and a headgroup (Figure 1.5) (López-Lara & Geiger, 2017). Only recently more lipids were discovered in the membranes of the *Roseobacter* group (Sohlenkamp & Geiger, 2015; López-Lara & Geiger, 2017). This discovery includes a third glycerophospholipid, specifically phosphatidylcholine (PtdCho). Other glycerolipids, like sulfoquinovosyl diacylglycerol (SQDG) and diacylglyceryl trimethylhomoserine (DGTS), share the diacylglycerol (DAG) backbone but have a P-free headgroup. Both SQDG and DGTS commonly replace phospholipids under P-limitation (Van Mooy et al., 2006; Sebastián et al., 2016). Another group of lipids was reported in marine *Roseobacters*: amino lipids contain an amino acid headgroup that is linked to a fatty acid chain via an amide bond, as in ornithine lipids (OL) and glutamine lipids (QL) (Geiger et al., 2010; Smith et al., 2019). Not long ago, a novel sulphur-containing amino lipid (SAL) was discovered in the membranes of *Roseobacters* (Smith et al., 2021). Here, homotaurine (3-aminopropane sulfonic acid) or a 2-aminopropane sulfonic acid is connected to two fatty acid chains via an amide bond. Glycerophospholipids are used as an internal source of P, allowing for survival during P-limited conditions.

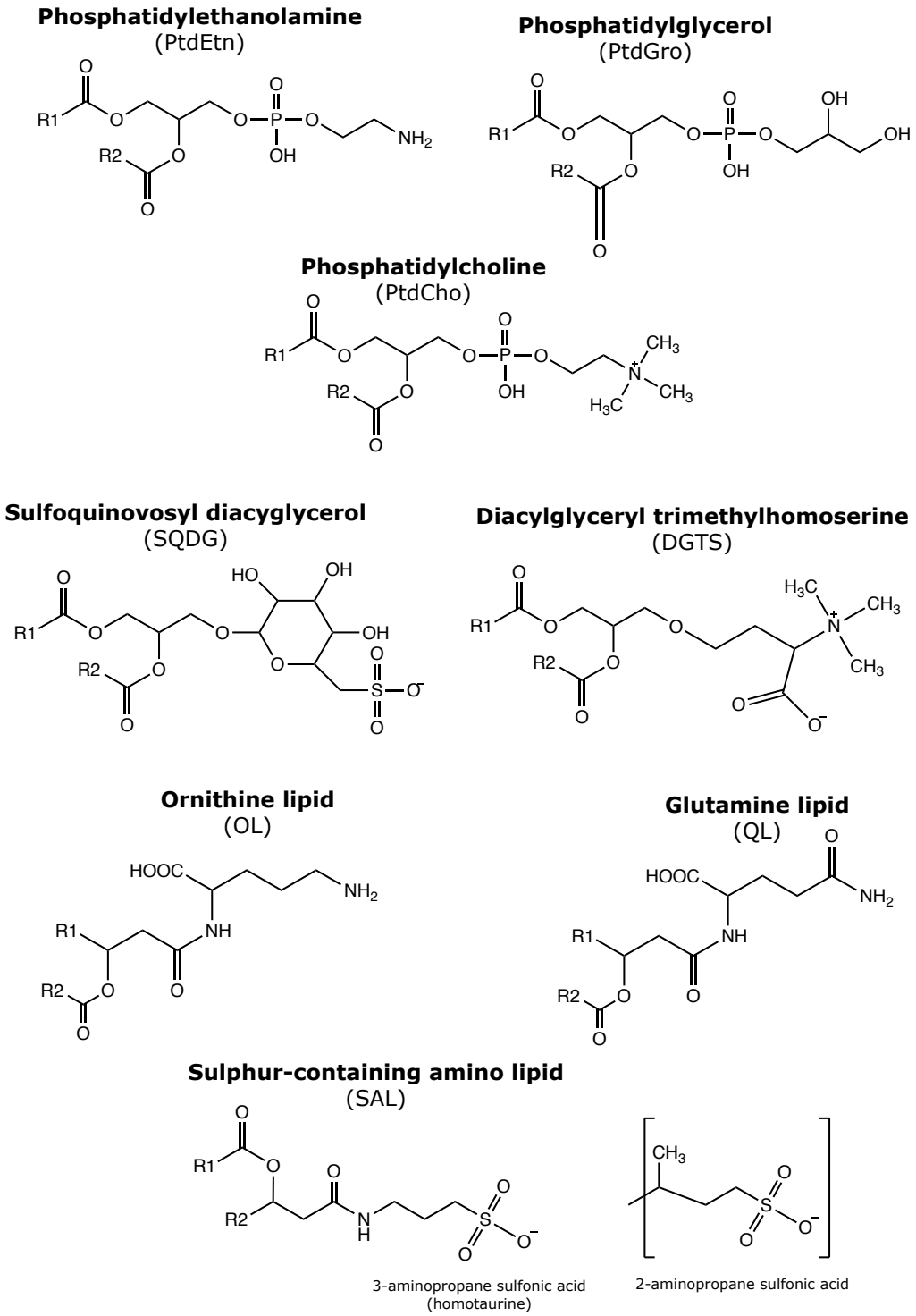

Figure 1.6 ***Chemical structures of selected membrane lipids of Phaeobacter sp. MED193.***
P-containing glycerolipids: PtdEtn, PtdGro, and PtdCho; P-free glycerolipids: SQDG and DGTS; amino lipids: OL, QL, and SAL with two possible headgroups: 3-aminopropane sulfonic acid (homotaurine) or 2-aminopropane sulfonic acid (in brackets). Adapted from López-Lara & Geiger, 2017; Smith et al., 2021.

But also other environmental stressors, such as changes in pH, temperature, or medium osmolarity, can alter the membrane lipid composition (Sohlenkamp & Geiger, 2015; López-Lara & Geiger, 2017).

Research investigating the intracellular and extracellular membrane lipid turnover is still scarce (Sahonero-Canavesi et al., 2019).

Sufficient reasons advised to use MED193 as a model organism for lipid-related studies in this work: 1. MED193 undertakes lipid remodelling as a P-stress response (Sebastián et al., 2016), 2. the MED193 membrane composition has been decoded (Sebastián et al., 2016), 3. MED193 is a specialist for P-limitation originating from the partially P-limited Mediterranean Sea (Brinkhoff et al., 2008), and 4. the cultivation of this strains has been optimised.

1.6.2 The role of phospholipids in the marine P cycle

Lipids are more resistant to degradation than other compounds of the DOM. They are frequently used as biomarkers to study recent and ancient biogeochemical cycles in marine environments and examine the composition of bacterial and archaeal communities (Law & Zhang, 2019). In marine heterotrophs, 20% of the cellular P content is stored in membrane phospholipids. In phytoplankton, phospholipids incorporate around 10% of the cellular P content (Van Mooy et al., 2008). Given this, phospholipids represent a lucrative source of organic P, and recent studies have estimated that phospholipids account for around 1.5% of the particulate organic carbon pool (Gašparović et al., 2018). Depending on the marine environment, between 10% and 55% of the total lipid pool are phospholipids (Frka et al., 2011; Marić et al., 2013; Gašparović et al., 2014). Latest studies on the lipid composition of POM have identified familiar phospholipids (see Figure 1.5), including PtdEtn, PtdGro, and PtdCho, but also novel and unknown saturated and unsaturated phospholipids. These novel phospholipids are not degraded in the ocean surface waters, but are transported to the deep sea (Suzumura, 2005; Gašparović et al., 2018). In marine sediments, the genus *Psychromonas* seems to be a crucial primary degrader of these lipids and proteins (Pelikan et al., 2021). In conclusion, phospholipids represent a viable source of P, but also carbon, nitrogen, and sulphur. Because of this, more research is needed to fully understand lipid degradation in the global oceans and their contribution to the marine food web.

1.7 PhD project overview and aims

The aims of this project were as follows:

1. To study the phosphate stress response in wild type *Phaeobacter* sp. MED193 and a *phoB* deletion mutant in which the Pho regulon is silenced (Chapter 3).
2. To investigate the ability of *Phaeobacter* sp. MED193 to utilise phospholipid headgroups as a sole source of P (Chapter 4).
3. To investigate the degradation pathway of glycerol-1-phosphate and glycerol-3-phosphate in *Phaeobacter* sp. MED193 (Chapter 5).
4. To determine the metal requirements of different phosphatases in *Phaeobacter* sp. MED193 and *Synechococcus* sp. WH8102 (Chapter 4 and Chapter 6).

Specific questions include:

1. Does the phosphate stress response of *Phaeobacter* sp. MED193 possess novelties due to its occupation of ultra-low P_i environments?
2. Is there genomic evidence that *Phaeobacter* sp. MED193 can utilise a variety of organic phosphates?
3. Does *Phaeobacter* sp. MED193 possess specific transporters for organic P compounds, such as phospholipid headgroups, or is an extracellular phosphatase required for cleavage before uptake?
4. Can marine bacteria utilise the archaeal lipid glycerol-1-phosphate?
5. What metal cofactors are required for phosphatase activity of *Phaeobacter* sp. MED193 and *Synechococcus* sp. WH8102?
6. What are the putative substrates of these phosphatases?

CHAPTER 2 MATERIALS & METHODS

2.1 Strains used and culture conditions

All strains that were used in this work are listed in Table 2.1. Stocks of all isolates were kept at -80 °C in 20% (v/v) glycerol.

Phaeobacter sp. MED193:

Glycerol stocks of *Phaeobacter* sp. MED193 (hereafter WT MED193) were revived by streak plating cells on 1.5% marine broth (MB) agar (A, Formedium Ltd., Norfolk, UK) plates followed by incubation at 30 °C for 24 to 48 hours. Colonies were then inoculated into 5 ml MB and incubated at 30 °C for 24 hours at 150 rpm shaking. For the MB media, 37.4 g L^{-1} of Difco™ Marine Broth 2216 (Becton, Dickinson and Company, Franklin Lakes, NJ, USA) was dissolved and autoclaved. For the maintenance of WT MED193, 100 µl of a 10^{-6} dilution was spread on MBA, incubated at 30 °C for 24 hours and kept at 4 °C afterwards. The same procedure applies to *Phaeobacter* sp. MED193 *ΔphoB* (hereafter *ΔphoB*). However, a final concentration of 10 µg ml^{-1} gentamicin was used for selection.

Table 2.1: ***List of bacterial strains used in this work.***
The antibiotic resistance is given for overexpression strains and deletion mutants.

Strain	*Antibiotic resistance*
Phaeobacter sp. MED193	
Phaeobacter sp. MED193 *ΔphoB*	10 µg ml^{-1} gentamicin
E. coli BL21	
E. coli BL21 (DE3)	
E. coli DH_5-Alpha	
E. coli BL21 SYNW0196 in pMAL-c4x SYNW2391 in pMAL-c4x	100 µg ml^{-1} ampicillin
E. coli BL21(DE3) SYNW1799 in pET-22b(+) SYNW2390 in pET151/D-TOPO MED193_05784 in pET151/D-TOPO	100 µg ml^{-1} ampicillin

E. coli: *E. coli* strains BL21, BL21(DE) and DH_5-Alpha were revived on Lysogeny Broth agar (LBA) and incubated at 37 °C for 24 hours. These colonies were then initially inoculated into 5 ml LB before following the protocol to make competent cells (see section 2.2.5). All *E. coli* strains containing overexpression plasmids were selected on LBA with 100 µg

ml^{-1} ampicillin. Details of growth conditions for these strains can be found in section 2.2.6.

2.1.1 Defined culture conditions for the growth of *Phaeobacter* sp. MED193 and *ΔphoB*

For the growth of WT MED193 in defined media, cells were revived by streak plating cells on MBA followed by incubation at 30 °C for 24 to 48 hours. Isolated colonies were picked and inoculated into 5 ml MB for overnight growth at 30 °C with shaking at 150 rpm. To achieve optimal growth afterwards, a dilution series was prepared and 100 µl of the 10^{-5}, 10^{-6} and 10^{-7} dilution was plated on MBA and incubated overnight at 30°C. As before, one single colony was inoculated into 10 ml MB and grown overnight at 30 °C in a shaking incubator. A 1% (v/v) inoculum of this initial culture was then transferred into artificial seawater (ASW). The defined media for MED193 (see Table 2.2 for details) derived from ASW medium in Wilson et al. (1996) was modified with a carbon source (10 mM sodium succinate), vitamins (1 ml L^{-1} MAMS vitamins, see Table 2.13) and a different nitrogen source (8.8 mM ammonium chloride). Growth was monitored by measuring the optical density (OD) at 540 nm (OD_{540}) on a Jenway 7305 (Cole-Parmer, Stone, UK) spectrophotometer. The same procedure applied to *ΔphoB*. However, a final concentration of 10 µg ml^{-1} gentamicin was used for selection.

2.1.2 Culture conditions for phosphate starvation of *Phaeobacter* sp. MED193 and *ΔphoB*

After 24 hours of growth of WT MED193 and *ΔphoB* in MB, the medium was visibly cloudy, and a 1% v/v inoculum of this culture was inoculated into 100 ml ASW (50 µM K_2HPO_4), and growth continued for another 24 hours. To prepare cultures for starvation, a 12.5% (v/v) inoculum of the overnight culture was spun down at room temperature (RT) for 10 min at 3,220 x g and inoculated into 100 ml P-free ASW. Cultures were then grown for 48 hours at 30 °C with shaking at 140 rpm to completely starve them for P. The growth was monitored by measuring OD_{540}. Again, a final concentration of 10 µg ml^{-1} gentamicin was used for *ΔphoB*.

Table 2.2: ***Composition of ASW medium.***

Chemical	*Stock solution (g L^{-1})*	*Stock conc.*	*Molecular weight (g mol^{-1})*	*Final conc. in 1 L of ASW*	*ml for 1 L of ASW*
NaCl			58.44	420.0 mM	25 g
*$MgCl_2$ * 6 H_2O*	200	0.98 M	203.30	9.8 mM	10
KCl	100	1.34 M	74.55	6.7 mM	5
*$CaCl_2$ * 2 H_2O*	100	0.68 M	147.01	3.4 mM	
$MgSO_4$	175	1.42 M	120.37	14.2 mM	10
K_2HPO_4	12.00	69.00 M	174.20	50 µM	724.64 µl
				172.3 µM	2.5
HEPES	43.32	0.182 M	238.30	1.0 mM	5.5
NH_4Cl	47.08	0.88 M	53.49	8.8 mM	10
*$C_4H_4Na_2O_4$ * 6 H_2O*	270.14	1.00 M	270.14	10.0 mM	10
Trace metals					
H_2BO_3	2.86	46.26 mM	61.83	46.26 µM	1
*$MnCl_2$ * 4 H_2O*	1.81	9.15 mM	197.91	9.15 µM	
*$ZnSO_4$ * 2 H_2O*	0.222	1.24 mM	179.46	1.24 µM	
*Na_2MoO_4 * 2 H_2O*	0.390	1.89 mM	205.92	1.89 µM	
*$CuSO_4$ * 5 H_2O*	0.008	32.04 µM	249.69	32.04 nM	
*$Co(NO_3)_2$ * 6 H_2O*	0.0494	169.74 µM	291.03	169.74 nM	
*$FeCl_3$ * 6 H_2O*	3.00	11.09 mM	270.30	11.09 µM	
EDTA(Na_2Mg)	0.50	1.39 mM	358.49	1.39 µM	

2.1.3 Growth on phospholipid headgroups

For the growth experiment on phospholipid headgroups, biological triplicates of WT MED193 and *ΔphoB* were prepared according to sections 2.1.1 and 2.1.2. Six conditions were used for the experiment and are described here:

- Pre-starved cultures supplemented with a phosphate source (final concentration of 172.3 µM)
  - phosphocholine (CAS no 72556-74-2, hereafter PC)
  - phosphoryl-ethanolamine (CAS no 1071-23-4, hereafter PE)
  - glycerol-phosphate (CAS no 927-20-8, hereafter PG)
  - inorganic phosphate (K_2HPO_4, hereafter +P)
- Pre-starved cultures as a negative control (hereafter -P)
- Cultures grown in ASW with a final concentration of 344 µM inorganic phosphate as a positive control (K_2HPO_4, hereafter HP control)

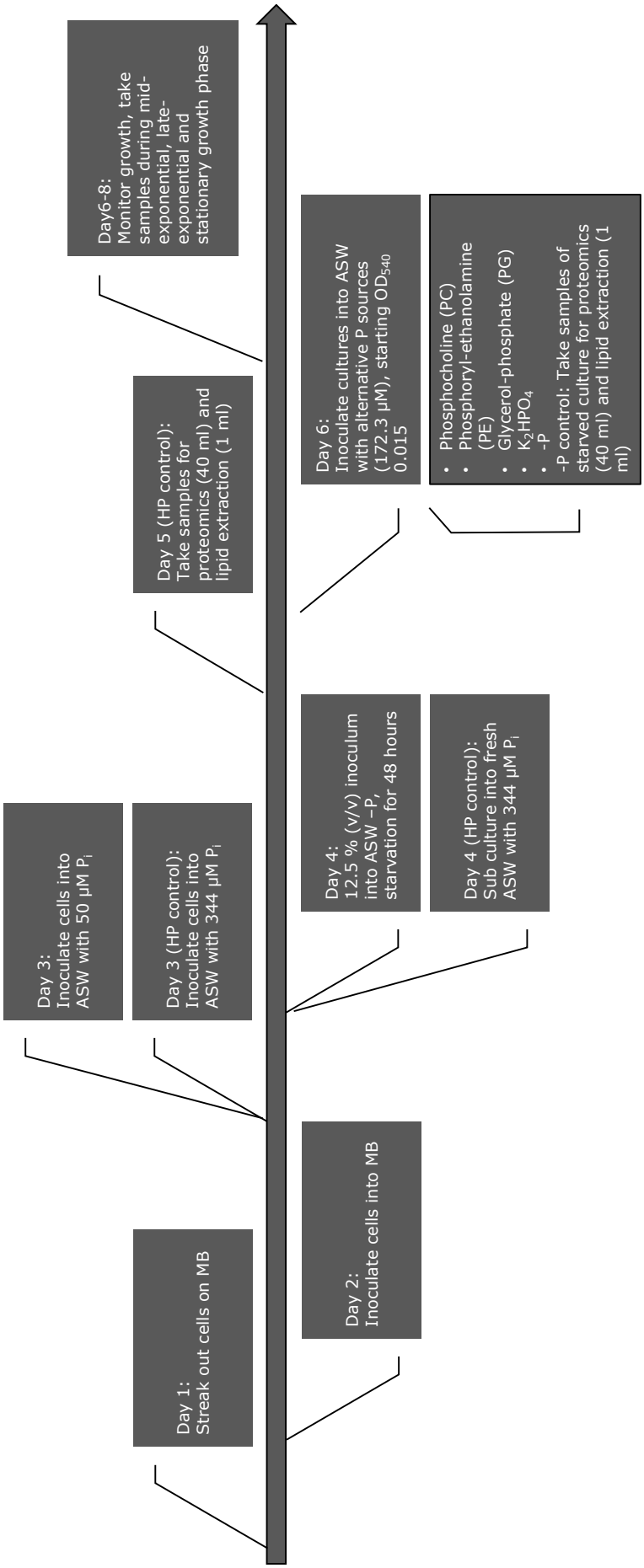

Figure 2.1: ***Timeline and description of the experimental setup for the growth experiment of marine heterotrophic bacteria on phospholipid headgroups as a sole source of phosphate.***

The phospholipid headgroups were purchased from Sigma-Aldrich (St. Louis, MO, USA). A timeline for the experimental setup can be found in Figure 2.1 and is described hereafter. The optical density of the pre-starved cultures was measured and inoculated into 400 ml ASW, containing either PC, PE, PG, P_i, or no P, to reach a final starting OD_{540} of 0.015. These cultures were incubated at 30 °C with shaking at 140 rpm and growth was monitored by measuring the OD_{540} over 48 hours. Furthermore, technical triplicates of each culture were loaded in a Falcon® 96-well clear flat bottom TC-treated culture microplate (Corning Inc., Corning, NY, USA) and growth was monitored in a FLUOstar Omega microplate reader (BMG Labtech, Ortenberg, Germany) over 48 hours. 40 ml samples for proteomics analysis (cellular and extracellular) and 1 ml samples for lipid analysis were taken shortly after cultures entered exponential growth, as well as late exponential phase and stationary phase. Samples were spun down at 3,220 x g at 4 °C for 10 min and the supernatant was poured into a new falcon tube. The pellets as well as the supernatant were snap-frozen in dry ice and kept at -20 °C until used.

2.1.3.1 Glycerol-phosphate degradation

To clarify the role of MED193_19449 (annotated as a periplasmic phosphonate binding protein) biological triplicates of WT MED193 and *ΔphoB* were prepared according to sections 2.1.1 and 2.1.2. These pre-starved cultures were then grown in ASW supplemented with either *sn*-glycerol-1-phosphate (CAS no 5746-57-6, hereafter G1P, Sigma-Aldrich) or *sn*-glycerol-3-phosphate (CAS no 17989-41-2, hereafter G3P, Sigma-Aldrich) with a final concentration of 172.3 µM. Cultures grown on inorganic phosphate (K_2HPO_4, hereafter +P) were used as a positive control and pre-starved cultures (hereafter -P) as a negative control. The growth experiment was performed according to the protocol described in section 2.1.3 and Figure 2.1.

2.2 Protein overexpression

2.2.1 Plasmid synthesis

Plasmids for the phosphatases from *Synechococcus* sp. WH8102 namely SYNW2390 (RefSeq WP_011129243,), SYNW2391 (RefSeq WP_011129244), SYNW0196 (RefSeq WP_011127072) and SYNW1799 (RefSeq WP_011128659) and from *Phaeobacter* sp. MED193 namely MED193_05784 (RefSeq CH902583) were synthesized via GeneArt™ (Thermo Fisher Scientific, Waltham, MA, USA). Initially, the overexpression cloning vector pET151/D- TOPO (Figure 2.2A) was used for all phosphatases except SYNW1799 (see section 2.2.3). pET151/D- TOPO contains a T7 and lacO promoter for high-level expression, an ampicillin resistance cassette, an N-terminal 6x polyhistidine (His)-Tag and a TEV protease recognition site, to cleave off the His-Tag after purification. As a non-constitutive system, the vector can be induced using Isopropyl β-d-1-thiogalactopyranoside (IPTG). Synthesizing a plasmid with GeneArt™ allows to codon optimize the gene sequence for *E. coli* to better guarantee good gene expression (Appendix 2.1 - Appendix 2.3). The phosphatase SYNW1799 was codon-optimized (Appendix 2.4) and cloned into pMA-T, a non-expression vector. More details on SYN1799 can be found in section 2.2.3.

2.2.2 Cloning work

2.2.2.1 SYNW2391 & SYNW0196

Overexpression of phosphatases encoded by the genes SYNW2391 and SYNW0196 in pET151/D- TOPO resulted only in the production of insoluble protein. Therefore, both genes were cloned into a pMAL™ vector which contains an N-terminal maltose-binding protein (MBP) fusion protein to help solubilise the protein (Figure 2.2B). The pMAL-c4x plasmid contains a Xa cleavage site to remove the MBP after purification as well as a tac promoter, which can be induced by IPTG. The plasmid was kindly provided by Dr Richard J. Puxty. The plasmid was cut with the restriction enzymes *Eco*RI and *Bam*HI according to the manufacturer's instructions. It was then purified by running the entire 50 µl reaction on a 1% (w/v) agarose gel, stained with ethidium bromide, for 30 min at 120 V. A 1 kilobase DNA

ladder (New England Biolabs (NEB), Ipswich, MA, USA) was used to verify the size of the fragments.

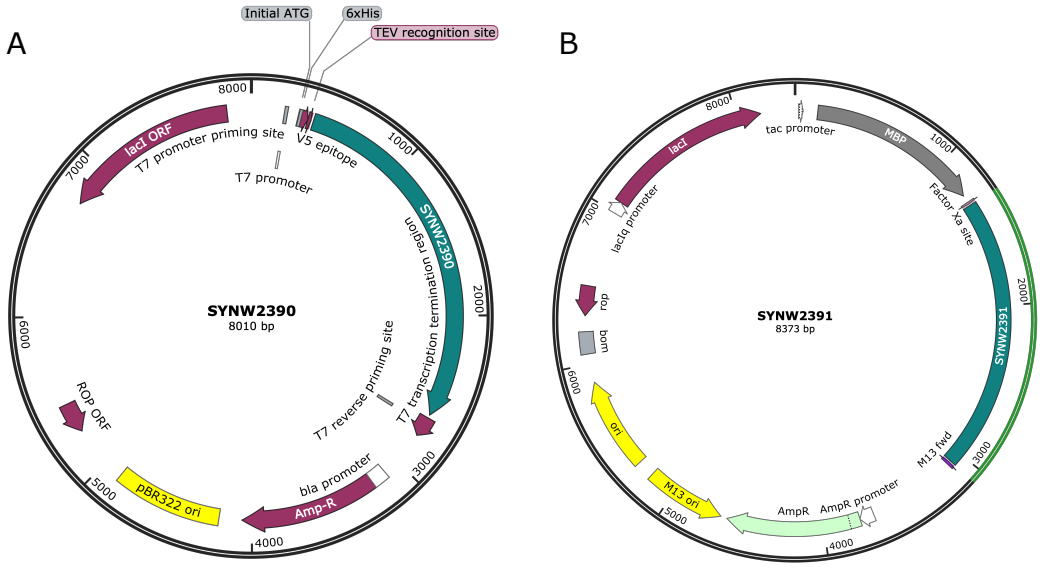

Figure 2.2: ***Plasmids used for the overexpression of SYNW2390 and SYNW2391.*** *(A) pET151/D-TOPO vector containing the gene for SYNW2390, synthesized with GeneArt™. The plasmid contains a T7 promoter, N-terminal His-Tag and a TEV cleavage site. Cell selection through ampicillin resistance. (B) pMAL-c4x vector containing the gene for SYNW2391. The plasmid contains a tac promoter but was modified with a T7 promoter, N-terminal maltose-binding protein (MBP) and a Xa cleavage site. Cell selection through ampicillin resistance.*

The bands on the gel were visualised on a UV visualiser and the strong plasmid band was removed with a clean scalpel and transferred to a 1.5 ml Eppendorf tube. The QIAquick gel extraction kit (Qiagen, Hilden, Germany) was used for the gel extraction. The *Phusion* polymerase high-fidelity PCR master mix with HF buffer (Thermo Fisher Scientific) was used to amplify both genes (SYNW0196 & SYNW2391). For more information about primer and PCR conditions see Table 2.3. Products were digested with *Dpn*I for 1 hour at 37 °C before an inactivation step at 65 °C for 20 min. The PCR product was then purified from the reaction mix using the QIAquick PCR purification kit (Qiagen). The concentration of the DNA (PCR fragment and plasmid) was measured using a NanoDrop 2000 (Thermo Fisher Scientific). The following calculation was used for the estimation of the fragment concentration for the cloning step:

$$pmols = \frac{weight\ in\ ng * 1000}{size\ of\ DNA\ in\ bp * 650\ daltons}$$

The recommended concentration of DNA fragments for the Gibson assembly of 2-3 fragments is 0.02-0.5 pmols. The highest efficiency is reached by assembling 50-100 ng of the vector with a 2-fold molar excess of the insert.

Table 2.3: ***List of primers (A) and PCR conditions (B, C) used for amplification and control of genes for Synechococcus sp. WH8102 phosphatases SYNW0196 & SYNW2391.***
PCR conditions used for amplification of (B) genes SYNW0196 and SYNW2391 (30 cycles) and (C) the T7 promoter (25 cycles).

A

Primer name	*Product*	*Sequence 5'-3'*
SYNW0196_fw	SYNW0196 with homologous regions to pMAL c4x	GATCGAGGGAAGGATTTCAGAATTCACCGCAAGCTTTCGTCATG
SYNW0196_rv		CCTGGCAGGTCGACTCTGAGGATCCTTAAATCAGTCCTTCAACCTGTTC
SYNW0196_PI_fw	SYNW0196 control primer from pMAL c4x into insert	GACGCGCAGACTAATTCGAG
SYNW0196_I1_rv	SYNW0196 control primer1 insert	GCATCACTACCTGCCAGACC
SYNW0196_I2_rv	SYNW0196 control primer2 insert	GAATATCTGCGGTGGTGGTT
SYNW0196_IP_rv	SYNW0196 control primer from insert into pMAL c4x	GTTTCCCAGTCACGACGTT
SYNW2391_fw	SYNW2391 with homologous regions to pMAL c4x	GATCGAGGGAAGGATTTCAGAATTCGCACGTATTAGCGATAGC
SYNW2391_rv		CCTGCAGGTCGACTCTAGAGGATCCTTATGCCAGATCTGCCTG
SYNW2391_PI_fw	SYNW2391 control primer from pMAL c4x into insert	TCGATGAAGCCCTGAAAGAC
SYNW2391_I_rv	SYNW2391 control primer insert	CCAGGTCTTTTGCACGAACT
SYNW2391_IP_rv	SYNW2391 control primer from insert into pMAL c4x	CCAGGGTTTTCCCAGTCAC
T7_fw	T7 promoter	TAATACGACTCACTATAGGG
T7_rv	T7 terminator	GCTAGTTATTGCTCAGCGG

B

	Temperature	*Time*
Initial denaturation	98 °C	30s
Denaturation	98 °C	10s
Primer annealing	60 °C	20s
Extension	72 °C	30s
Final extension	72 °C	5m

C

	Temperature	*Time*
Initial denaturation	95 °C	1m
Denaturation	95 °C	15s
Primer annealing	54 °C	15s
Extension	72 °C	10s
Final extension	72 °C	5m

The NEBuilder HiFi DNA assembly (NEB) mix was prepared according to the manufacturer's instructions. A concentration of 0.025 pmol vector and 0.05 pmol insert was used. The mixture was incubated at 50 °C for 1 hour. After the incubation step, the vector was transformed into chemically

competent NEB 5-alpha *E. coli* high-efficiency cells (NEB) according to the manufacturer's instructions. Transformants were selected by plating 100 µl cells on LBA – ampicillin (100 µg ml^{-1}). Furthermore, the remaining 900 µl were spun down at 435 x g for 5 min, supernatant eliminated, the cell pellet resuspended in 200 µl SOC media, and the whole suspension plated on LBA with ampicillin (100 µg ml^{-1}). Transformants were screened using T7 promoter primers (see Table 2.3A and B) and the MyTaq™ Red Mix (Bioline, London, UK). Colonies that showed the right product size were inoculated into 5 ml LB with ampicillin (100 µg ml^{-1}), plasmids were extracted by using the QIAprep spin miniprep kit (Qiagen), and plasmid was sent for sequencing (Figure 2.3), using the control primers listed in Table 2.3A.

```
SYNW0196   gacgttgatctgggcaccgatgatagtccgctgacacagggttttcgttcatttgatctggcagatctggttaccctgtat
Sequence   ------------------------------------------------------------------------------------
Sequence   GACGTTGATCTGGGCACCGATGATAGTCCGCTGACACAGGGTTTTCGTTCATTTGATCTGGCAGATCTGGTTACCCTGTAT
Sequence   ------------------------------GCTGACACAGGGTTTTCGTTCATTTGATCTGGCAGATCTGGTTACCCTGTAT
Sequence   ------------------------------------------------------------------------------------

SYNW0196   gttctggaaacccgtctgaccgcacgtgatgaacagctggcatatccgaatagtgatgcagttgcagcacgtattggtgat
Sequence   ------------------------------------------------------------------------------------
Sequence   GTTCTGGAAACCCGTCTGACCGCACGTGATGAACAGCTGGCATATCCGAATAGTGATGCAGTTGCAGCACGTATTGGTGAT
Sequence   GTTCTGGAAACCCGTCTGACCGCACGTGATGAACAGCTGGCATATCCGAATAGTGATGCAGTTGCAGCACGTATTGGTGAT
Sequence   ------------------------------------------------------------------------------------

SYNW0196   attctggccgatccgctgctgctggcaagctatgcagaaagcctgggtgttgcaccgcctgttagtgccgaagatctggat
Sequence   ------------------------------------------------------------------------------------
Sequence   ATTCTGGCCGATCCGCTGCTGCTGGCAAGCTATGCAGAAAGCCTGGGTGTTGCACCGCCTGTTAGTGCCGAAGATCTGGAT
Sequence   ATTCTGGCCGATCCGCTGCTGCTGGCAAGCTATGCAGAAAGCCTGGGTGTTGCACCGCCTGTTAGTGCCGAAGATCTGGAT
Sequence   ------------------------------------------------------------------------------------

SYNW0196   ggtgttaatgcactgagcgcagcactgattgatccggttacactggaactggttgcagcaaccgttgcagatggttggacc
Sequence   ------------------------------------------------------------------------------------
Sequence   GGTGTTAATGCACTGAGCGCAGCACTGATTGATCCGGTTACACTGGAACTGGTTGCAGCAACCGTTGCAGATGGTTGGACC
Sequence   GGTGTTAATGCACTGAGCGCAGCACTGATTGATCCGGTTACACTGGAACTGGTTGCAGCAACCGTTGCAGATGGTTGGACC
Sequence   ------------------------------------------------------------------------------------

SYNW0196   aatccgagccgtaatctgctgggtcaagatcagcagagctggctgcagagcggtctggcaggtagtgatgccgcatggcag
Sequence   ------------------------------------------------------------------------------------
Sequence   AATCCGAGCCGTAATCTGCTGG--------------------------------------------------------------
Sequence   AATCCGAGCCGTAATCTGCTGGGTCAAGATCAGCAGAGCTGGCTGCAGAGCGGTCTGGCAGGTAGTGATGCCGCATGGCAG
Sequence   ------------------------------------------------------------------------------------

SYNW0196   gttctgggtcagcaagttctgatgcagagcatggcaattccggcagaactgctgctgaatgcaaccgatccggatgttctg
Sequence   ------------------------------------------------------------------------------------
Sequence   ------------------------------------------------------------------------------------
Sequence   GTTCTGGGTCAGCAAGTTCTGATGCAGAGCATGGCAATTCCGGCAGAACTGCTGCTGAATGCAACCGATCCGGATGTTCTG
Sequence   ------------------------------------------------------------------------------------

SYNW0196   gcaaaatatagcgcaccgctggaaaaactggcaaccggtcagccgctgaatcaggatgaactggcactgtttgatgaagca
Sequence   ------------------------------------------------------------------------------------
Sequence   ------------------------------------------------------------------------------------
Sequence   GCAAAATATAGCGCACCGCTGGAAAAACTGGCAACCGGTCAGCCGCTGAATCAGGATGAACTGGCACTGTTTGATGAAGCA
Sequence   ------------------------------------------------------------------------------------

SYNW0196   accaaaattccgtataatctggatgcatgggatggttatggtgttgaacgtgaaaccattctgcagaccgcagcaggtctg
Sequence   ------------------------------------------------------------------------------------
Sequence   ------------------------------------------------------------------------------------
Sequence   ACCAAAATTCCGTATAATCTGGATGCATGGGATGGTTATGGTGTTGAACGTGAAACCATTCTGCAGACCGCAGCAGGTCTG
Sequence   ---------CCGTATAATCTGGATGCATGGGATGGTTATGGTGTTGAACGTGAAACCATTCTGCAGACCGCAGCAGGTCTG

SYNW0196   ggtaaaaaactggttagcctggcaggcgataccccataatgcctgggttggtgttctggatgccatgagtaccggtgcagca
Sequence   ------------------------------------------------------------------------------------
Sequence   ------------------------------------------------------------------------------------
Sequence   GGTAAAAAACTGGTTAGCCTGGCAGGCGATACCCATAATGCCTGGGTTGGTGTTCTGGATGCCATGAGTACCGGTGCAGCA
Sequence   GGTAAAAAACTGGTTAGCCTGGCAGGCGATACCCATAATGCCTGGGTTGGTGTTCTGGATGCCATGAGTACCGGTGCAGCA

SYNW0196   atgcctggtcaggttgttggtattgaatttgccacaccgggtgtgagcgcaccgggtattgaaacatatattgcacctggt
Sequence   ------------------------------------------------------------------------------------
Sequence   ------------------------------------------------------------------------------------
Sequence   ATGCCTGGTCAGGTTGTTGGTATTGAATTTGCCACACCGGGTGTGAGCGCACCGGGTATTGAAACATATATTGCACCTGGT
Sequence   ATGCCTGGTCAGGTTGTTGGTATTGAATTTGCCACACCGGGTGTGAGCGCACCGGGTATTGAAACATATATTGCACCTGGT

SYNW0196   ctggaaccgatttttctgagctataccgaaggtctgaaatataccgatctgagccgtcgcggttttctggatattacctt
Sequence   ------------------------------------------------------------------------------------
Sequence   ------------------------------------------------------------------------------------
Sequence   CTGGAACCGATTTTTCTGAGCTATACCGAAGGTCTGAAATATACCGATCTGAGCCGTCGCGGTTTTCTGGATATTACCTTT
Sequence   CTGGAACCGATTTTTCTGAGCTATACCGAAGGTCTGAAATATACCGATCTGAGCCGTCGCGGTTTTCTGGATATTACCTTT

SYNW0196   catgaagaacacatcaccagcagttatcagctgctggatcctgatgaaggttggattgcagatgttctgcagagtgatgat
Sequence   ------------------------------------------------------------------------------------
Sequence   ------------------------------------------------------------------------------------
Sequence   CATGAAGAACACATCACCAGCAGTTATCAGCTGCTGGATCCTGATGAAGGTTGGATTGCAGATGTTCTGCAGAGTGATGAT
Sequence   CATGAAGAACACATCACCAGCAGTTATCAGCTGCTGGATCCTGATGAAGGTTGGATTGCAGATGTTCTGCAGAGTGATGAT

SYNW0196   agctttagtccgcgtcagctgagccgtgtggatgcaaccaccaccgcagatattccgaccggttttgcacatggtcgtttt
Sequence   ------------------------------------------------------------------------------------
Sequence   ------------------------------------------------------------------------------------
Sequence   AGCT----------------------------------------------------------------------------
Sequence   AGCTTTAGTCCGCGTCAGCTGAGCCGTGTGGATGCAACCACCACCGCAGATATTCCGACCGGTTTTGCACATGGTCGTTTT

SYNW0196   cgtgaagttattcgtgccggtgcaggtaatgatcgtattgcagccggtgatcgtaaaggttatgttagcgcaggcggtggt
Sequence   ------------------------------------------------------------------------------------
Sequence   ------------------------------------------------------------------------------------
Sequence   ------------------------------------------------------------------------------------
Sequence   CGTGAAGTTATTCGTGCCGGTGCAGGTAATGATCGTATTGCAGCCGGTGATCGTAAAGGTTATGTTAGCGCAGGCGGTGGT

SYNW0196   aatgatgatattgatggtggtcgtcgtgcacagctgttactgggtgacgaaggtgatgatgtgattcgtggtcgtggtggt
Sequence   ------------------------------------------------------------------------------------
Sequence   ------------------------------------------------------------------------------------
Sequence   ------------------------------------------------------------------------------------
Sequence   AATGATGATATTGATGGTGGTCGTCGTGCACAGCTGTTACTGGGTGACGAAGGTGATGATGTGATTCGTGGTCGTGGTGGT

SYNW0196   ccagatgaactgcgtggcggtccgggtgcagatagcctgaatggtggtcctggtgatgacctgattttaggtggcgcaggc
Sequence   ------------------------------------------------------------------------------------
Sequence   ------------------------------------------------------------------------------------
Sequence   ------------------------------------------------------------------------------------
Sequence   CCAGATGAACTGCGTGGCGGTCCGGGTGCAGATAGCCTGAATGGTGGTCCTGGTGATGACCTGATTTTAGGTGGCGCAGGC

SYNW0196   gcagatagctttcgtattagcaaaggtgacgatcgcattgtggatctggatccgctggaaggtgacgttctgctgctgcct
Sequence   ------------------------------------------------------------------------------------
Sequence   ------------------------------------------------------------------------------------
Sequence   ------------------------------------------------------------------------------------
Sequence   GCAGATAGCTTTCGTATTAGCAAAGGTGACGATCGCATTGTGGATCTGGATCCGCTGGAAGGTGACGTTCTGCTGCTGCCT

SYNW0196   gccggtttagaaccgacactgaccagcgcagttagcggtgttctgctggccaccgatcgtggtacaaccctgctggaaggc
Sequence   ------------------------------------------------------------------------------------
Sequence   ------------------------------------------------------------------------------------
Sequence   ------------------------------------------------------------------------------------
Sequence   GCCGGTTTAGAACCGACACTGACCAGCGCAGTTAGCGGTGTTCTGCTGGCCACCGATCGTGGTACAACCCTGCTGGAAGGC

SYNW0196   ctgacgctggaacaggttgaaggactgatttaaggatcctctagagtcgacctgcaggcaagcttggcactggccgtcgtt
Sequence   ------------------------------------------------------------------------------------
Sequence   ------------------------------------------------------------------------------------
Sequence   ------------------------------------------------------------------------------------
Sequence   CTGACGCTGGAACAGGTTGAAGGACTGATTTAAGGATCCTCTAGAGTCGACCTGCAGGCAAGCT------------------
```

Figure 2.3: ***Multiple sequence alignment of SYNW0196 overexpression plasmid and sequenced fragments.***

2.2.3 SYNW1799

Synechococcus sp. WH8102 possesses a phosphatase of the PhoX-type (SYNW1799) which has a signal peptide in its sequence and is predicted to be secreted. To ensure the transport of the PhoX protein into the *E. coli* periplasm, the original signal peptide was replaced with one that is compatible with *E. coli*. Therefore, the *Synechococcus* sp. WH8102 *phoX* gene was cloned into a pET-22b(+) vector, which provides an N-terminal *pelB* signal sequence and a C-terminal His-Tag, kindly provided by Prof David I. Roper (Figure 2.4). The signal sequence of the SYNW1799 gene was determined using SignalP 3.0, SignalP 4.0, SignalP 4.1 and SignalP 5.0 (DTU Health Tech, Lyngby, Denmark). All servers predicted different cleavage sites. According to the result of SignalP 5.0, the cleavage site which cleaves off a signal sequence of 25 amino acids was used. For the cloning of the codon optimised SYNW1799 gene, firstly, the pET-22b(+) vector was sequenced. Secondly, two sets of primers were designed to amplify the plasmid in two fragments with homologous regions for ligation. Primers for the amplification of SYNW1799 had homologous regions to allow ligation into the multiple cloning site of the vector and a TEV cleavage site was added, which allows cleavage of the C-terminal His-Tag (see Table 2.4A). The PCR was performed using a proofreading *Phusion* polymerase. The conditions can be found in Table 2.4B.

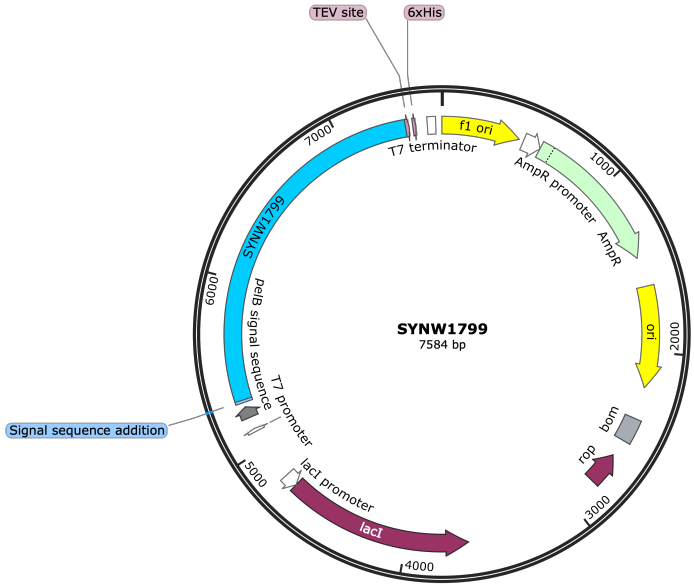

Figure 2.4: ***pET-22b(+) vector containing the gene for SYNW1799.***
The plasmid contains a T7 promoter, N-terminal pelB signal sequence and a C-terminal His-Tag with TEV cleavage site. Cell selection through Ampicillin resistance.

Table 2.4: ***List of primers (A) and PCR conditions (B) used for amplification of the Synechococcus sp. WH8102 PhoX gene SYNW1799 and the pET-22b(+) backbone.*** *Annealing temperature for SYNW1799 (B, 1) and pET-22b(+) backbone (B, 2) primers. 30 cycles were used for amplification.*

A

Primer name	*Product*	*Sequence 5'-3'*
pET-22b_frag1_fw	pET-22b(+) backbone fragment 1, homologous to SYNW1799 amplicon	CTTGGAGCGAACGACCTACA
pET-22b_frag1_rv		CGGATCCGAATTAATTCCGATATCC
pET-22b_frag2_fw	pET-22b(+) backbone fragment 2, homologous to SYNW1799 amplicon	TGCGGCCGCACTCGAGCACC
pET-22b_frag2_rv		TGTAGGTCGTTCGCTCCAAG
1799_pET-22b_fw	SYNW1799 with homologous region to pET-22b(+)	TCGGAATTAATTCGGATCCGTGTGTTGCACCGAGCGGTAATAGGGTG CGAGTGCGGCCGCAAGCT
1799_pET-22b_rv		TTCCCTGAAAATACAGGTTTTCGGCTCCAGCAGCGGCTG
1799_left_fw	SYNW1799 control primer from pet22b(+) into insert	ATGAAATACCTGCTGCCGAC
1799_right_rv	SYNW1799 control primer from insert into pet22b(+)	TTAGCAGCCGGATCTCAGTG

B

		Temperature	*Time*
Initial denaturation		98 °C	30s
Denaturation		98 °C	10s
Primer annealing	(1) (2)	64 °C 72 °C	30s
Extension		72 °C	1m 30s
Final extension		72 °C	10m

After purification of PCR products (QIAquick PCR purification kit), the concentration of the three fragments was measured using a NanoDrop. According to the formula stated in section 2.2.2.1, the concentration for the cloning step was calculated with a ratio of 1:1:2 of both vector fragments to the insert, using a final concentration of 0.046 pmol of each vector fragment and 0.092 pmol insert. The master mix was prepared according to the manufacturer's instructions and left for an incubation duration of 1 hour at 50 °C. The construct was cloned into DH_5-Alpha high-efficiency competent *E. coli* cells (NEB) and plated on LBA with ampicillin (100 µg ml^{-1}). Transformants were screened using T7 promoter primers (see Table 2.3A). Colonies that showed the correct product size were inoculated into 5 ml LB with ampicillin (100 µg ml^{-1}), plasmids were

extracted using the QIAprep spin miniprep kit (Qiagen) and sent for sequencing using control primers which can be found in Table 2.4A.

2.2.3.1 Site-directed mutagenesis

Overexpression of the *Synechococcus* sp. WH8102 PhoX using the pET-22b(+) vector did not produce any protein product (see section 2.2.3). This was potentially due to removing five amino acids that were part of the mature protein rather than the signal sequence. To assess this, these five amino acids were re-introduced by site-directed mutagenesis using the Q5® site-directed mutagenesis kit (NEB).

Table 2.5: ***List of primers (A) and conditions (B) used for the insertion of five amino acids (highlighted in red) into the pET-22b(+) plasmid containing the gene SYNW1799 via site-directed mutagenesis.***
25 cycles were set for the PCR to insert five amino acids into pET-22b(+)_SYNW1799.

A

Primer name	*Product*	*Sequence 5'-3'*
pET-22b-1799_SDM_fw	SDM mutagenesis of pET-22b(+) plasmid; insertion of 5 amino acids	GAGCGGTGTGTTGCACCAGCGGT
pET-22b-1799_SDM_rv		AGACCTTTCGGATCCGAATTAATTTCCGATATCC

B

	Temperature	*Time*
Initial denaturation	98 °C	30s
Denaturation	98 °C	10s
Primer annealing	66 °C	30s
Extension	72 °C	4m
Final extension	72 °C	2m

According to the manufacturer's instructions, primers were designed that contained the sequence of these five amino acids (see Table 2.5A). The PCR reaction conditions can be found in the same Table (B). After the PCR, the product was incubated with T4 kinase, DNA ligase and *Dpn*I at RT for 5 min. The ligation mix (5 µl) was then transformed in *E. coli* DH_5-Alpha chemically competent cells (NEB) according to the manufacturer's instructions (see section 2.2.4). Transformants were selected on LBA with 100 µg ml^{-1} ampicillin. Extracted plasmids were sent for sequencing (Figure 2.5) to confirm the correct insertion of the amino acids using the control primers that can be found in Table 2.4A.

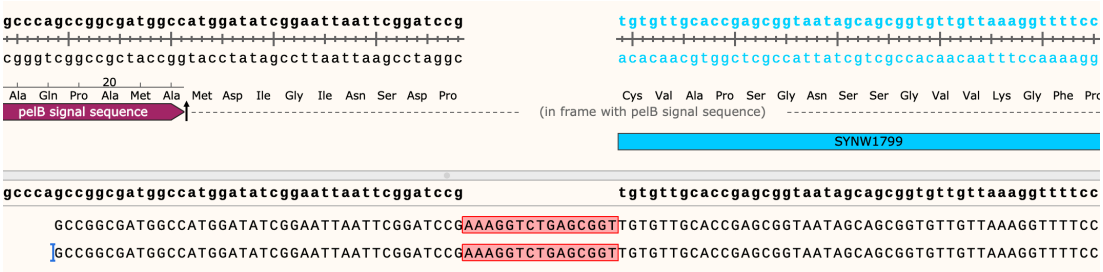

Figure 2.5: ***DNA sequence alignment confirming the insertion of five amino acids (red) into the SYNW1799 overexpression vector.***

2.2.4 Transformation and storage

All constructs were routinely transformed in either chemically competent non-expression (*E. coli* DH_5-Alpha) or expression strains (*E. coli* BL21(DE3) or BL21) according to the high-efficiency transformation protocol (NEB, C2987H/C2987I). Therefore, 50 µl competent cells were thawed on ice and 1 µl containing 100 ng plasmid DNA was added. The cells were carefully mixed and placed on ice for 30 min. A heat shock at 42 °C for exactly 30 s was performed and cells were immediately put back on ice afterwards. Preheated SOC media (950 µl) was added, and cells were incubated in a shaking incubator (250 rpm) at 37 °C for 1 hour. Transformants were selected on LBA with 100 µg ml^{-1} ampicillin. Therefore, 100 µl of an undiluted, a 10^{-2}, and a 10^{-3} dilution was spread on LBA – ampicillin (100 µg ml^{-1}) and incubated for 24 hours at 37 °C. Three single colonies were picked and inoculated into 5 ml LB with ampicillin (100 µg ml^{-1}) and incubated at 23 °C overnight with shaking at 180 rpm. These cultures were used to prepare 20% (v/v) glycerol stocks and stored at -80 °C. The stocks were used to extract the vector for further work using the QIAprep spin miniprep kit.

2.2.5 Chemically competent cell preparation

Chemically competent cells were either purchased from NEB or regularly made and stored at -80 °C. To make chemically competent cells, *E. coli* BL21(DE3), BL21 or DH_5-Alpha were streaked on LBA and incubated at 37 °C for 24 hours. Three single colonies were picked and inoculated into 5 ml LB in a 50 ml Falcon tube and incubated for 24 hours at 37 °C with shaking at 250 rpm. One ml of this culture was then inoculated into 100 ml preheated LB in a 250 ml flask and incubated at 37 °C with shaking at

180 rpm until OD_{600} reached 0.4. Cultures were cooled on ice for 10 min and centrifuged at 3,220 x g for 8 min at 4 °C. The supernatant was removed, and the cell pellet was carefully resuspended in 10 ml ice-cold filter sterile 0.1 M $CaCl_2$ solution and left on ice for 20 min. Cells were centrifuged for 8 min at 3,220 x g at 4 °C, the supernatant removed, and the pellet gently resuspended in 5 ml cold filter sterile 0.1 M $CaCl_2$ and 15% glycerol solution. Aliquots of 300 µl in 1.5 ml reaction tubes were prepared and kept at -80 °C.

2.2.6 Protein overexpression

For protein overexpression, the pET151-D/TOPO based constructs were transformed into chemically competent BL21(DE3) cells (NEB) per the manufacturer's instructions, whereas the pMAL c4x based constructs were transformed into BL21 competent cells (NEB) (see 2.2.4). For the overexpression, 2.5 L Thomson's Ultra Yield™ flasks (Thomson Instrument Company, Oceanside, CA, US) were used, prepared by rinsing them with 70% (v/v) ethanol and three times with ddH_2O before filling them with 500 ml of expression medium (see Table 2.6 and Table 2.7) and autoclaving. To avoid oxygen depletion, media volume was only 20% of the total flask volume. Before the overexpression experiment, flasks were left in a 37 °C incubator overnight to pre-heat the medium. Transformants were selected on LBA with ampicillin (100 µg ml^{-1}). To ensure growth of colonies containing the overexpression plasmid and to avoid potential satellite colonies, three single colonies were inoculated into 10 ml LB with 100 µg ml^{-1} ampicillin in 50 ml flasks which were incubated at 23 °C overnight with shaking at 180 rpm. A 2% (v/v) inoculum was then inoculated into the pre-heated overexpression medium and incubated for 25 hours with shaking at 180 rpm, using the following programme: 1 hour at 37 °C, 2 hours at 29 °C, 4 hours at 20 °C and 18 hours at 18 °C. Three different recipes for self-inducing media (see Table 2.6 and Table 2.7) were tested to find the optimal conditions for each construct to gain the highest yield of soluble protein. IPTG is a lactose metabolite and triggers the transcription of the *lac* operon and is therefore used as an induction substrate for overexpression in non-auto inductive media.

Table 2.6: ***Composition of Terrific Broth – Auto Induction Medium*.***

Chemical	*Stock solution ($g\ L^{-1}$)*	*Molecular weight ($g\ mol^{-1}$)*	*Final conc. in 1 L of Terrific broth*
Tryptone	12		1.2%
Yeast extract	24		2.4%
$MgSO_4$	0.15	246.48	608.56 µM
$(NH_4)_2SO_4$	3.30	132.14	24.97 mM
KH_2PO_4	6.50	136.09	47.76 mM
Na_2HPO_4	7.10	268.07	26.49 mM
Glucose	0.50	180.16	2.78 mM
alpha-lactose	2.00	360.31	5.55 mM
*Glycerol***	4.98	92.09	54.00 mM

* #GCM19.0500, GRiSP Research solutions, Porto, Portugal

** modified. Original recipe without glycerol.

Table 2.7: ***Composition of stock solutions for ZYM-5052 and MDA-5052 media*.***

Chemical	*Stock solution ($g\ L^{-1}$)*	*Stock conc.*	*Molecular weight ($g\ mol^{-1}$)*	*Final conc. in 1 L of ASW*	*ml for 1 L of media*
ZY**					**957 ml**
Tryptone	10.00			1%	
Yeast extract	5.00			0.5%	
50 x M					**20 ml**
Na_2HPO_4	335.00	1.25 M	268.07	25 mM	
KH_2PO_4	170.00	1.25 M	136.09	25 mM	
NH_4Cl	134.00	2.50 M	53.49	50 mM	
Na_2SO_4	35.50	0.25 M	142.04	5 mM	
50 x 5052					**20 ml**
Glycerol	250.00	2.72 M	92.09	54 mM	
Glucose	25.00	138.77 mM	180.16	2.78 mM	
Alpha-lactose	100.00	277.54 mM	360.31	5.55 mM	
$MgSO_4$	246.50	1.00 M	246.48	2 mM	**2 ml**
1000 x trace metals	**In 100 ml**				**0.2 ml**
$FeCl_3 * 6\ H_2O$	2.70	0.10 M	270.30	50 µM	
$CaCl_2 * 2\ H_2O$	15.80	1.00 M	158.20	20 µM	
$MnCl_2 * 4\ H_2O$	19.80	1.00 M	197.91	10 µM	
$ZnSO_4 * 7\ H_2O$	28.80	1.00 M	287.56	10 µM	
$CoCl_2 * 2\ H_2O$	4.76	0.20 M	237.93	2 µM	
$CuCl_2 * 2\ H_2O$	1.70	0.10 M	170.48	2 µM	
$NiCl_2 * 6\ H_2O$	4.76	0.20 M	237.69	2 µM	
$Na_2MoO_4 * 2\ H_2O$	2.42	0.10 M	241.95	2 µM	
Na_2SeO_3	1.73	0.10 M	172.94	2 µM	
H_3BO_3	0.62	0.10 M	61.83	2 µM	

* (Studier, 2005)

** For MDA-5052 media replace ZY with ddH_2O

In self-inducing media, glucose is added as a limited carbon source, which results in a high cell density before the protein overexpression is induced.

Once the glucose is depleted, cells take up the lactose which is converted into allolactose. This metabolite releases the T7lac/Lac repressor which leads to induction of the T7 RNA polymerase/Lac promoter (Studier, 2005).

2.2.7 SDS-PAGE

To confirm the overexpression of proteins, 500 µl of overexpression culture was mixed with 200 µl 2X Laemmli buffer (4% (w/v) SDS, 20% (v/v) glycerol, 120 mM Tris-Cl (pH 6.8), 0.02% bromophenol blue), proteins denatured at 98 °C for 15 min, and sample centrifuged for 5 min at 6,010 x g at RT to remove cell debris.

Table 2.8: ***Sizes of overexpressed proteins (original and expected) and plasmids used for overexpression.***

Protein	*Plasmid*	*Original size of protein (kDa)*	*Expected size of tagged protein (kDa)*
SYNW0196	pMAL-c4x	80.3	123.3
SYNW1799	pET-22b(+)	73.7	79.2
SYNW2390	pET151/D-TOPO	79.9	83.6
SYNW2391	pMAL-c4x	62.9	105.9
MED193_05784	pET151/D-TOPO	73.7	77.3

A precast Invitrogen™ NuPAGE Bis-Tris gel (Thermo Fisher Scientific) was placed into an Invitrogen™ mini gel tank (Thermo Fisher Scientific) and filled with SDS running buffer according to the manufacturer's instructions. Therefore, a ten-time concentrated running buffer (30.3 g Tris base, 144.4 g glycine, 10 g SDS, dissolved in 1 L ddH_2O) was prepared and diluted in ddH_2O. The SDS-PAGE gel was loaded with 10-30 µl of the sample, including a colour prestained protein standard (P7712S, NEB), and run at 140 V for 1 hour. After staining the gel with SimplyBlue™ SafeStain (Invitrogen™, Thermo Fisher Scientific) Coomassie stain, the gel was destained overnight in ddH_2O. Table 2.8 shows the original size of the proteins and the expected size after overexpression, including tags.

2.2.8 Verification of protein solubility

To verify protein solubility, cells were lysed, and soluble and insoluble fractions separated. The following steps were carried out on ice to avoid protein degradation. The overexpression culture was centrifuged at 11,325

x g for 15 min at 4°C and weighed afterwards. According to a 1 ml for 1 g ratio, cold and freshly prepared protein buffer (250 mM NaCl, 50 mM HEPES, 5% (v/v) Glycerol, pH 8.0) was added. The pellet was resuspended in the lysis buffer and sonicated using an Ultrasonic generator GM2070 connected to an Ultrasonic converter UW 2070, and a VS 70 T (Ø 13 mm) extended probe (BANDELIN electronic GmbH & Co. KG, Berlin, Germany). Cells were sonicated in 3x 30-sec intervals (pulsed cycle 3, active interval 0.3 sec, passive interval 0.7 sec) using 70% amplitude. Next, the lysate was centrifuged at 48,400 x g for 15 min at 4°C. The supernatant contains soluble proteins, whereas the pellet contains insoluble proteins. 50 µl soluble fraction was transferred into a reaction tube and 20 µl 2X Laemmli buffer was added. Samples were prepared and run on an SDS-PAGE gel according to the protocol in 2.2.7.

2.2.9 Preparation of gravity columns

Gravity columns for the His-Tag and MBP affinity purification were designed by assembling an Econo-column® (1.5 x 10 cm, # 7374151), an Econo-column funnel (250 ml, #7310003) and a 2-way stopcock (#7328102). The column parts were purchased from Bio-Rad Laboratories Inc. (Hercules, CA, USA). The column was filled with 5 ml Roche cOmplete™ His-Tag purification resin (#5893682001, Merck KGaA, Darmstadt, Germany). The resin was capped with an Econo alpha frit (25 mm, 30 µm, #12009472, Bio-Rad) filter to ensure resin stability when pouring in the sample. The column was stored in 20% (v/v) ethanol at 4°C.

2.2.10 Sample preparation for protein purification

After overexpressing the proteins according to the protocol in section 2.2.6, the cultures were spun down at 11,325 x g for 15 min at 4 °C. The supernatant was removed, and the pellet was resuspended in resuspension buffer (0.3 M NaCl in PBS), using a ratio of 20 ml buffer for 1 L of culture. The resuspended culture was split into 5 ml aliquots in 50 ml Falcon tubes, flash-frozen on dry ice and kept at -80 °C until used.

2.2.11 Affinity purification using His-Tag

Protein MED193_05784 was overexpressed in *E. coli* using a pet151/D-TOPO vector according to the protocol described in sections 2.2.6 and 2.2.10. For every purification, 500 ml culture was used. Therefore, two frozen aliquots were thawed in cold water and cold and freshly prepared lysis buffer (pH 8.0, filtered) was added (40 ml total). The recipe for the lysis buffer can be found in Table 2.9.

Table 2.9: ***Composition of lysis buffer (pH 8.0) for affinity purification of His-tagged proteins.***

Chemical	*Stock conc.*	*Volume to add in 40 ml*	*Final conc.*
HEPES	1 M	2 ml	50 mM
NaCl	2.5 M	4 ml	250 mM
Glycerol	50%	4 ml	5%
Proteinase inhibitor		2 tablets	
Benzonase®		1 µl	
BugBuster™	10X	4 ml	1X
ddH_2O		26 ml	

The Roche cOmplete™ ULTRA EDTA-free proteinase inhibitor tablets were purchased from Sigma Aldrich (#5892791001), as well as the Benzonase® Nuclease, ≥250 units μl^{-1} (#E1014-5KU). The Merck Millipore BugBuster™ 10X extraction buffer was purchased from Thermo Fisher Scientific (#10579953). After adding the lysis buffer, samples were left on a Luckham Multimix Model 840 tube roller for 20 min with frequent vortexing until the mixture was homogenous. Samples were sonicated on ice, using a probe sonicator and extended probe (for details see section 2.2.8). More sonication steps had to be done if the samples were not homogenous. In between the sonication steps, the Falcon tubes were inverted, and samples were properly cooled on ice to avoid protein precipitation. Afterwards, samples were centrifuged at 48,400 x g for 20 min at 4 °C. The supernatant, containing the soluble protein, was filtered by using a Whatman® Puradisc 0.2 µm syringe filter (Whatman plc, GE Healthcare, Chicago, IL, USA). For the purification step, the column was prepared by washing it with five column volumes of filtered and degassed ddH_2O and equilibrating it with five column volumes of protein buffer (50 mM HEPES, 250 mM NaCl, 5% glycerol, pH 8.0, filtered and degassed). The filtered

supernatant, containing the soluble protein, was poured onto the column. Five column volumes of protein buffer containing 10 mM imidazole were used to wash off unspecifically bound proteins. Then, the MED193 PhoX was eluted with 6 column volumes of protein buffer containing 250 mM imidazole. To clean the column, it was first washed with 5 column volumes of 250 mM imidazole buffer, then 5 column volumes of filtered and degassed ddH_2O, 5 column volumes of 1% SDS, water again and then 20% (v/v) ethanol.

2.2.12 Size exclusion chromatography

The purified MED193 PhoX from section 2.2.11 was analysed by SDS-PAGE (see section 2.2.7). As the eluted protein was contaminated with several different proteins, the protein was sequentially purified again by gel filtration on an ÄKTA purification system (GE Healthcare). Only 2.5 ml sample can be loaded onto the column. Hence, Amicon® ultra-15 centrifugal filter units with a 50 kDa cut-off (CAS no. UFC905024, Merck) were used to concentrate the protein in a 3 ml sample volume. In addition, some of the smaller proteins could be eliminated before the sample was loaded onto the gel filtration column (HiLoad™ 16/600 Superdex™ 200pg, GE Healthcare). Proteins were separated by size with 2.5 column volumes of washing buffer using a flow rate of 0.5 ml min^{-1}. Separated proteins were collected in fractions of 1 ml. Subsequently, three proteins of a high molecular weight gel filtration calibration kit (CAS no. 28-4038-42, GE Healthcare) were loaded and separated using the same conditions as described above. Next, plots were created for MED193_05874 (mAU against retention volume) and the proteins of the calibration kit. High mAU peaks indicate high protein concentration. Overlaying the plots of the separated candidate protein and proteins of the calibration kit can help to identify the retention volume of the candidate protein. Next, fractions of the identified peak containing the candidate protein were concentrated to 2 ml using Amicon® ultra-15 centrifugal filter units and protein concentration measured using a NanoDrop 2000. The protein was kept at -80 °C until used.

2.3 Protein biochemistry

2.3.1 Metal requirements of enzymes

To determine the metal requirements of the MED193 PhoX (MED193_05784) a standard alkaline phosphatase activity assay was used to verify enzyme activity. Therefore, the MED193 PhoX was overexpressed and purified as described in section 2.2.6 and sections 2.2.10 - 2.2.12. The protein concentration (triplicates) was measured using a NanoDrop and protein was diluted in protein buffer (50 mM HEPES, 250 mM NaCl, 5% glycerol, pH 8.0, filtered and degassed) to reach a final concentration of 25 ng protein for each reaction (100 µl). It is important to point out that although the NanoDrop is a time-saving method to measure protein concentrations, it is not a sensitive method. To allow for more accurate determinations, Bradford assay or inductively coupled plasma mass spectroscopy (ICP-MS) should be used (Bradford, 1976; Barnett et al., 2014). In the next step, metals (see metal stock solutions in Table 2.7) were added to the protein with a final concentration of 1 mM. Finally, samples were mixed with 10 µl *para*-nitrophenyl-phosphate (*p*NPP) (10 mM) in ddH_2O, loaded into a 96-well microplate, incubated at 30 °C, and colour change noted. Metals were tested either solely or in combination with a second metal.

2.3.1.1 Metal replacement

The MED193 PhoX (MED193_05784) showed no enzyme activity after purification. However, adding $CaCl_2$ restored enzyme activity. Previous studies have shown that PhoX-type phosphatases require calcium and iron for activity (e.g., Yong et al., 2014). To test if metals can be removed from the protein, a 2.5 ml sample containing 94 µM protein was mixed with 250 µM ethylenediaminetetraacetic acid (EDTA) and kept on a tube roller at 4 °C for 18 hours. EDTA has chelating properties and is commonly used to remove metals from proteins (Zaitoun & Lin, 1997). After incubation with EDTA, a PD-10 desalting column (GE Healthcare) was used for buffer exchange. Briefly, the column was washed four times with equilibration buffer, in this case protein buffer (see 2.3.1), loaded with 2.5 ml sample and eluted with 3.5 ml protein buffer. To ensure the removal of EDTA, only

3 ml eluate were collected. The eluate was concentrated using an Amicon column and protein activity was tested as described in section 2.3.1.

2.3.2 Enzyme kinetics

To measure enzyme kinetics for the MED193 PhoX (MED193_05784) the protein was overexpressed and purified as described in section 2.2.6 and sections 2.2.10-2.2.12. For the *p*NPP assay protein buffer (see 2.3.1) was used. However, the PiPer™ assay (see 2.3.2.2) required a specific reaction buffer (1X) that was included in the kit and diluted in ddH_2O accordingly. Nonetheless, both buffers were supplemented with $CaCl_2$ with a final concentration of 100 mM. Additionally, the concentration of the protein was measured using a NanoDrop and a final concentration of 25 ng MED193 PhoX was used in both assays, diluted in the respective buffer.

2.3.2.1 Assay for chromogenic phosphates – *p*NPP assay

The assay is based on the rate of conversion of *p*NPP to *para*-nitrophenol (*p*NP) and is adapted from Bessey et al. (1946). *p*NP has a yellow colour with a maximum absorbance at 405 nm. Hence, colour change can be measured spectrophotometrically. For the generation of a standard curve, *p*NP (in ddH_2O) was serially diluted in protein buffer, resulting in concentrations ranging from 3-267 µM (final concentration). Next, samples of 100 µl were loaded into a 96-well microplate, each containing 25 ng MED193 PhoX and serially diluted *p*NPP in protein buffer with final concentrations ranging from 9.8 µM-5 mM. Additionally, *p*NP samples for the standard curve were loaded. Samples without enzyme, with denatured enzyme, and without substrate were used as negative controls, and protein buffer was used as a blank. The plate was incubated for 1 hour at 30 °C in a microplate reader and colour change was monitored by continuously measuring OD_{405}.

2.3.2.2 Assay for non-chromogenic phosphates – PiPer™ assay

The PiPer™ assay (#P22061, Thermo Fisher Scientific) is used for the detection of P_i released from virtually any source of non-chromogenic organic P. Here, this assay was used to calculate the enzyme activity of the MED193 PhoX towards the two phospholipid headgroups PC and PE.

The assay requires the interaction of four proteins. In the presence of P_i maltose is converted to glucose and glucose-1-phosphate by a maltose phosphorylase. The next step involves the conversion of glucose to gluconolactone and H_2O_2 by a glucose oxidase. Finally, a horseradish peroxidase catalyses the reaction of H_2O_2 with the Amplex® red reagent (10-acetyl-3,7-dihydroxyphenoxazine) to generate resorufin, which can be detected spectrophotometrically by measuring OD_{575} (Figure 2.6).

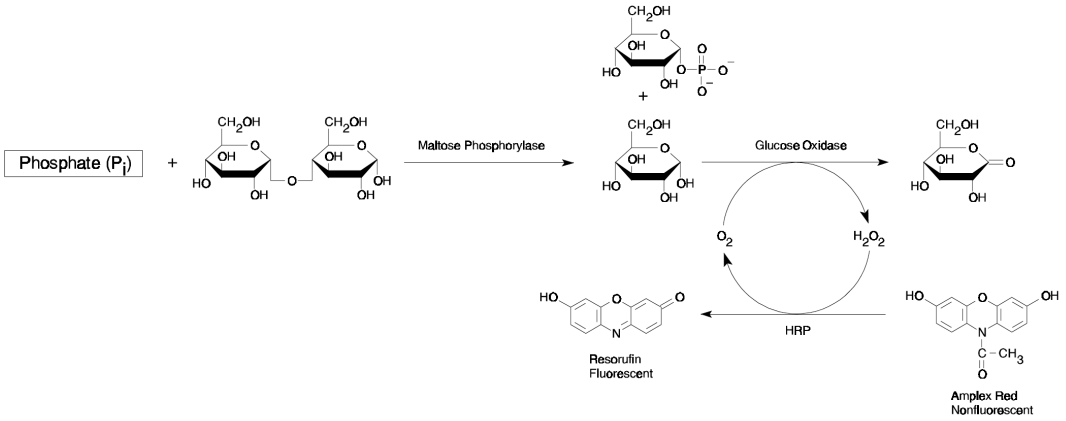

Figure 2.6: ***Principle of the PiPer™ phosphate assay.***
The Figure shows the reaction between the three enzymes maltose phosphorylase, glucose oxidase, and horseradish peroxidase (HRP) in the presence of P_i. P_i leads to the release of H2O2 which can react with Amplex® Red to generate resorufin. From the PiPer™ assay manual (Thermo Fisher Scientific).

The assay was performed according to the manufacturer's instructions (assay for enzyme activity). For the generation of a standard curve, a serial dilution of a phosphate standard (50 mM) in 1X reaction buffer was performed to reach concentrations ranging from 3.91-500 µM. Next, the two phospholipid headgroups PC and PE were serially diluted in reaction buffer (1X) to reach concentrations between 98 µM and 62.5 mM and the MED193 PhoX was diluted in 1X reaction buffer to reach a concentration of 50 ng. Finally, a modified working solution was prepared as listed in Table 2.10.

Samples were loaded into a 96-well microplate in the following chronological order:

1. 100 µl 1X reaction buffer (blank)
2. 50 µl protein or 50 µl 1X reaction buffer (negative control)
3. 10 µl working solution or 10 µl 1X reaction buffer (negative control)
4. 40 µl PE/PC or 40 µl 1X reaction buffer (negative control)

The plate was incubated in a microplate reader for 1 hour at 30°C and colour change was monitored by continuously measuring OD_{575}.

Table 2.10: ***Modified working solution for the PiPer™ assay.***

Chemical	*Volume to add in 1 ml*	*Final concentration*
Reaction buffer (1X)	730 µl	
Amplex red reagent	50 µl	100 µM
Maltose phosphorylase	100 µl	4 U ml^{-1}
Glucose oxidase	50 µl	2 U ml^{-1}
Horseradish peroxidase	20 µl	0.4 U ml^{-1}
Maltose	50 µl	0.4 mM

2.3.2.3 Calculation of enzyme kinetics

Enzyme kinetics was calculated in the same way for assays described in 2.3.2.1 and 2.3.2.2. First, all samples were normalised by the blank. Next, all samples were normalised by the negative controls (no colour change in *p*NPP reactions, natural colour change with time for the light-sensitive Amplex® red). Finally, standard curves were created by plotting the final concentrations of *p*NP or phosphate standard against OD_{504} or OD_{575} values retrieved from the experiment. A trend curve was added to determine the equation of the standard curve. Next, the slope for each sample containing either *p*NPP or a phospholipid headgroup was calculated using the simple linear regression function in Prism 9 (GraphPad Software, San Diego, CA, USA). The slope values, with R^2 >0.90, were further normalised by the reaction time, the standard curve equation, and the protein concentration. The resulting values (in nmol min^{-1} mg^{-1} protein) were then plotted against the substrate concentration to plot a Michaelis-Menten enzyme kinetics curve in Prism. In addition, Prism was used to calculate V_{max} and K_M of PhoX for *p*NPP, PC, and PE.

2.3.3 Sample preparation for electron paramagnetic resonance (EPR)

The MED193 PhoX protein MED193_05784 was overexpressed and purified as described in section 2.2.6 and sections 2.2.10-2.2.12. Next, the protein was concentrated in Amicon® ultra-15 centrifugal filter units to reach a protein concentration of 190 µM in 250 µl sample. Samples were flash-

frozen on dry ice and kept at -80°C until used. Upon transferring samples to EPR tubes, samples were thawed on ice. Protein buffer (see 2.3.1) was used for EPR analysis and the dithionite solution was prepared freshly.
Six conditions were prepared for EPR analysis:

1. Native PhoX
2. PhoX + 5 mM dithionite
3. PhoX + 20 mM dithionite
4. PhoX + 50 mM EDTA
5. PhoX + 1 mM PE
6. Buffer

After mixing the protein with dithionite, EDTA, or PE, samples were instantly transferred into EPR tubes and flash-frozen in liquid nitrogen. They were kept in a liquid nitrogen dewar and sent to the National EPR facility at the University of Manchester, where samples were analysed by Dr Muralidharan Shanmugam using EPR spectroscopy. The EPR spectra were measured at 10 K, 5 G modulation amplitude (MA) with a microwave power of -20 dB (~2.2 mW). Each spectrum was averaged over 4-6 scans to get a better signal to noise ratio.

2.3.4 MicroScale Thermophoresis (MST) assay

MST assays were performed by Chun-Yang Li at the College of Marine Life Sciences, Ocean University of China, Qingdao, China.
The MED193_19449 protein with a C-terminal His-tag was expressed in *E. coli* BL21 (DE3) and then purified by Ni^{2+} nitrilotriacetic acid (NTA) resin (Qiagen) and a Superdex-200 column (GE Healthcare). The binding affinity of the purified MED193_19449 to the substrate dihydroxyacetone phosphate (DHAP) was measured using the Monolith NT.115 (NanoTemper Technologies, Munich, Germany). The MED193_19449 protein was labelled in assay buffer (PBS buffer and TE buffer were mixed at a 1:1 volume ratio supplemented with 0.1% (v/v) Tween-20) using the Protein Labelling Kit RED-Tris-NTA (NanoTemper Technologies). For each assay, the labelled protein (about 2 µM) was mixed with the same volume of DHAP at 16 different serially diluted concentrations with the highest concentration in the assay being 30 mM. The samples were then loaded into standard capillaries (Monolith NT.115 Capillaries, NanoTemper Technologies) and measured at 25 °C using 60% excitation power and medium MST power. The data was analysed using the MO. Affinity Analysis v2.3 software

(NanoTemper Technologies). The same protocol was used for affinity measurements of MED193_10041 to ethanolamine.

2.4 Proteomics

2.4.1 Samples preparation for cellular proteomics

For the sample preparation of the cellular proteomics analysis, cell pellets of the growth experiments (see section 2.1.3) were resuspended in 1 ml ddH_2O and 200 µl 2X Laemmli buffer was added. Samples were boiled at 98 °C for 15 min and 5 µl was loaded on a precast NuPAGE Bis-Tris gel and a long run was done at 140 V for 1 hour (see section 2.2.7). Furthermore, a 30 µl sample was loaded on a precast NuPAGE Bis-Tris gel for a short run at 140 V for 15 min. After staining with Coomassie blue and destaining overnight in ddH_2O, the bands of the short-run gel were cut into small pieces and transferred into 1.5 ml Eppendorf tubes.

2.4.2 Samples preparation for extracellular proteomics

Proteins of the exoproteome (see growth experiments 2.1.3) had to be precipitated from the supernatant. The following protocol was used, as previously described (Christie-Oleza & Armengaud, 2010). First, the stock solutions 50% (w/v) trichloroacetic acid (TCA, CAS no. 76-03-9, Sigma-Aldrich) and 0.15% (w/v) sodium deoxycholate (DOC, CAS no. 302-95-4, Sigma-Aldrich) were prepared freshly and cooled down to 4 °C. 40 ml of the supernatant was filtered through a Whatman® Puradisc 0.2 µm syringe filter. 4 ml DOC was added to each sample and vortexed. Samples were incubated at RT for 10 min before adding 2.4 ml TCA and vortexing again. The samples were kept on ice for 30 min before centrifugation for 15 min at 3,220 x g at 4 °C, and the supernatant was discarded. The pellets were resuspended in 1 ml ddH_2O and transferred to a 2 ml Eppendorf tube. 150 µl DOC was added, the samples vortexed and then incubated for 10 min at RT. After adding 90 µl TCA the samples were vortexed and kept on ice for 30 min. Another centrifugation step at 6,010 x g, 4 °C for 10 min followed and the supernatant was discarded. Samples were then resuspended in 1 ml ethanol: ether (1:1 v/v) and centrifuged at 4 °C for 15 min at 15,871 x g. After eliminating the supernatant with a pipette, the

samples were dried in a fume hood. The pellet was kept at -20 °C until further use. For the gel run it was resuspended in ~50 µl of 2X Laemmli buffer. Here, the volume of the Laemmli depended on the size of the pellet. To facilitate resuspension, 5 min water bath sonication was alternated with 5 min incubation at 95 °C until the pellet was completely dissolved. Samples were then incubated for 5 min at 95 °C, centrifuged at 6,010 x g for 5 min, and the samples were loaded (5 µl for a long run and 30 µl for a short run) on a precast NuPAGE Bis-Tris gel. The short run was performed at 140 V for 15 min and the long run at 140 V for 1 hour. Gels were stained with Coomassie blue and destained in ddH_2O overnight. Protein bands from the short run were cut into small pieces and transferred into 1.5 ml Eppendorf tubes.

2.4.3 In-gel protein digestion

The in-gel protein digestion protocol was performed as described by the Proteomics Research Technology Platform, SLS, University of Warwick. Firstly, gel pieces were destained by adding a 50% ethanol (v/v) and 50 mM ammonium bicarbonate (ABC) solution and incubating at 55 °C with shaking at 650 rpm for 15 min. After removing the liquid, this step was repeated at least three times until all stain was removed. To dehydrate the gel pieces, 100% ethanol was added, and samples were incubated for 5 min at RT with shaking at 650 rpm. The liquid was removed, and a 10 mM Tris(2-carboxyethyl) phosphine (TCEP) and 40 mM 2-chloroacetamide solution was added to the samples, vortexed gently and incubated at 70 °C for 5 min. After washing the samples twice with a 50% ethanol (v/v) and 50 mM ABC solution for 20 min at RT with shaking at 650 rpm, the liquid was removed and the gel pieces were dehydrated with 100% ethanol for 5 min at RT with shaking at 650 rpm. The ethanol was removed, and a 2.5 ng μl^{-1} trypsin solution was added. Samples were then incubated at RT for 5 min. ddH_2O was added to cover the gel pieces with enough liquid to avoid dehydration and the samples were kept at 37 °C overnight. For peptide extraction, a 25% acetonitrile (ACN) and 5% formic acid solution was added, and the samples were sonicated for 5 min in a water bath sonicator. The liquid was transferred into a fresh 1.5 ml Eppendorf tube and the peptide extraction step was repeated another two times. To

concentrate the samples a Savant™ DNA SpeedVac™ (Thermo Fisher Scientific) was used to bring the volume down to 20 µl. Samples were kept at -20 °C. To prepare samples for analysis, samples were dried in the SpeedVac™ and then resuspended in a 2% ACN and 0.1% trifluoroacetic acid (TFA) solution. Before transferring the samples to a Mass Spec vial, Corning® Costar® Spin-X® centrifuge tube filters (CAS no. CLS8160-96EA, Sigma-Aldrich) were used to filter the samples. Samples were submitted to the Proteomics Research Technology Platform (Dr Andrew R. Bottrill and Dr Cleidiane Zampronio), SLS, at Warwick University and analysed by nanoLC-ESI-MS/MS using an Ultimate 2000 LC system (Dionez-LC Packings) coupled to an Orbitrap Fusion mass spectrometer (Thermo-Fisher). An LC separation of 60 min for exoproteomes and 120 min for cellular proteomes were performed on a 25 cm column before MS/MS analysis using settings as previously described (Christie-Oleza, Armengaud, et al., 2015).

2.4.4 Analysis of proteomics data

The recorded MS/MS spectra obtained from the Proteomics Research Technology Platform was processed using MaxQuant (v1.5.5.1) (Max Planck Institute of Biochemistry, Munich, Germany), a quantitative proteomics software package to analyse large mass-spectrometry data sets. The framework of the label-free quantification (LFQ) method described in Cox & Mann (2008) was used. All parameters were set by default. However, the 'match between run' function was selected. MS spectra were searched against the protein database of *Phaeobacter sp.* MED193 (A3X963_9RHOB). Subsequently, Perseus (v1.6.5.0, MPI of Biochemistry), a software to interpret protein quantification, was used for comparative proteomics analysis (Tyanova et al., 2016). The protein variations between the conditions were identified by using a two-sample *t*-test. Comparisons were made between each condition and either the high P_i control or the pre-starved culture to which phosphate in form the of P_i was added back. Statistical analysis was set using a false discovery rate (FDR) of 0.01 and 0.05 and a minimal $\log_2$ fold change of 2. A protein had to be present in every replicate of at least one condition to be considered valid.

2.5 Intact polar lipid extraction and analysis

2.5.1 Lipid extraction

The following protocol, a modified Folch extraction method, was used for lipid extraction (Folch et al., 1957). To allow comparison between samples grown in different conditions, it was necessary to collect the same amount of biomass at each sampling timepoint. The amount was calculated using the following formula:

Volume (ml) = 0.5 / OD_{540}

Samples were transferred into a clear glass wide opening screw-thread vial (CAS no. C4010-1, Thermo Fisher Scientific). Samples were centrifuged in the vials at 4 °C for 15 min at 4,025 x g and the supernatant was removed afterwards. 500 µl ice-cold methanol was added and the samples vortexed before adding 300 µl ddH_2O. One ml chloroform was then added and the samples vortexed again, followed by a centrifugation step at 4 °C for 5 min at 2,415 x g. Unscrewing the caps and switching off the breaks helped to get a clearer phase distinction. The two resulting phases are an upper methanol-water phase, containing hydrophilic metabolites and a lower chloroform phase, containing the lipids. The lower phase was transferred to a fresh glass vial using a glass Pasteur pipette. One ml chloroform was added to the remaining methanol-water phase and the lipids re-extracted. As before, the chloroform phase was aspirated to the same new vial. Samples were dried using a nitrogen stream in a Techne sample concentrator (Staffordshire, UK), making them storable at -80 °C. For immediate analysis samples were resuspended in 5% (v/v) 10 mM ammonium acetate (pH 9.2, reached by adding ammonium hydroxide) and 95% (v/v) acetonitrile.

2.5.2 Analysis of intact polar lipids

The liquid chromatography-mass spectrometry (LC-MS) method used in this thesis to analyse lipid extracts was based on Smith et al. (2021). Briefly, a Dionex 3400RS HPLC (Thermo Fisher Scientific) with a HILIC BEH amide XP column (2.5 µm, 3.0 x 150 mm, Waters Corp., Milford, MA, USA) was coupled with an amaZon SL ion trap MS (Bruker Corp., Billerica, MA, USA). Lipids were analysed via electrospray ionisation (ESI) in both

positive (+ve) and negative (-ve) ionisation modes. Solvents used in this protocol were A: HPLC-grade acetonitrile and B: ammonium acetate in ddH_2O, 10 mM, pH 9.2. Samples were run on a 15 min gradient from 95:5 (v/v) A-B ratio to 70:30 (v/v) A-B ratio, with 10 min equilibration between samples. The injection sample volume was set to 5 µl for the analysis. The flow rate was kept constantly at 150 µl min^{-1} and column temperature at 30 °C. The end cap voltage was set at 4,500 V in positive and 3,500 V in negative mode, both with a 500 V offset. The drying condition was kept the same: 8 L min^{-1} drying gas at 250 °C and nebulising gas pressure of 1 psi.

2.5.3 Identification of lipid classes

Initial lipid class identification was based on intact lipid masses. Various publications have identified the intact lipid masses of lipid classes (Table 2.11).

Table 2.11: ***Intact lipid masses for the identification of lipid classes.***
DGTS was identified by its $[M+H]^+$ ion in positive mode, all other lipids were identified by their $[M-H]^-$ ion in negative mode. Ornithine and glutamine lipid could be identified in both modes.

Lipid class	*Fatty acids*	*m/z*	*Retention time [min]*	*Reference*
DGTS $[M+H]^+$	36:2	764	10.3	(Popendorf et al., 2013)
Ornithine lipid $[M-H]^+$	38:2	705	12.6	(Zhang et al., 2009)
Glutamine lipid $[M-H]^+$	38:2	719	9.5	(Zhang et al., 2009)
PE $[M-H]^-$	36:2	743	12	(Han et al., 2005)
PG $[M-H]^-$	36:2	773	7	(Han et al., 2004)
Ornithine lipid $[M-H]^-$	38:2	703	13	(Zhang et al., 2009)
Glutamine lipid $[M-H]^-$	38:2	717	9.5	(Zhang et al., 2009)
Sulphur containing amino lipid (SAL) $[M-H]^-$	34:1	656	3.5	(Smith & Silvano et al., 2021)
SAL2 $[M-H]^-$	OH-34:1	672	3.7	(Smith & Silvano et al., 2021)

The software DataAnalysis 4.1 (Bruker Corp.), included in the Compass DataAnlaysis 4.1 software package, was used to identify lipid classes in the MS spectra.

2.5.4 Semi-quantification of membrane lipids

An external lipid standard was required for the semi-quantification of different lipid classes, as described in Cífková et al. (2012). The lipid

standard chosen for the work in this thesis was N-dodecanoyl-heptadecasphing-4-enine-1-phosphoethanolamine (sphingosyl-PE, d17:1/12:0), purchased from Avanti Polar Lipids (Alabaster, AL, USA). S-PE was used as lipid standard as it ionises well in both positive and negative ESI-MS and, with the method used in this work, elutes between 13.8 and 14 min, thereby separating well from other lipid classes identified in the LC-MS chromatogram. Lipids were extracted from culture samples as described in section 2.5.2 but with S-PE (final concentration of 25 µM) added before cell pelleting. Lipid extracts were analysed as described in section 2.5.2. Thereafter, QuantAnalysis (Bruker Corp.) was used to integrate signals of selected lipids. Here, the accuracy of the *m*/*z* was set to ± 0.05, the window for retention time was set to 1 min, and the signal/noise ratio was set at 10 for positive mode and 5 for negative mode. Each area was checked manually and adjusted if required. Integrated signals of selected lipids were extracted and normalised by the integrated signal of S-PE.

2.6 Metabolic assays – alkaline phosphatase assay

During the growth experiment analysing the WT MED193 and *ΔphoB* (see sections 2.1.2 and 2.1.3) alkaline phosphatase activity of the cultures was measured. This assay was performed to determine whether the cultures were phosphate stressed. The assay is based on the rate of conversion of *p*NPP to *p*NP and is adapted from Bessey et al. (1946). For the phosphatase activity assay, a 200 µl culture was mixed with 10 µl *p*NPP (100 mM) in ddH_2O and incubated at 30 °C until a colour change occurred. For a positive control, 1 µl of shrimp alkaline phosphatase (CAS no. M0371S, NEB) was added to 200 µl media used for the experiment and 10 µl 100 mM *p*NPP. The negative control, used as a blank, consisted of 200 µl medium and 10 µl 100 mM *p*NPP. After the incubation, 790 µl medium was added, the reaction was centrifuged for 5 min at 14,674 x g at RT and transferred to a cuvette before measuring the OD_{405} on a Jenway 7305 spectrophotometer.

2.7 Bioinformatics – phylogenetic relationships

Phylogenetic analyses of MED193_10041 (ethanolamine binding protein), MED193_10161 (C-P lyase, substrate-binding protein), and MED193_19449 (dihydroxyacetone phosphate binding protein) were performed using the NGPhylogeny.fr platform (Dereeper et al., 2008; Lemoine et al., 2019). Here, MUSCLE with default settings was used for multiple sequence alignment (Edgar, 2004b, 2004a), and sequences were trimmed using trimAI with default settings (Capella-Gutiérrez et al., 2009). Next, the IQ-TREE webserver (Nguyen et al., 2015; Trifinopoulos et al., 2016; Hoang et al., 2017; Kalyaanamoorthy et al., 2017) was used to create phylogenetic trees. Here, default settings were used, and sequence type was set to protein. Bootstrap analysis was set on ultrafast which includes 1000 bootstrap alignments. Next, iTOL was used to design phylogenetic trees (Letunic & Bork, 2021).

2.8 Mutagenesis in *Phaeobacter* sp. MED193

Dr Ian D.E.A. Lidbury kindly provided a *Phaeobacter* sp. MED193 *phoB* double cross-over mutant. The mutant was generated using a conjugation protocol as described in Lidbury et al., 2016 and 2017. First Gibson cloning (Gibson et al., 2009), using the NEBuilder HiFi DNA assembly (NEB) kit, was used to create a construct in pK18*mobSacB*, a mobilizable plasmid that doesn't replicate in *Roseobacters* (Schäfer et al., 1994). Before assembly, DNA fragments for regions A and B, and a gentamicin resistance (Gm^R) cassette were generated by PCR using a high-fidelity *Phusion* DNA polymerase PCR master mix (NEB). All amplified products had complementary overlap regions of 25 bp either with each other or with the plasmid (Table 2.12). Regions A and B were amplified by colony PCR of WT MED193 whereas Gm^R was amplified from purified stocks of p34S-Gm. In addition, the pk18*mobSacB* vector was cut with the restriction enzymes *Bam*HI and *Hind*III and gel-purified. According to the manufacturer's protocol, all four fragments were mixed and incubated, as described in section 2.2.2.1. The vector containing the construct Region A, Gm^R, and Region B (pk18::A-Gm^R-B) was transformed into *E. coli* DH5-Alpha (see section 2.2.4), plated on LBA containing 10 µg ml^{-1} gentamicin and 50 µg

ml^{-1} kanamycin, and incubated overnight at 37°C. Transformants were screened using M13 forward and Gm^R reverse primers, as well as Gm^R forward and M13 reverse primers (Table 2.12). Colonies that showed the correct product size were inoculated into 5 ml LB with gentamicin (10 µg ml^{-1}) and kanamycin (50 µg ml^{-1}), plasmids extracted using the QIAprep spin miniprep kit (Qiagen), and plasmids sent for sequencing using M13 primers (see Table 2.12).

Table 2.12: ***List of primers used for generating a phoB deletion mutant in Phaeobacter sp. MED193.***

Primer name	*Product*	*Sequence 5'-3'*
RegionA_fw RegionA_rv	Region A, homologous to genomic neighbourhood of *phoB*, pk18*mobSacB* and	TACGAATTCGAGCTCGGTACCCGGGGTAACCTGGAGCGTATTGG TCTAGAGTCGACAAGCCTTCTTCGCCGTTTTC
RegionB_fw RegionB_rv	Region B, homologous to genomic neighbourhood of *phoB*, pk18*mobSacB* and	ACGCCGCGGCCAACAGTTTGGTGGTGCTGATC CGTTGTAAAACGACGGCCAGTGCCACTCTTGCCGGTTTGTAGC
Gm^R_fw Gm^R_rv	Gentamicin resistance cassette, homologous to Region A and B	GCGAAGAAGGCTTGTCGACTCTAGAGGATCCCCGG ACCACCAAACTGTTGGCCGCGGCGTTGTGA
M13(-21)_fw M13(-40)_rv	Plasmid control primer from pk18*mobSacB* into inserted region (A, Gm^R, B)	TGTAAAACGACGGCCAGT CAGGAAACAGCTATGAC
Control_fw Control_rv	*phoB* control primer from MED193 genome into deleted region	AATTGTCGATTCAGCACGGG TCAATATGACCACGCGCTTG

Correct plasmids were then transformed into electrocompetent *E. coli* S17:1. *E. coli* S17:1 is capable of high-efficiency conjugation (R. Simon et al., 1983). Therefore, 50 µl cells were thawed on ice and 10 ng mini-prepped pk18::A-Gm^R-B was added. The mixture was then transferred into a pre-cooled electroporation cuvette (Gene Pulser®, 0.2 cm, BioRad) and kept on ice for a further 15 min. The cuvette was placed in a MicroPulser® (BioRad) and subjected to an electric pulse (2.5 kV, 25 µF, 200 Ω). Cells were recovered in 950 µl pre-warmed SOC medium for 1 hour at 37 °C with shaking before plating on LBA containing gentamicin (10 µg ml^{-1}) and kanamycin (50 µg ml^{-1}) and incubated overnight at 37 °C. Transformants were screened using M13 primers and single colonies that contained pk18::A-Gm^R-B were inoculated into 5 ml LB and grown overnight with shaking at 37 °C. Simultaneously, a single colony of WT MED193 was inoculated into MB and grown overnight with shaking at 30 °C. On the day

of conjugation, a 10% (v/v) inoculum of the pre-grown WT MED193 culture (receiver strain) was transferred into 10 ml MAMS (Table 2.13) and incubated at 30 °C and 150 rpm until OD_{540} of 0.5 was reached. At the same time, a 2% inoculum of the pre-grown *E. coli* S17:1 with pk18::A-Gm^R-B culture (donor strain) was transferred into 5 ml LB supplemented with gentamicin (10 µg ml^{-1}) and kanamycin (50 µg ml^{-1}) and grown at 37 °C and 150 rpm until an OD_{600} of 0.5 was reached. Thereafter, donor strain and receiver strain cultures were mixed and centrifuged at 2,415 x g for 10 min at RT, supernatant eliminated, and the pellet gently resuspended in 300 µl sea salts medium (-C/-N, Table 2.13). The homogenous mixture of donor and receiver strain was spotted on a ½ YTSS agar plate (Table 2.13) and left until the spot was completely dry before incubating it at 30 °C for 24 hours. 100 µl of serially diluted samples were plated on sea salts agar plates with 2 mM glycine betaine, 3 mM glucose, and 5 mM succinate (Table 2.13), containing either gentamicin (10 µg ml^{-1}) or kanamycin (50 µg ml^{-1}). Since *E. coli* is unable to grow on glycine betaine as a sole source of nitrogen, it is unable to grow on the sea salts agar plates. Plates were incubated at 30 °C for one to two weeks until colonies were visible. These colonies were streaked on fresh agar plates with the same sea salts medium conditions. Again, one plate was supplemented with 10 µg ml^{-1} gentamicin and one plate with 50 µg ml^{-1} kanamycin. Colonies that grew on gentamicin containing plates only were most likely double cross-over mutants. Therefore, they were screened using control primers (Table 2.12). A fragment size of 1930 bp was expected for the WT MED193 and fragment size of 2284 bp was expected for *ΔphoB*. In the double cross-over mutant, the *phoB* gene was interrupted by Gm^R. The deletion of the *phoB* gene in WT MED193 was confirmed by sequencing (see Appendix 3.1).

Table 2.13: ***Composition of different media used for mutagenesis of Phaeobacter sp. MED193.***
Stock solutions marked with an asterisk are added after autoclaving.

Chemical	*Stock solution ($g\ L^{-1}$)*	*Stock conc.*	*Molecular weight ($g\ mol^{-1}$)*	*Final conc. in 1 L of ddH_2O*	*ml for 1 L of media*
1/2 YTSS					
Yeast extract	2			0.2%	
Peptone	1.25			0.125%	
Sea salts (Sigma)	20			2%	
Sea salts agar					
Sea salts (Sigma)	30			3%	
Glucose	0.54		180.16	3 mM	
Succinate	1.35		270.14	5 mM	
Agar	15			1.5%	
HEPES pH 8	238.30	1 M	238.30	10 mM	10 *
Glycine betaine	117.15	1 M	117.15	2 mM	2 *
$FeCl_2$	0.06	0.5 mM	126.75	5 µM	10 *
KH_2PO_4	43.55	250 mM	174.20	1 mM	4 *
MAMS vitamins					1 *
Sea salts medium (-C, -N)					
Sea salts (Sigma)	30			3%	
HEPES pH 8	238.30	1 M	238.30	10 mM	10 *
Glycine betaine	117.15	1 M	117.15	2 mM	2 *
$FeCl_2$	0.06	0.5 mM	126.75	5 µM	10 *
KH_2PO_4	43.55	250 mM	174.20	1 mM	4 *
MAMS vitamins					1 *
MAMS - succinate					
NaCl	20		58.44	2%	
$(NH_4)_2SO_4$	100	756.77 mM	132.14	7.6 mM	10
*$CaCl_2$ * 2 H_2O*	29	136.05 mM	147.01	1.36 mM	10
*$MgSO_4$ * 7 H_2O*	20	81.15 mM	246.47	0.82 mM	10
*$FeSO_4$ * 7 H_2O*	0.2	719.40 µM	278.01	7.25 µM	
*Na_2MoO4 * 2 H_2O*	2	8.26 mM	241.95	82.6 µM	
KH_2PO_4	36	206.66 mM	174.20	2.67 mM	10 *
K_2HPO_4	234	1.34 M	174.18	13.4 mM	
Trace metals (see table 2.2)					1
MAMS vitamins					1 *
MAMS vitamins pH 4					
Thiamine hydrochloride	0.01				
Nicotinic acid	0.02				
Pyridoxine hydrochloride	0.02				
P-aminobenozoic acid	0.01				
Riboflavin	0.02				
Calcium panthotenate	0.02				
Biotin	0.001				
Cyanocobalamin	0.002				
Lipoic acid	0.005				
Folic acid	0.005				

CHAPTER 3 DECIPHERING THE PHO REGULON OF *PHAEOBACTER* SP. MED193

3.1 Introduction

Phosphorus (P) is a fundamental element of DNA and RNA, membrane phospholipids, and ATP, making it essential for living organisms (Koolman & Röhm, 2019). P-limitation often affects bacteria living in all kinds of environments. Therefore, evolution equipped these organisms with mechanisms to survive short-term and long-term P-shortages (Wanner & Chang, 1987; VanBogelen et al., 1996; Suzuki et al., 2004).

The Phosphate regulon (Pho regulon) is a regulatory mechanism involved in inorganic phosphate (P_i) management in bacteria and was first described in *E. coli* (Wanner, 1996; Santos-Beneit, 2015). It contains proteins required for P_i uptake, acquisition of P_i from organic phosphates and P-storage (Wanner, 1996; Scanlan & Wilson, 1999; Antelmann et al., 2000; Suzuki et al., 2004). In bacteria, expression of these proteins is regulated by a two-component system: PhoBR, composing a histidine kinase PhoR and a response regulator PhoB (Wanner, 1996; Antelmann et al., 2000). Upon P_i limitation, the histidine kinase PhoR phosphorylates the response regulator PhoB. PhoB sequentially binds specific regions on the DNA, so-called Pho boxes, to induce or inhibit gene expression (Makino et al., 1988; Karl, 2014; Santos-Beneit, 2015). As compared to P-replete conditions, gene expression can be more than 100-fold higher in P-deplete environments (Wanner, 1996; Suzuki et al., 2004).

Since the discovery of the Pho regulon, the phosphate stress response has been studied in various bacteria (Scanlan & Wilson, 1999; Antelmann et al., 2000; Schwarz & Forchhammer, 2005; Baek & Lee, 2007; Willis et al., 2019) and many proteins involved in the transport and metabolism of P_i and organic P have been identified. On the one hand, these proteins include phosphomonoesterases/phosphodiesterases (e.g., Larson et al., 1983; Wanner & Chang, 1987; Brzoska & Boos, 1989; Wanner, 1996; Antelmann et al., 2000; Baek & Lee, 2007; Pegos et al., 2017; Sosa et al., 2019; Willis et al., 2019) and phosphonate transporter and degradation proteins (e.g, Wanner & Metcalf, 1992; Ilikchyan et al.,

2009, 2010; Alicea et al., 2011; Seweryn et al., 2015; Sosa et al., 2017, 2019; Stosiek et al., 2020). On the other hand, it includes transporter systems for various organic and inorganic P compounds (e.g., Forward et al., 1997; Rees et al., 2009; Bisson et al., 2017) and proteins involved in P-storage, such as polyphosphate kinases (e.g., Ahn & Kornberg, 1990; Kulaev et al., 2005; Martin et al., 2014). Noteworthy, the discovery of lipid remodelling in P-depleted cells was found to be ubiquitous in marine bacteria and key enzymes have been described (Van Mooy et al., 2009; Zavaleta-Pastor et al., 2010; Carini et al., 2015; Ridgway, 2015; Sebastián et al., 2016; Wei et al., 2018).

Much is known about the P-stress response in marine bacteria. However, the P-stress response of members of the *Roseobacter* group has never been described before in detail. In this study, we used various methods to study the P-stress response of *Phaeobacter* sp. MED193 (MED193), a model organism of the *Roseobacter* group (Simon et al., 2017). Methods used to decipher the Pho regulon of MED193 include the physiological comparison between the MED193 wild type and a *phoB* knockout mutant, as well as cellular and exoproteome, membrane lipid, and bioinformatics analyses. We demonstrate that MED193 induces several well-known proteins during P-starvation and, using bioinformatics to predict putative pho boxes, confirm the dependency of the induced proteins on the Pho regulon.

3.2 Results

3.2.1 The Pho regulon controls P_i acquisition systems and lipid remodelling in *Phaeobacter* sp. MED193

In this chapter, a combination of assorted methods was exploited to decipher the Pho regulon of MED193 and identify proteins involved in the P-stress response. Wild type MED193 (WT MED193) and a MED193 *phoB* knockout mutant (*ΔphoB*) were used. The deletion mutant was kindly provided by Dr Ian D.E.A. Lidbury and confirmed by sequencing (see section 2.8, Appendix 3.1). Here, the *phoB* gene is interrupted by a Gentamicin resistance cassette.

First, as described in section 2.1.2, cultures were grown in triplicate in ASW, containing low P (50 µM), for 24 h and then transferred into P-free media for 48 h. Comparison of cultures grown in P-deplete media showed that OD_{540} of WT MED193 and *ΔphoB* cultures more than doubled within the first 24 hours of growth before decreasing again to the same final OD_{540} after 48 hours of P-starvation (Table 3.1). However, the OD_{540} reached after 24 hours was significantly different between WT MED193 and *ΔphoB* (*t*-test score, $p<0.01$).

Table 3.1: ***Growth of WT MED193 and ΔphoB in P-deplete media.***
Growth was monitored by measuring OD_{540} over 48 hours. Asterisk marks significant difference (t-test score, p<0.01).

	0 h	*24 h*	*48 h*
WT MED193	0.157	* 0.335	0.296
ΔphoB	0.161	0.412	0.298

A comparison of alkaline phosphatase activity towards the monoester *para*-nitrophenyl-phosphate (*p*NPP) and the diester *para*-nitrophenyl-phosphorylcholine (*p*NPPC) after 48 hours of P-starvation confirmed that phosphatase activity in *ΔphoB* was nearly abolished (Figure 3.1). This result affirms the hypothesis that most phosphatases of WT MED193 are Pho-regulated.

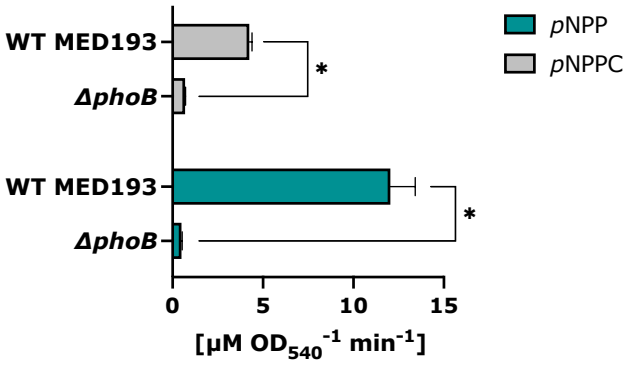

Figure 3.1: ***Alkaline phosphatase activity of WT MED193 and ΔphoB after 48 hours of P-depletion.***
Alkaline phosphatase activity was measured towards the monoester pNPP (green) and the diester pNPPC (grey). Whereas phosphatase activity was detected in WT MED193, it was nearly abolished in ΔphoB (p-value <0.05). Graph shows mean ± standard deviation of three biological replicates.

It has previously been reported that P-limited MED193 cells remodel membrane phospholipids, e.g. phosphatidylglycerol (PtdGro), to the P-free

betaine lipid diacylglyceryl-trimethylhomoserine (DGTS) (Sebastián et al., 2016). To confirm the hypothesis that this process is controlled by the Pho regulon membrane lipids of WT MED193 and *ΔphoB* samples after 48 hours of P-depletion, and P-replete WT MED193 cultures, were extracted. These lipids were sequentially analysed by liquid chromatography-mass spectrometry (LC-MS) (see section 2.5). Detected lipids were normalised against sphingosyl-PE d17:1/12:0 (SPE), commonly used as a lipid standard, and relative abundance of lipids/SPE ratios was plotted (Figure 3.2, Appendix 3.2). The figure displays the relative abundance of DGTS and the two phospholipids PtdGro and phosphatidyl-ethanolamine (PtdEtd). LC-MS data confirmed that lipid remodelling was non-existent in *ΔphoB*, verified by a high relative abundance of PtdGro/SPE and a low relative abundance of DGTS/SPE compared to WT MED193 -P. In addition, DGTS was barely detectable in *ΔphoB*. However, the lipid composition of WT MED193 showed a reduction in phospholipids and an increase in DGTS compared to the P-replete MED193 culture, confirming P-stress and associated lipid remodelling.

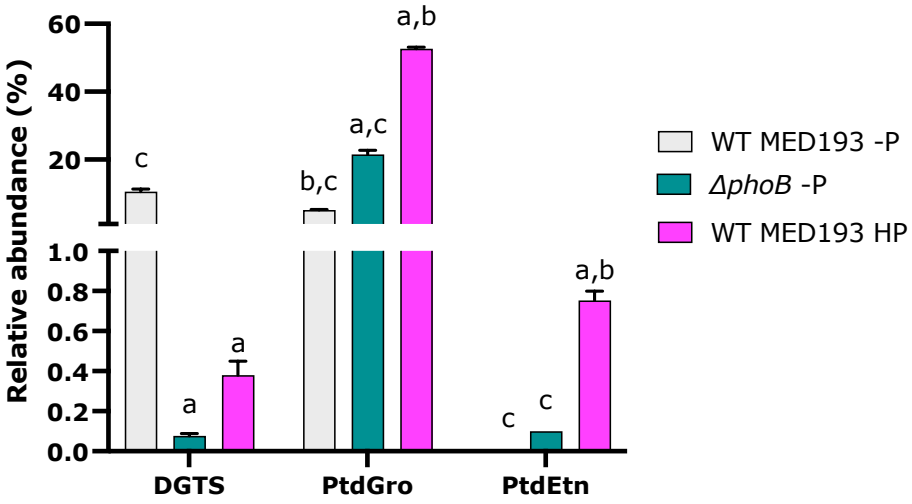

Figure 3.2: ***Membrane lipid composition as relative abundance (%) of WT MED193 and ΔphoB, normalised by SPE.***
Cultures used included P-deplete WT MED193 (WT MED193 -P), P-replete WT MED193 (WT MED193 HP), and P-deplete ΔphoB (ΔphoB -P). There is a significant difference (p-value <0.01) between WT MED193 -P (a) and ΔphoB (b) -P for DGTS and PtdGro, between WT MED193 -P (a) and WT MED193 HP (c) for DGTS, PtdGro, and PtdEtn, and between ΔphoB -P (b) and WT MED193 HP (c) for PtdGro, and PtdEtn. Graph shows mean ± standard deviation of biological triplicates. DGTS, diacylglyceryl-trimethylhomoserine; PtdGro, phosphatidyl-glycerol; PtdEtn, phosphatidylethanolamine.

3.2.2 Overview of the Pho regulon in *Phaeobacter* sp. MED193 – a proteomic approach

Additionally, proteomic analysis by liquid chromatography with tandem mass-spectrometry (LC-MS/MS, see section 2.4) of P-deplete cultures was used to identify proteins regulated by the Pho regulon. Whereas 2005 proteins were detected in the cellular proteome, only 1467 proteins were detected in the exoproteome. The comparison of the cellular proteomes and exoproteomes of WT MED193 and *ΔphoB* revealed several significantly upregulated and downregulated proteins (*p*-value <0.05, minimal $\log_2$ fold change (logFC 2), Figure 3.3). Where only 62 cellular proteins (3% of total proteins) of *ΔphoB* were significantly upregulated, 237 cellular proteins (12% of total proteins) were significantly downregulated (Figure 3.3A, Appendix 3.3, Appendix 3.4). A similar difference was found in the exoproteomes. Here, comparing the exoproteomes of P-deplete WT MED193 to *ΔphoB*, 164 *ΔphoB* proteins (11% of total proteins) were significantly upregulated and 531 proteins (36% of total proteins) were significantly downregulated (Figure 3.3B, Appendix 3.5, Appendix 3.6).

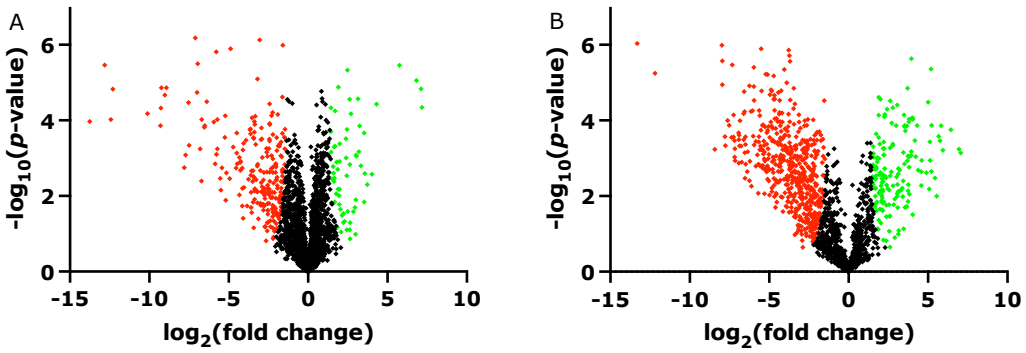

Figure 3.3: ***Volcano plots of cellular (A) and exo- (B) proteomic data comparing P-starved WT MED193 and ΔphoB cultures.***
WT MED193 and ΔphoB cultures were P-limited for 48 hours. Scatter points represent proteins. The x-axis is the fold change for the ratio between both cultures and the y-axis the statistical p-value. Green dots represent proteins that are significantly upregulated (A: 62, B: 164) and red dots represent proteins that are significantly downregulated (A:237, B: 531) in ΔphoB (p-value <0.05, logFC 2).

It was expected that most proteins involved in P-metabolism and transport would be undetectable in the *ΔphoB* proteomes. Therefore, it was hypothesised that looking into the significantly upregulated proteins of *ΔphoB* might give an idea of how the mutant handles P-stress when the

Pho regulon is inactive. Intriguingly, half of the ten most upregulated proteins in the cellular *ΔphoB* proteome are annotated as iron-related transporters, namely MED193_17504, MED193_22031, MED193_08013, MED193_08033, and MED193_17494 (Table 3.2). However, only MED193_08013 MED193_17504, and MED193_22031 share homology (08013/17504: protein sequence identity (Seq.ID) 29.33%, e-value $2e^{-08}$, 08013/22031: Seq.ID 22.86%, e-value 0.002, 17504/22031: Seq.ID 25.41%, e-value $3e^{-05}$). MED193_17504 is a homolog of *Silicibacter* sp. TrichCH4B HmuR (Table 3.3B, Seq.ID 52%, e-value 0.0). In the genome of *Silicibacter* sp. TrichCH4B two separate, neighbouring operons for complete heme uptake systems have been identified (Roe et al., 2013).

Table 3.2: ***Top 10 upregulated proteins in the cellular and exoproteome of P-deplete ΔphoB cultures.***
Proteins were significantly upregulated (p-value <0.05, logFC 2) in the proteomes of P-deplete ΔphoB cultures in comparison to P-deplete wild type MED193 cultures. White background; cellular proteome, grey background; exoproteome.

Identified proteins		*Accession number*	*Locus tag*	*Fold change*
Putative hemin receptor protein, iron uptake	*HmuR*	EAQ47012	MED193_17504	7.17
Hypothetical protein, DUF4856		EAQ45515	MED193_07678	7.11
Outer membrane TonB-dependent receptor, putative Fe siderophore transport		EAQ44834	MED193_22031	6.83
Outer membrane TonB-dependent receptor, putative Fe siderophore transport		EAQ45582	MED193_08013	5.75
Hypothetical protein		EAQ47013	MED193_17509	4.32
Putative ABC transporter, periplasmic binding protein, Fe siderophore transport	*FatB*	EAQ45586	MED193_08033	4.02
Sulfate permease, transmembrane protein	*Sul1*	EAQ45758	MED193_08893	3.73
Predicted membrane protein, nitric oxide reduction, potentially required for expression of *Nirk* and *Nor*	*NnrU*	EAQ44416	MED193_10518	3.57
S-adenosyl-L-methionine (SAM) methyltransferase	*BioC*	EAQ46319	MED193_14027	3.53
ABC-type transporter, periplasmic binding protein, putative Fe siderophore binding	*TroA-like*	EAQ47010	MED193_17494	3.53
Glycine cleavage system/decarboxylase complex, H protein	*GcvH*	EAQ44238	MED193_09370	7.06
Phosphogluconate dehydrates, 4Fe-4S cluster binding protein	*Edd*	EAQ46996	MED193_17424	6.95
Outer membrane TonB-dependent receptor, putative Fe siderophore transport		EAQ44834	MED193_22031	6.44
Lipopolysaccharide (LPS)-assembly protein, outer membrane protein	*LtpD*	EAQ44953	MED193_22626	5.93
UDP-N-acetylglucosamine acyltransferase, lipid A biosynthetic pathway		EAQ45140	MED193_04901	5.82
Type I secretion target repeat protein, Ca-binding		EAQ43596	MED193_03035	5.75
Creatinase, acting on C-N bonds, arginine/proline metabolism, metal-dependent		EAQ46665	MED193_15757	5.67
Malonyl-CoA synthase, AMP-dependent		EAQ46395	MED193_14407	5.55
Metallopeptidase, family M24		EAQ46197	MED193_07379	5.44
Taurine-pyruvate aminotransferase (class III), pyridoxal phosphate binding		EAQ43624	MED193_12173	5.23

As in MED193, these operons are transcribed in opposite directions (Table 3.3A). It has previously been described that these operons were

upregulated in *Silicibacter* under iron stress. In addition, growth experiments confirmed that *Silicibacter* acquires iron from several heme sources (Roe et al., 2013). The upregulation of several putative iron uptake systems indicates that *ΔphoB* might require iron as a metal cofactor for proteins synthesized upon P-limitation. MED193_17424 encodes a phosphogluconate dehydratase highly upregulated in the exoproteome of *ΔphoB* (Table 3.2). This protein binds one iron-sulphur (4Fe-4S) cluster and is predicted to be involved in carbohydrate metabolism. In addition, two proteins predicted to require metal co-factors were detected in the *ΔphoB* exoproteome, namely a metallopeptidase of the M24 family (MED193_07379) and a type I secretion target repeat protein (MED193_03035). However, both proteins are predicted to bind zinc, cobalt, manganese or nickel (Cerdà-Costa & Gomis-Rüth, 2014) and calcium (Delepelaire, 2004), respectively.

Table 3.3: ***Homology and genome neighbourhood of two heme uptake systems of Phaeobacter sp. MED193.***
(A) MED193 and Silicibacter sp. TrichCH4B share the same gene neighbourhood. Green; ABC transporter ATPase (HmuV) and periplasmic transmembrane protein (HmuT), turquoise; heme oxygenase (HmuS), light grey; outer membrane receptor (HmuR), dark grey; outer membrane energisation complex, white; not detected. The numbers above indicate fold change in ΔphoB compared to WT MED193 cellular proteome, numbers below show locus tag range. (B) Gene homology between MED193 heme uptake systems and Silicibacter sp. TrichCH4B. Listed are accession numbers, locus tags, Sequence identity (Seq.ID) in % and e-value.

A

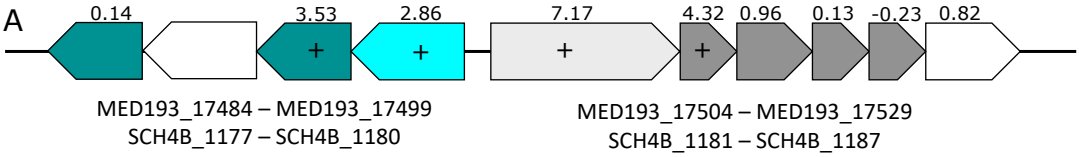

B

Identified proteins		*Accession number MED193*	*Locus tag MED193*	*Accession number TrichCH4B*	*Locus tag TrichCH4B*	*Seq.ID*	*e-value*
Hemin ABC transporter, ATP-binding protein	*HmuV*	EAQ47008	MED193_17484	EEW59515	SCH4B_1177	53%	$1e^{-97}$
Hemin ABC transporter, permease	*HmuU*	EAQ47009	MED193_17489	EEW60117	SCH4B_1178	69%	$4e^{-126}$
Hemin ABC transporter, periplasmic transmembrane protein	*HmuT*	EAQ47010	MED193_17494	EEW59380	SCH4B_1179	57%	$6e^{-97}$
Hemin transport protein, degrading factor	*HmuS*	EAQ47011	MED193_17499	EEW59923	SCH4B_1180	60%	$2e^{-156}$
TonB dependent hemin receptor	*HmuR*	EAQ47012	MED193_17504	EEW59184	SCH4B_1181	52%	0.0
Hypothetical protein		EAQ47013	MED193_17509	EEW59584	SCH4B_1182	46%	$2e^{-38}$
Outer membrane transport energisation protein	*ExbB*	EAQ47014	MED193_17514	EEW60097	SCH4B_1183	57%	$3e^{-67}$
Outer membrane transport energisation protein	*ExbD*	EAQ47015	MED193_17519	EEW59511	SCH4B_1184	54%	$2e^{-21}$
Biopolymer transport protein	*ExbD*	EAQ47016	MED193_17524	EEW59961	SCH4B_1185	46%	$1e^{-34}$
Outer membrane transport energisation protein	*TonB*	EAQ47017	MED193_17529	EEW59814	SCH4B_1187	38%	$4e^{-30}$

Apart from iron uptake through the heme transport system, it has been shown in other organisms that the Exb transport system (Table 3.3B) has a broad substrate specificity inclusive of various metals and macromolecules (Schauer et al., 2008).

To gain a better insight into the function of the differentially expressed proteins of cellular and exoproteomes of WT MED193 (Appendix 3.3, Appendix 3.5) and *ΔphoB* (Appendix 3.4, Appendix 3.6), functional prediction (Appendix 3.9) for each significantly upregulated and downregulated protein was extracted from the eggNOG database (Huerta-Cepas et al., 2019), clustered in groups, and plotted (Figure 3.4). Here, the number of proteins retrieved for each of the four categories is displayed. The plot confirms the differences already observed in the proteomic analysis described above.

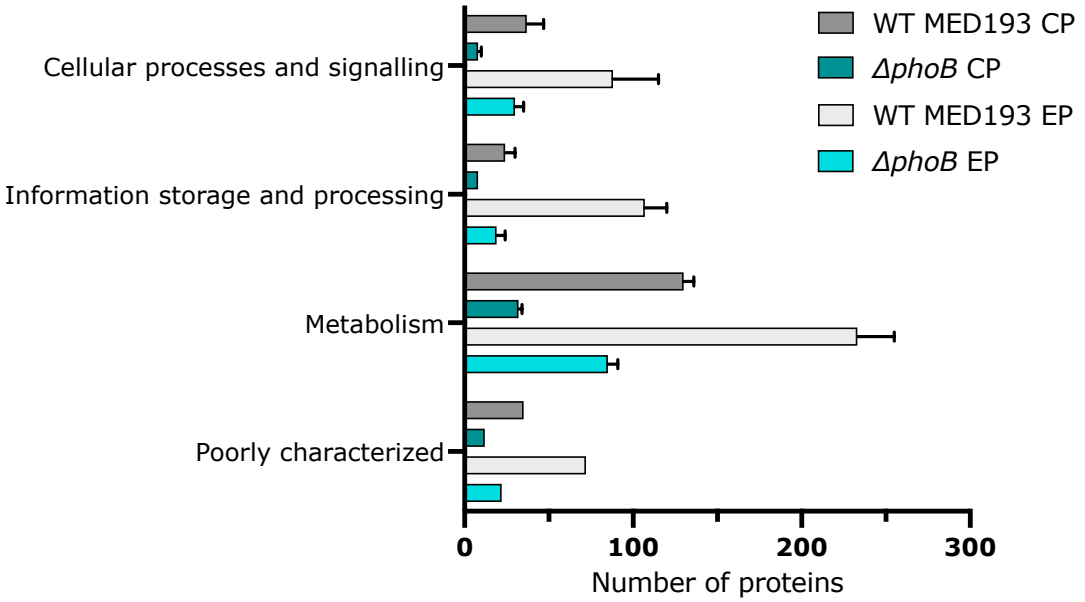

Figure 3.4: ***Functional comparison of upregulated proteins of WT MED193 and ΔphoB.***
Predicted protein functions from the eggNOG database were mined for proteins upregulated in WT MED193 (dark grey) and ΔphoB (dark green) cellular proteomes (CP), and WT MED193 (light grey) and ΔphoB (turquoise) exoproteomes (EP). Predicted functions were clustered in four general categories and plotted (y-axis), x-axis represents the number of upregulated proteins clustered in each category.

For cellular and exoproteomes, the difference between WT MED193 and *ΔphoB* was at least 65% in all four categories. Within the cellular proteome, proteins involved in 'cellular processes and signalling' pose the highest percentage difference between WT MED193 and *ΔphoB* (78.38%), directly followed by proteins assigned to 'metabolism' (75.38%). However,

regarding exoproteomes, the number of upregulated proteins belonging to 'information storage and processing' in WT MED193 is 82.24% higher compared to *ΔphoB*. In the remaining categories, there is a 66% difference between WT MED193 and *ΔphoB*.

3.2.3 The Pho regulon controls the P_i metabolism in *Phaeobacter* sp. MED193

Since cellular proteomics revealed a significant difference in the category 'metabolism', which also includes transporters for numerous substrates, the relative abundance was calculated for proteins of both cellular and exoproteomes of WT MED193 and *ΔphoB*. Calculations revealed clear differences. Therefore, relative abundances of the 50 most abundant proteins of WT MED193 and relative abundances of the corresponding proteins of *ΔphoB* were plotted (Figure 3.5, Appendix 3.7, Appendix 3.8). Additionally, cohesive proteins were connected via lines and six prominent proteins were highlighted in green.

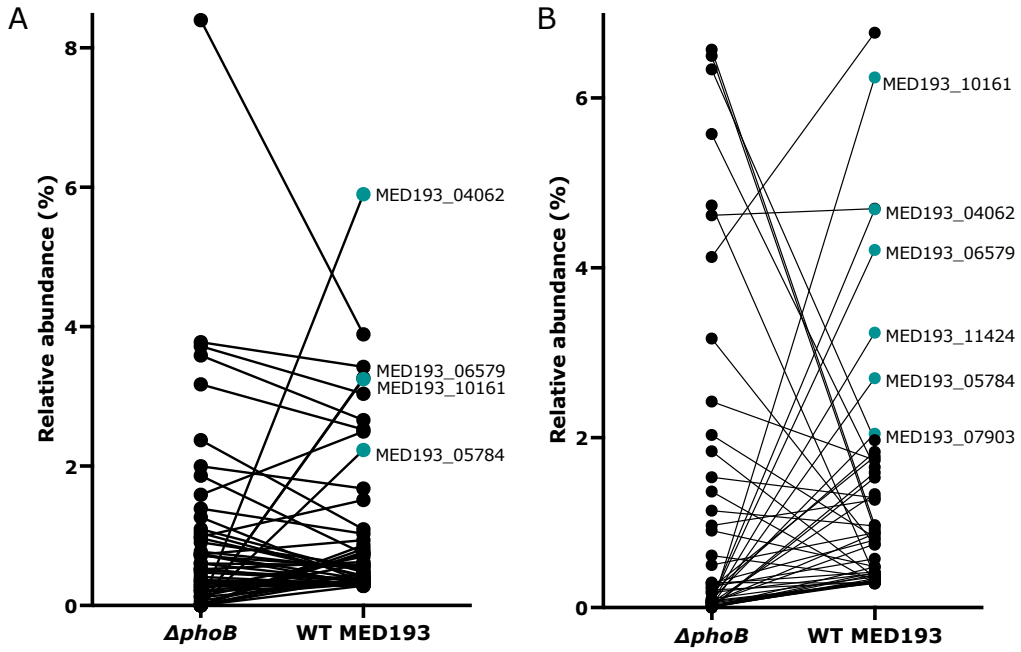

Figure 3.5: ***Comparison of 50 most abundant proteins identified in WT MED193 cellular (A) and exo- (B) proteomes and relative abundances of corresponding ΔphoB proteins.***
Lines connect cohesive proteins, indicating an increase or decrease of relative abundance. Six proteins, namely MED193_04062, MED193_05784, MED193_06579, MED193_07903, MED193_10161, and MED193_11424 show a clear difference between WT MED193 and ΔphoB and are highlighted in green.

These proteins showed a discrepancy in relative abundance between WT MED193 and *ΔphoB*, specifically MED193_04062, MED193_05784, MED193_06579, MED193_07903, MED193_10161, and MED193_11424 (Table 3.4).

Table 3.4: ***List of substrate-binding proteins and hydrolases that show a significant difference in relative abundance between WT MED193 and ΔphoB.***
Relative abundance is given in % for cellular (C), and exo- (E) proteomes of WT MED193 and ΔphoB, including accession numbers and locus tags.

Identified proteins		*Accession number*	*Locus tag*	*Relative abundance MED193 (%)*	*Relative abundance ΔphoB (%)*
Phosphate ABC transporter, PBP	*PstS*	EAQ44764	MED193_04062	C: 5.90 E: 4.69	C: <0.01 E: 0.09
Secreted phosphatase	*PhoX*	EAQ45878	MED193_05784	C: 2.23 E: 2.70	C: <0.01 E: 0.03
Glycerophosphoryl diester phosphodiesterase	*GlpQ*	EAQ46037	MED193_06579	C: 3.26 E: 4.21	C: <0.01 E: 0.08
SN-glycerol-3-phosphate ABC transporter, PBP	*UgpB*	EAQ45560	MED193_07903	C: 0.86 E: 2.04	C: <0.01 E: 0.09
Phosphonate ABC transporter, PBP	*PhnD*	EAQ43272	MED193_10161	C: 3.25 E: 6.24	C: <0.01 E: <0.01
Spermidine/putrescine ABC transporter, PBP	*PotD*	EAQ43393	MED193_11424	C: 0.60 E: 3.24	C: 0.13 E: 0.06

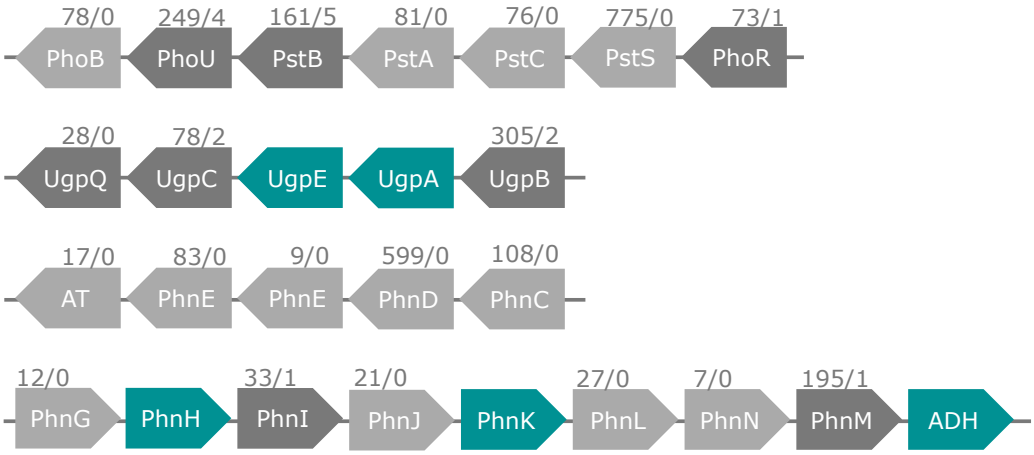

Figure 3.6: ***Genomic neighbourhood of highly abundant substrate-binding proteins found in the cellular proteome of WT MED193 in comparison to ΔphoB.***
The genomic neighbourhood of PstS (MED193_04062), UgpB (MED193_07903), and PhnD (MED193_10161), including second Phn operon. MS/MS count numbers, light grey; only detected in WT MED193, dark grey; detected in WT MED193 and ΔphoB, green; not detected. PhoB; transcriptional regulator Pho regulon, PhoU; phosphate uptake regulator, PstB; ATPase of Pst transporter, PstA/C; permease of Pst transporter, PstS; periplasmic substrate-binding protein (PSBP) of Pst transporter, PhoR; sensor histidine kinase, UgpQ; glycerophosphoryl diester phosphodiesterase, UgpC; ATPase of SN-G3P transporter, UgpA/E; permease of SN-G3P transporter, UgpB; PSBP of SN-G3P transporter, AT; acetyltransferase, PhnE1/2; permease of phosphonate transporter, PhnD; PSBP of phosphonate transporter, PhnC; ATPase of phosphonate transporter, PhnG/H/I/L; alpha-D-ribose 1-methylphosphonate 5-triphosphate synthase subunit, PhnJ; alpha-D-ribose 1-methylphosphonate 5-phosphate C-P lyase, PhnK; ATPase of ribophosphonate triphosphate synthase reaction, PhnN; ribose 1,5-biphosphate phosphokinase, PhnM; alpha-D-ribose-1-methylphosphonate 5-triphosphate diphosphatase, ADH; alcohol dehydrogenase.

Four of these proteins are annotated as substrate-binding proteins of ABC transporters, thereof three proteins are predicted to be involved in inorganic and organic P transport (PstS; MED193_04062, UpgB; MED193_07903, PhnD; MED193_10161). The fourth substrate-binding protein is annotated as PotD (MED193_11424), potentially involved in spermidine/putrescine transport. Furthermore, two proteins are annotated as phosphatases, specifically a phosphomonoesterase (PhoX; MED193_05784, see Chapter 4) and a putative phosphodiesterase (GlpQ; MED193_06579, Figure 3.6).

Examination of the genomic neighbourhood of the three P-related substrate-binding proteins demonstrated that the neighbouring proteins, mostly members of the ABC transporters, were either not detected or were barely detectable in the cellular proteome of *ΔphoB*. For example, proteins of the Pho operon, including proteins of the P_i ABC transporter Pst, the sensor histidine kinase PhoR and the phosphate uptake regulator PhoU, were represented in abundance in WT MED193, but barely or not detected in *ΔphoB* (Figure 3.6). Intriguingly, MED193 possesses two separate 'Phn' operons. Genes of these operons encode proteins predicted to be components of a phosphonate transporter (MED193_10146 to MED193_10166) and required for phosphonate degradation (MED193_17604 to MED193_17654). Out of all these proteins, two proteins were not detected in the cellular proteome of WT MED193, specifically PhnH and PhnK. Additionally, only two out of all proteins of both operons were detected in the cellular proteome of *ΔphoB*. However, the low MS/MS count of 1 indicates that both operons are regulated by PhoB (Figure 3.6). The substrate-binding protein PhnD (MED193_10161) belongs to the PhnD Superfamily (cl31344) associated with the C-P lyase system (Lu et al., 2020). MED193_10161 is a homolog (32% Seq.ID, e-value $2e^{-28}$) of the previously described PhnD in *E. coli* (EcPhnD) (Chen et al., 1990; Rizk et al., 2006; Alicea et al., 2011). Several conserved amino acids were identified in the proteins active site through crystallisation studies of EcPhnD, chemically bonded with 2-aminoethyl-phosphonic acid (2-AEP) (Alicea et al., 2011). These conserved amino acids were found in other C-P lyases (Figure 3.7, Appendix 3.10, Bisson et al., 2017), also in MED193_10161. However, not all amino acids are conserved in MED193.

```
                  80        90        100       110       120       130       140       150
Can.P.HTCC7211    FTFKDYAGTMESMLGGNLDYTWFGSSGYAGMYLKDPTAVVPVLTRMQPTGDMG-YYSVAVATKKSGIKS---------
Can.P.ubique      FTFKDYAGTMESMLGGNLDYTWFGSSGYAGMYLKDPTAVVPVLTRMQPTGDMG-YYSVAVATKKSGIKS----------
P.sp.MED193       FAPADYNGVIQGLLGGTLDMAWLGASGYAKTYLSDPEAVEPILVKVNVDGGYG-YYSVGFARADSGITS----------
D.phosphitoxidans YAPADYNGVIEGLLGGNLDMAWLGASGYAKVYMTNPDAVEPVLTKINKDGSFG-YYAIGFARVDSGIEN----------
S,JA23Ba213       FVAGDYTAVMVSQAQGQTHVAFYGPGSYVDAIEKANAPIEAFVKEDSLRSGTV-YHSLILSKKGSGIKT---------
M.magneticum      EVSADYAGAIWNLRSGRAQLAWLGNKTAIEA--VDLAGTEVFAKETYPSGLGG-YYTYLIVPRDSPLAS----------
N.PCC71201        FYVTQYAAVIEAMRFGKVQAAWLGGKSYIEA--ARVANAEAFAQVVSADGTRG-YYSHLIANKDNPITAEAKAVGGDKY
N.PCC71202        FYATQYSGVIEAMRFGQVHIAWYGGKSYIEA--ARIANAEAFAQTVATDGKKG-YYSHLIANKNNPITAAAKRQGGDKY
E.coli            FFAPDYAGIIQGMRFNKVDIAWYGNLSAMEA--VDRANGQVFAQTVAADGSPG-YWSVLIVNKDSPINN---------
P.aeruginosa      FFAPDYAGIIQGMRFDKVDIAWYGNKAAMEA--VDRAHGEIFAQTVAASGAPG-YWSLLIANKDSKIDS----------
T.erythraeum      FTATDYAGVIEAMRQDKVDIAWFGPLSYVLA--EQEAGAEAFATGVRTKTGKSTYKSILVVPGDSTVQS----------
B.japonicum       RIANDYAAVIEGQRAGNIQIASYGSASFARA-RLTGVKTDAFANDINADGSTG-YYSVFFVKASSAYKK----------
R.palustris       RIANDYAAVIEGQRAGNIHIGMYGPASYARAYLV-GAKVEPFAIEVNGDGSKG-YHSVLYVKKDSPYQK----------

                  160       170       180       190       200       210       220       230
Can.P.HTCC7211    -MED----LKGKSFGWADPNSTSGFLIPSIEL---KAMGM-DPDTYFSKTQFSGGHENNVLALMNGDVDAAVT-WVSGV
Can.P.ubique      -MED----LKGKSFGWADPNSTSGFLIPSIEL---KAMGM-DPDTYFSKTQFSGGHENNVLALMNGDVDAAVT-WVSGV
P.sp.MED193       -LED----MQGKVFGFGDPNSTSGFLIPSIEIPEITGSTM-TSGDYFGEVKFSGGHEQTIVGVNNGDFDGGVT-WADGL
D.phosphitoxidans -LED----MKGKVFGFGDPNSTSGYLIPSIEIPQ-AGYSM-KPGEYFKDVKFTGGHEQTIVAVFNGDIDGGVT-WACGL
S,JA23Ba213       -LED----AKGKDFAFVDPESTSGFKVPMAYFC--LEAKI-KPKEYFKRVAFAGTHESVILGIAQGTIPVGVT-W----
M.magneticum      -ADEVIAKAVDLTFAQGDVNSTSGTVVPGYYLF--ASRHL-EPRKLFKRVVHAN-HEDNIRAVAEGRSDAATV------
N.PCC71201        VIQN----AAKLTFAFNEPNSTSGFLVPSYYIF--TKNNI-EPKKAFKRLIFAGNHEACALAVANKQVDVATV------
N.PCC71202        VLQN----AAKLTFAFNEPNSTSGFLVPSYYVF--AKNKV-DPKKVFKRLIFSGSHEATALAVANNQVDVATN------
E.coli            -LNDLLAKRKDLTFGNGDPNSTSGFLVPGYYVF--AKNNI-SASD-FKRTVNAG-HETNALAVANKQVDVATN------
P.aeruginosa      -LEDMLANAKSLTFGNGDPNSTSGYLVPGYYVF--AKNNV-DPVKAFKRTLNSS-HEVNALAVANKQVDVATF------
T.erythraeum      -IQD----LKGKNVAFVDPASTSGGLVPSYLVL--KATGQ-KPKDFFGKLTYAGSHDAAGMAVKNQTVDAAGT------
B.japonicum       -VDD----LKGKNLGLVDPNSTSGNNVPRFEL---DKMGIPDADTYFSKVVFTGSHENAILALSQGTVDVAANQWTSDD
R.palustris       -IED----LKGKNLCLVDPNSTSGNNVPRFMM---NKMSI-DPDKFFAKVIYAGSHENAVIGVAQGTCDAAFN-W----

                  240       250       260       270       280       290       300       310
Can.P.HTCC7211    GSWEEGYSSGNLRKMVDKGILNMDDIVQIWSSKLIPNGPIVMPTFLPVRAHQVMIGLKQWIHEND--------PKCSEN
Can.P.ubique      GSWEEGYSSGNLRKMVDKGILNMDDIVQIWSSKLIPNGPIVMPTFLPVRAHQVMVGLKQWIHEND--------PKCSEN
P.sp.MED193       GNWEDGYNSGALRRAVDAGLVDMNDLVQIWQSKPIPEGPIVLRKDLPEDVKVKFTALMASLPAMD--------PECAYG
D.phosphitoxidans GDWVDGYNSGALRKAADAGIVDMTQIREIWRSKLIPEGPIVLRKDLPESVKLKITGMLASMPSMD--------PECAYG
S,JA23Ba213       -------DTGISIATNKGQIKGIEDLEVIWRSDPIPSSPWAYRKDLPEDLKEALRTAYLEYENT---------PEGQKW
M.magneticum      -------ASLIYDQLGRRDPGTLAATRIVWRSPLIPADPLVRRRDLPAADKERIAAFFFGYGQPAAGKSAMQLAEERRA
N.PCC71201        -------SNEALSRLERTNPTARQKIEIIWQSPLIPSDPIVYRQDLPADIKNRLQKFFYNY-------------KDAKV
N.PCC71202        -------NNESLERLEKTNPSARKKIEIIWTSPIIPSDPIAYRKDLPEDVKKKLRNFFYNF-------------KDRKI
E.coli            -------NTENLDKLKTSAPEKLKELKVIWKSPLIPGDPIVWRKNLSETTKDKIYDFFMNYGKT---------PEEKAV
P.aeruginosa      -------NTEGMERLELTQPEKARQLKVIWKSPLIPGDPLVWRNNLSDEQKNKLRDFFFKYGAN---------AEQKKV
T.erythraeum      -------NDITYNKMINKGLISEESNRILLESEPIPGSPLAYRQELDEQTKNNIRETVLNA------------HKDIKV
B.japonicum       DSTLAQMLTKNMLKNADGSAMKKDDFHIIHKSAPIINGPYAYNSDLPEDAKAAIAKAFFDAPAKD--------KAAFDR
R.palustris       --WNTEDESNLL-RMDRKGMVKAADFRIILKSDLIVNSPMAYLSDMPEDLKAAIRKAVLDLATND--------PETFNK
```

Figure 3.7: ***Multiple sequence alignment places MED193_10161 within the C-P lyases****.*
Y47 (turquoise), Y93 (turquoise), S127 (green), T128 (green), S129 (green), and H157 (blue), and an H_2O molecule coordinate the oxygen atoms of the 2-AEP phosphate group. The E.coli E177 (red) and D205 (red) coordinate the amino group of 2-AEP (Alicea et al., 2011). In MED193 the amino group coordinating glutamate and aspartate are replaced by two glycines (purple), potentially coordinating other phosphonate residues. Sequences retrieved from Bisson et al., 2017 and Poehlein et al., 2013.

Here, the amino group coordinating E177 and D205 are replaced by two glycines. The same conservation was identified in *Desulfotignum phosphitoxidans* (Figure 3.7). Moreover, *D. phosphitoxidans* can utilise several alkyl-, organo-, and phenyl-phosphonates as a sole source of P (Poehlein et al., 2013). It seems likely that MED193_10161 can bind one or more of these substrates, thereby introducing phosphonates to the C-P lyase complex.

The phosphodiesterase GlpQ (MED193_06579) was detected in the cellular and exoproteome of *ΔphoB*. However, the detection levels of GlpQ were distinctly higher in WT MED193 than *ΔphoB*. While the protein was counted 503 and 663 times in the WT MED193 cellular and exoproteome, GlpQ was only found 10 (-98%) and 52 times (-92%) in the *ΔphoB* cellular and exoproteome. Likewise, the phosphomonoesterase PhoX (MED193_05784) was detected in the cellular and exoproteome of *ΔphoB*.

While the MS/MS count for PhoX in the cellular and exoproteome of WT MED193 was 1340 and 1457, respectively, in *ΔphoB*, PhoX was only 1 (-99%) in the cellular and 56 (-96%) in the exoproteome. These results prove that both phosphatases are Pho-regulated. All proteins described above are either part of P-transporters or phosphatases, demonstrating the impact of the Pho regulon on the MED193 proteome. Likewise, the phospholipase C (PlcP) responsible for phospholipid remodelling in MED193 (Figure 3.2) was detected in the cellular proteome of WT MED193 with an MS/MS count of 17. However, the protein was not found in the cellular proteome of *ΔphoB*, confirming the hypothesis that lipid remodelling in MED193 is also Pho-regulated.

An additional seven proteins which are potentially involved in P metabolism were further analysed (Table 3.5). Two proteins, specifically a phosphodiesterase (GdpQ, MED193_11288) and a polyphosphate kinase (PpK2, MED193_11927) displayed a significant fold change between WT MED193 and *ΔphoB*. In addition, both proteins were detected in the cellular and exoproteome of WT MED193 but were non-existent in *ΔphoB*. This result indicates a Pho regulon dependency. Furthermore, two periplasmic substrate-binding proteins of a glycerol and G3P transporter, namely GlpV (MED193_09570) and UgpB (MED193_11293), were identified.

Table 3.5: ***List of MED193 proteins related to phosphate metabolism that show Pho-in/dependency.***
*The Table lists proteins that are related to organic phosphate metabolism, including dehydrogenases, periplasmic substrate-binding proteins, a phosphatase, and a kinase. Additionally, accession numbers, locus tags, fold change as the ratio between WT MED193 and ΔphoB, relative abundance (%) of protein within cellular (C) and exo- (E) proteomes, and MS/MS count values are given. *; significant fold change (p-value <0.05, logFC 2), N/D; not detected, in bold; Pho-regulated.*

Identified proteins		*Accession number*	*Locus tag*	*Fold change WT MED193/ ΔphoB*	*Rel. abundance (%) WT MED193*	*Rel. abundance (%) ΔphoB*	*MS/MS count WT MED193*	*MS/MS count ΔphoB*
G3P dehydrogenase	*GapA*	EAQ43254	MED193_10071	C: -0.59 E: 2.40 *	C: 0.0260 E: 0.0080	C: 0.0454 E: 0.0017	C: 49 E: 17	C: 49 E: 2
Phosphonate transporter, periplasmic binding protein	*PhnD*	EAQ47401	MED193_19449	C: -0.51 E: 2.65 *	C: 0.0005 E: 0.0205	C: 0.0008 E: 0.0038	C: 4 E: 19	C: 5 E: 11
G3P dehydrogenase	*GlpD*	EAQ47436	MED193_19624	C: -0.76	C: 0.0042	C: 0.0082	C: 9	C: 18
Glycerol transporter, periplasmic binding protein	*GlpV*	EAQ44278	MED193_09570	C: 1.57 E: 0.77	C: 0.0557 E: 0.4180	C: 0.0218 E: 0.2828	C: 119 E: 339	C: 63 E: 154
G3P transporter, periplasmic binding protein	*UgpB*	EAQ44571	MED193_11293	C: 5.71 * E: 4.09 *	C: 0.4698 E: 0.8720	C: 0.0104 E: 0.0590	C: 240 E: 246	C: 15 E: 41
Phosphodiesterase	*GdpQ*	EAQ44570	MED193_11288	C: 2.89 * E: 3.86 *	C: 0.0067 E: 0.0077	C: 0.0010 E: 0.0006	C: 24 E: 23	**C: N/D** **E: N/D**
Polyphosphate kinase	*PPK2*	EAQ43336	MED193_11927	C: 7.71 * E: 7.14 *	C: 0.1844 E: 0.0426	C: 0.0010 E: 0.0003	C: 178 E: 99	**C: 2** **E: N/D**

Whereas there was no significant fold change between WT MED193 and *ΔphoB* for GlpV, the fold change was significant for UgpB. Also, both proteins were found in the cellular and exoproteome of *ΔphoB*.

A reduced MS/MS count and a lower relative abundance of GlpV and UgpB in *ΔphoB* in comparison to WT MED193 indicate, that both proteins are presumably Pho-regulated but could be co-regulated by another transcriptional regulator. Finally, two dehydrogenases, namely GapA (MED193_10071) and GlpD (MED193_19624), and a periplasmic phosphonate-binding protein PhnD (MED193_19449) were discovered in the cellular and exoproteomes of WT MED193 and *ΔphoB*. Although GapA and GlpD were significantly upregulated in the WT MED193 exoproteome, the relative abundance and MS/MS count of both proteins didn't differ too much between WT MED193 and *ΔphoB*. These findings suggest that all three proteins are Pho-independent.

3.2.4 The identification of putative Pho boxes can help to identify more proteins that are Pho-regulated

A list of putative Pho boxes, kindly provided by Dr Marta Sebastián, was used to confirm the dependence of proteins mentioned above on the Pho regulon (Appendix 3.11, unpublished data). As described in the literature, 34 known Pho box sequences of *Sinorhizobium meliloti* and ten known Pho box sequences of *E. coli* were used to create a position-weight matrix (Yuan et al., 2006). The consensus sequence retrieved from the matrix was used to scan the intergenic regions of the WT MED193 genome for the highest score (log-odds), using an in-house Python script. Putative Pho boxes were divided into high-scoring (>10) and low-scoring Pho boxes, according to a threshold established from proteins known to be Pho-regulated (Sebastián et al., 2016). Next, proteins with a putative Pho box were compared to the proteomic dataset, comparing P-deplete WT MED193 and *ΔphoB* cultures. From the 120 proteins that possess a putative Pho box, only 17 proteins were significantly upregulated in the P-deplete WT MED193 condition. Unsurprisingly, three of the 17 Pho box-containing proteins were listed in Table 3.4, namely: PstS; MED193_04062, GlpQ; MED193_06579, and UgpB; MED193_07903. A Pho Box upstream of PlcP (MED193_17359) confirmed once again that

membrane phospholipid remodelling is Pho-regulated (Sebastián et al., 2016). Lastly, a 5'-nucleotidase/UDP-sugar hydrolase (MED193_18254, UshA) has a putative Pho box. Interestingly, this protein was around 6x higher upregulated in the cellular proteome of WT MED193 compared to *ΔphoB*, confirmed by the MS/MS count (MED193: 128, *ΔphoB*: 0).

The findings presented in this chapter demonstrate that the Pho regulon has a drastic impact on the MED193 proteome. Proteomics can be used as a tool to identify candidate proteins. However, biochemical studies of candidate proteins or the construction of deletion mutants are essential tools to clarify the roles of candidate proteins during P-limitation, e.g., the substrate specificity of substrate-binding proteins and hydrolases. More studies are needed to identify proteins that can complement silenced proteins.

3.3 Discussion

The Pho regulon is the regulatory machinery essential for the P-stress response in bacteria (Wanner, 1996; Santos-Beneit, 2015). It has been studied extensively in *E. coli* and several other bacteria (e.g., Wanner & Chang, 1987; Monds et al., 2006; Baek et al., 2007; Su et al., 2007). Many proteins involved in the P-stress response have been identified (e.g., Schweizer & Boos, 1985; Eder et al., 1996; Moore et al., 2005; Baek & Lee, 2006; Sebastián & Ammerman, 2009; Tetu et al., 2009). Here, for the first time, we used several techniques to decipher the Pho regulon of *Phaeobacter* sp. MED193, a member of the *Roseobacter* group. MED193 was first isolated from the Mediterranean Sea (Brinkhoff et al., 2008), an environment that is subject to spatial and seasonal P-depletion (Lazzari et al., 2016). Due to its habitat, MED193 became perfectly adapted to P-limitation, making it a favourable candidate to study P-stress.

Methods used to decipher the P-stress response of MED193 and *ΔphoB* included growth experiments, LC-MS analysis of membrane lipids, and cellular and exoproteome analysis. The *phoB* knockout mutant was kindly provided by Dr I. DEA Lidbury. *PhoB* encodes a transcriptional regulator and together with *phoR* (encoding a sensor histidine kinase), regulates the Pho regulon (Wanner & Chang, 1987; Wanner, 1996; Hirani et al., 2001). Deleting *phoB* abolishes the induction of the Pho regulon,

thereby suppressing the P-stress response. This method has previously been used in other studies to identify proteins involved in P-metabolism (e.g., Hirani et al., 2001; Baek & Lee, 2006, 2007; Lidbury et al., 2017).

Growth experiments showed that both WT MED193 and *ΔphoB* grow in P-deplete conditions. OD_{540} more than doubled within the first 24 hours of growth. However, a significant difference (t-test score, $p < 0.05$) was found between WT MED193 and *ΔphoB* (Table 3.1). A similar effect has been reported in *E. coli* and *Bradyrhizobium japonicum* (Minder et al., 1998; Baek & Lee, 2006, 2007). The Endpoint OD_{600} showed a significant difference in these studies between the wild type and *phoB* deletion mutant. In P-limited conditions, cultures reached a growth plateau at the end of exponential growth, and OD_{600} stayed constant for several hours. However, in this study OD_{540} dropped after 24 hours in P-depleted conditions by ~28% (WT MED193) and ~12% (*ΔphoB*), and both cultures resulted in the same final OD_{540} after 48 hours of growth. The drop demonstrates that cells can't survive a prolonged period of P-limitation. Cultures for this experiment were grown in MB for 24 hours, transferred to ASW with low P_i concentration (50 µM) for 24 hours and transferred again to P-free media for 48 hours. Prior experiments (unpublished data) have shown that MED193 becomes P-limited after overnight growth in MB. Adding the periods of P-limitation up means that WT MED193 and *ΔphoB* were P-limited for a total of 96 hours. Astonishingly, *ΔphoB* can survive and somehow adapt to such a long period of P-depletion, especially while not being able to make use of the Pho regulon. Contrarily, findings of this study suggest that WT MED193 uses P, scavenged from organic P sources like cell debris, to multiply rapidly, thereby increasing biomass. However, the rate of dying is slower in *ΔphoB*, indicating that the mutant can withstand limiting conditions better than the wild type. P obtained from unknown sources may be used for cell preservation rather than cell division. However, a more detailed growth experiment is needed to confirm these hypotheses.

Comparing alkaline phosphatase activity of WT MED193 and *ΔphoB* during the starvation period confirmed that phosphatase activity was almost abolished, demonstrated by the significantly lower alkaline phosphatase activity recorded in *ΔphoB* (Figure 3.1). This finding coincides

with data found in the literature, where several phosphatases have been described as Pho-regulated (e.g., Coleman, 1992; Baek & Lee, 2007; Lidbury et al., 2017). Additionally, MED193_06579, annotated as phosphodiesterase GlpQ, possesses a putative Pho box, further affirming its Pho-dependency (Appendix 3.11). In-depth analysis will most likely reveal more Pho boxes associated with other phosphatases.

Furthermore, membrane lipid quantification confirmed that lipid remodelling is indeed Pho-regulated (Figure 3.2). The substitute lipid DGTS was not detected in *ΔphoB*. Additionally, bioinformatics unveiled a putative Pho box close to *plcP* (unpublished data, Sebastián et al., 2016), and proteomics also confirmed that PlcP was undetectable in the cellular proteome of *ΔphoB*. It has previously been shown that the synthesis of DGTS in *Sinorhizobium meliloti* is Pho-dependent (Geiger et al., 1999). The phospholipid content was lower *ΔphoB* compared to WT MED193 HP. The relative abundance of both sulphur-containing aminolipids (SAL, SAL2, Appendix 3.2) was higher in the P-depleted WT MED193 cultures than in the P-replete WT MED193. It seems likely that *ΔphoB* is compensating for the lack of phospholipids with other lipids.

It was expected that the expression of most proteins involved in P uptake and metabolism would be abolished in the *ΔphoB* cellular and exoproteome. Since the mutant could withstand prolonged P-starvation, other mechanisms must be available to allow for survival. Interestingly, five transporter systems that are predicted to be involved in iron uptake are within the top ten most upregulated proteins of the cellular *ΔphoB* proteome (Table 3.2). Three of the five transporter proteins share a homology of around 25%. Not only is the highest upregulated protein MED193_17504, encoding a putative hemin receptor protein, a homolog of HmuR of *Silicibacter* sp. TrichCH4B, but their gene neighbourhood is identical (Table 3.3). The gene neighbourhood includes two complete heme uptake systems. Growth experiments of *Silicibacter* sp. TrichCH4B on various natural heme compounds, e.g., Fe(III)coproporphyrin, Fe(III)-heme, and haemoglobin A ferrous, demonstrated that the gene expression of the two heme uptake systems is induced by all three substrates (Roe et al., 2013). Iron can play a crucial part in the correct function of enzymes, serving as a metal cofactor for many proteins, often in the form of iron-

sulphur clusters (Camponeschi & Banci, 2019). Several proteins were found in the ten most upregulated proteins predicted to require metal cofactors for enzyme activity. A predicted nitric oxide reductase (MED193_10518, NnrU) is a homolog of NnrU of *Agrobacterium tumefaciens* C58 (Seq.ID 35%, e-value $2e^{-06}$) which has been shown by electron paramagnetic resonance spectroscopy to require heme *b* as a metal cofactor (Beltrán et al., 2015). Also, MED193_17424 annotated as phosphogluconate dehydratase has two conserved cysteines (pos. 155, 222) predicted to bind a 4Fe-4S cluster. Other metal-dependent proteins were upregulated in the exoproteome of *ΔphoB.* These proteins require different metals as cofactors, e.g., calcium, nickel, and manganese. However, no specific transporter systems for these metals have been detected in the most upregulated proteins. The ExbBD transport complex is situated in the inner membrane and linked to TonB that reaches the outer membrane. Here, TonB interacts with substrate-binding proteins, further transferring them to the ExbBD complex through structural conformation (Hickman et al., 2017). TonB dependent substrate-binding proteins have been shown to have broad substrate specificity, including various metals and macromolecules (Schauer et al., 2008). Findings regarding the coping mechanisms of *ΔphoB* demonstrate that the mutant can use alternative mechanisms to acquire essential nutrients. However, more studies are necessary to investigate the function of these transporters, e.g., TonB-ExbBD and HmuSTUV.

Looking into the proteomes of WT MED193 and *ΔphoB,* it was obvious that the Pho regulon controls many gene operons or single genes. Interestingly, *ΔphoB* lacks many proteins involved in 'information storage and processing' (WT MED193/*ΔphoB*: ~80%), 'metabolism' (WT MED193/*ΔphoB*: ~68%), and 'cellular processes and signalling' (WT MED193/*ΔphoB*: ~70%) (Figure 3.4). The 'information storage and processing' category includes proteins involved in DNA and RNA related processes, e.g., translation, transcription, and recombination. A comparison of the P-deplete WT MED193 and *ΔphoB* proteomes showed that more proteins are downregulated rather than upregulated, in the mutant, concluding in a lower translation and transcription rate. In the mutant, proteins belonging to the 'cellular processes and signalling'

category show lower detection levels. This category sums up proteins related to processes such as cell division and cell wall biogenesis. Therefore, downregulation of proteins of this category suggests that recombination and cell division is most likely downscaled.

Proteins belonging to various transporters, metabolism, and energy production and conversion are listed in the 'metabolism' category. Bacteria possess many transporters for P, most of which are Pho-regulated. A reduction of proteins in this category was expected. By exploring upregulated metabolism-related proteins in the WT MED193 proteome several substrate-binding proteins and hydrolases were revealed (Table 3.4). All these proteins are Pho-regulated in other organisms. PstS (MED193_04062), the periplasmic P_i binding protein of an ABC transporter, is situated in the Pho regulon and is induced by PhoBR (Wanner & Chang, 1987; Scanlan et al., 1993). Furthermore, the phosphomonoesterase PhoX (MED193_05784) has been described to be Pho-regulated (Monds et al., 2006; Zaheer et al., 2009). The protein GlpQ (MED193_06579) has a glycerophosphoryl diester phosphodiesterase domain, previously described in *Pseudomonas* (Lidbury et al., 2017). However, the MED193 GlpQ only shows 24% Seq.ID (e-value $1e^{-07}$) to the *P. strutzeri* DSM4166 GlpQ and no homology with the *P. fluorescens* SBW25 GlpQ. On the other side, MED193_06579 shows higher homology (39% Seq.ID, e-value $1e^{-07}$) to SCO1565, a GlpQ of *Streptomyces coelicolor*. A study has confirmed that this phosphodiesterase is PhoP-dependent (Santos-Beneit et al., 2009). The PhoPR two-component system of *Streptomyces* parallels the PhoBR system of *E. coli* (Sola-Landa et al., 2003), thereby confirming the Pho-dependency of MED193_06579. The *sn*-G3P ABC transporter Ugp, including the substrate-binding protein UgpB (MED193_07903), has been demonstrated to be Pho-regulated in *E. coli* K-12 and *Pseudovibrio* sp. strain FO-BEG1 (Schweizer & Boos, 1985; Yuan et al., 2006; Romano et al., 2015), and has been confirmed by a putative Pho box sequence upstream of UgpB.

The phosphonate-binding protein MED193_10161 belongs to an ABC transporter and is part of the C-P lyase machinery. Findings of this chapter have shown that the phosphonate binding protein MED193_10161, including all other proteins of the C-P lyase complex, was not detected in

ΔphoB, clearly demonstrating a PhoB-dependency. This operon is Pho-regulated in several bacteria (Wanner & Metcalf, 1992; White & Metcalf, 2004; Dyhrman et al., 2006; Stosiek et al., 2020). Noteworthy, the expression of the C-P lyase operon is fundamental for some *Prochlorococcus* strains in the Sargasso Sea (Ilikchyan et al., 2010). Unsurprisingly, the C-P lyase complex has a broad substrate specificity (Stosiek et al., 2020). Finally, a Pot ABC transporter was identified, potentially involved in spermidine and putrescine transport. It has recently been shown that this transporter was highly upregulated in *Pseudovibrio* sp. strain FO-BEG1 under P-limiting conditions (Romano et al., 2015). Putrescine and spermidine are polyamines with various functions in bacteria, e.g., as protection of DNA against free radicals or as the backbone of some bacterial siderophores to bind iron (Wortham et al., 2007).

In addition, seven proteins potentially involved in P-metabolism were identified (Table 3.5). Interestingly, a substrate-binding protein of a G3P transporter (UgpB, MED193_11293) shares an operon with a phosphodiesterase (GdpQ, MED193_11288). Of the whole operon, UgpB was the only protein detectable in the *ΔphoB* proteome, with a reduced MS/MS count (-88%) in comparison to WT MED193. This could mean that the whole operon is Pho-regulated, and only UgpB has an additional Pho-independent transcriptional regulator. Unfortunately, it doesn't have a high Seq.ID with any previously described UgpB proteins. Additionally, a putative polyphosphate kinase (PPK2, MED193_11927) was identified in WT MED193 but not in the *ΔphoB* proteome. Polyphosphate kinases are essential for P-storage (Achbergerová & Nahálka, 2011). They can synthesise long and linear polyphosphate chains from ATP, thereby conserving high amounts of energy in P-P bonds, releasable through hydrolysis (Ahn & Kornberg, 1990). The MED193 PPK2 is a homolog of two previously described PPK2s of *S. meliloti* Atu0418 (SMa0172, 73% Seq.ID, e-value $3e^{-167}$) and *P. aeruginosa* (PA2428, 65% Seq.ID, $1e^{-139}$) of the same study (Nocek et al., 2008). Both PPK2s could add P to nucleoside monophosphates and diphosphates. However, the reversible reaction was not detected. Likewise, Yuan et al. (2006) predicted Pho boxes in several bacteria and discovered a Pho box near PA2428. This discovery leads to

the conclusion that the MED193 PPK2 is Pho-regulated too. The substrate-binding protein of a glycerol transporter, namely GlpV (MED193_09570), was not significantly upregulated in the proteomes of MED193. However, the MS/MS count was halved in *ΔphoB* (MED193: 458, *ΔphoB*: 217). Unfortunately, not much is known about this protein. The transporter belongs to the **C**arbohydrate **U**ptake **T**ransporter-1 (CUT1) family. It has been demonstrated in *Rhizobium leguminosarum* VF39SM that this transporter is involved in the transport of glycerol and G3P (Ding et al., 2012). Furthermore, the MED193 and VF39SM GlpVs are homologs (Seq.ID 61%, e-value 0.0). To get a better insight into MED193_09570, collaborators in China overexpressed this protein and tested its binding affinity towards glycerol, G1P, and G3P. However, the protein didn't bind any of the substrates. In addition, Chapter 5 will focus on the substrate-binding protein MED193_19449. This protein shows no Pho-dependency. Finally, two dehydrogenases, namely GapD (MED193_10071) and GlpD (MED193_19624), clearly showed Pho-independency. GapA is potentially involved in the glycolytic pathway and further in carbohydrate degradation (Soukri et al., 1989). The MED193 GlpD is a homolog of a previously described G3P dehydrogenase of *E. coli* (Seq.ID 45%, e-value $2e^{-143}$). This protein is involved in the aerobic synthesis of glycerone from G3P, a step in the glycerol degradation pathway (Yeh et al., 2008).

Results of this chapter demonstrate that MED193 possesses a comprehensive P-stress response. Many of the detected proteins discussed in this chapter have been described in the literature. In the future, more work is still required to decipher the entire Pho regulon of MED193. This work will include the biochemical analysis of candidate proteins mentioned in this section. Studying the biochemistry of substrate-binding proteins and hydrolases, including substrate specificity, will help to understand how bacteria like MED193 adapted to their nutrient-depleted environment. In addition, a genetic complementation of the *phoB* gene in MED193 is required to confirm that changes observed in the lipidome and proteome, as described in this chapter, are the result of the deletion of the *phoB* gene.

CHAPTER 4 IDENTIFICATION OF ORGANIC PHOSPHATE TRANSPORTERS IN *PHAEOBACTER* SP. MED193

4.1 Introduction

Open ocean surface waters are well known for being scarce in nutrients (Cavender-Bares et al., 2001; Karl et al., 2001; Ammerman et al., 2003; Paytan & McLaughlin, 2007). One of these nutrients essential for growth is P (Paytan & McLaughlin, 2007; Karl, 2014; Koolman & Röhm, 2019). Bacteria that had to adapt to these conditions developed strategies to increase their P-uptake (e.g. see Casey et al., 2016). They can either express transport proteins that have a high-affinity for P_i (Scanlan et al., 1993; Hirani et al., 2001; Pitt et al., 2010; Cox & Saito, 2013) or use organic P-sources as an alternative supply (Tetu et al., 2009; Cox & Saito, 2013; Lin et al., 2018).

These strategies include the degradation of internal P-resources. Apart from nucleic acids, membrane phospholipids are a rich organic P-source, containing up to 20% of the P content in heterotrophic bacteria and about 10% of the P content in some phytoplankton (Van Mooy et al., 2008). Many marine bacteria have recently been described to recycle phospholipids internally as an adaptation to P-limitation. For instance, photoautotrophic bacteria synthesize a sulphur and sugar-containing lipid (SQDG) in response to reduced P-concentrations (Van Mooy et al., 2006, 2009; Peng et al., 2019; Peng & Miao, 2020).

In addition, the *Alphaproteobacterium Phaeobacter* sp. MED193 (MED193) possesses a PlcP that shows 57% similarity to the recently discovered PlcP of *S. meliloti* (Zavaleta-Pastor et al., 2010; Sebastián et al., 2016). The MED193 PlcP was shown to be responsible for the remodelling of phospholipids, replacing them with the betaine lipid DGTS. It has been shown that the phospholipid content of membranes in MED193 decreased by half under P_i-stress, whereas the amount of non-P lipids, e.g., betaine lipids, glycolipids and putative aminolipids, increased (Sebastián et al., 2016). Also, P-starvation experiments showed that PlcP is regulated by P-availability. The ability to remodel phospholipids as a response to P-limitation shows that MED193, which was isolated from the

nutrient-depleted Mediterranean Sea (Brinkhoff et al., 2008; Lazzari et al., 2016), is well adapted to these conditions, making it a model organism for further studies regarding P-limitation.

It has been shown that phospholipids are an important source of P during P-limitation. As these lipids represent a major component of membrane lipids, which are released after cell death, it is assumed that phospholipids contribute considerably to the global marine P-pool. Still, little is known about the concentration of phospholipids in open ocean waters and their degradation pathways (Suzumura, 2005; Gašparović et al., 2018).

In this study, we use the marine heterotrophic bacterium *Phaeobacter* sp. MED193 as a model organism to investigate the ability to utilize phospholipid headgroups as the sole source of P. Using a proteomic approach, we identified key enzymes that are involved in the transport and degradation of the phospholipid headgroups phosphoryl-ethanolamine (PE), phosphocholine (PC) and glycerol-phosphate (PG). An extracellular PhoX-type phosphatase was identified that is involved in the extracellular cleavage of PE and PC, thereby making the substituents ethanolamine and choline available for import. Collaborators in China helped to confirm the substrate-binding protein of ethanolamine in MED193 through protein overexpression and substrate-binding assays.

4.2 Results

4.2.1 *Phaeobacter* sp. MED193 uses phospholipid headgroups as a source of P

P-starved MED193 cells were fed with three different phospholipid headgroups to determine if phospholipid headgroups can be used as a source of P. Cell cultures of MED193 were grown under P-limiting conditions before P was added back in the form of PC, PE, and PG, as described in the experimental setup (see sections 2.1.2 and 2.1.3). Growth was monitored by measuring the OD_{540} over time. Growth experiments showed that MED193 was able to grow on all alternative P-sources (Figure 4.1 and Figure 4.2A). However, irrespective of whether cultures were grown in flasks or microplates, cultures supplemented with each

phospholipid headgroup didn't reach the same final cell yield as those grown on inorganic P. To some extent, this might be due to the requirement of an adaptation period for MED193 to grow on these organic P-compounds, including the activation of alternative P-transport systems and degradation pathways though this is more likely to cause a growth lag rather than a growth yield difference.

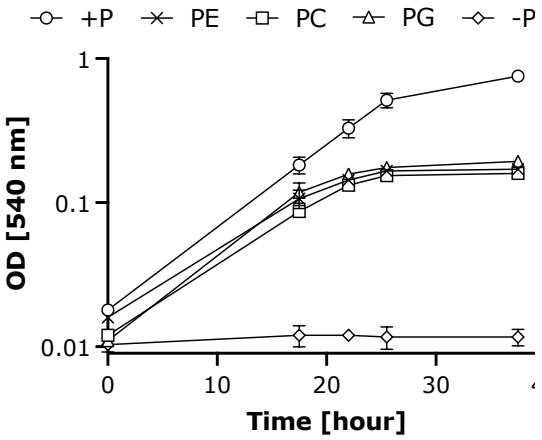

Figure 4.1: ***Growth of pre-starved MED193 cultures in different P-conditions, flask experiment.*** *ASW was supplemented with P_i (+P, O), phosphoryl-ethanolamine (PE, x), phosphocholine (PC, □), glycerol-phosphate (PG, Δ), and no P (◇). Graph shows mean ± standard deviation of three biological replicates.*

Cultures that had reached the stationary phase, following growth on each headgroup, were sequentially transferred into fresh medium containing the same headgroup. These cultures were grown again and monitored by measuring the OD_{540} (Figure 4.2B and C). This experiment was performed to assess whether MED193 requires time to adapt to each phospholipid headgroup as the sole P source and whether, for example, specific transporters need inducing to optimize growth on each headgroup. This 'resubbing' experiment showed that the lag phase either fluctuated (P_i, PC), steadily decreased (PG) or stayed constant (PE).

In the initial (IG) and first sequential growth experiment (FT), the growth rate was highest in +P (P_i) cultures (IG: +28% - +111%, FT: +37% - +72%, Table 4.1). However, growth rates of cultures supplemented with P_i (+P), PE, and PG were the same after the second sequential transfer (ST) (PC ~ -30%). Additionally, the final yield remained constant in the +P culture and was on average more than 60% higher than the final yield of the other conditions (+83% PE, +116% PC, +62% PG). An interesting pattern was found within cultures with added P_i (+P) and PC. Here, a shortened lag phase resulted in a higher growth rate (FT), whereas an elongated lag phase led to a reduced growth rate (ST).

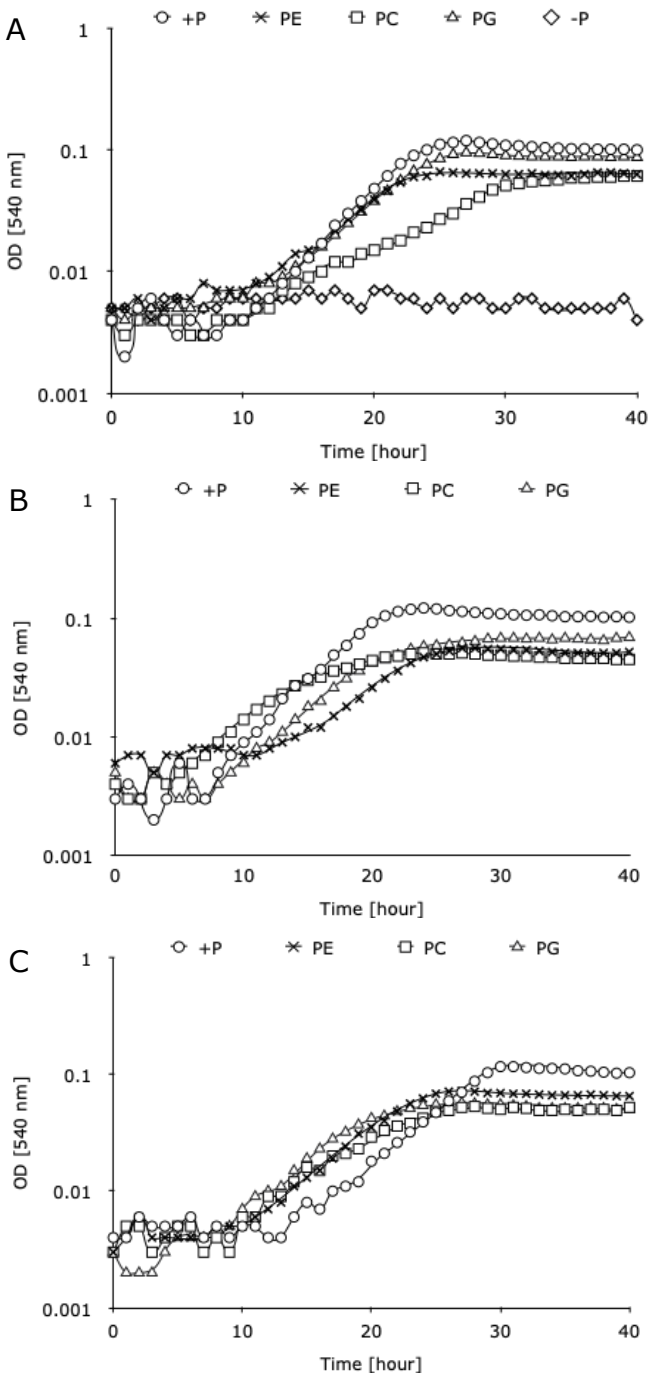

Figure 4.2: ***Adaptation of MED193 cultures to different organic P sources.***
(A) Initial growth of pre-starved MED193 cultures in different P conditions, (B) first sequential transfer of MED193 cultures, (C) second sequential transfer of MED193 cultures. ASW was supplemented with P_i (+P, O), PE (x), PC (□), PG (Δ) and no P (◇). Data points represent the mean value of 54 samples taken within one hour: OD_{540} measurements every 10 minutes, three biological replicates with three technical replicates each. Standard deviation was calculated but is not shown due to complexity.

In PG cultures instead, the lag phase and final yield decreased throughout the experiment while the growth rate stayed constant. Although the lag phase of cultures supplied with PE didn't change, a lower final yield followed a slower growth rate (FT), and a higher final yield was gained with a faster growth rate (ST).

Table 4.1: ***Growth kinetics of pre-starved MED193 cultures grown in different P conditions.***
Comparison between initial (IG) and two sequential growth experiments (FT, ST) of MED193 cultures supplemented with P_i (+P), PE, PC, and PG after P-starvation. Lag phase [hour], growth rate [$hour^{-1}$], final yield [OD_{540}]. Red arrow: decrease, green arrow: increase, yellow cross: difference to the prior growth experiment is < 5%. Asterix indicates significant difference to the prior experiment (t-tests, p-value < 0.05).

Culture (IG = initial growth, FT = first transfer, ST = second transfer)	*Lag phase [hour]*	*Growth rate [$hour^{-1}$]*	*Final yield [OD_{540}]*
+P (IG)	8	0.255	0.119
+P (FT)	↓ 6	↑ 0.268	✕ 0.122
+P (ST)	* ↑ 13	* ↓ 0.198	✕ 0.116
PE (IG)	11	0.171	0.066
PE (FT)	✕ 11	↓ 0.156	↓ 0.056
PE (ST)	✕ 11	↑ 0.192	↑ 0.072
PC (IG)	10	0.121	0.061
PC (FT)	* ↓ 4	* ↑ 0.192	↓ 0.051
PC (ST)	↑ 9	* ↓ 0.137	✕ 0.053
PG (IG)	10	0.199	0.095
PG (FT)	↓ 7	✕ 0.196	* ↓ 0.068
PG (ST)	↓ 4	✕ 0.201	* ↓ 0.057

4.2.2 Membrane lipid composition of *Phaeobacter* sp. MED193 under different growth conditions

It has previously been shown that MED193 recycles membrane phospholipids, which are then replaced with DGTS (Sebastián et al., 2016). To assess whether lipid modifications took place following growth on each headgroup, culture samples were taken after 17.5, 22, 26.5 and 37.5 hours of growth. Bacterial membrane lipids were extracted from collected samples and analysed by LC-MS (see section 2.5). It has previously been shown that proteins involved in cell growth, cell division, and protein biosynthesis dominate the proteome of marine bacteria during exponential growth. However, there is a clear shift towards proteins involved in scavenging nutrients when entering the stationary growth phase

(Muthusamy et al., 2017). Therefore, samples taken after 17.5 hours were primarily focused on, since these represent the earliest samples taken during exponential growth phase. However, it is to be noted that these samples don't represent the mid-exponential phase but rather the late exponential phase.

The appearance of DGTS and the reduction of phospholipids would be an indication of P-starvation. The subsequent transfer of the P-deplete culture to each phospholipid headgroup would assess if changes in the membrane lipid composition, as mentioned above, were reversed. While the P-deplete culture was incubated in P-free media for 48 hours, the P-replete culture was supplemented with 344 µM P and grown for 24 hours. The high concentration of P used here was to ensure the culture would not get P-limited, since previous experiments have revealed that MED193 becomes P-limited after 24 hours of growth with 172.3 µM P_i (data not shown). A mixture of phospholipids and non-P lipids was discovered in the lipidome of all conditions (Figure 4.3). Phospholipids detected were PtdEtn and PtdGro.

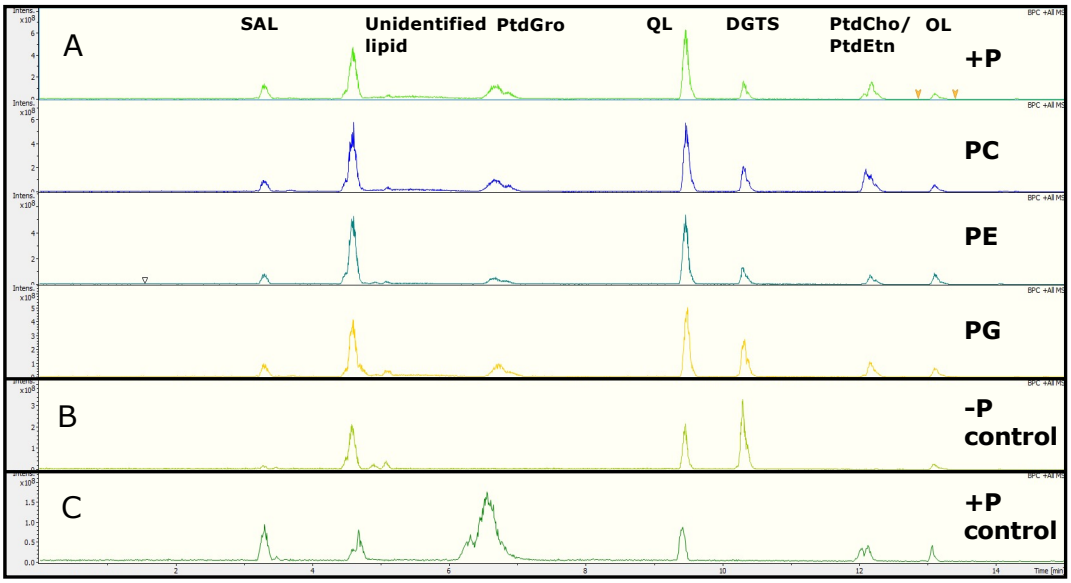

Figure 4.3: ***Lipid composition of Phaeobacter sp. MED193 cultures grown in ASW with different P supplements.***
Supplementation with a final concentration of 172.3 µM P as follows: K_2HPO_4 for +P, phosphocholine for PC, phosphoryl-ethanolamine for PE, glycerol-phosphate for PG (A). The -P culture (B) was pre-starved, whereas the +P culture (C) was grown in high P (344µM) to avoid P limitation. Phospholipid abundance (PtdGro, PtdCho/PtdEtn) significantly decreased in P-depleted cultures while betaine lipid (DGTS) abundance increased. The figure shows representative positive chromatograms of whole lipid extracts from MED193 cultures.

The non-P lipids found in the whole-cell lipid extracts consisted of the following amino acid-containing lipids: ornithine lipid (OL), glutamine lipid (QL) and sulphur-containing amino lipid (SAL) (Smith et al., 2021). Furthermore, the P-free betaine lipid DGTS was abundant in P-starved cultures. The proportion of the phospholipids PtdEtn and PtdGro decreased following P-starvation. However, the non-P lipid DGTS became more abundant in the P-starved cultures and even became the prevalent lipid (Figure 4.3B). Additionally, PtdGro was the dominant lipid in the P-replete positive control and no DGTS could be detected (Figure 4.3C). After adding phosphate back to pre-starved cultures, either in the form of inorganic phosphate or phospholipid headgroups, the proportion of PtdGro and PtdEtn slowly increased again, whereas DGTS decreased (Figure 4.3A). The chromatogram confirms that MED193 uses P_i, acquired from phospholipid headgroups, to restore phospholipids in the membrane.

4.2.3 Phosphate stress response in *Phaeobacter* sp. MED193

Samples from the growth experiment in Figure 4.1 were subjected to a cellular and exoproteome analysis using LC-MS/MS (see section 2.4). A total of 2458 cellular and 1357 extracellular proteins were identified. To identify proteins that are induced in P-deplete MED193 cultures, samples from the P-deplete and P-replete (supplemented with 344 µM P_i to avoid P starvation) cultures were compared.

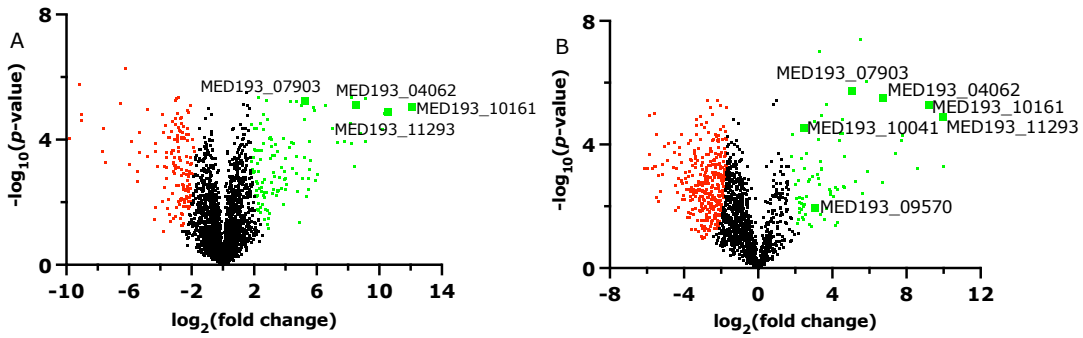

Figure 4.4: ***Volcano plots of cellular (A) and exo- (B) proteomic data comparing P-deplete and P-replete (high P) MED193 cultures.***
P-deplete MED193 cultures vs P-replete cultures grown in high P (344 µM). Scatter points represent proteins. The x-axis is the fold change for the ratio between both growth conditions and the y-axis is the statistical p-value. Green dots represent proteins that are significantly upregulated in the -P growth condition whereas red dots represent those proteins that are significantly downregulated (p-value <0.01, logFC 2). Four (A) or five (B) proteins namely MED193_04062, MED193_07903, MED193_09570, MED193_10161, and MED193_11293 are substrate-binding proteins of P transporters.

In the cellular proteome, 275 (~11%) out of 2458 identified proteins were significantly upregulated or downregulated (*p*-value <0.01, logFC of 2, Figure 4.4A, Appendix 4.1). A higher number of significantly upregulated or downregulated proteins were found in the exoproteome. Here, 419 (~31%) of the 1357 identified proteins showed a significant fold change (*p*-value <0.01, logFC 2, Figure 4.4B, Appendix 4.2). Interestingly, five proteins, significantly upregulated in the P-depleted growth condition, are annotated as substrate-binding proteins of P-transporters, namely MED193_04062, MED193_07903, MED193_09570, MED193_10161 and MED193_11293.

Moreover, the comparison of P-deplete to P-replete cultures showed that proteins belonging to the Pho regulon were affected by P-limitation. The Pho regulon contains genes that encode proteins involved in the P stress response, such as high-affinity P_i transporter systems, phosphatases and regulatory proteins (Moore et al., 2005; Santos-Beneit, 2015). One of these proteins (MED193_04062) is annotated as PstS. This protein encodes a periplasmic P_i-binding protein and is a component of the high-affinity phosphate transporter Pst. This protein is highly upregulated in the cellular and exoproteome when P is limited. Here, it represents the most abundant protein in the cellular proteome and the second most abundant protein in the exoproteome (Table 4.2). In addition, two periplasmic *sn*-glycerol-3-phosphate (G3P) binding proteins (UgpB, MED193_07903 and MED193_11293), components of *sn*-G3P ABC transporters, were upregulated in the cellular and exoproteome of P-deplete cultures. The protein GlpV (MED193_09570), annotated as substrate-binding protein of a glycerol ABC transporter, was more upregulated in the exoproteome than in the cellular proteome. Intriguingly, a periplasmic phosphonate binding protein, PhnD (MED193_10161), was one of the most abundant cellular and extracellular proteins in the P-limited condition. This protein is a component of a phosphonate ABC transport system (Table 4.2).

To gain a better insight into the expression of these substrate-binding proteins in different growth conditions, a heatmap was created based on the logFC 2 of the substrate-binding proteins and their genomic environment.

Table 4.2: ***Identified substrate-binding proteins in the P-deplete compared to the P-replete condition.***
*These proteins were significantly upregulated in the P-deplete condition (p-value <0.01, logFC 2) and are components of P transporters. The Table shows the fold change (logFC 2) and relative abundance of the proteins in the MED193 cellular and exoproteome, as well as the accession numbers and locus tags. Significant fold changes of proteins are marked with ** for p-value <0.01 or * for p-value <0.05.*

Identified substrate-binding proteins		*Accession number*	*Locus tag*	*Fold change cellular*	*Relative abundance P-deplete cultures*	*Relative abundance P-replete cultures*	*Fold change extracellular*	*Relative abundance P-deplete cultures*	*Relative abundance P-replete cultures*
Phosphonate ABC transporter	*PhnD*	EAQ43272	MED193_10161	** 12.07	3.39%	0.07%	** 9.21	6.27%	0.01%
G3P ABC-type transporter	*UgpB*	EAQ44571	MED193_11293	** 10.58	0.47%	0.03%	** 9.97	1.09%	0.001%
Phosphate ABC transporter	*PstS*	EAQ44764	MED193_04062	** 8.52	5.96%	0.30%	** 6.73	6.00%	0.06%
SN-G3P ABC transporter	*UgpB*	EAQ45560	MED193_07903	** 5.23	0.95%	0.06%	** 5.06	2.79%	0.08%
Glycerol ABC transporter	*GlpV*	EAQ44278	MED193_09570	1.25	0.06%	0.01%	** 3.06	0.80%	0.01%

It shows the comparison between pre-starved -P cultures supplemented with P_i and the P-deplete, P-replete, and the pre-starved P-deplete cultures supplemented with PE, PC and PG (Figure 4.5). The heatmap clearly shows that all substrate-binding proteins (highlighted in bold) were more upregulated in the P-deplete culture condition, except GlpV. Unsurprisingly, the top seven proteins in the heatmap were all highly upregulated in the P-deplete condition but only barely or not detected in the other conditions. These seven proteins are encoded by genes that belong to the Pho regulon, and the expression of these proteins is commonly used as a P stress indicator (Santos-Beneit, 2015).

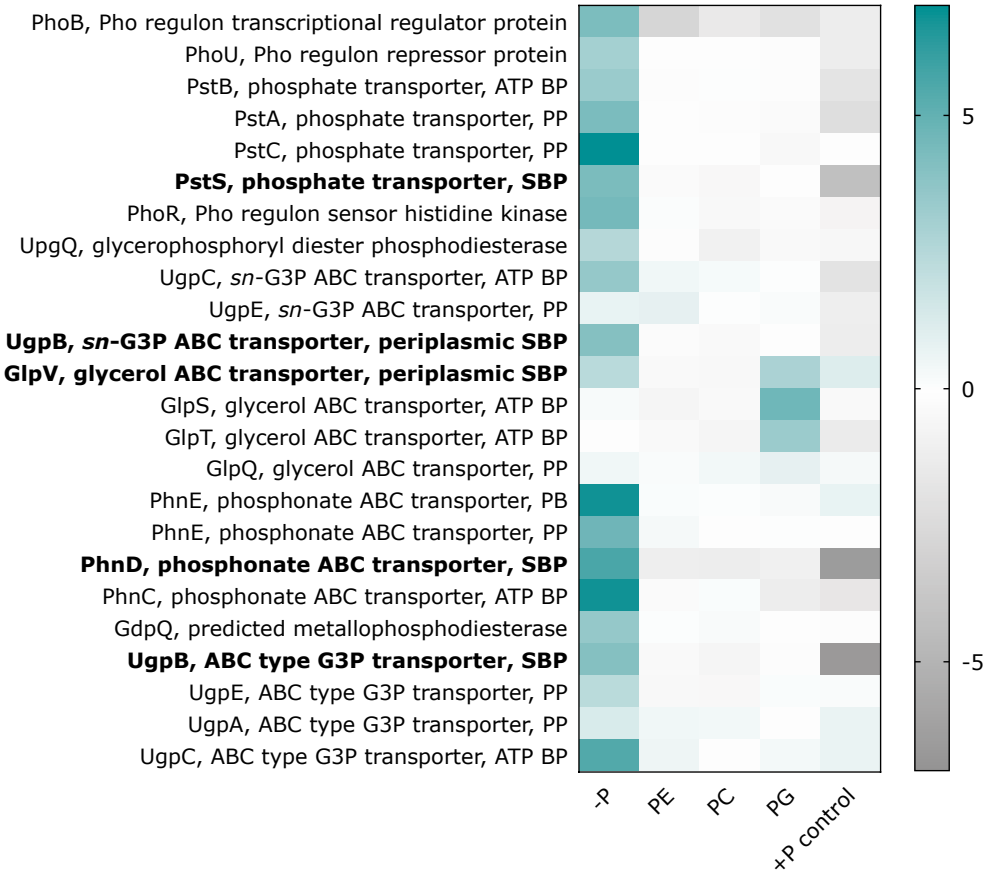

Figure 4.5: ***LogFC 2 based heatmap on transporters that were upregulated in different growth conditions of Phaeobacter sp. MED193 cultures.***
The heatmap shows logFC 2 based comparison between pre-starved -P cultures that were supplemented with P_i and P-deplete cultures, P-replete cultures (HP control), and pre-starved -P cultures supplemented with phosphoryl-ethanolamine (PE), phosphocholine (PC), and glycerol-phosphate (PG). Proteins were significantly upregulated in P-deplete cultures compared to P-replete cultures (HP control) (p-value <0.01, minimal log2 fold change (logFC) of 2). The logFC 2 extends from -7 (dark grey) over 0 (white) to 7 (green).

Three proteins annotated as components of a glycerol ABC transporter were highly upregulated in the pre-starved -P culture

supplemented with PG. These three proteins are annotated as a substrate-binding protein (GlpV) and two ATP binding proteins (GlpS and GlpT). The permease protein GlpQ, however, shows only a minor upregulation like the P-deplete and P-replete cultures. Furthermore, in the P-deplete condition, only the substrate-binding protein GlpV was upregulated. Proteins of the Ugp transport system were highly upregulated in the -P cultures as compared to the pre-starved -P culture supplemented with P_i. However, no upregulation, or only a minor upregulation, was found in the pre-starved -P cultures supplemented with the phospholipid headgroups.

Another ABC transporter system, potentially involved in the uptake of phosphonates (gene name *Phn*), was highly upregulated in the P-deplete culture. There was no detection, or only minor detection, of this protein in the other conditions. The substrate-binding protein PhnD was slightly downregulated in cultures that were supplemented with phospholipid headgroups and even more downregulated in the P-replete culture condition. Another potential ABC type *sn*-G3P transporter was highly upregulated in P-deplete cultures. This transporter didn't show a significant change in detection level in pre-starved cultures supplemented with any of the phospholipid headgroups. Additionally, this substrate-binding protein (UpgB) was drastically downregulated in the P-replete condition. The data shown above shows that MED193 has a clear response to phosphate stress, including the induction of several transporters. However, these transporters showed no indication that they were involved in the transport of phospholipid headgroups (except the Glp transporter). The potential transport pathways and degradation of phospholipid headgroups will be presented in the following sections.

4.2.4 Discovery of a phosphoryl-ethanolamine degradation pathway in *Phaeobacter* sp. MED193

Growth experiments confirmed that MED193 can grow with PE as a sole source of P (Figure 4.1). The lag phase of cultures grown on PE didn't differ much from the +P control. However, cultures supplemented with PE didn't reach the same final yield when entering the stationary phase (Table 4.1). Growing pre-starved MED193 cultures on PE restored membrane phospholipids, indicated by a decreasing DGTS/PtdGro ratio (Figure 4.3A,

B). A proteomic approach was used to identify key enzymes that are involved in the catabolism of PE. Cellular and exoproteomes of PE cultures were compared to pre-starved cultures that were supplemented with P_i. Only 15 (or 47 with *p*-value 0.05) out of 2458 identified proteins in the cellular proteome were significantly up- or downregulated (*p*-value 0.01, logFC 2, Figure 4.6A, Appendix 4.3).

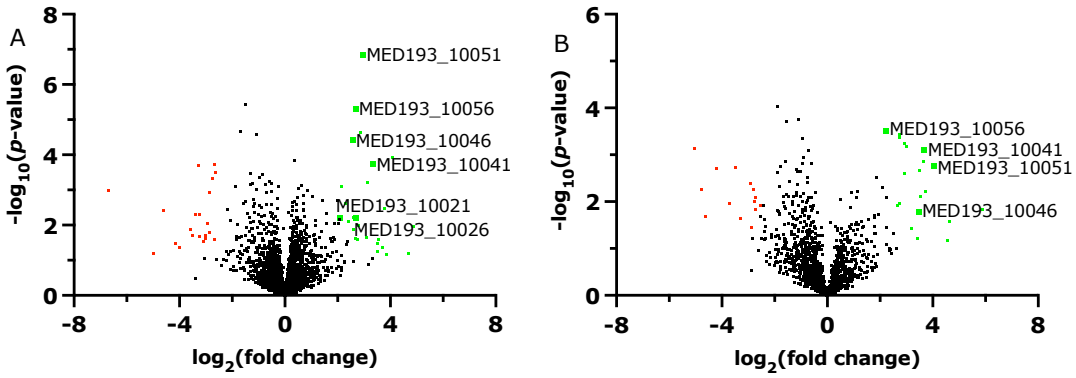

Figure 4.6: ***Volcano plots of cellular (A) and exo- (B) proteomic data comparing PE to +P MED193 cultures.***
Pre-starved MED193 cultures that were supplemented with P_i vs cultures supplemented with phosphoryl-ethanolamine (PE). Scatter points represent proteins. The x-axis is the fold change for the ratio between both growth conditions and the y-axis is the statistical p-value. Green dots represent proteins that are significantly upregulated in the PE growth condition whereas red dots represent those proteins that are significantly downregulated (p-value <0.05, logFC 2). Six proteins namely MED193_10021, MED193_10026, MED193_10041, MED193_10046, MED193_10051, and MED193_10056 are involved in the catabolism of ethanolamine.

Furthermore, 15 (or 34 with *p*-value 0.05) out of 1357 identified proteins were significantly up- or downregulated in the exoproteome (*p*-value 0.01, logFC 2, Figure 4.6B, Appendix 4.4). Six proteins were identified which were significantly upregulated in both cellular and exoproteome, namely MED193_10021, MED193_10026, MED193_10041, MED193_10046, MED193_10051 and MED193_10056 (Figure 4.6).

Interestingly, the protein encoded by MED193_10041 shows 83% amino acid sequence identity to a substrate-binding protein (Csal_0678) from *Chromohalobacter salexigens*, previously described as an ethanolamine binding protein (Vetting et al., 2015). To test the hypothesis that MED193_10041 is a periplasmic ethanolamine binding protein, collaborators in China overexpressed this protein and used MicroScale Thermophoresis (MST) to show the binding affinity of MED193_10041 to ethanolamine (see section 2.3.4). For this purpose, the purified protein

was first labelled in assay buffer, mixed with serially diluted concentrations of ethanolamine, and the binding affinity measured. Results were analysed and plotted (Figure 4.7). MST analysis showed a binding affinity (K_d) of 7.88 ± 1.88 µM ethanolamine for MED193_10041.

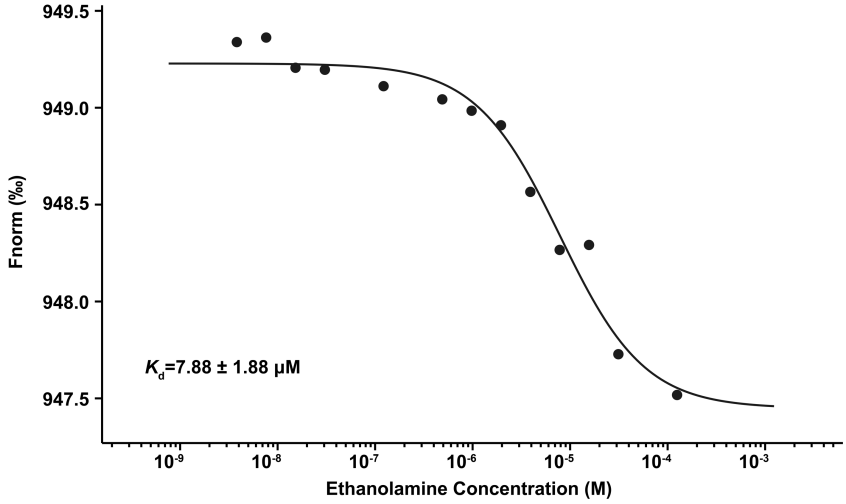

Figure 4.7: ***MicroScale Thermophoresis analysis defining binding affinity of MED193_10041 to ethanolamine.***
Purified protein was mixed with serially diluted concentrations of ethanolamine, and binding affinity was measured. The x-axis represents the logarithmic concentration of serially diluted ethanolamine (M); the y-axis represents the normalised fluorescence (Fnorm). Binding affinity was calculated with K_d of 7.88 ± 1.88 µM. n=3.

It has previously been shown that *C. salexigens* doesn't possess the canonical ethanolamine utilisation pathway (EUT) (Vetting et al., 2015), and this has been best studied and described in *Salmonella typhimurium* strain LT2 (Kofoid et al., 1999). The genomic environment of MED193_10041, comprised of seven neighbouring genes, was compared to *C. salexigens* and *S. typhimurium* LT2 (Table 4.3). Intriguingly, two genes namely MED193_10051 and MED193_10056 are predicted to encode an aldehyde dehydrogenase (24% Seq.ID) and an alcohol dehydrogenase (32% Seq.ID) respectively, that are part of the EUT operon in *S. typhimurium* LT2. However, all seven genes of MED193 have close homologs in *C. salexigens* (Table 4.3). Furthermore, the genomic environment of *C. salexigens* is identical to MED193 (Figure 4.8). Two of these genes, namely MED193_10031 and MED193_10036, are annotated as TRAP transporter permease components, DctQ and DctM, respectively. However, neither protein is present in the MED193 cellular or exoproteome data.

Table 4.3: ***Proteins of Phaeobacter sp. MED193 that are upregulated in cultures grown in ASW supplemented with phosphoryl-ethanolamine.*** *The Table shows the logFC and relative abundance of the proteins in MED193 (C: cellular, E: exoproteome), as well as the protein identity with homologs in C. salexigens and S. typhimurium LT2, including e-value and bit score.*

Identified proteins		*Accession number*	*Locus tag MED193*	*Fold change*	*Relative abundance*	*Locus tag*	*E-value*	*Identity*	*Bit score*
RpiR regulator		EAQ43244	MED193_10021	2.09	0.004	Csal_0674*	9.2E-161	72%	446
N-formylglutamate amidohydrolase		EAQ43245	MED193_10026	2.71	0.009	Csal_0675*	1E-105	62%	304
TRAP transporter, small permease component	*DctQ*	EAQ43246	MED193_10031	-	-	Csal_0676*	9.7E-105	71%	296
TRAP transporter, large permeate component	*DctM*	EAQ43247	MED193_10036	-	-	Csal_0677*	2.8E-127	86%	375
TRAP transporter, ethanolamine binding protein	*DctP*	EAQ43248	MED193_10041	C: 3.35 E: 3.68	C: 0.124 E: 0.211	Csal_0678*	0	83%	599
L-glutamine synthetase		EAQ43249	MED193_10046	C: 2.56 E: 3.46	C: 0.058 E: 0.031	Csal_0679*	0	75%	738
Aldehyde dehydrogenase	*EutE*	EAQ43250	MED193_10051	C: 2.97 E: 4.05	C: 0.166 E: 0.097	Csal_0680*	0	79%	717
Alcohol dehydrogenase	*EutG*	EAQ43251	MED193_10056	C: 2.68 E:2.23	C: 0.152 E: 0.129	Csal_0681*	0	79%	634
Aldehyde oxidoreductase	*EutE*	EAQ43250	MED193_10051	C: 2.97 E: 4.05	C: 0.166 E: 0.097	AAC78118**	8E-09	24%	54
Alcohol dehydrogenase	*EutG*	EAQ43251	MED193_10056	C: 2.68 E:2.23	C: 0.152 E: 0.129	AAC78120**	4E-40	32%	143

* *Chromohalobacter salexigens* (Vetting et al., 2015)

** *Salmonella typhimurium* strain LT2 (Kofoid et al., 1999)

Figure 4.8: ***Genomic environment of the ethanolamine catabolism genes in Phaeobacter sp. MED193.***
RpiR: RpiR regulator (MED193_10021, Csal_0674); FGase: N-formylglutamate amidohydrolase (MED193_10026, Csal_0675), DctQ: TRAP transporter, small permease component (MED193_10031, Csal_0676); DctM: TRAP transporter, large permease component (MED193_10036, Csal_0677); DctP: TRAP transporter, ethanolamine binding protein (MED193_10041, Csal_0678); GS: L-glutamine synthetase (MED193_10046, Csal_0679); ALDH: Aldehyde dehydrogenase (MED193_10051, Csal_0680); ADH: Alcohol dehydrogenase (MED193_10056, Csal_0681). Figure is adapted from Vetting et al., 2015.

C. salexigens deletion mutants in the substrate-binding protein (Csal_0676) of the TRAP transporter or the L-glutamine synthetase (Csal_0679) are unable to grow on ethanolamine as a sole source of nitrogen (Vetting et al., 2015). Using this finding, Vetting et al. (2015) predicted an ethanolamine utilisation pathway in *C. salexigens* and re-annotated the enzymes according to their function. The MED193 data showed that the putative proteins L-glutamine synthetase (MED193_10046), alcohol dehydrogenase (MED193_10056), aldehyde dehydrogenase (MED193_10056) and N-formylglutamate amidohydrolase (MED193_10026) were upregulated in both cellular and exoproteomes of cultures grown in ASW supplemented with PE. These four proteins are predicted to catalyse the degradation of ethanolamine to glycine (Figure 4.9). The ethanolamine utilisation pathway includes a TRAP transporter (MED193_10031, MED193_10036, MED193_10041) which has not been described in MED193 before.

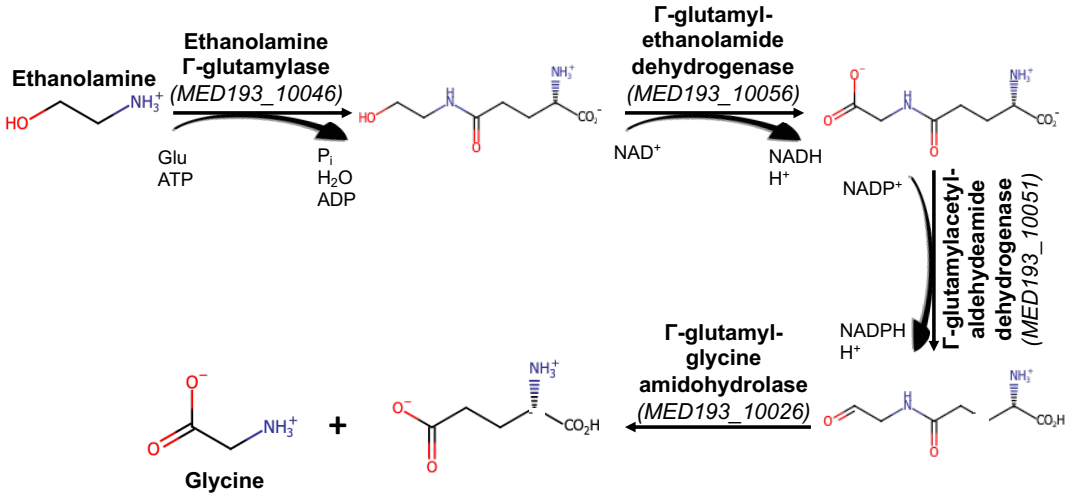

Figure 4.9: ***Predicted cytoplasmic ethanolamine degradation pathway in Phaeobacter sp. MED193.***
The enzymes have been re-annotated to match their predicted function. Locus tags represent enzymes in MED193 that are upregulated in cultures grown with phosphoryl-ethanolamine. Figure is adapted from Vetting et al., 2015.

MED193_10041 is the substrate-binding protein of a transporter that belongs to the **Tr**ipartite **A**TP-independent **P**eriplasmic **T**ransporter (TRAP-T) family. Members of this family have been described before, including substrate specificity. Phylogenetic analyses were used to show the evolutionary relationship within the TRAP-T family.

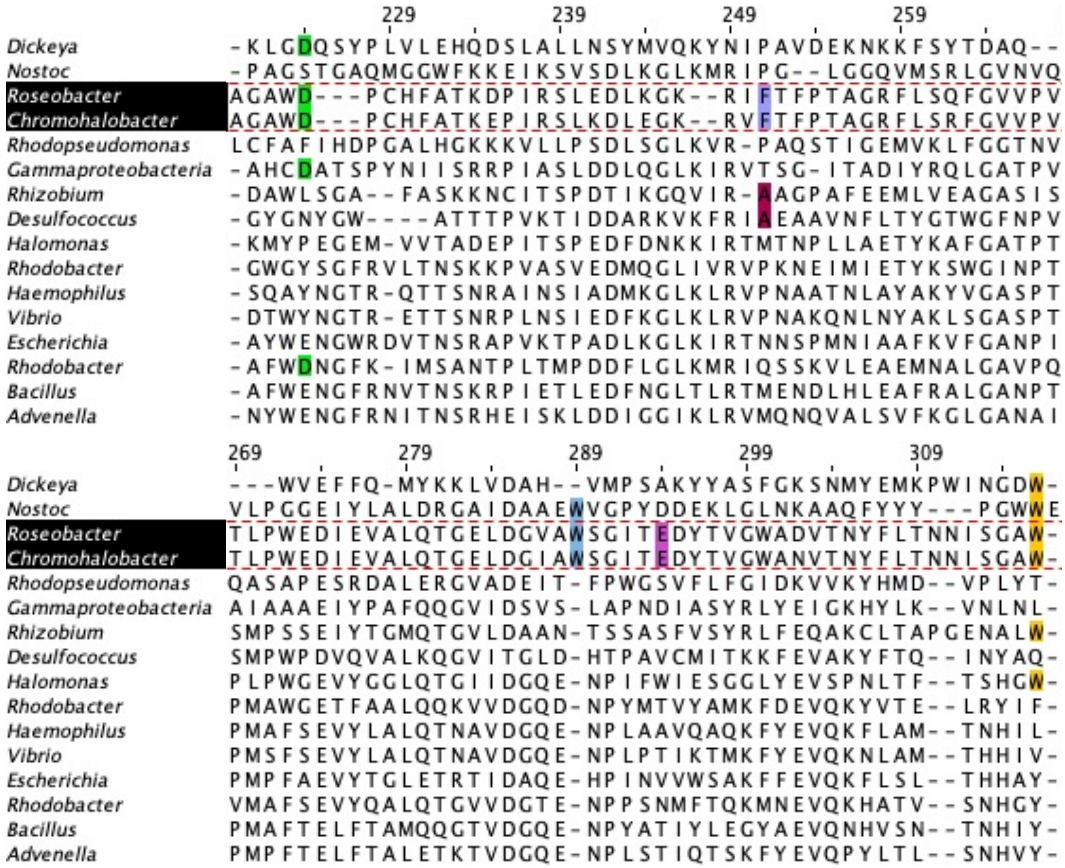

Figure 4.10: ***The ethanolamine binding protein MED193_10041 and Csal_0678 represent a new member of the Tripartite ATP-independent Periplasmic Transporter (TRAP-T) family.***
Multiple sequence alignment of the ethanolamine binding protein (BP) MED193_10041/Csal_0678 from Phaeobacter sp. MED193 and Chromohalobacter salexigens (Vetting et al., 2015), 2-oxo monocarboxylate BP from Nostoc sp. PCC7120 (Uniprot Number: Q8YSQ6, Pernil et al., 2010), lignin derived aromatic compounds BP from Rhodopseudomonas palustris ATCC BAA98 (UN: Q6N8XO, Salmon et al., 2013), dicarboxylic acids BP from a Gammaproteobacteria bacterium (UP: A0A2E5VB86, Tully et al., 2018), phenylacetate/pyruvate BP from Desulfococcus multivorans DSM 2059 (Accesion Number: AOY59254, Dörries et al., 2016), galacturonides BP from Dickeya didantii 3937 (UN: E0SDC9, Hugouvieux-Cotte-Pattat et al., 2001), sialic acid BP from Haemophilus influenzae ATCC 51907 (UN: P44542, Hopkins et al., 2013) and Vibrio cholerae serotype 01 N16961 (UN: Q9KR64, Mulligan et al., 2012), 2,3-diketo-L-gulonate (2,3-DKG) BP from Escherichia coli K12 (UN: P37676, Thomas et al., 2006), disulfide 3,3'-dithiodipropionic acid (DTDP) BP from Bacillus halodurans ATCC BAA125 (UN: Q9K9H4, Kelly & Thomas, 2001; Takami et al., 2000) and Advenella mimigardefordensis DPN7 (UN: R4JTF7, Meinert et al., 2017; Wübbeler et al., 2014), dicarboxylate BP from Rhodobacter capsulatus (UN: P37735, Forward et al., 1997), taurine BP from Rhodobacter sphaeroides ATCC 17023 (UN: Q3IVI6, Brüggemann et al., 2004; Denger et al., 2006), ectoine/hydroxyectoine BP from Halomonas elongata ATCC 33173 (UN: E1VBK1, Grammann et al., 2002), malonate BP from Sinorhizobium meliloti 1021 (UN: Q930W1, Chen et al., 2010). The ethanolamine amine group is coordinated by the carbonyl of Trp215 (blue) and the side chains of Glu220 (pink) and Asp155 (green), Tyr242 (yellow) and Glu220 coordinate the oxygen. The highly conserved TRAP SBP protein arginine (red) is only present in Rhizobium meliloti 1021 and Desulfococcus sulfovorans, however, it is replaced by phenylalanine (Phe177, purple) in MED193 and C. salexigens.

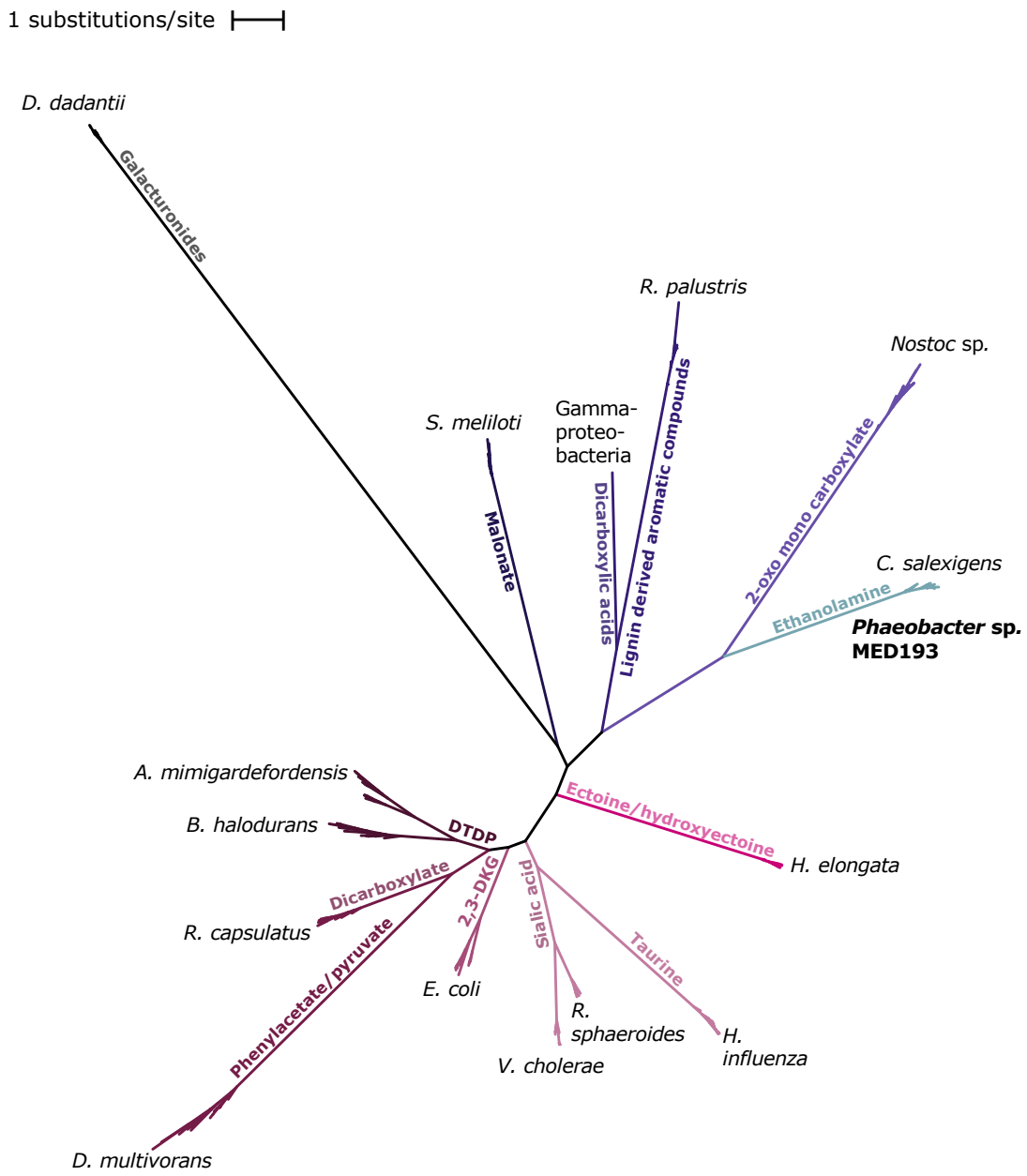

Figure 4.11 ***Phylogeny of the ethanolamine binding protein from Phaeobacter sp. MED193 within the TRAP-T family.***
The phylogenetic tree represents characterised members of the TRAP-T family including 10 of their closest homologs retrieved through BLAST. The ethanolamine binding proteins of Phaeobacter sp. MED193 and Chromohalobacter salexigens cluster together and form a new group within the TRAP-T family. The 2-oxo monocarboxylate binding protein of Nostoc sp. PCC 7120 appears to be the closest relative to the ethanolamine binding protein of MED193 and C. salexigens. Branch length represents the expected number of substitutions per site.

Therefore, multiple sequence alignment (MSA) (Edgar, 2004b, 2004a) was performed to compare sequences of TRAP-T family members and ten close homologs each (retrieved through the Transporter Classification Database (Saier et al., 2021) and BLAST) (Figure 4.10). Hereafter, the MSA was used to create a neighbour-joining tree, for more details see section 2.7 (Capella-Gutiérrez et al., 2009; Trifinopoulos et al., 2016; Letunic & Bork, 2021). This phylogenetic tree shows a clear separation between family members (Figure 4.11), supported by conserved amino acids in the active ethanolamine binding site (Vetting et al., 2015, Figure 4.10). Co-purification of Csal_0678 and ethanolamine showed that the ethanolamine amine group is coordinated by the carbonyl of Trp215 (blue) and the side chains of Glu220 (pink) and Asp155 (green). Furthermore, Tyr242 (yellow) and Glu220 coordinate the ethanolamine oxygen. The highly conserved arginine (red) of the TRAP-T substrate-binding protein is only present in *Rhizobium meliloti* 1021 and *Desulfococcus sulfovorans*. However, it is replaced by phenylalanine (Phe177, purple) in MED193 and *C. salexigens* (Figure 4.10).

Primary production in ocean surface waters is, among other factors, controlled by nitrogen availability and accessibility, especially for non-diazotrophic bacteria. However, diazotrophic bacteria can fix atmospheric nitrogen and are more prone to be limited by P or iron (Moore et al., 2008, 2013; Peter & Sommer, 2015). The newly described pathway in MED193 enables bacteria to utilise ethanolamine, a degradation product of the membrane phospholipid PtdEtn, as a source of nitrogen and/or carbon. To further investigate the abundance of the substrate-binding protein MED193_10041 in the marine environment, genomes and transcriptomes of the Ocean Gene Atlas (OGA) database (Sunagawa et al., 2015; Villar et al., 2018) were mined. Additionally, a hidden Markov model (hmm) file was created containing the sequences of MED193_10041, Csal_0678 and ten close homologs each. This hmm file was used as a query for a BLAST search to find homologs with an e-value cut-off of e^{-35} in the OM_RGCv2_metaG (metagenomics) and OM-RGCv2_metaT (metatranscriptomics) databases. The e-value was determined experimentally, ensuring that proteins within the cut-off belong to MED193_10041/Csal_0678 and not to other members of the TRAP-T

family. The protein was found to be moderately represented in the Tara oceans metagenomes (452 hits). Then, abundance was calculated as a percentage of the median abundance of ten prokaryotic single-copy marker genes/transcripts (Villar et al., 2018; Milanese et al., 2019). Boxplots represent the relationship between gene abundance (%) and sampling depths (Figure 4.12A). A combination of the Kruskal-Wallis test and the post-hoc Dunn's test (*p*-value <0.05) was used for multiple comparison. Therefore, an in-house R-script was used.

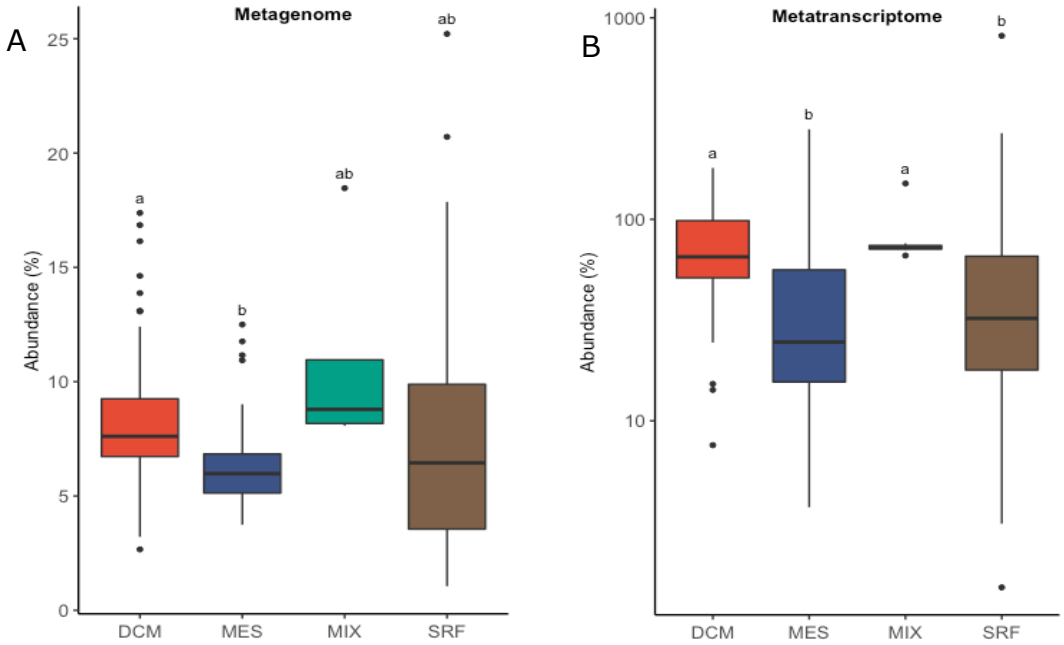

Figure 4.12: ***The abundance and distribution of the ethanolamine binding protein in the Tara oceans database – metagenomic and metatranscriptomic analysis.*** *The OGA database was searched using MED193_10041 of Phaeobacter sp. MED193 with an e-value cut-off of e^{-35}. Abundance was calculated as a percentage of the median abundance of ten prokaryotic single-copy marker genes/transcripts (Milanese et al., 2019). DCM, deep chlorophyll maximum; MES, mesopelagic zone; MIX, mixed layer; SRF, surface water.*

Additionally, the Tara Oceans metatranscriptomes database (Sunagawa et al., 2015; Villar et al., 2018) was searched and analysed using the same criteria as described above (Figure 4.12B). Metagenomics analysis revealed that on average, about 5-10% of microbial cells in the environmental dataset possess the ethanolamine binding protein (Figure 4.12A), predominantly represented by *Alphaproteobacteria* (Figure 4.13, Appendix 4.10). However, metatranscriptomics analysis showed that it is highly expressed (Figure 4.12B). Since the abundance was calculated as a percentage of the median expression of ten prokaryotic single-copy marker genes, Figure 4.12B shows that the ethanolamine binding protein is highly

active, on average around 50-100% of the marker transcripts. Eight of the marker genes are involved in ribosomal structure, biogenesis, and translation processes. The other two marker genes are part of intracellular trafficking, secretion, and vesicular transport (Milanese et al., 2019).

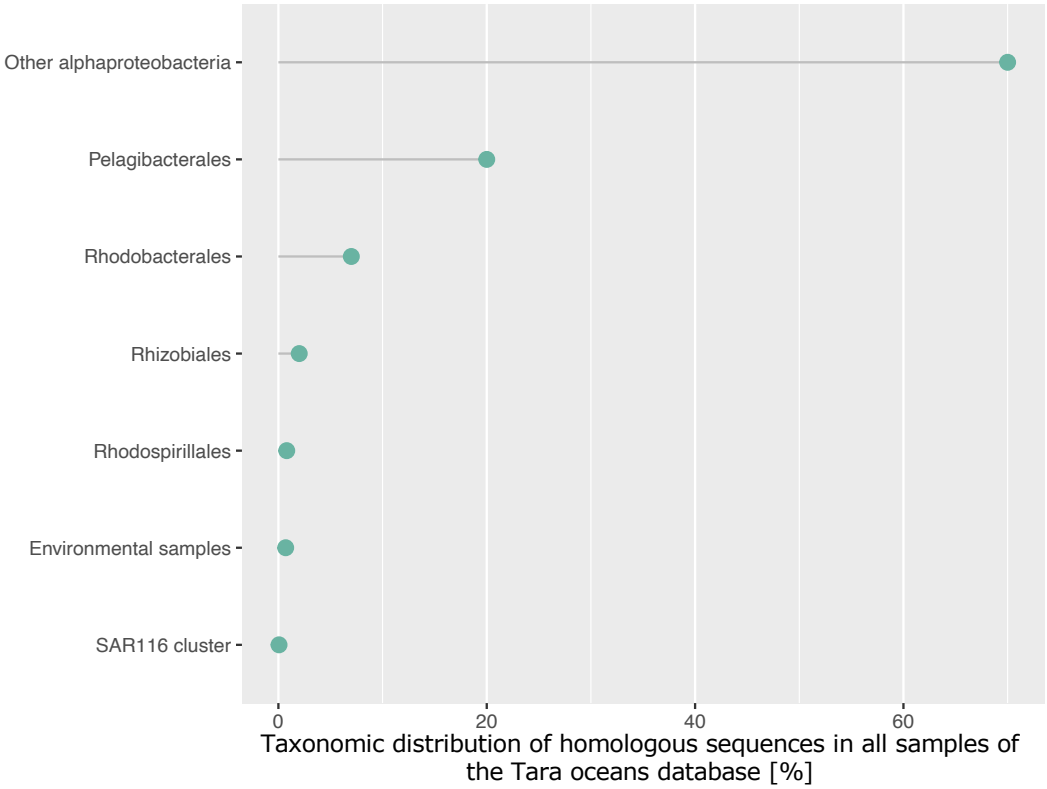

Figure 4.13: ***The distribution of the ethanolamine binding protein and homologs in the Tara oceans database.***
The weighted taxonomic distribution of homologs is modified from Krona plots (see Appendix 4.10), retrieved from the OGA interphase, according to the OGA catalogue 2. The OGA database was searched using MED193_10041 of Phaeobacter sp. MED193 with an e-value cut-off of e^{-35}. 94% of the homologs were found within the class of Alphaproteobacteria. Only 7% of the homologs accounted for members of the marine Roseobacter group (Rhodobacterales).

These single-copy marker genes are model genes that can span more than one domain and are usually protein encoding genes (Milanese et al., 2019; Lu et al., 2020). Using the same approach as before (see section 2.7), a phylogenetic tree was created to demonstrate the relationship between members of the TRAP-T family including ten of the closest homologs and environmental samples retrieved from the BLAST search of ethanolamine binding protein homologs in the Tara oceans database (Figure 4.14). Furthermore, Krona plots retrieved from the OGA interphase (Appendix 4.9) were used to identify the distribution of the protein and its homologs within the database. Interestingly, 94% of all homologs belong to members of the *Alphaproteobacteria*.

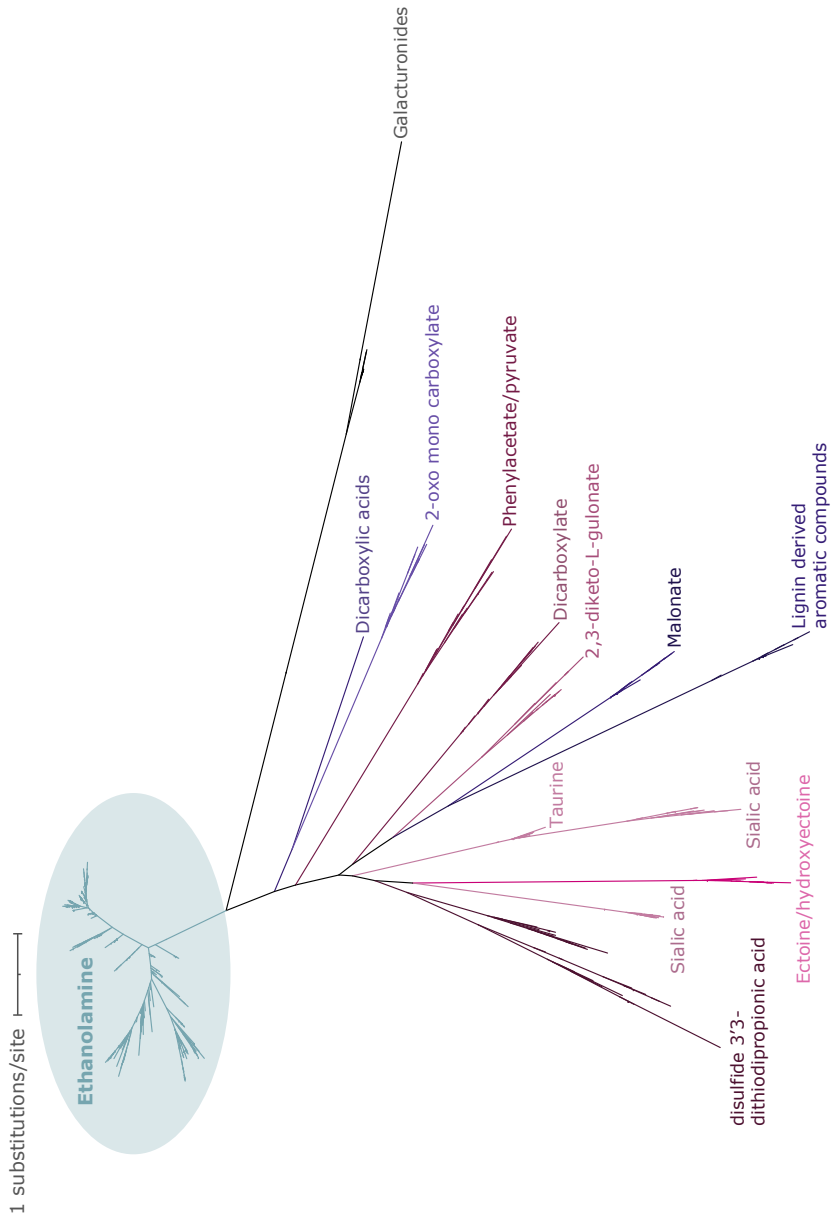

Figure 4.14: ***Phylogenetic tree of characterised TRAP-T family members and homologs of MED193_10041 and Csal_0678 retrieved from the OGA database.***
The phylogenetic tree represents characterised members of the TRAP-T family including 10 of their closest homologs obtained through BLAST. Furthermore, the OGA database was searched for homologs of the ethanolamine binding proteins MED193_10041 and Csal_0678 with an e-value cut-off of e^{-33}. The tree shows a clear clustering of ethanolamine binding proteins found in environmental samples, representing a new member of the TRAP-T family (highlighted in green). Tree branches are labelled with the substrate each protein binds to. Branch length represents the expected number of substitutions per site.

However, the marine *Roseobacter* group contributes only 7% of all homologs (Figure 4.13). The findings in this section highlight the ability of MED193 to acquire P_i from PE as a sole source of P. Enzymes that are upregulated in this condition are likely to be involved in the cellular catabolism of ethanolamine. In addition, the substrate-binding protein of a TRAP transporter (MED193_10041) was demonstrably shown to bind ethanolamine but not PE. It is still not fully understood how MED193 makes ethanolamine accessible for transport, i.e., how the P_i group is cleaved off. I hypothesize that an extracellular phosphatase, a member of the PhoX family, is involved in this process.

4.2.5 The choline/betaine degradation pathway is involved in the uptake and catabolism of phosphocholine

To determine if MED193 can utilise PC as a sole organic source of P, -P pre-starved MED193 cultures were supplemented with PC. As shown in Figure 4.1, MED193 was able to utilise PC and entered the exponential growth phase after a similar lag phase, compared to the +P culture. Interestingly, the cultures didn't reach the same final yield as the cultures that were supplemented with P_i. The cultures adapted to the organic P source, as shown in the 'resubbing' experiment (Figure 4.2B, C). The lag phase was shorter, as compared to the initial growth on PC. However, the final yield of these cultures didn't increase and stayed below the final yield of the +P culture (Table 4.1). Furthermore, the phospholipids in the membranes were restored, shown by the decreased DGTS/ PtdGro ratio in Figure 4.3A, B. As above, a proteomic approach was used to identify key enzymes that are involved in the utilisation and degradation of PC. In the cellular proteome one (or 52 with *p*-value 0.05) out of 2458 identified proteins was significantly upregulated (or downregulated (*p*-value 0.05), *p*-value 0.01, logFC 2, Figure 4.15A, Appendix 4.5).

However, only two (or four with *p*-value 0.05) out of 1357 identified proteins were significantly up- or downregulated in the exoproteome of cultures grown in ASW with PC compared to cultures that were supplemented with P_i (*p*-value 0.01, logFC, Figure 4.15B, Appendix 4.6). Comparing both proteomic datasets, five proteins were identified that were significantly upregulated only in the PC condition, namely MED193_19144,

MED193_21671, MED193_21676, MED193_ 21681 and MED193_21686 (Figure 4.15).

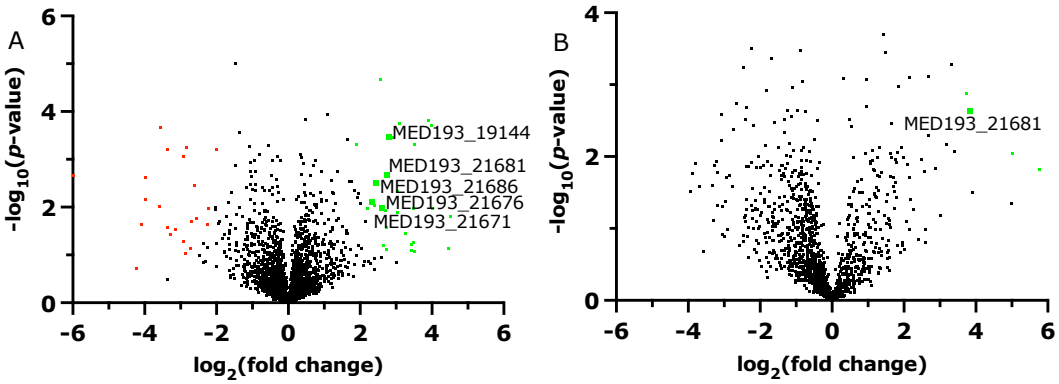

Figure 4.15: ***Volcano plots of cellular (A) and exo- (B) proteomic data comparing PC to +P MED 193 cultures.***
Pre-starved MED193 cultures that were supplemented with P_i vs cultures supplemented with phosphocholine (PC). Scatter points represent proteins. The x-axis is the fold change for the ratio between both growth conditions and the y-axis is the statistical p-value. Green dots represent proteins that are significantly upregulated in the PC growth condition whereas red dots represent those proteins that are significantly downregulated (p-value 0.05, logFC 2). Five proteins namely MED193_19144, MED193_21671, MED193_21676, MED193_21681, and MED193_21686 are involved in the degradation of choline.

One of these proteins, MED193_21681, was annotated as a betaine aldehyde dehydrogenase. Betaine is the oxidation product of choline; hence they share a similar chemical structure. Comparison was made to a *Roseobacter* group bacterium with a published choline degradation pathway. *SPO0084*, annotated as a betaine aldehyde dehydrogenase (BetB), from *Ruegeria pomeroyi* DSS-3, is a close homolog of MED193_21681 (79% Seq.ID, Table 4.4). This protein has previously been shown to be involved in choline catabolism, catalysing the oxidation of choline O-sulfate to glycine betaine (Lidbury et al., 2015). The comparison of the genomic environment of *betB* (MED193_21681) to *SPO0084* in *R. pomeroyi* DSS-3 showed that the gene neighbourhood looks similar, with four genes sharing the same annotation closely together (Figure 4.16).

A proposed choline degradation pathway in *R. pomeroyi* DSS-3 was described by Lidbury et al., 2015. Comparing the sequence identity of all proteins which were predicted to be part of the catabolic pathway in *R. pomeroyi* DSS-3 versus MED193 revealed that MED193 possesses a homolog to each *R. pomeroyi* DSS-3 gene with high sequence identity (Table 4.4).

Table 4.4: ***Phaeobacter sp. MED193 proteins that are involved in the catabolism of PC.***
*The Table shows the fold change and relative abundance of these proteins in MED193, as well as the sequence identity with homologs in R. pomeroyi, including e-value and bit score. Significant fold changes of proteins are marked with ** for p-value <0.01 or * for p-value <0.05.*

Identified proteins		*Accession number*	*Locus tag*	*Fold change cellular*	*Relative abundance in %*	*Locus tag (Ruegeria pomeroyi DSS-3)*	*E-value (Ruegeria pomeroyi DSS-3)*	*Identity (Ruegeria pomeroyi DSS-3)*	*Bit score (Ruegeria pomeroyi DSS-3)*
Choline transporter, membrane protein	*BetT*	EAQ43510	MED193_21671	* 2.60	0.0034	SPO1087	0	72%	577
Choline sulfatase	*BetC*	EAQ43511	MED193_21676	* 2.34	0.0019	SPO1083	0	85%	905
Choline dehydrogenase	*BetA*	EAQ43513	MED193_21686	* 2.45	0.0088	SPO1088	0	77%	873
Betaine aldehyde dehydrogenase	*BetB*	EAQ43512	MED193_21681	* 2.74	0.0143	SPO0084	0	79%	772
Glycine betaine:homocysteine methyltransferase	*BHMT*	EAQ46471	MED193_14787	-0.04	0.0008	SPO3398	4.7E-138	66%	389
Glycine betaine:homocysteine methyltransferase	*BHMT*	EAQ43526	MED193_02685	-0.18	0.0107	SPO1884	2.4E-100	86%	291
Dimethylglycine dehydrogenase	*DMGDH*	EAQ47340	MED193_19144	* 2.80	0.0374	SPO0635	0	93%	1624
Sarcosine dehydrogenase	*MMGDH*	EAQ46473	MED193_14797	-0.05	0.0011	SPO3396	0	82%	1400
5,10-methylene-H_4F dehydrogenase/methenyl-H_4F cyclehydrolase	*FolD*	EAQ45801	MED193_09108	0.29	0.0518	SPO1559	0	83%	499
Formyl-H_4F synthstase	*Fhs*	EAQ45802	MED193_09113	0.63	0.2654	SPO1557	0	90%	1023
Formate dehydrogenase	*Fdh*	EAQ43299	MED193_11742	0.52	0.0005	SPO1555	0	82%	921
Formate dehydrogenase	*Fdh*	EAQ43298	MED193_11737	0.33	0.0003	SPO1556	0	75%	1456

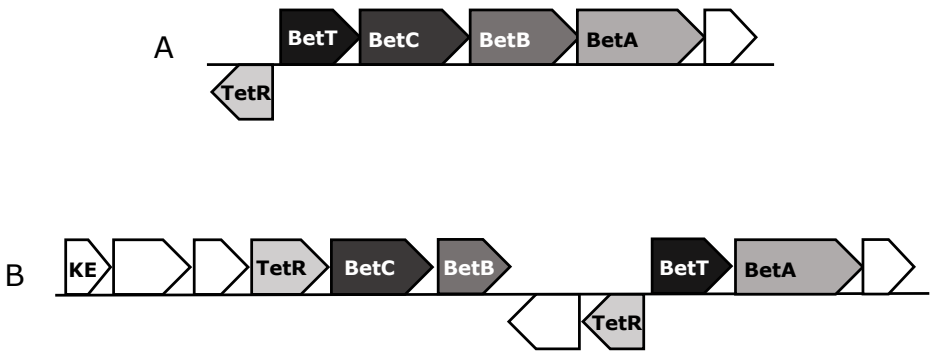

Figure 4.16: ***Genomic environment of choline catabolism genes in Phaeobacter sp. MED193 (A) and Ruegeria pomeroyi DSS-3 (B).***
TetR: transcriptional regulator (MED193_21666, SPO1082 & SPO1086); BetT: choline transporter (MED193_21671, SPO1087), BetC: choline sulfatase (MED193_21676, SPO1083); BetB: betaine aldehyde dehydrogenase (MED193_21681, SPO0084); BetA: choline dehydrogenase (MED193_21686, SPO1088); KE: putative L-lysine exporter (SPO1079).

As all proteins of the choline catabolism pathway in *R. pomeroyi* DSS-3 have homologs with high sequence identity in MED193, the pathway predicted by Lidbury et al. (2015) was used to propose a pathway for the degradation of choline in MED193 (Figure 4.17).

Five MED193 proteins shown in Table 4.4 are upregulated in the cellular proteome (highlighted in dark green, Figure 4.17). Four of these proteins, namely a membrane protein of the choline transporter (BetT, MED193_21671), a choline dehydrogenase (BetA, MED193_ 21686), a betaine aldehyde dehydrogenase (BetB, MED193_ 21681), and a choline sulfatase (BetC, MED193_21676) are predicted to be directly involved in the uptake and initial transformation of choline (Figure 4.17).

Furthermore, a dimethylglycine dehydrogenase (DMGDH, MED193_19144), which is believed to catalyse the demethylation of dimethylglycine to sarcosine is highly upregulated (Table 4.4). However, a glycine betaine: homocysteine methyltransferase (BHMT, MED193_14787 and MED193_14787) and a sarcosine dehydrogenase (MMGDH, MED193_ 14797), said to catalyse the previous and following steps to DMGDH, are downregulated in the PC growth condition. The degradation of methylene tetrahydrofolate to carbon dioxide is predicted to be initiated by three genes, a 5,10-methylene-H4F dehydrogenase/ methenyl-H4F cyclohydrolase (FolD, MED193_09108), a formyl-H4F synthetase (Fhs, MED193_09113 & MED193_11742) and a formate dehydrogenase (Fdh, MED193_11737) which are slightly upregulated in the cellular proteome.

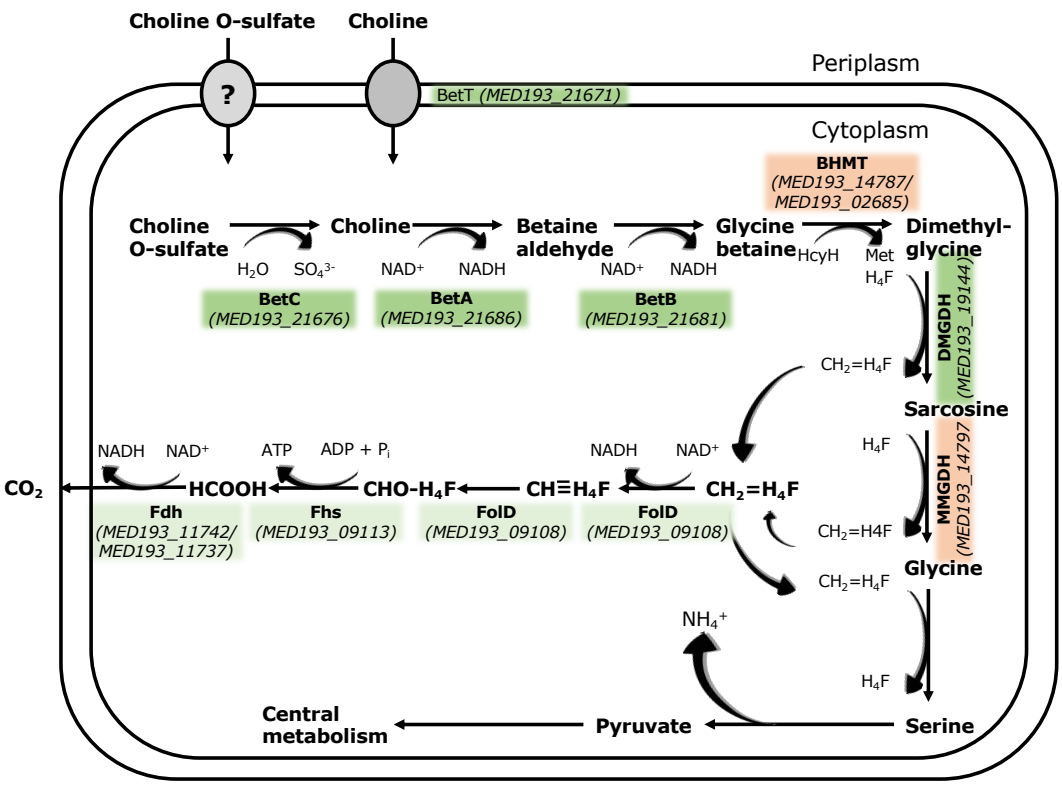

Figure 4.17: ***Predicted choline catabolism in Phaeobacter sp. MED193.*** *BetT, choline transporter; BetA, choline dehydrogenase; BetB, betaine aldehyde dehydrogenase; BetC, choline sulfatase; BHMT, glycine betaine: homocysteine methyltransferase; DMGDH, dimethylglycine dehydrogenase; MMGDH, sarcosine dehydrogenase; HcyH, homocysteine; Met, Methionine, FolD, 5,10-methylene-H_4F dehydrogenase/ methenyl-H_4F cyclohydrolase; Fhs, formyl-H_4F synthetase; Fdh, formate dehydrogenase; CH_2=H_4F, methylene tetrahydrofolate; CHO≡H_4F, 5, 10-methenyl-tetrahydrofolate; CHO-H_4F, formyl-tetrahydrofolate; HCOOH, formate; H_4F, tetrahydrofolate; CO_2, carbon dioxide. Adapted from Lidbury et al., 2015.*

The results presented show that MED193 can grow on PC as a sole source of phosphorus. The proteomic approach revealed that the choline catabolism pathway, which was previously proposed in *R. pomeroyi* DSS-3 (Lidbury et al., 2015), is upregulated in MED193. MED193 uses choline as a source of nitrogen and carbon. However, it is still unclear if an extracellular phosphatase of the PhoX family cleaves PC outside the cell, hereby making choline accessible for the transporter system.

4.2.6 Identification of organic transporters that are potentially involved in the uptake and catabolism of glycerol-phosphate in *Phaeobacter* sp. MED193

As shown in growth experiments on different phospholipid headgroups, pre-starved -P MED193 cultures were able to utilize PG as the sole source of P (Figure 4.1). Cultures grown on PG had a similar lag phase

as the control group (+P, supplemented with P_i after pre-starvation for P) before reaching the exponential growth phase. However, compared to the +P control, cultures supplemented with PG didn't reach the same final OD (Figure 4.1, Table 4.1). Sequential re-subbing in fresh media, supplemented with the same P source as before, showed that the lag phase was shorter, and the exponential growth rate was reached faster. Interestingly, cultures still couldn't reach the same final yield as the control cultures (+P) when entering the stationary growth phase (Figure 4.2B, C, Table 4.1). Membrane lipid analysis by LC-MS revealed that PG was restored, as shown by the decreasing DGTS/ PtdGro ratio in the chromatogram in Figure 4.3A, B.

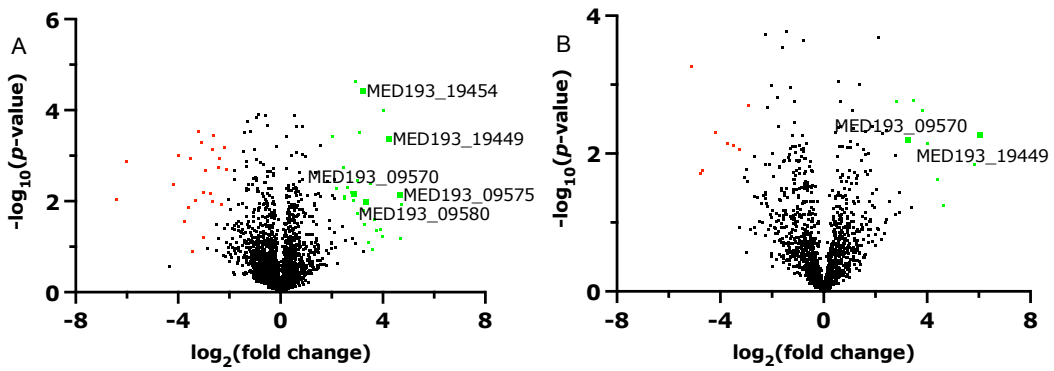

Figure 4.18: ***Volcano plots of cellular (A) and exo- (B) proteomic data comparing PG to +P MED193 cultures.***
Pre-starved MED193 cultures that were supplemented with P_i vs cultures supplemented with glycerol-phosphate (PG). Scatter points represent proteins. The x-axis is the fold change for the ratio between both growth conditions and the y-axis is the statistical p-value. Green dots represent proteins that are significantly upregulated in the PG growth condition whereas red dots represent those proteins that are significantly downregulated (p-value 0.05, logFC 2). Two proteins namely MED193_09570 and MED193_19449 are substrate-binding proteins of ABC transporters and were found in both, the cellular and exoproteome.

A proteomic approach (see section 2.4) was used to identify key enzymes that are potentially involved in the transport, uptake, and catabolism of PG. Therefore, the abundance of proteins found in the PG condition was compared to proteins of the pre-starved -P culture that was supplemented with P_i. Of the 2458 identified cellular proteins, only two (or 52 with *p*-value 0.05) were significantly upregulated (or downregulated (*p*-value 0.05), *p*-value 0.01, logFC 2, Figure 4.18A, Appendix 4.7). By comparison, out of the 1357 identified extracellular proteins, 11 (or 17 with *p*-value 0.05) were significantly up- or downregulated (*p*-value 0.01,

log FC2, Figure 4.18B, Appendix 4.8). Comparison of the cellular and exoproteome data highlighted two proteins, namely MED193_09570 and MED193_19449 that were significantly upregulated in both datasets. As described above (see section 4.2.3 and Figure 4.5), MED193_09570 encodes the protein GlpV, which is annotated as a substrate-binding protein of a glycerol ABC transporter.

Looking specifically at proteins which were upregulated in the cellular proteome, there are a few proteins of interest. Two ATP-binding proteins were identified as significantly upregulated in the cellular proteome which are part of the same ABC transporter, namely MED193_09575 (GlpS) and MED193_09580 (GlpT). However, only one of the two permeases, identified in the cellular proteome, namely MED193_09590 (GlpQ), was detected with minor upregulation. The second permease encoded by MED193_09585 (GlpP), was not detected in the proteome. Looking closer at the detection levels of GlpV in the cellular and exoproteome dataset, there is no significant difference between the PG and the -P cultures (Table 4.5). However, both ATP-binding proteins GlpS (MED193_09575) and GlpT (MED193_09580) were highly upregulated in the PG condition but are only slightly upregulated or even downregulated in the -P control. In contrast, there was no significant difference between cultures grown on PG and the -P control regarding detection levels of the permease GlpQ (MED193_09590) (Table 4.5).

The second significantly upregulated protein found in both the cellular and exoproteome is encoded by MED193_19449 and is annotated as a phosphonate binding protein (PhnD) of an ABC transporter. One of the ATP-binding proteins encoded by MED193_19454 (PhnC) was significantly upregulated in the cellular proteome. However, both permease components encoded by MED193_19459 (PhnE2) and MED193_19464 (PhnE1) were either not significantly upregulated or not detected by LC-MS/MS. In comparison to the Glp-ABC-transporter described above, PhnD (MED193_19449), PhnC (MED193_19454), and PhnE2 (MED193_19459) were significantly upregulated in the PG condition only but showed no upregulation in the -P control (Table 4.5).

Table 4.5: ***Phaeobacter sp. MED193 substrate-binding proteins that are upregulated in cultures grown with PG.***
*The Table shows the fold change of these proteins in the cellular and exoproteome, comparing the proteomes of the -P control and the cultures supplemented with PG to the pre-starved -P culture supplemented with P_i. Significant fold changes of proteins are marked with ** for p-value <0.01 or * for p-value <0.05. Proteins that are marked with N/D (not detected) were not detected by LC-MS-MS.*

Identified proteins		*Accession number*	*Locus tag*	*Fold change -P control cellular*	*Fold change PG cellular*	*Fold change -P control extracellular*	*Fold change PG extracellular*
Glycerol ABC transporter, substrate-binding protein	*GlpV*	EAQ44278	MED193_09570	* 2.41	* 2.88	** 3.38	* 3.27
Glycerol ABC transporter, ATP-binding protein	*GlpS*	EAQ44279	MED193_09575	0.24	* 4.67	N/D	N/D
Glycerol ABC transporter, ATP-binding protein	*GlpT*	EAQ44280	MED193_09580	-0.05	* 3.35	N/D	N/D
Glycerol ABC transporter, permease	*GlpQ*	EAQ44282	MED193_09590	0.46	0.86	N/D	N/D
Phosphonate ABC transporter, substrate-binding protein	*PhnD*	EAQ47401	MED193_19449	0.01	* 4.25	* 2.27	** 6.06
Phosphonate ABC transporter, ATP-binding protein	*PhnC*	EAQ47402	MED193_19454	-0.46	* 3.24	N/D	N/D
Phosphonate ABC transporter, permease	*PhnE2*	EAQ47403	MED193_19459	-0.01	1.49	N/D	N/D

These findings suggest that this transporter is induced by the presence of PG and is not regulated by the Pho regulon as the Glp-ABC-transporter. Hence, the substrate-binding protein was overexpressed and purified by collaborators in China. However, the transporter didn't show any binding affinity towards glycerol, G1P, or G3P. More work regarding PG catabolism in MED193 will be discussed in Chapter 5.

4.2.7 The extracellular alkaline phosphatase PhoX of *Phaeobacter* sp. MED193 has monoesterase activity towards phospholipid headgroups

The results in this chapter demonstrate that MED193 can grow on phospholipid headgroups as a sole source of P (Figure 4.1). However, the findings in sections 4.2.4 and 4.2.5 only describe pathways in MED193 for the transport and catabolism of ethanolamine and choline and not for the intact headgroup. Since there was no evidence for transporters of the intact headgroup, it seems likely that some type of phosphatase is involved in the extracellular cleavage of these compounds, thereby making ethanolamine, choline, and P bioavailable for cells. It has previously been shown that members of the PhoX family are extracellular phosphatases (Wu et al., 2007; Kathuria & Martiny, 2011; Sebastián & Ammerman, 2011) that are widespread in the marine environment (Sebastián & Ammerman, 2009). Furthermore, the relative abundance of MED193 PhoX was moderately high, ranking it in the top 50 of the most abundant proteins (Figure 4.19).

These findings suggest that the MED193 PhoX (MED193_05784) phosphatase plays a crucial role in the extracellular cleavage of phospholipid headgroups. To determine metal requirements, substrate specificity, and enzyme kinetics of PhoX, an overexpression plasmid for MED193_05784 was synthesized in a pET151/D-TOPO vector (see section 2.2.1). This plasmid was used to overexpress PhoX in *E. coli* using an auto-induction media (see section 2.2.6). The 'Compute pI/Mw' tool (ExPASy server) was used to calculate the theoretical molecular weight of the protein as 73728.95 Dalton (Bjellqvist et al., 1993, 1994; Gasteiger et al., 2005).

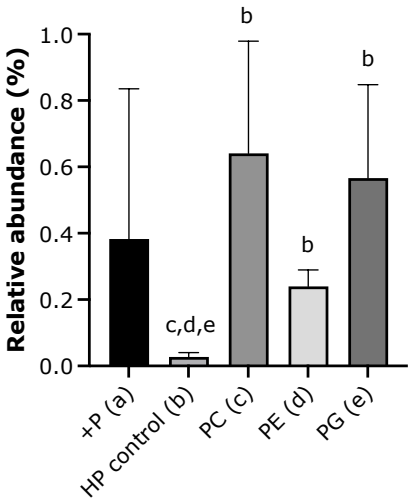

Figure 4.19: ***Relative abundance of the alkaline phosphatase PhoX in the exoproteome of pre-starved MED193 cultures grown on P_i, PC, PE, and PG.*** *Pre-starved MED193 cultures that were supplemented with P_i, phosphocholine (PC), phosphoryl-ethanolamine (PE), glycerol-phosphate (PG), and MED193 cultures grown in high P_i (HP control). The x-axis displays the growth conditions and the y-axis the relative abundance in %. PhoX abundance is highest in PC, followed by PG, P_i, and PC and is barely detectable in the HP control. Graph shows mean ± standard deviation of triplicates. Significant differences are labelled (t-test, p-value <0.05).*

Verification of the overexpressed protein was done through SDS-PAGE (see section 2.2.7). A band of around 75 kDa was visible in the induced (PhoX) compared to the uninduced (negative control) culture (Figure 4.20). Next, PhoX was first purified by His-Tag affinity chromatography and sequentially by size-exclusion chromatography (see sections 2.2.10 - 2.2.12). A gel filtration calibration kit for high molecular weight proteins was used to confirm the size of PhoX. Standards used for the calibration were Ovalbumin (44 kDa), Conalbumin (75 kDa), and Aldolase (158 kDa) (Figure 4.21). After size exclusion chromatography, purified PhoX was concentrated using an Amicon column, and the concentration was measured using a NanoDrop 2000.

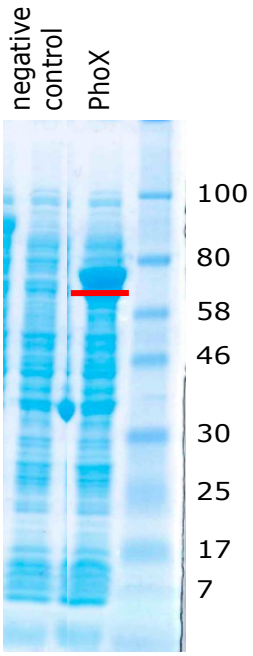

Figure 4.20: ***MED193 PhoX overexpressed in E. coli.*** *The protein was overexpressed in E. coli using a pET151-D/TOPO plasmid and auto-induction media. Induced (PhoX, highlighted in red) and uninduced (negative control) cultures. Protein standard for protein size identification.*

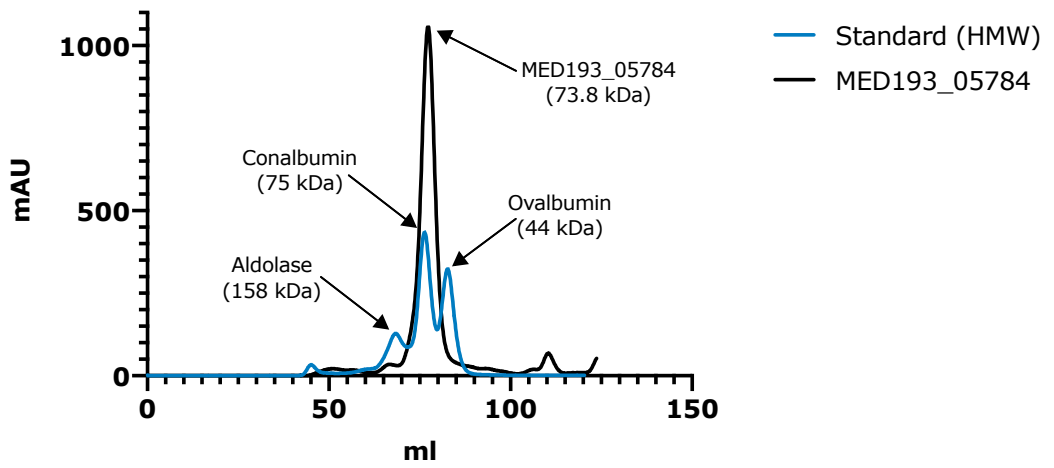

Figure 4.21: ***Size exclusion chromatography of MED193 PhoX, including protein standards.***
Gel filtration chromatogram of PhoX and protein standards. Retention volume of MED193 PhoX was 77.5 ml (73.8 kDa); retention volume for the standards was as follows: Aldolase, 67.5 ml (158 kDa); Conalbumin, 75 ml (75 kDa); Ovalbumin, 82.5 ml (44 kDa).

Additionally, bioinformatics analysis was used to further investigate the MED193_05784 protein. The Phyre^2 protein fold recognition server (Kelley et al., 2016) predicted 43% identity with 83% coverage (558 residues with 100% confidence) with the PhoX of *Pseudomonas fluorescens* Pf0-1. This protein has recently been demonstrated to be a monomer (Wu et al., 2007; Luo et al., 2010). Interestingly, active-site cofactors of multiple PhoX phosphatases have recently been characterized as iron-calcium clusters (Wu et al., 2007; Kathuria & Martiny, 2011), including the PhoX identified by Phyre^2 (Yong et al., 2014). After purification, no enzyme activity was detectable. The substrate *p*NPP is routinely used for phosphatase activity assays. Here, the substrate gets hydrolysed, resulting in free P_i and the release of *p*NP. *p*NP has a yellow colour with a maximum absorbance at 405 nm, and this colour change can be measured spectrophotometrically (Bessey et al., 1946). Since no colour change was detectable for the native protein, it was supplemented with a variety of metals (Wu et al., 2007; Kathuria & Martiny, 2011; Yong et al., 2014).

In MED193, the addition of $CaCl_2$ only or in combination with several other metals restored activity of the PhoX phosphatase, except the combination of $CaCl_2$ and $ZnSO_4$. The addition of $FeCl_3$ resulted in precipitated iron, and no activity could be measured in this case (Figure 4.22, Appendix 4.11). Although it has been previously described that PhoX

requires iron and calcium as metal cofactors, the data above (Figure 4.22) showed that the addition of Ca^{2+} was enough to restore activity. Given this, it was possible that the purified protein already contained iron.

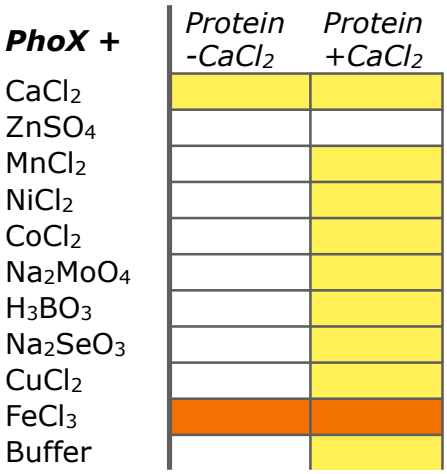

Figure 4.22: ***Colorimetric phosphatase activity assay with pNPP to test metal requirements of the MED193 PhoX.***
The addition of $CaCl_2$ could restore phosphatase activity in the native protein and in combination with all metals tested, except $ZnSO_4$. Protein -$CaCl_2$: native protein, protein +$CaCl_2$: native protein supplemented with $CaCl_2$. Rows list all metals tested. Yellow: release of pNP (PhoX activity), orange: precipitation of iron, white: no pNP release (no PhoX activity).

To test this hypothesis, the protein was treated with EDTA, buffer exchanged, and PhoX tested for enzyme activity (see section 2.3.1.1). Enzyme activity towards *p*NPP was abolished. However, activity could be restored by adding Ca^{2+} (data not shown). This result reinforced the hypothesis that iron atoms are bound covalently to the enzyme.

To further confirm this hypothesis, collaborators at the National Service for Electron Paramagnetic Resonance Spectroscopy (EPR) at the University of Manchester used EPR to determine the oxidation state of the MED193 PhoX iron atoms, thus, confirming the presence of iron in the active site of the protein (Figure 4.23). The EPR conditions and concentrations of reagents used for analysis and sample preparation were the same as used previously for *P. fluorescens* Pf0-1 PhoX (Yong et al., 2014) and are briefly described in section 2.3.3. Compared to the Yong et al. (2014) data, as-isolated MED193 PhoX was not EPR silent (black trace). The addition of 5 mM dithionite (red trace) did not influence the EPR signal of MED193 PhoX. However, the addition of 20 mM dithionite (blue trace) reduced the EPR signal, which is comparable to *P. fluorescens* PhoX. Supplementation with 50 mM EDTA (green trace) enhanced the EPR signal. In contrast, the addition of the phospholipid headgroup PE (1 mM, cyan trace) did not influence the Fe^{3+} cluster, hence, no change in the EPR signal was observed.

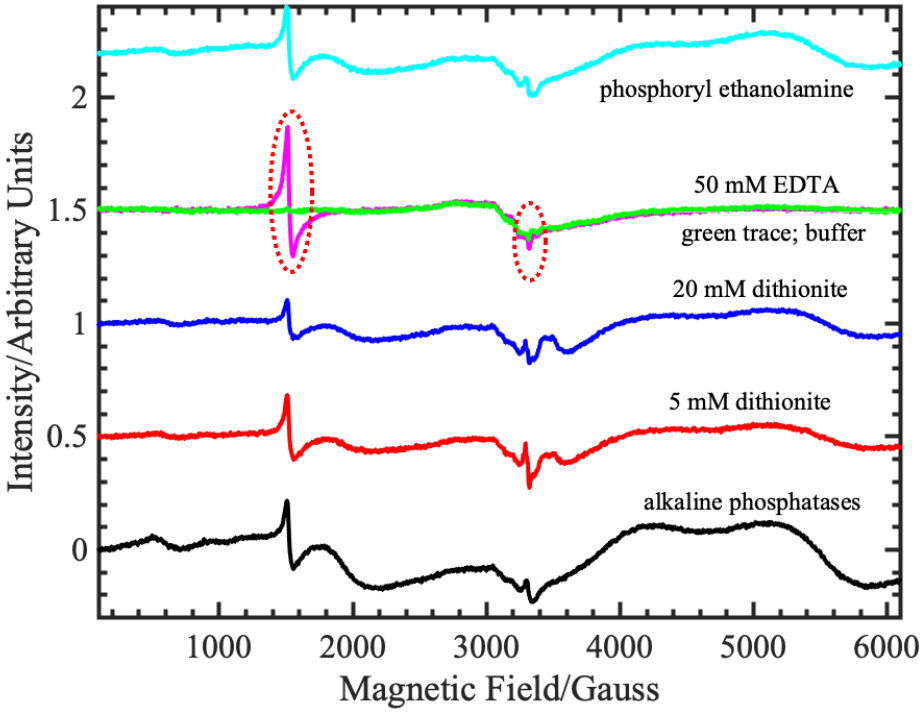

Figure 4.23: ***Spectroscopic analysis of MED193 PhoX.***
EPR spectra of PhoX. Native protein was expected to have a binuclear Fe^{3+}- Fe^{3+} cluster and no EPR signal. EPR signal of as-isolated protein (black trace) suggests loss of one Fe^{3+}. EPR signal decreased with increasing dithionite concentration (red and blue trace), reducing some Fe^{3+} to EPR silent Fe^{2+}. EDTA enhanced the EPR signal (green trace), confirming the hypothesis that high-spin Fe^{3+} was covalently bound to the protein. The addition of phosphoryl-ethanolamine (cyan trace) did not influence the EPR signal, and the substrate does not bind to the Fe^{3+}-centre.

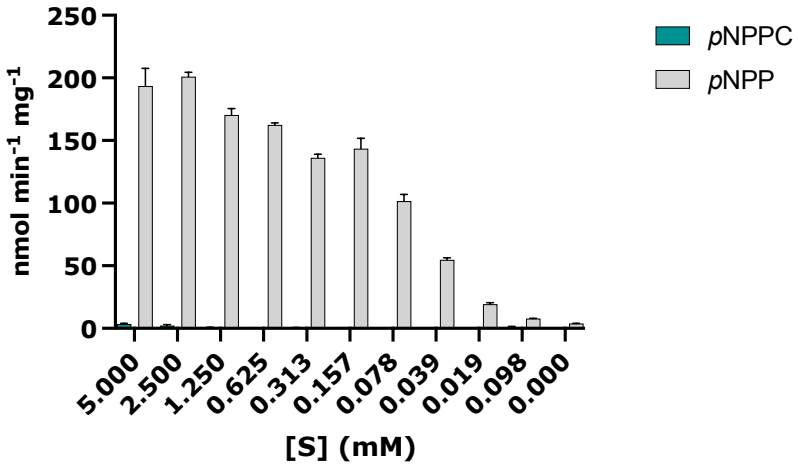

Figure 4.24: ***Alkaline phosphatase activity assay to determine the substrate specificity of MED193 PhoX.***
pNPP (blue) and pNPPC (grey) were used to determine the substrate specificity of MED193 PhoX towards mono- and diester. The activity was measured for different substrate concentrations (x-axis) and normalised against time and concentration of protein (y-axis). Minor activity/background noise was detected for pNPPC; increasing activity was measured with increasing pNPP concentration. Graph shows mean ± standard deviation of triplicates.

The experiments described above confirm that the MED193 PhoX requires iron and calcium for enzyme activity. Additionally, enzyme activity assays were performed to determine substrate specificity and enzyme kinetics. Initially, two widely-applied substrates were used for the detection of alkaline phosphatase activity to demonstrate substrate specificity towards phosphate monoester and phosphate diester bonds. Whereas the assay with the phosphate monoester *p*NPP showed high enzyme activity, the phosphate diester *p*NPPC showed no colour change, indicating that *p*NPPC could not be hydrolysed by PhoX (Figure 4.24).

Subsequently, three phosphate monoesters, specifically *p*NPP, PE and PC, were used for enzyme activity assays to calculate enzyme kinetics using the Michaelis-Menten equation. The experimental setup is described in section 2.3.2. The rate of enzyme activity was plotted against substrate concentration (Figure 4.25) and plots were used to calculate V_{max} and K_m. Here, V_{max} is defined as the maximum velocity of the reaction when the enzyme is saturated with the substrate, K_M is the substrate concentration at which half V_{max} is reached (Roskoski, 2015). V_{max} was calculated as follows: *p*NPP 194.60 nmol min^{-1} mg $protein^{-1}$, PC 7.89 nmol min^{-1} mg $protein^{-1}$, PE 180.00 nmol min^{-1} mg $protein^{-1}$ and K_M resulted in: *p*NPP 90.89 µM, PC 16.50 µM, PE 192.30 µM (Table 4.6).

Table 4.6: ***V_{max} and K_M values calculated for Phaeobacter sp. MED193 PhoX for substrates pNPP, PC, and PE.***
V_{max} and K_M values were calculated from best fit Michaelis-Menten curves for initial enzyme velocity plotted against substrate concentration.

Michaelis Menten	[*p*NPP]	[PC]	[PE]
V_{max} (nmol min^{-1} mg $^{-1}$)	194.60	7.89	180.00
K_M (µM)	90.89	16.50	192.30

Findings in this chapter suggest that MED193 PhoX is indeed involved in the extracellular cleavage of the phospholipid headgroups PE and PC consistent given the fact that no transporters for the intact headgroups have been found. The cleavage process makes ethanolamine, choline, and P_i bioavailable for cells. Furthermore, biochemical analysis of PhoX showed that the active site has an iron-calcium cluster cofactor which is required for enzyme activity.

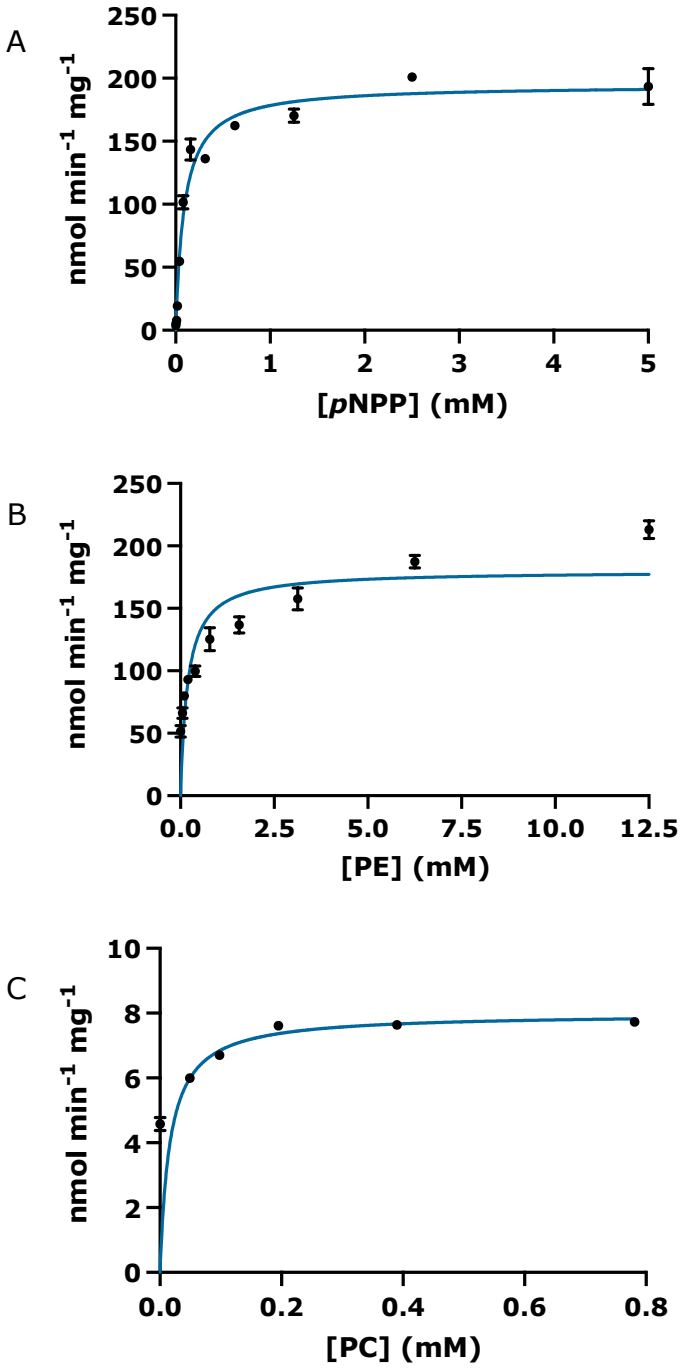

Figure 4.25: ***Michaelis-Menten curves to determine enzyme kinetics for MED193 PhoX with substrates pNPP, PE, and PC.***
Initial velocity (y-axis) plotted against increasing substrate concentration (x-axis). The best fit Michaelis-Menten curve was used to calculate V_{max} and K_M for pNPP (A), PE (B), and PC (C). Standard error (n=3).

4.3 Discussion

MED193 is a member of the *Roseobacter* group (Brinkhoff et al., 2008; Simon et al., 2017). This *Alphaproteobacterium* was isolated from the Mediterranean Sea, which is known to be scarce in nutrients that are essential for growth, including P (Lazzari et al., 2016). Because of this, MED193 is used as a model organism to study adaptation mechanisms to P-starvation. For the first time, a proteomic approach was used to investigate the response of MED193 to P-limitation and to identify key enzymes/transporters that are required to acquire P_i from organic phosphates, in particular phospholipid headgroups. To do this, MED193 cultures were first starved for P, before adding P back in the forms of P_i, PE, PC and PG. As a positive control, cultures were also grown under high P_i-replete conditions to assure continuous P-availability. For this study, lipidomic and proteomic analysis was performed, and growth experiments were monitored by measuring OD_{540}.

4.3.1 Growth of *Phaeobacter* sp. MED193 on phospholipid headgroups and changes in the membrane lipid composition

Growth experiments performed in this study have shown for the first time that the marine heterotrophic *Alphaproteobacterium* MED193 can grow on phospholipid headgroups as a sole source of P. Unsurprisingly, the -P control didn't grow, demonstrating that P is essential for bacterial growth. Interestingly, in comparing the length of the lag phase of all growth conditions in the initial growth experiment, there was not a very large difference detected (Table 4.1). Independent of the P-source, whether organic or inorganic, cultures entered the exponential growth phase at a similar time (± 3 hours) and reached a growth plateau after approximately 12 hours of exponential growth. However, cultures supplemented with phospholipid headgroups didn't reach the same final OD_{540} as the control group (Figure 4.1 and Figure 4.2, Table 4.1). This indicates that, although provided with an alternative P-source, MED193 cells are not supplied with enough P_i to restore normal growth as hydrolysis of organic P and subsequent transport may be too costly (Zhang et al.,

2014). The same effect was seen in both sequential growth experiments (Figure 4.2B, C).

All growth experiments were conducted for 40 hours before transferring cultures to fresh media. Comparing all three growth experiments of the +P and PC cultures, it becomes obvious that they share the same pattern. In both cases, the lag phase is shortened by 25-60% after the first sequential transfer but increases again by 116-125% after the second sequential transfer. In the initial growth experiment, both PC and P_i (to some extent) cultures reached the stationary growth phase shortly before being transferred to fresh media. This explains the shorter lag phase and faster growth rate in the first sequential growth experiment. Since cultures reached the stationary phase earlier in the first sequential growth experiment, cells potentially became limited for nutrients again before transfer to fresh media occurred. The second sequential growth experiments demonstrate a longer lag phase and reduced growth rate. In P_i and PC cultures, the final yield stayed almost the same throughout the growth experiments with a variance of 5-16%. This means that the P_i retrieved from the inorganic and organic P-source is continuously and equally invested in bacterial growth (Table 4.1). Cultures grown on PG demonstrate a steadily decreasing lag phase (-60%) with decreasing final yield (-40%) but a constant growth rate. This indicates that cells adapted to the uptake of PG, resulting in a reduced lag phase. However, as stated above, P_i obtained from PG was either not enough to restore cell yield or was used for other processes rather than bacterial growth (Zhang et al., 2014). Intriguingly, the lag phase of cultures supplemented with PE was constant throughout all three growth experiments. However, the growth rate and final yield both fluctuated by ~20%. Both growth rate and final yield seem to positively correlate as a higher growth rate resulted in a higher final yield and vice versa (Table 4.1).

Once cells reached the stationary growth phase, OD_{540} was stable for more than 10 hours, indicating that cells entered a balanced equilibrium between cell division and cell death. This effect was described before in *Symbiodinium voratum* supplemented with 2-AEP and glyphosate groups (Tian-Tian et al., 2019).

Proteomic analysis showed that a PhoX-type alkaline phosphatase (MED193_05784) was upregulated in cultures supplemented with P_i and phospholipid headgroups in comparison to the culture grown on high P (344 µM P_i). Interestingly, this enzyme was described to be a secreted phosphate monoesterase (Wu et al., 2007; Luo et al., 2009; Yong et al., 2014). We believe that the MED193 PhoX is involved in the hydrolysis of phospholipid headgroups, making the substituents ethanolamine, choline, and glycerol, as well as P_i accessible for transport. Hence, it is surprising that MED193 still shows signs of P-stress while the same concentration of P (172 µM) was provided in all conditions. The periplasmic phosphate-binding protein PstS was upregulated in all conditions compared to the high P control. Since *pstS* is used as a universal marker gene for P-stress (Scanlan et al., 1993), this result indicates that MED193 was still P-limited despite being provided with different P-sources.

It has previously been described in *Trichodesmium* ISM101 that P uptake from different organic P-compounds or DOP and the resulting P-content per cell is lower compared to cultures treated with DIP (White et al., 2010). Furthermore, a study on several marine algae and the cyanobacterium *Synechococcus* grown on glucose-6-phosphate (G6P) showed that cultures utilising G6P didn't reach the same final OD as cultures grown with P_i. In the same study, it was shown through ^{14}C experiments that G6P was hydrolysed to acquire P_i and that a transport system for the sugar-phosphate is unlikely to exist (Kuenzler, 1965). These results confirm that growth on organic P-sources is not necessarily comparable to growth on P_i, highlighting P_i as the preferred bioavailable P-source. Additionally, it affirms the importance of extracellular phosphomonoesterases, e.g., PhoX, in acquiring P_i from organic P-compounds.

This study revealed that MED193 utilises phospholipid headgroups as a sole source of P and restores phospholipids in its membrane (Figure 4.3). As previously described (Sebastián et al., 2016), phospholipids are remodelled to DGTS when cells are P-limited, as clearly demonstrated in the lipid composition by a high DGTS/ PtdGro ratio in P-limited cultures (Figure 4.3B). However, once pre-starved cultures were supplied with a P-source, the DGTS/PtdGro ratio decreased, proving that phospholipids in

membranes are restored. The chromatogram (Figure 4.3A) highlights an increase in PtdGro and PtdCho/PtdEtn as compared to the -P control independent of the P-source, whether organic or inorganic. However, compared to the high P control (Figure 4.3C), PtdGro in membrane lipids has not been restored completely. It is unclear if PtdGro can be restored entirely in later stages of exponential growth, thereby mirroring the membrane composition of P-replete cultures. It has not been described before to what extent the lipid status in bacteria can be reversed (Sahonero-Canavesi et al., 2019) and, as such, it remains unclear if DGTS is actively degraded by MED193 or if the DGTS/PtdGro ratio decreases as part of a dilution process.

4.3.2 Phosphate stress response in *Phaeobacter* sp. MED193

For many years, the P stress response has been studied in *E. coli* as a model organism for bacterial P stress (Baek & Lee, 2006, 2007; Gardner et al., 2014). It is known that the PhoBR two-component system regulates the P_i stress response in bacteria. The PhoBR system controls the Pho regulon which encodes enzymes that are involved in P_i uptake and acquisition of P_i from organic phosphate (Baek & Lee, 2006; Monds et al., 2006; Su et al., 2007; Santos-Beneit, 2015). However, not much is known about organic phosphate transporter systems. The response of MED193 to phosphate stress, as seen in the proteomic data, is comparable to *E. coli*. P-limitation triggered the induction of the Pho regulon, indicated by the upregulation of PhoB, PhoR, and the Pst transporter system (-P, Figure 4.5).

Furthermore, four putative organic P-transporters were found to be significantly upregulated in P-limited conditions. Firstly, proteins encoded by the *ugp* operon were upregulated, including a glycerophosphoryl diester phosphodiesterase (UgpQ) and an *sn*-G3P ABC transporter (UgpC, UgpE, and UgpB). It has previously been shown that the *ugp* operon is a member of the Pho regulon (Schweizer & Boos, 1985; Brzoska & Boos, 1989; VanBogelen et al., 1996). Interestingly, this transporter is believed to be inhibited by high intra- and extracellular concentrations of P_i (Brzoska & Boos, 1989). Additional studies showed that many marine bacteria retrieved from the GOS metagenome database possess *ugp* transporter

genes, allowing the uptake of glycerol phosphate monoesters and phosphate diesters. However, approximately half of these bacteria were found not to have the gene *ugpQ*, and, therefore, are unable to hydrolyse phosphodiesters (Luo et al., 2009).

Secondly, the substrate-binding protein of an ABC transporter (GlpV), annotated as a glycerol transporter, was highly upregulated under P-limited conditions. Only this protein was upregulated whereas both ATP-binding proteins (GlpS and GlpT) and the permease (GlpQ) of the ABC transporter were not significantly different to the P-replete control group. However, all members of this transporter were significantly upregulated in the culture supplied with PG. Intriguingly, not much is known about this transporter. A recent study on *Rhizobium leguminosarum* bv. viciae strain VF39SM showed that the *glp* operon consists of genes encoding an ABC transporter, a kinase and dehydrogenase (Ding et al., 2012). Apart from the regulatory gene *glpR*, all other genes are organised in one single operon. This operon was highly induced by both glycerol and G3P. In the Ding et al. (2012) study, radiolabelled glycerol was used to demonstrate that deletion of these transporter genes abolishes transport of glycerol and G3P.

Thirdly, a protein annotated as PhnD, with gene name MED193_10161, was upregulated in the P-limited condition. As demonstrated in Chapter 3, this protein is most likely a member of the C-P lyase machinery. Through proteomic analyses, several utilisation pathways for organic P have been discovered in P-deplete MED193 cultures. Three of the most upregulated proteins have been described and analysed in this section, further highlighting the ability of MED193 to cope with long-term P-limitation. These results indicate that phospholipid headgroups derived from lysed bacteria can be a common source of P for bacteria in oligotrophic environments.

4.3.3 Discovery of a phosphoryl-ethanolamine degradation pathway in *Phaeobacter* sp. MED193

For the first time, it has been demonstrated that MED193 can utilise PE as a sole source of P, potentially by hydrolysing this organic compound outside the cell, thereby making P_i and ethanolamine accessible.

Interestingly, phosphate acquired from extracellular PE was used to reinstate cell growth and partially restore membrane phospholipids as indicated by a decreasing DGTS/PtdGro ratio (Figure 4.3A).

In this study, a proteomic approach was used to identify key enzymes that are involved in the transport and degradation of PE. A substrate-binding protein, MED193_10041, was upregulated in the cellular and exoproteome of cultures supplemented with PE (Figure 4.6). Subsequent bioinformatics analysis linked this protein to a previously described ethanolamine binding protein (Csal_0678) of *Chromohalobacter salexigens* (Vetting et al., 2015). To conduct biochemical studies on this protein, collaborators in China overexpressed MED193_10041 and used MST to demonstrate the binding affinity of the protein to ethanolamine. The protein was found to bind ethanolamine with a K_d of around 7.88 µM (Figure 4.7). The low concentration indicates that ethanolamine is a natural substrate of MED193_10041. Furthermore, the genomic environment of MED193 and *C. salexigens* are identical, both gene clusters comprising seven genes that are potentially involved in the catabolism of ethanolamine (Figure 4.8). Data retrieved from the phenotypical characterisation of deletion mutants in the ethanolamine binding protein and L-glutamine synthetase was used to predict an ethanolamine degradation pathway in *C. salexigens* (Vetting et al., 2015). The similarity between MED193_10041 and Csal_0678 (Figure 4.8) and high sequence identity between all proteins of both gene clusters (Table 4.5) allowed mapping of the predicted ethanolamine degradation pathway of *C. salexigens* to MED193 (Figure 4.9).

The ethanolamine binding protein is part of a TRAP transporter. Several transporters of the TRAP-T family have been described previously and the substrate specificity determined (Forward et al., 1997; Takami et al., 2000; Kelly & Thomas, 2001; Hugouvieux-Cotte-Pattat et al., 2001; Grammann et al., 2002; Brüggemann et al., 2004; Thomas et al., 2006; Denger et al., 2006; Chen et al., 2010; Pernil et al., 2010; Mulligan et al., 2012; Salmon et al., 2013; Hopkins et al., 2013; Wübbeler et al., 2014; Dörries et al., 2016; Meinert et al., 2017; Tully et al., 2018). Phylogenetic studies of MED193_10041 demonstrated a clear clustering with *C. salexigens* Csal_0678, both being distinct to other members of the TRAP-

T family (Figure 4.11). MSA of TRAP-T family members confirmed the distinctions between MED193_10041 and Csal_0678 to other family members (Figure 4.10). It has previously been shown which amino acids are involved in the coordination of ethanolamine in the active site of Csal_0678 (Vetting et al., 2015). Unsurprisingly, the same amino acids are present in the protein structure of MED193_10041, indicating the composition of the active site coincides. However, the structures of other TRAP-T family members distinguish themselves from the ethanolamine binding proteins described. These findings lead to the assumption that MED193_10041 and Csal_0678 form a new group of substrate-binding proteins within the TRAP-T family.

Ocean primary production can be limited by nitrogen availability. Therefore, it seems likely that ethanolamine can be used by marine microorganisms as a source of nitrogen. To determine the distribution of MED193_10041 in the marine environment, a BLAST search using a hmm file of MED193_10041 and Csal_0678 was used to find homologs in the Ocean Gene Atlas (OGA). The metagenomics analysis revealed that the gene is evenly distributed between different sampling depths. Here, it was found in around 10% of the genomes in the database (Figure 4.12). Moreover, looking into the taxonomic distribution of this protein, 94% of organisms that possess this substrate-binding protein belong to the *Alphaproteobacteria*, dominatingly in the order *Pelagibacterales*, known as SAR11 (19%, Figure 4.13, Appendix 4.9). Within the *Alphaproteobacteria*, the *Roseobacter* group only contributes 7%. Although the sequence of MED193_10041 and Csal_0678 and 10 close homologs each were included in the hmm file that was used as a query for the BLAST search, only 1% of retrieved homologs belong to *Gammaproteobacteria* (Appendix 4.10). Whilst metagenomics analysis showed that the gene was present in only around 10% of all searched genomes, metatranscriptomics revealed that the gene was highly expressed (Figure 4.12B). Since the abundance was calculated as a percentage of the median abundance of ten prokaryotic single-copy marker transcripts, the boxplot shows that the ethanolamine binding protein is highly active, on average around 50% of the marker transcripts or same transcription level as the marker transcripts. Most marker genes used for normalisation are involved in ribosomal processes.

Ribosomal genes are commonly used as so-called housekeeping genes as their expression is relatively stable (Thorrez et al., 2008). These genes are ubiquitously distributed between domains (Lu et al., 2020). In a few cases, transcription was higher than the marker gene expression. Finally, sequences retrieved from the OGA were included in the phylogenetic tree of the TRAP-T family, presenting a clear and distinct clustering of the ethanolamine binding proteins (Figure 4.13).

Findings in this section describe a novel ethanolamine degradation pathway in MED193. The substrate-binding protein has been demonstrated to bind ethanolamine, transporting it from the periplasm to the cytoplasm where it potentially is further degraded to glycine. However, more work is needed to confirm the degradation pathway. It is still unclear if MED193 possesses an organic transporter system for PE or if PhoX is involved in the cleavage of the headgroup before transport. The construction of a PhoX deletion mutant would help to assess whether MED193 can still grow on PE, assuming all extracellular phosphatase activity has been abolished.

4.3.4 The choline/betaine degradation pathway is involved in the uptake and catabolism of phosphocholine

The results of this section demonstrate that MED193 can utilise PC as a sole source of P (Figure 4.1 & Figure 4.2). Furthermore, membrane phospholipids could partially be restored after adding P, in the form of PC, back to the media (Figure 4.3A). In the cellular and exoproteome, five proteins were highlighted, namely MED193_19144, MED193_21671, MED193_21676, MED193_21681, and MED193_21686, that were significantly upregulated (Figure 4.15). All these proteins have homologs in *Ruegeria pomeroyi* DSS-3 (Table 4.4). Here, these proteins are involved in choline metabolism (Lidbury et al., 2015).

MED193_19144 is annotated as a dimethylglycine dehydrogenase (SPO0635 in DSS-3), putatively involved in the demethylation of dimethylglycine to sarcosine (Figure 4.17). In *R. pomeroyi* DSS-3, it was predicted that this step is catalysed by SPO3400 (Lidbury et al., 2015). SPO3400 has a close homolog in MED193 (MED193_14777, 80% Seq.ID, e-value 0.0). However, this protein was downregulated in the PC condition. This result suggests, that MED193_19144 is involved in the catabolism of

choline in MED193, potentially replacing MED193_14777. Additionally, MED193_21671 annotated as a choline membrane transport protein (*BetT*), is a close homolog to SPO1087 in *R. pomeroyi* DSS-3 (72% Seq.ID, Table 4.4). *BetT* was first described in *E. coli* (b0314), where it was shown to be a high-affinity choline transporter (Andresen et al., 1988; Lamark et al., 1991). Deletion mutations in *E. coli* (Lamark et al., 1991) and *R. pomeroyi* DSS-3 (Lidbury et al., 2015) demonstrated that *BetT* is responsible for choline uptake. Inferring from the homology of MED193_21671 to SPO1087 and b0314 (30% Seq.ID, e-value $4.3e^{-51}$), it seems likely that MED193_21671 is the choline transporter *BetT* in MED193.

Another protein potentially involved in the choline catabolism is MED193_21676, highly upregulated under PC conditions and annotated as choline sulfatase (*BetC*). MED193_21676 shares high sequence identity with SPO1083 of *R. pomeroyi* DSS-3 (Table 4.4). It has been confirmed that *BetC* is essential for the growth of *R. pomeroyi* DSS3-3 (Lidbury et al., 2015) and *Sinorhizobium meliloti* (Østerås et al., 1998) on choline-*O*-sulfate (COS). Interestingly, in *S. meliloti* it has been demonstrated that *BetC* has substrate specificity towards both substrates, COS and phosphorylcholine (Østerås et al., 1998). Hence, MED193_21676 may be responsible for the conversion of phosphocholine to choline (Figure 4.17). However, no transporter for PC has been described.

MED193_21681 encodes a putative betaine aldehyde dehydrogenase (BADH, *BetB*). In *E. coli* a K_M of around 1 µM for betaine aldehyde was determined for the BADH (Falkenberg & Strøm, 1990). In additional studies, it was discovered that *BetB* is regulated by choline (Lamark et al., 1991). Furthermore, no BADH activity was detected in *S. meliloti BetB2* deletion mutants (Østerås et al., 1998). MED193_21681 has 79% Seq ID with *BetB* from *R. pomeroyi* DSS-3. Here, the deletion of SPO0084 (*BetB*) led to an accumulation of betaine aldehyde when grown on choline (Lidbury et al., 2015). According to high sequence identity with *BetB* of *R. pomeroyi* DSS-3 (79% Seq.ID, Table 4.4), *E.coli* (54% Seq.ID, e-value $2.9e^{-178}$), and *S. meliloti* (61% Seq.ID, e-value 0.0) it is obvious that MED193_21681 encodes *BetB*, an oxidoreductase that oxidises betaine aldehyde to glycine betaine (Figure 4.17).

The last upregulated protein discovered in the proteome of cultures supplemented with PC is a putative choline dehydrogenase (CDH, *BetA*), encoded by MED193_21686. Choline dehydrogenase has been extensively studied (Landfald & Strøm, 1986; Styrvold et al., 1986; Pocard et al., 1997; Rosenstein et al., 1999). Deletion of *BetA* in *E.coli* (Landfald & Strøm, 1986; Styrvold et al., 1986) and *S. meliloti* (Østerås et al., 1998), and *CudB* in *Staphylococcus xylosus* C2A (Rosenstein et al., 1999) abolished CDH activity. MED193_21686 is a homolog of *E. coli BetA* (b0311, 49% Seq.ID, e-value $3.6e^{-178}$), *S. meliloti* (SMc00093, 67% Seq.ID, e-value 0), and *S. xylosus* (Ga0069509_11229, 48% Seq.ID, e-value $4e^{-180}$). It is also a homolog of SPO1088 (77% Seq.ID, Table 4.4), CDH of *R. pomeroyi* DSS-3. Here, a SPO1088 deletion mutant couldn't utilise choline as a sole source of carbon. Hence, no CDH activity was detected (Lidbury et al., 2015). These findings suggest that MED193_21686 encodes a choline dehydrogenase in MED193, completing the initial choline degradation pathway, thereby converting choline or phosphocholine to sarcosine.

Proteomic analysis of MED193 cultures grown on PC uncovered a gene operon that is directly induced by the compound. The *bet* operon of MED193 and *R. pomeroyi* DSS-3 are similar (Figure 4.16) and all proteins encoded by the *bet* operon have a homolog in *R. pomeroyi* DSS-3 (Table 4.4). The results presented in this chapter indicate that MED193 possesses a similar choline degradation pathway as predicted in *R. pomeroyi* DSS-3 (Lidbury, 2015, Figure 4.17). However, neither the predicted pathway nor the proteomics data had evidence for an organic PC transporter. Hence, it is still unclear if such a transporter exists or if a phosphatase is necessary for phosphate cleavage before choline uptake.

4.3.5 Identification of organic transporters that are potentially involved in the uptake and catabolism of glycerol-phosphate in *Phaeobacter* sp. MED193

The findings of this section confirmed that MED193 can grow on PG as a sole source of P (Figure 4.1 and Figure 4.2). Furthermore, PG utilisation causes the reinstatement of membrane phospholipids (Figure 4.3). A proteomic approach was used to identify key enzymes which are

potentially involved in PG catabolism in MED193. Two substrate-binding proteins were identified that were highly upregulated in the exo- and cellular proteomes, specifically MED193_09570 and MED193_19449 (Figure 4.18). As described in section 4.2.3, including Figure 4.5, MED193_09570 is annotated as GlpV, a substrate-binding protein of a glycerol ABC transporter. Both ATP-binding proteins of the same ABC transporter, MED193_09575 (GlpS) and MED193_09580 (GlpT), were also significantly upregulated. However, only one of the two permeases, MED193_09590 (GlpQ), was detected by MS/MS. According to Table 4.5, GlpV is upregulated in the P-deplete and PG conditions. However, both ATP-binding proteins are only upregulated in the PG and not in the P-deplete condition. As discussed in section 4.3.2 little is known about this transporter. In *Rhizobium leguminosarum* bv. *viciae* strain VF39SM GlpV was found to be part of the *glp* operon. This operon consists of multiple genes encoding an ABC transporter, a kinase, and dehydrogenase (H. Ding et al., 2012). Interestingly, the operon was induced by glycerol and G3P. MED193_09570 is a homolog of the *R. leguminosarum* GlpV (61% Seq.ID, e-value 0.0). Because of this, MED193_09570 was overexpressed and tested for substrate specificity by collaborators in China. However, MED193_09570 didn't have a binding affinity towards glycerol, G1P, or G3P.

The other protein found in cultures supplemented with PG was MED193_19449, annotated as PhnD. Although this protein was detected in the proteomes of the P-deplete and PG cultures, it was more highly upregulated in the PG condition (Table 4.5). PhnD is the substrate-binding protein of an ABC transporter, including the ATP-binding proteins PhnB (not detected) and PhnC (MED193_19454), and the permeases PhnE1 (MED193_19464) and PhnE2 (MED193_19459). Many proteins that are annotated as PhnD have been described before (Chen et al., 1990; Wanner & Metcalf, 1992; Ilikchyan et al., 2009, 2010; Alicea et al., 2011; Willis et al., 2019). However, most of these proteins belong to the C-P lyase machinery, like MED193_10161 (Figure 3.7). Since the substrate specificity of this protein is still unclear, collaborators in China have overexpressed and purified this protein to conduct biochemical analyses. However, no binding affinity towards glycerol, G1P, or G3P was detected.

The substrate PG used in the growth experiment was a mixture of G1P and G3P. It is perhaps unlikely that bacteria can utilise G1P since unless bioengineered, bacteria have not been described to synthesise G1P (Caforio et al., 2018) and G1P represents the backbone of archaeal phospholipids (Nishihara et al., 1999; Caforio & Driessen, 2017). Since no sufficient proof for a specific PG transport pathway was found in the proteomics data shown here, more research is needed. Further results are summarised in Chapter 5. However, the data in this section indicates that MED193_19449 and MED193_09570 are substrate-binding proteins involved in PG catabolism.

4.3.6 The extracellular alkaline phosphatase PhoX of *Phaeobacter* sp. MED193 has monoesterase activity towards phospholipid headgroups

Phosphatases play a crucial role in the adaptation of bacteria to P-limitation, especially in the acquisition of P_i from organic P-sources. One of these phosphatases belongs to the PhoX-type phosphatases, an extracellular enzyme that has been described in several studies (Wu et al., 2000; Monds et al., 2006; Luo et al., 2009; Sebastián & Ammerman, 2011; Cox & Saito, 2013; Pegos et al., 2014, 2017; Lin et al., 2018; Tian-Tian et al., 2019). This protein is more widely distributed in marine organisms than previously thought (Sebastián & Ammerman, 2009).

The results presented in this chapter demonstrate that MED193 can use phospholipid headgroups as a source of P (Figure 4.1). However, there is no sufficient evidence that MED193 possesses organic transporters for PE and PC. Therefore, it seems likely that an alkaline phosphatase is cleaving P_i off extracellularly, thereby making P_i and the substituents ethanolamine and choline bioavailable for cells. The exoproteome of cultures supplemented with PC, PE and PG support this hypothesis. Here, PhoX was detected in the exoproteome, ranking the phosphatase in the top 50 of the most abundant proteins (Figure 4.19). To prove the hypothesis MED193 PhoX, encoded by MED193_05784, was overexpressed and purified.

Interestingly, MED193 PhoX didn't have any enzyme activity after purification. Several metals and metal combinations were tested. However, $CaCl_2$ was the only additive that could reinstate enzyme activity.

Furthermore, Zn^{2+} seemed to inhibit the protein, as the combination of $ZnCl_2$ and $CaCl_2$ couldn't restore enzyme activity (Figure 4.22). This coincides with previous reports that reported inhibition of the protein through zinc (Wu et al., 2007; Zaheer et al., 2009; Kathuria & Martiny, 2011; Sebastián & Ammerman, 2011; Yong et al., 2014). Previous studies have identified cysteine, aspartate, and glutamate as zinc-ligating residues (Ireland & Martin, 2019). The MED193 and *P. fluorescens* PhoX both possess one cysteine, three aspartates, and five glutamates in their active centre. Therefore, zinc may compete with calcium for the active site. Also, these studies characterised the active-site cofactors as an iron-calcium cluster (Wu et al., 2007; Zaheer et al., 2009; Kathuria & Martiny, 2011; Yong et al., 2014).

EPR was used to further confirm the oxidation state of iron ions in the active centre of MED193 PhoX. *P. fluorescens* Pf0-1 PhoX was used for comparison purposes. Here, the cofactors of the active centre were demonstrated to consist of two antiferromagnetically coupled ferric iron ions (Fe^{3+}) and three calcium ions (Ca^{2+}) (Yong et al., 2014). The EPR results of MED193 PhoX differed slightly from *P. fluorescens* PhoX (Figure 4.23). Whereas a binuclear Fe^{3+}- Fe^{3+} anti-ferromagnetically coupled-cluster was confirmed in *P. fluorescens* PhoX (EPR-silent), the spectra of native MED193 PhoX showed a peak, indicating that the enzyme was not fully metallated and some protein was lacking a second Fe^{3+} in the active site. The addition of the reducing agent dithionite (5 mM and 20 mM) resulted in a reduced peak in both MED193 and *P. fluorescens* PhoX. However, the reduction in *P. fluorescens* was stronger compared to MED193. In conclusion, the addition of 5 mM and 20 mM dithionite indicates that only one Fe^{3+} is present in native MED193 PhoX which can't be reduced by low concentrations of dithionite. However, higher concentrations can reduce iron atoms and thereby reduce the EPR signal. Interestingly, the same result as in *P. fluorescens* PhoX was achieved when adding 50 mM EDTA. Also, in the MED193 PhoX EPR spectra, the signal was drastically increased, confirming that only a small fraction of the high-spin Fe^{3+} can be removed by EDTA, leading to an increased signal by the remaining Fe^{3+} (Yong et al., 2014).

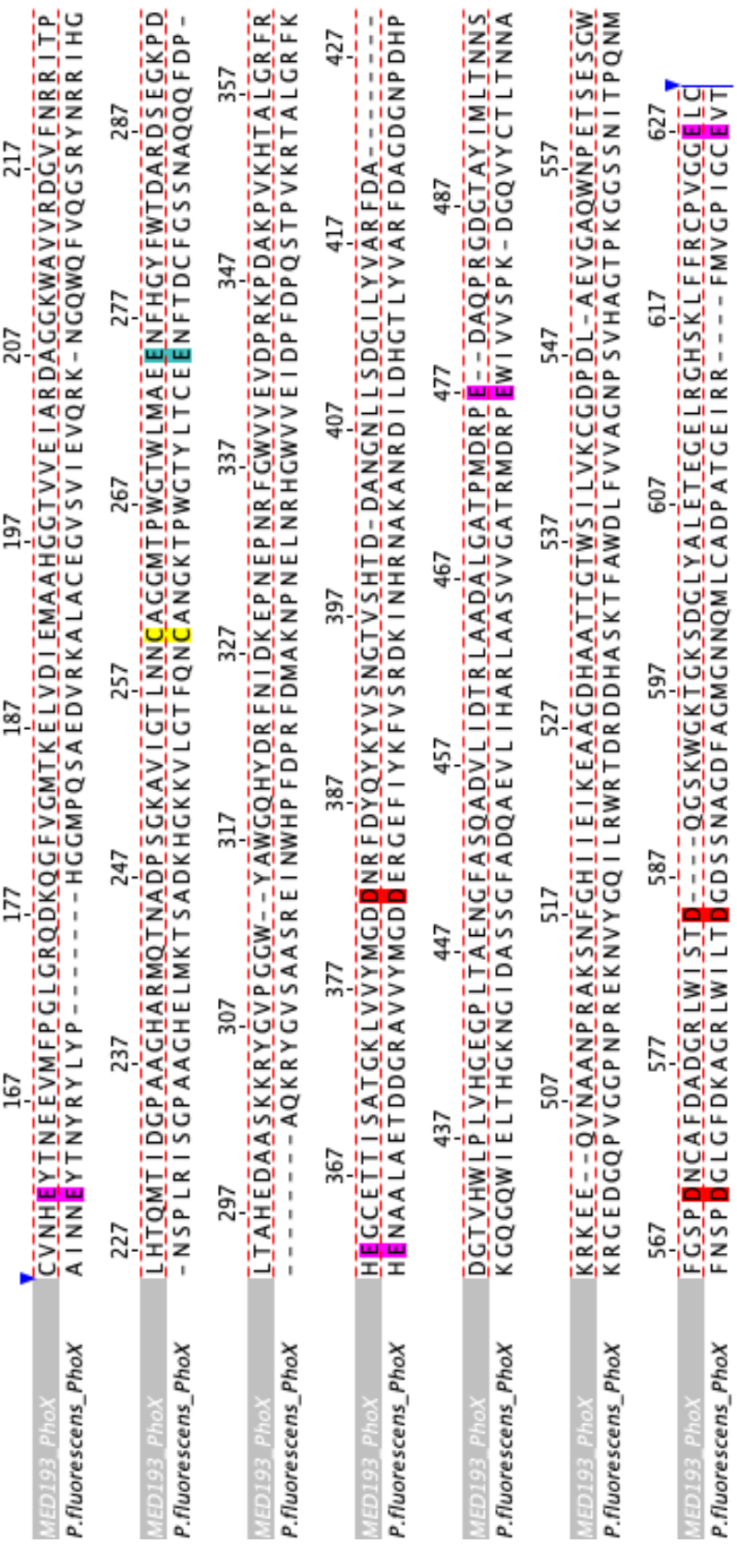

Figure 4.26: ***The active site of MED193_05784 (PhoX) and P. fluorescens Pf0-1 PhoX.*** *Sequence alignment of MED193 and P. fluorescens PhoX. Highlighted are amino acids that coordinate the iron-calcium cluster. Glutamates 90,273, 387, and 532 (pink), cysteine 179 (yellow), aspartates 292, 479, and 494 (red). Aspartate 194 is replaced by glutamate (turquoise)* (Yong et al., 2014).

However, the addition of PE didn't influence the EPR signal. This suggests that the substrate does not bind directly to Fe^{3+} or both iron atoms are needed for binding. Enzyme kinetics was conducted to determine the V_{max} and K_M of MED193 PhoX. Initially, two substrates were used to test for substrate specificity towards phosphate monoesters and phosphate diesters. Whereas the phosphate monoester *p*NPP could be hydrolysed by MED193_05784, the phosphate diester *p*NPPC could not be utilised (Figure 4.24). Following these tests, the three phosphate monoesters *p*NPP, PE and PC were used to calculate enzyme kinetics using the Michaelis-Menten equation (Figure 4.25). The K_M value of MED193_05784 for *p*NPP was 90.89 µM. In the literature, the following kinetic parameters for several purified PhoX were found: K_M 7.9 µM in *P. fluorescens* Pf0-1 (Yong et al., 2014), K_M 66-95 µM in *Pasteurella multocida* strain X_{-73} (Wu et al., 2007), 85.3 ± 4.5 µM in *Sinorhizobium meliloti* (Zaheer et al., 2009), K_M 180 µM in a metagenome-derived alkaline phosphatase (mAP) of the PhoX-II cluster (Lee et al., 2015), and K_M 240 µM in *Vibrio cholerae* (Roy et al., 1982). The K_M value calculated for MED193 PhoX fits well in the values retrieved for other purified PhoX. The relatively low K_M indicates that PhoX is crucial for use of organic phosphates at low concentrations.

The K_M values of MED193 PhoX for the two phospholipid headgroups PC and PE were 16.50 µM and 192.30 µM, respectively (Table 4.6). Although PC and PE have a similar structure, PhoX has a more than 12 times higher binding affinity for PC than for PE. However, MED193 PhoX got inhibited by PC with concentrations above 750 µM, whereas the limit for PE was 12 mM. In purified *S. meliloti* PhoX, the K_M for phosphoserine was 26.6 ± 1.3 µM (Zaheer et al., 2009).

4.3.7 Summary and future work

Phaeobacter sp. MED193, a member of the *Roseobacter* group (Brinkhoff et al., 2008) isolated from the P-limited Mediterranean Sea (Lazzari et al., 2016), is used here as a model organism to study the P stress response. For the first time, a proteomic approach was used to investigate the mechanistic response of MED193 to P-limitation and to identify key enzymes/transporters that are needed to acquire P_i from

organic P, in particular phospholipid headgroups. In this study, it was demonstrated that MED193 indeed can utilise the phospholipid headgroups PE, PC and PG as a sole source of P. Furthermore, pathways for the catabolism of PC and PE were elucidated, and a new group of ethanolamine TRAP transporters was identified. Importantly, this work has demonstrated the importance of phosphatases for the survival of organisms in oligotrophic environments. A PhoX-type phosphatase from MED193 plays a crucial role in the hydrolysis of phospholipid headgroups, thereby making P_i and ethanolamine/choline bioavailable for cells. However, more work is needed to confirm that the PhoX-type phosphatase is indeed cleaving the phospholipid headgroups extracellularly. Therefore, it will be crucial to generate a deletion mutation in WT MED. This approach will help to understand if the PhoX phosphatase is essential for the growth of MED193 on phospholipid headgroups.

Although no breakthrough was made in the discovery of the degradation and transport of PG, potential enzymes/transporters were found that might be involved in this process (see also Chapter 5). In addition, more experiments are required to demonstrate if the phospholipid headgroups used in this study are used as a sole source of P or carbon as well. Although a high concentration of carbon was used for the experimental setup, there is the possibility the transporters found for choline and ethanolamine are regulated by the carbon availability.

Finally, samples taken for the analyses in this chapter were taken after 17.5 h of growth. Figure 4.1 shows that this time point represent the late exponential growth phase rather than the early or mid-exponential growth phase. It is to be considered to investigate the proteomes of samples taken during early growth to better understand the initial response to phospholipid headgroups.

CHAPTER 5 IDENTIFICATION OF A NOVEL TRANSPORTER INVOLVED IN GLYCEROL-PHOSPHATE UPTAKE IN *PHAEOBACTER* SP. MED193

5.1 Introduction

Phosphorus (P) is essential for the growth of all living organisms, as it is a fundamental element within DNA and RNA, ATP, and membrane phospholipids (Paytan & McLaughlin, 2007; Karl, 2014; Koolman & Röhm, 2019). In 1811, Vauquelin was the first to discover P in lipids extracted from brain tissues (Suzumura, 2005). Shortly afterwards, Gobley extracted a P-containing lipid from egg-yolk and brain tissues and named this lipid lecithin/phosphatidylcholine (Gobley, 1874a, 1874b). This lipid belongs to the group of glycerophospholipids derived from *sn*-glycerol-3-phosphatidic acid (Suzumura, 2005).

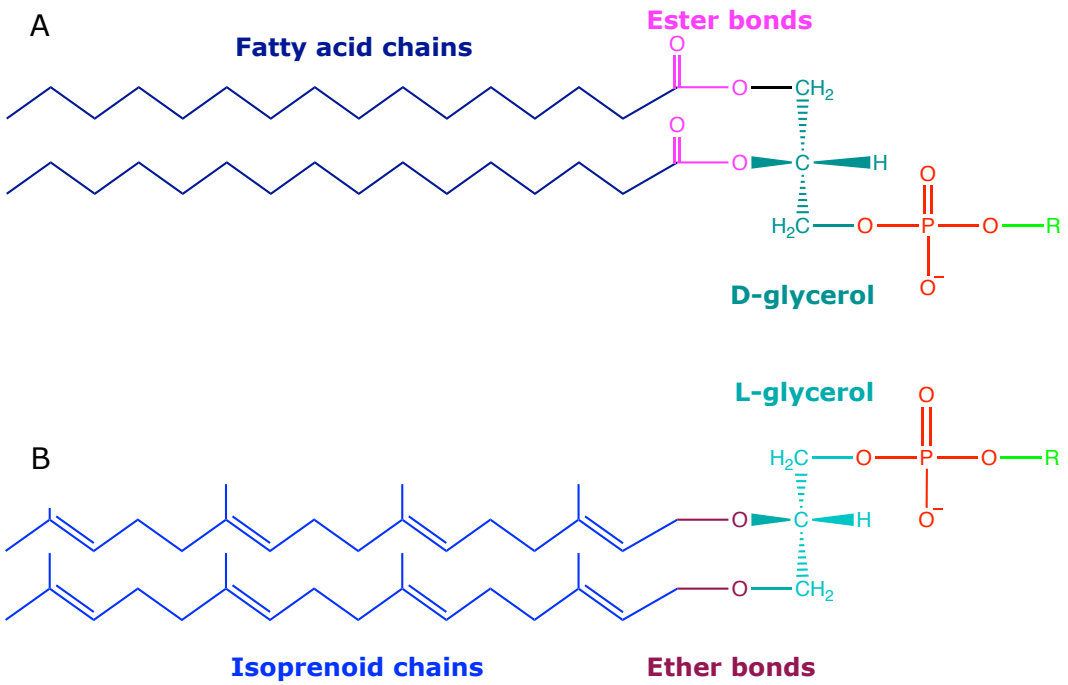

Figure 5.1: ***Chemical structure of bacterial (A) and archaeal (B) membrane phospholipids.***
(A) Bacterial phospholipid which consists of two fatty acid chains that are connected to a D-glycerol and phosphate backbone via ester bonds. (B) Archaeal phospholipid consists of two unsaturated isoprenoid chains that are connected to an L-glycerol and phosphate backbone via ether bonds. Both phospholipid structures contain a polar headgroup (light green). Adapted from Harayama & Riezman, 2018 and Coleman et al., 2019.

Glycerophospholipids are characterised by two fatty acid chains that are connected via ester bonds to a G3P backbone, which is connected to a polar head group (Figure 5.1A). The polar headgroup comprises either a nitrogenous base, glycerol, or an inositol unit (Suzumura, 2005; Schouten et al., 2013; Moellering et al., 2017; Harayama & Riezman, 2018; Coleman et al., 2019).

These glycerophospholipids have not only been found in the domains of Bacteria and Eukaryota; but they have also been isolated from Archaea (Caforio & Driessen, 2017; Coleman et al., 2019; Law & Zhang, 2019; Exterkate et al., 2021). Although a study suggested that archaea and bacteria descended from a common ancestor (Weiss et al., 2016), major differences between the two domains have been well characterised (Kandler, 1995; Reeve et al., 1997; Bell & Jackson, 1998; Kelman & Kelman, 2014). One of these differences is the structure of membrane phospholipids. In archaea, a G1P backbone connects the polar headgroup to highly methylated isoprenoid chains via ether bonds (Figure 5.1B) (Caforio & Driessen, 2017; Moellering et al., 2017; Law & Zhang, 2019; Exterkate et al., 2021). Intriguingly, G1P and G3P are enantiomers which means they are mirror images of each other but not identical (Figure 5.2) (Muller, 1994; Moss, 1996).

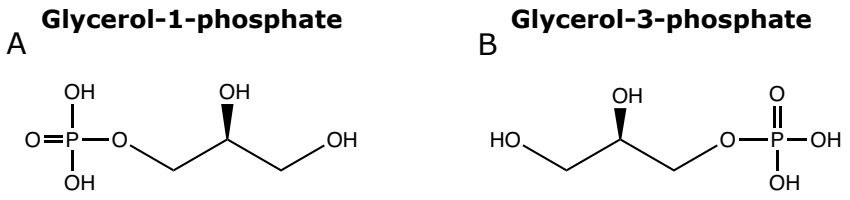

Figure 5.2: ***Chemical structure of glycerol-1-phosphate (A) and glycerol-3-phosphate (B).***
G1P and G3P are enantiomers. Although both structures are mirror images of each other, the molecules are not identical. Whereas G1P is naturally synthesised in Archaea, G3P is a natural compound of Bacteria and Eukaryota.

Two different enzymes have been identified that synthesize these compounds. Whereas a G1P dehydrogenase (G1PDH) has been reported to be involved in G1P synthesis in archaea (Carbone et al., 2015), a G3P dehydrogenase (G3PDH) is responsible for the synthesis of G3P in bacteria (Caforio et al., 2018; Coleman et al., 2019). Although homologs of G1PDH and G3PDH have been discovered in bacteria and archaea, respectively,

the resulting phospholipids have not been reported in the opposing domain (Coleman et al., 2019).

Interestingly, the findings described in Chapter 4 showed that MED193 can utilise PG as a sole source of P. However, the compound used in this study was a mixture of G1P and G3P, and it remains unclear if MED193 can use both forms of PG, or only the bacterial G3P. In this chapter, we demonstrate that MED193 can acquire P_i from both the archaeal G1P as well as the bacterial G3P. Using a proteomic approach, we identified potential key enzymes that are putatively involved in the modification, binding, transport, and degradation of G1P and G3P. Collaborators in China determined the substrate of a prominent substrate-binding protein through protein overexpression and MicroScale Thermophoresis. Additionally, we used a *phoB* deletion mutant to prove that the utilisation of both substrates is independent of the Pho regulon.

5.2 Results

5.2.1 *Phaeobacter* sp. MED193 can utilise both glycerol-1-phosphate and glycerol-3-phosphate

In this chapter, both enantiomers of GP were used as a sole source of P in separate experiments to distinguish differences in transport and metabolism. In addition to the MED193 wild type (WT MED193), a *phoB* deletion mutant (*ΔphoB*), kindly provided by Dr Ian D.E.A. Lidbury (see section 2.8), was cultivated in the same conditions to determine if proteins involved in G1P/G3P catabolism are Pho-regulated.

Therefore, cell cultures of WT MED193 and *ΔphoB* were grown under P-limiting conditions before P was added back, with a final concentration of 172 µM, in the form of P_i, G1P, and G3P as described in the experimental setup (see sections 2.1.2 and 2.1.3). Growth was monitored by measuring OD_{540} over 44 hours (Figure 5.3). The data clearly showed growth of WT MED193 and *ΔphoB* on both G1P and G3P as sole P-source though with a reduction in final cell yield in cultures supplemented with G1P and G3P compared to cultures grown on P_i, demonstrated by a significant difference (t-test, p-value <0.01) in final OD_{540}. WT MED193 and *ΔphoB* cultures supplemented with P_i reached a similar final OD_{540} after 44 hours of

growth, with no significant difference (t-test, *p*-value <0.01). Differences in growth curves between WT MED193 and *ΔphoB* G1P and G3P cultures are not significant (t-test, *p*-value <0.01).

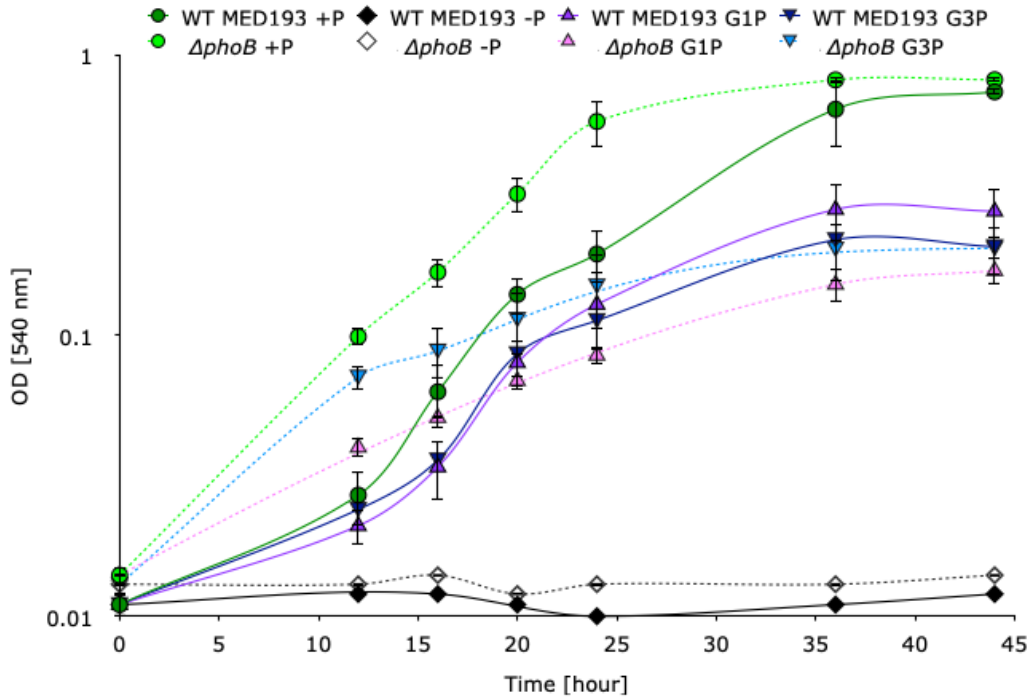

Figure 5.3: ***Growth of pre-starved WT MED193 and ΔphoB on G1P and G3P.*** *WT MED193 and ΔphoB were grown in ASW supplemented with P_i (O), G1P (△), G3P (▽) and no P (◇). P was added back with a final concentration of 172 µM. WT MED193 represented in dark colours and continuous connection lines: P_i, dark green; no P, black; G1P, purple; G3P, dark blue; ΔphoB represented in light colours and dotted connection lines: P_i, light green; no P, white; G1P, pink; G3P, light blue. Graph shows mean ± standard deviation of three biological replicates.*

Alkaline phosphatase activity towards the phosphate monoester *p*NPP and the phosphate diester *p*NPPC was measured after 24 hours of growth, during the mid-exponential growth phase (Figure 5.4). Alkaline phosphatase activity measurement showed a significant difference only between WT MED193 +P (a) and *ΔphoB* +P € as well as WT MED193 G1P (c) and *ΔphoB* G1P (g, t-test, *p*-value <0.05). Higher alkaline phosphatase activity was detected in WT MED193 -P cultures only. This indicates that no elevated phosphomonoesterase and/or phosphodiesterase activity was required for the catabolism of G1P and G3P.

In addition, membrane lipids of pre-starved WT MED193 and *ΔphoB* samples grown on P_i, no P, G1P, and G3P were extracted and analysed by LC-MS (see section 2.5). Detected lipids were normalised against SPE, and relative abundance of lipids/SPE ratios was plotted (Figure 5.5).

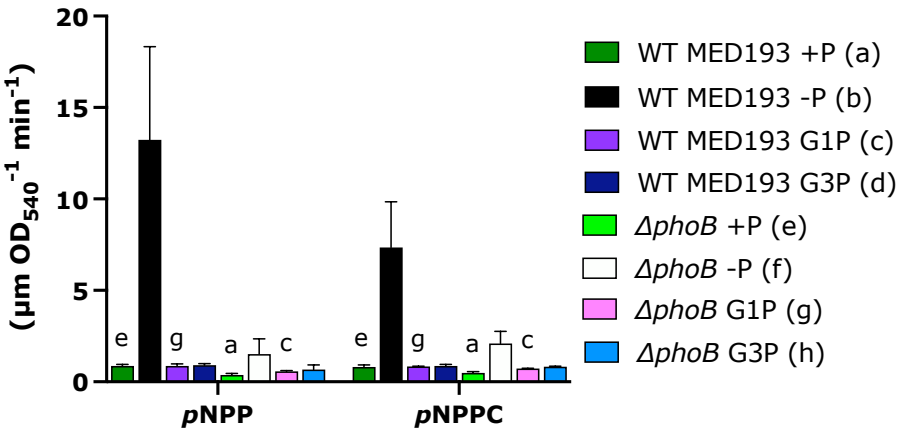

Figure 5.4: ***Alkaline phosphatase activity of pre-starved WT MED193 and ΔphoB cultures after 24 hours of growth in ASW supplemented with different P sources.*** *Alkaline phosphatase activity was measured towards the phosphate monoester pNPP and the phosphate diester pNPPC. Significant differences were found between WT MED193 +P (a) and ΔphoB +P (e) as well as WT MED193 G1P (c) and ΔphoB G1P (g) (t-test, p-value <0.05). High activity was detected in WT MED193 -P cultures only. Graph shows mean ± standard deviation of triplicates.*

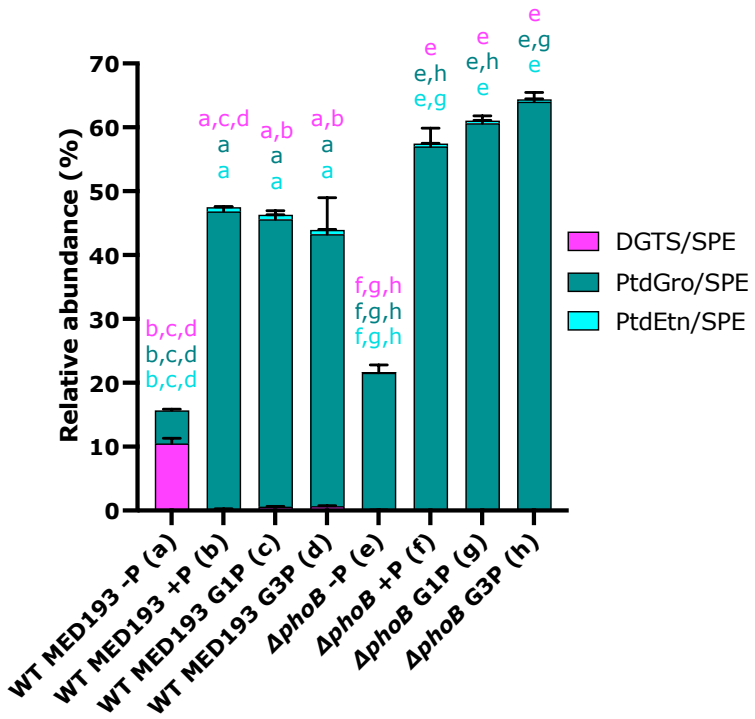

Figure 5.5: ***Membrane lipid composition as relative abundance (%) of pre-starved WT MED193 and ΔphoB grown on different P-sources.***
Pre-starved WT MED193 and ΔphoB cultures were grown in ASW supplemented with Pi, G1P, G3P, and no P. Membrane lipid composition shows a significant difference (t-test, p-value <0.05) between differentially labelled cultures. Numbering is specific for cultures; colouring refers to lipid. ΔphoB cultures supplemented with G1P and G3P show a higher relative abundance of PtdGro than WT MED193. Graph shows mean ± standard deviation of triplicates. DGTS, diacylglyceryl-trimethylhomoserine; PtdGro, phosphatidyl-glycerol; PtdEtn, phosphatidylethanolamine.

Figure 5.5 displays the relative abundance of DGTS, PtdGro, and PtdEtn. LC-MS data demonstrated that membrane phospholipids were restored in pre-starved WT MED193 and *ΔphoB* cultures when supplemented with P_i, G1P and G3P. Furthermore, whereas DGTS was detected in WT MED193 -P with a high relative abundance it was barely detectable in all other conditions, confirming that WT MED193 cultures supplemented with organic P in the forms of G1P and G3P can overcome P limitation and that lipid remodelling was abolished in *ΔphoB* cultures.

5.2.2 *Phaeobacter* sp. MED193 can utilise the archaeal phospholipid backbone G1P as a sole source of P

Additionally, a proteomic approach was used to identify enzymes that are potentially involved in the catabolism of G1P and G3P. Samples of pre-starved WT MED193 and *ΔphoB* cultures supplemented with P_i, G1P, and G3P were taken after 24 hours of growth and analysed by MS/MS as described in section 2.4. A total of 1387 proteins were detected in the cellular proteome, but only 629 proteins were detected in the exoproteome. The growth data (Figure 5.3) showed that both WT MED193 and *ΔphoB* can utilise G1P as a sole source of P. Next, cellular and exoproteomics were used to identify enzymes that are putatively involved in the catabolism of G1P.

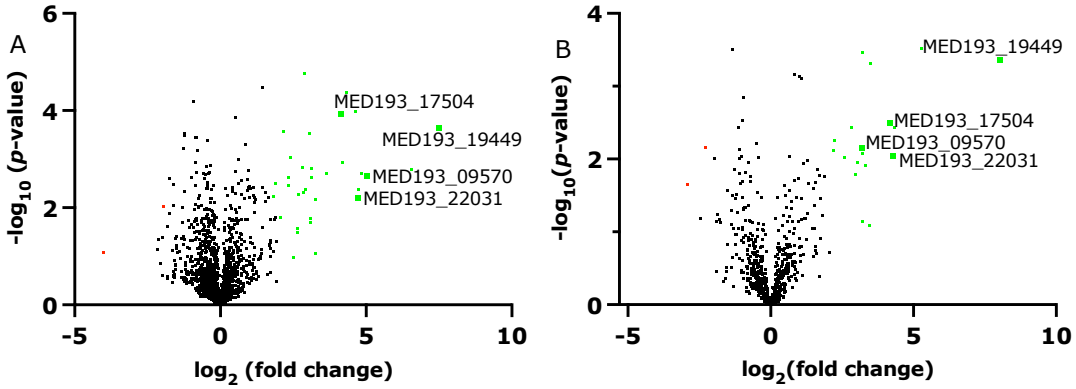

Figure 5.6: ***Volcano plots of cellular (A) and exo- (B) proteomic data comparing WT MED193 G1P to WT MED193 +P cultures.***
Pre-starved WT MED193 cultures that were supplemented with P_i vs WT MED193 cultures supplemented with G1P. Scatter points represent proteins. The x-axis is the fold change for the ratio between both growth conditions and the y-axis is the statistical p-value. Green dots represent proteins that are significantly upregulated in the G1P growth condition whereas red dots represent those proteins that are significantly downregulated (p-value <0.05, logFC 2). Four proteins namely MED193_09570, MED193_17504, MED193_19449, and MED193_22031 are potentially involved in the catabolism of G1P.

Thereafter, the cellular and exoproteomes of WT MED193 and *ΔphoB* grown on G1P were compared to the cellular and exoproteomes of WT MED193 supplemented with P_i (WT MED193 +P). In comparing WT MED193 G1P to WT MED193 +P, 33 proteins were deemed significantly up- and two proteins significantly downregulated in the cellular proteome (Figure 5.6A, Appendix 5.1, *p*-value <0.05, logFC 2). Similarly, in the exoproteome 18 proteins were significantly up- and two proteins significantly downregulated (Figure 5.6B, Appendix 5.2, *p*-value <0.05, logFC 2).

However, in comparing the cellular proteome of *ΔphoB* G1P to WT MED193 +P 51 proteins were significantly up- and 108 significantly downregulated (Figure 5.7A, Appendix 5.3, *p*-value <0.05, logFC 2). In the exoproteome, only 17 proteins were significantly up- and 31 significantly downregulated (Figure 5.7B, Appendix 5.4, *p*-value <0.05, logFC 2).

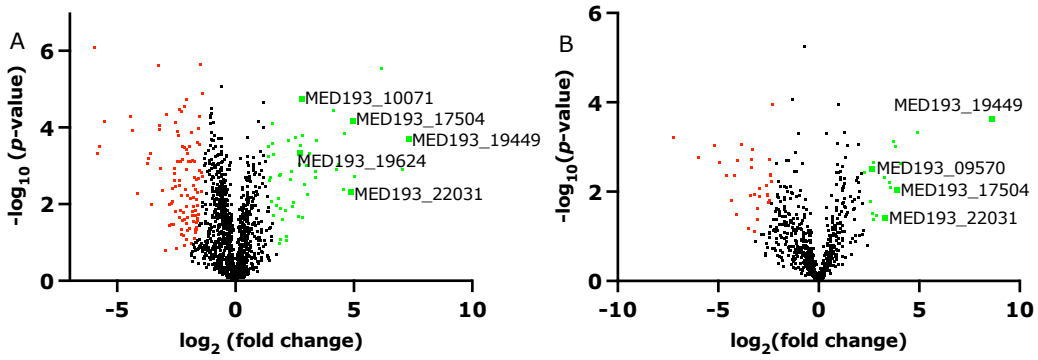

Figure 5.7: ***Volcano plots of cellular (A) and exo- (B) proteomic data comparing ΔphoB G1P to WT MED193 +P cultures.***
Pre-starved WT MED193 cultures that were supplemented with P_i vs ΔphoB cultures supplemented with G1P. Scatter points represent proteins. The x-axis is the fold change for the ratio between both growth conditions and the y-axis is the statistical p-value. Green dots represent proteins that are significantly upregulated in the G1P growth condition whereas red dots represent those proteins that are significantly downregulated (p-value <0.05, logFC 2). Six proteins namely MED193_09570, MED193_10071, MED193_17504, MED193_19449, MED193_19624, and MED193_22031 are potentially involved in the catabolism of G1P.

Several predicted substrate-binding proteins were found to be significantly upregulated in the cellular and exoproteomes of WT MED193 and *ΔphoB*, when comparing the G1P versus the +P condition, namely MED193_09570, MED193_MED193_17504, MED193_19449, and MED193_22031. Of these four proteins, MED193_19449 (annotated PhnD)

was the highest upregulated protein in WT MED193 and *ΔphoB* confirming Pho-independency. MED193_19454 (PhnC, ATPase) and MED193_19459 (PhnE, permease) were also highly upregulated in the cellular proteomes of both WT MED193 and *ΔphoB*. Together, the three proteins form an ABC transporter, annotated as phosphonate transporter (dark blue rows in Table 5.1).

MED193_17504 and another four proteins of the same operon were significantly upregulated in WT MED193 and *ΔphoB*, specifically MED193_17484, MED193_17494, MED193_17499, MED193_17509, and MED193_17514 (green rows Table 5.1). This group of proteins is predicted to form a TonB dependent transporter complex. A second TonB dependent transduction complex was detected in both cellular proteomes, formed by five proteins of the same operon, genes MED193_22031, MED193_22046, MED193_22051, MED193_22056, and MED193_22061 (purple rows in Table 5.1). In addition, MED193_09570 (GlpV), annotated as the glycerol binding protein of an ABC transporter, was more highly upregulated in WT MED193 than in *ΔphoB*. Despite this, this protein does not seem to be Pho-regulated. However, GlpS (MED193_09575), annotated as the ATPase of the same ABC glycerol transporter, was upregulated in the proteome of WT MED193 only, whilst other proteins of this transporter were not detected in either proteome (yellow rows in Table 5.1). Additionally, a G3PDH (GlpA, MED193_19624) was upregulated in WT MED193 and the *ΔphoB* mutant cellular proteome (Table 5.1). This protein is predicted to convert G3P to dihydroxyacetone phosphate (DHAP) (Hartley et al., 2017). Comparing the top upregulated proteins in the cellular proteomes of WT MED193 and *ΔphoB*, no large differences were discovered between the wild type and the deletion mutant.

Three proteins of the 30 most upregulated proteins of the cellular proteome of *ΔphoB* were identified to be downregulated in the wild type, namely MED193_14797 (fold change *ΔphoB* 6.17, WT MED193 -0.85), MED193_15777 (fold change *ΔphoB* 3.41, WT MED193 -0.18), and MED193_19144 (fold change *ΔphoB* 2.55, WT MED193 -0.01) (Appendix 5.3). MED193_14797 is annotated as an oxidoreductase/ aminomethyl transferase involved in the pyridine pathway, MED193_15777 is predicted to encode a glycosyltransferase with an EpsK domain, and MED193_19144

is annotated as aminomethyl transferase involved in the glycine betaine degradation, converting dimethylglycine to sarcosine.

Table 5.1: ***Top 30 most upregulated proteins in the cellular proteomes of WT MED193 and ΔphoB supplemented with G1P.***
Table lists fold change of 30 most upregulated proteins (p-value <0.05) in the cellular proteomes of WT MED193 and ΔphoB in comparison to WT MED193 +P, including locus tags, accession numbers, and annotations. Proteins of the same gene cluster are marked in the same colour.

Identified proteins		*Accession number*	*Locus tag*	*WT MED193 fold change*	*ΔphoB fold change*
TonB dependent iron siderophore receptor		EAQ45582	MED193_08013	3.6305	4.3705
TonB dependent iron siderophore receptor, plug		EAQ45588	MED193_08043	4.3237	4.1541
ABC glycerol transporter, periplasmic substrate binding protein	*GlpV*	EAQ44278	MED193_09570	5.0190	3.3905
ABC glycerol transporter, ATPase	*GlpS*	EAQ44279	MED193_09575	2.6570	0.9877
Glyceraldehyde-3-phosphate dehydrogenase	*GapA*	EAQ43254	MED193_10071	2.4205	2.7960
ABC iron/B12 (?) transporter, periplasmic substrate binding protein		EAQ46986	MED193_17374	2.8319	1.4628
Inner membrane transport system, binding protein dependent	*FecCD*	EAQ46987	MED193_17379	2.1808	-0.8798
ABC iron transporter, ATPase		EAQ46988	MED193_17384	3.1195	2.7334
ABC-type heme transporter, ATPase	*HmuV*	EAQ47008	MED193_17484	4.6360	4.5870
Transmembrane protein, putative periplasmic hemin binding protein		EAQ47010	MED193_17494	2.6677	2.3175
Hemin degrading factor	*HemS*	EAQ47011	MED193_17499	4.8561	5.0098
TonB dependent hemin receptor protein, plug	*HmuR*	EAQ47012	MED193_17504	4.1582	4.9551
Uncharacterized protein		EAQ47013	MED193_17509	2.9212	2.9343
TonB dependent transduction complex, outer membrane	*ExbB*	EAQ47014	MED193_17514	4.1783	4.2749
Antibiotic biosynthesis monooxygenase domain		EAQ47108	MED193_17984	4.7421	4.5462
Uncharacterized protein		EAQ47308	MED193_18984	2.8356	-0.9687
ABC phosphonate transporter, periplasmic substrate binding protein	*PhnD*	EAQ47401	MED193_19449	7.4876	7.3127
ABC phosphonate transporter, ATPase	*PhnC*	EAQ47402	MED193_19454	6.5733	7.0391
ABC phosphonate transporter, permease	*PhnE*	EAQ47403	MED193_19459	3.1188	3.3698
Haloacid dehalogenase-like hydrolase		EAQ47405	MED193_19469	2.8932	2.8274
Glycerol-3-phosphate dehydrogenase	*GlpA*	EAQ47436	MED193_19624	2.3341	2.7035
Uncharacterized protein		EAQ47443	MED193_19659	2.6260	0.2366
Putative imelysin, peptidase M75 family		EAQ47444	MED193_19664	3.2417	2.9763
Putative hemin uptake system	*HemP*	EAQ47446	MED193_19674	3.0926	3.0284
Inner membrane protein, inhibitor of apoptosis-promoting Bax1	*BI1*	EAQ43490	MED193_21571	2.5192	0.9490
Outer membrane TonB dependent receptor protein, plug		EAQ44834	MED193_22031	4.7050	4.8866
TonB dependent transduction complex, outer membrane	*ExbD*	EAQ44837	MED193_22046	3.0520	3.1059
TonB dependent transduction complex, outer membrane	*ExbB*	EAQ44838	MED193_22051	3.1016	2.8392
Siderophore interacting protein, oxidoreductase		EAQ44839	MED193_22056	3.2479	2.4704
ABC iron transporter, ATPase		EAQ44840	MED193_22061	2.3195	1.6030

The findings in this section demonstrate that MED193 possesses several proteins that are potentially involved in the catabolism of G1P. Additionally, these proteins are not controlled by the Pho regulon, as all proteins are equally upregulated in the wild type and *phoB* deletion mutant cultures. However, biochemical studies of the candidate protein MED193_19449 are needed to confirm the substrate specificity of the periplasmic substrate-binding protein.

5.2.3 Glycerol-3-phosphate catabolism in *Phaeobacter* sp. MED193

Growth experiments (Figure 5.3) and analysis of the membrane lipid composition (Figure 5.5) showed that MED193 can utilise G3P after a prolonged duration of P-starvation to restore both growth and membrane phospholipids. Cellular and exoproteomics were used to understand which enzymes play a crucial role in the catabolism of G3P in MED193. Here, the proteomes of WT MED193 and *ΔphoB* supplemented with G3P were compared to WT MED193 cultures grown on P_i (WT MED193 +P). Thirty-nine proteins were significantly upregulated, and eight proteins significantly downregulated in the cellular proteome of WT MED193 grown on G3P (Figure 5.8A, Appendix 5.5, *p*-value <0.05, logFC 2) in comparison to WT MED193 +P. However, in the exoproteome, only 11 proteins were significantly upregulated, but 62 proteins were significantly downregulated (Figure 5.8B, Appendix 5.6, *p*-value <0.05, logFC 2).

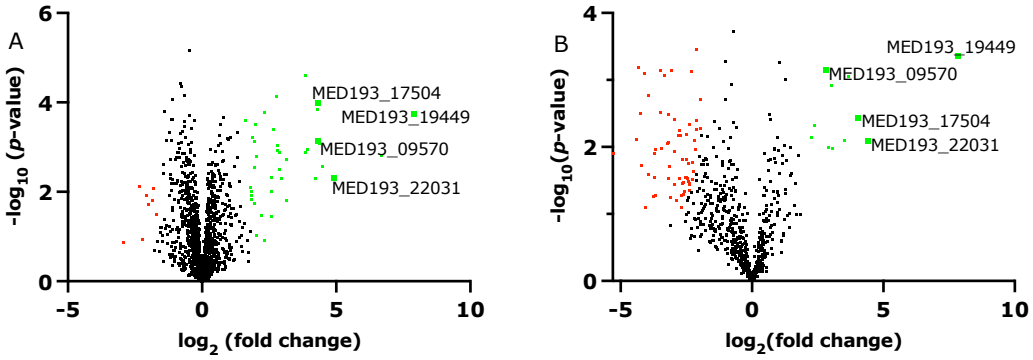

Figure 5.8: ***Volcano plots of cellular (A) and exo- (B) proteomic data comparing WT MED193 G3P to WT MED193 +P cultures.***
Pre-starved WT MED193 cultures that were supplemented with P_i vs WT MED193 cultures supplemented with G3P. Scatter points represent proteins. The x-axis is the fold change for the ratio between both growth conditions and the y-axis is the statistical p-value. Green dots represent proteins that are significantly upregulated in the G3P growth condition whereas red dots represent those proteins that are significantly downregulated (p-value <0.05, logFC 2). Four proteins namely MED193_09570, MED193_17504, MED193_19449, and MED193_22031 are potentially involved in the catabolism of G3P.

Four proteins highly upregulated in both the cellular and exoproteome were identified: MED193_09570, MED193_17504, MED193_19449, and MED193_22031.

In comparing the cellular proteome of *ΔphoB* G3P to WT MED193 +P, 35 proteins were significantly upregulated, and 46 proteins were significantly downregulated (Figure 5.9A, Appendix 5.7, *p*-value <0.05, logFC 2). In the exoproteome of *ΔphoB*, 20 proteins were significantly

upregulated, and 32 proteins were significantly downregulated (Figure 5.9B, Appendix 5.8, *p*-value <0.05, logFC 2).

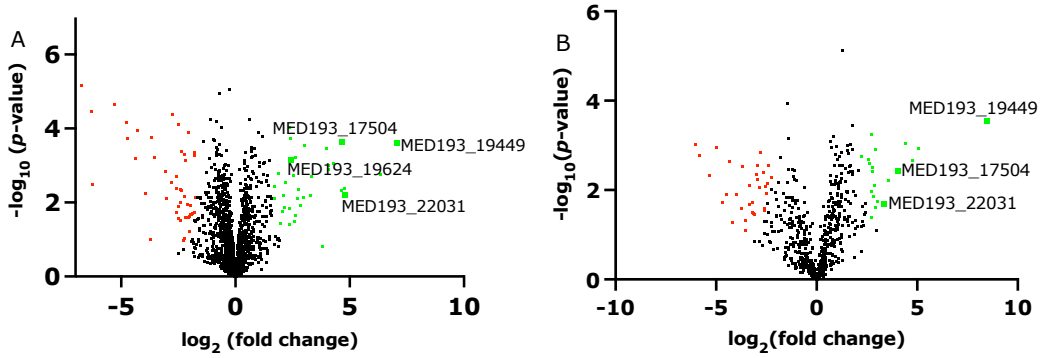

Figure 5.9: ***Volcano plots of cellular (A) and exo- (B) proteomic data comparing ΔphoB G3P to WT MED193 +P cultures.***
Pre-starved WT MED193 cultures that were supplemented with P_i vs ΔphoB cultures supplemented with G3P. Scatter points represent proteins. The x-axis is the fold change for the ratio between both growth conditions and the y-axis is the statistical p-value. Green dots represent proteins that are significantly upregulated in the G3P growth condition whereas red dots represent those proteins that are significantly downregulated (p-value <0.05, logFC 2). Four proteins namely MED193_17504, MED193_19449, MED193_19624, and MED193_22031 are potentially involved in the catabolism of G3P.

Four proteins were upregulated in both the cellular and exoproteomes of *ΔphoB* when grown on G3P compared to WT MED193 +P, namely MED193_17504, MED193_19449, MED193_19624, and MED193_22031. Interestingly, three of these proteins coincided with proteins discovered in the proteomes of WT MED193, namely MED193_17504, MED193_19449, and MED193_22031. In contrast, whilst the periplasmic substrate-binding protein (annotated as GlpV) of a glycerol ABC transporter (MED193_09570) was the sixth highest upregulated protein in the cellular proteome of WT MED193, it was significantly downregulated in *ΔphoB* (yellow rows in Table 5.2). This was of particular interest as this protein was upregulated in the proteome of *ΔphoB* G1P (see section 5.2.2) and *ΔphoB* -P (see Chapter 3), confirming that it is Pho independent. These findings suggest that in *ΔphoB* this protein is induced by the presence of G1P but not by G3P.

The 30 most upregulated proteins in the cellular proteomes of WT MED193 and *ΔphoB*, when comparing growth on G3P to the WT MED193 +P condition, were identical except for four proteins that were downregulated in *ΔphoB*, including the glycerol ABC transporter proteins

GlpV (MED193_09570) and GlpS (MED193_09575) (yellow rows in Table 5.2).

Table 5.2: ***Top 30 most upregulated proteins in the cellular proteomes of WT MED193 and ΔphoB supplemented with G3P.***
Table lists fold change of 30 most upregulated proteins (p-value <0.05) in the cellular proteomes of WT MED193 and ΔphoB in comparison to WT MED193 +P, including locus tags, accession numbers, and annotations. Proteins of the same gene cluster are marked in the same colour.

Identified proteins		*Accession number*	*Locus tag*	*WT MED193 fold change*	*ΔphoB fold change*
TonB dependent iron siderophore receptor		EAQ45582	MED193_08013	3.8598	4.0689
ABC iron siderophore transporter, periplasmic substrate binding protein		EAQ45586	MED193_08033	2.0354	1.7085
TonB dependent iron siderophore receptor, plug		EAQ45588	MED193_08043	3.8558	3.9727
ABC glycerol transporter, periplasmic substrate binding protein	*GlpV*	EAQ44278	MED193_09570	4.3403	-0.8297
ABC glycerol transporter, ATPase	*GlpS*	EAQ44279	MED193_09575	2.5900	0.8757
Peptidoglycan binding domain containing protein		EAQ43729	MED193_12698	2.2029	2.6237
ABC iron/B12 (?) transporter, periplasmic substrate binding protein		EAQ46986	MED193_17374	2.8194	2.0649
ABC iron transporter, ATPase		EAQ46988	MED193_17384	2.7851	2.2120
ABC-type heme transporter, ATPase	*HmuV*	EAQ47008	MED193_17484	4.3159	4.2996
Transmembrane protein, putative periplasmic hemin binding protein		EAQ47010	MED193_17494	2.9053	2.7273
Hemin degrading factor	*HemS*	EAQ47011	MED193_17499	4.4914	4.7661
TonB dependent hemin receptor protein, plug	*HmuR*	EAQ47012	MED193_17504	4.3153	4.6599
Uncharacterized protein		EAQ47013	MED193_17509	2.8744	3.3076
TonB dependent transduction complex, outer membrane	*ExbB*	EAQ47014	MED193_17514	3.9424	4.0950
Antibiotic biosynthesis monooxygenase domain		EAQ47108	MED193_17984	4.2484	4.6397
Uncharacterized protein		EAQ47308	MED193_18984	2.6056	-0.2521
ABC phosphonate transporter, periplasmic substrate binding protein	*PhnD*	EAQ47401	MED193_19449	7.8864	7.0897
ABC phosphonate transporter, ATPase	*PhnC*	EAQ47402	MED193_19454	6.6694	6.3570
ABC phosphonate transporter, permease	*PhnE*	EAQ47403	MED193_19459	3.1347	2.7649
Haloacid dehalogenase-like hydrolase		EAQ47405	MED193_19469	2.6502	2.3440
Glycerol-3-phosphate dehydrogenase	*GlpA*	EAQ47436	MED193_19624	2.8085	2.4261
Putative imelysin, peptidase M75 family		EAQ47444	MED193_19664	4.3752	2.8250
Putative hemin uptake system	*HemP*	EAQ47446	MED193_19674	2.5737	3.2824
Inner membrane protein, inhibitor of apoptosis-promoting Bax1	*BI1*	EAQ43490	MED193_21571	2.3235	0.2283
Outer membrane TonB dependent receptor protein, plug		EAQ44834	MED193_22031	4.9229	4.7965
TonB dependent transduction complex, outer membrane	*ExbD*	EAQ44837	MED193_22046	2.0273	3.0265
TonB dependent transduction complex, outer membrane	*ExbB*	EAQ44838	MED193_22051	3.1404	2.5690
Siderophore interacting protein, oxidoreductase		EAQ44839	MED193_22056	2.9577	2.3800
ABC iron transporter, ATPase		EAQ44840	MED193_22061	1.9767	1.7138
ABC iron/B12 (?) transporter, periplasmic substrate binding protein	*FecB2*	EAQ44843	MED193_22076	2.3396	2.6082

By comparison, three significantly upregulated proteins in the cellular proteome of *ΔphoB* were down- or only slightly upregulated in WT MED193, namely MED193_15777 (fold change *ΔphoB* 3.79, WT MED193 -0.62), MED193_19144 (fold change *ΔphoB* 2.55, WT MED193 0.19), and MED193_16924 (fold change *ΔphoB* 2.40, WT MED193 0.84) (Appendix 5.7). MED193_15777 is annotated as a glycosyltransferase with EpsK domain, MED193_19144 is a putative dimethylglycine dehydrogenase involved in the glycine betaine degradation, and MED193_16924 encodes a putative allophanate hydrolase. Intriguingly, the two highest upregulated

proteins in the cellular proteome of WT MED193 and *ΔphoB* when comparing growth on G3P to the WT MED193 +P condition belong to a putative ABC phosphonate transporter, namely the periplasmic binding protein PhnD (MED193_19449) and an ATPase PhnC (MED193_19454).

Another two proteins of the same operon were upregulated in both proteomes: a permease PhnE (MED193_19459) and a haloacid dehalogenase-like hydrolase (MED193_19469) which includes carbon and phosphorus hydrolases (dark blue rows in Table 5.2). Additionally, two operons encoding TonB dependent transduction complexes were found within the top 30 upregulated proteins of WT MED193 and *ΔphoB* (green and purple rows in Table 5.2). Finally, a G3PDH (GlpA, MED193_19624) was significantly upregulated in the wild type and the *phoB* deletion mutant (Table 5.2).

The data presented in this section demonstrates that several proteins are potentially involved in the catabolism of G3P. Abolishing the phosphate stress response in the *phoB* deletion mutant didn't influence the transport process of G3P which confirmed that G3P catabolism is not Pho regulated. However, more studies are needed to confirm substrate-binding proteins and other proteins involved in the G3P metabolism.

5.2.4 Identification of identical proteins that are involved in G1P and G3P transport in *Phaeobacter* sp. MED193

Proteomic analysis revealed that several proteins that were significantly upregulated in WT MED193 and *ΔphoB* cultures supplemented with G1P were also significantly upregulated in WT MED193 and *ΔphoB* G3P cultures in comparison to WT MED193 +P cultures. This included four periplasmic substrate-binding proteins and two dehydrogenases (Table 5.3). MED193_09570 (annotated as GlpV) is a component of an ABC glycerol transporter, MED193_19449 (annotated as PhnD) is the substrate-binding protein of an ABC phosphonate transporter. Both transporters are not Pho-regulated and are induced in both WT MED193 and the *ΔphoB* mutant. However, clear differences can be seen in the fold change of both transporters.

Table 5.3: ***Proteins that were upregulated in the cellular proteomes of wild type Phaeobacter sp. MED193 and ΔphoB cultures supplemented with G1P and G3P.***
Table lists fold change of proteins that were significantly upregulated (p-value <0.05) in the cellular proteomes of WT MED193 and ΔphoB supplemented with G1P and G3P in comparison to WT MED193 +P, including locus tags, accession numbers, and annotations.

Identified proteins		*Accession number*	*Locus tag*	*G1P WT MED193 fold change*	*G1P ΔphoB fold change*	*G3P WT MED193 fold change*	*G3P ΔphoB fold change*
ABC glycerol transporter, periplasmic substrate-binding protein	*GlpV*	EAQ44278	MED193_09570	5.019	3.391	4.340	-0.830
ABC glycerol transporter, ATPase	*GlpS*	EAQ44279	MED193_09575	2.657	0.988	2.590	0.876
Glyceraldehyde-3-phosphate dehydrogenase	*GapA*	EAQ43254	MED193_10071	2.420	2.796	1.888	1.868
ABC-type heme transporter, ATPase	*HmuV*	EAQ47008	MED193_17484	4.636	4.587	4.316	4.300
Transmembrane protein, putative periplasmic hemin binding protein		EAQ47010	MED193_17494	2.668	2.318	2.905	2.727
Hemin degrading factor	*HemS*	EAQ47011	MED193_17499	4.856	5.010	4.491	4.766
TonB dependent hemin receptor protein, plug	*HmuR*	EAQ47012	MED193_17504	4.158	4.955	4.315	4.660
Uncharacterized protein		EAQ47013	MED193_17509	2.921	2.934	2.874	3.308
TonB dependent transduction complex, outer membrane	*ExbB*	EAQ47014	MED193_17514	4.178	4.275	3.942	4.095
TonB dependent transduction complex, outer membrane	*ExbD*	EAQ47016	MED193_17524	1.665	2.709	1.799	2.122
ABC phosphonate transporter, periplasmic substrate-binding protein	*PhnD*	EAQ47401	MED193_19449	7.488	7.313	7.886	7.090
ABC phosphonate transporter, ATPase	*PhnC*	EAQ47402	MED193_19454	6.573	7.039	6.669	6.357
ABC phosphonate transporter, permease	*PhnE*	EAQ47403	MED193_19459	3.119	3.370	3.135	2.765
Haloacid dehalogenase-like hydrolase		EAQ47405	MED193_19469	2.893	2.827	2.650	2.344
Glycerol-3-phosphate dehydrogenase	*GlpA*	EAQ47436	MED193_19624	2.334	2.704	2.808	2.426
Outer membrane TonB dependent receptor protein, plug	*ExbB*	EAQ44834	MED193_22031	4.705	4.887	4.923	4.796
Transport energization protein TonB, outer membrane	*HemP*	EAQ44835	MED193_22036	2.045	2.095	1.958	2.160
TonB dependent transduction complex, outer membrane	*ExbD*	EAQ44837	MED193_22046	3.052	3.106	2.027	3.027
TonB dependent transduction complex, outer membrane	*ExbB*	EAQ44838	MED193_22051	3.102	2.839	3.140	2.569
Siderophore interacting protein, oxidoreductase		EAQ44839	MED193_22056	3.248	2.470	2.958	2.380
ABC iron transporter, ATPase		EAQ44840	MED193_22061	2.320	1.603	1.977	1.714
ABC iron/B12 (?) transporter, periplasmic substrate-binding protein	*FeBC*	EAQ44843	MED193_22076	1.876	1.537	2.340	2.608

Where MED193_19449 is highly upregulated in all four conditions tested, MED193_09570 is downregulated in *ΔphoB* G3P. However, the ATPase (GlpS, MED193_09575) of this transporter was downregulated in the *ΔphoB* mutant supplemented with G1P and G3P. Another ATPase of this transporter (GlpT, MED193_09580) and the two permeases (GlpP, MED193_09585 and GlpQ, MED193_09590) were not detected in the proteomes of WT MED193 and *ΔphoB* grown on G1P and G3P. In contrast, the components of the ABC phosphonate transporter, namely the periplasmic substrate-binding protein PhnD (MED193_19449), the ATPase PhnC (MED193_19454), and the permease PhnE (MED193_19459), as well as a haloacid dehalogenase-like phosphatase (MED193_19469) were highly upregulated in the WT MED193 and *ΔphoB* cultures supplemented with G1P and G3P. The other two transporters that were upregulated in cultures supplemented with G1P and G3P in comparison to WT MED193 +P cultures are annotated as TonB dependent outer membrane transporters. Additionally, two dehydrogenases were upregulated in WT MED193 and were highly upregulated in the WT MED193 and *ΔphoB* cultures supplemented with G1P and G3P, namely MED193_10073 (annotated as GapA) and MED193_19624 (annotated as GlpA).

5.2.5 Description of a novel periplasmic dihydroxyacetone phosphate-binding protein of *Phaeobacter* sp. MED193, correlated to the transport of G1P and G3P

Findings of this chapter and section 4.2.6 identified a periplasmic substrate-binding protein that was significantly upregulated in all growth experiments supplemented with PG, independent of the substrate chirality and Pho regulon. MED193_19449 was overexpressed by collaborators in China and substrate specificity biochemically determined. Here, MST was used to show the binding affinity of MED193_19449 towards DHAP, an oxidation product of G3P (Hartley et al., 2017). For this purpose, the protein was overexpressed and purified. Next, it was labelled in assay buffer, mixed with serially diluted concentrations of DHAP, and the binding affinity was measured (see section 2.3.4). Results were analysed and plotted (Figure 5.10). MST analysis showed a binding affinity (K_d) of 288.9 ± 47.4 µM DHAP for MED193_19449. Other tested substrates, including

P_i, phosphite, PE, PC, G1P, G3P, and 2-AEP showed no binding affinity to the MED193_19449 protein.

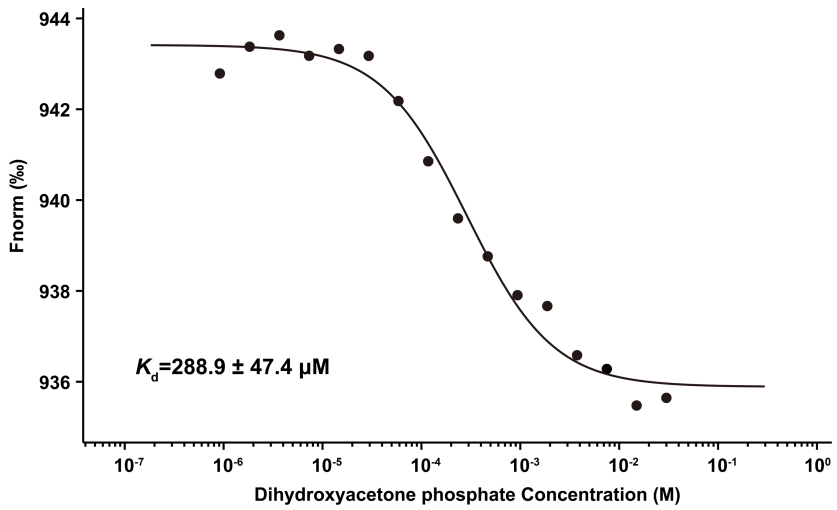

Figure 5.10: ***MicroScale Thermophoresis analysis defining binding affinity of MED193_19449 to dihydroxyacetone phosphate.***
Purified protein was mixed with serially diluted concentrations of DHAP, and binding affinity was measured. The x-axis represents the logarithmic concentration of serial diluted DHAP (M); the y-axis represents the normalised fluorescence (Fnorm). Binding affinity was calculated with K_d of 288.9 ± 47.4 µM. n=3.

As proven by MST, MED193_19449 is a novel DHAP binding protein component of a transporter belonging to the **A**TP-**B**inding **C**assette (ABC) superfamily. This superfamily includes uptake and efflux transporters (Saurin et al., 1999), where transport is energized by ATP hydrolysis. Members of the ABC superfamily are grouped by substrate specificity. Several members associated with inorganic and organic phosphate transport have been characterised and classified before (Bisson et al., 2017). In marine environments, P occurs in either inorganic or organic forms with various valance states (Karl, 2014). The DIP pool is dominated by variably protonated orthophosphates like H_2PO^{4-}, HPO_4^{2-}, and PO_4^{3-}. In these orthophosphates, P occurs in the fully oxidised (P^{5+}) valance state (Van Mooy et al., 2015; Ruttenberg, 2019).

Similarly, the DOP pool is dominated by phosphomonoesters and phosphodiesters (C-O-P) where P also occurs in its (P^{5+}) valence state (Van Mooy et al., 2015; Ruttenberg, 2019). Then, around 20 years ago, phosphonates (C-P) have been discovered in the marine DOP pool (Quinn et al., 2007; McGrath et al., 2013). In phosphonates, P exists in the (P^{3+}) valence state (Van Mooy et al., 2015; Bisson et al., 2017; Ruttenberg,

2019). Since the discovery of phosphonates in the marine environment, many proteins have been identified and characterized that are involved in the so-called C-P lyase machinery, proteins that are required for the transport and degradation of phosphonates (e.g., Rizk et al., 2006; Alicea et al., 2011; Villarreal-Chiu et al., 2012; Seweryn et al., 2015). More recently, a new type of inorganic phosphate has been reported in the DIP pool, namely phosphite (PO_3^{3-}) and hypophosphite ($H_2PO_2^-$). In phosphite, the P atom exists in the (P^{3+}) valence state, identical to phosphonates, whereas the P atom of hypophosphite occurs in its (P^{1+}) valence state (Van Mooy et al., 2015; Bisson et al., 2017; Sosa, 2017; Ruttenberg, 2019). It has recently been reported that many bacterial species can utilise phosphite and hypophosphite as a source of P, often oxidising it to phosphate first (e.g., White & Metcalf, 2004; Poehlein et al., 2013; Polyviou et al., 2015). However, only recent studies have identified high-affinity binding proteins of phosphite and hypophosphite (Bisson et al., 2017).

In the work by Bisson et al. (2017), proteins of the phosphonate/phosphite/phosphate periplasmic substrate-binding protein family Pfam12974 that bind selenophosphate (Sel-P), hypophosphite (HxtB), phosphite (PtxB), C-P substrates (C-P), and phosphonates (PhnD) have been selected to create a phylogenetic tree and demonstrate the relationship between members of this protein family. However, substrates of several substrate-binding proteins annotated as PhnD remain unclear. To understand the phylogeny of MED193_19449, the list of proteins investigated by Bisson et al. (2017) was included with MED193_19449, close homologs of this protein (retrieved through BLAST), and the C-P lyase binding protein MED193_10161 (Appendix 5.9). Next, a MSA was used to create a neighbour-joining tree, for more details see section 2.7 (Edgar, 2004a, 2004b; Capella-Gutiérrez et al., 2009; Trifinopoulos et al., 2016). The phylogenetic tree displayed a clear separation between ABC superfamily members (Figure 5.11). MED193_19449 clusters together with its homologs and apart from other groups and is closest related to the group of phosphite binding proteins (PtxB).

In this section a novel substrate-binding protein from MED193 linked to the transport of G1P and G3P is described. This substrate-binding

protein demonstrably binds DHAP, an oxidation product of G3P. Interestingly, this protein is Pho-independent and was shown to be induced by the presence of G1P and G3P. Furthermore, MED193_19449 was the highest upregulated protein in the cellular and exoproteomes of WT MED193 and *ΔphoB* supplemented with G1P, G3P, and a mixture of both enantiomers. However, it is still unclear which dehydrogenase is involved in the conversion of G3P and potentially G1P to DHAP. Candidate proteins have been identified but more work, including mutagenesis and biochemical studies, is needed to confirm the complete catabolism of G1P and G3P in MED193.

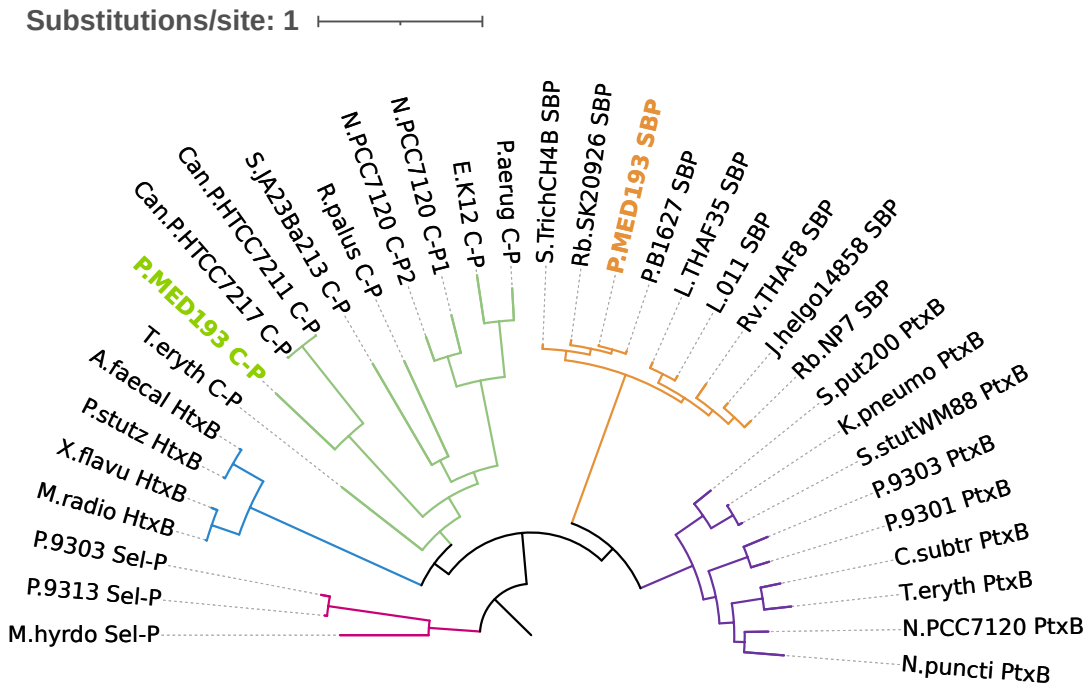

Figure 5.11: ***Phylogeny of the dihydroxyacetone phosphate binding protein from MED193 within the ATP-Binding Cassette (ABC) superfamily.***
The phylogenetic tree represents members of the ABC superfamily associated with organic phosphate transport, including phosphite (PtxB), hypophosphate (HtxB), selenophosphate (Sel-P), C-P lyase substrates (C-P), and unknown substrates of proteins annotated as phosphonate binding proteins (SBP). The DHAP binding protein of MED193 (P.MED193 SBP) clusters within the group of other SBPs of unknown substrates. PtxB, associated with phosphite binding, is related closest to SBPs. Branch length represents the expected number of substitutions per site (see scale bar).

5.3 Discussion

Membrane glycerophospholipids are ubiquitous in all three domains of life. However, structural differences have been discovered between Bacteria and Archaea (Suzumura, 2005; Schouten et al., 2013; Caforio &

Driessen, 2017; Moellering et al., 2017; Harayama & Riezman, 2018; Coleman et al., 2019; Law & Zhang, 2019; Exterkate et al., 2021).

The results of section 4.2.6 showed that MED193 can utilise a mixture of G1P and G3P as a sole source of P. Since this bacterium was first isolated from the spatially P-depleted Mediterranean Sea (Lazzari et al., 2016), it qualifies as a model organism for P-limitation studies. Adaptation to P-limitation includes mechanisms to acquire P_i from organic P-sources (Tetu et al., 2009; Cox & Saito, 2013; Lin et al., 2018), including membrane phospholipids that are released by marine organisms, i.e., archaea, upon cell death. It seems likely that marine bacteria can scavenge P from these 'waste products'. Archaea conduct crucial processes within the microbial loop, such as ammonia oxidation (Jarrell et al., 2011). In addition, new studies suggest that archaea contribute more than 20% of the total marine microbial community (Karner et al., 2001). For example, in the Mediterranean seas, archaea account for around 40-60% of the prokaryotic cell count (Fuhrman & Campbell, 1998; Chaban et al., 2006). Archaea are ubiquitous and play an important part in the marine food web. Therefore, more research is needed to understand the interactions between archaea and other microorganisms. This work sheds some light on how the marine model organism *Phaeobacter* sp. MED193 can acquire P from bacterial and archaeal phospholipids.

For the first time, we used several methods, including lipidomics to study the membrane lipid composition of MED193, a proteomic approach to identify enzymes that are required for the acquisition of P_i from G1P and G3P, and enzyme kinetics to determine the substrate of a periplasmic binding protein involved in PG transport. Furthermore, apart from the wild type (WT MED193), we studied the lipidome and proteome of a *phoB* deletion mutant (*ΔphoB*) to understand if the transport of PG is Pho regulated.

First, the findings of this chapter confirmed that pre-starved -P WT MED193 and *ΔphoB* cultures can grow on G1P and G3P as a sole source of P and equally use both compounds (Figure 5.3). There was no significant difference between the growth of WT MED193 G1P and WT MED193 G3P, as well as *ΔphoB* G1P and *ΔphoB* G3P. Previous studies have demonstrated that G3P can be used as a sole source of P by various bacteria. For

example, the growth of several *Pseudomonas* strains supplemented with G3P showed no distinction from cultures grown on P_i (Lidbury et al., 2017). Wild type *Staphylococcus aureus* was grown on 58 P-containing compounds, including a mixture of G1P and G3P, and G3P only (Kelliher et al., 2020). Here, endpoint OD_{600} was reduced by ~5-15% in cultures supplemented with PG in comparison to control cultures grown on P_i. In contrast, the difference between endpoint OD_{540} of WT MED193 cultures supplemented with G3P and P_i was more than 50%. Importantly, *S. aureus* was not exposed to a prolonged period of P-starvation as the cultures in this study. Furthermore, the final OD_{600} of a *S. aureus phoB* deletion mutant grown on G3P was reduced by ~ 30% in comparison to the wild type, similar to the results obtained here. To date, no growth experiments in other prokaryotes have been conducted using G1P as a sole source of P.

Next, alkaline phosphatase activity was measured to investigate if phosphatases are required for the growth of pre-starved WT MED193 and *ΔphoB* cultures on PG (Figure 5.4). As expected, high alkaline phosphatase activity was measured in P-deplete WT MED193 cultures, where alkaline phosphatase activity exceeded 12.5 μM OD_{540}^{-1} min^{-1} for samples incubated with *p*NPP and 7 μM OD_{540}^{-1} min^{-1} for samples incubated with *p*NPPC. However, in all other conditions, alkaline phosphatase activity stayed below 2.5 μM OD_{540}^{-1} min^{-1} independent of the addition of the phosphate monoester or phosphate diester. This suggests that the G1P and G3P pathway doesn't induce general phosphatase activity. In addition, the low alkaline phosphatase activity measured in P-deplete *ΔphoB* cultures confirms that silencing the Pho regulon abolishes almost all phosphatase activity.

Exploring the membrane lipid composition of WT MED193 and *ΔphoB* cultures after 24 hours of growth, data confirmed that glycerophospholipids were restored in pre-starved -P WT MED193 cultures grown on G1P, G3P, and P_i and lipid remodelling was abolished in the *ΔphoB* mutant (Figure 5.5). Independent of the substrate chirality both G1P and G3P can be used to reinstate growth and membrane phospholipids. There was no significant difference in the relative abundance of lipids between WT MED193 and between *ΔphoB* cultures

supplemented with a source of P after P-starvation (*t*-test, *p*-value <0.05). This confirms that P_i and both PG forms can equally reinstate or preserve glycerophospholipids. Comparing the lipid composition of *ΔphoB* cultures, the relative abundance of PtdGro was around three times higher in cultures supplemented with P_i, G1P, and G3P than in P-starved cultures. Studies using isotope labelled G1P and G3P would help to understand if both compounds are equally incorporated into the backbone or polar headgroup of membrane phospholipids.

To investigate the response of MED193 to G1P and G3P, a proteomic approach was used to determine key enzymes that are potentially involved in the catabolism of both P-compounds. Thereafter, LC-MS/MS was used to identify proteins of WT MED193 and *ΔphoB* that are synthesised during the mid-exponential growth phase when cultures were supplemented with G1P and G3P as a sole source of P. Comparing WT MED193 and *ΔphoB* cellular and exoproteomes to the proteome of the control WT MED193 +P culture, proteins were highlighted that were specifically induced by PG. Here, the most upregulated protein in WT MED193 and *ΔphoB* cultures supplemented with G1P and G3P was MED193_19449. This protein is annotated as PhnD, a phosphonate binding protein of an ABC transporter. The operon consists of another four proteins, including an ATPase (PhnC, MED193_19454), two permeases (PhnE MED193_19459 and MED193_19464) and a putative phosphatase of the haloacid dehalogenase hydrolase (MED193_19469). Of the five proteins of this operon, MED193_19464 was not detected in the proteome of WT MED193 and *ΔphoB*, implying that both permeases are not required for the functionality of the ABC transporter. MS/MS counts confirmed that this operon is induced by G1P and G3P (Table 5.4). Where proteins of this operon were detected in cultures supplemented with G1P and G3P, these proteins were not found in control cultures grown on P_i.

It is noteworthy, that, although proteomics allows for large-scale and high-throughput analyses of proteomes, there are still significant limitations to this method. One of these limitations is the complexity of the proteome. Several million proteins have been discovered to date and it is unlikely that the whole proteome of an organism can be detected through proteomics (Betzen et al., 2015). It seems likely, that proteomics primarily

detects highly abundant proteins but finds its limits in detecting lower abundant components (Chandramouli & Qian, 2009). Concerning data discussed in this work, it is important to factor in detection limits for proteins that are not or barely detectable in the proteomes of MED193 and *ΔphoB*.

Interestingly, MED193_19469 is a homolog (Seq.ID 30%, e-value $4e^{-07}$) of Rv1692, a recently described G3P phosphatase of *Mycobacterium tuberculosis* (Larrouy-Maumus et al., 2013). Here, Rv1692 was shown to be involved in phospholipid polar headgroup recycling, degrading G3P to glycerol and P_i. In comparison to MED193, *M. tuberculosis* is not known to use lipid remodelling as a P-stress response. The predicted pathway in *M. tuberculosis* indicates that the interaction of ten proteins is needed to recycle phospholipids.

Table 5.4: ***MS/MS count of phosphonate ABC transporter proteins detected in cellular proteome of WT MED193 and ΔphoB.***
MED193_19449 (PhnD), periplasmic substrate-binding protein; MED193_19454_PhnC, ATPase; MED193_19459 (PhnE), permease; MED193_19469, haloacid dehalogenase hydrolase.

Protein / MS/MS count	*PhnD, MED193_10071*	*PhnC, MED193_10071*	*PhnE, MED193_19624*	*MED193_19469*
MS/MS count *ΔphoB* G1P	58	64	20	11
MS/MS count *ΔphoB* G3P	51	48	13	10
MS/MS count *ΔphoB* +P	0	0	0	0
MS/MS count WT G1P	70	58	29	9
MS/MS count WT G3P	98	80	26	10
MS/MS count WT +P	4	0	0	0

All findings indicated that MED193_19449 is the substrate-binding protein of an ABC transporter involved in the uptake of G1P and G3P. Therefore, our collaborators in China overexpressed this protein and tested the binding affinity of MED193_19449 towards various substrates, including G1P, G3P, glycerol, 2-AEP, and DHAP. However, MST confirmed binding of MED193_19449 for DHAP only, with an affinity K_d of 288.9 ± 47.4 µM (Figure 5.10). DHAP is the oxidation product of G1P and G3P.

Oxidation of PG is catalysed by a G3PDH (Hartley et al., 2017). It has been demonstrated that human and *Dunaliella salina* G3PDH can work bidirectionally, also reversing the oxidation process (Ou et al., 2006; Chen et al., 2012). For example, the G3PDH in humans is required for the conversion of DHAP to G3P, an intermediate product of the Embden-Meyerhof glucose glycolysis pathway (Ou et al., 2006).

However, in humans and *E. coli*, uptake of G3P doesn't require a preceding oxidation step as required in MED193. In *E. coli*, a protein named GlpT functions as a G3P/P_i antiporter and is driven by a P_i gradient (Huang et al., 2003; Lemieux et al., 2004). In humans, two orthologs of GlpT exist, namely a G3P permease that transports G3P into mitochondria, and a microsomal G6P transporter, found in the lungs and kidneys (Bartoloni et al., 2000; Lemieux et al., 2004; Almqvist et al., 2004). However, the GlpT transporter protein from *E. coli* doesn't have a homolog in MED193. Two different dehydrogenases were detected in the exo- and cellular proteome of WT MED193 and *ΔphoB*, a G3PDH (MED193_19624, GlpA) and a glyceraldehyde-3-phosphate dehydrogenase (GAPDH, MED193_10071, GapA). MS/MS count showed that the detection level of both proteins was higher in WT MED193 and *ΔphoB* cultures supplemented with G1P and G3P than in control cultures grown on P_i.

Table 5.5: ***MS/MS count of G3PDH detected in the exo- (EP) and cellular proteome (CP) of WT MED193 and ΔphoB.***
MED193_10071 (GapA), glyceraldehyde-3-phosphate dehydrogenase; MED193_19624 (GlpA), G3P dehydrogenase.

Protein / MS/MS count	*GapA, MED193_10071 EP*	*GapA, MED193_10071 CP*	*GlpA, MED193_19624 CP*
MS/MS count *ΔphoB* G1P	9	60	18
MS/MS count *ΔphoB* G3P	15	57	19
MS/MS count *ΔphoB* +P	3	12	8
MS/MS count WT G1P	29	74	32
MS/MS count WT G3P	9	54	54
MS/MS count WT +P	11	23	9

However, only the GAPDH GapA (MED193_10071) was detected in the exoproteome. Here, GapA was significantly upregulated in WT MED193 G1P cultures solely (fold change +2.22, p-value <0.05, logFC 2, Appendix 5.2). By comparison, both GapA and GlpA were significantly upregulated in the cellular proteome of WT MED193 and *Δpho* cultures supplemented with G1P and G3P, confirmed by higher MS/MS count in these conditions (Table 5.5, Appendix 5.1, Appendix 5.3, Appendix 5.5, Appendix 5.7). Specifically, GlpA had a higher detection level in WT MED193 cultures grown on G3P.

We hypothesise that an extracellular, but membrane bound G3PDH (MED193_19624) dehydrogenates G3P to DHAP in *Phaeobacter* sp. MED193 (Figure 5.12). G1P is potentially dehydrogenated to DHAP by an extracellular GAPDH (MED193_10071). Thereafter, MED193_19449 binds DHAP and transports it across the inner membrane. Intracellularly, a membrane-bound G3PDH (MED193_19624) reverses the oxidation process and converts DHAP back to G1P and G3P, respectively. Finally, a G3P phosphatase (MED193_19469) of the HAD family hydrolases G1P and G3P, hereby releasing P_i.

However, more studies are needed to confirm this hypothesis, including biochemical studies of both dehydrogenases, G3PDH (MED193_19624) and GAPDH (MED193_10071), and the G3P phosphatase (MED193_19469). Furthermore, phylogenetic studies revealed that MED193_19449 and its homologs form a new group of substrate-binding proteins within the ABC transporter superfamily (Figure 5.11). Further studies are needed to define if there are any more substrates of this binding protein, and crystallography can help to identify key amino acids of the active site of MED193_19449. Finally, a combination of these results will help to complement the phylogenetic tree and describe this new ABC transporter group.

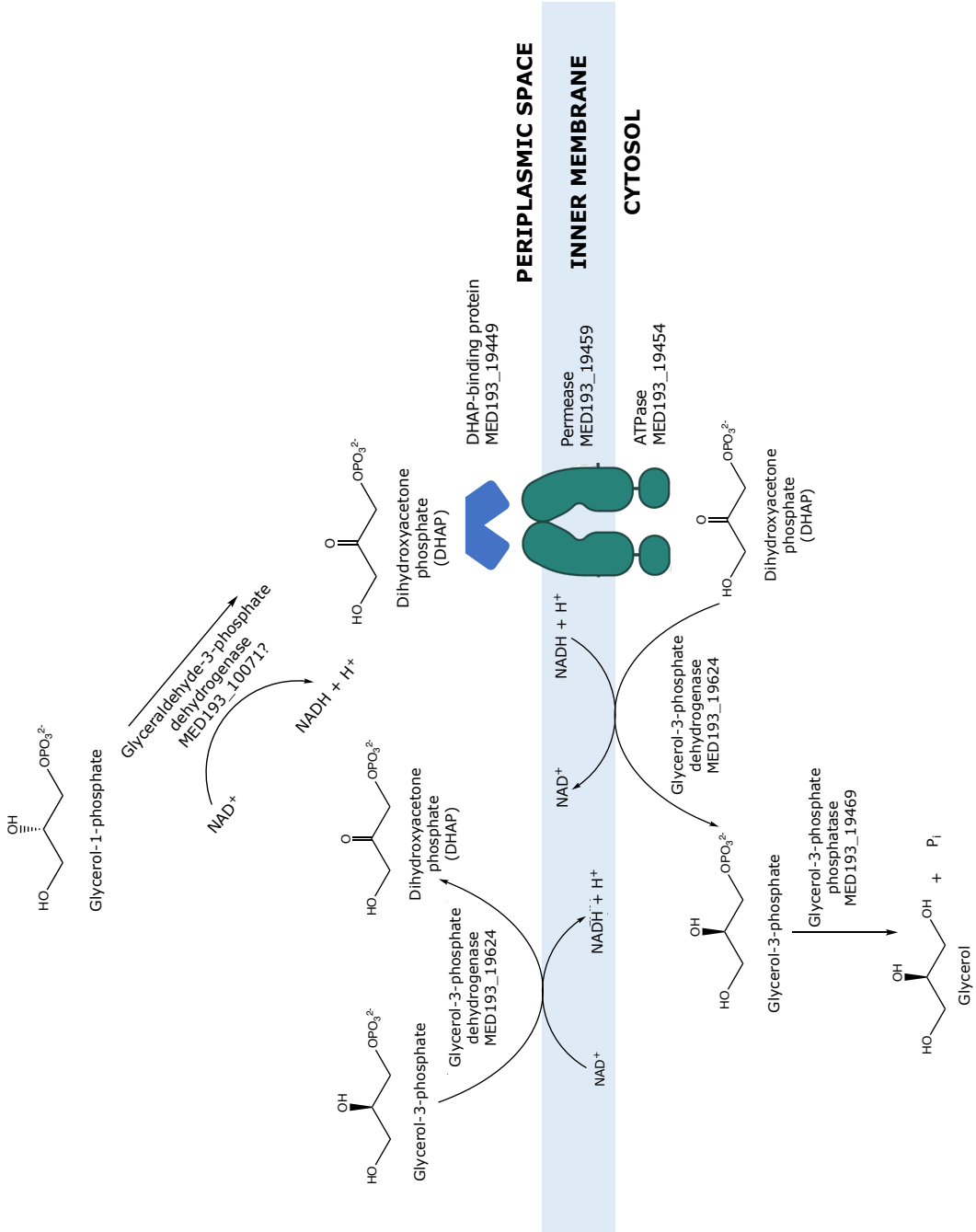

Figure 5.12: ***Proposed pathway for the degradation of G3P and G1P in MED193.***
First, G3P is oxidised to DHAP by a membrane-bound G3PDH (MED193_19624). In contrast, G1P is converted to DHAP by a GAPDH (MED193_10071?). Thereafter, MED193_19449 binds DHAP and transports it, together with the permease MED193_19459 and the ATPase MED193_19454, across the inner membrane. Here, a membrane-bound G3PDH (MED193_19624) reverses the oxidation and converts DHAP back to G3P and G1P (represented by G3P only). Finally, a G3P phosphatase (MED193_19469) hydrolyses G3P, hereby releasing glycerol and P_i. Adapted from Larrouy-Maumus et al., (2013) and Hartley et al., (2017).

CHAPTER 6 HUNTING THE ELEMENTS – UNRAVELLING THE BIOCHEMISTRY OF PHOSPHATASES IN *SYNECHOCOCCUS* SP. WH8102

6.1 Introduction

Even though phosphorus (P) is one of the most common elements in the Earth's crust, its availability is limited. P is essential for all living organisms (Koolman & Röhm, 2019); hence, P-limitation can drastically influence growth. In marine environments, P occurs in different inorganic and organic forms (Karl, 2014). Inorganic phosphate (P_i), the preferred source of P for organisms, constitutes only a small fraction of the total P pool, which is dominated by dissolved organic P (Wu et al., 2000; Cavender-Bares et al., 2001; Kelly et al., 2013; Karl, 2014).

As a result of limiting P-environments, organisms have had to adapt to those conditions, including synthesis of specific P_i acquisition systems (Scanlan et al., 1993; Hirani et al., 2001; Pitt et al., 2010; Cox & Saito, 2013), the development of mechanisms to reduce P-requirements (e.g., lipid remodelling) (Van Mooy et al., 2006, 2009; Sebastián et al., 2016), or the ability to utilise alternative organic P-sources (Tetu et al., 2009; Cox & Saito, 2013; Lin et al., 2018). These adaptation mechanisms are of great importance since major parts of the global oceans are P-deplete (Ammerman et al., 2003; Paytan & McLaughlin, 2007; Karl, 2014). Here, the marine primary production is dominated by photoautotrophic organisms (Field et al., 1998; Flombaum et al., 2013; Grob et al., 2013).

The two major primary producers are members of the genera *Synechococcus* and *Prochlorococcus*. Even though *Synechococcus* is more widely distributed, its abundance is generally about one order of magnitude lower than *Prochlorococcus* in regions where they co-occur (Li, 1995; Ahlgren & Rocap, 2012; Flombaum et al., 2013). Members of the marine *Synechococcus* genus are characterised as small, unicellular, and ovoid cylindrical cyanobacteria (Waterbury et al., 1986). In addition, *Synechococcus* is widely distributed in the global marine environment, with habitats ranging from tropical waters to the polar circle. Adaptation to various environmental conditions is evident, resulting in a rich diversity of

strains and ecological niche adaptation (Scanlan et al., 2009; Palenik, 2012). Within the genus *Synechococcus*, the development of generalists and specialists resulted in the evolution of new variants which are divided into several lineages and clades. It is suggested that all *Synechococcus* strains share a 'core' genome, a potential clade-specific genome and a strain-specific genome (Palenik, 2012).

Synechococcus sp. WH8102 (hereafter *Syn.* WH8102), a model organism of *Synechococcus* clade III, dominates warm and oligotrophic environments (Palenik et al., 2003; Scanlan et al., 2009; Ahlgren & Rocap, 2012). The P-stress response of *Syn.* WH8102 has been studied extensively (e.g., Hirani et al., 2001; Scanlan & West, 2002; Palenik et al., 2003; Moore et al., 2005; Tetu et al., 2009). Interestingly, one of the adaptation mechanisms of *Syn.* WH8102 to limiting P-conditions is the synthesis of different phosphatases to release P_i from organic P-sources (Aiba & Mizuno, 1994; Hirani et al., 2001; Suzuki et al., 2004; Moore et al., 2005; Tetu et al., 2009; Casey et al., 2016). Bioinformatics analysis revealed that for this purpose, *Syn.* WH8102 possesses multiple genes that encode four putative 'alkaline' phosphatases (SYNW0120, SYNW0196, SYNW2391, SYNW2390) (Palenik et al., 2003; Tetu et al., 2009) and one PhoX-type phosphatase (SYNW1799) (Scanlan et al., 2009; Kathuria & Martiny, 2011). Whilst on the face of it the function of these enzymes during P-limitation is relatively well understood, in fact, nothing is known about their biochemistry, such as metal cofactors and substrate specificity. For example, zinc, calcium, and iron are believed to be common metal cofactors for most 'alkaline' phosphatases (Majumdar et al., 2005; Shaked et al., 2006; Cox & Saito, 2013; Yong et al., 2014).

In this chapter, we used a combination of bioinformatics studies, such as sequence analysis and protein modelling, and biochemical analysis to confirm the presence of a PhoD and PhoX type phosphatase in *Syn.* WH8102.

6.2 Results

Syn. WH8102 possesses four putative 'alkaline' phosphatases (SYNW0120, SYNW0196, SYNW2390, and SYNW2391), and one PhoX-type phosphatase (SYNW1799). Although the general function of these

phosphatases is relatively well understood, nothing is known about their biochemistry, including metal requirement and substrate specificity. In this chapter, a combination of bioinformatics and protein overexpression was used to answer some of these questions. Moreover, only four of these phosphatases SYNW0196, SYNW1799, SYNW2390, and SYNW2391 were focused upon. Even though SYNW0120 is annotated as a putative alkaline phosphatase-like protein, with an estimated molecular weight of only 24 kDa, conserved domain analysis revealed that the protein most likely belongs to the DedA family (Lu et al., 2020), consisting of uncharacterised membrane proteins. This protein family is associated with various cell processes, such as antibiotic resistance, cell division, temperature sensitivity, and altered membrane composition (Doerrler et al., 2013; Kumar & Doerrler, 2014; Panta et al., 2019), and hence was left out of the analysis here.

First, to gain a better understanding of the four phosphatases SYNW0196, SYNW1799, SYNW2390, and SYNW2391, the software tool ProtParam in Expasy was used to retrieve some biochemical information about these phosphatases (Table 6.1) (Gasteiger et al., 2005). The ProtParam data showed that the number of amino acids ranges from 576 to 750 and that all four proteins are relatively large with a minimum size of 63 kDa and a maximum size of 80 kDa. The theoretical isoelectric point (pI) is similar for all four proteins and lies within the range of 4.1 and 5.0. At this pH, the net charge of the protein is zero. For example, if the pH of the purification buffer is higher than the pI of the protein, the protein charge becomes negative. The charge of the protein can be important for affinity purification (Ritchie, 2012). Sulphur atoms count is important for proper calculation of protein concentration through inductively coupled plasma optical emission spectrometry (ICP-OES) (Suzuki et al., 2014). The number of sulphur atoms was 20 in SYNW1799 and between six and nine in the other three phosphatases. In addition, the instability index estimates the stability of the protein in a test tube. If the calculated value is below 40, the protein is most likely stable, whereas a value higher than 40 indicates that the protein might be unstable (Gasteiger et al., 2005). According to the calculated instability index, only SYNW1799 is unstable, indicating that this protein might be difficult to overexpress and purify.

Table 6.1: ***Parameters retrieved from the ProtParam tool by Expasy regarding the Synechococcus phosphatases SYNW0196, SYNW2390, SYNW2391, and SYNW1799.***
Parameters include the number of amino acids, predicted molecular weight of the protein in Dalton, the theoretical isoelectric point (pI), number of Sulphur atoms, and the instability index which determines if a protein is probably stable (<40) in a test tube.

Parameters	*SYNW0196*	*SYNW2390*	*SYNW2391*	*SYNW1799*
Number of amino acids	749	750	576	716
Molecular weight (Da)	80393.83	79947.12	63036.21	76186.89
Theoretical pI	4.26	4.16	4.39	5.00
Sulphur atoms	9	8	6	20
Instability index	38.07	31.44	29.15	43.09
Stability	stable	stable	stable	unstable

6.2.1 Protein overexpression and purification

Protein biochemistry is a field of research that is used to characterise proteins like pH optimum, metal requirements, substrate specificity, and protein localization. Therefore, overexpression and purification of candidate proteins are required. Plasmids for all four phosphatases (SYNW0196, SYNW1799, SYNW2390, and SYNW2391) were synthesised via GeneArt™. Sequences were codon optimised for *E. coli* and sequences of SYNW0196, SYNW2390, and SYNW2391 cloned into a pET151/D-TOPO expression vector with N-terminal His-Tag (see section 2.2.1). These expression vectors were then transformed into the chemically competent T7 *E. coli* expression strain BL21 (DE3) (see section 2.2.4). Importantly for purification, the protein must be soluble. Therefore, overexpression was tested in various growth and expression conditions, as summarized in Table 6.2 (a detailed list can be found in Appendix 6.1) and solubility verified by SDS-PAGE (see 2.2.8). In the beginning, the expression of SYNW0196 and SYNW2391 resulted in insoluble protein only (Table 6.2a, e). The insoluble fraction mostly consists of inclusion bodies, containing misfolded proteins, and hydrophobic membrane proteins (Trimpin & Brizzard, 2018). Because of this, the codon optimised sequences of SYNW0196 and SYNW2391 were cloned into a pMAL c4x vector which co-expressed a maltose-binding protein that can increase the solubility of the overexpressed protein (see section 2.2.2.1). In doing so the expected protein size increased by around 43 kDa. Thereafter, the solubility of

SYNW0196 and SYNW2391, cloned into a pMAL c4x vector, was reached in three overexpression conditions: in self-inducing minimal medium (MDA-5052), self-inducing rich medium (ZYM-5052), and self-inducing terrific broth (TB-5052) (Table 6.2b, f). SYNW2390 was soluble in almost all conditions tested (Table 6.2). However, SYNW1799 could not be overexpressed in any of the conditions, independent of the expression vector and gene sequence used (for more details see section 2.2.3, Table 6.2c, d).

Table 6.2: ***Conditions used for overexpression of Synechococcus sp. WH8102 phosphatases in E. coli.***
The first column lists conditions used for overexpression: Formedium™; LB, lysogeny broth; M9, minimal standard medium; MDA-5052, minimal self-inducing medium; TaKaRa, LB and M9 co-expressed with different TaKaRa chaperones; TB-5052, self-inducing terrific broth; ZYM-5052, rich self-inducing medium. Genes of phosphatases were cloned in different expression vectors: SYNW0196, pET151/D-TOPO (a) and pMAL c4x (b); SYNW1799, pET151/D-TOPO (c) and pet22b(+) (d); SYNW2390, pET151/D-TOPO; SYNW2391, pET151/D-TOPO (e) and pMAL c4x (f). Protein was either insoluble, soluble (highlighted in green), or not expressed (no protein).

Protein / Condition	**SYNW0196**	**SYNW1799**	**SYNW2390**	**SYNW2391**
Expression vector and strain	pET151/D-TOPO (a) pMAL c4x (b)	pET151/D-TOPO (c) pet22b(+) (d)	pET151/D-TOPO	pET151/D-TOPO (e) pMAL c4x (f)
Formedium™: various temperatures, self-inducing	insoluble protein (a)		insoluble protein	insoluble protein (e)
LB: various temperatures, IPTG concentrations, and additives	insoluble protein (a, b)		soluble protein	insoluble protein (e, f)
M9: various temperatures, IPTG concentrations, and additives	insoluble protein (a, b)		soluble protein	insoluble protein (e, f)
MDA-5052: 18 °C, 18 hours, self-inducing	soluble protein (b)	no protein (c, d)	soluble protein	soluble protein (f)
TaKaRa: LB and M9, various temperatures, and IPTG concentrations				insoluble protein (e)
TB-5052: 18 °C, 18 hours, self-inducing	soluble protein (b)	no protein (c, d)	soluble protein	soluble protein (f)
ZYM-5052: 18 °C, 18 hours, self-inducing	soluble protein (b)	no protein (c, d)	soluble protein	soluble protein (f)

Not only is protein solubility essential, but protein yield is also another important criterion for protein purification since small amounts of protein can get lost during the purification process. It is of great advantage if an overexpression condition results in a high protein yield. Comparison

of the three self-inducing conditions mentioned above showed that the highest protein yield was reached in the self-inducing rich medium (ZYM-5052), for the three phosphatases SYNW0196, SYNW2390, and SYNW2391 (Figure 6.1B). A detailed protocol for the overexpression of all three phosphatases can be found in section 2.2.6.

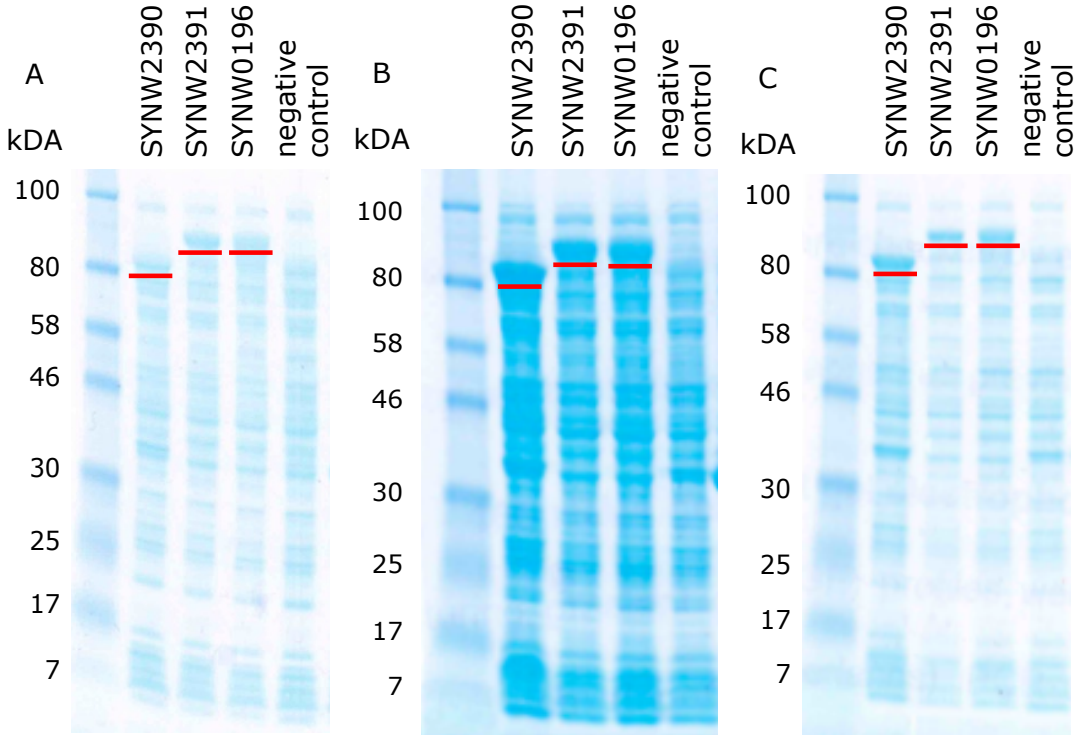

Figure 6.1: ***Protein overexpression of phosphatases SYNW0196, SYNW2390, and SYNW2391 in three different self-inducing media conditions.***
Protein yield reached after 25 hours of overexpression using either MDA-5052 (A), ZYM-5052 (B), or TB-5052 (C). SDS-PAGE gel of whole-cell protein extracts.

Although a high protein yield was reached, the SYNW2390 phosphatase could not be purified using the same protocol as described in section 2.2.10 and 2.2.11. SDS-PAGE revealed that the His-Tag was cleaved off during the purification process (data not shown). Since protein purification was unsuccessful, bioinformatic analysis was used to predict metal requirements and functions of the four phosphatases SYNW0196, SYNW1799, SYNW2390, and SYNW2391. Interestingly, only SYNW0196 and SYNW2390 are homologs (30% Seq.ID, e-value $9e^{-10}$). However, where SYNW0196 is annotated as a PhoD-type phosphatase, SYNW2390 doesn't share the same conserved domain (Lu et al., 2020). Further examination of all four phosphatases was needed.

6.2.2 Bioinformatics analysis and homology modelling of SYNW0196, a PhoD phosphatase

To further investigate the phosphatase SYNW0196 using bioinformatics tools, Phyre^2 was used to search for crystallised and characterised homologs of the protein. The Phyre^2 protein fold recognition folder predicted 34% identity with 59% coverage (444 residues with 100% confidence) with the PhoD phosphatase of *Bacillus subtilis* (Kelley et al., 2016). Furthermore, SYNW0196 had 11% identity with a purple acid phosphatase (PAP) of *Ipomoea batatas* (sweet potato). The PhoD phosphatase family consists of extra-cellular phosphodiesterases which also have phosphomonoesterase activity (Yamane & Maruo, 1978). Protein crystallography revealed that the *B. subtilis* PhoD phosphatase requires one Fe^{3+} and two Ca^{2+} ions for activity (Rodriguez et al., 2014). In comparison, PAPs hydrolyse phosphate monoesters and phosphoanhydride bonds and require a Fe^{3+}-Mn^{2+} or a Fe^{3+}-Zn^{2+} co-factor for activity (Klabunde et al., 1996; Schenk et al., 2005).

To determine if SYNW0196 belongs to the PhoD or PAP family, sequences of five close homologs of SYNW0196, sequences of four previously described PhoD type phosphatases, and sequences of three characterised PAPs were extracted (Appendix 6.2), and multiple sequence alignment (MSA) was performed using MUSCLE with default settings (Edgar, 2004a, 2004b; Lemoine et al., 2019). The alignment shows a clear separation between the PhoD type phosphatases and the PAPs (Figure 6.2). In all three PAPs, only three of the conserved amino acids of the active site coincide with PhoD type phosphatases, namely Asp163, Tyr166, and His324 (*I. batatas*). This clearly shows that SYNW0196 belongs to the PhoD type phosphatases. In addition, the alignment shows that SYNW0196 possesses eight of the nine conserved amino acids that are involved in metal coordination in the catalytic site. Only the Ca^{2+}-coordinating Asn216 of *B. subtilis* is replaced by an aspartic acid (Asp212) in *Syn.* WH8102. Intriguingly, this difference was found in all five homologs of SYNW0196, distinguishing cyanobacteria from heterotrophic bacteria. This variation has been described before. Nonetheless, aspartic acid can bind Ca^{2+} as effectively as asparagine (Rodriguez et al., 2014).

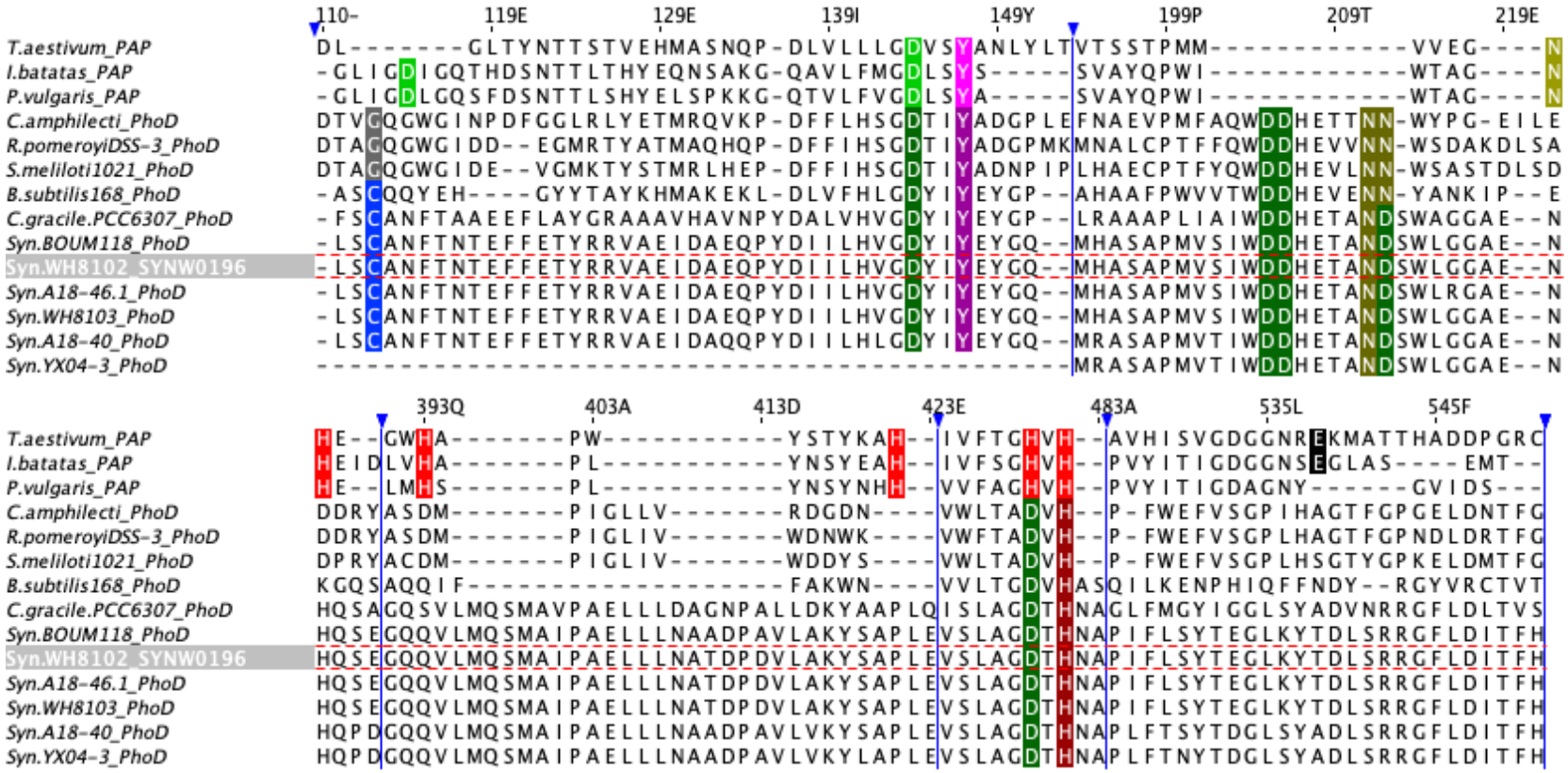

Figure 6.2: ***Multiple sequence alignment of Synechococcus sp. WH8102 phosphatase SYNW0196 with PhoD and purple acid phosphatases.*** *MSA of SYNW0196 and five close homologs with two characterised phosphatases; a PhoD phosphatase from Bacillus subtilis (PDBe 2YEQ, Rodriguez et al., 2014) and a purple acid phosphatase from Ipomoea batatas (PDBe 1XZW, Schenk et al., 2005). Coordinating amino acids of the catalytic site of SYNW0196 are highlighted: Asn169 in dark yellow; Asp144, Asp163, Asp164, Asp170, and Asp221 in dark green; Cys112 in blue; His223 in dark red; and Tyr210 in dark purple. Coordinating amino acids of the catalytic site of I. batatas are highlighted: Asn200 in yellow; Asp134 and Asp163 in light green, His201, His285, His295, His322, and His324 in light red; and Tyr147 in light purple.*

Since multiple sequence alignment demonstrated that SYNW0196 is most likely a member of the PhoD phosphatase family, the predicted model of SYNW0196 based on the *B. subtilis* PhoD, as well as the *B. subtilis* PhoD model were extracted from the Phyre[2] server and the RCSB protein data bank (rcsb.org, Berman et al., 2000; Burley et al., 2021). Next, UCSF Chimera (Pettersen et al., 2004) was used to analyse both PhoD models. Thereafter, MatchMaker (with default settings) was used to overlay the models of SYNW0196 and *B. subtilis* PhoD. Then, the sequence of SYNW0196 was used to label all amino acids of the catalytic site that are involved in the coordination of the $2Ca^{2+}$-Fe^{3+} metal-cofactor and the phosphate (PO_4^{3-}) ion (Figure 6.3).

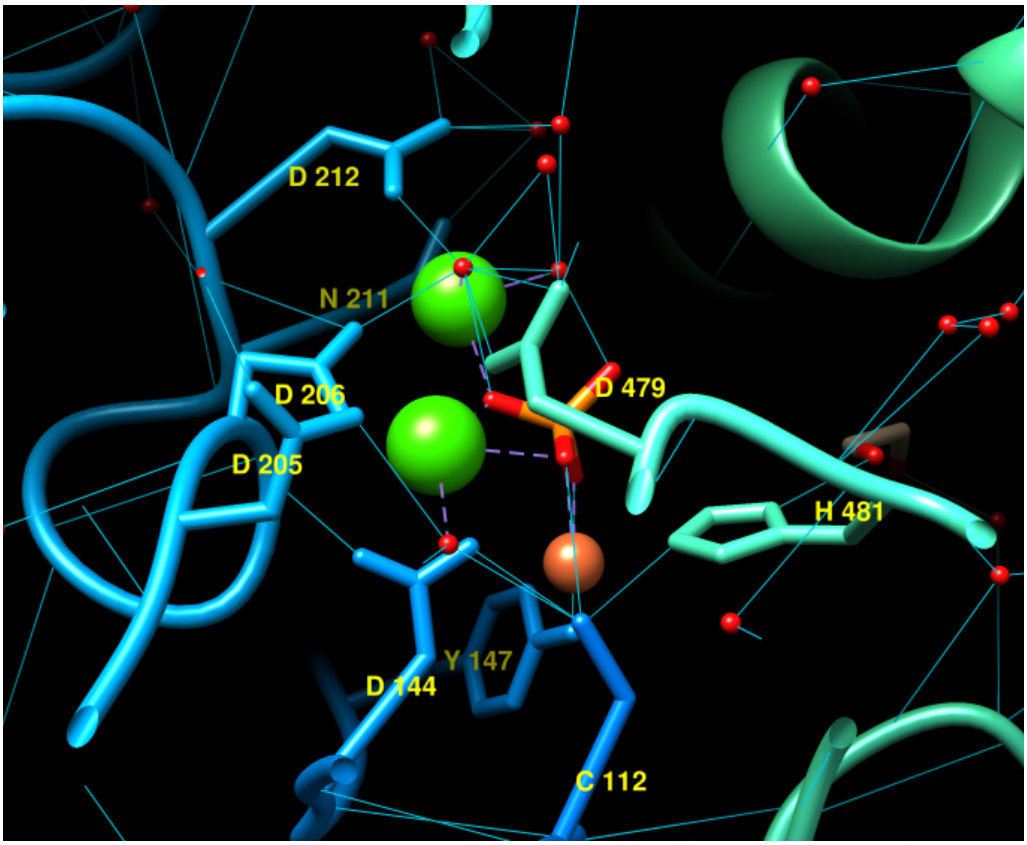

Figure 6.3: ***Predicted catalytic site of SYNW0196.***
The active site of SYNW0196 is based on the B. subtilis PhoD (PDBe 2YEQ, Rodriguez et al., 2014). Amino acids that coordinate two Ca^{2+} ions (green) and one Fe^{3+} (orange), and the PO_4^{3-} ion (orange tetrahedral shape with red tips) are labelled in yellow. Molecular graphics and analyses were performed with the UCSF Chimera package. Chimera is developed by the Resource for Biocomputing, Visualization, and Informatics at the University of California, San Francisco (supported by NIGMS P41-GM103311).

The findings in this section confirm that SYNW0196 is most likely a member of the PhoD phosphatase family. However, more biochemical

studies are necessary to assess its substrate specificity, verify the metal requirements of this phosphatase, and determine its localisation.

6.2.3 Bioinformatics analysis and homology modelling of SYNW1799, a PhoX phosphatase

To gain a better understanding of the phylogeny of SYNW1799, the same approach was used as before (see section 6.2.2). The Phyre[2] protein fold recognition server predicted 33% identity with 73% coverage (523 residues with 100% coverage) with the PhoX-type phosphatase of *Pseudomonas fluorescens* Pf0-1. PhoX-type phosphatases form a family of alkaline phosphatases that are commonly found in the periplasm of bacteria (Wanner, 1996; Yong et al., 2014). With few exceptions (Wu et al., 2007), PhoX phosphatases have been reported to hydrolyse solely phosphate monoester bonds with broad substrate specificity (Majumdar et al., 2005; Zaheer et al., 2009; Sebastián & Ammerman, 2011). In addition, prior studies have demonstrated that PhoX phosphatases require two Fe^{3+} and three Ca^{2+} ions for enzyme activity (Wu et al., 2007; Zaheer et al., 2009; Kathuria & Martiny, 2011; Yong et al., 2014).

To confirm that SYNW1799 belongs to the PhoX family, sequences of six close homologs of SYNW1799 and sequences of four previously described PhoX phosphatases were extracted (Appendix 6.3), and MSA was performed using MUSCLE with default settings. The alignment showed clear conformity between all sequences examined (Figure 6.4). This verifies that SYNW1799 belongs to the PhoX-type phosphatases. The alignment showed that SYNW1799 possesses all conserved amino acids that have been demonstrated to be involved in the metal cofactor coordination in the active site. PhoX phosphatases have been subdivided into two groups, depending on the conserved amino acid adjacent to the Ca^{2+}-binding Asp575. Where phosphatases with a flanking glycine belong to group I, phosphatases with a neighbouring asparagine belong to group II (Zaheer et al., 2009). In this analysis, only the *P. fluorescens* and *Pasteurella multocida* PhoX phosphatases belong to group I, all other phosphatases are members of group II.

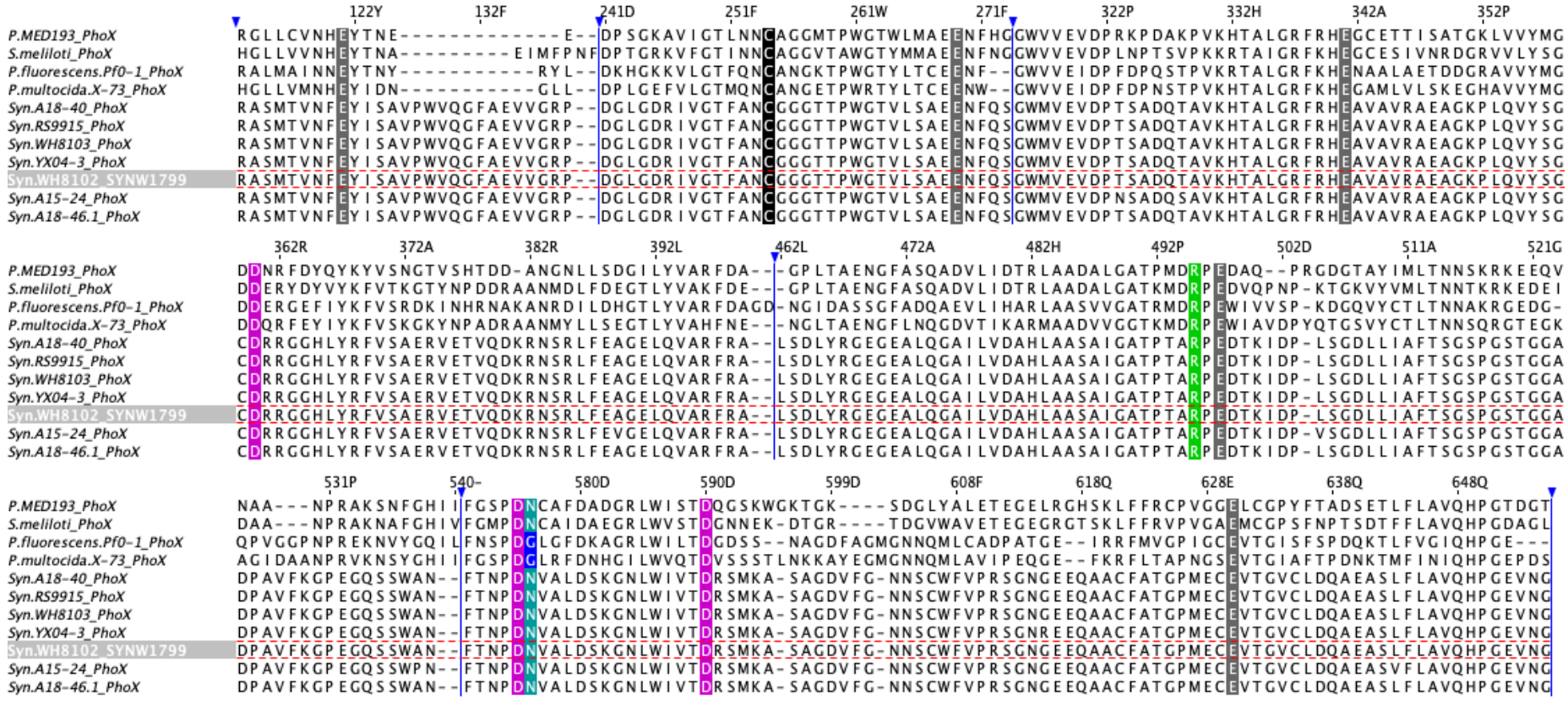

Figure 6.4: ***Multiple sequence alignment of Synechococcus sp. WH8102 phosphatase SYNW01799 with homologs and characterised PhoX-type phosphatases.***
MSA of SYNW01799 and six close homologs with four characterised phosphatases; PhoX phosphatases from Pseudomonas fluorescens Pf0-1 (PDBe 3ZWU, Yong et al., 2014), Sinorhizobium meliloti 1021 (Zaheer et al., 2009), Pasteurella multocida X-73 (J. R. Wu et al., 2007), and Phaeobacter sp. MED193 (Chapter 4). Coordinating amino acids of the catalytic site of SYNW1799 are highlighted: Arg495 in green; Asp360, Asp575, and Asp590 in purple; Cys254 in black; and Glu121, Glu269, Glu341, Glu497, and Glu630 in dark grey. The PhoX-family is subdivided into two groups: group I with conserved G (blue) and group II with conserved N (turquoise) adjacent to the PhoX-conserved Asp575, required for Ca^{2+} binding (Zaheer et al., 2009).

In conclusion, MSA confirmed that SYNW1799 is most likely a member of the PhoX phosphatase family. Therefore, the predicted model of SYNW1799 based on the *P. fluorescens* PhoX and the *P. fluorescens* PhoX model itself were extracted from the Phyre[2] server and the RCSB protein data bank. UCSF Chimera was used to analyse both PhoX models. Here, MatchMaker (with default settings) was used to overlay the model of the model of *P. fluorescens* PhoX and SYNW1799, and the sequence of SYNW1799 was used to label amino acids of the catalytic site involved in the coordination of the two Fe^{3+} and three Ca^{2+} ions and the vanadate (VO_4^{3-}) ion (Figure 6.5)

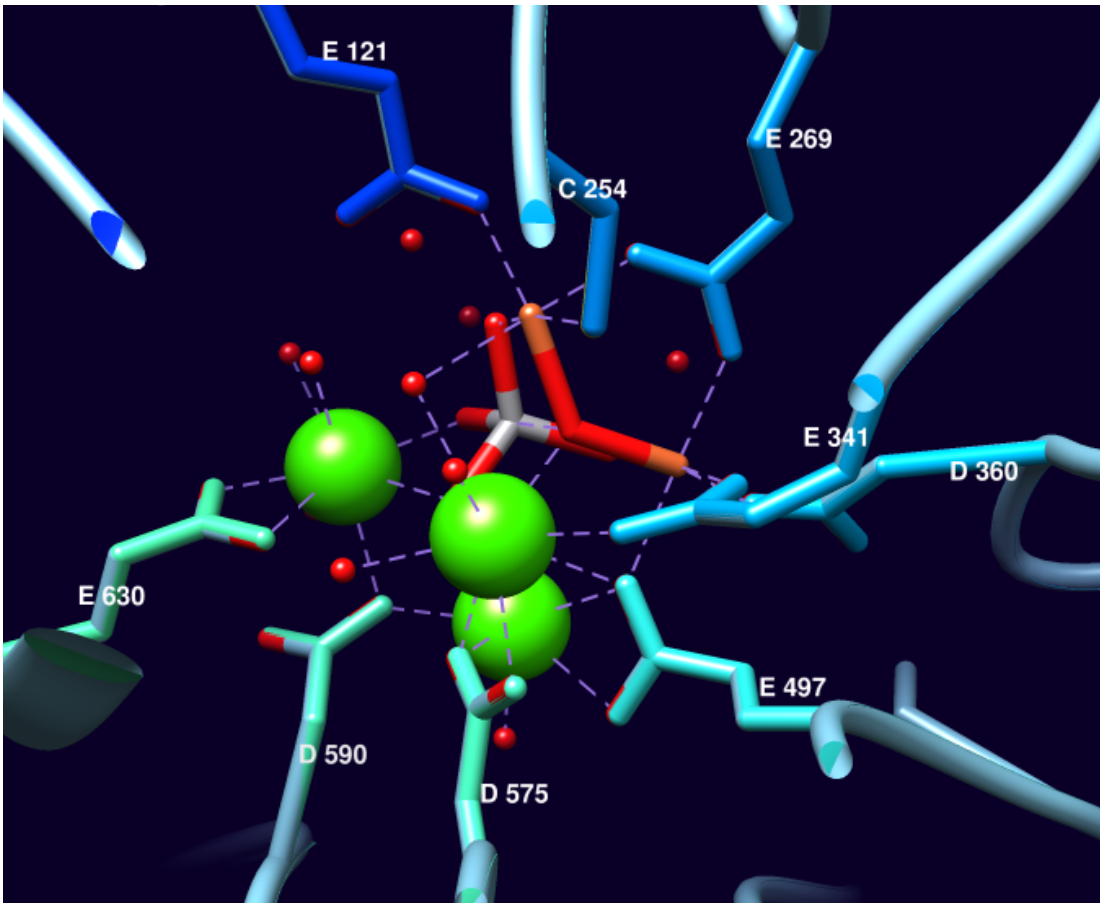

Figure 6.5: ***Predicted catalytic site of SYNW1799.***
The catalytic site of SYNW1799 is based on the P. fluorescens PhoX (PDBe 3ZWU, Yong et al., 2014). Amino acids that coordinate the three Ca^{2+} ions (green), the mu-Oxo-Diiron ion (orange-red structure), and the VO_4^{3-} ion (a grey tetrahedral shape with red tips) are labelled in white. Molecular graphics and analyses were performed with the UCSF Chimera package. Chimera is developed by the Resource for Biocomputing, Visualization, and Informatics at the University of California, San Francisco (supported by NIGMS P41-GM103311).

The results of this section demonstrate that SYNW1799 is most likely a extracellular phosphomonoesterase of the PhoX-type family. However,

more studies are needed to fully understand the substrate specificity of this protein, as well as confirmation of metals required for enzyme activity.

6.2.4 Using bioinformatics to determine the phylogeny of SYNW2390 and SYNW2391

SYNW2390 and SYNW2391 are two phosphatases of *Syn*. WH8102 that have not been described in detail before. Because of this, the same approach was used as before (see section 6.2.2). Phyre^2 was used to find homologs of both proteins. However, the results of both homology searches were inconclusive. Where SYNW2390 had between 10-30% identity with various 5'-nucleotidases, SYNW2391 only had 10-20% identity with several hydrolases and reductases. MSA of SYNW2390 and SYNW2391 with corresponding proteins retrieved from the Phyre^2 server didn't identify any conserved amino acids that are involved in metal-binding within the active centre. Therefore, the family of phosphatases both these proteins belong to couldn't be identified. For further analysis, sequences of previously described phosphatases of various families (Zaheer et al., 2009; Kageyama et al., 2011; Lee et al., 2015; Lin et al., 2015) and close homologs of SYNW0196, SYNW1799, SYNW2390, and SYNW2391 were mined to create a phylogenetic tree (Figure 6.6, Appendix 6.4), as described in section 2.7 (Edgar, 2004b, 2004a; Capella-Gutiérrez et al., 2009; Trifinopoulos et al., 2016; Letunic & Bork, 2021). It was expected that the tree would help to assign SYNW2390 and SYNW2391 to a group of phosphatases.

The tree showed a clear clustering of three groups: the PhoX, the PhoD and the PhoA phosphatase families. As expected, SYNW1799 and MED193_05784 were assigned to the PhoX-type family (Figure 6.6, red) within the PhoX-II group of phosphatases. Within the PhoX-type family, a clear clustering was found between the PhoX-I and PhoX-II groups. SYNW0196 grouped with other members of the PhoD-type family (Figure 6.6, blue). In addition, SYNW2390 and SYNW2391 clustered within a broad group of PhoA-type phosphatases, including PhoA phosphatases, atypical PhoA phosphatases, and RTX-containing phosphatases.

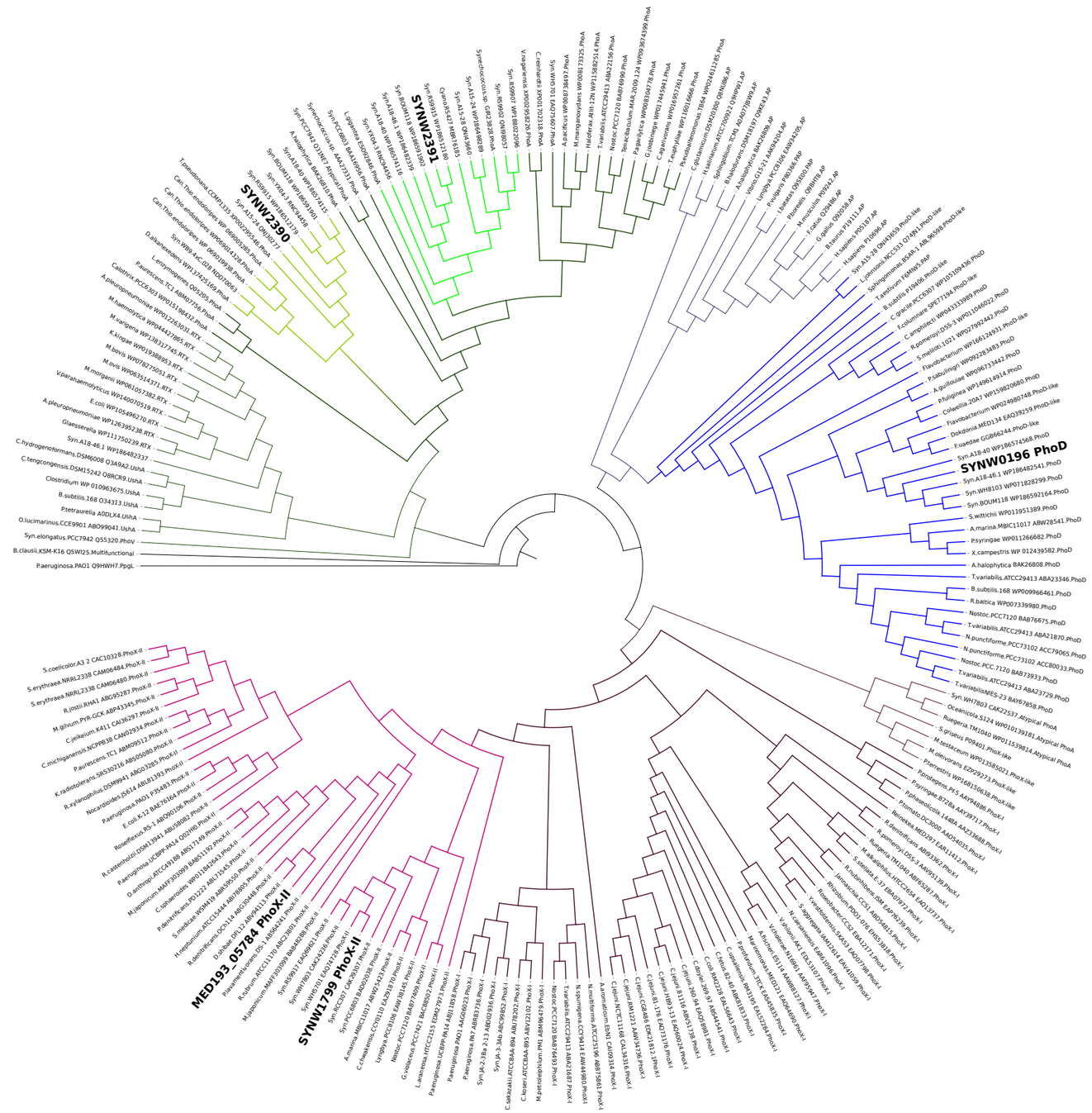

Figure 6.6: ***Phylogenetic tree of alkaline phosphatases.*** *The phylogenetic tree clusters phosphatases belonging to the PhoX (red), PhoD (blue), and PhoA (green) phosphatase families in three big groups. Sequences of the phylogenetic tree were retrieved from previous publications (Zaheer et al., 2009; Kageyama et al., 2011; Lee et al., 2015; X. Lin et al., 2015). Additionally, it includes close homologs of the Synechococcus sp. WH8102 phosphatases SYNW0196, SYNW1799, SYNW2390, and SYNW2391 (Appendix 6.4). The tree assigns SYNW1799 and the MED193 PhoX (see chapter 4.2.7) within the PhoX-II group, characterized by an asparagine adjacent to the conserved Ca^{2+} binding Asp575. Where SYNW0196 clusters within the PhoD family, SYNW2390 and SYNW2391 are grouped with PhoA-type phosphatases. Neighbour-joining tree with 1000 bootstraps using Maximum-Likelihood.*

These repeats in toxin (RTX) proteins (Welch, 2001) form a big family of various extracellular proteins that are described to bind Ca^{2+} ions and are secreted via the type I secretion system (Linhartová et al., 2010).

According to the phylogenetic tree, SYNW2390 and SYNW2391 are most likely PhoA-type phosphatases that primarily hydrolyse phosphomonoester bonds (Luo et al., 2010; Lin et al., 2015) and require zinc and magnesium or calcium for enzyme activity (Zaheer et al., 2009; Luo et al., 2010; Li et al., 2018). However, more work is needed to confirm the structure of both proteins, including protein purification and crystallisation to confirm the enzyme type and metal requirements. Moreover, studies are required to understand the substrate specificity and localisation of both proteins.

6.3 Discussion

Synechococcus sp. WH8102 is a model organism because it is well adapted to oligotrophic environments, including P-limitation (Palenik et al., 2003; Scanlan et al., 2009; Ahlgren & Rocap, 2012). One of the adaptation mechanisms to P-depletion is the expression of alkaline phosphatases which are required to release P_i from organic phosphate (Tetu et al., 2009; Cox & Saito, 2013; Lin et al., 2018). Therefore, *Syn.* WH8102 has multiple genes for four putative alkaline phosphatases, namely SYNW0196, SYNW1799, SYNW2390, and SYNW2391 (Palenik et al., 2003; Scanlan et al., 2009; Tetu et al., 2009; Kathuria & Martiny, 2011).

6.3.1 Protein overexpression and purification

This study aimed to unravel the biochemistry of all four phosphatases, including metal requirements and substrate specificity. Therefore, several overexpression conditions were tested for all four phosphatases (Table 6.2). Where SYNW2390 could be overexpressed using a pET151/D-TOPO expression vector, a pMAL c4x vector, which fuses a co-expressed maltose-binding protein (MBP) to the recombinant protein, was required to gain solubility of SYNW0196 and SYNW2391. Prior studies have demonstrated that fusing recombinant proteins to an MBP, a highly soluble protein, can promote the solubility of aggregation-prone proteins (Kapust & Waugh, 1999; Chen et al., 2005). After testing various

conditions, a rich self-inducing medium (ZYM-5052) and a specific overexpression protocol was used for these three proteins (for details see section 2.2.6), resulting in high protein yield (Figure 6.1). However, initial protein purification didn't work and SYNW2390 couldn't be purified following the protocol described in sections 2.2.10 and 2.2.11.

In contrast, SYNW1799 could not be overexpressed, independent of the construct used and overexpression medium tested. According to ProtParam, SYNW1799 contains 20 sulphur atoms (Table 6.1) and a predicted signal sequence (see section 2.2.3). It seems likely that this protein requires the oxidizing microenvironment of the of *E. coli* periplasm to allow the development of disulphide bonds and thereby accurate formation of the mature protein (Brosnan & Brosnan, 2006; Berkman, 2012; Manta et al., 2019). The PelB signal sequence of the pET-22b(+) expression vector has been shown to effectively transport mature proteins into the periplasm, cleaving off the signal sequence in the process (Mirzadeh et al., 2020). However, in the study conducted by Mirzadeh et al. (2020) a mild induction protocol was used, specifically 0.05 mM IPTG for 2 hours at 30 °C. To date, SYNW1799 has been overexpressed only once before. Thus, in the study conducted by Kathuria and Martiny (2011) a pEcoli-N-term 6xHN plasmid was used for overexpression and the protein was not purified but the crude extract was used for biochemical analysis. Unfortunately, the sequence cloned into the plasmid was not published. Since a plasmid with an N-terminal His-Tag was used it seems likely that the N-terminal signal sequence of the protein was removed. However, the N-terminal His-Tag might have been cleaved off naturally after protein synthesis, a potential reason why the protein was not purified but the crude extract was used in the study by Kathuria and Martiny (2011).

Unfortunately, in this study, none of the overexpressed proteins could be purified and biochemical analysis conducted. Hence, bioinformatics was used as an alternative tool to describe the four phosphatases SYNW0196, SYNW1799, SYNW2390, and SYNW2391.

6.3.2 Bioinformatics analysis and homology modelling of SYNW0196, a PhoD phosphatase

The Phyre[2] server was used to search for already crystallised and characterised homologs of SYNW0196. This protein had high identity with a PhoD phosphatase of *Bacillus subtilis* but also had some homology with a purple acid phosphatase (PAP) of *Ipomoea batatas*. Both types of phosphatases are closely related to each other (Rodriguez et al., 2014), and require two iron ions for enzyme activity. However, where PhoD phosphatases require two additional Ca^{2+} ions (Rodriguez et al., 2014; Browning et al., 2017), Mn^{2+} or Zn^{2+} is essential for enzyme activity in PAPs (Klabunde et al., 1996; Schenk et al., 2000). PhoD phosphatases have generally been defined as extracellular phosphodiesterases that also show phosphomonoesterase activity (Yamane & Maruo, 1978; Sosa et al., 2019). PhoD phosphatases are widely abundant in ocean environments, especially in regions with low P_i concentrations (<10 nM) (Sebastián & Ammerman, 2009; Kathuria & Martiny, 2011), and are believed to be responsible for high dissolved organic P turnover in these areas (Sosa et al., 2019). In addition, P-limited marine environments often show a tendency towards metal depletion as well, specifically zinc and cobalt (Lohan et al., 2002; Shaked et al., 2006; Jakuba et al., 2008; Kathuria & Martiny, 2011). Zinc is not just essential for the growth of organisms; it is essential for the proper functioning of around 300 enzyme systems, including extracellular phosphatases (Lohan et al., 2002; Barnett et al., 2014). For example, the classical PhoA phosphomonoesterase, extensively studied in *E. coli*, requires Mg^{2+} and Zn^{2+} for enzyme activity (Coleman, 1992; Wanner, 1996; Luo et al., 2010). Since PhoD phosphatases have an affinity towards phosphate diesters but also phosphate monoesters, it is believed that these phosphatases are a replacement for the classical PhoA phosphatase in marine environments that are low in P and zinc concentrations.

In contrast, PAPs have an affinity towards phosphate monoester and phosphoanhydride bonds (Klabunde et al., 1996; Schenk et al., 2005; Pabis et al., 2016). They are ubiquitous in mammalian cells and plants but have not been discovered in many prokaryotes, except for cyanobacteria

and mycobacteria, but with low homology (Schenk et al., 2000). Cyanobacterial PAPs are closest related to mammalian and low-molecular-weight PAPs of plants (Schenk et al., 2000). However, the function of these proteins has not been identified yet.

To determine the phylogeny of SYNW0196, sequences of close homologs of SYNW0196, characterised PhoD phosphatases, and purple acid phosphatases were used for multiple sequence alignment (MSA) (Figure 6.2, Appendix 6.2). The MSA confirmed that SYNW0196 belongs to the PhoD phosphatase family, sharing eight of the nine conserved amino acids that are required for the metal coordination in the active centre, as described in *B. subtills*. Furthermore, the substitution of the Ca^{2+}-binding Asn216 of *B. subtilis* by an aspartic acid has been described before (Rodriguez et al., 2014) and is a common structural variation. Indeed, the carboxylates of aspartic acid or the oxygens of asparagine can bind Ca^{2+} to the same measures (Kretsinger, 2013).

6.3.3 Bioinformatics analysis and homology modelling of SYNW1799, a PhoX phosphatase

SYNW1799 was the only phosphatase in this study that couldn't be overexpressed. Because of this, bioinformatics was used to confirm that this protein is indeed a member of the PhoX family. As described before, the Phyre^2 server was used to identify homologs of SYNW1799 that have already been crystallised and characterised. SYNW1799 is closely related to the PhoX-type phosphatase of *Pseudomonas fluorescens* Pf0-1, the same protein that was used as a comparison for the *Phaeobacter* sp. MED193 PhoX (MED193 PhoX) in section 4.2.7. This protein has been studied thoroughly and conserved amino acids involved in the coordination of metal ions have been identified (Yong et al., 2014). For comparison purposes, sequences of close homologs of SYNW1799 and previously described PhoX phosphatases, including the *Phaeobacter* sp. MED193 PhoX were extracted and MSA was performed (Figure 6.4, Appendix 6.3). The alignment confirmed that SYNW1799 shares all conserved amino acids with the *P. fluorescens* PhoX that have been identified by Yong et al., (2014). These amino acids are involved in the coordination of the two Fe^{3+} and three Ca^{2+} ions that are required for enzyme activity in the active

centre (Wu et al., 2007; Zaheer et al., 2009; Kathuria & Martiny, 2011; Yong et al., 2014). In addition, Zaheer et al. (2009) subdivided PhoX phosphatases into two groups, characterised by different conserved amino acids adjacent to the Ca^{2+} binding Asp575. Where proteins of the PhoX-I group contain a conserved glycine, members of the PhoX-II group all share an asparagine following Asp575. The alignment clusters SYNW1799, all homologs of SYNW1799, MED193 PhoX, and the *Sinorhizobium meliloti* PhoX within the PhoX-II group. In comparison, the *P. fluorescens* and *Pasteurella multocida* PhoX phosphatases are members of the PhoX-I group.

It is believed that the adjacent conserved amino acids can influence the metal specificity of the PhoX phosphatase (Zaheer et al., 2009). Where PhoX-I phosphatases have shown the ability to reinstate enzyme activity to some degree by substituting Ca^{2+} ions with Co^{2+}, Mn^{2+}, or Ni^{2+} ions (Roy et al., 1982; Majumdar et al., 2005; Wu et al., 2007), PhoX-II phosphatases are strictly restricted to Ca^{2+} ions as a metal cofactor (Zaheer et al., 2009; Yong et al., 2014). A study on metal requirements of SYNW1799 confirmed this theory (Kathuria & Martiny, 2011). Here, it has been demonstrated that the enzyme had phosphate monoester activity towards *p*NPP in the crude extract after overexpression. The crude extract was treated with EDTA to remove metals, thereby abolishing enzyme activity. The activity was reinstated by adding Ca^{2+} ions back. Apart from calcium, Cu^{2+}, Mg^{2+}, Mn^{2+}, and Ni^{2+} ions could be used to restore some enzyme activity. A similar trend was reported for a *Prochlorococcus* PhoX (Kathuria & Martiny, 2011). However, this theory doesn't coincide with findings reported for MED193 PhoX. Although this protein is a member of the PhoX-I group, enzyme activity could only be restored after the addition of Ca^{2+} alone (see 4.2.7). Therefore, more studies are needed to confirm the correlation between the adjacent conserved amino acids and metal specificity.

6.3.4 Using bioinformatics to determine the phylogeny of SYNW2390 and SYNW2391

Both alkaline phosphatases SYNW2390 and SYNW2391 have been overexpressed using a pET151/D-TOPO151 and pMAL c4x vector,

respectively. However, SYNW2390 could not be purified. Therefore, the same strategy, as described above, was used and the Phyre[2] server was searched for close homologs of both proteins. Since results were inconclusive and no high identity towards any characterised proteins was found, phylogeny was used to determine the family of phosphatases these two proteins belong to. Sequences of previously described phosphatases (Zaheer et al., 2009; Kageyama et al., 2011; Lee et al., 2015; Lin et al., 2015) and close homologs of SYNW2390 and SYNW2391 were extracted and used to create a phylogenetic tree (Figure 6.6, Appendix 6.4). The tree shows a clear clustering of three large groups: PhoX-type, PhoD-type, and PhoA-type phosphatases. Where SYNW1799 and MED193 PhoX cluster within the PhoX-II phosphatases (see section 6.2.3), SYNW0196 groups with other PhoD-type phosphatases (see section 6.2.2). In addition, SYNW2390 and SYNW2391 cluster with a large group of PhoA-type phosphatases.

SYNW2390 and six close homologs formed a branch with PhoA phosphatases of *Thalassiosira pseudonana CCMP1335* (Accession number XP_002295546), *Candidatus Thiodiazotropha endoloripes* (Accession numbers WP_069014328, WP_069019938, and WP_069005285), and *Desulfoglaeba alkanexedens* (Accession number WP_137425169). Looking into the conserved domains of these proteins a pattern was found (Figure 6.7) (Lu et al., 2020; Mistry et al., 2021). The homologs of SYNW2390 all contained a metallophosphatase superfamily and a 5’ nucleotidase family domain. Where *D. alkanexedens* and *Can. T. endoloripes* have a signal peptide to allow transport of the mature protein into the periplasm, the proteins of *Syn.* WH8102 and *T. pseudonana* don’t. Therefore, proteins must be secreted differently. Interestingly, SYNW2390 has a C-terminal RTX-domain. These proteins are commonly exported via the type I secretion system (Linhartová et al., 2010). However, the specific phosphatase function of this protein is still unclear.

Analysis of SYNW2391 revealed that there are no conserved domains in this protein or any of the close homologs within the same branch (Lu et al., 2020; Mistry et al., 2021). According to the phylogenetic tree, the next closest branch includes an atypical PhoA (Pho^{Aty}) phosphatase from *Synechococcus elongatus* PCC 7942 (Accession number

WP_011242477). This unusual phosphatase is larger than most phosphatases characterised to date and has similarities with the α-subunit of the ATPase from bacteria and chloroplasts and the UshA sugar phosphatase of *E. coli* (Ray et al., 1991). Conserved domains of this protein include a PhoA-like, a 5'nucleotidase, a YncE, and a DUF4214 domain (Figure 6.7). Interestingly, SYNW2391 and the Pho^{Aty} share 37.50% Seq.ID (e-value $3e^{-32}$). SYNW2391 is similar to the second half of the Pho^{Aty} protein sequence which contains the conserved domains for a YncE domain and a domain of unknown function (4214). The YncE domain is associated with DNA-binding. However, more studies are required to understand the function of both SYNW2390 and SYNW2391.

Figure 6.7: ***Comparative structural analysis of alkaline phosphatases in different organisms.***
Sequence comparison of phosphatases among homologs that form a branch with SYNW2390 and organisms of adjacent branches. PQQ, catabolism of alcohols; RTX, extracellular Ca^{2+} binding proteins; LTD, lamin tail domain, DNA-binding; Exo/Endonuclease, intracellular signalling; MPP-super family, metallophosphatase superfamily; 5'nucleotidase, degradation of extracellular nucleotides; SP, signal peptide; PhoA, alkaline phosphomonoesterase; YncE, DNA-binding beta-propeller fold protein; DUF4212.

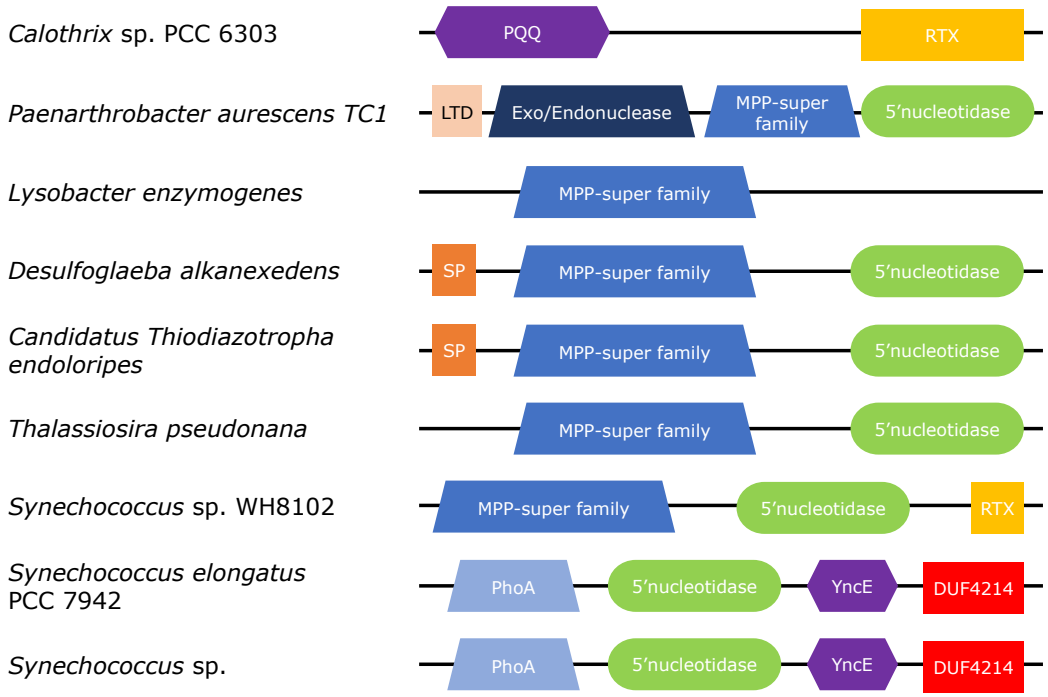

6.3.5 Summary and future work

The results of this chapter confirmed that the phosphatases SYNW0196 and SYNW1799 of *Syn.* WH8102 belong to the PhoD and the

PhoX phosphatase family, respectively. However, the phosphatase family affiliation for SYNW2390 and SYNW2391 is still unclear. Therefore, it is of great importance to overexpress both phosphatases to conduct biochemical analyses, to fully understand the substrate specificity, the metal requirement and localisation of all four phosphatases. It seems likely that SYNW2390 and SYNW2391 require different metal cofactors in comparison to the *Syn.* WH8102 PhoD and PhoX. This would confer *Syn.* WH8102 an advantage in P-limited environments that are co-limited by metals.

CHAPTER 7 FINAL CONCLUSIONS AND FUTURE PERSPECTIVES

7.1 Conclusions

The aim of this thesis was to investigate the role of phospholipid headgroups as the sole source of P for P-depleted marine heterotroph *Phaeobacter* sp. MED193 cultures (Chapter 4 and Chapter 5). In addition, we examined the P-stress response of MED193 to unravel novelties due to its occupation of ultra-low P_i environments (Chapter 3). Finally, we used various methods to characterise phosphatases of MED193 and *Synechococcus* sp. WH8102 (Chapter 4 and Chapter 6).

7.1.1 The Pho regulon of *Phaeobacter* sp. MED193

In Chapter 3 a MED193 *phoB* deletion mutant was utilised to better understand which MED193 proteins are Pho-regulated by comparing the proteomes of P-depleted *ΔphoB* and WT MED193 cultures (Table 3.4). Many of the proteins, upregulated in P-depleted WT MED193 cultures, have been described before, for example the Pst transporter (Wanner & Chang, 1987; Scanlan et al., 1993), various phosphatases (e.g., Monds et al., 2006; Santos-Beneit et al., 2009; Zaheer et al., 2009; Lidbury et al., 2017), and several P-related transporters (Schweizer & Boos, 1985; Wanner & Metcalf, 1992; White & Metcalf, 2004; Yuan et al., 2006; Romano et al., 2015). In addition, lipidomics analysis confirmed that lipid remodelling is Pho-regulated as DGTS synthesis was abolished in the *phoB* mutant (Figure 3.2). We also identified proteins that were upregulated in P-depleted WT MED193 cultures whose protein function is still unclear. One of these proteins was MED193_09570, annotated as GlpV. To date, only one study has focused on this protein isolated from *Rhizobium leguminosarum* VF39SM. In *Rhizoboum leguminosarum* VF39SM, GlpV is involved in the transport of glycerol and G3P (Ding et al., 2012). However, substrate specificity assays conducted by collaborators in China couldn't identify any substrates that MED193_09570 can bind. In addition, a substrate-binding protein (PotD), predicted to be involved in spermidine and putrescine transport (Romano et al., 2015), was identified in the WT MED193 proteome. However, the role of putrescine and spermidine in

MED193 is only predicted (Wortham et al., 2007). Future work should focus on identifying the function and substrate specificity of GlpV (MED193_09570) and PotD (MED193_11424) to understand their role during P-limitation in MED193. In this study we examined proteomes and lipidomes of MED193 and *ΔphoB* cultures that were P-starved for 48 hours. A time series of samples could help to understand the progress of P-starvation, comparing early P-stress to late P-stress response. In doing so, more proteins that are Pho-regulated and required for survival in limited P-conditions could be identified. In *Arabidopsis* genes involved in the P-stress response are classified as early and late in expression. Where early genes encode for proteins involved in rapid P_i uptake, late genes encode proteins that are required for metabolic bypass processes (Ajmera et al., 2019).

7.1.2 Novel transporters involved in the phospholipid headgroup uptake in *Phaeobacter* sp. MED193

In Chapter 4 and Chapter 5 of this thesis a proteomic approach was used to investigate the ability of MED193 to utilise the four phospholipid headgroups PC, PE, G1P, and G3P. MED193 was able to grow on all four compounds (Figure 4.1, Figure 4.2, and Figure 5.3). Lipidomics analysis further demonstrated that the synthesis of membrane phospholipids was restored after the addition of the phospholipid headgroups as a sole source of P (Figure 4.3A and Figure 5.5) and lipid remodelling as a response to P-limitation (Sebastián et al., 2016) was reversed. Proteomics analysis highlighted key enzymes that are involved in the transport and degradation of these phospholipid headgroups. Section 4.2.4 describes the catabolism of PE. Although no transporter for PE was identified, an ethanolamine binding protein (MED193_10041) was discovered and described. Collaborators in China confirmed ethanolamine as a substrate of this binding protein (Figure 4.7). The intracellular catabolism of ethanolamine was previously described in *Chromohalobacter salexigens* (Vetting et al., 2015) and adapted for MED193 (Figure 4.9), but requires further molecular confirmation. MED193_10041 forms a new cluster of substrate-binding proteins within the TRAP-T family (Figure 4.14) and although this protein was only moderately present in the Tara oceans

metagenomes (5-10%), the gene encoding the protein was highly expressed (Figure 4.12). Results in section 4.2.5 describe the degradation pathway of PC in MED193, which was recently proposed in *Ruegeria pomeroyi* DSS-3, a fellow member of the *Roseobacter* group (Figure 4.17 Lidbury et al., 2015). Finally, section 4.2.6 and Chapter 5 discuss the identification of a substrate-binding protein (MED193_19449) of DHAP (Figure 5.10), an oxidation product of G3P and potentially G1P (Hartley et al., 2017). This substrate-binding protein forms a new cluster within the ABC superfamily (Figure 5.11). A G3PDH (MED193_19624) and a GAPDH (10071) were prominent in the proteomics data (Table 5.5). G3PDHs have been reported to not only oxidise G3P to DHAP, but to reverse the oxidation process as well (Ou et al., 2006; Chen et al., 2012). Within the operon of MED193_19449 we identified a putative G3P phosphatase (MED193_19464) which was previously described in *Mycobacterium tuberculosis* (Larrouy-Maumus et al., 2013). In connection with the discovery of the substrate-binding protein MED193_19449, a G3PDH, a GAPDH, and a G3P phosphatase, we proposed a degradation pathway of G1P/G3P in MED193 (Figure 5.12). Although we reported a PhoX phosphatase to be involved in the extracellular cleavage of PC and PE prior to uptake, molecular evidence it still required to confirm this hypothesis. In addition, the catabolism of G1P/G3P still demands further research. For example, the extracellular oxidation of G1P/G3P to DHAP and the intracellular substrate degradation process. Deleting the gene for the substrate-binding protein will help to understand its role in G1P/G3P uptake. Since phospholipids of marine bacteria account for around 10-20% of cellular P content (Van Mooy et al., 2008) and make up circa 1.5% of the particulate organic carbon pool (Gašparović et al., 2018), they represent an important source of P in oligotrophic oceans. Not only are phospholipids a lucrative source of P, but also for nitrogen and carbon. Our findings support the importance of phospholipids in the marine P cycle. However, further research is still needed to fully understand the role of phospholipids within the marine P cycle.

7.1.3 Metal requirements of phosphatases of *Phaeobacter* sp. MED193 and *Synechococcus* sp. WH8102

In Chapter 4 and Chapter 6 overexpression, EPR, enzyme activity assays, and bioinformatics were used to study the metal requirements of the PhoX phosphatase of MED193 (see section 4.2.7) and four phosphatases of *Syn*. WH8102 (Chapter 6). The MED193 PhoX (MED193_05784) showed phosphomonoesterase activity towards *p*NPP, PC, and PE (Figure 4.25) and K_M values (Table 4.6) were determined that fell within the range of previously reported PhoX K_Ms of other organisms (Roy et al., 1982; Wu et al., 2007; Zaheer et al., 2009; Yong et al., 2014; Lee et al., 2015). Phosphomonoesterase activity was previously described for PhoX-type phosphatases, e.g., see Wu et al. (2000); Monds et al. (2006); Yong et al. (2014). Metal replacement experiments (Figure 4.22) and EPR (4.23) confirmed that iron and calcium are required for MED193 PhoX enzyme activity, as has been found for other bacteria (e.g., Zaheer et al., 2009; Kathuria & Martiny, 2011; Yong et al., 2014). In addition, we developed plasmid constructs and growth conditions (Table 6.2) to successfully overexpress the three *Syn.* WH8102 phosphatases SYNW0196, SYNW2390, and SYNW2391 in *E. coli* (Figure 6.1). More work is required to optimise the purification of these three phosphatases. Additionally, a suitable vector (Mergulhão et al., 2005; Mirzadeh et al., 2020) and growth condition need to be established for the overexpression of SYNW1799, the *Syn.* WH8102 PhoX. Enzyme activity assays and metal replacement studies are required to determine substrate specificity and metal requirements for all these proteins. This will allow me to confirm the results obtained through bioinformatic studies (Figure 6.2 and Figure 6.4), specifically that SYNW0196 is a PhoD-type phosphatase and SYNW1799 is a PhoX-type phosphatase, and that both enzymes require an iron-calcium cofactor for enzyme activity (e.g., Zaheer et al., 2009; Rodriguez et al., 2014; Yong et al., 2014; Browning et al., 2017). Further work is required to identify the family of phosphatases SYNW2390 and SYNW2391 belong to. Apart from biochemical studies, as mentioned above, protein crystallisation qualifies as a suitable method to determine the structure and function of both phosphatases (Ronda et al., 2015). In addition,

identifying the localisation of the four *Syn.* WH8102 phosphatases and other phosphatases of MED193 could help to better understand the adaptation mechanisms of both strains to their ultra-low P_i environments. Bioinformatic studies predict that PhoX phosphatases are in general extracellular and associate PhoD and PhoA phosphatases with the cytoplasm (Luo et al., 2009).

7.2 Future perspectives

This work has not only highlighted the importance of phospholipid headgroups as a source of P for bacteria, but also the requirement of various phosphatases to make these compounds bioavailable. Combining the results of all chapters it is obvious that MED193 and *Syn.* WH8102 possess comprehensive mechanisms to overcome P-limitation in their natural environment. In recent years, improved LC-MS methods to detect intact polar lipids in the marine environment allowed the discovery of novel lipids in the oceans and the modelling of lipid distributions (Ding et al., 2021; and references within). In addition, recent studies have focused on the role of lipids in the marine ecosystem (Suzumura, 2005; Frka et al., 2011; Marić et al., 2013; Gašparović et al., 2014, 2018; Pelikan et al., 2021). Using a combination of proteomics and lipidomics, as a single or meta-omics approach, will help to gain further insights into the marine P cycle and to unravel new links within it.

REFERENCES

Achbergerová, L. & Nahálka, J. 2011. Polyphosphate - an ancient energy source and active metabolic regulator. *Microbial Cell Factories*, *10*, 1–14.

Ahlgren, N. A. & Rocap, G. 2012. Diversity and distribution of marine *Synechococcus*: multiple gene phylogenies for consensus classification and development of qPCR assays for sensitive measurement of clades in the ocean. *Frontiers in Microbiology*, *3*, 1–24.

Ahn, K. & Kornberg, A. 1990. Polyphosphate kinase from *Escherichia coli*. *The Journal of Biological Chemistry*, *265*, 11734–11739.

Aiba, H. & Mizuno, T. 1994. A novel gene whose expression is regulated by the response-regulator, SphR, in response to phosphate limitation in *Synechococcus* species PCC 7942. *Molecular Microbiology*, *13*, 25–34.

Ajmera, I., Hodgman, T. C., & Lu, C. 2019. An integrative systems perspective on plant phosphate research. *Genes*, *10*.

Alicea, I., Marvin, J. S., Miklos, A. E., Ellington, A. D., Looger, L. L., & Schreiter, E. R. 2011. Structure of the *Escherichia coli* phosphonate binding protein PhnD and rationally optimized phosphonate biosensors. *Journal of Molecular Biology*, *414*, 356–369.

Almqvist, J., Huang, Y., Hovmöller, S., & Wang, D.-N. 2004. Homology modeling of the human microsomal glucose 6-phosphate transporter explains the mutations that cause the glycogen storage disease type Ib. *Biochemistry*, *43*, 9289–9297.

Ammerman, J. W., Hood, R. R., Case, D. A., & Cotner, J. B. 2003. Phosphorus deficiency in the Atlantic: an emerging paradigm in oceanography. *EOS*, *84*, 165–170.

Anderson, G. C. & Zeutschel, R. P. 1970. Release of dissolved organic matter by marine phytoplankton in coastal and offshore areas of the Northeast Pacific Ocean. *Limnology and Oceanography*, *15*.

Andresen, P. A., Kaasen, I., Styrvold, O. B., Boulnois, G., & Strøm, A. R. 1988. Molecular cloning, physical mapping and expression of the *bet* genes governing the osmoregulatory choline-glycine betaine pathway of *Escherichia coli*. *Journal of General Microbiology*, *134*, 1737–1746.

Antelmann, H., Scharf, C., & Hecker, M. 2000. Phosphate starvation-inducible proteins of *Bacillus subtilis*: proteomics and transcriptional analysis. *Journal of Bacteriology*, *182*, 4478–4490.

Azam, F., Fenchel, T., Field, J. G., Gray, J. S., Meyer-Reil, L. A., & Thingstad, F. 1983. The ecological role of water-column microbes in the Sea. *Marine*

Ecology Progress Series, *10*, 257–263.

Baek, J. H., Kang, Y. J., & Lee, S. Y. 2007. Transcript and protein level analyses of the interactions among PhoB, PhoR, PhoU and CreC in response to phosphate starvation in *Escherichia coli*. *FEMS Microbiology Letters*, *277*, 254–259.

Baek, J. H. & Lee, S. Y. 2006. Novel gene members in the Pho regulon of *Escherichia coli*. *FEMS Microbiology Letters*, *264*, 104–109.

Baek, J. H. & Lee, S. Y. 2007. Transcriptome analysis of phosphate starvation response in *Escherichia coli*. *Journal of Microbiology and Biotechnology*, *17*, 244–252.

Barnett, J. P., Scanlan, D. J., & Blindauer, C. A. 2014. Identification of major zinc-binding proteins from a marine cyanobacterium: insight into metal uptake in oligotrophic environments. *Metallomics*, *6*, 1254–1268.

Bartoloni, L., Wattenhofer, M., Kudoh, J., Berry, A., Shibuya, K., Kawasaki, K., Wang, J., Asakawa, S., Talior, I., Bonne-Tamir, B., Rossier, C., Michaud, J., McCabe, E. R. B., Minoshima, S., Shimizu, N., Scott, H. S., & Antonarakis, S. E. 2000. Cloning and characterization of a putative human glycerol 3-phosphate permease gene (SLC37A1 or G3PP) on 21q22.3: mutation analysis in two candidate phenotypes, DFNB10 and a glycerol kinase deficiency. *Genomics*, *70*, 190–200.

Baturin, G. 2003. Phosphorus cycle in the ocean. *Lithology and Mineral Resources*, *38*, 101–119.

Behrenfeld, M. J., Bale, A. J., Kolber, Z. S., Aiken, J., & Falkowski, P. G. 1996. Confirmation of iron limitation of phytoplankton photosynthesis in the Equatorial Pacific Ocean. *Nature*, *383*, 508–511.

Bell, S. D. & Jackson, S. P. 1998. Transcription and translation in Archaea: a mosaic of eukaryal and bacterial features. *Trends in Microbiology*, *6*, 222–228.

Beltrán, J., Kloss, B., Hosler, J. P., Geng, J., Liu, A., Modi, A., Dawson, J. H., Sono, M., Shumskaya, M., Ampomah-Dwamena, C., Love, J. D., & Wurtzel, E. T. 2015. Control of carotenoid biosynthesis through a heme-based *cis-trans* isomerase. *Nature Chemical Biology*, *11*, 598–605.

Benitez-Nelson, C. R. 2000. The biogeochemical cycling of phosphorus in marine systems. *Earth-Science Reviews*, *51*, 109–135.

Bennett, E. M., Carpenter, S. R., & Caraco, N. F. 2001. Human impact on erodable phosphorus and eutrophication: a global perspective: increasing accumulation of phosphorus in soil threatens rivers, lakes, and coastal oceans with eutrophication. *BioScience*, *51*, 227–234.

Bergametti, G., Remoudaki, E., Losno, R., Steiner, E., Chatenet, B., & Buat-Menard, P. 1992. Source, transport and deposition of atmospheric phosphorus over the northwestern Mediterranean. *Journal of Atmospheric Chemistry*, *14*, 501–513.

Berkman, M. 2012. Production of disulfide-bonded proteins in *Escherichia coli*. *Protein Expression and Purification*, *82*, 240–251.

Berman, H. M., Westbrook, J., Feng, Z., Gilliland, G., Bhat, T. N., Weissig, H., Shindyalov, I. N., & Bourne, P. E. 2000. The Protein Data Bank. *Nucleic Acids Research*, *28*, 235–242.

Berner, E. K. & Berner, R. A. 1996. *Global environment water, air, and geochemical cycles* (Prentice-H). Englewood Cliffs, New Jersey.

Bessey, O. A., Lowky, O. H., & Brock, M. J. 1946. A method for the rapid determination of alkaline phosphatase with five cubic millimeters of serum. *Journal of Biological Chemistry*, *164*, 321–329.

Betzen, C., Alhamdani, M. S. S., Lueong, S., Schröder, C., Stang, A., & Hoheisel, J. D. 2015. Clinical proteomics: promises, challenges and limitations of affinity arrays. *Proteomics Clinical Applications*, *9*, 342–347.

Biddanda, B. A., Dila, D., Weinke, A., Mancuso, J., Villar-Argaiz, M., Medina-Sánchez, J. M., González-Olalla, J. M., & Carrillo, P. 2021. Housekeeping in the hydrosphere: microbial cooking, cleaning, and control under stress. *Life*, *11*, 1–19.

Bisson, C., Adams, N. B. P., Stevenson, B., Brindley, A. A., Polyviou, D., Bibby, T. S., Baker, P. J., Hunter, C. N., & Hitchcock, A. 2017. The molecular basis of phosphite and hypophosphite recognition by ABC-transporters. *Nature Communications*, *8*, 1–12.

Bjellqvist, B., Basse, B., Olsen, E., & Celis, J. E. 1994. Reference points for comparisons of two-dimensional maps of proteins from different human cell types defined in a pH scale where isoelectric points correlate with polypeptide compositions. *Electrophoresis*, *15*, 529–539.

Bjellqvist, B., Hughes, G. J., Pasquali, C., Paquet, N., Ravier, F., Sanchez, J. C., Frutiger, S., & Hochstrasser, D. 1993. The focusing positions of polypeptides in immobilized pH gradients can be predicted from their amino acid sequences. *Electrophoresis*, *14*, 1023–1031.

Björkman, K. M. & Karl, D. M. 2003. Bioavailability of dissolved organic phosphorus in the euphotic zone at Station ALOHA, North Pacific Subtropical Gyre. *Limnology and Oceanography*, *48*, 1049–1057.

Björkman, K. M., Thomson-Bulldis, A. L., & Karl, D. M. 2000. Phosphorus dynamics in the North Pacific subtropical gyre. *Aquatic Microbial Ecology*, *22*, 185–198.

Bradford, M. M. 1976. A rapid and sensitive method for the quantitation of microgram quantities of protein utilizing the principle of protein-dye binding. *Analytical Biochemistry*, *72*, 248–254.

Brinkhoff, T., Giebel, H. A., & Simon, M. 2008. Diversity, ecology, and genomics of the *Roseobacter* clade: a short overview. *Archives of Microbiology*, *189*, 531–539.

Brosnan, J. T. & Brosnan, M. E. 2006. The sulfur-containing amino acids: an overview. *The Journal of Nutrition*, *136*, 1636S-1640S.

Browning, T. J., Achterberg, E. P., Yong, J. C., Rapp, I., Utermann, C., Engel, A., & Moore, C. M. 2017. Iron limitation of microbial phosphorus acquisition in the tropical North Atlantic. *Nature Communications*, *8*.

Brüggemann, C., Denger, K., Cook, A. M., & Ruff, J. 2004. Enzymes and genes of taurine and isethionate dissimilation in *Paracoccus denitrificans*. *Microbiology*, *150*, 805–816.

Bruna, R. E., Kendra, C. G., Groisman, E. A., & Pontes, M. H. 2021. Limitation of phosphate assimilation maintains cytoplasmic magnesium homeostasis. *PNAS*, *118*.

Brzoska, P. & Boos, W. 1989. The *ugp*-encoded glycerophosphoryldiester phosphodiesterase, a transport-related enzyme of *Escherichia coli*. *FEMS Microbiology Reviews*, *63*, 115–124.

Buchan, A., González, J. M., & Moran, M. A. 2005. Overview of the marine *Roseobacter* lineage. *Applied and Environmental Microbiology*, *71*, 5665–5677.

Buchan, A., LeCleir, G. R., Gulvik, C. A., & González, J. M. 2014. Master recyclers: features and functions of bacteria associated with phytoplankton blooms. *Nature Reviews Microbiology*, *12*, 686–698.

Burley, S. K., Bhikadiya, C., Bi, C., Bittrich, S., Chen, L., Crichlow, G. V., Christie, C. H., Dalenberg, K., Di Costanzo, L., Duarte, J. M., Dutta, S., Feng, Z., Ganesan, S., Goodsell, D. S., Ghosh, S., Kramer Green, R., Guranovic, V., … Zhuravleva, M. 2021. RCSB Protein Data Bank: Powerful new tools for exploring 3D structures of biological macromolecules for basic and applied research and education in fundamental biology, biomedicine, biotechnology, bioengineering and energy sciences. *Nucleic Acids Research*, *49*, D437–D451.

Burrows, M. T., Schoeman, D. S., Richardson, A. J., Molinos, J. G., Hoffmann, A., Buckley, L. B., Moore, P. J., Brown, C. J., Bruno, J. F., Duarte, C. M., Halpern, B. S., Hoegh-Guldberg, O., Kappel, C. V., Kiessling, W., O'Connor, M. I., Pandolfi, J. M., Parmesan, C., … Poloczanska, E. S. 2014. Geographical limits to species-range shifts are suggested by climate velocity. *Nature*, *507*, 492–

495.

Caforio, A. & Driessen, A. J. M. 2017. Archaeal phospholipids: Structural properties and biosynthesis. *Biochimica et Biophysica Acta*, *1862*, 1325–1339.

Caforio, A., Siliakus, M. F., Exterkate, M., Jain, S., Jumde, V. R., Andringa, R. L. H., Kengen, S. W. M., Minnaard, A. J., Driessen, A. J. M., & van der Oost, J. 2018. Converting *Escherichia coli* into an archaebacterium with a hybrid heterochiral membrane. *PNAS*, *115*, 3704–3709.

Camponeschi, F. & Banci, L. 2019. Metal cofactors trafficking and assembly in the cell: a molecular view. *Pure and Applied Chemistry*, *91*, 231–245.

Capella-Gutiérrez, S., Silla-Martínez, J. M., & Gabaldón, T. 2009. trimAl: a tool for automated alignment trimming in large-scale phylogenetic analyses. *Bioinformatics*, *25*, 1972–1973.

Carbone, V., Schofield, L. R., Zhang, Y., Sang, C., Dey, D., Hannus, I. M., Martin, W. F., Sutherland-Smith, A. J., & Ronimus, R. S. 2015. Structure and evolution of the archaeal lipid synthesis enzyme *sn*-glycerol-1-phosphate dehydrogenase. *Journal of Biological Chemistry*, *290*, 21690–21704.

Carini, P., Van Mooy, B. A. S., Thrash, J. C., White, A., Zhao, Y., Campbell, E. O., Fredricks, H. F., & Giovannoni, S. J. 2015. SAR11 lipid renovation in response to phosphate starvation. *PNAS*, *112*, 7767–7772.

Carpenter, S. R., Caraco, N. F., Correll, D. L., Howarth, R. W., Sharpley, A. N., & Smith, V. H. 1998. Nonpoint pollution of surface waters with phosphorus and nitrogen. *Ecological Applications*, *8*, 559–568.

Carr, N. G. & Wyman, M. 1994. Cyanobacteria: their biology in relation to the oceanic picoplankton. In D. A. Bryant (Ed.), *The molecular biology of cyanobacteria. Advances in photosynthesis* (Vol. 1, pp. 27–44). Dordrecht: Springer.

Casey, J. R., Mardinoglu, A., Nielsen, J., & Karl, D. M. 2016. Adaptive evolution of phosphorus metabolism in *Prochlorococcus*. *MSystems*, *1*, 1–15.

Cavender-Bares, K. K., Karl, D. M., & Chisholm, S. W. 2001. Nutrient gradients in the western North Atlantic Ocean: relationship to microbial community structure and comparison to patterns in the Pacific Ocean. *Deep-Sea Research I*, *48*, 2373–2395.

Cerdà-Costa, N. & Gomis-Rüth, F. X. 2014. Architecture and function of metallopeptidase catalytic domains. *Protein Science*, *23*, 123–144.

Chaban, B., Ng, S. Y. M., & Jarrell, K. F. 2006. Archaeal habitats - From the extreme to the ordinary. *Canadian Journal of Microbiology*, *52*, 73–116.

Chandramouli, K. & Qian, P.-Y. 2009. Proteomics: challenges, techniques and

possibilities to overcome biological sample complexity. *Human Genomics & Proteomics*, *2009*, 22.

Chen, A.-M., Wang, Y.-B., Jie, S., Yu, A.-Y., Luo, L., Yu, G.-Q., Zhu, J.-B., & Wang, Y.-Z. 2010. Identification of a TRAP transporter for malonate transport and its expression regulated by *GtrA* from *Sinorhizobium meliloti*. *Research in Microbiology*, *161*, 556–564.

Chen, C. M., Ye, Q. Z., Zhu, Z., Wanner, B. L., & Walsh, C. T. 1990. Molecular biology of carbon-phosphorus bond cleavage. *Journal of Biological Chemistry*, *265*, 4461–4471.

Chen, H., Lu, Y., & Jiang, J. G. 2012. Comparative analysis on the key enzymes of the glycerol cycle metabolic pathway in *Dunaliella salina* under osmotic stresses. *PLoS ONE*, *7*, 3–9.

Chen, Y. & Schäfer, H. 2019. Towards a systematic understanding of structure–function relationship of dimethylsulfoniopropionate-catabolizing enzymes. *Molecular Microbiology*, *111*, 1399–1403.

Chen, Y., Xing, X. H., & Lou, K. 2005. Construction of recombinant *Escherichia coli* for over-production of soluble heparinase I by fusion to maltose-binding protein. *Biochemical Engineering Journal*, *23*, 155–159.

Christie-Oleza, J. A. & Armengaud, J. 2010. In-depth analysis of exoproteomes from marine bacteria by shotgun liquid chromatography-tandem mass spectrometry: The *Ruegeria pomeroyi* DSS-3 case-study. *Marine Drugs*, *8*, 2223–2239.

Christie-Oleza, J. A., Armengaud, J., Guerin, P., & Scanlan, D. J. 2015. Functional distinctness in the exoproteomes of marine *Synechococcus*. *Environmental Microbiology*, *17*, 3781–3794.

Christie-Oleza, J. A., Scanlan, D. J., & Armengaud, J. 2015. "You produce while I clean up", a strategy revealed by exoproteomics during *Synechococcus*-*Roseobacter* interactions. *Proteomics*, *15*, 3454–3462.

Christie-Oleza, J. A., Sousoni, D., Lloyd, M., Armengaud, J., & Scanlan, D. J. 2017. Nutrient recycling facilitates long-term stability of marine microbial phototroph–heterotroph interactions. *Nature Microbiology*, *2*.

Chróst, R. J. 1990. Microbial Ectoenzymes in Aquatic Environments (pp. 47–78).

Cífková, E., Holčapek, M., Lísa, M., Ovčačíková, M., Lyčka, A., Lynen, F., & Sandra, P. 2012. Nontargeted quantitation of lipid classes using hydrophilic interaction liquid chromatography–electrospray ionization mass spectrometry with single internal standard and response factor approach. *Analytical Chemistry*, *84*, 10064–10070.

Coleman, G. A., Pancost, R. D., Williams, T. A., & Dagan, T. 2019. Investigating

the origins of membrane phospholipid biosynthesis genes using outgroup-free rooting. *Genome Biology and Evolution*, *11*, 883–898.

Coleman, J. E. 1992. Structure and Mechanism of Alkaline Phosphatase. *Annual Review of Biophysics and Biomolecular Structure*, *21*, 441–483.

Coleman, M. L. & Chisholm, S. W. 2007. Code and context: *Prochlorococcus* as a model for cross scale biology. *Trends in Microbiology*, *15*, 398–407.

Compton, J., Mallinson, D., Glenn, C. R., Filippelli, G. M., Follmi, K., Shields, G., & Zanin, Y. 2000. Variations in the global phosphoruscycle. In C. R. Glenn, L. Prévôt-Lucas, & J. Lucas (Eds.), *Marine Authigenesis: from Global to Microbial* (66th ed.). SEPM Society for Sedimentary Geology.

Cotner, J. B. & Biddanda, B. A. 2002. Small players, large role: microbial influence on biogeochemical processes in pelagic aquatic ecosystems. *Ecosystems*, *5*, 105–121.

Cotner, J. B. & Wetzel, R. G. 1992. Uptake of dissolved inorganic and organic phosphorus compounds by phytoplankton and bacterioplankton. *Limnology and Oceanography*, *37*, 232–243.

Cox, A. D. & Saito, M. A. 2013. Proteomic responses of oceanic *Synechococcus* WH8102 to phosphate and zinc scarcity and cadmium additions. *Frontiers in Microbiology*, *4*, 1–17.

Cox, J. & Mann, M. 2008. MaxQuant enables high peptide identification rates, individualized p.p.b.-range mass accuracies and proteome-wide protein quantification. *Nature Biotechnology*, *26*, 1367–1372.

Daniel, R., Simon, M., & Wemheuer, B. 2018. Editorial: molecular ecology and genetic diversity of the *Roseobacter* clade. *Frontiers in Marine Science*, *9*, 1–3.

Delaney, M. L. 1998. Phosphorus accumulation in marine sediments and the oceanic phosphorus cycle. *Global Biogeochemical Cycles*, *12*, 563–572.

Delepelaire, P. 2004. Type I secretion in gram-negative bacteria. *Biochimica et Biophysica Acta (BBA) - Molecular Cell Research*, *1694*, 149–161.

Denger, K., Smits, T. H. M., & Cook, A. M. 2006. Genome-enabled analysis of the utilization of taurine as sole source of carbon or of nitrogen by *Rhodobacter sphaeroides* 2.4.1. *Microbiology*, *152*, 3197–3206.

Deppeler, S. L. & Davidson, A. T. 2017. Southern Ocean phytoplankton in a changing climate. *Frontiers in Marine Science*, *4*.

Dereeper, A., Guignon, V., Blanc, G., Audic, S., Buffet, S., Chevenet, F., Dufayard, J.-F., Guindon, S., Lefort, V., Lescot, M., Claverie, J.-M., & Gascuel, O. 2008. Phylogeny.fr: robust phylogenetic analysis for the non-specialist. *Nucleic Acids Research*, *36*, W465-9.

Diaz, J. M., Steffen, R., Sanders, J. G., Tang, Y., & Duhamel, S. 2019. Preferential utilization of inorganic polyphosphate over other bioavailable phosphorus sources by the model diatoms *Thalassiosira* spp. *Environmental Microbiology*, *21*, 2415–2425.

Ding, H., Yip, C. B., Geddes, B. A., Oresnik, I. J., & Hynes, M. F. 2012. Glycerol utilization by *Rhizobium leguminosarum* requires an ABC transporter and affects competition for nodulation. *Microbiology*, *158*, 1369–1378.

Ding, S., Bale, N. J., Hopmans, E. C., Villanueva, L., Arts, M. G. I., Schouten, S., & Damsté, J. S. S. 2021. Lipidomics of environmental microbial communities. II: characterization using molecular networking and information theory. *Frontiers in Microbiology*, *12*.

Doerrler, W. T., Sikdar, R., Kumar, S., & Boughner, L. A. 2013. New functions for the ancient DedA membrane protein family. *Journal of Bacteriology*, *195*, 3–11.

Dörries, M., Wöhlbrand, L., Kube, M., Reinhardt, R., & Rabus, R. 2016. Genome and catabolic subproteomes of the marine, nutritionally versatile, sulfate-reducing bacterium *Desulfococcus multivorans* DSM 2059. *BMC Genomics*, *17*, 918.

Duarte, C. M. 2014. Global change and the future ocean: a grand challenge for marine sciences. *Frontiers in Marine Science*, *1*, 1–16.

Duce, R. A., Liss, P. S., Merrill, J. T., Atlas, E. L., Buat-Menard, P., Hicks, B. B., Miller, J. M., Prospero, J. M., Arimoto, R., Church, T. M., Ellis, W., Galloway, J. N., Hansen, L., Jickells, T. D., Knap, A. H., Reinhardt, K. H., Schneider, B., … Zhou, M. 1991. The atmospheric input of trace species to the world ocean. *Global Biogeochemical Cycles*, *5*, 193–259.

Dufresne, A., Ostrowski, M., Scanlan, D. J., Garczarek, L., Mazard, S., Palenik, B., Paulsen, I. T., de Marsac, N. T., Wincker, P., Dossat, C., Ferriera, S., Johnson, J., Post, A. F., Hess, W. R., & Partensky, F. 2008. Unraveling the genomic mosaic of a ubiquitous genus of marine cyanobacteria. *Genome Biology*, *9*.

Dyhrman, S. T., Chappell, P. D., Haley, S. T., Moffett, J. W., Orchard, E. D., Waterbury, J. B., & Webb, E. A. 2006. Phosphonate utilization by the globally important marine diazotroph *Trichodesmium*. *Nature*, *439*, 68–71.

Eder, S., Shi, L., Jensen, K., Yamane, K., & Hulett, F. M. 1996. A *Bacillus subtilis* secreted phosphodiesterase/alkaline phosphatase is the product of a Pho regulon gene, *phoD*. *Microbiology*, *142*, 2041–2047.

Edgar, R. C. 2004a. MUSCLE: a multiple sequence alignment method with reduced time and space complexity. *BMC Bioinformatics*, *5*, 1–19.

Edgar, R. C. 2004b. MUSCLE: multiple sequence alignment with high accuracy and

high throughput. *Nucleic Acids Research*, *32*, 1792–1797.

Exterkate, M., de Kok, N. A. W., Andringa, R. L. H., Wolbert, N. H. J., Minnaard, A. J., & Driessen, A. J. M. 2021. A promiscuous archaeal cardiolipin synthase enables construction of diverse natural and unnatural phospholipids. *Journal of Biological Chemistry*, 104743.

Faba-Rodriguez, R., Brearley, C. A., & Hemmings, A. M. 2019. *Crystal structure of a cereal purple acid phytase provides insights to phytate degradation in plants*.

Falkenberg, P. & Strøm, A. R. 1990. Purification and characterization of osmoregulatory betaine aldehyde dehydrogenase of *Escherichia coli*. *Biochimica et Biophysica Acta*, *1034*, 253–259.

Falkowski, P. G., Fenchel, T., & Delong, E. F. 2008. The microbial engines that drive earth's biogeochemical cycles. *Science*, *320*, 1034–1039.

Faul, K. L., Paytan, A., & Delaney, M. L. 2005. Phosphorus distribution in sinking oceanic particulate matter. *Marine Chemistry*, *97*, 307–333.

Feng, X., Chu, X., Qian, Y., Henson, M. W., Lanclos, V. C., Qin, F., Barnes, S., Zhao, Y., Thrash, J. C., & Luo, H. 2021. Mechanisms driving genome reduction of a novel *Roseobacter* lineage. *The ISME Journal*, *15*, 3576–3586.

Field, C. B., Behrenfeld, M. J., Randerson, J. T., & Falkowski, P. G. 1998. Primary production of the biosphere: integrating terrestrial and oceanic components. *Science*, *281*, 237–240.

Filippelli, G. M. & Delaney, M. L. 1996. Phosphorus geochemistry of equatorial Pacific sediments. *Geochimica et Cosmochimica Acta*, *60*, 1479–1495.

Flombaum, P., Gallegos, J. L., Gordillo, R. A., Rincón, J., Zabala, L. L., Jiao, N., Karl, D. M., Li, W. K. W., Lomas, M. W., Veneziano, D., Vera, C. S., Vrugt, J. A., & Martiny, A. C. 2013. Present and future global distributions of the marine cyanobacteria *Prochlorococcus* and *Synechococcus*. *PNAS*, *110*, 9824–9829.

Folch, J., Lees, M., & Sloane Stanley, G. H. 1957. A simple method for the isolation and purification of total lipids from animal tissues. *Journal of Biological Chemistry*, *226*, 497–509.

Föllmi, K. B. 1996. The phosphorus cycle, phosphogenesis and marine phosphate-rich deposits. *Earth-Science Reviews*, *40*, 55–124.

Forward, J. A., Behrendt, M. C., Wyborn, N. R., Cross, R., & Kelly, D. J. 1997. TRAP transporters: a new family of periplasmic solute transport systems encoded by the *dctPQM* genes of *Rhodobacter capsulatus* and by homologs in diverse gram-negative bacteria. *Journal of Bacteriology*, *179*, 5482–5493.

Frischkorn, K. R., Krupke, A., Rouco, M., Salazar Estrada, A. E., Van Mooy, B. A.

S., & Dyhrman, S. T. 2018. *Trichodesmium* physiological ecology and phosphate reduction in the western Tropical South Pacific. *Biogeosciences*, *15*, 5761–5778.

Frka, S., Gašparović, B., Marić, D., Godrijan, J., Djakovac, T., Vojvodić, V., Dautović, J., & Kozarac, Z. 2011. Phytoplankton driven distribution of dissolved and particulate lipids in a semi-enclosed temperate sea (Mediterranean): spring to summer situation. *Estuarine, Coastal and Shelf Science*, *93*, 290–304.

Froelich, P. N. 1988. Kinetic control of dissolved phosphate in natural rivers and estuaries: a primer on the phosphate buffer mechanism. *Limnology and Oceanography*, *33*, 649–668.

Fuhrman, J. A. & Campbell, L. 1998. Marine ecology - microbial microdiversity. *Nature*, *393*, 410–411.

Gajewski, E., Steckler, D. K., & Goldberg, R. N. 1986. Thermodynamics of the Hydrolysis of Adenosine 5′ - triphosphate to Adenosine 5′ - diphosphate. *The Journal of Biological Chemistry*, *261*, 12733–12737.

Gardner, S. G., Johns, K. D., Tanner, R., & McCleary, W. R. 2014. The PhoU protein from *Escherichia coli* interacts with PhoR, PstB, and metals to form a phosphate-signaling complex at the membrane. *Journal of Bacteriology*, *196*, 1741–1752.

Gašparović, B., Frka, S., Koch, B. P., Zhu, Z. Y., Bracher, A., Lechtenfeld, O. J., Neogie, S. B., Larag, R. J., & Kattnerb, G. 2014. Factors influencing particulate lipid production in the East Atlantic Ocean. *Deep-Sea Research I*, *89*, 56–67.

Gašparović, B., Penezić, A., Lampitt, R. S., Sudasinghe, N., & Schaub, T. 2018. Phospholipids as a component of the oceanic phosphorus cycle. *Marine Chemistry*, *250*, 70–80.

Gasteiger, E., Hoogland, C., Gattiker, A., Duvaud, S., Wilkins, M. R., Appel, R. D., & Bairoch, A. 2005. Protein identification and analysis tools on the ExPASy server. In *The Proteomics Protocols Handbook* (pp. 571–608).

Geiger, O., González-Silva, N., López-Lara, I. M., & Sohlenkamp, C. 2010. Amino acid-containing membrane lipids in bacteria. *Progress in Lipid Research*, *49*, 46–60.

Geiger, O., Röhrs, V., Weissenmayer, B., Finan, T. M., & Thomas-Oates, J. E. 1999. The regulator gene *phoB* mediates phosphate stress-controlled synthesis of the membrane lipid diacylglyceryl-N,N,N-trimethylhomoserine in *Rhizobium* (*Sinorhizobium*) *meliloti*. *Molecular Microbiology*, *32*, 63–73.

Gibson, D. G., Young, L., Chuang, R.-Y., Venter, J. C., Hutchison, C. A., & Smith,

H. O. 2009. Enzymatic assembly of DNA molecules up to several hundred kilobases. *Nature Methods*, *6*, 343–345.

Gobley, M. 1874a. Recherches chimiques sur le cerveau. *Journal de Pharmacie et de Chimie*, *4*, 346–354.

Gobley, M. 1874b. Sur la lécithine et la cérébrine. *Journal de Pharmacie et de Chimie*, *20*, 161–166.

Grammann, K., Volke, A., & Kunte, H. J. 2002. New type of osmoregulated solute transporter identified in halophilic members of the bacteria domain: TRAP transporter TeaABC mediates uptake of ectoine and hydroxyectoine in *Halomonas elongata* DSM 2581. *Journal of Bacteriology*, *184*, 3078–3085.

Grob, C., Ostrowski, M., Holland, R. J., Heldal, M., Norland, S., Erichsen, E. S., Blindauer, C. A., Martin, A. P., Zubkov, M. V., & Scanlan, D. J. 2013. Elemental composition of natural populations of key microbial groups in Atlantic waters. *Environmental Microbiology*, *15*, 3054–3064.

Grossman, A. R., Schaefer, M. R., Chiang, G. G., & Collier, J. L. 1994. The responses of cyanobacteria to environmental conditions: light and nutrients. In D. A. Bryant (Ed.), *The molecular biology of cyanobacteria. Advances in photosynthesis* (1st ed., pp. 641–675). Springer Netherlands.

Harayama, T. & Riezman, H. 2018. Understanding the diversity of membrane lipid composition. *Nature Reviews Molecular Cell Biology*, *19*, 281–296.

Hartley, C. J., French, N. G., Scoble, J. A., Williams, C. C., Churches, Q. I., Frazer, A. R., Taylor, M. C., Coia, G., Simpson, G., Turner, N. J., & Scott, C. 2017. Sugar analog synthesis by *in vitro* biocatalytic cascade: a comparison of alternative enzyme complements for dihydroxyacetone phosphate production as a precursor to rare chiral sugar synthesis. *PLoS ONE*, *12*.

Hickman, S. J., Cooper, R. E. M., Bellucci, L., Paci, E., & Brockwell, D. J. 2017. Gating of TonB-dependent transporters by substrate-specific forced remodelling. *Nature Communications*, *8*, 14804.

Hirani, T. A., Suzuki, I., Murata, N., Hayashi, H., & Eaton-Rye, J. J. 2001. Characterization of a two-component signal transduction system involved in the induction of alkaline phosphatase under phosphate-limiting conditions in *Synechocystis* sp. PCC 6803. *Plant Molecular Biology*, *45*, 133–44.

Hoang, D. T., Chernomor, O., von Haeseler, A., & Minh, B. Q. 2017. UFBoot2: Improving the ultrafast bootstrap approximation. *Molecular Biology and Evolution*, *35*, 518–522.

Hopkins, A. P., Hawkhead, J. A., & Thomas, G. H. 2013. Transport and catabolism of the sialic acids *N*-glycolylneuraminic acid and 3-keto-3-deoxy-D-glycero-D-galactonononic acid by *Escherichia coli* K-12. *FEMS Microbiology Letters*,

347, 14–22.

Huang, Y., Lemieux, M. J., Song, J., Auer, M., & Wang, D.-N. 2003. Structure and mechanism of the glycerol-3-phosphate transporter from *Escherichia coli*. *Science*, *301*, 616–620.

Huerta-Cepas, J., Szklarczyk, D., Heller, D., Hernández-Plaza, A., Forslund, S. K., Cook, H., Mende, D. R., Letunic, I., Rattei, T., Jensen, L. J., von Mering, C., & Bork, P. 2019. eggNOG 5.0: a hierarchical, functionally and phylogenetically annotated orthology resource based on 5090 organisms and 2502 viruses. *Nucleic Acids Research*, *47*, D309–D314.

Hugouvieux-Cotte-Pattat, N., Blot, N., & Reverchon, S. 2001. Identification of TogMNAB, an ABC transporter which mediates the uptake of pectic oligomers in *Erwinia chrysanthemi* 3937. *Molecular Microbiology*, *41*, 1113–1123.

Ilikchyan, I. N., McKay, R. M. L., Kutovaya, O. A., Condon, R., & Bullerjahn, G. S. 2010. Seasonal expression of the picocyanobacterial phosphonate transporter gene *phnD* in the Sargasso sea. *Frontiers in Microbiology*, *1*, 1–8.

Ilikchyan, I. N., McKay, R. M. L., Zehr, J. P., Dyhrman, S. T., & Bullerjahn, G. S. 2009. Detection and expression of the phosphonate transporter gene *phnD* in marine and freshwater picocyanobacteria. *Environmental Microbiology*, *11*, 1314–1324.

Ireland, S. M. & Martin, A. C. R. 2019. ZincBind - the database of zinc binding sites. *Database*, 1–8.

Jakuba, R. W., Moffett, J. W., & Dyhrman, S. T. 2008. Evidence for the linked biogeochemical cycling of zinc, cobalt, and phosphorus in the western North Atlantic Ocean. *Global Biogeochemical Cycles*, *22*, 1–13.

James, W. F., Barko, J. W., & Eakin, H. L. 2002. Labile and refractory forms of phosphorus in runoff of the Redwood river basin, Minnesota. *Journal of Freshwater Ecology*, *17*, 297–304.

Jarrell, K. F., Walters, A. D., Bochiwal, C., Borgia, J. M., Dickinson, T., & Chong, J. P. J. 2011. Major players on the microbial stage: why archaea are important. *Microbiology*, *157*, 919–936.

Kageyama, H., Tripathi, K., Rai, A. K., Cha-um, S., Waditee-Sirisattha, R., & Takabe, T. 2011. An alkaline phosphatase/phosphodiesterase, PhoD, induced by salt stress and secreted out of the cells of Aphanothece halophytica, a halotolerant cyanobacterium. *Applied and Environmental Microbiology*, *77*, 5178–5183.

Kalyaanamoorthy, S., Minh, B. Q., Wong, T. K. F., von Haeseler, A., & Jermiin, L. S. 2017. Fast model selection for accurate phylogenetic estimatesNo Title.

Nature Methods, *14*, 587–589.

Kandler, O. 1995. Cell wall biochemistry in Archaea and its phylogenetic implications. *Journal of Biological Physics*, *20*, 165–169.

Kapust, R. B. & Waugh, D. S. 1999. Escherichia coli maltose-binding protein is uncommonly effective at promoting the solubility of polypeptides to which it is fused. *Protein Science*, *8*, 1668–1674.

Karl, D. M. 2014. Microbially mediated transformations of phosphorus in the sea: new views of an old cycle. *Annual Review of Marine Science*, *6*, 279–337.

Karl, D. M., Bidigare, R. R., & Letelier, R. M. 2001. Long-term changes in plankton community structure and productivity in the North Pacific Subtropical Gyre: the domain shift hypothesis. *Deep-Sea Research II*, *48*, 1449–1470.

Karl, D. M. & Björkman, K. M. 2001. Phosphorus cycle in seawater: dissolved and particulate pool inventories and selected phosphorus fluxes. In J. H. Paul (Ed.), *Methods Microbiology* (30th ed., pp. 239–270). San Diego: Academics.

Karl, D. M., Björkman, K. M., Dore, J. E., Fujieki, L., Hebel, D. V., Houlihan, T., Letelier, R. M., & Tupas, L. M. 2001. Ecological nitrogen-to-phosphorus stoichiometry at station ALOHA. *Deep-Sea Research II*, *48*, 1529–1566.

Karner, M. B., Delong, E. F., & Karl, D. M. 2001. Archaeal dominance in the mesopelagic zone of the Pacific Ocean. *Nature*, *409*, 507–510.

Kathuria, S. & Martiny, A. C. 2011. Prevalence of a calcium-based alkaline phosphatase associated with the marine cyanobacterium Prochlorococcus and other ocean bacteria. *Environmental Microbiology*, *13*, 74–83.

Kaur, A., Hernandez-Fernaud, J. R., Aguilo-Ferretjans, M. d. M., Wellington, E. M., & Christie-Oleza, J. A. 2017. 100 Days of marine *Synechococcus–Ruegeria pomeroyi* interaction: a detailed analysis of the exoproteome. *Environmental Microbiology*, *20*, 785–799.

Kelley, L. A., Mezulis, S., Yates, C. M., Wass, M. N., & Sternberg, M. J. E. 2016. The Phyre2 web portal for protein modeling, prediction and analysis. *Nature Protocols*, *10*, 845–858.

Kelliher, J. L., Leder Macek, A. J., Grudzinski, K. M., Radin, J. N., & Kehl-Fie, T. E. 2020. *Staphylococcus aureus* preferentially liberates inorganic phosphate from organophosphates in environments where this nutrient is limiting. *Journal of Bacteriology*, *202*.

Kelly, D. J. & Thomas, G. H. 2001. The tripartite ATP-independent periplasmic (TRAP) transporters of bacteria and archaea. *FEMS Microbiology Reviews*, *25*, 405–424.

Kelly, L., Ding, H., Huang, K. H., Osburne, M. S., & Chisholm, S. W. 2013. Genetic diversity in cultured and wild marine cyanomyoviruses reveals phosphorus

stress as a strong selective agent. *The ISME Journal*, *7*, 1827–1841.

Kelman, L. M. & Kelman, Z. 2014. Archaeal DNA replication. *Annual Review of Genetics*, *48*, 71–97.

Klabunde, T., Sträter, N., Fröhlich, R., Witzel, H., & Krebs, B. 1996. Mechanism of Fe(III)-Zn(II) purple acid phosphatase based on crystal structures. *Journal of Molecular Biology*, *259*, 737–748.

Kofoid, E., Rappleye, C., Stojiljkovic, I., & Roth, J. 1999. The 17-gene ethanolamine (*eut*) operon of *Salmonella typhimurium* encodes five homologues of carboxysome shell proteins. *Journal of Bacteriology*, *181*, 5317–5329.

Kolber, Z. S., Barber, R. T., Coale, K. H., Fitzwater, S. E., Greene, R. M., Johnson, K. S., Lindley, S., & Falkowski, P. G. 1994. Iron limitation of phytoplankton photosynthesis in the equatorial Pacific Ocean. *Nature*, *371*, 145–149.

Koolman, J. & Röhm, K.-H. 2019. *Taschenatlas der Biochemie*. (J. Wirth, Ed.) (5th ed.). Stuttgart: Georg Thieme Verlag KG.

Kornberg, S. R. 1957. Adenosine triphosphate synthesis from polyphosphate by an enzyme from *Escherichia coli*. *Biochimica et Biophysica Acta*, *26*, 294–300.

Kremling, K. & Streu, P. 1993. Saharan dust influenced trace element fluxes in deep North Atlantic subtropical waters. *Deep-Sea Research I*, *40*, 1155–1168.

Kretsinger, R. H. 2013. Calcium-binding proteins, overview. In R. H. Kretsinger, V. N. Uversky, & E. . Permyakov (Eds.), *Encyclopedia of Metalloproteins* (pp. 521–536). Springer, New York, NY.

Kuenzler, E. J. 1965. Glucose-6-phosphate utilization by marine algae. *Journal of Phycology*, *1*, 156–164.

Kulaev, I. S., Vagabov, V. M., & Kulakovskaya, T. V. 2005. *The biochemistry of inorganic polyphosphates* (Vol. 2). John Wiley & Sons.

Kumar, S. & Doerrler, W. T. 2014. Members of the conserved DedA family are likely membrane transporters and are required for drug resistance in *Escherichia coli*. *Antimicrobial Agents and Chemotherapy*, *58*, 923–930.

Lamark, T., Kaasen, I., Eshoo, M. W., Falkenberg, P., McDougall, J., & Strøm, A. R. 1991. DNA sequence and analysis of the *bet* genes encoding the osmoregulatory choline—glycine betaine pathway of *Escherichia coli*. *Molecular Microbiology*, *5*, 1049–1064.

Landfald, B. & Strøm, A. R. 1986. Choline-glycine betaine pathway confers a high level of osmotic tolerance in *Escherichia coli*. *Journal of Bacteriology*, *165*, 849–855.

Larrouy-Maumus, G., Biswas, T., Hunt, D. M., Kelly, G., Tsodikov, O. V., & de Carvalho, L. P. S. 2013. Discovery of a glycerol 3-phosphate phosphatase reveals glycerophospholipid polar head recycling in *Mycobacterium tuberculosis*. *PNAS*, *110*, 11320–11325.

Larson, T. J., Ehrmann, M., & Boos, W. 1983. Periplasmic glycerophosphodiester phosphodiesterase of *Escherichia coli*, a new enzyme of the *glp* regulon. *Journal of Biological Chemistry*, *258*, 5428–5432.

Law, K. P. & Zhang, C. L. 2019. Current progress and future trends in mass spectrometry-based archaeal lipidomics. *Organic Geochemistry*, *134*, 45–61.

Lazzari, P., Solidoro, C., Salon, S., & Bolzon, G. 2016. Spatial variability of phosphate and nitrate in the Mediterranean Sea: a modeling approach. *Deep-Sea Research I*, *108*, 39–52.

Lee, D. H., Choi, S. L., Rha, E., Kim, S. J., Yeom, S. J., Moon, J. H., & Lee, S. G. 2015. A novel psychrophilic alkaline phosphatase from the metagenome of tidal flat sediments. *BMC Biotechnology*, *15*, 1–13.

Legendre, L., Rivkin, R. B., Weinbauer, M. G., Guidi, L., & Uitz, J. 2015. The microbial carbon pump concept: potential biogeochemical significance in the globally changing ocean. *Progress in Oceanography*, *134*, 432–450.

Lemieux, M. J., Huang, Y., & Wang, D.-N. 2004. Glycerol-3-phosphate transporter of *Escherichia coli*: structure, function and regulation. *Research in Microbiology*, *155*, 623–629.

Lemoine, F., Correia, D., Lefort, V., Doppelt-Azeroual, O., Mareuil, F., Cohen-Boulakia, S., & Gascuel, O. 2019. NGPhylogeny.fr: new generation phylogenetic services for non-specialists. *Nucleic Acids Research*, *47*, W260–W265.

Letunic, I. & Bork, P. 2021. Interactive Tree Of Life (iTOL) v5: an online tool for phylogenetic tree display and annotation. *Nucleic Acids Research*, *49*, W293–W296.

Li, T., Guo, C., Zhang, Y., Wang, C., Lin, X., & Lin, S. 2018. Identification and expression analysis of an atypical alkaline phosphatase in *Emiliania huxleyi*. *Frontiers in Microbiology*, *9*, 1–13.

Li, W. K. W. 1995. Composition of ultraphytoplankton in the central North Atlantic. *Marine Ecology Progress Series*, *122*, 1–8.

Li, W. K. W. 1998. Annual average abundance of heterotrophic bacteria and *Synechococcus* in surface ocean waters. *Limnology and Oceanography*, *43*, 1746–1753.

Lidbury, I. D. E. A., Kimberley, G., Scanlan, D. J., Murrell, J. C., & Chen, Y. 2015. Comparative genomics and mutagenesis analyses of choline metabolism in

the marine *Roseobacter* clade. *Environmental Microbiology*, *17*, 5048–5062.

Lidbury, I. D. E. A., Murphy, A. R. J., Fraser, T. D., Bending, G. D., Jones, A. M. E., Moore, J. D., Goodall, A., Tibbett, M., Hammond, J. P., Scanlan, D. J., & Wellington, E. M. H. 2017. Identification of extracellular glycerophosphodiesterases in *Pseudomonas* and their role in soil organic phosphorus remineralisation. *Scientific Reports*, *7*.

Lidbury, I. D. E. A., Murphy, A. R. J., Scanlan, D. J., Bending, G. D., Jones, A. M. E., Moore, J. D., Goodall, A., Hammond, J. P., & Wellington, E. M. H. 2016. Comparative genomic, proteomic and exoproteomic analyses of three *Pseudomonas* strains reveals novel insights into the phosphorus scavenging capabilities of soil bacteria. *Environmental Microbiology*, *18*, 3535–3549.

Lin, S., Litaker, R. W., & Sunda, W. G. 2016. Phosphorus physiological ecology and molecular mechanisms in marine phytoplankton. *Journal of Phycology*, *52*, 10–36.

Lin, W., Zhao, D., & Luo, J. 2018. Distribution of alkaline phosphatase genes in cyanobacteria and the role of alkaline phosphatase on the acquisition of phosphorus from dissolved organic phosphorus for cyanobacterial growth. *Journal of Applied Phycology*, *30*, 839–850.

Lin, X., Wang, L., Shi, X., & Lin, S. 2015. Rapidly diverging evolution of an atypical alkaline phosphatase (PhoA<superscript>aty</superscript>) in marine phytoplankton: insights from dinoflagellate alkaline phosphatases. *Frontiers in Microbiology*, *6*, 1–12.

Linhartová, I., Bumba, L., Mašín, J., Basler, M., Osička, R., Kamanová, J., Procházková, K., Adkins, I., Hejnová-Holubová, J., Sadílková, L., Morová, J., & Šebo, P. 2010. RTX proteins: a highly diverse family secreted by a common mechanism. *FEMS Microbiology Reviews*, *34*, 1076–1112.

Lohan, M. C., Statham, P. J., & Crawford, D. W. 2002. Total dissolved zinc in the upper water column of the subarctic North East Pacific. *Deep-Sea Research II*, *49*, 5793–5808.

López-Lara, I. M. & Geiger, O. 2017. Bacterial lipid diversity. *Biochimica et Biophysica Acta*, *1862*, 1287–1299.

Lougheed, T. 2011. Phosphorus paradox. *Environmental Health Perspectives*, *119*, A 209-A 213.

Lu, S., Wang, J., Chitsaz, F., Derbyshire, M. K., Geer, R. C., Gonzales, N. R., Gwadz, M., Hurwitz, D. I., Marchler, G. H., Song, J. S., Thanki, N., Yamashita, R. A., Yang, M., Zhang, D., Zheng, C., Lanczycki, C. J., & Marchler-Bauer, A. 2020. CDD/SPARCLE: the conserved domain database in 2020. *Nucleic Acids Research*, *48*, D265–D268.

Luo, H., Benner, R., Long, R. A., & Hu, J. 2009. Subcellular localization of marine bacterial alkaline phosphatases. *PNAS*, *106*, 21219–21223.

Luo, H. & Moran, M. A. 2014. Evolutionary ecology of the marine *Roseobacter* clade. *Microbiology and Molecular Biology Reviews*, *78*, 573–587.

Luo, M., Guo, Y.-C., Deng, J.-Y., Wei, H.-P., Zhang, Z.-P., Leng, Y., Men, D., Song, L.-R., Zhang, X.-E., & Zhou, Y.-F. 2010. Characterization of a monomeric heat-labile classical alkaline phosphatase from *Anabaena* sp. PCC7120. *Biochemistry (Moscow)*, *75*, 655–664.

Mahaffey, C., Reynolds, S., Davis, C. E., & Lohan, M. C. 2014. Alkaline phosphatase activity in the subtropical ocean: insights from nutrient, dust and trace metal addition experiments. *Frontiers in Marine Science*, *1*, 1–13.

Majumdar, A., Ghatak, A., & Ghosh, R. K. 2005. Identification of the gene for the monomeric alkaline phosphatase of *Vibrio cholerae* serogroup O1 strain. *Gene*, *344*, 251–258.

Makino, K., Shinagawa, H., Amemura, M., Kimura, S., Nakata, A., & Ishihama, A. 1988. Regulation of the phosphate regulon of *Escherichia coli*. Activation of *pstS* transcription by PhoB protein in vitro. *Journal of Molecular Biology*, *203*, 85–95.

Manta, B., Boyd, D., & Berkman, M. 2019. Disulfide bond formation in the perisplasm of *Escherichia coli*. *EcoSal Plus*, *8*.

Marić, D., Frka, S., Godrijan, J., Tomažić, I., Penezić, A., Djakovac, T., Vojvodić, V., Precali, R., & Gašparović, B. 2013. Organic matter production during late summer–winter period in a temperate sea. *Continental Shelf Research*, *55*, 52–65.

Martin, J. H., Coale, K. H., Johnson, K. S., Fitzwater, S. E., Gordon, R. M., Tanner, S. J., Hunter, C. N., Elrod, V. A., Nowicki, J. L., Coley, T. L., Barber, R. T., Lindley, S., Watson, A. J., Scoy, K. Van, Law, C. S., Liddicoat, M. I., Ling, R., … Tindale, N. W. 1994. Testing the iron hypothesis in ecosystems of the Equatorial Pacific Ocean. *Nature*, *371*, 123–129.

Martin, P., Dyhrman, S. T., Lomas, M. W., Poulton, N. J., & Van Mooy, B. A. S. 2014. Accumulation and enhanced cycling of polyphosphate by Sargasso Sea plankton in response to low phosphorus. *PNAS*, *111*, 8089–94.

McGrath, J. W., Chin, J. P., & Quinn, J. P. 2013. Organophosphonates revealed: New insights into the microbial metabolism of ancient molecules. *Nature Reviews Microbiology*, *11*, 412–419.

Meinert, C., Senger, J., Witthohn, M., Wübbeler, J. H., & Steinbüchel, A. 2017. Carbohydrate uptake in *Advenella mimigardefordensis* strain DPN7(T) is mediated by periplasmic sugar oxidation and a TRAP-transport system.

Molecular Microbiology, *104*, 916–930.

Mergulhão, F. J. M., Summers, D. K., & Monteiro, G. A. 2005. Recombinant protein secretion in *Escherichia coli*. *Biotechnology Advances*, *23*, 177–202.

Migon, C., Sandroni, V., & Béthoux, J.-P. 2001. Atmospheric input of anthropogenic phosphorus to the northwest mediterranean under oligotrophic conditions. *Marine Environmental Research*, *52*, 413–426.

Milanese, A., Mende, D. R., Paoli, L., Salazar, G., Ruscheweyh, H. J., Cuenca, M., Hingamp, P., Alves, R., Costea, P. I., Coelho, L. P., Schmidt, T. S. B., Almeida, A., Mitchell, A. L., Finn, R. D., Huerta-Cepas, J., Bork, P., Zeller, G., & Sunagawa, S. 2019. Microbial abundance, activity and population genomic profiling with mOTUs2. *Nature Communications*, *10*.

Minder, A. C., Narberhaus, F., Fischer, H. M., & Hennecke, H. 1998. The *Bradyrhizobium japonicum phoB* gene is required for phosphate-limited growth but not for symbiotic nitrogen fixation. *FEMS Microbiology Letters*, *161*, 47–52.

Mirzadeh, K., Shilling, P. J., Elfageih, R., Cumming, A. J., Cui, H. L., Renning, M., Nørholm, M. H. H., & Daley, D. O. 2020. Increased production of periplasmic proteins in *Escherichia coli* by directed evolution of the translation initiation region. *Microbial Cell Factories*, *19*.

Mistry, J., Chuguransky, S., Williams, L., Qureshi, M., Salazar, G. A., Sonnhammer, E. L. L., Tosatto, S. C. E., Paladin, L., Raj, S., Richardson, L. J., Finn, R. D., & Bateman, A. 2021. Pfam: the protein families database in 2021. *Nucleic Acids Research*, *49*, D412–D419.

Moellering, E. R., Prince, V. L., & Prince, R. C. 2017. Fatty acids: introduction. In O. Geiger (Ed.), *Handbook of Hydrocarbon and Lipid Microbiology*.

Monds, R. D., Newell, P. D., Schwartzman, J. A., & O'Toole, G. A. 2006. Conservation of the Pho regulon in *Pseudomonas fluorescens* Pf0-1. *Applied and Environmental Microbiology*, *72*, 1910–1924.

Moore, C. M., Mills, M. M., Arrigo, K. R., Berman-Frank, I., Bopp, L., Boyd, P. W., Galbraith, E. D., Geider, R. J., Guieu, C., Jaccard, S. L., Jickells, T. D., La Roche, J., Lenton, T. M., Mahowald, N. M., Marañón, E., Marinov, I., Moore, J. K., … Ulloa, O. 2013. Processes and patterns of oceanic nutrient limitation. *Nature Geoscience*, *6*, 701–710.

Moore, C. M., Mills, M. M., Langlois, R., Milne, A., Achterberg, E. P., La Roche, J., & Geider, R. J. 2008. Relative influence of nitrogen and phosphorus availability on phytoplankton physiology and productivity in the oligotrophic sub-tropical North Atlantic Ocean. *Limnology and Oceanography*, *53*, 291–305.

Moore, L. R., Ostrowski, M., Scanlan, D. J., Feren, K., & Sweetsir, T. 2005. Ecotypic variation in phosphorus-acquisition mechanisms within marine picocyanobacteria. *Aquatic Microbial Ecology*, *39*, 257–269.

Morel, F. M. M. & Price, N. M. 2003. The biogeochemical cycles of trace metals in the oceans. *Science*, *300*, 944–947.

Morohoshi, T., Maruo, T., Shirai, Y., Kato, J., Ikeda, T., Takiguchi, N., Ohtake, H., & Kuroda, A. 2002. Accumulation of inorganic polyphosphate in *phoU* mutants of *Escherichia coli* and *Synechocystis* sp . strain PCC6803. *Applied and Environmental Microbiology*, *68*, 4107–4110.

Morrissey, J. & Bowler, C. 2012. Iron utilization in marine cyanobacteria and eukaryotic algae. *Frontiers in Microbiology*, *3*, 43.

Moss, G. P. 1996. Basic terminology of stereochemistry (IUPAC Recommendations 1996). *Pure and Applied Chemistry*, *68*, 2193–2222.

Muller, P. 1994. Glossary of terms used in physical organic chemistry (IUPAC Recommendations 1994). *Pure and Applied Chemistry*, *66*, 1077–1184.

Mulligan, C., Leech, A. P., Kelly, D. J., & Thomas, G. H. 2012. The membrane proteins SiaQ and SiaM form an essential stoichiometric complex in the sialic acid tripartite ATP-independent periplasmic (TRAP) transporter SiaPQM (VC1777-1779) from *Vibrio cholerae*. *The Journal of Biological Chemistry*, *287*, 3598–3608.

Muthusamy, S., Lundin, D., Mamede Branca, R. M., Baltar, F., González, J. M., Lehtiö, J., & Pinhassi, J. 2017. Comparative proteomics reveals signature metabolisms of exponentially growing and stationary phase marine bacteria. *Environmental Microbiology*, *19*, 2301–2319.

Nguyen, L. T., Schmidt, H. A., von Haeseler, A., & Minh, B. Q. 2015. IQ-TREE: a fast and effective stochastic algorithm for estimating maximum likelihood phylogenies. *Molecular Biology and Evolution*, *32*, 268–274.

Nishihara, M., Yamazaki, T., Oshima, T., & Koga, Y. 1999. *sn*-glycerol-1-phosphate-forming activities in *Archaea*: Separation of archaeal phospholipid biosynthesis and glycerol catabolism by glycerophosphate enantiomers. *Journal of Bacteriology*, *181*, 1330–1333.

Nocek, B., Kochinyan, S., Proudfoot, M., Brown, G., Evdokimova, E., Osipiuk, J., Edwards, A. M., Savchenko, A., Joachimiaka, A., & Yakunin, A. F. 2008. Polyphosphate-dependent synthesis of ATP and ADP by the family-2 polyphosphate kinases in bacteria. *PNAS*, *105*, 17730–17735.

Noskova, Y., Likhatskaya, G., Terentieva, N., Son, O., Tekutyeva, L., & Balabanova, L. 2019. A novel alkaline phosphatase/phosphodiesterase, CamPhoD, from marine bacterium *Cobetia amphilecti* KMM 296. *Marine*

Drugs, *17*, 1–20.

Østerås, M., Boncompagni, E., Vincent, N., Poggi, M. C., & Le Rudulier, D. 1998. Presence of a gene encoding choline sulfatase in *Sinorhizobium meliloti bet* operon: choline-*O*-sulfate is metabolized into glycine betaine. *PNAS*, *95*, 11394–11399.

Ostrowski, M., Mazard, S., Tetu, S. G., Phillippy, K., Johnson, A., Palenik, B., Paulsen, I. T., & Scanlan, D. J. 2010. PtrA is required for coordinate regulation of gene expression during phosphate stress in a marine Synechococcus. *The ISME Journal*, *4*, 908–921.

Ou, X., Ji, C., Han, X., Zhao, X., Li, X., Mao, Y., Wong, L. L., Bartlam, M., & Rao, Z. 2006. Crystal structures of human glycerol 3-phosphate dehydrogenase 1 (GPD1). *Journal of Molecular Biology*, *357*, 858–869.

Pabis, A., Duarte, F., & Kamerlin, S. C. L. 2016. Promiscuity in the enzymatic catalysis of phosphate and sulfate transfer. *Biochemistry*, *55*, 3061–3081.

Palenik, B. 2012. Recent functional genomics studies in marine *Synechococcus*. In R. L. Burnap & W. F. J. Vermaas (Eds.), *Funtional Genomics and Evolution of Photosynthetic Systems* (33rd ed., pp. 103–118). Dordrecht: Springer.

Palenik, B., Brahamsha, B., Larimer, F. W., Land, M., Hauser, L., Chain, P., Lamerdin, J., Regala, W., Allen, E. E., McCarren, J., Paulsen, I. T., Dufresne, A., Partensky, F., Webb, E. A., & Waterbury, J. B. 2003. The genome of a motile marine *Synechococcus*. *Nature*, *424*, 1037–1042.

Pandey, V. D. & Parveen, S. 2011. Alkaline phosphatase activity in cyanobacteria. *Indian Journal of Fundamenal and Applied Life Sciences*, *1*, 295–303.

Panta, P. R., Kumar, S., Stafford, C. F., Billiot, C. E., Douglass, M. V., Herrera, C. M., Trent, M. S., & Doerrler, W. T. 2019. A DedA family membrane protein is required for *Burkholderia thailandensis* Colistin resistance. *Frontiers in Microbiology*, *10*, 2532.

Pasek, M. A. 2008. Rethinking early Earth phosphorus geochemistry. *PNAS*, *105*, 853–858.

Paytan, A. & McLaughlin, K. 2007. The oceanic phosphorus cycle. *Chemical Reviews*, *107*, 563–576.

Pegos, V. R., Medrano, F. J., & Balan, A. 2014. Crystallization and preliminary X-ray diffraction analysis of the phosphate-binding protein PhoX from *Xanthomonas citri*. *Acta Crystallographica Section F: Structural Biology Communications*, *70*, 1604–1607.

Pegos, V. R., Santos, R. M. L., Medrano, F. J., & Balan, A. 2017. Structural features of PhoX, one of the phosphate-binding proteins from Pho regulon of *Xanthomonas citri*. *PLoS ONE*, *12*, 1–16.

Pelikan, C., Wasmund, K., Glombitza, C., Hausmann, B., Herbold, C. W., Flieder, M., & Loy, A. 2021. Anaerobic bacterial degradation of protein and lipid macromolecules in subarctic marine sediment. *The ISME Journal*, *15*, 833–847.

Peng, Z., Feng, L., Wang, X., & Miao, X. 2019. Adaptation of *Synechococcus* sp. PCC 7942 to phosphate starvation by glycolipid accumulation and membrane lipid remodeling. *Biochimica et Biophysica Acta*, *1864*, 158522.

Peng, Z. & Miao, X. 2020. Monoglucosyldiacylglycerol participates in phosphate stress adaptation in *Synechococcus* sp. PCC 7942. *Biochemical and Biophysical Research Communications*, *522*, 662–668.

Pernil, R., Herrero, A., & Flores, E. 2010. A TRAP transporter for pyruvate and other monocarboxylate 2-oxoacids in the cyanobacterium *Anabaena* sp. strain PCC 7120. *Journal of Bacteriology*, *192*, 6089–6092.

Peter, K. H. & Sommer, U. 2015. Interactive effect of warming, nitrogen and phosphorus limitation on phytoplankton cell size. *Ecology and Evolution*, *5*, 1011–1024.

Peterson, C. N., Mandel, M. J., & Silhavy, T. J. 2005. *Escherichia coli* starvation diets: essential nutrients weigh in distinctly. *Journal of Bacteriology*, *187*, 7549–7553.

Pettersen, E. F., Goddard, T. D., Huang, C. C., Couch, G. S., Greenblatt, D. M., Meng, E. C., & Ferrin, T. E. 2004. UCSF Chimera - a visualization system for exploratory research and analysis. *Journal of Computational Chemistry*, *25*, 1605–12.

Pitchford, J. W. & Brindley, J. 1999. Iron limitation, grazing pressure and oceanic high nutrient-low chlorophyll (HNLC) regions. *Journal of Plankton Research*, *21*, 525–547.

Pitt, F. D., Mazard, S., Humphreys, L., & Scanlan, D. J. 2010. Functional characterization of *Synechocystis* sp. strain PCC 6803 *pst1* and *pst2* gene clusters reveals a novel strategy for phosphate uptake in a freshwater cyanobacterium. *Journal of Bacteriology*, *192*, 3512–3523.

Pocard, J. A., Vincent, N., Boncompagni, E., Tombras Smith, L., Poggi, M. C., & Le Rudulier, D. 1997. Molecular characterization of the *bet* genes encoding glycine betaine synthesis in *Sinorhizobium meliloti* 102F34. *Microbiology*, *143*, 1369–1379.

Poehlein, A., Daniel, R., Schink, B., & Simeonova, D. D. 2013. Life based on phosphite: a genome-guided analysis of *Desulfotignum phosphitoxidans*. *BMC Genomics*, *14*.

Polyviou, D., Hitchcock, A., Baylay, A. J., Moore, C. M., & Bibby, T. S. 2015.

Phosphite utilization by the globally important marine diazotroph *Trichodesmium*. *Environmental Microbiology Reports*, *7*, 824–830.

Prospero, J. M., Barrett, K., Church, T., Dentener, F., Duce, R. A., Galloway, J. N., Levy, H., Moody, J., & Quinn, P. 1996. Atmospheric deposition of nutrients to the North Atlantic Basin. In R. W. Howarth (Ed.), *Nitrogen Cycling in the North Atlantic Ocean and its Watersheds* (1st ed., pp. 27–73). Dordrecht: Springer Netherlands.

Quinn, J. P., Kulakova, A. N., Cooley, N. A., & McGrath, J. W. 2007. New ways to break an old bond: the bacterial carbon-phosphorus hydrolases and their role in biogeochemical phosphorus cycling. *Environmental Microbiology*, *9*, 2392–2400.

Ray, J. M., Bhaya, D., Block, M. A., & Grossman, A. R. 1991. Isolation, transcription, and inactivation of the gene for an atypical alkaline phosphatase of *Synechococcus* sp. strain PCC 7942. *Journal of Bacteriology*, *173*, 4297–4309.

Rees, D. C., Johnson, E., & Lewinson, O. 2009. ABC transporters: the power to change. *Nature Reviews. Molecular Cell Biology*, *10*, 218–227.

Reeve, J. N., Sandman, K., & Daniels, C. J. 1997. Archaeal histones, nucleosomes, and transcription initiation. *Cell*, *89*, 999–1002.

Resing, J. A. & Sanson, F. J. 1999. The chemistry of lava–seawater interactions: the generation of acidity. *Geochimica et Cosmochimica Acta*, *63*, 2183–2198.

Ridame, C. & Guieu, C. 2002. Saharan input of phosphate to the oligotrophic water of the open western Mediterranean Sea. *Limnology and Oceanography*, *47*, 856.

Ridgway, N. D. 2015. *Phospholipid synthesis in mammalian cells*. *Biochemistry of Lipids, Lipoproteins and Membranes: Sixth Edition* (Sixth Edit). Elsevier.

Ritchie, C. 2012. An in-depth review of column chromatography for protein purification and survey result from formal publications. *Materials and Methods*, *2*.

Rizk, S. S., Cuneo, M. J., & Hellinga, H. W. 2006. Identification of cognate ligands for the *Escherichia coli phnD* protein product and engineering of a reagentless fluorescent biosensor for phosphonates. *Protein Science*, *15*, 1745–1751.

Rodriguez, F., Lillington, J., Johnson, S., Timmel, C. R., Lea, S. M., & Berks, B. C. 2014. Crystal structure of the Bacillus subtilis phosphodiesterase PhoD reveals an iron and calcium-containing active site. *Journal of Biological Chemistry*, *289*, 30889–30899.

Roe, K. L., Hogle, S. L., & Barbeau, K. A. 2013. Utilization of heme as an iron source by marine *Alphaproteobacteria* in the *Roseobacter* clade. *Applied and*

Environmental Microbiology, *79*, 5753–5762.

Romano, S., Schulz-Vogt, H. N., González, J. M., & Bondarev, V. 2015. Phosphate limitation induces drastic physiological changes, virulence-related gene expression, and secondary metabolite production in *Pseudovibrio* sp. strain FO-BEG1. *Applied and Environmental Microbiology*, *81*, 3518–3528.

Ronda, L., Bruno, S., Bettati, S., Storici, P., & Mozzarelli, A. 2015. From protein structure to function via single crystal optical spectroscopy. *Frontiers in Molecular Biosciences*, *2*.

Rosenstein, R., Futter-Bryniok, D., & Götz, F. 1999. The choline-converting pathway in *Staphylococcus xylosus* C2A: genetic and physiological characterization. *Journal of Bacteriology*, *181*, 2273–2278.

Roskoski, R. B. T. 2015. Michaelis-Menten Kinetics. In *Biomedical Sciences*. Elsevier.

Roy, N. K., Ghosh, R. K., & Das, J. 1982. Monomeric alkaline phosphatase of *Vibrio cholerae*. *Journal of Bacteriology*, *150*, 1033–1039.

Ruttenberg, K. C. 2019. Phosphorus cycle. In J. K. Cochran, H. J. Bokuniewicz, & P. L. B. T. Yager (Eds.), *Encyclopedia of Ocean Sciences* (3rd ed., pp. 447–460). Oxford: Academic Press.

Sahonero-Canavesi, D. X., López-Lara, I. M., & Geiger, O. 2019. Membrane lipid degradation and lipid cycles in microbes. In *Handbook of Hydrocarbon and Lipid Microbiology* (pp. 231–254).

Saier, M. H., Reddy, V. S., Moreno-Hagelsieb, G., Hendargo, K. J., Zhang, Y., Iddamsetty, V., Lam, K. J. K., Tian, N., Russum, S., Wang, J., & Medrano-Soto, A. 2021. The Transporter Classification Database (TCDB): 2021 update. *Nucleic Acids Research*, *8*, D461–D467.

Salmon, R. C., Cliff, M. J., Rafferty, J. B., & Kelly, D. J. 2013. The CouPSTU and TarPQM transporters in *Rhodopseudomonas palustris*: redundant, promiscuous uptake systems for lignin-derived aromatic substrates. *PLoS ONE*, *8*, e59844.

Santos-Beneit, F. 2015. The Pho regulon: a huge regulatory network in bacteria. *Frontiers in Microbiology*, *6*.

Santos-Beneit, F., Rodríguez-García, A., Apel, A. K., & Martín, J. F. 2009. Phosphate and carbon source regulation of two PhoP-dependent glycerophosphodiester phosphodiesterase genes of *Streptomyces coelicolor*. *Microbiology*, *155*, 1800–1811.

Saurin, W., Hofnung, M., & Dassa, E. 1999. Getting in or out: early segregation between importers and exporters in the evolution of ATP-binding cassette (ABC) transporters. *Journal of Molecular Evolution*, *48*, 22–41.

Scanlan, D. J., Mann, N. H., & Carr, N. G. 1993. The response of the picoplanktonic marine cyanobacterium *Synechococcus* species WH7803 to phosphate starvation involves a protein homologous to the periplasmic phosphate-binding protein of *Escherichia coli*. *Molecular Microbiology*, *10*, 181–191.

Scanlan, D. J., Ostrowski, M., Mazard, S., Dufresne, A., Garczarek, L., Hess, W. R., Post, A. F., Hagemann, M., Paulsen, I. T., & Partensky, F. 2009. Ecological genomics of marine picocyanobacteria. *Microbiology and Molecular Biology Reviews*, *73*, 249–299.

Scanlan, D. J. & West, N. J. 2002. Molecular ecology of the marine cyanobacteria genera *Prochlorococcus* and *Synechococcus*. *FEMS Microbiology Ecology*, *40*, 1–12.

Scanlan, D. J. & Wilson, W. H. 1999. Application of molecular techniques to addressing the role of P as a key effector in marine ecosystems. *Hydrobiologia*, *401*, 149–175.

Schäfer, A., Tauch, A., Jäger, W., Kalinowski, J., Thierbach, G., & Pühler, A. 1994. Small mobilizable multi-purpose cloning vectors derived from the *Escherichia coli* plasmids pK18 and pK19: selection of defined deletions in the chromosome of *Corynebacterium glutamicum*. *Gene*, *1*, 69–73.

Schauer, K., Rodionov, D. A., & de Reuse, H. 2008. New substrates for TonB-dependent transport: do we only see the 'tip of the iceberg'? *Trends in Biochemical Sciences*, *33*, 330–338.

Schenk, G., Gahan, L. R., Carrington, L. E., Mitić, N., Valizadeh, M., Hamilton, S. E., De Jersey, J., & Guddat, L. W. 2005. Phosphate forms an unusual tripodal complex with the Fe-Mn center of sweet potato purple acid phosphatase. *PNAS*, *102*, 273–278.

Schenk, G., Korsinczky, M. L. J., Hume, D. A., Hamilton, S., & Dejersey, J. 2000. Purple acid phosphatases from bacteria: similarities to mammalian and plant enzymes. *Gene*, *255*, 419–424.

Schouten, S., Hopmans, E. C., & Sinninghe Damsté, J. S. 2013. The organic geochemistry of glycerol dialkyl glycerol tetraether lipids: a review. *Organic Geochemistry*, *54*, 19–61.

Schwarz, R. & Forchhammer, K. 2005. Acclimation of unicellular cyanobacteria to macronutrient deficiency: emergence of a complex network of cellular responses. *Microbiology*, *151*, 2503–2514.

Schweizer, H. & Boos, W. 1985. Regulation of *ugp*, the *sn*-glycerol-3-phosphate transport system of *Escherichia coli* K-12 that is part of the Pho regulon. *Journal of Bacteriology*, *163*, 392–394.

Sebastián, M. & Ammerman, J. W. 2009. The alkaline phosphatase PhoX is more

widely distributed in marine bacteria than the classical PhoA. *The ISME Journal*, *3*, 563–572.

Sebastián, M. & Ammerman, J. W. 2011. Role of the phosphatase PhoX in the phosphorus metabolism of the marine bacterium *Ruegeria pomeroyi* DSS-3. *Environmental Microbiology Reports*, *3*, 535–542.

Sebastián, M., Smith, A. F., González, J. M., Fredricks, H. F., Van Mooy, B. A. S., Koblížek, M., Brandsma, J., Koster, G., Mestre, M., Mostajir, B., Pitta, P., Postle, A. D., Sánchez, P., Gasol, J. M., Scanlan, D. J., & Chen, Y. 2016. Lipid remodelling is a widespread strategy in marine heterotrophic bacteria upon phosphorus deficiency. *The ISME Journal*, *10*, 968–978.

Sellner, K. G. 1986. Physiology, ecology, and toxic properties of marine cyanobacteria blooms. *Limnology and Oceanography*, *42*, 1089–1104.

Seweryn, P., Van, L. B., Kjeldgaard, M., Russo, C. J., Passmore, L. A., Hove-Jensen, B., Jochimsen, B., & Brodersen, D. E. 2015. Structural insights into the bacterial carbon-phosphorus lyase machinery. *Nature*, *525*, 68–72.

Shaked, Y., Xu, Y., Leblanc, K., & Morel, F. M. M. 2006. Zinc availability and alkaline phosphatase activity in *Emiliania huxleyi*: Implications for Zn-P co-limitation in the ocean. *Limnology and Oceanography*, *51*, 299–309.

Shemi, A., Schatz, D., Fredricks, H. F., Van Mooy, B. A. S., Porat, Z., & Vardi, A. 2016. Phosphorus starvation induces membrane remodeling and recycling in *Emiliania huxleyi*. *New Phytologist*, *211*, 886–898.

Simon, M., Scheuner, C., Meier-Kolthoff, J. P., Brinkhoff, T., Wagner-Döbler, I., Ulbrich, M., Klenk, H. P., Schomburg, D., Petersen, J., & Göker, M. 2017. Phylogenomics of *Rhodobacteraceae* reveals evolutionary adaptation to marine and non-marine habitats. *The ISME Journal*, *11*, 1483–1499.

Simon, R., Priefer, U., & Pühler, A. 1983. A broad host range mobilization system for *in vivo* genetic engineering: transposon mutagenesis in gram negative bacteria. *Nature Biotechnology*, *1*, 784–791.

Smith, A. F., Rihtman, B., Stirrup, R., Silvano, E., Mausz, M. A., Scanlan, D. J., & Chen, Y. 2019. Elucidation of glutamine lipid biosynthesis in marine bacteria reveals its importance under phosphorus deplete growth in *Rhodobacteraceae*. *The ISME Journal*, *13*, 39–49.

Smith, A. F., Silvano, E., Päuker, O., Guillonneau, R., Quareshy, M., Murphy, A., Mausz, M. A., Stirrup, R., Rihtman, B., Aguilo-Ferretjans, M. d. M., Brandsma, J., Petersen, J., Scanlan, D. J., & Chen, Y. 2021. A novel class of sulfur-containing aminolipids widespread in marine roseobacters. *The ISME Journal*.

Sohlenkamp, C. & Geiger, O. 2015. Bacterial membrane lipids: diversity in structures and pathways. *FEMS Microbiology Reviews*, *40*, 133–159.

Sola-Landa, A., Moura, R. S., & Martin, J. F. 2003. The two-component PhoR-PhoP system controls both primary metabolism and secondary metabolite biosynthesis in *Streptomyces lividans*. *PNAS*, *100*, 6133–6138.

Sosa, O. A. 2017. Phosphorus redox reactions as pinch hitters in microbial metabolism. *PNAS*, *115*, 201719600.

Sosa, O. A., Repeta, D. J., DeLong, E. F., Ashkezari, M. D., & Karl, D. M. 2019. Phosphate-limited ocean regions select for bacterial populations enriched in the carbon–phosphorus lyase pathway for phosphonate degradation. *Environmental Microbiology*, *21*, 2402–2414.

Sosa, O. A., Repeta, D. J., Ferrón, S., Bryant, J. A., Mende, D. R., Karl, D. M., & DeLong, E. F. 2017. Isolation and characterization of bacteria that degrade phosphonates in marine dissolved organic matter. *Frontiers in Microbiology*, *8*, 1–16.

Soukri, A., Mougin, A., Corbier, C., Wonacott, A., Branlant, C., & Branlant, G. 1989. Role of the histidine 176 residue in glyceraldehyde-3-phosphate dehydrogenase as probed by site-directed mutagenesis. *Biochemistry*, *28*, 2586–2592.

Stosiek, N., Talma, M., & Klimek-Ochab, M. 2020. Carbon-phosphorus lyase — the state of the art. *Applied Biochemistry and Biotechnology*, *190*, 1525–1552.

Strom, S. L. 2008. Microbial ecology of ocean biogeochemistry: a community perspective. *Science*, *320*, 1043–1045.

Studier, F. W. 2005. Protein production by auto-induction in high density shaking cultures. *Protein Expression and Purification*, *41*, 207–234.

Styrvold, O. B., Falkenberg, P., Landfald, B., Eshoo, M. W., Bjørnsen, T., & Strøm, A. R. 1986. Selection, mapping, and characterization of osmoregulatory mutants of *Escherichia coli* blocked in the choline-glycine betaine pathway. *Journal of Bacteriology*, *165*, 856–863.

Su, Z., Olman, V., & Xu, Y. 2007. Computational prediction of Pho regulons in cyanobacteria. *BMC Genomics*, *8*, 1–12.

Sunagawa, S., Coelho, L. P., Chaffron, S., Kultima, J. R., Labadie, K., Salazar, G., Djahanschiri, B., Zeller, G., Mende, D. R., Alberti, A., Cornejo-Castillo, F. M., Costea, P. I., Cruaud, C., D'Ovidio, F., Engelen, S., Ferrera, I., Gasol, J. M., … Bork, P. 2015. Structure and function of the global ocean microbiome. *Science*, *348*, 1261359.

Sundareshwar, P. V. & Morris, J. T. 1999. Phosphorus sorption characteristics of intertidal marsh sediments along an estuarine salinity gradient. *Limnology and Oceanography*, *44*.

Suzuki, S., Ferjani, A., Suzuki, I., & Murata, N. 2004. The SphS-SphR two component system is the exclusive sensor for the induction of gene expression in response to phosphate limitation in *Synechocystis*. *Journal of Biological Chemistry*, *279*, 13234–13240.

Suzuki, Y., Nobusawa, A., & Furuta, N. 2014. Quantification of proteins by measuring the sulfur content of their constituent peptides by means of nano HPLC-ICPMS. *Analytical Sciences*, *30*, 551–559.

Suzumura, M. 2005. Phospholipids in marine environments: a review. *Talanta*, *66*, 422–434.

Suzumura, M., Hashihama, F., Yamada, N., & Kinouchi, S. 2012. Dissolved phosphorus pools and alkaline phosphatase activity in the euphotic zone of the western North Pacific Ocean. *Frontiers in Microbiology*, *3*, 1–13.

Takami, H., Nakasone, K., Takaki, Y., Maeno, G., Sasaki, R., Masui, N., Fuji, F., Hirama, C., Nakamura, Y., Ogasawara, N., Kuhara, S., & Horikoshi, K. 2000. Complete genome sequence of the alkaliphilic bacterium *Bacillus halodurans* and genomic sequence comparison with *Bacillus subtilis*. *Nucleic Acids Research*, *28*, 4317–4331.

Tetu, S. G., Brahamsha, B., Johnson, D. A., Tai, V., Phillippy, K., Palenik, B., & Paulsen, I. T. 2009. Microarray analysis of phosphate regulation in the marine cyanobacterium *Synechococcus* sp. WH8102. *The ISME Journal*, *3*, 835–849.

Thomas, G. H., Southworth, T., León-Kempis, M. R., Leech, A., & Kelly, D. J. 2006. Novel ligands for the extracellular solute receptors of two bacterial TRAP transporters. *Microbiology*, *152*, 187–198.

Thomson, N., Bentley, S., Holden, M., & Parkhill, J. 2003. Fitting the niche by genomic adaptation. *Nature Reviews. Microbiology*, *1*, 92–93.

Thorrez, L., Van Deun, K., Tranchevent, L. C., Van Lommel, L., Engelen, K., Marchal, K., Moreau, Y., Van Mechelen, I., & Schuit, F. 2008. Using ribosomal protein genes as reference: a tale of caution. *PLoS ONE*, *3*.

Tian-Tian, L., Ping, H., Jia-Xing, L., Zhi-Xin, K., & Ye-Hui, T. 2019. Utilization of different dissolved organic phosphorus sources by *Symbiodinium voratum* in vitro. *FEMS Microbiology Ecology*, *95*.

Trifinopoulos, J., Nguyen, L. T., von Haeseler, A., & Minh, B. Q. 2016. W-IQ-TREE: a fast online phylogenetic tool for maximum likelihood analysis. *Nucleic Acids Research*, *44*, W232–W235.

Trimpin, S. & Brizzard, B. 2018. Analysis of insoluble proteins. *BioTechniques*, *46*.

Tully, B. J., Graham, E. D., & Heidelberg, J. F. 2018. The reconstruction of 2,631 draft metagenome-assembled genomes from the global oceans. *Scientific Data*, *5*, 170203.

Tyanova, S., Temu, T., Sinitcyn, P., Carlson, A., Hein, M. Y., Geiger, T., Mann, M., & Cox, J. 2016. The Perseus computational platform for comprehensive analysis of (prote)omics data. *Nature Methods*, *13*, 731–740.

van den Meersche, K., Middelburg, J. J., Soetaert, K., van Rijswijk, P., Boschker, H. T. S., & Heip, C. H. R. 2004. Carbon-nitrogen coupling and algal-bacterial interactions during an experimental bloom: modeling a ^{13}C tracer experiment, *49*, 862–878.

Van Mooy, B. A. S., Fredricks, H. F., Pedler, B. E., Dyhrman, S. T., Karl, D. M., Koblížek, M., Lomas, M. W., Mincer, T. J., Moore, L. R., Moutin, T., Rappé, M. S., & Webb, E. A. 2009. Phytoplankton in the ocean use non-phosphorus lipids in response to phosphorus scarcity. *Nature*, *458*, 69–72.

Van Mooy, B. A. S., Krupke, A., Dyhrman, S. T., Fredricks, H. F., Frischkorn, K. R., Ossolinski, J. E., Repeta, D. J., Rouco, M., Seewald, J. D., & Sylva, S. P. 2015. Major role of planktonic phosphate reduction in the marine phosphorus redox cycle. *Science*, *348*, 783–785.

Van Mooy, B. A. S., Moutin, T., Duhamel, S., Rimmelin, P., & Van Wambeke, F. 2008. Phospholipid synthesis rates in the eastern subtropical South Pacific Ocean. *Biogeosciences*, *5*, 133–139.

Van Mooy, B. A. S., Rocap, G., Fredricks, H. F., Evans, C. T., & Devol, A. H. 2006. Sulfolipids dramatically decrease phosphorus demand by picocyanobacteria in oligotrophic marine environments. *PNAS*, *103*, 8607–8612.

VanBogelen, R. A., Olson, E. R., Wanner, B. L., & Neidhardt, F. C. 1996. Global analysis of proteins synthesized during phosphorus restriction in *Escherichia coli*. *Journal of Bacteriology*, *178*, 4344–4366.

Vetting, M. W., Al-Obaidi, N., Zhao, S., San Francisco, B., Kim, J., Wichelecki, D. J., Bouvier, J. T., Solbiati, J. O., Vu, H., Zhang, X., Rodionov, D. A., Love, J. D., Hillerich, B. S., Seidel, R. D., Quinn, R. J., Osterman, A. L., Cronan, J. E., … Almo, S. C. 2015. Experimental strategies for functional annotation and metabolism discovery: targeted screening of solute binding proteins and unbiased panning of metabolomes. *Biochemistry*, *54*, 909–931.

Villar, E., Vannier, T., Vernette, C., Lescot, M., Cuenca, M., Alexandre, A., Bachelerie, P., Rosnet, T., Pelletier, E., Sunagawa, S., & Hingamp, P. 2018. The Ocean Gene Atlas: exploring the biogeography of plankton genes online. *Nucleic Acids Research*, *46*, W289–W295.

Villarreal-Chiu, J. F., Quinn, J. P., & McGrath, J. W. 2012. The genes and enzymes of phosphonate metabolism by bacteria, and their distribution in the marine environment. *Frontiers in Microbiology*, *3*, 1–13.

Walsh, C. T. 2020. Introduction to phosphorus chemical biology. In K. J. Weissman

(Ed.), *The Chemical Biology of Phosphorus* (pp. 3–26). Royal Society of Chemistry.

Wang, X.-J., Zhang, N., Teng, Z.-J., Wang, P., Zhang, W.-P., Chen, X.-L., Zhang, Y.-Z., Chen, Y., Fu, H.-H., & Li, C.-Y. 2021. Structural and mechanistic insights into dimethylsulfoxide formation through dimethylsulfide oxidation. *Frontiers in Microbiology*, *12*.

Wanner, B. L. 1996. Phosphorus assimilation and control of the phosphate regulon. In F. C. Neidhardt (Ed.), *Escherichia coli and Salmonella: Cellular and Molecular Biology* (2nd ed., pp. 1357–1381). Washington D.C.: ASM Press.

Wanner, B. L. & Chang, B. D. 1987. The *phoBR* operon in *Escherichia coli* K-12. *Journal of Bacteriologyacteriology*, *169*, 5569–5574.

Wanner, B. L. & Metcalf, W. W. 1992. Molecular genetic studies of a 10.9-kb operon in *Escherichia coli* for phosphonate uptake and biodegradation. *FEMS Microbiology Letters*, *100*, 133–140.

Waterbury, J. B., Watson, S. W., Valois, F. W., & Franks, D. G. 1986. Biological and ecological characterization of the marine cyanobacterium *Synechococcus*. *Can. Bull. Fish. Aquat. Sci.*, 71–120.

Wei, T., Quareshy, M., Zhang, Y. -z., Scanlan, D. J., & Chen, Y. 2018. Manganese is essential for PlcP metallophosphoesterase activity involved in lipid remodelling in abundant marine heterotrophic bacteria. *Applied and Environmental Microbiology*, *84*, 1–10.

Weiss, M. C., Sousa, F. L., Mrnjavac, N., Neukirchen, S., Roettger, M., Nelson-Sathi, S., & Martin, W. F. 2016. The physiology and habitat of the last universal common ancestor. *Nature Microbiology*, *1*, 16116.

Welch, R. A. 2001. RTX toxin structure and function: a story of numerous anomalies and few analogies in toxin biology. In F. G. van der Goot (Ed.), *Pore-Forming Toxins* (Current To, pp. 85–111). Springer Berlin Heidelberg.

White, A. E., Karl, D. M., Björkman, K. M., Beversdorf, L. J., & Leteliera, R. M. 2010. Production of organic matter by *Trichodesmium* IMS101 as a function of phosphorus source. *Limnology and Oceanography*, *55*, 1755–1767.

White, A. K. & Metcalf, W. W. 2004. Two C-P lyase operons in *Pseudomonas stutzeri* and their roles in the oxidation of phosphonates, phosphite, and hypophosphite. *Journal of Bacteriology*, *186*, 4730–4739.

Willis, A., Chuang, A. W., Dyhrman, S., & Burford, M. A. 2019. Differential expression of phosphorus acquisition genes in response to phosphorus stress in two *Raphidiopsis raciborskii* strains. *Harmful Algae*, *82*, 19–25.

Wilson, W. H., Carr, N. G., & Mann, N. H. 1996. The effect of phosphate status on

the kinetics of cyanophage infection in the oceanic cyanobacterium *Synechococcus* sp. WH7803. *Journal of Phycology*, *32*, 506–516.

Wollast, R. 1983. The Major Biogeochemical Cycles and Their Interactions. In B. Bolin & R. B. Cook (Eds.), *The major biogeochemical cycles and their interactions*. Chinchester, UK: Wiley-Interscience.

Wortham, B. W., Oliveira, M. A., & Patel, C. N. 2007. Polyamines in bacteria: pleiotropic effects yet specific mechanisms. In R. D. Perry & J. D. Fetherston (Eds.), *The Genus Yersinia. Advances in Experimental Medicine and Biology* (pp. 106–115). New York, NY: Springer New York.

Wu, J. R., Shien, J.-H., Shieh, H. K., Hu, C. C., Gong, S. R., Chen, L. Y., & Chang, P. C. 2007. Cloning of the gene and characterization of the enzymatic properties of the monomeric alkaline phosphatase (PhoX) from *Pasteurella multocida* strain X-73. *FEMS Microbiology Letters*, *267*, 113–120.

Wu, J., Sunda, W., Boyle, E. A., & Karl, D. M. 2000. Phosphate depletion in the Western North Atlantic Ocean. *Science*, *289*, 759–762.

Wübbeler, J. H., Hiessl, S., Schuldes, J., Thürmer, A., Daniel, R., & Steinbüchel, A. 2014. Unravelling the complete genome sequence of *Advenella mimigardefordensis* strain DPN7T and novel insights in the catabolism of the xenobiotic polythioester precursor 3,3′-dithiodipropionate. *Microbiology*, *160*, 1401–1416.

Yamagata, Y., Watanabe, H., Saitoh, M., & Namba, T. 1991. Volcanic production of polyphosphates and its relevance to prebiotic evolution. *Nature*, *352*, 516–519.

Yamane, K. & Maruo, B. 1978. Purification and characterization of extracellular soluble and membrane-bound insoluble alkaline phosphatases possessing phosphodiesterase activities in *Bacillus subtilis*. *Journal of Bacteriology*, *134*, 100–7.

Yeh, J. I., Chinte, U., & Du, S. 2008. Structure of glycerol-3-phosphate dehydrogenase, an essential monotopic membrane enzyme involved in respiration and metabolism. *PNAS*, *105*, 3280–3285.

Yong, S. C., Roversi, P., Lillington, J., Rodriguez, F., Krehenbrink, M., Zeldin, O. B., Garman, E. F., Lea, S. M., & Berks, B. C. 2014. A complex iron-calcium cofactor catalyzing phosphotransfer chemistry. *Science*, *345*, 1170–1173.

Young, C. L. & Ingall, E. D. 2010. Marine dissolved organic phosphorus composition: insights from samples recovered using combined electrodialysis/reverse osmosis. *Aquatic Geochemistry*, *16*, 563–574.

Yuan, Z. C., Zaheer, R., Morton, R., & Finan, T. M. 2006. Genome prediction of PhoB regulated promoters in *Sinorhizobium meliloti* and twelve

proteobacteria. *Nucleic Acids Research*, *34*, 2686–2697.

Zaheer, R., Morton, R., Proudfoot, M., Yakunin, A., & Finan, T. M. 2009. Genetic and biochemical properties of an alkaline phosphatase PhoX family protein found in many bacteria. *Environmental Microbiology*, *11*, 1572–1587.

Zaitoun, M. A. & Lin, C. T. 1997. Chelating behavior between metal ions and EDTA in sol−gel matrix. *The Journal of Physical Chemistry B*, *101*, 1857–1860.

Zavaleta-Pastor, M., Sohlenkamp, C., Gao, J.-L., Guan, Z., Zaheer, R., Finan, T. M., Raetz, C. R. H., Lopez-Lara, I. M., & Geiger, O. 2010. *Sinorhizobium meliloti* phospholipase C required for lipid remodeling during phosphorus limitation. *PNAS*, *107*, 302–307.

Zeng, Q. & Chisholm, S. W. 2012. Marine viruses exploit their host's two-component regulatory system in response to resource limitation. *Current Biology*, *22*, 124–128.

Zhang, C., Lin, S., Huang, L., Lu, W., Li, M., & Liu, S. 2014. Suppression subtraction hybridization analysis revealed regulation of some cell cycle and toxin genes in *Alexandrium catenella* by phosphate limitation. *Harmful Algae*, *39*, 26–39.

Zhang, Y. M. & Rock, C. O. 2008. Membrane lipid homeostasis in bacteria. *Nature Reviews Microbiology*, *6*, 222–233.

Zubkov, M. V., Mary, I., Woodward, E. M. S., Warwick, P. E., Fuchs, B. M., Scanlan, D. J., & Burkill, P. H. 2007. Microbial control of phosphate in the nutrient-depleted North Atlantic Subtropical Gyre. *Environmental Microbiology*, *9*, 2079–2089.

APPENDICES

Appendix I CHAPTER 2

Appendix 2.1 Codon optimised nucleotide sequence of SYNW0196

ACCGCAAGCTTTCGTCATGGTGTTGCAAGCGGTGATCCGTATCAGGATAGCTTTGTTATTTG
GAGCCGTGTTAGTGATGTTGATGGTAGCAGCGCAAGCGTTAATTGGGAAGTTAGCAGCAGCC
CGAAATTCAAAAAACGTACCATTCTGGATAGCGGCACCATTAGCACCAGCAGCGATCGTGAT
TGGACCGTTAAAGCACTGCCGGAAGGTCTGCAGGCAGGCGAAGATTATTACTATCGTTTTGA
AGTTGATGGTGTTGTTAGTCCGGTTGGTCATGCAAGCACCCTGCCGGATAAAGCAGCAAGCG
TTCGTATGGCCGTTCTGAGCTGTGCAAATTTTACCAACACCGAATTCTTTGAAACCTATCGT
CGTGTTGCAGAAATTGATGCAGAACAGCCGTATGATATTATTCTGCATGTGGGCGATTATAT
CTATGAATATGGTCAAGGTGGTTATCCGAGCGCAGAAAGCGCAGTTGAAAATCGTGGTTTTG
AACCGGATAGCGAACTGCTGAGCCTGGATGATTATCGTCAGCGTTATGCACAGTATCATTCA
GATGCAGGTCTGCGTGAAATGCATGCAAGCGCACCGATGGTTAGCATTTGGGATGATCATGA
AACCGCAAATGATAGCTGGTTAGGTGGTGCAGAAAATCATCAGAGCGAAGTTGAAGGTGATT
GGGCAAGCCGTCGTGATGCAGCACTGCAGGCATACTATGAATGGATGCCGATTCGTGAACCG
GCACTGCGTCGTGACGTTGATCTGGGCACCGATGATAGTCCGCTGACACAGGGTTTTCGTTC
ATTTGATCTGGCAGATCTGGTTACCCTGTATGTTCTGGAAACCCGTCTGACCGCACGTGATG
AACAGCTGGCATATCCGAATAGTGATGCAGTTGCAGCACGTATTGGTGATATTCTGGCCGAT
CCGCTGCTGCTGGCAAGCTATGCAGAAAGCCTGGGTGTTGCACCGCCTGTTAGTGCCGAAGA
TCTGGATGGTGTTAATGCACTGAGCGCAGCACTGATTGATCCGGTTACACTGGAACTGGTTG
CAGCAACCGTTGCAGATGGTTGGACCAATCCGAGCCGTAATCTGCTGGGTCAAGATCAGCAG
AGCTGGCTGCAGAGCGGTCTGGCAGGTAGTGATGCCGCATGGCAGGTTCTGGGTCAGCAAGT
TCTGATGCAGAGCATGGCAATTCCGGCAGAACTGCTGCTGAATGCAACCGATCCGGATGTTC
TGGCAAAATATAGCGCACCGCTGGAAAAACTGGCAACCGGTCAGCCGCTGAATCAGGATGAA
CTGGCACTGTTTGATGAAGCAACCAAAATTCCGTATAATCTGGATGCATGGGATGGTTATGG
TGTTGAACGTGAAACCATTCTGCAGACCGCAGCAGGTCTGGGTAAAAAACTGGTTAGCCTGG
CAGGCGATACCCATAATGCCTGGGTTGGTGTTCTGGATGCCATGAGTACCGGTGCAGCAATG
CCTGGTCAGGTTGTTGGTATTGAATTTGCCACACCGGGTGTGAGCGCACCGGGTATTGAAAC
ATATATTGCACCTGGTCTGGAACCGATTTTTCTGAGCTATACCGAAGGTCTGAAATATACCG
ATCTGAGCCGTCGCGGTTTTCTGGATATTACCTTTCATGAAGAACACATCACCAGCAGTTAT
CAGCTGCTGGATCCTGATGAAGGTTGGATTGCAGATGTTCTGCAGAGTGATGATAGCTTTAG
TCCGCGTCAGCTGAGCCGTGTGGATGCAACCACCACCGCAGATATTCCGACCGGTTTTGCAC
ATGGTCGTTTTCGTGAAGTTATTCGTGCCGGTGCAGGTAATGATCGTATTGCAGCCGGTGAT
CGTAAAGGTTATGTTAGCGCAGGCGGTGGTAATGATGATATTGATGGTGGTCGTCGTGCACA
GCTGTTACTGGGTGACGAAGGTGATGATGTGATTCGTGGTCGTGGTGGTCCAGATGAACTGC
GTGGCGGTCCGGGTGCAGATAGCCTGAATGGTGGTCCTGGTGATGACCTGATTTTAGGTGGC

GCAGGCGCAGATAGCTTTCGTATTAGCAAAGGTGACGATCGCATTGTGGATCTGGATCCGCT
GGAAGGTGACGTTCTGCTGCTGCCTGCCGGTTTAGAACCGACACTGACCAGCGCAGTTAGCG
GTGTTCTGCTGGCCACCGATCGTGGTACAACCCTGCTGGAAGGCCTGACGCTGGAACAGGTT
GAAGGACTGATTTAA

Appendix 2.2 Codon optimised nucleotide sequence of SYNW2390

ATGAGCTTCAAACTGCAGCTGATTCATAGCAGCGATAACGAAAGCAACTTCAAAGATGTTAA
CACCCTGGAAGATAAGGTGGTTAATTATGCAGCAATTACCGATGGTCTGCAGGATGAAGCAG
CAGCACAAGGTTGGGCAAGCCTGCATGTTACCGCAGGCGATCATACCCTGCCGAACCTGTTT
TATAGTGCCGGTGAAACCACCGAAGGTAAACCTGGTCTGGCAGATATCAAAATCTTTAATGC
CATGGGTGTGAAAGCCAATGGTATTGGTAATCATGAAATGGATGGCAACATCGGCGAATTTA
TTGATATGGTTAATGCCAGCGATTATGTTCATCTGAGCGCAAATCTGGATTTTAGCAGCGTT
GTTGATACCGATGGCAATGCAGCACCGTTTGTTAGCTATGCAGCAGATGAACCGGCACAGAG
CGTTGAAGAACTGGCAGGTAAAATTGCACCGAGCGCATATGTTGAAATTGATGGTGAGCAGA
TTGGTCTGATTGGTCGTAGCCCGAGCGAAATGTTTAGCCTGGTTGCAGATGGTAATCTGCCA
GGTCTGGATTATGTTGGTGGCACCAGCGGTGAAGGCACCGCACGTGAACCGGTGCTGGAACC
GCTGCCGCTGATCCAGGCAGAAATTGATCGTCTGACAAATCAGGGCATCAACAAGATCATCT
TTATTGATCATGCCCAGGATTATACCGATCAGAGCGTTCTGCCTGCAGAACTGGATGGTGTT
GATGTTATTATTCAGGCAGGTATGACCGGTTATATGAGCGCAGAAACCCCGAGCGGTCCGTT
TAATCTGCTGCGTACCGAAGAAGCAGGTAATCCGATTACACATAATTATCCGCTGGAAAGCA
AAGATTCAGCCGGTAAAACCGTTCTGATTACAAATACAGAGCAGATTTGGCGTTATGTTGGC
CATCTGCTGGTTCATTTTGATGATAATGGTGAGATCACCAGCTATGATGCAGATAATAGCGG
TCCGGTTCCGACCAATGATGAAGGTGTTGCAGCACTGCGTGCATGGACCAGTGGTGATGCAG
TTGCAGATCCGGTTGTTGTTAGCACCTATGAAGCACTGCTGGCAACCGATGAACTGAATGCA
GCATTTGCAGAAGTTGGCACCACCACCGATAGCCTGAATGGTGTTCGTGCAGATATTCGTAG
CCGTGAAACCAATCTGGGTCGTCTGGCAGCAGATAGCACCCTGTGGTATGCAAATCAGTATC
TGGAAGAAATTGGCGAAACCAAACGTGCCGATATTGCACTGAAAAATGGTGGTGGTATTCGT
GATACCATTGCAGGTCTGAGCCCGATTACGCAGCTGCAGGTTAATGCAGCCCTGGCATTTGA
TAATAAACTGACCATTATGGATCTGACCGGTGCAGAATTTCTGGCCATTGTTGAAAATGGTG
TTAGCCGTGCTCCGGCACTGGATGGCCGTTTTCCGCATTTTGCCGGTGCCGAACTGGATTTT
GTTACCTATCGTCCGGGTATTGAAGAAGCACTGAGCCTGACCGAAGCAAGCCGTGTTCAGAA
TCTGACCGTTAATCGTGATGATGGTAGCACCGTTGAACTGGTTAGCGATTTTTTTGTTAATG
CCGATGCACTGGAAGAGACATTTACCCTGGCAACCAATAACTATCAGGCAGGCGGTGGTGAT
GGTTATCAGGCATTTGTTCCTCTGGAAAACAAAATCGAAACCGTGATTGGCGAACAAGAAAT
CCTGGCCACCTATATTAGCGAAGAATTAGCCGGTGCAGTGGATATTTCAGATGCAGATGTTA
TTGCAAGTCCGCGTACCGATCTGATTCGTCCGCAGCTGGATGATCTGATTAATCCGAGCGAC
GAACTGATTGGTACAAGCGGTGATGATGAGCTGAAAGGTAAACGTCGTTTAGGTGGTAATAG
CCTGTATGGCAAAGAAGGTGACGATTCACTGAAAGGTCGTAAAGGTGATGATCTGCTGGATG

GCGGTAGCGGAGATGACGTTCTGAAAGGTTTTGGTGGTAGTGATGTTTATGTGGGTAGCGCA
GGCACCGATCGTATTAATGGTTTTAGCTTTGATCAGGGTGATGTGGTTGCAATTGATAGCAG
CATTAACTTTGAAATTGTGCAGAGCGCCAATCCGAATAAAAACCTGCGTGTTGAACATGATC
TGGGCGAAATTATCTTCAAAGGTATTAAAGCAGACCAGCTGATTGATCTGCAGAATAGCATT
CAGATTACCGAAGCCATCTAA

Appendix 2.3 Codon optimised nucleotide sequence of SYNW2391

GCACGTATTAGCGATAGCATTATTAGTCCGCTGCAGAGCGTTAGCCCTGGTGGTGCAGAAAA
AGTTGATTGGTATGCACCGACCAAAACCGCATTTGTTATTACCGGTGAGTATACCGATGATA
AAGGTGGTCAGGTTGTTGCCATTGATTATAGCAATGGTTATGGTAAAGGCACCGCCATCGAT
GAGTATTATTTCGAAGGTGATGTTAGTGATGTTCGTGTTAGCAGCCAGGGTCTGATTGCAGC
AAGCGTTTTTGATAAAGTTACCCGTGAAGGCACCGTTCAGTTTCTGGATTTTACCAAAGAAA
GCGGTTTTACCAGCCTGGGTAGCGTTGAAGTTGGTTATCAGCCGGATCAGCTGGCATTTACC
AAAAATGGTAAAAAACTGGTGACCGCCAATGAAGGTGAACCGCTGATGTTTTATGGTAGTGA
TGAAACCAGCCAGAATCCGCGTGGTAGCATTAGCATTATCAATATTGCAAACGACCTGACCA
AAAGCAAAGTGAACACCCTGTATTTTACGAAAAGCAACAAGTACTATGAGAAACGTGGTGTT
CGTCTGTATGGTCCGGAAATGGATAGCAATAGCAAATTTGGCGAATATGATATCGAGCCGGA
ATATGTTGGTATTACCGGCAATAATACCGCACTGGTTGCACTGCAAGAAAACAATGCACTGG
CACGTGTTAATCTGAAAAAAGAAAAAATCACCGGTGTGTTTGGCCTGGGTTATAAAGATTGG
AGCGGTATTCCGTTTGATACCACCGATAAAGATGATGGTTATAATCCGACCGTTAAAGAAGG
TGTTACCAGCGCACGTATGCCGGATGGTATTGATACCTTTCAGATCAAATTAGGTGGCAAGA
AGCAGATCCTGTTTATTAGCCCGAATGAAGGCGACGGTCGTGTTCGTCCGGATGATGTTAAT
TTTGAAGCACCGGCAGATGGTGTTTATAGCTGGGGCACCAATAGTACCGGTGCCGAAATTGA
AAGCTTTACCGATCCGCTGACACTGACCGATGAAATTTACATTTATGACAAAGCCGGTGTGG
GTAACAGCGGTGATATTGAAGATGTTGAAGAGGGTGATGAATTCTTCATCACGCAGAAATAT
GGTGTGAGCAGCGACGATGAATTTTGGAGTGATGAAGTTCGTGCAAAAGACCTGGAAGATTT
TGGTGATGTGAGCAAATATGATAGCCAGATTATTGGTGAAGGTCGCATGAAAACCCTGGCAG
ATCAGAATGATCCGGTTACCGGTGGTCTGGTTGGTTTTGGTGGTCGTGGTTTTAGCATTCAT
GCAAATGATGGTAGCGTGATTTATGATAGCGGTAATCTGACAGAAGAAATTGCAGCAGAACT
GGGTTATTATCCTGATAATCGCAGTGATGACAAAGGTACAGAACCGGAAACCGTTGAATATT
TCAGCTTCGGCAAAAAAAAGAACAAACGCCATTATATTGCAGTGGCACTGGAACGTTGTTTT
AACAATGGTGATGAGGATCGTCTGGGTACAATTGTTCCGATTTTTGAAGTTGTTGATCTGGA
AGCAGCCGATAATGATGAACGTGTTAAACATGTTGCAACCCTGCAGAGTCCGGAAAGCCTGT
CACCGGAAGGTCTGCTGTTTGTTAATGATACCAATACCAGCGGTCATATGTTTGTGACCAAT
GAAGTTAGTCGTACCCTGGATACCTATGCAATTAGCCAGGCAGATCTGGCATAAGGATCCTC
TAGAGTCGACCTGCAGG

Appendix 2.4 Codon optimised nucleotide sequence of SYNW1799

CGTCGTCGTAGCGTTCTGAGCCTGTTAGGTTTAGGTGGTGTTGGTGTTCTGACCGCAAAAGG
TCTGAGCGGTTGTGTTGCACCGAGCGGTAATAGCAGCGGTGTTGTTAAAGGTTTTCCGTTTC
AGCCGGTTCGTGTTCCGCTGCCGGTTAATAGTGATGGTCTGCAGGCAAGCGAACAGCAGAGC
ACCTATCGTGAACTGGCAGTTGAAGATCGTCTGACCGTTCCGGAAGGTTTTCAGAGCCAGCT
GCTGGCAGCATGGGGTGATCGTCTGGGTGATAGCCGTTTTGGTTTTAACAATGATCATCTGG
GTTTTGTTCAGCATGCACCGGATCGTGCAAGCATGACCGTTAATTTTGAATATATCAGCGCA
GTTCCGTGGGTTCAGGGTTTTGCAGAAGTTGTTGGTCGTCCGCTGCCTTTTGCAGCACTGGT
TAGCGCACTGCAGAGCAGTGATGGTGTTATTGATTGTACCGCACTGCCTGCCGGTGATCGCC
GTCTGCAGCAGATTCGTACCGTTGCAGATGAAGCAATGACCGATTTAGGTATTGGTGTGATG
ACCCTGGAACGTGATGGTCAAGGTCGTTGGAAACGTGCACAGGCACCGCAGGATCGTCGTAT
TACCGGTATTAGCGGTCTGGATGAACCGGAACAGCAACTGCTGAGCACCGGTCCGGCAGCAG
CAGTTTTTCGTGCCAGCAATCGTCAGGGTTATGATGATGGCCTGGGTGATCGCATTGTTGGC
ACCTTTGCAAATTGTGGTGGTGGTACAACCCCGTGGGGTACAGTTCTGAGCGCAGAAGAAAA
CTTTCAGAGTCAGGTGCCGGAACCGGTTTATGCAGATGGTAGCGCAGCACCGCCTAGCGAAC
GTCCGTTTGTTTGTAAAGATGGTAAATTAGGTGGTCTGGGTAATGTTTATGGTCTGGCAGGT
AACAAATATGGTTGGATGGTTGAAGTTGATCCGACCAGCGCAGATCAGACCGCAGTTAAACA
CACCGCACTGGGTCGTTTTCGTCATGAAGCCGTTGCAGTTCGTGCAGAAGCAGGTAAACCGC
TGCAGGTTTATAGCGGTTGCGATCGTCGTGGTGGTCATCTGTATCGTTTTGTTAGCGCAGAA
CGTGTTGAAACCGTTCAGGATAAACGTAATAGCCGTCTGTTTGAAGCCGGTGAACTGCAGGT
TGCACGTTTTCGTGCGGATGGTAGTGGTGAATGGCTGGCAGTTACACCGGAAAGCGTTGTTG
ATCCGTTTCGTCCGAGCCGTTTTAGTGATGCAGATCTGGGTTGTCCGGTTGAACTGCCGCAT
CGTGATCGTAGCCAGGCAGGGGCAGAACTGTTTCGTGAAGATGCAGCCGTTGAAGATTATTG
TCGTCGTTTTGCAACCCTGAGCGATCTGTACCGTGGTGAAGGTGAAGCACTGCAGGGTGCAA
TTCTGGTTGATGCCCATCTGGCAGCAAGCGCAATTGGTGCAACCCCGACCGCACGTCCGGAA
GATACCAAAATTGATCCGCTGAGCGGTGATCTGCTGATTGCATTTACCAGCGGTAGTCCGGG
TAGCACCGGTGGTGCAGATCCGGCAGTTTTTAAAGGTCCGGAAGGCCAGAGCAGCTGGGCAA
ATGGTTGGGTTATGCGTCTGAGCGAAAGCGGTGAAAATGGTTTTACCTGGCGTATGGCCGTT
ACCGGTGGTACACCGTGGGCAGGCGGTCTGGGCTTTACCAATCCGGATAATGTTGCACTGGA
TAGCAAAGGTAATCTGTGGATTGTTACCGATCGTAGCATGAAAGCATCAGCCGGTGATGTTT
TTGGTAATAATAGCTGTTGGTTTGTTCCGCGTAGCGGTAATGGTGAAGAACAGGCAGCATGT
TTTGCGACCGGTCCGATGGAATGTGAAGTGACCGGTGTTTGTCTGGATCAGGCAGAAGCAAG
CCTGTTTCTGGCAGTTCAGCATCCGGGTGAAGTTAATGGTAGCCGTAGTCAGGGTGATGAAG
AAATTCAGGCACATGAACTGGTTGATCGTGATGGTGGTGTTTTTCAGCAGCTGCGTACCGTG
CCGCTGGGTAGCAATTGGCCTGGTCAGGCACCGGCACGTCCGCCTCGTCCGGGTGTTGTTGC
AATTCAGCGTAGCAATGGTCAGCCGCTGCTGGAAGCC

Appendix II CHAPTER 3

Appendix 3.1 Multiple sequence alignment to confirm PhoB mutant. Blue; forward and reverse control primers, yellow; region A and region B, pink; PhoB sequence, light green; forward and reverse gentamicin primers, dark green; Gentamicin resistance cassette.

```
PhoB_mutant/376-26  376 GGCAATTGTCGATTCAGCACGGGCTCTGGAAACCCGCGACGAGGAACTGGCACAAAAGGTGCGTCTAGGCGACA  449
Control_fw/1-1217     1 ----------------------------------------------------AAAGGTGCGTCTAGGCGACA   20
Control_rv/1-1191       ------------------------------------------------------------------------
Gent_fw/1-1241          ------------------------------------------------------------------------
Gent_rv/1-1202          ------------------------------------------------------------------------

PhoB_mutant/376-26  450 AGGCCATTGATGGACTGGAAGAGCTGATTAACGAAGAATCCGCCCGCGTCATTGCGATGCGGGCCCCGGCTGCG  523
Control_fw/1-1217    21 AGGCCATTGATGGACTGGAAGAGCTGATTAACGAAGAATCCGCCCGCGTCATTGCGATGCGGGCCCCGGCTGCG   94
Control_rv/1-1191       ------------------------------------------------------------------------
Gent_fw/1-1241          ------------------------------------------------------------------------
Gent_rv/1-1202        1 -------------------------------------------------GTTATCNCG-------------------    9

PhoB_mutant/376-26  524 GTTGATCTGCGGGTCGTTCTGTCCGTGATGAAGATTGCAGGTAACCTGGAGCGTATTGGCGACTATTCAAAAAA  597
Control_fw/1-1217    95 GTTGATCTGCGGGTCGTTCTGTCCGTGATGAAGATTGCAGGTAACCTGGAGCGTATTGGCGACTATTCAAAAAA  168
Control_rv/1-1191       ------------------------------------------------------------------------
Gent_fw/1-1241          ------------------------------------------------------------------------
Gent_rv/1-1202          ------------------------------------------------------------------------

PhoB_mutant/376-26  598 CATTGCCAAGCGCACGGGTGTTTTGGTGCAGTGGCATGACAATACAGACAGCTCTGCCGCCCTGCGCCGCATGG  671
Control_fw/1-1217   169 CATTGCCAAGCGCACGGGTGTTTTGGTGCAGTGGCATGACAATACAGACAGCTCTGCCGCCCTGCGCCGCATGG  242
Control_rv/1-1191       ------------------------------------------------------------------------
Gent_fw/1-1241          ------------------------------------------------------------------------
Gent_rv/1-1202          ------------------------------------------------------------------------

PhoB_mutant/376-26  672 CTCGTGAAGTCGAGCTGATGCTAAAGGACGCTTTGGATGCCTATATTCAACGCGATACAGAACTGGCTGCCGAT  745
Control_fw/1-1217   243 CTCGTGAAGTCGAGCTGATGCTAAAGGACGCTTTGGATGCCTATATTCAACGCGATACAGAACTGGCTGCCGAT  316
Control_rv/1-1191       ------------------------------------------------------------------------
Gent_fw/1-1241          ------------------------------------------------------------------------
Gent_rv/1-1202          ------------------------------------------------------------------------

PhoB_mutant/376-26  746 GTAATCACGCGGGATCGTGAGGTGGACCAGATGTACAACGCACTGTTCCGCGAGTTCTTGACCCATATGATGGA  819
Control_fw/1-1217   317 GTAATCACGCGGGATCGTGAGGTGGACCAGATGTACAACGCACTGTTCCGCGAGTTCTTGACCCATATGATGGA  390
Control_rv/1-1191       ------------------------------------------------------------------------
Gent_fw/1-1241          ------------------------------------------------------------------------
Gent_rv/1-1202       10 ----------GGGGTTNGGANGTGGCCCAAAT-NACAACGCATTTTTCCGCGAGTTCTTGACCCAT-TGATGGA   71

PhoB_mutant/376-26  820 AGATCCGCGCAACATTACAGCCTGTATGCATCTGCACTTCATTGCAAAAAACATCGAACGCATGGGGGATCACG  893
Control_fw/1-1217   391 AGATCCGCGCAACATTACAGCCTGTATGCATCTGCACTTCATTGCAAAAAACATCGAACGCATGGGGGATCACG  464
Control_rv/1-1191       ------------------------------------------------------------------------
Gent_fw/1-1241          ------------------------------------------------------------------------
Gent_rv/1-1202       72 AGATCCGCGCAACATTACAGCCTGTAAGCATCTGCACTTCATTGCAAAAAACATCGAACGCATGGGGGATCACG  145

PhoB_mutant/376-26  894 TCACCTCCATCGCTGAAGAGCTAATCTATCTGGTGACCGGTCGTCGGCCAGAGGATGACCGGCCCAAAGCAGAT  967
Control_fw/1-1217   465 TCACCTCCATCGCTGAAGAGCTAATCTATCTGGTGACCGGTCGTCGGCCAGAGGATGACCGGCCCAAAGCAGAT  538
Control_rv/1-1191       ------------------------------------------------------------------------
Gent_fw/1-1241          ------------------------------------------------------------------------
Gent_rv/1-1202      146 TCACCTCCATCGCTGAAGAGCTAATCTATCTGGTGACCGGTCGTCGGCCAGAGGATGACCGGCCCAAAGCAGAT  219

PhoB_mutant/376-26  968 TTCACCTCCATTTCGACAGAGGAGGCCTGATCCATGACTGCCGATCAGCCGACAGTTCTGATCATCGAGGATGA 1041
Control_fw/1-1217   539 TTCACCTCCATTTCGACAGAGGAGGCCTGATCCATGACTGCCGATCAGCCGACAGTTCTGATCATCGAGGATGA  612
Control_rv/1-1191       ------------------------------------------------------------------------
Gent_fw/1-1241          ------------------------------------------------------------------------
Gent_rv/1-1202      220 TTCACCTCCATTTCGACAGAGGAGGCCTGATCCATGACTGCCGATCAGCCGACAGTTCTGATCATCGAGGATGA  293

PhoB_mutant/376-26 1042 GTTAGCCCAGCGAGAGGTCCTTGCCTACAATCTTGAGGCCGATGGCTTTCGTGTCATCCGGGCAGAAAACGGCG 1115
Control_fw/1-1217   613 GTTAGCCCAGCGAGAGGTCCTTGCCTACAATCTTGAGGCCGATGGCTTTCGTGTCATCCGGGCAGAAAACGGCG  686
Control_rv/1-1191       ------------------------------------------------------------------------
Gent_fw/1-1241          ------------------------------------------------------------------------
Gent_rv/1-1202      294 GTTAGCCCAGCGAGAGGTCCTTGCCTACAATCTTGAGGCCGATGGCTTTCGTGTCATCCGGGCAGAAAACGGCG  367

PhoB_mutant/376-26 1116 AAGAAGGCTTGTCGACTCTAGAGGATCCCCGGGTACCGAGCTCGAATTGACATAAGCCTGTTCGGTTCGTAAAC 1189
Control_fw/1-1217   687 AAGAAGGCTTGTCGACTCTAGAGGATCCCCGGGTACCGAGCTCGAATTGACATAAGCCTGTTCGGTTCGTAAAC  760
Control_rv/1-1191       ------------------------------------------------------------------------
Gent_fw/1-1241        1 ----------------------------------------GAGCTCGAATTGACATAAGCCTGTTCGGTTCGTAAAC   37
Gent_rv/1-1202      368 AAGAAGGCTTGTCGACTCTAGAGGATCCCCGGGTACCGAGCTCGAATTGACATAAGCCTGTTCGGTTCGTAAAC  441

PhoB_mutant/376-26 1190 TGTAATGCAAGTAGCGTATGCGCTCACGCAACTGGTCCAGAACCTTGACCGAACGCAGCGGTGGTAACGGCGCA 1263
Control_fw/1-1217   761 TGTAATGCAAGTAGCGTATGCGCTCACGCAACTGGTCCAGAACCTTGACCGAACGCAGCGGTGGTAACGGCGCA  834
Control_rv/1-1191       ------------------------------------------------------------------------
Gent_fw/1-1241       38 TGTAATGCAAGTAGCGTATGCGCTCACGCAACTGGTCCAGAACCTTGACCGAACGCAGCGGTGGTAACGGCGCA  111
Gent_rv/1-1202      442 TGTAATGCAAGTAGCGTATGCGCTCACGCAACTGGTCCAGAACCTTGACCGAACGCAGCGGTGGTAACGGCGCA  515

PhoB_mutant/376-26 1264 GTGGCGGTTTTCATGGCTTGTTATGACTGTTTTTTTGTACAGTCTATGCCTCGGGCATCCAAGCAGCAAGCGCG 1337
Control_fw/1-1217   835 GTGGCGGTTTTCATGGCTTGTTATGACTGTTTTTTTGTACAGTCTATGCCTCGGGCATCCAAGCAGCAAGCGCG  908
Control_rv/1-1191       ------------------------------------------------------------------------
Gent_fw/1-1241      112 GTGGCGGTTTTCATGGCTTGTTATGACTGTTTTTTTGTACAGTCTATGCCTCGGGCATCCAAGCAGCAAGCGCG  185
Gent_rv/1-1202      516 GTGGCGGTTTTCATGGCTTGTTATGACTGTTTTTTTGTACAGTCTATGCCTCGGGCATCCAAGCAGCAAGCGCG  589

PhoB_mutant/376-26 1338 TTACGCCGTGGGTCGATGTTTGATGTTATGGAGCAGCAACGATGTTACGCAGCAGCAACGATGTTACGCAGCAG 1411
Control_fw/1-1217   909 TTACGCCGTGGGTCGATGTTTGATGTTATGGAGCAGCAACGATGTTACGCAGCAGCAACGATGTTACGCAGCAG  982
Control_rv/1-1191       1 ----------------------------------------------------ACGATTTTTCCCAGCAG   17
Gent_fw/1-1241      186 TTACGCCGTGGGTCGATGTTTGATGTTATGGAGCAGCAACGATGTTACGCAGCAGCAACGATGTTACGCAGCAG  259
Gent_rv/1-1202      590 TTACGCCGTGGGTCGATGTTTGATGTTATGGAGCAGCAACGATGTTACGCAGCAGCAACGATGTTACGCAGCAG  663

PhoB_mutant/376-26 1412 GGCAGTCGCCCTAAAACAAAGTTAGGTGGCTCAAGTATGGGCATCATTCGCACATGTAGGCTCGGCCCTGACCA 1485
Control_fw/1-1217   983 GGCAGTCGCCCTAAAACAAAGTTAGGTGGCTCAAGTATGGGCATCATTCGCACATGTAGGCTCGGCCCTGACCA 1056
Control_rv/1-1191    18 GGCAGNCGCCCTAAAACAAAGTTAGGTGG-TCAAGTATGGGCATCATT-GCACATGTAGG-TTGGGCCTGACCA   88
Gent_fw/1-1241      260 GGCAGTCGCCCTAAAACAAAGTTAGGTGGCTCAAGTATGGGCATCATTCGCACATGTAGGCTCGGCCCTGACCA  333
Gent_rv/1-1202      664 GGCAGTCGCCCTAAAACAAAGTTAGGTGGCTCAAGTATGGGCATCATTCGCACATGTAGGCTCGGCCCTGACCA  737

PhoB_mutant/376-26 1486 AGTCAAATCCATGCGGGCTGCTCTTGATCTTTTCGGTCGTGAGTTCGGAGACGTAGCCACCTACTCCCAACATC 1559
Control_fw/1-1217  1057 AGTCAAATCCATGCGGGCTGCTCTTGATCTTTTCGGTCGTGAGTTCGGAGACGTAGCCACCTACTCCCAACATC 1130
Control_rv/1-1191     89 AGTCAAATCCATGCGGG-TGGTTTTGATCTTTTC-GTTGGGAGTTCGGAGACGTAGCCACTTACTCCCAACATC  160
Gent_fw/1-1241      334 AGTCAAATCCATGCGGGCTGCTCTTGATCTTTTCGGTCGTGAGTTCGGAGACGTAGCCACCTACTCCCAACATC  407
Gent_rv/1-1202      738 AGTCAAATCCATGCGGGCTGCTCTTGATCTTTTCGGTCGTGAGTTCGGAGACGTAGCCACCTACTCCCAACATC  811
```

```
PhoB_mutant/376-26! 1560 AGCCGGACTCCGATTACCTCGGGAACTTGCTCCGTAGTAAGACATTCATCGCGCTTGCTGCCTTCGACCAAGAA 1633
Control_fw/1-1217   1131 AGCCGGACTCCGATTACCTCGGGAACTTGCTCCGAATAAAGAATTTCTTCCCCCTTGCTGCNTTNNAACAAAAA 1204
Control_rv/1-1191    161 AGCCGGACTCCGATTACCTCGGGAACTTGCTCCGTAGTAAGACATTCATCGCGCTTGCTGCCTTCGACCAAGAA  234
Gent_fw/1-1241       408 AGCCGGACTCCGATTACCTCGGGAACTTGCTCCGTAGTAAGACATTCATCGCGCTTGCTGCCTTCGACCAAGAA  481
Gent_rv/1-1202       812 AGCCGGACTCCGATTACCTCGGGAACTTGCTCCGTAGTAAGACATTCATCGCGCTTGCTGCCTTCGACCAAGAA  885

PhoB_mutant/376-26! 1634 GCGGTTGTTGGCGCTCTCGCGGCTTACGTTCTGCCCAGGTTTGAGCAGCCGCGTAGTGAGATCTATATCTATGA 1707
Control_fw/1-1217   1205 ANGG------------------------------------------------------------------------ 1208
Control_rv/1-1191    235 GCGGTTGTTGGCGCTCTCGCGGCTTACGTTCTGCCCAAGTTTGAGCAGCCGCNTAGTGAGATCTATATCTATGA  308
Gent_fw/1-1241       482 GCGGTTGTTGGCGCTCTCGCGGCTTACGTTCTGCCCAAGTTTGAGCAGCCGCGTAGTGAGATCTATATCTATGA  555
Gent_rv/1-1202       886 GCGGTTGTTGGCGCTCTCGCGGCTTACGTTCTGCCCAAGTTTGAGCAGCCGCGTAGTGAGATCTATATCTATGA  959

PhoB_mutant/376-26! 1708 TCTCGCAGTCTCCGGCGAGCACCGGAGGCAGGGCATTGCCACCGCGCTCATCAATCTCCTCAAGCATGAGGCCA 1781
Control_fw/1-1217   1209 -------GTTTTTGGC------------------------------------------------------------ 1217
Control_rv/1-1191    309 TCTCGCAGTCTCCGGCGAGCACCGGAGGCAGGGCATTGCCACCGCGCTCATCAATCTCCTCAAGCATGAGGCCA  382
Gent_fw/1-1241       556 TCTCGCAGTCTCCGGCGAGCACCGGAGGCAGGGCATTGCCACCGCGCTCATCAATCTCCTCAAGCATGAGGCCA  629
Gent_rv/1-1202       960 TCTCGCAGTCTCCGGCGAGCACCGGAGGCAGGGCATTGCCACCGCGCTCATCAATCTCCTCAAGCATGAGGCCA 1033

PhoB_mutant/376-26! 1782 ACGCGCTTGGTGCTTATGTGATCTACGTGCAAGCAGATTACGGTGACGATCCCGCAGTGGCTCTCTATACAAAG 1855
Control_fw/1-1217        ------------------------------------------------------------------------
Control_rv/1-1191    383 ACGCGCTTGGTGCTTATGTGATCTACGTGCAAGCAGATTACGGTGACGATCCCGCAGTGGCTCTCTATACAAAG  456
Gent_fw/1-1241       630 ACGCGCTTGGTGCTTATGTGATCTACGTGCAAGCAGATTACGGTGACGATCCCGCAGTGGCTCTCTATACAAAG  703
Gent_rv/1-1202      1034 ACGCGCTTGGTGCTTATGTGATCTACGTGCAAGCAGATTACGGTGACGATCCCGCAGTGGCTCTCTATACAAAG 1107

PhoB_mutant/376-26! 1856 TTGGGCATACGGGAAGAAGTGATGCACTTTGATATCGACCCAAGTACCGCCACCTAACAATTCGTTCAAGCCGA 1929
Control_fw/1-1217        ------------------------------------------------------------------------
Control_rv/1-1191    457 TTGGGCATACGGGAAGAAGTGATGCACTTTGATATCGACCCAAGTACCGCCACCTAACAATTCGTTCAAGCCGA  530
Gent_fw/1-1241       704 TTGGGCATACGGGAAGAAGTGATGCACTTTGATATCGACCCAAGTACCGCCACCTAACAATTCGTTCAAGCCGA  777
Gent_rv/1-1202      1108 TTGGGCATACGGGAAGAAGTGATGCACTTTGATATCGACCCAAGTACCGCCACCTAACAATTCG-TCAAGCCGA 1180

PhoB_mutant/376-26! 1930 GATCGGCTTCCCGGCCGCGGAGTTGTTCGGTAAATTGTCACAACGCCGCGGCCAACAGTTTGGTGGTGCTGATC 2003
Control_fw/1-1217        ------------------------------------------------------------------------
Control_rv/1-1191    531 GATCGGCTTCCCGGCCGCGGAGTTGTTCGGTAAATTGTCACAACGCCGCGGCCAACAGTTTGGTGGTGCTGATC  604
Gent_fw/1-1241       778 GATCGGCTTCCCGGCCGCGGAGTTGTTCGGTAAATTGTCACAACGCCGCGGCCAACAGTTTGGTGGTGCTGATC  851
Gent_rv/1-1202      1181 GATCGGC-TCCCGGCCGCGAGTT------------------------------------------------- 1202

PhoB_mutant/376-26! 2004 CGGTGCGCACGGTGCGCGGCGCGGGCTACGCTTTAGGCTAAGGCCTCGCCAGACCGTATGAACACTTCAATGGG 2077
Control_fw/1-1217        ------------------------------------------------------------------------
Control_rv/1-1191    605 CGGTGCGCACGGTGCGCGGCGCGGGCTACGCTTTAGGCTAAGGCCTCGCCAGACCGTATGAACACTTCAATGGG  678
Gent_fw/1-1241       852 CGGTGCGCACGGTGCGCGGCGCGGGCTACGCTTTAGGCTAAGGCCTCGCCAGACCGTATGAACACTTCAATGGG  925
Gent_rv/1-1202           ------------------------------------------------------------------------

PhoB_mutant/376-26! 2078 CGTCACTCGGCGCCCGTTTGCTGTCGCGGTCGATCACAGGCAGCGCCTATCGCGGTAGCGGGTCTTCTGGCTGT 2151
Control_fw/1-1217        ------------------------------------------------------------------------
Control_rv/1-1191    679 CGTCACTCGGCGCCCGTTTGCTGTCGCGGTCGATCACAGGCAGCGCCTATCGCGGTAGCGGGTCTTCTGGCTGT  752
Gent_fw/1-1241       926 CGTCACTCGGCGCCCGTTTGCTGTCGCGGTCGATCACAGGCAGCGCCTATCGCGGTAGCGGGTCTTCTGGCTGT  999
Gent_rv/1-1202           ------------------------------------------------------------------------

PhoB_mutant/376-26! 2152 GCTTGACCTTCAAGCCAGAGCCGAAACTTTGTCAGCGCCGGATCACGCGATTTATTCTTTGGCCAGACCAGAAA 2225
Control_fw/1-1217        ------------------------------------------------------------------------
Control_rv/1-1191    753 GCTTGACCTTCAAGCCAGAGCCGAAACTTTGTCAGCGCCGGATCACGCGATTTATTCTTTGGCCAGACCAGAAA  826
Gent_fw/1-1241      1000 GCTTGACCTTCAAGCCAGAGCCGAAACTTTGTCAGCGCCGGATCACGCGATTTATTCTTTGGCCAGACCAGAAA 1073
Gent_rv/1-1202           ------------------------------------------------------------------------

PhoB_mutant/376-26! 2226 ATAGGCGCCTGCGGCCTCACT-GGGGCGTGATTGTAGCGCAGCCAACCTACCGGTGGCGATATCCTGTTCCACA 2298
Control_fw/1-1217        ------------------------------------------------------------------------
Control_rv/1-1191    827 ATAGGCGCCTGCGGCCTCACT-GGGGCGTGATTGTAGCGCAGCCAACCTACCGGTGGCGATATCCTGTTCCACA  899
Gent_fw/1-1241      1074 ATAGGCGCCTGCGGCCTCACTGGGGGCGTGATTGTAGCGCAGCCAACCTACCGGTGGCGATATCCTGTTCCAAA 1147
Gent_rv/1-1202           ------------------------------------------------------------------------

PhoB_mutant/376-26! 2299 AGATAATCCGGCATCAAGGCCACCCCCAACCCGTGCAATGCAGCCTGGGTAATGGTTGAGAATTGATCATACAT 2372
Control_fw/1-1217        ------------------------------------------------------------------------
Control_rv/1-1191    900 AGATAATCCGGCATCAAGGCCACCCCCAACCCGTGCAATGCAGCCTGGGTAATGGTTGAGAATTGATCATACAT  973
Gent_fw/1-1241      1148 AAATAATCCGGCATCAAGG-CAACCCCAACCCGGGCAATGCACCCTGGGTAATGGTTGAAAATTGATCAT-NAT 1219
Gent_rv/1-1202           ------------------------------------------------------------------------

PhoB_mutant/376-26! 2373 TGTCCCGCCCAGACCCTCTGGGCTGGCCGAAACACTATGCTGCTCAAACCAATCCAGCCAGGCCTTGGGCCGGG 2446
Control_fw/1-1217        ------------------------------------------------------------------------
Control_rv/1-1191    974 TGTCCCGCCCAGACCCTCTGGGCTGGCCGAAACACTATGTAGCTCAAACCAATCCAGCCAGGCCTTGGGCCGGG 1047
Gent_fw/1-1241      1220 TGTCCCGCCCAA--CCCCTGGGNT------------------------------------------------- 1241
Gent_rv/1-1202           ------------------------------------------------------------------------

PhoB_mutant/376-26! 2447 TCTGAATATGTAACAGCGGCATGTCCAATATGTTCTTGGGGGCAACATAGGTTCCAATCGGGACCATTTGCGGG 2520
Control_fw/1-1217        ------------------------------------------------------------------------
Control_rv/1-1191   1048 TCTGAATATGTAACAGCGGCATGTCCAATATGTTCTTGGGGGCAACATAGGTTCCAATCGGGACCATTTGCGGG 1121
Gent_fw/1-1241           ------------------------------------------------------------------------
Gent_rv/1-1202           ------------------------------------------------------------------------

PhoB_mutant/376-26! 2521 CTACAAACCGGCAAGAGCTGCTCAGATTTTAGCAGCATGGATTCGGT-GCCCGGCCAATCAGCAGTACCAAAAT 2593
Control_fw/1-1217        ------------------------------------------------------------------------
Control_rv/1-1191   1122 CTACAAACCGGCAAGAGCTGCTCAGATTTTAGCAGCATGGATTCGGTCGCCCGGCCAATCAGCAGTACCA---- 1191
Gent_fw/1-1241           ------------------------------------------------------------------------
Gent_rv/1-1202           ------------------------------------------------------------------------

PhoB_mutant/376-26! 2594 GAATTGCTGCATCAATAGGTTCGCTGCCAAAACTAAAGGCCTGCAAGCGCGTGGTCATATTGATGG        2659
Control_fw/1-1217        ------------------------------------------------------------
Control_rv/1-1191        ------------------------------------------------------------
Gent_fw/1-1241           ------------------------------------------------------------
Gent_rv/1-1202           ------------------------------------------------------------
```

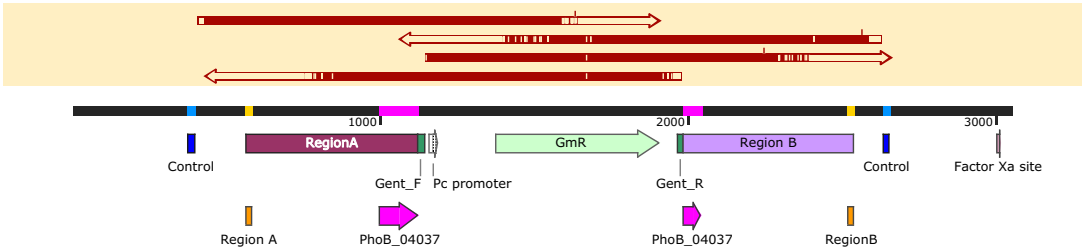

Appendix 3.2 Relative abundance of lipid/SPE ratios in samples taken from P-replete WT MED193 (MED193 HP), P-deplete WT MED193 (MED193 -P), and P-deplete ΔphoB (ΔphoB -P) cultures. Multiple t-test analyses between MED193 -P (a), ΔphoB -P (b), and MED193 HP (c) with p-value <0.01. SAL/SAL2; sulfur containing aminolipid, OL; ornithine lipid, QL; glutamine lipid; DGTS, diacylglyceryl-trimethylhomoserine; PtdGro, phosphatidyl-glycerol; PtdEtn, phosphatidylethanolamine.

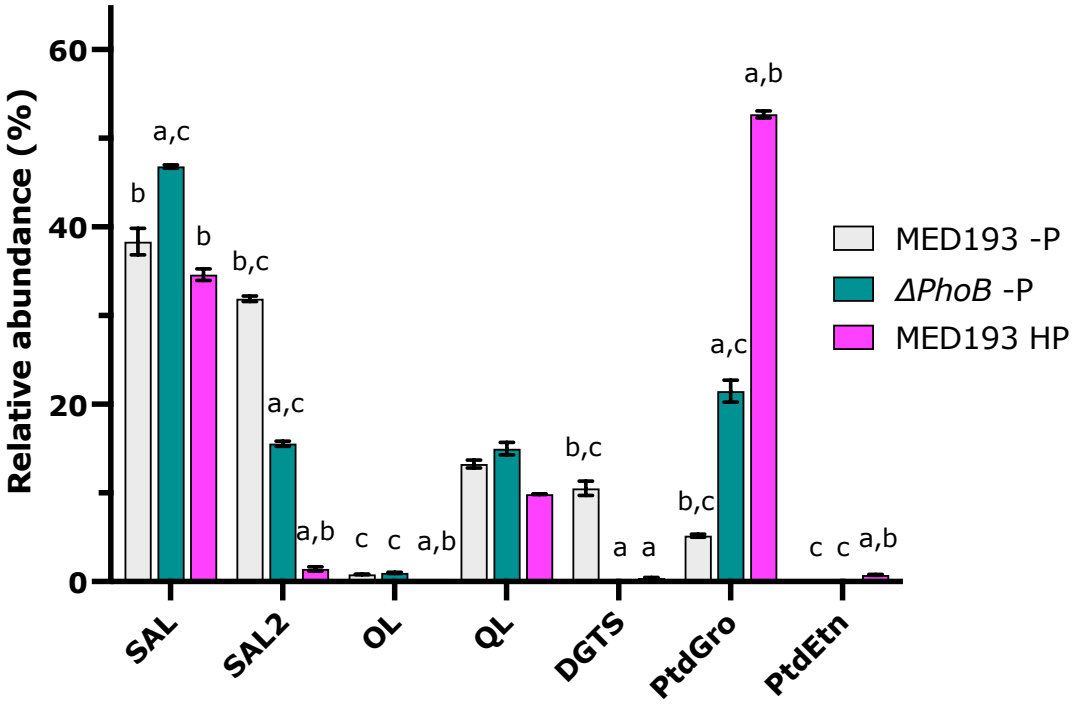

Appendix 3.3 Significantly upregulated proteins (p-value <0.05) in the cellular proteome of P-deplete MED193 cultures in comparison to ΔphoB. Colours represent COGs: yellow; metabolism, blue; cellular processes and signalling, green; information storage and processing, no colour; poorly characterised.

Protein ID	*p-value <0.05*	*-log$_{10}$ (p-value)*	*Log$_2$ (fold change)*	*Locus tag*	*Uniprot annotation*
A3XBP0	+	3.968	13.754	MED193_04062	Phosphate ABC transporter, periplasmic phosphate-binding protein
A3X8H3	+	5.463	12.818	MED193_05784	Uncharacterized protein
A3X815	+	4.023	12.426	MED193_06579	Glycerophosphoryl diester phosphodiesterase
A3XFY2	+	4.828	12.297	MED193_10161	Phosphonate ABC transporter, periplasmic phosphonate-binding protein
A3XBZ9	+	4.177	10.112	MED193_03507	Iron-binding periplasmic protein
A3X9P6	+	3.858	9.299	MED193_01855	Putative periplasmic solute-binding protein
A3X9J4	+	4.323	9.273	MED193_07903	SN-glycerol-3-phophate ABC transporter, periplasmic SN-glycerol-3-phosphate-binding protein
A3X7T5	+	4.859	9.238	MED193_06969	NADH dehydrogenase subunit L
A3X3K4	+	4.667	9.021	MED193_17649	Alkylphosphonate utilization protein PhnM
A3XFW0	+	4.862	8.925	MED193_11712	N-methylproline demethylase, putative
A3XAW5	+	2.752	7.802	MED193_04391	CaiB/BaiF family protein
A3XFR8	+	3.085	7.714	MED193_11927	Polyphosphate kinase, putative
A3XAA0	+	4.470	7.533	MED193_00825	Glyceraldehyde-3-phosphate dehydrogenase (EC 1.2.1.-)
A3XFY3	+	3.342	7.494	MED193_10166	Phosphonates import ATP-binding protein PhnC (EC 7.3.2.2)
A3XC77	+	6.179	7.105	MED193_03127	2',3'-cyclic nucleotide 2'-phosphodiesterase/3'-nucleotidase bifunctional periplasmic protein (EC 3.1.4.16)
A3X9J7	+	4.738	6.987	MED193_07888	sn-glycerol-3-phosphate import ATP-binding protein UgpC (EC 3.6.3.20)
A3XBP2	+	5.496	6.950	MED193_04052	Phosphate transport system permease protein PstA
A3X7Z6	+	3.245	6.797	MED193_06674	Carbon monoxide dehydrogenase, large subunit
A3X388	+	2.393	6.718	MED193_18239	Putative binding domain protein
A3XBN9	+	4.023	6.698	MED193_04057	Phosphate transport system permease protein
A3XBP1	+	3.819	6.537	MED193_04047	Phosphate import ATP-binding protein PstB (EC 7.3.2.1) (ABC phosphate transporter) (Phosphate-transporting ATPase)
A3XA99	+	3.858	6.504	MED193_00820	Transcriptional regulator/arsenate reductase
A3XBP3	+	4.493	6.388	MED193_04042	Phosphate-specific transport system accessory protein PhoU
A3X384	+	3.956	5.934	MED193_18254	UshA protein
A3XA24	+	2.852	5.854	MED193_01200	UDP-glucose 6-dehydrogenase (EC 1.1.1.22)

A3XA04	+	5.813	5.779	MED193_01305	Na(+)-translocating NADH-quinone reductase subunit A (Na(+)-NQR subunit A) (Na(+)-translocating NQR subunit A) (EC 7.2.1.1) (NQR complex subunit A) (NQR-1 subunit A)
A3XDT6	+	3.098	5.772	MED193_00725	Chloroacetaldehyde dehydrogenase
A3XFY0	+	3.247	5.718	MED193_10151	Phosphonate ABC transporter, permease protein
A3XC84	+	4.022	5.714	MED193_11293	Sugar ABC transporter, periplasmic sugar-binding protein
A3X844	+	2.466	5.535	MED193_06444	ABC transporter, periplasmic substrate-binding protein
A3XBP5	+	2.157	5.494	MED193_04037	Phosphate regulon transcriptional regulatory protein PhoB
A3XA11	+	2.747	5.429	MED193_01280	Na(+)-translocating NADH-quinone reductase subunit F (Na(+)-NQR subunit F) (Na(+)-translocating NQR subunit F) (EC 7.2.1.1) (NQR complex subunit F) (NQR-1 subunit F)
A3XBN7	+	3.551	5.248	MED193_04067	Phosphate regulon sensor histidine kinase, putative
A3X5K9	+	4.123	5.211	MED193_19059	Uncharacterized protein
A3XDT0	+	1.887	5.194	MED193_00745	Probable 1,4-butanediol diacrylate esterase
A3XBX7	+	2.608	5.143	MED193_03622	Indolepyruvate ferredoxin oxidoreductase (EC 1.2.7.8)
A3X8G7	+	2.459	4.942	MED193_05814	Periplasmic glucan biosynthesis protein MdoG
A3X3A1	+	5.892	4.880	MED193_18169	Uncharacterized protein
A3XDV2	+	3.292	4.718	MED193_00665	Uncharacterized protein
A3X3L3	+	2.741	4.534	MED193_17614	Alkylphosphonate utilization protein PhnI
A3XE52	+	3.137	4.493	MED193_00125	Dioxygenase
A3X532	+	3.669	4.491	MED193_19939	Uncharacterized protein
A3XAW2	+	2.850	4.465	MED193_04416	Glucose-6-phosphate 1-dehydrogenase (G6PD) (EC 1.1.1.49)
A3XFX2	+	3.020	4.333	MED193_10201	Acyl-CoA dehydrogenase family protein
A3XCQ4	+	2.026	4.324	MED193_10448	Methylmalonyl-CoA mutase
A3X937	+	2.885	4.282	MED193_08703	Caspase-1, p20
A3X6T0	+	2.682	4.261	MED193_14802	Uncharacterized protein
A3X670	+	2.914	4.237	MED193_15857	Type I secretion membrane fusion protein, HlyD family protein
A3XAK2	+	1.737	4.148	MED193_04966	Oligopeptide/dipeptide ABC transporter, periplasmic substrate-binding protein
A3XFY1	+	2.737	4.144	MED193_10156	Phosphonate ABC transporter, permease protein
A3XF83	+	2.202	4.126	MED193_21716	Uncharacterized protein
A3XDV1	+	3.215	4.110	MED193_00660	Uncharacterized protein
A3X3R1	+	1.411	4.090	MED193_17364	S-adenosylmethionine-diacylglycerol 3-amino-3-carboxypropyltransferase
A3XAW1	+	3.393	4.061	MED193_04411	6-phosphogluconolactonase
A3XC79	+	2.225	4.039	MED193_11308	Sugar ABC transporter, ATP-binding protein

A3XC02	+	3.475	3.908	MED193_03497	ATP-binding component of transport system
A3XFZ7	+	1.737	3.838	MED193_10096	Formate dehydrogenase, alpha subunit, putative
A3X3K7	+	2.443	3.754	MED193_17644	Uncharacterized protein
A3X9N9	+	3.755	3.666	MED193_01875	3',5'-cyclic adenosine monophosphate phosphodiesterase CpdA (3',5'-cyclic AMP phosphodiesterase) (cAMP phosphodiesterase) (EC 3.1.4.53)
A3X9U7	+	3.771	3.626	MED193_01590	Chemotaxis response regulator
A3X755	+	3.640	3.620	MED193_14152	UDP-glucose pyrophosphate
A3X835	+	2.546	3.604	MED193_06474	TRAP-T family transporter, DctP (Periplasmic binding) subunit
A3XA62	+	1.692	3.595	MED193_01025	Uncharacterized protein
A3X9P3	+	2.100	3.588	MED193_01870	ABC spermidine/putrescine transporter, ATPase subunit
A3XA68	+	2.665	3.560	MED193_00995	Uncharacterized protein
A3XDU3	+	1.562	3.545	MED193_00670	Uncharacterized protein
A3X421	+	4.067	3.532	MED193_16829	Phosphoglycerate mutase family protein
A3XFX1	+	2.386	3.489	MED193_10196	Acyl-CoA dehydrogenase family protein
A3X3E4	+	2.666	3.470	MED193_17959	Integration host factor subunit beta (IHF-beta)
A3XDK1	+	1.833	3.461	MED193_13118	Aldehyde dehydrogenase family protein
A3X728	+	3.547	3.436	MED193_14292	AMP nucleosidase (EC 3.2.2.4)
A3XEW0	+	2.509	3.421	MED193_12248	Transglycosylase, Slt family protein
A3X8U2	+	3.521	3.419	MED193_07578	Uncharacterized protein
A3XD40	+	1.159	3.419	MED193_09640	Cold shock family protein
A3X4Q5	+	3.687	3.378	MED193_20584	Putative 3-oxoacyl-acyl carrier protein reductase
A3XDZ9	+	3.972	3.375	MED193_00410	Uncharacterized protein
A3XE22	+	2.466	3.374	MED193_00310	Replication protein a
A3X7Z9	+	1.907	3.363	MED193_06669	Carbon monoxide dehydrogenase, medium subunit, putative
A3X3K9	+	2.132	3.362	MED193_17634	Alkylphosphonate utilization protein PhnL
A3X7P9	+	3.893	3.356	MED193_07164	Amidohydrolase family protein
A3XA00	+	2.191	3.347	MED193_01335	CBS domain protein
A3X4N5	+	2.175	3.340	MED193_20664	DnaK suppressor protein
A3XFW3	+	4.112	3.331	MED193_10246	Uncharacterized protein
A3XFD7	+	3.365	3.297	MED193_21431	Peptide/nickel/opine uptake family ABC transporter, ATP-binding protein
A3X974	+	2.432	3.272	MED193_08508	Uncharacterized protein
A3X8I0	+	2.126	3.225	MED193_05749	Sulfur oxidation protein SoxY
A3XCJ4	+	2.791	3.205	MED193_10723	TPR domain protein
A3XBS0	+	2.108	3.191	MED193_03902	Uncharacterized protein

A3X9L3	+	1.816	3.186	MED193_07818	Probable binding protein component of ABC sugar transporter
A3XFL5	+	5.096	3.182	MED193_11419	Polyamine transport protein PotA
A3X8K8	+	2.838	3.175	MED193_05624	Branched-chain amino acid ABC transporter, ATP-binding protein
A3X8A3	+	1.396	3.128	MED193_06134	Lactoylglutathione lyase, putative
A3X4R3	+	6.126	3.053	MED193_20524	Uncharacterized protein
A3XF89	+	1.804	3.011	MED193_21691	Uncharacterized protein
A3XA64	+	2.673	3.010	MED193_01010	Uncharacterized protein
A3XF72	+	1.751	2.977	MED193_02700	Uncharacterized protein
A3XA92	+	3.491	2.970	MED193_00870	5-carboxy-2-hydroxymuconate semialdehyde dehydrogenase
A3X8I3	+	2.351	2.948	MED193_05744	Sulfur oxidation Z protein
A3XEY5	+	2.116	2.936	MED193_12123	Microcystin dependent protein MdpB
A3XA54	+	3.801	2.932	MED193_01065	Uncharacterized protein
A3XB36	+	3.508	2.905	MED193_22116	Poly(3-hydroxyalkanoate) polymerase
A3XC83	+	2.244	2.894	MED193_11288	Phosphodiesterase
A3X7B2	+	2.094	2.878	MED193_13887	Peptide methionine sulfoxide reductase MsrA (Protein-methionine-S-oxide reductase) (EC 1.8.4.11) (Peptide-methionine (S)-S-oxide reductase) (Peptide Met(O) reductase)
A3X945	+	3.018	2.876	MED193_08648	Uncharacterized protein
A3XFW1	+	1.749	2.855	MED193_11717	Methyltransferase (EC 2.1.1.-)
A3X899	+	1.778	2.848	MED193_06169	Polyphosphate kinase 2
A3XBH6	+	1.778	2.833	MED193_22461	Integration host factor subunit alpha (IHF-alpha)
A3XCB2	+	2.425	2.815	MED193_11133	Glycosyl hydrolase, family 25
A3X7S1	+	2.146	2.814	MED193_07074	Hydroxymethylglutaryl-CoA lyase (EC 4.1.3.4)
A3X8T2	+	1.626	2.806	MED193_07643	Phosphoribosyl-ATP pyrophosphatase (PRA-PH) (EC 3.6.1.31)
A3XCQ1	+	2.622	2.785	MED193_10433	Crotonyl-CoA reductase
A3X4T5	+	2.202	2.761	MED193_20429	Methylmalonyl-CoA epimerase
A3X567	+	1.743	2.756	MED193_19764	Hydrolase, NUDIX family protein
A3X7N2	+	2.018	2.743	MED193_07254	Kynureninase (EC 3.7.1.3) (L-kynurenine hydrolase)
A3X8M7	+	1.185	2.725	MED193_05534	Pyridine nucleotide-disulphide oxidoreductase family protein
A3XF87	+	1.934	2.721	MED193_21681	Betaine aldehyde dehydrogenase
A3X612	+	1.187	2.687	MED193_16152	Signal recognition particle protein (Fifty-four homolog)
A3XC01	+	2.085	2.675	MED193_03492	Metallo-beta-lactamase family protein
A3X390	+	0.813	2.640	MED193_18224	AMP-binding enzyme
A3X3L1	+	3.258	2.614	MED193_17624	Alpha-D-ribose 1-methylphosphonate 5-phosphate C-P lyase (PRPn C-P lyase) (EC 4.7.1.1)

A3XFE0	+	3.157	2.602	MED193_21446	Peptide/nickel/opine uptake family ABC transporter, periplasmic substrate-binding protein
A3X8T4	+	2.634	2.585	MED193_07618	Uncharacterized protein
A3XDF8	+	1.293	2.582	MED193_13353	Uncharacterized protein
A3X429	+	1.075	2.581	MED193_16774	Phospho-2-dehydro-3-deoxyheptonate aldolase (EC 2.5.1.54)
A3X7G6	+	1.793	2.568	MED193_13632	YCII-related domain protein
A3XFC0	+	2.190	2.564	MED193_21546	50S ribosomal protein L33
A3XDC7	+	3.048	2.560	MED193_13478	Spermidine/putrescine import ATP-binding protein PotA (EC 3.6.3.31)
A3XBZ2	+	1.619	2.553	MED193_03542	CBS domain protein
A3X6H2	+	2.282	2.551	MED193_15352	Uncharacterized protein
A3XCA6	+	1.520	2.537	MED193_11193	Iron-sulfur-binding protein, RdxA/RdxB/FixG family protein
A3XF80	+	1.613	2.525	MED193_21746	Propionyl-CoA carboxylase, alpha subunit
A3X736	+	1.310	2.504	MED193_14287	DNA-binding protein HU
A3XFB4	+	2.182	2.495	MED193_21566	Uncharacterized protein
A3XCJ2	+	3.252	2.472	MED193_10748	Uncharacterized protein
A3XEY6	+	2.050	2.467	MED193_12128	Hypothetical microcystin dependent protein
A3X975	+	2.131	2.465	MED193_08513	Uncharacterized protein
A3X442	+	1.805	2.460	MED193_16719	50S ribosomal protein L30
A3X8I4	+	2.035	2.456	MED193_05734	Sulfur oxidation B protein
A3X3R3	+	2.184	2.454	MED193_17359	Metallo-phosphoesterase, PlcP
A3XD38	+	3.501	2.442	MED193_09675	Universal stress family protein
A3XA05	+	3.917	2.430	MED193_01295	Na(+)-translocating NADH-quinone reductase subunit C (Na(+)-NQR subunit C) (Na(+)-translocating NQR subunit C) (EC 7.2.1.1) (NQR complex subunit C) (NQR-1 subunit C)
A3X4D9	+	2.630	2.428	MED193_21149	Acetolactate synthase (EC 2.2.1.6)
A3XFK5	+	3.456	2.423	MED193_11424	Spermidine/putrescine ABC transporter,spermidine/putrescine-binding protein
A3X7K4	+	4.439	2.422	MED193_07384	Uncharacterized protein
A3XFE1	+	2.391	2.414	MED193_21451	Peptide/nickel/opine uptake family ABC transporter, periplasmic substrate-binding protein
A3X756	+	3.890	2.403	MED193_14157	UDP-glucose 4-epimerase
A3XFZ3	+	1.342	2.379	MED193_10121	Iron-sulfur cluster-binding protein
A3X687	+	1.188	2.368	MED193_15757	Creatinase
A3XC00	+	1.952	2.336	MED193_03512	Glycerol-3-phosphate regulon repressor
A3XD10	+	2.723	2.325	MED193_09780	Cold shock family protein

A3XBU0	+	3.067	2.302	MED193_03812	Universal stress protein family protein
A3X9K3	+	4.127	2.300	MED193_07883	Glycerophosphoryl diester phosphodiesterase, putative
A3XF96	+	2.099	2.263	MED193_21631	Uncharacterized protein
A3X6I0	+	1.658	2.262	MED193_15312	Translation initiation factor IF-1
A3X889	+	1.960	2.250	MED193_06209	Thioesterase family protein
A3X9X3	+	1.454	2.228	MED193_01450	Uncharacterized protein
A3X636	+	4.211	2.227	MED193_16027	2,4-dienoyl-CoA reductase
A3X7R6	+	1.155	2.226	MED193_07094	Acetyl-coenzyme A synthetase
A3X8H1	+	1.754	2.223	MED193_05804	Uncharacterized protein
A3XFY8	+	2.984	2.220	MED193_10146	Chloramphenicol acetyltransferase, putative
A3XFP8	+	3.624	2.218	MED193_12017	Pyruvate kinase (EC 2.7.1.40)
A3XBU3	+	2.621	2.215	MED193_03792	L-fuculose phosphate aldolase
A3XA06	+	1.652	2.212	MED193_01300	Na(+)-translocating NADH-quinone reductase subunit B (Na(+)-NQR subunit B) (Na(+)-translocating NQR subunit B) (EC 7.2.1.1) (NQR complex subunit B) (NQR-1 subunit B)
A3XFV8	+	1.570	2.208	MED193_11702	Oxidoreductase, FMN-binding/pyridine nucleotide-disulfideoxidoreductase
A3XE23	+	0.871	2.207	MED193_00315	Uncharacterized protein
A3XA89	+	2.770	2.207	MED193_00880	Fumarylacetoacetate hydrolase family protein
A3XG05	+	2.344	2.179	MED193_10041	Bacterial extracellular solute-binding protein, family 7
A3X337	+	0.910	2.175	MED193_18484	TRAP transporter solute receptor, TAXI family protein
A3X9W9	+	1.338	2.156	MED193_01485	NG,NG-dimethylarginine dimethylaminohydrolase, putative
A3X9J0	+	1.547	2.142	MED193_07938	Oligopeptide/dipeptide ABC transporter, periplasmic substrate-binding protein
A3XF23	+	1.118	2.130	MED193_02975	Sensor histidine kinase/response regulator
A3X433	+	1.711	2.130	MED193_16764	50S ribosomal protein L17
A3X460	+	1.677	2.122	MED193_16614	50S ribosomal protein L23
A3X839	+	1.064	2.122	MED193_06459	ABC transporter, ATP-binding protein
A3X6M0	+	2.092	2.119	MED193_15087	3-methyl-2-oxobutanoate hydroxymethyltransferase (EC 2.1.2.11) (Ketopantoate hydroxymethyltransferase) (KPHMT)
A3XDF9	+	1.535	2.052	MED193_13313	ATP-dependent Clp protease proteolytic subunit (EC 3.4.21.92) (Endopeptidase Clp)
A3X669	+	1.673	2.049	MED193_15852	Type I secretion system ATPase
A3X6L5	+	2.623	2.043	MED193_15112	Cytochrome c family protein
A3XFS4	+	1.938	2.039	MED193_11912	30S ribosomal protein S21
A3X4N1	+	2.818	2.037	MED193_20704	Uncharacterized protein

A3X729	+	2.855	2.035	MED193_14297	Adenine deaminase (Adenase) (Adenine aminase) (EC 3.5.4.2)
A3XBU1	+	2.770	2.027	MED193_03797	Methylthioribose-1-phosphate isomerase (M1Pi) (MTR-1-P isomerase) (EC 5.3.1.23) (S-methyl-5-thioribose-1-phosphate isomerase)
A3XCX9	+	1.577	2.023	MED193_09975	Bifunctional uridylyltransferase/uridylyl-removing enzyme (UTase/UR) (Bifunctional [protein-PII] modification enzyme) (Bifunctional nitrogen sensor protein) [Includes: [Protein-PII] uridylyltransferase (PII uridylyltransferase) (UTase) (EC 2.7.7.59); [Protein-PII]-UMP uridylyl-removing enzyme (UR) (EC 3.1.4.-)]
A3X8B3	+	1.554	2.017	MED193_06099	Uncharacterized protein
A3XAM0	+	1.270	2.012	MED193_04871	DNA-binding response regulator CtrA
A3X579	+	2.425	2.002	MED193_19724	Uncharacterized protein
A3X3J2	+	2.424	1.989	MED193_17714	Oligopeptide ABC transporter, periplasmic oligopeptide-binding protein
A3XFL3	+	1.488	1.977	MED193_11409	Probable spermidine/putrescine transport system permease, component of ATP-transporter system
A3X8E8	+	3.542	1.975	MED193_05924	Thioesterase family protein
A3XF07	+	3.199	1.963	MED193_03045	Aminomethyl transferase family protein
A3X802	+	1.138	1.962	MED193_06639	Sulfite reductase, putative
A3X7N3	+	2.495	1.956	MED193_07244	D-beta-hydroxybutyrate dehydrogenase
A3XF82	+	2.270	1.937	MED193_21711	Propionyl-CoA carboxylase, beta subunit
A3XBR1	+	2.203	1.926	MED193_03947	Oxidoreductase, zinc-binding dehydrogenase family protein
A3X6X3	+	1.116	1.924	MED193_14577	Inositol monophosphatase family protein
A3X4U0	+	4.155	1.909	MED193_20389	Uncharacterized protein
A3XDS4	+	3.323	1.879	MED193_12748	Glutamate synthase family protein
A3XFE5	+	1.921	1.870	MED193_21421	Uncharacterized protein
A3X619	+	1.443	1.851	MED193_16092	50S ribosomal protein L19
A3XBW3	+	1.905	1.844	MED193_03697	Cyclic pyranopterin monophosphate synthase (EC 4.6.1.17) (Molybdenum cofactor biosynthesis protein C)
A3XEN2	+	1.526	1.830	MED193_12663	Uncharacterized protein
A3X444	+	1.394	1.825	MED193_16709	50S ribosomal protein L18
A3X8M4	+	1.836	1.804	MED193_05544	UPF0335 protein MED193_05544
A3XBR4	+	3.369	1.802	MED193_03927	Elongation factor Ts (EF-Ts)
A3X3Q2	+	3.324	1.798	MED193_17409	Putative sulfatase
A3XB41	+	1.970	1.769	MED193_22111	Polyhydroxyalkanoate depolymerase, intracellular
A3X6C8	+	1.526	1.740	MED193_15547	Feruloyl-CoA synthase
A3XCK6	+	2.013	1.728	MED193_10693	Uncharacterized protein

A3XDK7	+	2.104	1.726	MED193_13098	Glycosyl transferase, family 25
A3X6W8	+	3.067	1.721	MED193_14597	Enoyl-CoA hydratase/isomerase family protein
A3X496	+	3.427	1.707	MED193_16454	Isobutyryl-CoA dehydrogenase
A3X6P4	+	2.382	1.705	MED193_14957	TRAP dicarboxylate transporter, DctP subunit
A3X8M9	+	1.631	1.701	MED193_05519	N-carbamoyl-L-amino acid amidohydrolase
A3X6K8	+	1.543	1.701	MED193_15177	UPF0246 protein MED193_15177
A3X3J1	+	1.916	1.699	MED193_17719	ATP-binding component of a ABC transport system (Oligopeptide)
A3XBD1	+	1.713	1.698	MED193_22681	Cytochrome P450 family protein
A3XFG2	+	2.209	1.690	MED193_11684	Uncharacterized protein
A3XFG1	+	3.035	1.660	MED193_11679	Carboxyl-terminal protease family protein
A3X7T2	+	1.599	1.651	MED193_06994	NADH dehydrogenase subunit I (EC 1.6.5.3)
A3X4Q9	+	2.680	1.626	MED193_20554	Acetylornithine aminotransferase (ACOAT) (EC 2.6.1.11)
A3X7D0	+	3.653	1.623	MED193_13797	Shikimate dehydrogenase (NADP(+)) (SDH) (EC 1.1.1.25)
A3XCN9	+	4.616	1.621	MED193_10523	Citrate lyase, beta subunit
A3XCY5	+	2.529	1.620	MED193_09900	Molybdopterin biosynthesis protein MoeB, putative
A3X891	+	2.629	1.613	MED193_06194	Uncharacterized protein
A3XBQ7	+	2.035	1.598	MED193_03962	Oxidoreductase, short chain dehydrogenase/reductase family protein
A3XCI9	+	2.711	1.592	MED193_10763	Molybdenum cofactor guanylyltransferase (MoCo guanylyltransferase) (EC 2.7.7.77) (GTP:molybdopterin guanylyltransferase) (Mo-MPT guanylyltransferase) (Molybdopterin guanylyltransferase) (Molybdopterin-guanine dinucleotide synthase) (MGD synthase)
A3X5U5	+	2.005	1.590	MED193_18619	Uncharacterized protein
A3XG06	+	5.989	1.585	MED193_10046	Gamma-glutamylisopropylamide synthetase, putative
A3X709	+	2.386	1.575	MED193_14382	Branched-chain-amino-acid aminotransferase (BCAT) (EC 2.6.1.42)
A3X997	+	1.975	1.570	MED193_08403	Pseudouridine synthase (EC 5.4.99.-)
A3X886	+	2.354	1.542	MED193_06239	Lipoprotein-releasing system ATP-binding protein LolD (EC 3.6.3.-)
A3X497	+	2.368	1.522	MED193_16429	Ribonuclease 3 (EC 3.1.26.3) (Ribonuclease III) (RNase III)
A3XA25	+	3.549	1.494	MED193_01205	Glycosyl transferase, group 1
A3X414	+	3.552	1.478	MED193_16849	Sensor histidine kinase
A3X8H4	+	2.834	1.462	MED193_05789	Uncharacterized protein
A3XC90	+	3.247	1.461	MED193_11233	Universal stress protein family protein
A3XB20	+	3.767	1.451	MED193_22191	Uncharacterized protein

Appendix 3.4 Significantly upregulated proteins (p-value <0.05) in the cellular proteome of P-deplete ΔphoB cultures in comparison to MED193. Colours represent COGs: yellow; metabolism, blue; cellular processes and signalling, green; information storage and processing, no colour; poorly characterised.

Protein ID	*p-value <0.05*	*-log$_{10}$ (p-value)*	*Log$_2$ (fold change)*	*Locus tag*	*Uniprot annotation*
A3X3N5	+	4.344	7.171	MED193_17504	Putative Hemin receptor protein HmuR
A3X8S2	+	4.832	7.114	MED193_07678	Uncharacterized protein
A3XB54	+	5.053	6.827	MED193_22031	Outer membrane protein
A3X9H4	+	5.455	5.751	MED193_08013	TonB dependent-iron siderophore receptor
A3X3N2	+	4.430	4.318	MED193_17509	Uncharacterized protein
A3X9G8	+	2.577	4.020	MED193_08033	Putative ABC transporter, periplasmic Fe+3 siderophore binding protein
A3X8Z9	+	2.301	3.734	MED193_08893	Sulfate transporter family protein
A3XCN8	+	2.592	3.571	MED193_10518	NnrU family protein
A3X786	+	3.666	3.533	MED193_14027	Uncharacterized protein
A3X3N7	+	1.843	3.530	MED193_17494	Putative hemin binding periplasmic transmembrane protein
A3X4L3	+	2.795	3.320	MED193_20779	Preprotein translocase, SecG subunit
A3X7U0	+	3.854	3.238	MED193_06959	NADH-quinone oxidoreductase subunit N (EC 1.6.5.11) (NADH dehydrogenase I subunit N) (NDH-1 subunit N)
A3X3E0	+	3.172	3.206	MED193_17969	N-(5'-phosphoribosyl)anthranilate isomerase (PRAI) (EC 5.3.1.24)
A3XDR6	+	4.572	3.145	MED193_12793	Ferric iron ABC transporter, periplasmic ferric iron-binding protein
A3X6N6	+	3.056	3.047	MED193_15017	Heavy metal-(Cd/Co/Hg/Pb/Zn)-translocating P-type ATPase:Heavy metal translocating P-type ATPase
A3X752	+	3.081	3.027	MED193_14187	Ribosome hibernation promoting factor (HPF)
A3XAV2	+	1.897	3.003	MED193_04451	Heme A synthase (HAS) (EC 1.3.-.-) (Cytochrome aa3-controlling protein)
A3X4R1	+	0.987	2.987	MED193_20539	Uncharacterized protein
A3XFQ3	+	1.696	2.954	MED193_11987	Putative adenylate/guanylate cyclase transmembrane protein
A3X3N4	+	1.584	2.856	MED193_17499	Hemin degrading factor
A3X544	+	4.177	2.699	MED193_19859	Methyltransferase
A3X923	+	1.294	2.652	MED193_08768	Uncharacterized protein
A3X586	+	0.869	2.647	MED193_19659	Uncharacterized protein
A3X8V0	+	2.830	2.629	MED193_07543	FMN-dependent alpha-hydroxy acid dehydrogenase family protein
A3X775	+	1.103	2.623	MED193_14067	Ribosome maturation factor RimP
A3X8X8	+	4.558	2.612	MED193_08988	3-oxoadipate CoA-succinyl transferase, alpha subunit
A3XB89	+	1.589	2.499	MED193_21866	Amidase (EC 3.5.1.4)

A3X4Z0	+	5.326	2.473	MED193_20139	Ribose-phosphate pyrophosphokinase (RPPK) (EC 2.7.6.1) (5-phospho-D-ribosyl alpha-1-diphosphate) (Phosphoribosyl diphosphate synthase) (Phosphoribosyl pyrophosphate synthase) (P-Rib-PP synthase) (PRPP synthase) (PRPPase)
A3XA42	+	3.761	2.445	MED193_01125	Acyl-CoA synthase (EC 2.3.1.86)
A3XAM3	+	2.536	2.442	MED193_04861	ATP-dependent DNA helicase RecG
A3XB39	+	1.105	2.439	MED193_22101	Hydrolase, alpha/beta fold family protein
A3XB53	+	3.007	2.398	MED193_22036	Putative TonB protein
A3XCE0	+	3.517	2.388	MED193_10983	Molybdopterin converting factor, subunit 1
A3X590	+	1.325	2.295	MED193_19634	Uncharacterized protein
A3X4V3	+	1.296	2.234	MED193_20329	Uncharacterized protein
A3XAE8	+	1.536	2.226	MED193_05226	Transporter, AcrB/AcrD/AcrF family protein
A3X8L5	+	1.482	2.143	MED193_05574	Uncharacterized protein
A3XBN1	+	1.046	2.072	MED193_04097	Transcriptional regulator, AraC family protein
A3XCQ9	+	1.646	2.032	MED193_10408	Uncharacterized protein
A3XBF2	+	3.383	1.994	MED193_22581	Agmatinase
A3X591	+	2.913	1.985	MED193_19639	Uncharacterized protein
A3X4D1	+	2.180	1.983	MED193_21199	Uncharacterized protein
A3X7N6	+	1.777	1.964	MED193_07234	Isoprenylcysteine carboxyl methyltransferase family protein
A3XEX2	+	2.007	1.950	MED193_12208	Uncharacterized protein
A3X7X8	+	4.880	1.910	MED193_06759	Orotate phosphoribosyltransferase (OPRT) (OPRTase) (EC 2.4.2.10)
A3XBM2	+	2.178	1.883	MED193_22221	Uncharacterized protein
A3XAX9	+	2.705	1.864	MED193_04321	Iron-sulfur cluster assembly transcription factor IscR, putative
A3XAX2	+	1.172	1.843	MED193_04356	Uncharacterized protein
A3XBZ3	+	2.899	1.802	MED193_03547	Phosphopantetheine adenylyltransferase (EC 2.7.7.3) (Dephospho-CoA pyrophosphorylase) (Pantetheine-phosphate adenylyltransferase) (PPAT)
A3X904	+	2.058	1.770	MED193_08868	Uncharacterized protein
A3X8X9	+	4.248	1.705	MED193_08993	3-oxoadipate CoA-transferase, beta subunit
A3X8V3	+	3.314	1.700	MED193_09113	Formate--tetrahydrofolate ligase (EC 6.3.4.3) (Formyltetrahydrofolate synthetase) (FHS) (FTHFS)
A3X6I8	+	1.842	1.670	MED193_15262	ABC transporter, ATP-binding protein
A3XD94	+	2.473	1.664	MED193_09370	Glycine cleavage system H protein
A3XAU5	+	3.296	1.646	MED193_04491	D-beta-hydroxybutyrate dehydrogenase
A3X4N3	+	2.386	1.635	MED193_20684	Uncharacterized protein
A3XAF9	+	2.607	1.608	MED193_05171	Protein-export membrane protein SecF
A3XBF3	+	2.781	1.576	MED193_22586	Agmatinase

A3X3D5	+	2.454	1.521	MED193_17999	Peptidyl-tRNA hydrolase (PTH) (EC 3.1.1.29)
A3X983	+	3.158	1.458	MED193_08468	Riboflavin synthase subunit alpha (EC 2.5.1.9)
A3XC89	+	4.330	1.441	MED193_11273	Prephenate dehydratase (EC 4.2.1.51)
A3X8V6	+	3.701	1.436	MED193_09108	Bifunctional protein FolD [Includes: Methenyltetrahydrofolate cyclohydrolase (EC 3.5.4.9); Methylenetetrahydrofolate dehydrogenase (EC 1.5.1.5)]

Appendix 3.5 Significantly upregulated proteins (p-value <0.05) in the exoproteome of P-deplete MED193 cultures in comparison to ΔphoB. Colours represent COGs: yellow: metabolism, blue: cellular processes and signalling, green: information storage and processing, no colour: poorly characterised.

Protein ID	*p-value <0.05*	*-log$_{10}$ (p-value)*	*Log$_2$ (fold change)*	*Locus tag*	*Uniprot annotation*
A3XFY2	+	6.037	13.308	MED193_10161	Phosphonate ABC transporter, periplasmic phosphonate-binding protein
A3XBZ9	+	5.245	12.185	MED193_03507	Iron-binding periplasmic protein
A3X9P6	+	3.235	8.429	MED193_01855	Putative periplasmic solute-binding protein
A3XD38	+	5.986	7.984	MED193_09675	Universal stress family protein
A3X6C4	+	4.946	7.949	MED193_15572	Universal stress protein family protein
A3XC90	+	5.574	7.945	MED193_11233	Universal stress protein family protein
A3XBP3	+	3.571	7.782	MED193_04042	Phosphate-specific transport system accessory protein PhoU
A3X6J7	+	3.332	7.762	MED193_15212	ATPase, MoxR family protein
A3XCK7	+	4.001	7.624	MED193_10648	Thiol:disulfide interchange protein, putative
A3X755	+	3.873	7.527	MED193_14152	UDP-glucose pyrophosphate
A3X6T7	+	3.549	7.368	MED193_14742	Acetyl-CoA C-acetyltransferase
A3X9Z4	+	5.468	7.331	MED193_01365	TRAP dicarboxylate transporter-DctP subunit
A3X647	+	3.562	7.247	MED193_15942	50S ribosomal protein L11
A3X3K4	+	4.144	7.245	MED193_17649	Alkylphosphonate utilization protein PhnM
A3XCK2	+	3.466	7.181	MED193_10673	Acetoacetyl-CoA reductase
A3X736	+	3.029	7.177	MED193_14287	DNA-binding protein HU
A3X6V3	+	3.251	7.154	MED193_14672	Putative ATP-dependent protease La, LON
A3XFR8	+	2.939	7.143	MED193_11927	Polyphosphate kinase, putative
A3X8H3	+	3.670	6.917	MED193_05784	Uncharacterized protein
A3X443	+	3.493	6.905	MED193_16704	50S ribosomal protein L6
A3X479	+	2.874	6.904	MED193_16534	Electron transfer flavoprotein, alpha subunit

A3X769	+	3.612	6.894	MED193_14082	Translation initiation factor IF-2
A3X384	+	3.329	6.869	MED193_18254	UshA protein
A3X4R1	+	3.996	6.834	MED193_20539	Uncharacterized protein
A3XCL1	+	3.320	6.765	MED193_10668	Acetyl-CoA acetyltransferase (EC 2.3.1.9)
A3X4Q9	+	2.897	6.728	MED193_20554	Acetylornithine aminotransferase (ACOAT) (EC 2.6.1.11)
A3XFS0	+	3.491	6.606	MED193_11892	Uncharacterized protein
A3X441	+	4.177	6.601	MED193_16714	30S ribosomal protein S5
A3XBX6	+	4.761	6.577	MED193_03632	Glutamate racemase (EC 5.1.1.3)
A3XBP1	+	4.232	6.545	MED193_04047	Phosphate import ATP-binding protein PstB (EC 7.3.2.1) (ABC phosphate transporter) (Phosphate-transporting ATPase)
A3XCP6	+	3.150	6.531	MED193_10473	Succinate dehydrogenase iron-sulfur subunit (EC 1.3.5.1)
A3XCX0	+	2.472	6.519	MED193_09145	Cell division coordinator CpoB
A3X9A5	+	3.360	6.493	MED193_08358	Helicase, putative
A3XBB1	+	3.568	6.491	MED193_22786	Uncharacterized protein
A3X476	+	2.845	6.476	MED193_16539	Electron transfer flavoprotein, beta subunit
A3XFQ1	+	2.645	6.383	MED193_12007	50S ribosomal protein L35
A3X442	+	3.169	6.356	MED193_16719	50S ribosomal protein L30
A3XA57	+	4.917	6.247	MED193_01050	Uncharacterized protein
A3XAK2	+	2.404	6.247	MED193_04966	Oligopeptide/dipeptide ABC transporter, periplasmic substrate-binding protein
A3X8C6	+	2.918	6.212	MED193_06029	Uracil phosphoribosyltransferase (EC 2.4.2.9) (UMP pyrophosphorylase) (UPRTase)
A3X435	+	4.237	6.148	MED193_16754	30S ribosomal protein S11
A3X8T4	+	2.260	6.123	MED193_07618	Uncharacterized protein
A3XFK5	+	4.254	6.055	MED193_11424	Spermidine/putrescine ABC transporter,spermidine/putrescine-binding protein
A3XE74	+	3.583	6.003	MED193_00045	TRAP dicarboxylate transporter, DctP subunit
A3XBP0	+	5.404	5.972	MED193_04062	Phosphate ABC transporter, periplasmic phosphate-binding protein
A3X815	+	4.898	5.964	MED193_06579	Glycerophosphoryl diester phosphodiesterase
A3X388	+	3.349	5.958	MED193_18239	Putative binding domain protein
A3XF83	+	4.532	5.948	MED193_21716	Uncharacterized protein
A3XBD4	+	2.793	5.844	MED193_22671	Nucleoside diphosphate kinase (NDK) (NDP kinase) (EC 2.7.4.6) (Nucleoside-2-P kinase)
A3X464	+	3.446	5.841	MED193_16599	30S ribosomal protein S10
A3XBH6	+	3.091	5.741	MED193_22461	Integration host factor subunit alpha (IHF-alpha)

A3X3N2	+	2.075	5.686	MED193_17509	Uncharacterized protein
A3XFS4	+	2.843	5.667	MED193_11912	30S ribosomal protein S21
A3X902	+	3.436	5.661	MED193_08883	Uncharacterized protein
A3XCC0	+	3.574	5.646	MED193_11123	Porphobilinogen deaminase (PBG) (EC 2.5.1.61) (Hydroxymethylbilane synthase) (HMBS) (Pre-uroporphyrinogen synthase)
A3XAJ4	+	4.263	5.627	MED193_05001	Single-stranded DNA-binding protein (SSB)
A3X7B2	+	3.223	5.597	MED193_13887	Peptide methionine sulfoxide reductase MsrA (Protein-methionine-S-oxide reductase) (EC 1.8.4.11) (Peptide-methionine (S)-S-oxide reductase) (Peptide Met(O) reductase)
A3XAI4	+	4.126	5.594	MED193_05036	Nitrogen regulatory protein P-II
A3XFP1	+	2.805	5.590	MED193_12062	Acetyl-coenzyme A carboxylase carboxyl transferase subunit alpha (ACCase subunit alpha) (Acetyl-CoA carboxylase carboxyltransferase subunit alpha) (EC 2.1.3.15)
A3X3D4	+	3.322	5.554	MED193_18009	50S ribosomal protein L25 (General stress protein CTC)
A3X447	+	3.745	5.523	MED193_16689	50S ribosomal protein L5
A3XDK0	+	5.894	5.509	MED193_13113	Thiol-specific antioxidant protein
A3X7J7	+	2.792	5.496	MED193_07414	Cell division protein FtsZ
A3XFY3	+	4.782	5.485	MED193_10166	Phosphonates import ATP-binding protein PhnC (EC 7.3.2.2)
A3X8I5	+	3.231	5.473	MED193_05739	SoxAX cytochrome complex subunit A (EC 2.8.5.2) (Protein SoxA) (Sulfur oxidizing protein A) (Thiosulfate-oxidizing multienzyme system protein SoxA)
A3X413	+	3.227	5.460	MED193_16864	50S ribosomal protein L34
A3X6W7	+	3.868	5.427	MED193_14592	20-beta-hydroxysteroid dehydrogenase, putative
A3XA60	+	3.224	5.419	MED193_01015	Probable ClpA/B-type chaperone
A3X3P3	+	2.809	5.414	MED193_17454	Uncharacterized protein
A3X937	+	2.739	5.411	MED193_08703	Caspase-1, p20
A3XAA0	+	3.881	5.380	MED193_00825	Glyceraldehyde-3-phosphate dehydrogenase (EC 1.2.1.-)
A3X450	+	3.110	5.374	MED193_16669	30S ribosomal protein S17
A3X4D9	+	3.454	5.337	MED193_21149	Acetolactate synthase (EC 2.2.1.6)
A3X4L2	+	2.982	5.316	MED193_20799	Adenylosuccinate synthetase (AMPSase) (AdSS) (EC 6.3.4.4) (IMP--aspartate ligase)
A3X3N7	+	3.338	5.312	MED193_17494	Putative hemin binding periplasmic transmembrane protein
A3X7Z6	+	2.059	5.303	MED193_06674	Carbon monoxide dehydrogenase, large subunit
A3X4T5	+	3.162	5.303	MED193_20429	Methylmalonyl-CoA epimerase

A3X3E4	+	2.929	5.276	MED193_17959	Integration host factor subunit beta (IHF-beta)
A3X7Z8	+	2.706	5.266	MED193_06664	Translation initiation factor IF-3
A3X768	+	2.936	5.255	MED193_14122	Chaperone protein DnaJ
A3XFU7	+	3.827	5.252	MED193_11787	NADH-ubiquinone oxidoreductase family protein
A3XCG1	+	5.223	5.219	MED193_10908	Uncharacterized protein
A3X8D1	+	2.757	5.187	MED193_06009	AMP-binding protein
A3X7C0	+	3.374	5.160	MED193_13837	Chromosome partitioning protein parB
A3X4R0	+	2.640	5.157	MED193_20559	Ornithine carbamoyltransferase (OTCase) (EC 2.1.3.3)
A3XA99	+	3.677	5.148	MED193_00820	Transcriptional regulator/arsenate reductase
A3X708	+	2.794	5.108	MED193_14422	Chorismate synthase (CS) (EC 4.2.3.5) (5-enolpyruvylshikimate-3-phosphate phospholyase)
A3XBY3	+	5.212	5.104	MED193_03587	Uncharacterized protein
A3XFC0	+	2.446	5.102	MED193_21546	50S ribosomal protein L33
A3X6X0	+	3.734	5.087	MED193_14607	Glutathione S-transferase family protein
A3X649	+	3.249	5.077	MED193_15952	50S ribosomal protein L10
A3X6F2	+	2.990	5.066	MED193_15437	2-dehydro-3-deoxyphosphogluconate
A3X5M1	+	3.843	5.029	MED193_18989	Uncharacterized protein
A3XB36	+	3.099	5.018	MED193_22116	Poly(3-hydroxyalkanoate) polymerase
A3X4W5	+	2.401	5.017	MED193_20284	Adenylyl-sulfate kinase (EC 2.7.1.25) (APS kinase) (ATP adenosine-5'-phosphosulfate 3'-phosphotransferase) (Adenosine-5'-phosphosulfate kinase)
A3XA72	+	2.709	5.006	MED193_00965	Uncharacterized protein
A3X337	+	2.700	4.981	MED193_18484	TRAP transporter solute receptor, TAXI family protein
A3X8D7	+	2.029	4.981	MED193_05969	Fatty oxidation complex, alpha subunit
A3XBD2	+	3.548	4.971	MED193_22686	DNA-binding response regulator, LuxR family protein
A3X420	+	4.683	4.945	MED193_16824	Glutamate/glutamine/aspartate/asparagine ABC transporter, ATP-binding protein
A3X5J5	+	3.957	4.899	MED193_19124	2-hydroxyacid dehydrogenase (EC 1.1.1.272)
A3X8E2	+	4.812	4.888	MED193_05939	Acyl-CoA dehydrogenase family protein
A3X3K7	+	4.779	4.845	MED193_17644	Uncharacterized protein
A3XE52	+	3.845	4.837	MED193_00125	Dioxygenase
A3X5W4	+	2.213	4.824	MED193_16367	Uncharacterized protein
A3X8I0	+	2.121	4.823	MED193_05749	Sulfur oxidation protein SoxY

A3XF74	+	3.456	4.806	MED193_02710	Phosphoribosylformylglycinamidine synthase subunit PurS (FGAM synthase) (EC 6.3.5.3) (Formylglycinamide ribonucleotide amidotransferase subunit III) (FGAR amidotransferase III) (FGAR-AT III) (Phosphoribosylformylglycinamidine synthase subunit III)
A3X7D0	+	2.908	4.802	MED193_13797	Shikimate dehydrogenase (NADP(+)) (SDH) (EC 1.1.1.25)
A3X8A1	+	3.797	4.787	MED193_06154	Aminotransferase (EC 2.6.1.-)
A3XB74	+	2.707	4.778	MED193_21936	Putative copper resistance (CopC-like)
A3X639	+	3.480	4.770	MED193_15997	30S ribosomal protein S12
A3X6I2	+	3.028	4.758	MED193_15277	Uncharacterized protein
A3XA00	+	2.620	4.744	MED193_01335	CBS domain protein
A3XC77	+	4.559	4.720	MED193_03127	2',3'-cyclic nucleotide 2'-phosphodiesterase/3'-nucleotidase bifunctional periplasmic protein (EC 3.1.4.16)
A3XDT0	+	5.175	4.711	MED193_00745	Probable 1,4-butanediol diacrylate esterase
A3XF67	+	2.467	4.697	MED193_02725	C4-dicarboxylate transport transcriptional regulatory protein DctD
A3X8Z1	+	2.950	4.693	MED193_08933	Threonine synthase (EC 4.2.3.1)
A3XFP4	+	2.283	4.688	MED193_12037	Uncharacterized protein
A3X3F7	+	4.661	4.680	MED193_17894	Hemolysin, putative
A3X3D8	+	1.988	4.674	MED193_17979	Tryptophan synthase beta chain (EC 4.2.1.20)
A3X4S1	+	4.266	4.664	MED193_20489	Phosphomannomutase/phosphoglucomutase
A3X8I3	+	3.425	4.650	MED193_05744	Sulfur oxidation Z protein
A3X926	+	4.047	4.649	MED193_08748	Carbamoyl-phosphate synthase small chain (EC 6.3.5.5) (Carbamoyl-phosphate synthetase glutamine chain)
A3X9J4	+	4.563	4.645	MED193_07903	SN-glycerol-3-phophate ABC transporter, periplasmic SN-glycerol-3-phosphate-binding protein
A3XB84	+	2.840	4.608	MED193_21871	Propionate--CoA ligase
A3X5V1	+	1.702	4.598	MED193_18599	Thymidylate kinase (EC 2.7.4.9) (dTMP kinase)
A3X4Z1	+	3.788	4.585	MED193_20144	2-hydroxychromene-2-carboxylate isomerase (EC 5.99.1.4)
A3XAP4	+	2.420	4.564	MED193_04736	30S ribosomal protein S9
A3XC66	+	3.059	4.559	MED193_03167	30S ribosomal protein S18
A3X429	+	2.075	4.557	MED193_16774	Phospho-2-dehydro-3-deoxyheptonate aldolase (EC 2.5.1.54)
A3X8H4	+	2.044	4.552	MED193_05789	Uncharacterized protein
A3X458	+	4.049	4.539	MED193_16644	50S ribosomal protein L16
A3X974	+	2.364	4.534	MED193_08508	Uncharacterized protein

A3X6Y3	+	1.839	4.527	MED193_14522	Uncharacterized protein
A3XDH4	+	3.654	4.525	MED193_13248	30S ribosomal protein S20
A3XBR8	+	3.418	4.475	MED193_03922	30S ribosomal protein S2
A3XF02	+	3.972	4.469	MED193_03065	Uncharacterized protein
A3XCP9	+	2.649	4.444	MED193_10458	Purine nucleoside phosphorylase DeoD-type (PNP) (EC 2.4.2.1)
A3X665	+	3.370	4.434	MED193_15882	AhpC/TSA family protein
A3X6H2	+	4.737	4.427	MED193_15352	Uncharacterized protein
A3X7L3	+	2.795	4.409	MED193_07349	DnaJ domain protein
A3X8T5	+	2.367	4.405	MED193_07623	1-(5-phosphoribosyl)-5-[(5-phosphoribosylamino)methylideneamino] imidazole-4-carboxamide isomerase (EC 5.3.1.16) (Phosphoribosylformimino-5-aminoimidazole carboxamide ribotide isomerase)
A3XA52	+	3.361	4.392	MED193_01055	Uncharacterized protein
A3XC01	+	4.170	4.372	MED193_03492	Metallo-beta-lactamase family protein
A3XE23	+	3.406	4.367	MED193_00315	Uncharacterized protein
A3X672	+	2.823	4.352	MED193_15817	Thiosulfate sulfurtransferase, putative
A3X7L6	+	4.532	4.343	MED193_07339	Uncharacterized protein
A3X791	+	2.969	4.338	MED193_14007	ErfK/YbiS/YcfS/YnhG family protein/Tat domain protein
A3XB34	+	4.209	4.337	MED193_22131	Polyhydroxyalkanoate synthesis repressor PhaR
A3X7R7	+	3.968	4.319	MED193_07054	NADH-quinone oxidoreductase subunit C (EC 1.6.5.11) (NADH dehydrogenase I subunit C) (NDH-1 subunit C)
A3XA70	+	2.781	4.315	MED193_00980	FHA domain protein, putative
A3XFL5	+	3.032	4.315	MED193_11419	Polyamine transport protein PotA
A3XBN7	+	3.504	4.304	MED193_04067	Phosphate regulon sensor histidine kinase, putative
A3XB93	+	3.860	4.299	MED193_21831	Uncharacterized protein
A3XDK9	+	2.420	4.298	MED193_13063	30S ribosomal protein S15
A3X597	+	2.643	4.288	MED193_19619	Corrinoid adenosyltransferase (EC 2.5.1.17) (Cob(II)alamin adenosyltransferase) (Cob(II)yrinic acid a,c-diamide adenosyltransferase)
A3X7S1	+	3.546	4.283	MED193_07074	Hydroxymethylglutaryl-CoA lyase (EC 4.1.3.4)
A3X973	+	2.956	4.277	MED193_08518	Uncharacterized protein
A3XAH2	+	2.886	4.268	MED193_05106	Uncharacterized protein
A3X616	+	1.981	4.256	MED193_16127	30S ribosomal protein S16
A3X4Q1	+	3.088	4.250	MED193_20599	50S ribosomal protein L28

A3X916	+	3.712	4.250	MED193_08813	Dihydropteroate synthase (DHPS) (EC 2.5.1.15) (Dihydropteroate pyrophosphorylase)
A3X3A1	+	3.498	4.245	MED193_18169	Uncharacterized protein
A3X8J5	+	4.785	4.244	MED193_05679	NADH-ubiquinone oxidoreductase (EC 1.6.5.3)
A3X7T3	+	2.677	4.201	MED193_06999	NADH-quinone oxidoreductase subunit I (EC 1.6.5.11) (NADH dehydrogenase I subunit I) (NDH-1 subunit I)
A3X9B4	+	3.342	4.200	MED193_08308	Uncharacterized protein
A3X5K9	+	4.196	4.191	MED193_19059	Uncharacterized protein
A3XDH2	+	1.969	4.167	MED193_13283	Beta-ketothiolase
A3X436	+	3.960	4.167	MED193_16739	Adenylate kinase (AK) (EC 2.7.4.3) (ATP-AMP transphosphorylase) (ATP:AMP phosphotransferase) (Adenylate monophosphate kinase)
A3XBE9	+	3.226	4.146	MED193_22606	Uncharacterized protein
A3XA65	+	1.592	4.132	MED193_01000	Uncharacterized protein
A3XBB3	+	2.991	4.131	MED193_22776	Corrinoid methyltransferase protein, putative
A3XCJ5	+	3.533	4.129	MED193_10728	Electrotransfer ubiquinone oxidoreductase family protein
A3XC84	+	3.057	4.093	MED193_11293	Sugar ABC transporter, periplasmic sugar-binding protein
A3XFQ2	+	2.951	4.080	MED193_11982	Phenylalanine--tRNA ligase alpha subunit (EC 6.1.1.20) (Phenylalanyl-tRNA synthetase alpha subunit) (PheRS)
A3X482	+	2.442	4.068	MED193_16524	3-hydroxybutyryl-CoA dehydrogenase (EC 1.1.1.157)
A3X8L5	+	5.348	4.045	MED193_05574	Uncharacterized protein
A3X613	+	3.232	4.043	MED193_16112	Ribosome maturation factor RimM
A3X6Z8	+	3.604	4.024	MED193_14467	Ubiquinol--cytochrome c reductase, cytochrome c1
A3X740	+	3.776	4.013	MED193_14257	Glutathione S-transferase family protein
A3X9U7	+	2.083	4.008	MED193_01590	Chemotaxis response regulator
A3X4F0	+	3.326	4.001	MED193_21094	Peptidase, M48 family protein
A3XDS6	+	3.613	3.996	MED193_12758	Chaperone protein ClpB
A3XA56	+	2.465	3.964	MED193_01045	Uncharacterized protein
A3XAK7	+	3.207	3.962	MED193_04951	Uridylate kinase (UK) (EC 2.7.4.22) (Uridine monophosphate kinase) (UMP kinase) (UMPK)
A3X773	+	1.734	3.938	MED193_14102	Protein translocase subunit SecA
A3X7K8	+	2.300	3.931	MED193_07369	Cobalt chelatase, pCobT subunit
A3X975	+	3.201	3.911	MED193_08513	Uncharacterized protein
A3XEM5	+	3.273	3.898	MED193_12673	Uncharacterized protein
A3X6U6	+	4.995	3.893	MED193_14692	Aminotransferase, classes I and II

A3XB37	+	1.713	3.887	MED193_22121	Phasin, PhaP
A3X7X6	+	3.220	3.870	MED193_06789	ABC transporter, ATP-binding protein
A3XAQ1	+	2.535	3.864	MED193_04721	Homoserine O-acetyltransferase (HAT) (EC 2.3.1.31) (Homoserine transacetylase) (HTA)
A3XC83	+	3.716	3.859	MED193_11288	Phosphodiesterase
A3XDV1	+	2.923	3.850	MED193_00660	Uncharacterized protein
A3XD22	+	1.860	3.846	MED193_09740	Uncharacterized conserved secreted protein
A3XDP7	+	2.419	3.838	MED193_12903	Saccharopine dehydrogenase, putative
A3X6P5	+	3.144	3.824	MED193_14962	Fumarylacetoacetate hydrolase family protein
A3X8X2	+	2.303	3.820	MED193_09003	Transglycosylase, Slt family protein
A3XFX3	+	3.837	3.815	MED193_10206	Acetyl-CoA acyltransferase/thiolase family protein
A3XDV2	+	1.856	3.795	MED193_00665	Uncharacterized protein
A3X648	+	1.967	3.792	MED193_15947	50S ribosomal protein L1
A3X752	+	2.187	3.791	MED193_14187	Ribosome hibernation promoting factor (HPF)
A3X618	+	4.169	3.788	MED193_16087	50S ribosomal protein L31
A3X826	+	2.496	3.786	MED193_06524	DNA-binding protein HU, putative
A3X438	+	5.858	3.773	MED193_16729	50S ribosomal protein L15
A3XBJ7	+	3.591	3.762	MED193_22361	Uncharacterized protein
A3XAI1	+	2.177	3.762	MED193_05061	Uncharacterized protein
A3XDS7	+	1.573	3.743	MED193_12763	Orotidine 5'-phosphate decarboxylase (EC 4.1.1.23)
A3XB31	+	5.714	3.726	MED193_22146	Glutamine synthetase family protein
A3XC32	+	3.409	3.720	MED193_03347	Phosphoglycerate kinase (EC 2.7.2.3)
A3X625	+	2.823	3.720	MED193_16072	Molybdenum cofactor biosynthesis domain protein
A3X7R8	+	2.818	3.719	MED193_07059	NADH-quinone oxidoreductase subunit B (EC 1.6.5.11) (NADH dehydrogenase I subunit B) (NDH-1 subunit B)
A3X6Z5	+	2.700	3.711	MED193_14452	Glutathione S-transferase family protein
A3X3R1	+	2.094	3.711	MED193_17364	S-adenosylmethionine-diacylglycerol 3-amino-3-carboxypropyltransferase
A3X7I9	+	3.962	3.705	MED193_07469	UDP-N-acetylglucosamine--N-acetylmuramyl-(pentapeptide) pyrophosphoryl-undecaprenol N-acetylglucosamine transferase (EC 2.4.1.227) (Undecaprenyl-PP-MurNAc-pentapeptide-UDPGlcNAc GlcNAc transferase)
A3XFD6	+	3.111	3.705	MED193_21476	Uncharacterized protein
A3X8C3	+	2.737	3.704	MED193_06054	Phosphate acetyltransferase (EC 2.3.1.8)
A3X567	+	2.901	3.700	MED193_19764	Hydrolase, NUDIX family protein

A3XC61	+	2.535	3.693	MED193_03202	3-oxoacyl-(Acyl-carrier-protein) reductase
A3X7E3	+	5.559	3.686	MED193_13752	ATP-dependent protease ATPase subunit HslU (Unfoldase HslU)
A3X4F4	+	4.539	3.672	MED193_21089	27 kDa outer membrane protein, putative
A3XA30	+	3.306	3.658	MED193_01180	Uncharacterized protein
A3XG05	+	3.166	3.653	MED193_10041	Bacterial extracellular solute-binding protein, family 7
A3X626	+	2.533	3.651	MED193_16077	Uncharacterized protein
A3XAW5	+	3.118	3.630	MED193_04391	CaiB/BaiF family protein
A3X651	+	3.001	3.628	MED193_15962	DNA-directed RNA polymerase subunit beta (RNAP subunit beta) (EC 2.7.7.6) (RNA polymerase subunit beta) (Transcriptase subunit beta)
A3XBJ8	+	1.700	3.603	MED193_22366	ATPase, AAA family protein
A3X835	+	1.814	3.601	MED193_06474	TRAP-T family transporter, DctP (Periplasmic binding) subunit
A3X4W8	+	2.020	3.600	MED193_20249	N5-carboxyaminoimidazole ribonucleotide mutase (N5-CAIR mutase) (EC 5.4.99.18) (5-(carboxyamino)imidazole ribonucleotide mutase)
A3X6A9	+	2.217	3.598	MED193_15632	3-isopropylmalate dehydrogenase (EC 1.1.1.85) (3-IPM-DH) (Beta-IPM dehydrogenase) (IMDH)
A3X4P5	+	3.234	3.596	MED193_20629	Uncharacterized protein
A3XAM7	+	1.587	3.585	MED193_04826	Enoyl-CoA hydratase (EC 4.2.1.17)
A3XBY0	+	2.758	3.585	MED193_03617	Transcriptional regulator, LysR family protein
A3X4X9	+	3.168	3.583	MED193_20209	10 kDa chaperonin (GroES protein) (Protein Cpn10)
A3XFW3	+	2.349	3.565	MED193_10246	Uncharacterized protein
A3XDT6	+	2.621	3.551	MED193_00725	Chloroacetaldehyde dehydrogenase
A3X671	+	2.886	3.550	MED193_15862	Endoribonuclease L-PSP family protein
A3XF34	+	2.885	3.546	MED193_02890	Cytosine deaminase
A3XFW9	+	2.426	3.528	MED193_10236	Uncharacterized protein
A3XBW8	+	2.806	3.521	MED193_03657	Enoyl-CoA hydratase/isomerase family protein
A3X5X6	+	2.009	3.505	MED193_16322	Methionyl-tRNA formyltransferase (EC 2.1.2.9)
A3XAS5	+	2.500	3.495	MED193_04601	Nitrogen assimilation regulatory protein NtrX
A3X7H1	+	4.314	3.468	MED193_13612	Uncharacterized protein
A3XCS1	+	3.017	3.462	MED193_10353	Universal stress family protein
A3XBV9	+	2.474	3.459	MED193_03702	Indole-3-glycerol phosphate synthase (IGPS) (EC 4.1.1.48)
A3X5X3	+	4.848	3.457	MED193_16307	Peptide deformylase (PDF) (EC 3.5.1.88) (Polypeptide deformylase)
A3X7L1	+	1.896	3.446	MED193_07359	Cobalt chelatase, CobS subunit

A3XCG2	+	2.428	3.444	MED193_10893	Dihydroorotase, multifunctional complex type
A3X6W6	+	1.989	3.444	MED193_14637	Pyridoxal phosphate homeostasis protein (PLP homeostasis protein)
A3XDA1	+	2.820	3.435	MED193_09355	2-hydroxyacid dehydrogenase
A3XFC8	+	3.901	3.434	MED193_21486	Tellurite resistance protein
A3X7R5	+	1.456	3.421	MED193_07089	Methylcrotonyl-CoA carboxylase, beta subunit
A3XA04	+	3.315	3.397	MED193_01305	Na(+)-translocating NADH-quinone reductase subunit A (Na(+)-NQR subunit A) (Na(+)-translocating NQR subunit A) (EC 7.2.1.1) (NQR complex subunit A) (NQR-1 subunit A)
A3XFH0	+	2.668	3.397	MED193_11634	Acetyl-coenzyme A carboxylase carboxyl transferase subunit beta (ACCase subunit beta) (Acetyl-CoA carboxylase carboxyltransferase subunit beta) (EC 2.1.3.15)
A3X5H3	+	0.980	3.381	MED193_19244	ATP phosphoribosyltransferase regulatory subunit
A3XAC9	+	4.434	3.381	MED193_05331	Putative pre-16S rRNA nuclease (EC 3.1.-.-)
A3X3H2	+	3.068	3.376	MED193_17814	Haloacid dehalogenase, type II
A3X640	+	2.619	3.353	MED193_16002	30S ribosomal protein S7
A3X8S5	+	2.064	3.351	MED193_07663	RNA methyltransferase, TrmH family, group 3
A3XBU3	+	1.570	3.349	MED193_03792	L-fuculose phosphate aldolase
A3X445	+	1.440	3.346	MED193_16694	30S ribosomal protein S14
A3X4U1	+	2.461	3.343	MED193_20394	Carbamoyl-phosphate synthase large chain (EC 6.3.5.5) (Carbamoyl-phosphate synthetase ammonia chain)
A3X9N9	+	3.052	3.339	MED193_01875	3',5'-cyclic adenosine monophosphate phosphodiesterase CpdA (3',5'-cyclic AMP phosphodiesterase) (cAMP phosphodiesterase) (EC 3.1.4.53)
A3X497	+	3.237	3.338	MED193_16429	Ribonuclease 3 (EC 3.1.26.3) (Ribonuclease III) (RNase III)
A3X5W9	+	3.270	3.319	MED193_16342	Ribonuclease H (RNase H) (EC 3.1.26.4)
A3XDP9	+	1.508	3.317	MED193_12863	Uncharacterized protein
A3X952	+	1.667	3.314	MED193_08628	Homoserine dehydrogenase
A3XB11	+	2.800	3.314	MED193_04161	Peptidoglycan binding protein, putative
A3XCW8	+	3.339	3.302	MED193_09135	ATP-dependent zinc metalloprotease FtsH (EC 3.4.24.-)
A3XAX3	+	2.389	3.301	MED193_04361	Alanine--tRNA ligase (EC 6.1.1.7) (Alanyl-tRNA synthetase) (AlaRS)
A3XCB3	+	3.568	3.298	MED193_11138	Coproporphyrinogen oxidase (EC 1.3.3.3)
A3XDI1	+	1.620	3.273	MED193_13238	Beta sliding clamp
A3XD16	+	1.846	3.270	MED193_09770	Thioredoxin

A3XAX9	+	1.027	3.253	MED193_04321	Iron-sulfur cluster assembly transcription factor IscR, putative
A3XDM7	+	2.270	3.247	MED193_13003	Bifunctional purine biosynthesis protein PurH [Includes: Phosphoribosylaminoimidazolecarboxamide formyltransferase (EC 2.1.2.3) (AICAR transformylase); IMP cyclohydrolase (EC 3.5.4.10) (Inosinicase) (IMP synthase) (ATIC)]
A3XBU1	+	2.333	3.244	MED193_03797	Methylthioribose-1-phosphate isomerase (M1Pi) (MTR-1-P isomerase) (EC 5.3.1.23) (S-methyl-5-thioribose-1-phosphate isomerase)
A3XF56	+	2.958	3.234	MED193_02770	Fumarate hydratase class II (Fumarase C) (EC 4.2.1.2) (Aerobic fumarase) (Iron-independent fumarase)
A3X8J3	+	2.469	3.224	MED193_05694	ATP-dependent Clp protease ATP-binding subunit ClpX
A3XBV3	+	3.052	3.221	MED193_03742	Xanthine phosphoribosyltransferase (EC 2.4.2.22) (Xanthine-guanine phosphoribosyltransferase) (XGPRT)
A3X8H5	+	2.375	3.210	MED193_05794	Acetolactate synthase, catabolic, putative
A3X4M1	+	1.235	3.188	MED193_20734	Aminotransferase, classes I and II
A3X6L5	+	2.306	3.186	MED193_15112	Cytochrome c family protein
A3X444	+	2.631	3.179	MED193_16709	50S ribosomal protein L18
A3X496	+	2.328	3.166	MED193_16454	Isobutyryl-CoA dehydrogenase
A3XA92	+	1.109	3.156	MED193_00870	5-carboxy-2-hydroxymuconate semialdehyde dehydrogenase
A3XBB2	+	3.702	3.155	MED193_22791	Uncharacterized protein (Fragment)
A3XAX2	+	1.185	3.152	MED193_04356	Uncharacterized protein
A3X4R3	+	4.151	3.135	MED193_20524	Uncharacterized protein
A3XE46	+	2.399	3.130	MED193_00190	Putative extracellular solute-binding protein
A3X8E1	+	1.682	3.119	MED193_05959	Acetyl-CoA acetyltransferase (EC 2.3.1.9)
A3XAU2	+	3.958	3.114	MED193_04506	DNA-binding protein, putative
A3XA24	+	2.864	3.110	MED193_01200	UDP-glucose 6-dehydrogenase (EC 1.1.1.22)
A3XD03	+	2.579	3.109	MED193_09840	2-isopropylmalate synthase (EC 2.3.3.13) (Alpha-IPM synthase) (Alpha-isopropylmalate synthase)
A3XCW9	+	2.085	3.108	MED193_09140	tRNA(Ile)-lysidine synthase (EC 6.3.4.19) (tRNA(Ile)-2-lysyl-cytidine synthase) (tRNA(Ile)-lysidine synthetase)
A3X756	+	1.752	3.099	MED193_14157	UDP-glucose 4-epimerase
A3XBC1	+	3.038	3.078	MED193_22746	Ribonuclease D (RNase D) (EC 3.1.13.5)
A3XFX5	+	1.459	3.077	MED193_10171	Ribulose-phosphate 3-epimerase (EC 5.1.3.1)

A3X5W6	+	2.163	3.073	MED193_16377	DNA-directed RNA polymerase subunit omega (RNAP omega subunit) (EC 2.7.7.6) (RNA polymerase omega subunit) (Transcriptase subunit omega)
A3XBA5	+	1.214	3.072	MED193_21786	DnaJ-like protein DjlA, putative
A3X6I7	+	1.367	3.071	MED193_15257	Uncharacterized protein
A3XFE2	+	2.188	3.071	MED193_21406	Acyl-CoA synthase (EC 2.3.1.86)
A3XAQ4	+	2.249	3.055	MED193_04696	Methyltransferase (EC 2.1.1.-)
A3X9J7	+	2.389	3.052	MED193_07888	sn-glycerol-3-phosphate import ATP-binding protein UgpC (EC 3.6.3.20)
A3XF82	+	3.383	3.046	MED193_21711	Propionyl-CoA carboxylase, beta subunit
A3X8B8	+	2.127	3.046	MED193_06079	Threonine--tRNA ligase (EC 6.1.1.3) (Threonyl-tRNA synthetase) (ThrRS)
A3XBP5	+	1.966	3.045	MED193_04037	Phosphate regulon transcriptional regulatory protein PhoB
A3X8W3	+	1.761	3.041	MED193_09058	Lipoprotein, putative
A3XC20	+	2.459	3.037	MED193_03407	AhpC/TSA family protein
A3X417	+	3.796	3.036	MED193_16839	Acetylglutamate kinase (EC 2.7.2.8) (N-acetyl-L-glutamate 5-phosphotransferase) (NAG kinase) (NAGK)
A3X638	+	2.537	3.032	MED193_15992	Uncharacterized protein
A3X7W5	+	2.114	3.025	MED193_06839	Oxidoreductase, short-chain dehydrogenase/reductase family protein
A3XD90	+	3.386	3.013	MED193_09395	Uncharacterized protein
A3XA46	+	3.043	3.002	MED193_01090	Uncharacterized protein
A3X716	+	1.401	2.996	MED193_14367	Histone deacetylase family protein
A3X7B5	+	1.075	2.992	MED193_13857	Ribonuclease PH (RNase PH) (EC 2.7.7.56) (tRNA nucleotidyltransferase)
A3XE22	+	2.197	2.976	MED193_00310	Replication protein a
A3XEV8	+	2.003	2.973	MED193_12288	Kinase, pfkB family protein
A3X4I5	+	1.192	2.971	MED193_20934	Putative glutathione s-transferase protein
A3X431	+	2.759	2.966	MED193_16784	ATPase, AAA family protein
A3X453	+	0.988	2.956	MED193_16664	50S ribosomal protein L29
A3XBN0	+	2.381	2.937	MED193_04117	Branched-chain amino acid ABC transporter, ATP-binding protein
A3X9A1	+	1.905	2.925	MED193_08368	Sterol carrier family protein
A3XCZ6	+	2.606	2.924	MED193_09850	Rod shape-determining protein MreB
A3X6A3	+	2.947	2.919	MED193_15697	Uncharacterized protein
A3X8A9	+	0.826	2.918	MED193_06104	ArsC family protein
A3X970	+	2.080	2.915	MED193_08543	RNA polymerase sigma factor RpoD (Sigma-70)

A3X931	+	3.224	2.915	MED193_08723	HIT family protein
A3XB88	+	1.801	2.896	MED193_21861	NAD kinase (EC 2.7.1.23)
A3XFR0	+	3.479	2.896	MED193_11977	Phenylalanine--tRNA ligase beta subunit (EC 6.1.1.20) (Phenylalanyl-tRNA synthetase beta subunit) (PheRS)
A3XEW0	+	1.340	2.891	MED193_12248	Transglycosylase, Slt family protein
A3XCL5	+	0.643	2.886	MED193_10643	Argininosuccinate lyase (ASAL) (EC 4.3.2.1) (Arginosuccinase)
A3X801	+	2.430	2.876	MED193_06659	Uncharacterized protein
A3XAJ3	+	2.715	2.875	MED193_04996	Transglycosylase SLT domain protein
A3X8R3	+	2.424	2.868	MED193_07723	Biotin synthase (EC 2.8.1.6)
A3X8T8	+	1.955	2.856	MED193_07608	Uncharacterized protein
A3XDF9	+	2.963	2.846	MED193_13313	ATP-dependent Clp protease proteolytic subunit (EC 3.4.21.92) (Endopeptidase Clp)
A3XF76	+	3.259	2.826	MED193_02685	Methionine synthase I (Fragment)
A3X8R6	+	2.598	2.823	MED193_07713	ATP-dependent dethiobiotin synthetase BioD (EC 6.3.3.3) (DTB synthetase) (DTBS) (Dethiobiotin synthase)
A3X3I9	+	3.134	2.807	MED193_17724	Uncharacterized protein
A3X3Z2	+	1.531	2.806	MED193_16969	Uncharacterized protein
A3XAY4	+	2.295	2.790	MED193_04291	FeS assembly ATPase SufC
A3X8X9	+	3.861	2.789	MED193_08993	3-oxoadipate CoA-transferase, beta subunit
A3X5A4	+	2.494	2.787	MED193_19564	Precorrin-4 C11-methyltransferase
A3X7A0	+	1.117	2.771	MED193_13927	Argininosuccinate synthase (EC 6.3.4.5) (Citrulline--aspartate ligase)
A3XFQ0	+	2.643	2.769	MED193_12027	Uncharacterized protein
A3X421	+	3.463	2.766	MED193_16829	Phosphoglycerate mutase family protein
A3X3K6	+	2.276	2.758	MED193_17639	Ribose 1,5-bisphosphate phosphokinase PhnN (EC 2.7.4.23) (Ribose 1,5-bisphosphokinase)
A3X642	+	3.993	2.757	MED193_15967	DNA-directed RNA polymerase subunit beta' (RNAP subunit beta') (EC 2.7.7.6) (RNA polymerase subunit beta') (Transcriptase subunit beta')
A3X7K3	+	2.434	2.756	MED193_07399	DNA repair protein RecN (Recombination protein N)
A3X500	+	3.430	2.739	MED193_20094	ATP synthase subunit delta (ATP synthase F(1) sector subunit delta) (F-type ATPase subunit delta) (F-ATPase subunit delta)
A3X5K3	+	2.522	2.738	MED193_19079	Isocitrate dehydrogenase [NADP] (EC 1.1.1.42) (Oxalosuccinate decarboxylase)
A3XBH9	+	1.304	2.734	MED193_22456	Transcriptional regulator, MerR family protein
A3X456	+	3.275	2.733	MED193_16634	50S ribosomal protein L22

A3X693	+	1.756	2.732	MED193_15747	Possible esterase/lipase/thioesterase
A3X490	+	1.677	2.729	MED193_16479	Phosphoenolpyruvate carboxykinase (ATP) (PCK) (PEP carboxykinase) (PEPCK) (EC 4.1.1.49)
A3XBS3	+	2.861	2.721	MED193_03887	GTPase Obg (EC 3.6.5.-) (GTP-binding protein Obg)
A3XAH5	+	1.710	2.706	MED193_05096	Adenylosuccinate lyase (ASL) (EC 4.3.2.2) (Adenylosuccinase)
A3X4L6	+	1.332	2.705	MED193_20774	CTP synthase (EC 6.3.4.2) (Cytidine 5'-triphosphate synthase) (Cytidine triphosphate synthetase) (CTP synthetase) (CTPS) (UTP--ammonia ligase)
A3XA76	+	3.228	2.703	MED193_00955	Ser/Thr protein phosphatase, putative
A3XAU9	+	1.960	2.689	MED193_04461	Thiamine-phosphate pyrophosphorylase, putative
A3X9V5	+	1.019	2.679	MED193_01555	Cystathionine gamma-synthase
A3X904	+	3.199	2.675	MED193_08868	Uncharacterized protein
A3X9A8	+	3.018	2.673	MED193_08333	Nicotinate-nucleotide--dimethylbenzimidazole phosphoribosyltransferase (NN:DBI PRT) (EC 2.4.2.21) (N(1)-alpha-phosphoribosyltransferase)
A3XCW5	+	1.425	2.673	MED193_09160	TonB domain protein, putative
A3X6Y4	+	3.032	2.665	MED193_14527	Uncharacterized protein
A3X6V2	+	1.743	2.663	MED193_14667	Thioredoxin
A3X8C1	+	3.449	2.657	MED193_06044	Cytidine deaminase (EC 3.5.4.5) (Cytidine aminohydrolase)
A3X8M8	+	0.947	2.654	MED193_05514	Dihydropyrimidinase (EC 3.5.2.2)
A3X5C8	+	3.450	2.652	MED193_19449	Phosphonate-binding periplasmic protein
A3XFL6	+	3.869	2.632	MED193_11374	Metallo-beta-lactamase family protein
A3X8A0	+	2.202	2.630	MED193_06149	DNA-binding protein, putative
A3XE06	+	3.114	2.629	MED193_00390	Uncharacterized protein
A3XAF7	+	1.497	2.622	MED193_05191	Uncharacterized protein
A3X8B0	+	1.152	2.620	MED193_06109	Cold shock family protein
A3XBZ0	+	1.647	2.616	MED193_03557	Glyceraldehyde-3-phosphate dehydrogenase, type I
A3X7C4	+	2.063	2.612	MED193_13812	Transcription termination factor Rho (EC 3.6.4.-) (ATP-dependent helicase Rho)
A3X785	+	1.392	2.611	MED193_14022	Ferrochelatase (EC 4.99.1.1) (Heme synthase) (Protoheme ferro-lyase)
A3XFQ6	+	3.455	2.610	MED193_12002	50S ribosomal protein L20
A3XFS1	+	3.243	2.597	MED193_11897	Ribonuclease T2 family protein
A3XBR9	+	1.826	2.592	MED193_03897	Gamma-glutamyl phosphate reductase (GPR) (EC 1.2.1.41) (Glutamate-5-semialdehyde dehydrogenase) (Glutamyl-gamma-semialdehyde dehydrogenase) (GSA dehydrogenase)

A3XAW9	+	2.390	2.587	MED193_04366	Protein RecA (Recombinase A)
A3X5J3	+	1.290	2.577	MED193_19134	Oxidoreductase, FAD-binding
A3XA55	+	3.381	2.571	MED193_01040	Uncharacterized protein
A3X8P5	+	2.066	2.570	MED193_05439	Acetyl-coenzyme A synthetase (AcCoA synthetase) (Acs) (EC 6.2.1.1) (Acetate--CoA ligase) (Acyl-activating enzyme)
A3X8R9	+	2.231	2.568	MED193_07703	Glycine betaine/proline ABC transporter, periplasmic substrate-binding protein
A3XFD0	+	4.026	2.567	MED193_21496	Pseudouridine synthase (EC 5.4.99.-)
A3X7S0	+	3.316	2.561	MED193_07069	Enoyl-CoA hydratase (EC 4.2.1.17)
A3X4N5	+	2.432	2.558	MED193_20664	DnaK suppressor protein
A3X9X3	+	2.778	2.552	MED193_01450	Uncharacterized protein
A3X6P9	+	1.388	2.549	MED193_14932	Transcriptional regulator, LacI family protein
A3XA98	+	1.655	2.541	MED193_00845	TRAP dicarboxylate transporter, DctP subunit
A3X8K1	+	3.317	2.534	MED193_05659	Biotin carboxylase (EC 6.3.4.14) (EC 6.4.1.2)
A3XFG2	+	2.264	2.526	MED193_11684	Uncharacterized protein
A3X8L3	+	2.748	2.514	MED193_05594	Response regulator
A3XBQ8	+	0.935	2.472	MED193_03967	Uncharacterized protein
A3XBZ8	+	1.292	2.460	MED193_03527	ErfK/YbiS/YcfS/YnhG family protein
A3XAS1	+	1.541	2.456	MED193_04611	Nitrogen regulation protein NtrC
A3XA53	+	1.531	2.443	MED193_01060	Uncharacterized protein
A3X6J5	+	2.723	2.441	MED193_15202	Uncharacterized protein
A3X4C2	+	1.209	2.428	MED193_21249	ABC transporter, periplasmic binding protein
A3X6L6	+	1.892	2.427	MED193_15117	Peptidase, T4 family protein
A3XB53	+	1.511	2.423	MED193_22036	Putative TonB protein
A3X6P3	+	1.075	2.414	MED193_15002	Glycine cleavage system T protein
A3X3F3	+	1.739	2.406	MED193_17904	S-adenosylmethionine synthase (AdoMet synthase) (EC 2.5.1.6) (MAT) (Methionine adenosyltransferase)
A3X9R2	+	1.898	2.403	MED193_01770	Uncharacterized protein
A3X790	+	1.153	2.402	MED193_14002	Lipoprotein, putative
A3X5Q6	+	2.167	2.401	MED193_18819	Uncharacterized protein
A3XG01	+	1.838	2.400	MED193_10071	Glyceraldehyde-3-phosphate dehydrogenase (EC 1.2.1.-)
A3XBG0	+	3.503	2.400	MED193_22551	Enolase (EC 4.2.1.11) (2-phospho-D-glycerate hydro-lyase) (2-phosphoglycerate dehydratase)
A3X3G9	+	2.530	2.396	MED193_17834	Enoyl-[acyl-carrier-protein] reductase [NADH] (EC 1.3.1.9)

A3XAP6	+	2.409	2.389	MED193_04746	Carboxypeptidase
A3XA41	+	2.170	2.386	MED193_01120	DNA-binding protein, putative
A3XBW5	+	2.010	2.384	MED193_03687	LexA repressor (EC 3.4.21.88)
A3X5U1	+	1.648	2.380	MED193_18639	Uncharacterized protein
A3XCS0	+	1.917	2.378	MED193_10348	Aminotransferase, class IV
A3X4P9	+	2.152	2.377	MED193_20609	Uncharacterized protein
A3XBV7	+	1.931	2.350	MED193_03717	Anthranilate synthase component II
A3XB14	+	1.458	2.347	MED193_04136	Uncharacterized protein
A3XFX4	+	3.064	2.344	MED193_10211	Enoyl-CoA hydratase/isomerase/3-hydroxyacyl-CoA dehydrogenase
A3XDM8	+	2.217	2.343	MED193_13008	Uncharacterized protein
A3X517	+	2.475	2.342	MED193_20014	Uncharacterized protein
A3XFZ7	+	1.290	2.337	MED193_10096	Formate dehydrogenase, alpha subunit, putative
A3XD37	+	3.351	2.318	MED193_09670	Uncharacterized protein
A3XFJ8	+	2.663	2.317	MED193_11494	Uncharacterized protein
A3X612	+	1.158	2.309	MED193_16152	Signal recognition particle protein (Fifty-four homolog)
A3X3H3	+	1.107	2.305	MED193_17809	Hydrolase, alpha/beta fold family protein
A3X8F0	+	0.945	2.300	MED193_05904	Dihydroorotate dehydrogenase (quinone) (EC 1.3.5.2)
A3X7Z7	+	1.490	2.292	MED193_06679	Carbon-monoxide dehydrogenase, small subunit
A3XEN0	+	1.174	2.286	MED193_12653	Uncharacterized protein
A3XBC3	+	0.903	2.282	MED193_22736	Phosphoribosylformylglycinamidine cyclo-ligase (EC 6.3.3.1) (AIR synthase) (AIRS) (Phosphoribosyl-aminoimidazole synthetase)
A3XAW2	+	2.432	2.282	MED193_04416	Glucose-6-phosphate 1-dehydrogenase (G6PD) (EC 1.1.1.49)
A3X583	+	1.953	2.266	MED193_19694	Uncharacterized protein
A3XDI2	+	1.312	2.265	MED193_13198	Transcriptional regulator, IclR family protein
A3X3X0	+	1.021	2.256	MED193_17079	TRAP dicarboxylate transporter, DctP subunit
A3X4Y6	+	0.797	2.253	MED193_20179	HAD-superfamily subfamily IIA hydrolase
A3XDL4	+	1.440	2.253	MED193_13038	Ribosome-binding factor A
A3X449	+	2.862	2.246	MED193_16684	50S ribosomal protein L24
A3XC67	+	2.660	2.241	MED193_03172	30S ribosomal protein S6
A3XC71	+	2.176	2.240	MED193_03162	50S ribosomal protein L9
A3XFB4	+	1.827	2.237	MED193_21566	Uncharacterized protein

A3XBX9	+	1.339	2.229	MED193_03612	Phosphoribosylformylglycinamidine synthase subunit PurL (FGAM synthase) (EC 6.3.5.3) (Formylglycinamide ribonucleotide amidotransferase subunit II) (FGAR amidotransferase II) (FGAR-AT II) (Glutamine amidotransferase PurL) (Phosphoribosylformylglycinamidine synthase subunit II)
A3X599	+	2.600	2.225	MED193_19584	Putative precorrin-3B C17-methyltransferase
A3X6L8	+	4.018	2.223	MED193_15127	3-ketoacyl-(Acyl-carrier-protein) reductase (EC 1.1.1.100)
A3XFV2	+	0.764	2.215	MED193_11767	Probable DSBA oxidoreductase
A3X7H6	+	2.551	2.211	MED193_07524	Iron-sulfur cluster carrier protein
A3X3E0	+	2.034	2.209	MED193_17969	N-(5'-phosphoribosyl)anthranilate isomerase (PRAI) (EC 5.3.1.24)
A3X5L9	+	1.219	2.209	MED193_18999	Uncharacterized protein
A3XAS4	+	2.715	2.208	MED193_04596	Uncharacterized protein
A3XDR5	+	2.138	2.206	MED193_12788	50S ribosomal protein L36
A3XE07	+	1.397	2.187	MED193_00395	ATPase of the AAA+ class
A3XEM6	+	1.237	2.185	MED193_12678	Uncharacterized protein
A3X6Y8	+	1.221	2.183	MED193_14497	Haloalkane dehalogenase (EC 3.8.1.5)
A3X7Q3	+	3.472	2.183	MED193_07134	Glutamine--fructose-6-phosphate aminotransferase [isomerizing] (EC 2.6.1.16) (D-fructose-6-phosphate amidotransferase) (GFAT) (Glucosamine-6-phosphate synthase) (Hexosephosphate aminotransferase) (L-glutamine--D-fructose-6-phosphate amidotransferase)
A3X6J1	+	0.825	2.178	MED193_15232	DNA polymerase I (EC 2.7.7.7)
A3XBH8	+	1.255	2.171	MED193_22451	2'-deoxycytidine 5'-triphosphate deaminase (EC 3.5.4.13)
A3XB21	+	0.950	2.168	MED193_22196	Uncharacterized protein
A3X3I1	+	1.537	2.150	MED193_17764	Mandelate racemase/muconate lactonizing enzyme family protein
A3X4T0	+	3.379	2.146	MED193_20444	Nitroreductase family protein
A3X6A0	+	0.979	2.145	MED193_15682	Ribosomal silencing factor RsfS
A3X928	+	1.466	2.144	MED193_08758	Transcriptional regulator, GntR family protein
A3XF72	+	1.492	2.140	MED193_02700	Uncharacterized protein
A3XF98	+	2.789	2.139	MED193_21641	Probable transcriptional regulatory protein MED193_21641
A3X727	+	1.566	2.137	MED193_14332	Carnitinyl-CoA dehydratase (EC 4.2.1.-)
A3XBN5	+	1.963	2.137	MED193_04077	Guanylate kinase (EC 2.7.4.8) (GMP kinase)
A3XBS6	+	3.605	2.133	MED193_03872	50S ribosomal protein L21
A3X4W6	+	1.133	2.133	MED193_20264	Heat shock protein, Hsp20 family protein
A3X6V0	+	3.182	2.129	MED193_14712	Uncharacterized protein

A3X5U9	+	3.197	2.129	MED193_18609	Lipoprotein, putative
A3X6Z6	+	2.088	2.126	MED193_14457	Ubiquinol-cytochrome c reductase iron-sulfur subunit (EC 1.10.2.2)
A3X5H0	+	1.165	2.115	MED193_19249	ATP phosphoribosyltransferase (EC 2.4.2.17)
A3X455	+	2.337	2.100	MED193_16629	30S ribosomal protein S19
A3X8B4	+	3.007	2.099	MED193_06084	Uncharacterized protein
A3X806	+	1.360	2.092	MED193_06634	Uncharacterized protein
A3X8K9	+	1.784	2.083	MED193_05604	Branched-chain amino acid ABC transporter, periplasmic substrate-binding protein
A3X6S2	+	2.268	2.064	MED193_14857	Uncharacterized protein
A3X720	+	1.301	2.059	MED193_14342	Uncharacterized protein
A3XBA7	+	0.872	2.059	MED193_21771	Methylmalonyl-CoA mutase (EC 5.4.99.2)
A3X399	+	1.991	2.055	MED193_18174	Uncharacterized protein
A3X6L3	+	2.541	2.054	MED193_15152	Penicillin-insensitive murein endopeptidase (EC 3.4.-.-)
A3X6C7	+	1.236	2.040	MED193_15542	Amidohydrolase 2
A3X463	+	3.145	2.033	MED193_16609	50S ribosomal protein L4
A3XF53	+	1.021	2.025	MED193_02805	Oxidoreductase, zinc-binding dehydrogenase family protein
A3X6R0	+	3.097	2.023	MED193_14897	Probable DctP (Periplasmic C4-dicarboxylate binding protein)
A3XAG7	+	2.305	2.012	MED193_05141	Periplasmic protein thiol:disulfide oxidoreductase, DsbE subfamily protein
A3X472	+	1.422	2.009	MED193_16569	DNA topoisomerase 4 subunit A (EC 5.99.1.3) (Topoisomerase IV subunit A)
A3XD11	+	2.520	2.004	MED193_09785	Acyl-CoA thioesterase, putative
A3X7A5	+	3.479	1.998	MED193_13902	Uncharacterized protein
A3XBW7	+	3.685	1.995	MED193_03672	Citrate synthase
A3X7E5	+	3.103	1.990	MED193_13717	Thioredoxin
A3XAU7	+	2.025	1.967	MED193_04476	Kinase, pfkB family protein
A3X3G0	+	1.806	1.964	MED193_17879	Lipoprotein, putative
A3X8G7	+	3.678	1.962	MED193_05814	Periplasmic glucan biosynthesis protein MdoG
A3XFE1	+	1.863	1.941	MED193_21451	Peptide/nickel/opine uptake family ABC transporter, periplasmic substrate-binding protein
A3X9Z5	+	1.006	1.938	MED193_01340	Regulatory protein, IclR
A3XAU5	+	3.188	1.929	MED193_04491	D-beta-hydroxybutyrate dehydrogenase
A3XCP8	+	1.534	1.912	MED193_10453	DNA-binding protein, H-NS family protein

A3X7S4	+	1.518	1.897	MED193_07044	NADH-quinone oxidoreductase subunit D (EC 1.6.5.11) (NADH dehydrogenase I subunit D) (NDH-1 subunit D)
A3X7F8	+	1.143	1.896	MED193_13637	Uncharacterized protein
A3X473	+	1.371	1.896	MED193_16549	ATP:cob(I)alamin adenosyltransferase, putative
A3X9Y1	+	1.732	1.885	MED193_01415	ParA family ATPase
A3XC36	+	1.537	1.874	MED193_03337	Pyruvate dehydrogenase E1 component subunit alpha (EC 1.2.4.1)
A3XFQ4	+	1.288	1.864	MED193_11992	50S ribosomal protein L20
A3XFZ6	+	3.704	1.846	MED193_10091	Formate dehydrogenase, iron-sulfur subunit, putative
A3XCE6	+	1.911	1.830	MED193_10963	OmpA domain protein
A3X930	+	1.542	1.813	MED193_08738	TPR repeat protein
A3XFB9	+	2.142	1.812	MED193_21541	N-acetylmuramoyl-L-alanine amidase, putative
A3X3R6	+	1.850	1.805	MED193_17339	Probable acyl-CoA dehydrogenase
A3XD12	+	1.830	1.790	MED193_09790	ABC transporter, ATP-binding protein
A3X4J7	+	2.171	1.784	MED193_20864	Transcriptional regulator, Crp/Fnr family protein
A3XC17	+	1.447	1.778	MED193_03427	Uncharacterized protein
A3XCG4	+	1.768	1.769	MED193_10873	Aspartate carbamoyltransferase (EC 2.1.3.2) (Aspartate transcarbamylase) (ATCase)
A3XBG3	+	1.951	1.768	MED193_22526	Uncharacterized protein
A3XCM6	+	1.720	1.761	MED193_10593	Pyridoxamine 5'-phosphate oxidase family protein
A3X891	+	1.466	1.755	MED193_06194	Uncharacterized protein
A3X9V0	+	3.468	1.750	MED193_01575	Uncharacterized protein
A3XDM5	+	3.611	1.739	MED193_12993	Uncharacterized protein
A3XBV0	+	2.162	1.734	MED193_03752	Pyridoxine/pyridoxamine 5'-phosphate oxidase (EC 1.4.3.5) (PNP/PMP oxidase) (PNPOx) (Pyridoxal 5'-phosphate synthase)
A3XCN4	+	2.884	1.654	MED193_10543	Succinate--CoA ligase [ADP-forming] subunit beta (EC 6.2.1.5) (Succinyl-CoA synthetase subunit beta) (SCS-beta)
A3X5J4	+	2.170	1.646	MED193_19129	Gamma-glutamyltranspeptidase
A3X650	+	1.833	1.640	MED193_15957	50S ribosomal protein L7/L12
A3XD23	+	1.835	1.637	MED193_09745	ABC transporter, ATP-binding protein
A3X7V0	+	2.073	1.631	MED193_06904	Oxidoreductase, short chain dehydrogenase/reductase family protein
A3X7V8	+	2.544	1.621	MED193_06854	LysM domain/M23/M37 peptidase
A3XAP5	+	3.505	1.614	MED193_04741	50S ribosomal protein L13
A3XFQ5	+	3.053	1.598	MED193_11997	Uncharacterized protein

A3XFE0	+	1.977	1.583	MED193_21446	Peptide/nickel/opine uptake family ABC transporter, periplasmic substrate-binding protein
A3XAD0	+	3.287	1.579	MED193_05316	Sarcosine oxidase, delta subunit family protein
A3X4I0	+	2.547	1.546	MED193_20959	Phosphoenolpyruvate-protein phosphotransferase
A3XFR1	+	4.522	1.531	MED193_11942	Alanine dehydrogenase (EC 1.4.1.1)
A3XCW3	+	2.983	1.489	MED193_09150	Peptidoglycan-associated protein

Appendix 3.6 Significantly upregulated proteins (p-value <0.05) in the exoproteome of P-deplete ΔphoB cultures in comparison to MED193. Colours represent COGs: yellow; metabolism, blue; cellular processes and signalling, green; information storage and processing, no colour; poorly characterised.

Protein ID	*p-value <0.05*	*-log$_{10}$ (p-value)*	*Log$_2$ (fold change)*	*Locus tag*	*Uniprot annotation*
A3XD94	+	3.143	7.057	MED193_09370	Glycine cleavage system H protein
A3X3Q1	+	3.239	6.947	MED193_17424	Phosphogluconate dehydratase (EC 4.2.1.12)
A3XB54	+	3.752	6.441	MED193_22031	Outer membrane protein
A3XBE4	+	3.214	5.932	MED193_22626	LPS-assembly protein LptD
A3XAL2	+	3.856	5.821	MED193_04901	Acyl-[acyl-carrier-protein]--UDP-N-acetylglucosamine O-acyltransferase (EC 2.3.1.129)
A3XF05	+	3.460	5.754	MED193_03035	Type I secretion target repeat protein
A3X687	+	3.580	5.670	MED193_15757	Creatinase
A3X705	+	2.000	5.548	MED193_14407	Malonyl-CoA synthase
A3X7K7	+	2.475	5.443	MED193_07379	Metallopeptidase, family M24
A3XEX5	+	3.872	5.234	MED193_12173	Taurine--pyruvate aminotransferase
A3XFC4	+	2.651	5.220	MED193_21516	Metallo-beta-lactamase family protein
A3X7Q1	+	5.358	5.190	MED193_07174	Amidohydrolase family protein
A3X9B5	+	2.943	5.137	MED193_08313	4-hydroxyphenylpyruvate dioxygenase
A3XBQ2	+	3.433	5.125	MED193_03992	Acetoacetyl-CoA synthase
A3X6I1	+	2.185	5.072	MED193_15272	UDP-N-acetylglucosamine 1-carboxyvinyltransferase (EC 2.5.1.7) (Enoylpyruvate transferase) (UDP-N-acetylglucosamine enolpyruvyl transferase) (EPT)
A3XAK9	+	4.485	5.001	MED193_04916	Outer membrane protein assembly factor BamA
A3XG06	+	2.614	4.894	MED193_10046	Gamma-glutamylisopropylamide synthetase, putative
A3X4I2	+	2.941	4.608	MED193_20944	GTP cyclohydrolase FolE2 (EC 3.5.4.16)
A3X9H4	+	2.275	4.577	MED193_08013	TonB dependent-iron siderophore receptor
A3XAE7	+	2.643	4.572	MED193_05221	Efflux transporter, RND family, MFP subunit

A3X4H1	+	2.685	4.384	MED193_20989	Benzoate-coenzyme A ligase
A3X8V3	+	3.866	4.308	MED193_09113	Formate--tetrahydrofolate ligase (EC 6.3.4.3) (Formyltetrahydrofolate synthetase) (FHS) (FTHFS)
A3X861	+	3.044	4.222	MED193_06364	Type I restriction system specificity protein
A3X4K3	+	3.467	4.171	MED193_20839	Glutathione reductase (GRase) (EC 1.8.1.7)
A3XFN3	+	4.026	4.055	MED193_12107	Uncharacterized protein (Fragment)
A3XFH7	+	4.069	4.040	MED193_11574	S-formylglutathione hydrolase (EC 3.1.2.12)
A3XAM8	+	1.508	4.033	MED193_04831	Methylenetetrahydrofolate--tRNA-(uracil-5-)-methyltransferase TrmFO (EC 2.1.1.74) (Folate-dependent tRNA (uracil-5-)-methyltransferase) (Folate-dependent tRNA(M-5-U54)-methyltransferase)
A3XD01	+	4.052	3.969	MED193_09830	Glutamine-dependent NAD(+) synthetase (EC 6.3.5.1) (NAD(+) synthase [glutamine-hydrolyzing])
A3X860	+	3.177	3.957	MED193_06359	Type I site-specific deoxyribonuclease HsdM
A3XEZ2	+	5.634	3.951	MED193_03105	Uncharacterized protein
A3XFM9	+	3.079	3.944	MED193_11339	Saccharopine dehydrogenase
A3X3N5	+	2.048	3.830	MED193_17504	Putative Hemin receptor protein HmuR
A3X7S7	+	4.037	3.818	MED193_07014	NADH-quinone oxidoreductase (EC 1.6.5.11)
A3X960	+	2.760	3.808	MED193_08583	Glutamate dehydrogenase
A3XBI7	+	3.030	3.804	MED193_22416	Arginine--tRNA ligase (EC 6.1.1.19) (Arginyl-tRNA synthetase) (ArgRS)
A3X3A3	+	3.966	3.799	MED193_18154	S-(hydroxymethyl)glutathione dehydrogenase (EC 1.1.1.284)
A3X4Z0	+	2.303	3.762	MED193_20139	Ribose-phosphate pyrophosphokinase (RPPK) (EC 2.7.6.1) (5-phospho-D-ribosyl alpha-1-diphosphate) (Phosphoribosyl diphosphate synthase) (Phosphoribosyl pyrophosphate synthase) (P-Rib-PP synthase) (PRPP synthase) (PRPPase)
A3XB18	+	3.059	3.744	MED193_22216	Xanthine dehydrogenase family protein, large subunit
A3XEM3	+	2.136	3.742	MED193_12713	Exonuclease I
A3X6G6	+	1.856	3.742	MED193_15367	Uncharacterized protein
A3XB22	+	4.850	3.713	MED193_22201	Valine--tRNA ligase (EC 6.1.1.9) (Valyl-tRNA synthetase) (ValRS)
A3XD95	+	2.930	3.706	MED193_09375	Probable glutamine synthetase (EC 6.3.1.2)
A3XEN2	+	3.855	3.663	MED193_12663	Uncharacterized protein
A3X5I0	+	1.722	3.655	MED193_19209	Xanthine dehydrogenase, B subunit
A3XD02	+	3.725	3.579	MED193_09835	MORN repeat protein
A3X7E1	+	1.700	3.545	MED193_13742	ATP-dependent protease subunit HslV (EC 3.4.25.2)
A3XB95	+	3.867	3.539	MED193_21821	Proline--tRNA ligase (EC 6.1.1.15) (Prolyl-tRNA synthetase) (ProRS)

A3XD93	+	2.852	3.515	MED193_09365	Glycine dehydrogenase (decarboxylating) (EC 1.4.4.2) (Glycine cleavage system P-protein) (Glycine decarboxylase) (Glycine dehydrogenase (aminomethyl-transferring))
A3XC21	+	3.844	3.509	MED193_03402	Uncharacterized protein
A3X7L8	+	4.145	3.497	MED193_07324	Aspartyl/glutamyl-tRNA(Asn/Gln) amidotransferase subunit B (Asp/Glu-ADT subunit B) (EC 6.3.5.-)
A3XEW4	+	1.134	3.459	MED193_12268	Uncharacterized protein
A3XBM8	+	3.155	3.447	MED193_04107	ABC branched amino acid transporter family, periplasmic substrate-binding protein
A3XBF2	+	2.401	3.440	MED193_22581	Agmatinase
A3XCN7	+	1.989	3.416	MED193_10513	Uncharacterized protein
A3XD79	+	2.207	3.375	MED193_09435	Outer membrane protein, OMP85 family protein
A3XAU6	+	2.151	3.282	MED193_04496	ABC transporter, periplasmic substrate-binding protein
A3XDM4	+	2.687	3.221	MED193_12988	Peptidase, M16 family protein
A3X454	+	1.090	3.159	MED193_16654	Uncharacterized protein
A3XEM0	+	0.992	3.136	MED193_12698	Uncharacterized protein
A3X4W2	+	2.728	3.134	MED193_20294	Thioredoxin reductase (EC 1.8.1.9)
A3X4X2	+	2.127	3.132	MED193_20244	N5-carboxyaminoimidazole ribonucleotide synthase (N5-CAIR synthase) (EC 6.3.4.18) (5-(carboxyamino)imidazole ribonucleotide synthetase)
A3X8C2	+	2.587	3.130	MED193_06049	Uncharacterized protein
A3XBH7	+	1.692	3.089	MED193_22466	3-oxoacyl-[acyl-carrier-protein] synthase 3 (EC 2.3.1.180) (3-oxoacyl-[acyl-carrier-protein] synthase III) (Beta-ketoacyl-ACP synthase III) (KAS III)
A3XAL9	+	2.305	3.082	MED193_04866	DNA ligase (EC 6.5.1.2) (Polydeoxyribonucleotide synthase [NAD(+)])
A3XFM5	+	4.407	3.065	MED193_11369	Fumarylacetoacetase
A3XA68	+	1.994	3.065	MED193_00995	Uncharacterized protein
A3XAC5	+	2.071	3.057	MED193_05341	tRNA-dihydrouridine(20/20a) synthase (EC 1.3.1.-) (EC 1.3.1.91) (U20-specific dihydrouridine synthase) (U20-specific Dus) (tRNA-dihydrouridine synthase A)
A3XB72	+	2.507	3.017	MED193_21951	Amidohydrolase domain protein
A3X7Q2	+	3.865	3.000	MED193_07129	Bifunctional protein GlmU [Includes: Glucosamine-1-phosphate N-acetyltransferase (EC 2.3.1.157); UDP-N-acetylglucosamine pyrophosphorylase (EC 2.7.7.23) (N-acetylglucosamine-1-phosphate uridyltransferase)]
A3X8C4	+	0.904	2.908	MED193_06034	Phosphopentomutase (EC 5.4.2.7) (Phosphodeoxyribomutase)
A3XD89	+	1.923	2.906	MED193_09390	Probable glyoxylate induced protein
A3X666	+	1.771	2.837	MED193_15887	Pyridine nucleotide-disulphide oxidoreductase family protein
A3X4A9	+	2.271	2.792	MED193_21299	Uncharacterized enzyme involved in inositol metabolism, IolB
A3X4N2	+	4.339	2.790	MED193_20679	Type I secretion outer membrane protein, TolC family protein

A3XB15	+	3.374	2.782	MED193_04141	Invasion associated family protein
A3XDE5	+	3.338	2.779	MED193_13383	2,3,4,5-tetrahydropyridine-2,6-dicarboxylate N-succinyltransferase (EC 2.3.1.117) (Tetrahydrodipicolinate N-succinyltransferase) (THDP succinyltransferase) (THP succinyltransferase) (Tetrahydropicolinate succinylase)
A3XAI6	+	3.931	2.713	MED193_05046	6-aminohexanoate-cyclic-dimer hydrolase, putative
A3X5C0	+	2.637	2.690	MED193_19509	6-phosphogluconate dehydrogenase domain protein
A3X593	+	2.535	2.620	MED193_19649	Bacterioferritin (EC 1.16.3.1)
A3XG08	+	3.274	2.616	MED193_10006	Endoribonuclease L-PSP family protein
A3X6W5	+	4.518	2.612	MED193_14632	Outer membrane porin
A3X9F9	+	1.472	2.602	MED193_08083	Uncharacterized protein
A3X4J2	+	0.649	2.600	MED193_20894	Phosphoribosylamine--glycine ligase (EC 6.3.4.13) (GARS) (Glycinamide ribonucleotide synthetase) (Phosphoribosylglycinamide synthetase)
A3X754	+	1.465	2.574	MED193_14197	Uncharacterized protein
A3X4H9	+	1.073	2.567	MED193_20954	Aspartokinase (EC 2.7.2.4)
A3XAD8	+	2.159	2.551	MED193_05276	Superoxide dismutase (EC 1.15.1.1)
A3X4G2	+	1.769	2.543	MED193_21049	Uncharacterized protein
A3X917	+	2.202	2.459	MED193_08793	Ketol-acid reductoisomerase (NADP(+)) (KARI) (EC 1.1.1.86) (Acetohydroxy-acid isomeroreductase) (AHIR) (Alpha-keto-beta-hydroxylacyl reductoisomerase)
A3X430	+	4.293	2.430	MED193_16779	Periplasmic serine protease, DO/DeqQ family protein
A3XD80	+	2.290	2.392	MED193_09440	Uncharacterized protein
A3XEN1	+	1.457	2.386	MED193_12658	Uncharacterized protein
A3XFH5	+	1.757	2.379	MED193_11609	Ornithine cyclodeaminase/mu-crystallin family protein
A3X852	+	0.818	2.372	MED193_06404	Uncharacterized protein
A3XAX0	+	2.483	2.368	MED193_04371	Uncharacterized protein
A3X4N0	+	2.531	2.293	MED193_20699	Elongation factor P (EF-P)
A3XFB7	+	4.158	2.285	MED193_21531	Glutamyl-tRNA(Gln) amidotransferase subunit A (Glu-ADT subunit A) (EC 6.3.5.7)
A3X8S2	+	2.726	2.273	MED193_07678	Uncharacterized protein
A3X8A7	+	4.098	2.259	MED193_06124	Thymidylate synthase (TS) (TSase) (EC 2.1.1.45)
A3X4K1	+	3.260	2.238	MED193_20854	Periplasmic serine endoprotease DegP-like (EC 3.4.21.107)
A3XDG8	+	2.511	2.225	MED193_13308	Serine/threonine protein phosphatase family protein
A3X3G5	+	3.087	2.223	MED193_17844	3-hydroxydecanoyl-[acyl-carrier-protein] dehydratase (EC 4.2.1.59)
A3X8F3	+	3.426	2.222	MED193_05889	Ser/Thr protein phosphatase/nucleotidase, putative
A3XFN2	+	1.849	2.222	MED193_12102	D-amino acid aminotransferase, putative
A3X9S0	+	3.083	2.210	MED193_01725	Polysaccharide biosynthesis protein
A3X5E6	+	0.838	2.193	MED193_19374	Uncharacterized protein

A3X8N3	+	3.259	2.179	MED193_05484	ABC transporter, periplasmic substrate-binding protein
A3X5F0	+	2.387	2.179	MED193_19344	Extracellular solute-binding protein, family 5
A3XAI5	+	2.162	2.162	MED193_05041	Glutamine synthetase (EC 6.3.1.2)
A3X948	+	1.815	2.160	MED193_08633	Fructose-1,6-bisphosphatase
A3XA90	+	1.611	2.149	MED193_00885	2-oxo-hepta-3-ene-1,7-dioic acid hydratase, putative
A3XBQ4	+	2.121	2.144	MED193_03977	Phosphotransferase family protein
A3X3Q2	+	2.470	2.135	MED193_17409	Putative sulfatase
A3XEW3	+	2.575	2.133	MED193_12263	Oxidoreductase, FAD-binding
A3X3Z1	+	1.629	2.133	MED193_16964	Uncharacterized protein
A3X7B3	+	1.834	2.119	MED193_13892	Putative IlvE, Branched-chain amino acidaminotransferase/4-amino-4-deoxychorismate lyase
A3XFM4	+	1.955	2.111	MED193_11364	Homogentisate 1,2-dioxygenase (EC 1.13.11.5)
A3X641	+	2.359	2.109	MED193_16007	Elongation factor G (EF-G)
A3X907	+	2.458	2.100	MED193_08858	Peptidoglycan binding domain protein
A3X8M9	+	2.017	2.087	MED193_05519	N-carbamoyl-L-amino acid amidohydrolase
A3X9A3	+	1.873	2.079	MED193_08378	Oligoendopeptidase F
A3X509	+	2.149	2.059	MED193_20074	Peptidase, M23/M37 family protein
A3XBY6	+	2.566	2.051	MED193_03577	Transketolase
A3XFN8	+	2.272	2.049	MED193_12092	Uncharacterized protein
A3X4H4	+	1.287	2.032	MED193_20979	Enoyl-CoA hydratase (EC 4.2.1.17)
A3X985	+	2.140	2.012	MED193_08458	3,4-dihydroxy-2-butanone 4-phosphate synthase (DHBP synthase) (EC 4.1.99.12)
A3XDP4	+	4.560	2.011	MED193_12888	N-carbamoyl-L-amino acid amidohydrolase
A3XC15	+	2.623	1.997	MED193_03437	Dihydrolipoyl dehydrogenase (EC 1.8.1.4)
A3X3E3	+	1.660	1.985	MED193_17954	30S ribosomal protein S1
A3XAY7	+	3.373	1.969	MED193_04271	Cysteine desulfurase (EC 2.8.1.7)
A3XBK3	+	2.570	1.928	MED193_22326	Uncharacterized protein
A3XAY0	+	2.078	1.916	MED193_04326	Uncharacterized protein
A3XBG4	+	2.994	1.909	MED193_22531	UPF0061 protein MED193_22531
A3XDN0	+	1.363	1.897	MED193_12968	Zinc/manganese/iron ABC transporter, periplasmic zinc/manganese/iron-binding protein
A3XBQ6	+	4.139	1.895	MED193_03987	Beta-lactamase
A3XCF0	+	3.548	1.890	MED193_10938	Glutamate--cysteine ligase (EC 6.3.2.2)
A3X7P5	+	4.613	1.889	MED193_07194	Peptide/opine/nickel uptake family ABC transporter, periplasmic substrate-binding protein
A3XA86	+	1.116	1.864	MED193_00890	2,4-dihydroxyhept-2-ene-1, 7-dioic acid aldolase, hypothetical

A3X7S9	+	1.134	1.830	MED193_07024	Uncharacterized protein
A3XFJ2	+	3.013	1.818	MED193_11509	Aspartate-semialdehyde dehydrogenase (ASA dehydrogenase) (ASADH) (EC 1.2.1.11) (Aspartate-beta-semialdehyde dehydrogenase)
A3XFA2	+	2.909	1.797	MED193_21606	Guanine deaminase
A3XBT0	+	3.001	1.787	MED193_03852	Uncharacterized protein
A3X5V2	+	1.849	1.779	MED193_18584	Uncharacterized protein
A3X4A2	+	1.612	1.756	MED193_16409	Pyridoxine 5'-phosphate synthase (PNP synthase) (EC 2.6.99.2)
A3X531	+	3.642	1.748	MED193_19934	Uncharacterized protein
A3XC87	+	2.767	1.744	MED193_11263	Oligopeptide/dipeptide uptake family ABC transporter, periplasmic substrate-binding protein
A3XD40	+	2.720	1.741	MED193_09640	Cold shock family protein
A3XEZ3	+	2.457	1.719	MED193_03110	Trigger factor (TF) (EC 5.2.1.8) (PPIase)
A3XFS2	+	2.533	1.718	MED193_11902	Alcohol dehydrogenase, zinc-containing
A3XC29	+	1.997	1.689	MED193_03357	Peptidyl-prolyl cis-trans isomerase (PPIase) (EC 5.2.1.8)
A3XD32	+	1.798	1.688	MED193_09700	Lysine--tRNA ligase (EC 6.1.1.6) (Lysyl-tRNA synthetase) (LysRS)
A3X7Y3	+	2.214	1.683	MED193_06754	Dihydroorotase (DHOase) (EC 3.5.2.3)
A3X8V6	+	2.200	1.681	MED193_09108	Bifunctional protein FolD [Includes: Methenyltetrahydrofolate cyclohydrolase (EC 3.5.4.9); Methylenetetrahydrofolate dehydrogenase (EC 1.5.1.5)]
A3XF38	+	2.722	1.674	MED193_02865	Probable binding protein component of ABC transporter
A3XDE3	+	1.716	1.663	MED193_13418	Succinyl-diaminopimelate desuccinylase (SDAP desuccinylase) (EC 3.5.1.18) (N-succinyl-LL-2,6-diaminoheptanedioate amidohydrolase)
A3X9B6	+	2.454	1.653	MED193_08293	O-acetylhomoserine aminocarboxypropyltransferase
A3XFU2	+	2.713	1.629	MED193_11812	Bordetella uptake gene family protein
A3X7D2	+	3.125	1.561	MED193_13782	Protein-export protein SecB
A3XDN3	+	3.308	1.550	MED193_12983	Peptidase, M16 family protein
A3XCW4	+	2.826	1.549	MED193_09155	Tol-Pal system protein TolB
A3X4X6	+	2.310	1.546	MED193_20214	60 kDa chaperonin (GroEL protein) (Protein Cpn60)
A3X7W2	+	3.033	1.543	MED193_06844	5'-nucleotidase SurE (EC 3.1.3.5) (Nucleoside 5'-monophosphate phosphohydrolase)
A3X7U4	+	2.213	1.521	MED193_06944	Metallo-beta-lactamase family protein
A3X4U7	+	2.513	1.505	MED193_20374	Efflux transporter, RND family, MFP subunit
A3X6D7	+	2.357	1.487	MED193_15502	Alpha-D-glucose-1-phosphate cytidylyltransferase

Appendix 3.7 50 most abundant proteins (relative abundance in %) in cellular proteome of P-deplete MED193 cultures and corresponding proteins (rel. abundance in %) of P-deplete ΔphoB cultures.

Protein ID	*Rel. abundance (%) MED193*	*Rel. abundance (%) PhoB*	*Locus tag*	*Uniprot annotation*
A3XBP0	5.900	0.001	MED193_04062	Phosphate ABC transporter, periplasmic phosphate-binding protein
A3X6W5	3.891	8.398	MED193_14632	Outer membrane porin
A3XFN8	3.422	3.777	MED193_12092	Uncharacterized protein
A3X815	3.263	0.001	MED193_06579	Glycerophosphoryl diester phosphodiesterase
A3XFY2	3.247	0.001	MED193_10161	Phosphonate ABC transporter, periplasmic phosphonate-binding protein
A3X4X6	3.037	3.720	MED193_20214	60 kDa chaperonin (GroEL protein) (Protein Cpn60)
A3XFR1	2.660	3.588	MED193_11942	Alanine dehydrogenase (EC 1.4.1.1)
A3X468	2.524	3.171	MED193_16017 MED193_16584	Elongation factor Tu (EF-Tu)
A3XB37	2.497	1.589	MED193_22121	Phasin, PhaP
A3X8H3	2.231	0.000	MED193_05784	Uncharacterized protein
A3XEZ2	1.679	1.996	MED193_03105	Uncharacterized protein
A3X4X9	1.513	0.986	MED193_20209	10 kDa chaperonin (GroES protein) (Protein Cpn10)
A3X4Z8	1.092	2.372	MED193_20109	ATP synthase subunit beta (EC 7.1.2.2) (ATP synthase F1 sector subunit beta) (F-ATPase subunit beta)
A3X501	1.030	1.391	MED193_20099	ATP synthase subunit alpha (EC 7.1.2.2) (ATP synthase F1 sector subunit alpha) (F-ATPase subunit alpha)
A3X814	0.937	0.732	MED193_06604	TRAP transporter solute receptor, DctP family protein
A3X9J4	0.864	0.002	MED193_07903	SN-glycerol-3-phophate ABC transporter, periplasmic SN-glycerol-3-phosphate-binding protein
A3XBZ9	0.812	0.001	MED193_03507	Iron-binding periplasmic protein
A3X9P6	0.763	0.001	MED193_01855	Putative periplasmic solute-binding protein
A3X424	0.744	1.863	MED193_16809	Glutamate/glutamine/aspartate/asparagine ABC transporter, periplasmic substrate-binding protein
A3XC77	0.743	0.006	MED193_03127	2',3'-cyclic nucleotide 2'-phosphodiesterase/3'-nucleotidase bifunctional periplasmic protein (EC 3.1.4.16)
A3XBR4	0.702	0.234	MED193_03927	Elongation factor Ts (EF-Ts)
A3XAD8	0.624	0.521	MED193_05276	Superoxide dismutase (EC 1.15.1.1)
A3XFK5	0.603	0.131	MED193_11424	Spermidine/putrescine ABC transporter,spermidine/putrescine-binding protein

A3X7G0	0.577	0.603	MED193_13647	Uncharacterized protein
A3X4D7	0.566	0.906	MED193_21164	Bacterial extracellular solute-binding protein, family 7
A3XCN3	0.543	0.714	MED193_10538	Malate dehydrogenase (EC 1.1.1.37)
A3XFN2	0.520	0.775	MED193_12102	D-amino acid aminotransferase, putative
A3X4Y3	0.479	1.096	MED193_20189	Putative manganese-dependent inorganic pyrophosphatase (EC 3.6.1.1)
A3XC84	0.470	0.010	MED193_11293	Sugar ABC transporter, periplasmic sugar-binding protein
A3X4R3	0.467	0.065	MED193_20524	Uncharacterized protein
A3XDG0	0.429	0.968	MED193_13318	D-3-phosphoglycerate dehydrogenase (EC 1.1.1.95)
A3X650	0.415	0.212	MED193_15957	50S ribosomal protein L7/L12
A3X479	0.408	1.040	MED193_16534	Electron transfer flavoprotein, alpha subunit
A3XBP3	0.395	0.006	MED193_04042	Phosphate-specific transport system accessory protein PhoU
A3XBD4	0.377	0.735	MED193_22671	Nucleoside diphosphate kinase (NDK) (NDP kinase) (EC 2.7.4.6) (Nucleoside-2-P kinase)
A3X8P8	0.376	0.506	MED193_05429	TRAP dicarboxylate transporter, DctP subunit
A3XCL1	0.360	0.474	MED193_10668	Acetyl-CoA acetyltransferase (EC 2.3.1.9)
A3X960	0.347	0.603	MED193_08583	Glutamate dehydrogenase
A3XDK0	0.336	0.286	MED193_13113	Thiol-specific antioxidant protein
A3X8V3	0.335	1.265	MED193_09113	Formate--tetrahydrofolate ligase (EC 6.3.4.3) (Formyltetrahydrofolate synthetase) (FHS) (FTHFS)
A3X8J4	0.329	0.322	MED193_05699	ATP-dependent Clp protease proteolytic subunit (EC 3.4.21.92) (Endopeptidase Clp)
A3XC64	0.326	0.364	MED193_03182	Uncharacterized protein
A3XA55	0.317	0.122	MED193_01040	Uncharacterized protein
A3X476	0.306	0.729	MED193_16539	Electron transfer flavoprotein, beta subunit
A3XDR4	0.305	0.198	MED193_12828	Branched-chain amino acid ABC transporter, periplasmic branched-chain amino acid binding protein, putative
A3XCN4	0.301	0.409	MED193_10543	Succinate--CoA ligase [ADP-forming] subunit beta (EC 6.2.1.5) (Succinyl-CoA synthetase subunit beta) (SCS-beta)
A3XBP1	0.285	0.004	MED193_04047	Phosphate import ATP-binding protein PstB (EC 7.3.2.1) (ABC phosphate transporter) (Phosphate-transporting ATPase)
A3XCU5	0.283	0.273	MED193_09260	Probable transaldolase (EC 2.2.1.2)
A3X760	0.281	0.534	MED193_14127	Chaperone protein DnaK (HSP70) (Heat shock 70 kDa protein) (Heat shock protein 70)
A3XDD1	0.280	0.352	MED193_13453	Polyamine ABC trasnporter, periplasmic polyamine-binding protein

Appendix 3.8 50 most abundant proteins (relative abundance in %) in exoproteome of P-deplete MED193 cultures and corresponding proteins (rel. abundance in %) of P-deplete ΔphoB cultures.

Protein ID	*Rel. abundance (%) MED193*	*Rel. abundance (%) PhoB*	*Locus tag*	*Uniprot annotation*
A3X4D7	6.768	4.128	MED193_21164	Bacterial extracellular solute-binding protein, family 7
A3XFY2	6.243	0.001	MED193_10161	Phosphonate ABC transporter, periplasmic phosphonate-binding protein
A3X814	4.697	4.620	MED193_06604	TRAP transporter solute receptor, DctP family protein
A3XBP0	4.691	0.086	MED193_04062	Phosphate ABC transporter, periplasmic phosphate-binding protein
A3X815	4.212	0.078	MED193_06579	Glycerophosphoryl diester phosphodiesterase
A3XFK5	3.237	0.056	MED193_11424	Spermidine/putrescine ABC transporter,spermidine/putrescine-binding protein
A3X8H3	2.700	0.026	MED193_05784	Uncharacterized protein
A3X9J4	2.048	0.095	MED193_07903	SN-glycerol-3-phophate ABC transporter, periplasmic SN-glycerol-3-phosphate-binding protein
A3X424	1.972	6.337	MED193_16809	Glutamate/glutamine/aspartate/asparagine ABC transporter, periplasmic substrate-binding protein
A3X4X9	1.832	0.177	MED193_20209	10 kDa chaperonin (GroES protein) (Protein Cpn10)
A3X4R3	1.777	0.234	MED193_20524	Uncharacterized protein
A3XDD1	1.737	2.427	MED193_13453	Polyamine ABC trasnporter, periplasmic polyamine-binding protein
A3X4X6	1.652	5.577	MED193_20214	60 kDa chaperonin (GroEL protein) (Protein Cpn60)
A3X9P6	1.588	0.005	MED193_01855	Putative periplasmic solute-binding protein
A3XBZ9	1.529	0.000	MED193_03507	Iron-binding periplasmic protein
A3XC77	1.335	0.059	MED193_03127	2',3'-cyclic nucleotide 2'-phosphodiesterase/3'-nucleotidase bifunctional periplasmic protein (EC 3.1.4.16)
A3X4Z8	1.292	1.535	MED193_20109	ATP synthase subunit beta (EC 7.1.2.2) (ATP synthase F1 sector subunit beta) (F-ATPase subunit beta)
A3X8P8	1.268	0.967	MED193_05429	TRAP dicarboxylate transporter, DctP subunit
A3XAD8	0.970	6.570	MED193_05276	Superoxide dismutase (EC 1.15.1.1)
A3XDR4	0.962	1.142	MED193_12828	Branched-chain amino acid ABC transporter, periplasmic branched-chain amino acid binding protein, putative
A3X6W5	0.919	6.496	MED193_14632	Outer membrane porin
A3XBU2	0.880	0.502	MED193_03802	TRAP transporter solute receptor, TAXI family protein
A3XC84	0.872	0.059	MED193_11293	Sugar ABC transporter, periplasmic sugar-binding protein
A3XDR6	0.827	2.033	MED193_12793	Ferric iron ABC transporter, periplasmic ferric iron-binding protein

A3XD08	0.796	0.287	MED193_09820	Metallo-beta-lactamase family protein
A3X975	0.748	0.058	MED193_08513	Uncharacterized protein
A3X7P5	0.740	3.169	MED193_07194	Peptide/opine/nickel uptake family ABC transporter, periplasmic substrate-binding protein
A3X468	0.574	0.249	MED193_16017 MED193_16584	Elongation factor Tu (EF-Tu)
A3X5I5	0.481	0.906	MED193_19179	Bmp family protein
A3XDK0	0.477	0.012	MED193_13113	Thiol-specific antioxidant protein
A3XD56	0.418	0.283	MED193_09570	Sugar ABC transporter, periplasmic sugar-binding protein
A3XBD4	0.410	0.008	MED193_22671	Nucleoside diphosphate kinase (NDK) (NDP kinase) (EC 2.7.4.6) (Nucleoside-2-P kinase)
A3X433	0.400	0.176	MED193_16764	50S ribosomal protein L17
A3XBP3	0.388	0.002	MED193_04042	Phosphate-specific transport system accessory protein PhoU
A3XBM8	0.376	4.736	MED193_04107	ABC branched amino acid transporter family, periplasmic substrate-binding protein
A3X7E5	0.362	0.105	MED193_13717	Thioredoxin
A3XAI5	0.356	1.841	MED193_05041	Glutamine synthetase (EC 6.3.1.2)
A3X9B8	0.353	0.612	MED193_08303	Outer membrane protein, 28Kda
A3X442	0.340	0.005	MED193_16719	50S ribosomal protein L30
A3XCL1	0.325	0.004	MED193_10668	Acetyl-CoA acetyltransferase (EC 2.3.1.9)
A3X8I3	0.317	0.015	MED193_05744	Sulfur oxidation Z protein
A3X456	0.313	0.054	MED193_16634	50S ribosomal protein L22
A3X8T4	0.313	0.005	MED193_07618	Uncharacterized protein
A3X465	0.302	0.209	MED193_16604	50S ribosomal protein L3
A3X6L5	0.300	0.038	MED193_15112	Cytochrome c family protein
A3X6V0	0.299	0.079	MED193_14712	Uncharacterized protein
A3XDK9	0.293	0.017	MED193_13063	30S ribosomal protein S15
A3XDF7	0.287	0.295	MED193_13348	Uncharacterized protein
A3XFN8	0.286	1.367	MED193_12092	Uncharacterized protein
A3X449	0.284	0.069	MED193_16684	50S ribosomal protein L24

Appendix 3.9 General categories of the Clusters of Orthologous Groups (COGs) including specific functional descriptions.

Metabolism	***Cellular processes and signalling***	***Information storage and processing***
Energy production and conversion	Cell cycle control, cell division, chromosome partitioning	Chromatin structure and dynamics
Amino acid transport and metabolism	Cell wall/membrane/ envelope biogenesis	Translation, ribosomal structure and biogenesis
Nucleotide transport and metabolism	Cell motility	Transcription
Carbohydrate transport and metabolism	Post-translational modification, protein turnover, and chaperones	Replication, recombination and repair
Coenzyme transport and metabolism	Signal transduction mechanisms	
Lipid transport and metabolism	Intracellular trafficking, secretion, and vesicular transport	
Inorganic ion transport and metabolism	Defense mechanisms	
Secondary metabolites biosynthesis, transport, and catabolism	Cytoskeleton	

Appendix 3.10 List of proteins used for multiple sequence alignment of C-P lyases, retrieved from Bisson, 2017.

Protein and organism	**Abbreviation**	**Locus tag**	**NCBI Accession**	**UniProtKB**
Pseudomonas aeruginosa ATCC 15692	P.aeruginosa	PA3383	NP_252073	Q9HYL8
Escherichia coli K12	E.coli	b4105	NP_418529	P16682
Nostoc sp. PCC7120	N.PCC71201	all2228	BAB73927	Q8YUV3
Nostoc sp. PCC7120	N.PCC71202	all2229	BAB73928	Q8YUV2
Rhodopseudomonas palustris ATCC BAA-98	R.palustris	RPA0699	CAE26143	Q6NBX7
Trichodesmium erythraeum IMS101	T.erythraeum	Tery_4993	ABG53907	Q10V17
Synechococcus sp. JA-2-3B'a(2-13)	S.JA23Ba213	CYB_0160	ABD01161	Q2JPW5
Candidatus Pelagibacter sp. HTCC7211	Can.P.HTCC7211	PB7211_926	WP_008545354	B6BPP6
Candidatus Pelagibacter ubique HTCC7217	Can.P.ubique	P773DRAFT_0391	WP_029455242	N/A
Phaeobacter sp. MED193	P.sp.MED193	MED193_10161	EAQ43272	A3XFY2
Bradyrhizobium japonicum SEMIA 5079	B.japonicum	N/A	WP_039154563	A0A023XSC0
Magnetospirillum magneticum ATCC 700264	M.magneticum	amb1105	WP_011383518	Q2W8B6
Desulfotignum phosphitoxidan DSM 13687	D.phosphitoxidan	Dpo_1c07940	EMS81653	S0G2S3

Appendix 3.11 List of MED193 proteins with putative pho boxes. The score describes the accuracy of consensus sequence binding, only pho box sequences with scores ≥ 10 are listed. Method based on Yuan et al., 2006, data retrieved from Dr Marta Sebastián.

Label	**Putative pho box sequence**	**Score**	**bp between end of target and beginning of gene (neg. value means the pho box is within the gene)**
MED193_21741 hypothetical protein	TTTTTACAGCCCTGTCAG	10.0	-52
MED193_08048 PAS	CTGTCGCTTTACTATCTT	10.0	-123
MED193_20294 thioredoxin-disulfide reductase	ATTTCACAACCGCGAAAT	10.0	164
MED193_00685 hypothetical protein	CTGGCATTCGACCTTCAC	10.0	-189
MED193_01895 glycine betaine transporter	CTGTCAAAGTGTCGCAAT	10.0	-47
MED193_10096 formate dehydrogenase, alpha subunit, putative	CTGTCACTCAGGCGACGG	10.0	-172
MED193_10021 hypothetical protein	CTGTCAATATAATTTCAG	10.1	94
MED193_16052 transcriptional regulator, LysR family protein	TTGTGAAAACCCTGCAAT	10.1	77
MED193_08693 hypothetical protein	CATTCGTCGACCCTTCAT	10.1	72
MED193_20519 hypothetical protein	ATGACAAAGAGCTGCCAG	10.2	-118
MED193_02815 tellurite resistance protein	CTTTCATATTAATGTCGC	10.2	-128

MED193_14542 adenylate/guanylate cyclase	CTGACACCGCAATGACAC	10.2	-22
MED193_10743 transcription elongation factor GreA	CTTTGGTAGACCCGACAT	10.2	51
MED193_18289 SIS domain protein	ATGGCACAAATGTATCAT	10.2	-31
MED193_11048 enoyl-CoA hydratase	ATGTCATGGTGCTTTCGG	10.3	-160
MED193_07658 hypothetical protein	CTGTCAAAAAGCCCAAAC	10.3	-31
MED193_01365 TRAP dicarboxylate transporter- DctP subunit	ATGTCGCCATAGTGAAAC	10.3	212
MED193_17724 hypothetical protein	ATGTCGTGGTCCGGTCAT	10.3	266
MED193_03507 iron-binding periplasmic protein	TCGTTACAAAACCGTCAG	10.3	66
MED193_11374 metallo-beta-lactamase family protein	CGGTGATGACTCTGTCAT	10.3	-137
MED193_06894 hypothetical protein	CTTTCACAGCTTTGTCAG	10.3	111
MED193_07568 putative regulatory protein	CTGTCCTTTCCCTTTCAC	10.4	50
MED193_16499 putative kinase/phosphatase	CTGGCAGCAAGGTGCCAC	10.4	-179
MED193_05599 transcriptional regulator, putative	CTGACAGGCAGCCGTATT	10.5	-33
MED193_10241 transcriptional regulator, IclR family protein	CTGTCAACAAAATATCAA	10.5	36
MED193_19869 hypothetical protein	CTGACAGAAAACTGTTCT	10.5	-28
MED193_17174 peptidase, M24 family protein	TTGTGACTGATCCGTCAA	10.5	-115
MED193_10998 UvrABC system protein C	AGGTCACAGATCTGTTAC	10.6	238
MED193_16934 hypothetical protein	ATGTCGCAGACATGTCCC	10.6	-160
MED193_20854 periplasmic serine protease, DO/DeqQ family protein	TTGTTATCAAGCGGTTAT	10.6	254
MED193_00130 transcriptional regulator CatR	ATTTCAAACAGCTGACCT	10.6	-22
MED193_19394 putative AsnC-family transcriptional regulator	TCGTCAAAATGGCGTAAT	10.6	14
MED193_12148 hypothetical protein	CCTTCACAGCCCTGTCTT	10.7	45
MED193_15697 hypothetical protein	CTGTCACTGCGGTGCAGT	10.7	-94
MED193_19774 EF hand domain protein	CTGTGATTTTGCTGCAAT	10.7	185
MED193_05371 Transcriptional Regulator, AraC family protein	CTGACATCTACCCGTCTG	10.7	50
MED193_17359 Metallo-phosphoesterase	CTGTCACGGTTCTGTTAA	10.7	49
MED193_03442 hypothetical protein	CTGTTGCAAACACGACAT	10.7	154
MED193_18254 UshA protein	CTGACGCATGACTGTCTT	10.7	57
MED193_08888 streptogramin acetyltransferase, putative	CTGTCACAAGCCCTTGAT	10.7	-93
MED193_05549 hypothetical protein	CGGTCACACAGCTGCAGT	10.8	165
MED193_20924 hypothetical protein	CTGCCGCCTCGCTTTCAT	10.8	80
MED193_11504 hypothetical protein	CTGACACCGCAGTTTCAA	10.8	-147
MED193_15762 CDP-diacylglycerol--serine O-phosphatidyltransferase	TTGGCGCGGTGCTGTCAC	10.9	238
MED193_17029 hypothetical protein	CCTTCGTGAACCCTTCAT	10.9	109

MED193_00360 hypothetical protein	ATTTCAATGAGCTGTATT	10.9	129
MED193_18194 putative transcriptional activator of the pca operon, LysR family protein	ACGTCAAACCAGTGTCAC	10.9	-74
MED193_02370 putative suppressor for copper-sensitivity B precursor	CTGTCGGCCGGGCTTCAT	11.0	-186
MED193_17684 glycosyl transferase, group 1 family protein	CTTTCAGAGACCTTTATC	11.0	-48
MED193_16479 phosphoenolpyruvate carboxykinase	CAGTCATGGAAACGTCAT	11.0	109
MED193_05256 lysM domain protein	CTTTCACTGAGTTTTCAA	11.0	60
MED193_22676 TfoX domain protein	CTGTCAACAAGATGTCCA	11.0	69
MED193_12968 zinc/manganese/iron ABC transporter, periplasmiczinc/manganese/iron-binding protein	ATGTCACAGAAGTTTTGT	11.0	85
MED193_00305 hypothetical protein	TTGTCACCGATCTTTTTC	11.0	138
MED193_00435 hypothetical protein	TTGTCACCGATCTTTTTC	11.0	151
MED193_02310 cobalt/cadmium/zinc transporter, CDF family protein	CTGTCGGATGCGTTTCAC	11.1	-147
MED193_18964 hypothetical protein	CTGTCACGGTAATTACAT	11.1	-2
MED193_05609 branched-chain amino acid ABC transporter, permease protein	CTGACATCGCGGTTTCTC	11.1	104
MED193_14942 probable 4-hydroxybenzoyl CoA thioesterase	ATGTCACAACAGCTTAGC	11.1	-18
MED193_19224 hypothetical protein	ATTTCACCTAACTTTATT	11.1	78
MED193_10121 iron-sulfur cluster-binding protein	TTTTGACTCACCCGTCAC	11.2	383
MED193_08238 hypothetical protein	CCGTCACCTCTCTGTCCT	11.2	-41
MED193_09640 cold shock family protein	ATGTCGACCTGCTGTCTC	11.3	-67
MED193_07069 enoyl-CoA hydratase	CTGACGTTGAACCGTCCT	11.3	-66
MED193_05011 probable chemoreceptor (methyl-accepting chemotaxis) transmembrane protein	CTGACAGCGACCTTTCTC	11.3	-114
MED193_08733 hypothetical protein	CTGCCAAAGACCCTTCAT	11.3	-2
MED193_12863 hypothetical protein	TTTTCGTGAAGTTTTCAC	11.4	150
MED193_00050 hypothetical protein	TTTTAAAACAACTGTCAC	11.4	210
MED193_13887 methionine-S-sulfoxide reductase	TTTTCAAAACCCTGAAAC	11.4	-25
MED193_20139 ribose-phosphate pyrophosphokinase	CTGTCACATAGCCATTGC	11.4	18
MED193_05829 hypothetical protein	CCGTCACATAGCTGTAGG	11.5	5
MED193_03627 acyltransferase domain protein	TTGTCATGTCGCTGTTAA	11.5	54
MED193_08228 hypothetical protein	GTGTCACTGATTTGTCAC	11.5	144
MED193_21626 trkA domain protein	TTGTCATGGAGCCGCAGT	11.6	76
MED193_17424 phosphogluconate dehydratase	CTGTCAGACACCCGAAAG	11.6	9

MED193_14797 FAD dependent oxidoreductase/aminomethyl transferase	CTTTCGGAGTGCTGACAT	11.7	-2
MED193_21691 hypothetical protein	CCGTCACCGCTGTTTCAC	11.7	169
MED193_11812 bordetella uptake gene family protein	CTTTCGCACAGTTGTCAA	11.8	31
MED193_15937 hypothetical protein	ATGTCATTCAGTTTTCAA	11.8	72
MED193_05181 preprotein translocase, YajC subunit	CTGTCGCGCCCGTGTCAG	12.0	225
MED193_05469 exonuclease, DNA polymerase III, epsilon subunit family protein	CTGTGGCTGAGCTATCAC	12.0	-105
MED193_15942 ribosomal protein L11	CTGACATTGAGTTTTAAC	12.0	161
MED193_03227 hypothetical protein	TTGTCGTGCCCCTGCCAC	12.0	226
MED193_15497 CDP-glucose-4,6-dehydratase	CGGTCATACAGGTTTCAA	12.0	-56
MED193_21781 hypothetical protein	CTGTCGTCATGGTTTCCC	12.1	104
MED193_18169 hypothetical protein	CTGTCAAAAATCCATTAC	12.1	44
MED193_15227 hypothetical protein	TTGTAGCACCTCTGTCAT	12.1	18
MED193_12898 glutathione S-transferase, putative	CTGACATGCAGCTTTACT	12.2	-13
MED193_14297 adenine deaminase	CTGTCATCCTCTTGCCAT	12.2	73
MED193_01850 probable LacI-family transcriptional regulator	CTGTCACACTCCTGTAGA	12.5	46
MED193_21656 L-lysine exporter, putative	TTGTCACATCCCTGCCGC	12.5	-25
MED193_06579 Glycerophosphoryl diester phosphodiesterase	TGGTCATAAAAGCTTCAC	12.5	-19
MED193_12858 AMP-binding enzyme	CTGACATCCCCCCGTCTT	12.5	214
MED193_21886 Integrase, catalytic region	ATTTGACACAGCCTTCAT	12.6	-23
MED193_15047 nicotinate phosphoribosyltransferase	TTGTGACCCAACTTACAT	12.7	-2
MED193_09780 cold shock family protein	CTGTCATCGCGAGGTCAT	12.8	107
MED193_03577 transketolase	CTGTCACTCACCCCTCAT	12.9	245
MED193_21941 cytochrome c family protein	ATGTCAAAAAACTGTTTT	12.9	363
MED193_08143 sugar ABC transporter permease protein	TTGTCATCTCGGTGAAAC	12.9	-100
MED193_06934 ATP-dependent RNA helicase RhlE	CTGTCACACCGCAGTCCC	12.9	62
MED193_20694 hypothetical protein	TCGTCACAGTTCCGTCAT	12.9	51
MED193_17544 glutaryl 7-ACA acylase-like protein	CTTTCAAAGTGCTTACAT	13.0	91
MED193_19214 xanthine dehydrogenase, A subunit	ATGACAATCACCTTTCAT	13.1	-18
MED193_01880 hypothetical protein	CTCTCATCGAACCGTCAT	13.3	43
MED193_07519 MraZ, putative	CTGTCAGCCTGCTGAAAC	13.4	635
MED193_17999 peptidyl-tRNA hydrolase	TGGTCATACAGCCTTAAT	13.5	67
MED193_03927 elongation factor Ts	TTGTCACAGATTTGACAT	13.9	55
MED193_04946 ribosome recycling factor	CTGTCATATTGCTGATAC	14.0	287

MED193_03797 translation initiation factor IF-2B subunit alpha	CTGTCAAAACTCCGTTAC	14.1	103
MED193_03127 2',3'-cyclic nucleotide 2'-phosphodiesterase/3'-nucleotidase bifunctional periplasmic precursor protein	TTGTCATTTTGCTGTTAT	14.3	45
MED193_06174 hydrolase, alpha/beta fold family protein	GTGTCAAGAAACTGTCAT	15.6	114
MED193_11644 ABC transporter, permease protein	CTGTCATGCAGCTTTTAT	16.6	16
MED193_06874 twin-arginine translocation protein, TatA/E family protein	CTGACATAAACCTGTCAG	16.7	159
MED193_13098 glycosyl transferase, family 25	CTGTCACCACGCCGTCCT	16.8	233
MED193_19239 histidyl-tRNA synthetase	CTGTCACTCAGCTGTTAC	17.4	149
MED193_04062 phosphate ABC transporter, periplasmic phosphate-binding protein	CTGTTACATAGCCGTCAC	17.9	71
MED193_04671 lipoyl synthase	CTGTTACGAAACTGTCAT	17.9	221
MED193_07903 SN-glycerol-3-phophate ABC transporter, periplasmic SN-glycerol-3-phosphate-binding protein	ATGTCAAAAAACTTTCAC	18.1	58
MED193_11807 DNA-binding response regulator	CTGACACAGACCTGTCAT	18.9	24
MED193_04216 HNH endonuclease family protein	CTGTCACAGGGCTGTCAT	19.5	146

Appendix 4.1 Significantly up- and downregulated proteins (p-value <0.01) in the cellular proteome of P-deplete MED193 cultures.

Protein ID	*p-value <0.01*	*-log$_{10}$ (p-value)*	*Log$_2$ (fold change)*	*Locus tag*	*Uniprot annotation*
A3XFY2	+	5.049	12.072	MED193_10161	Phosphonate ABC transporter, periplasmic phosphonate-binding protein
A3XC84	+	4.885	10.581	MED193_11293	Sugar ABC transporter, periplasmic sugar-binding protein
A3X9P6	+	4.847	10.322	MED193_01855	Putative periplasmic solute-binding protein
A3XBZ9	+	4.317	10.205	MED193_03507	Iron-binding periplasmic protein
A3X815	+	3.931	9.138	MED193_06579	Glycerophosphoryl diester phosphodiesterase
A3X3K4	+	5.327	9.101	MED193_17649	Alkylphosphonate utilization protein PhnM
A3XB37	+	4.191	8.805	MED193_22121	Phasin, PhaP
A3XBP0	+	5.106	8.525	MED193_04062	Phosphate ABC transporter, periplasmic phosphate-binding protein
A3XFY3	+	3.160	8.415	MED193_10166	Phosphonates import ATP-binding protein PhnC (EC 7.3.2.2)
A3XA99	+	3.888	8.253	MED193_00820	Transcriptional regulator/arsenate reductase
A3X8H3	+	5.343	8.240	MED193_05784	Uncharacterized protein
A3XAW5	+	4.504	8.137	MED193_04391	CaiB/BaiF family protein
A3XFW0	+	3.958	7.784	MED193_11712	N-methylproline demethylase, putative
A3X384	+	3.909	7.353	MED193_18254	UshA protein
A3XBN9	+	4.353	6.990	MED193_04057	Phosphate transport system permease protein
A3XBP2	+	5.083	6.552	MED193_04052	Phosphate transport system permease protein PstA
A3XFY0	+	2.889	6.042	MED193_10151	Phosphonate ABC transporter, permease protein
A3X844	+	2.699	5.920	MED193_06444	ABC transporter, periplasmic substrate-binding protein
A3XAA0	+	4.918	5.845	MED193_00825	Glyceraldehyde-3-phosphate dehydrogenase (EC 1.2.1.-)
A3XB41	+	5.015	5.814	MED193_22111	Polyhydroxyalkanoate depolymerase, intracellular
A3X3A1	+	3.342	5.633	MED193_18169	Uncharacterized protein
A3XC02	+	3.943	5.568	MED193_03497	ATP-binding component of transport system
A3XBP5	+	3.057	5.524	MED193_04037	Phosphate regulon transcriptional regulatory protein PhoB
A3X9J7	+	2.750	5.467	MED193_07888	sn-glycerol-3-phosphate import ATP-binding protein UgpC (EC 3.6.3.20)
A3X3R1	+	2.396	5.444	MED193_17364	S-adenosylmethionine-diacylglycerol 3-amino-3-carboxypropyltransferase
A3X8G7	+	2.176	5.352	MED193_05814	Periplasmic glucan biosynthesis protein MdoG
A3XBP1	+	4.639	5.237	MED193_04047	Phosphate import ATP-binding protein PstB (EC 7.3.2.1) (ABC phosphate transporter) (Phosphate-transporting ATPase)

A3X9J4	+	5.226	5.226	MED193_07903	SN-glycerol-3-phophate ABC transporter, periplasmic SN-glycerol-3-phosphate-binding protein
A3XBN7	+	3.427	5.224	MED193_04067	Phosphate regulon sensor histidine kinase, putative
A3X3K7	+	2.750	5.071	MED193_17644	Uncharacterized protein
A3XFW1	+	5.085	5.005	MED193_11717	Methyltransferase (EC 2.1.1.-)
A3XAQ9	+	1.363	4.895	MED193_04676	Peroxiredoxin/glutaredoxin family protein
A3XC79	+	2.346	4.757	MED193_11308	Sugar ABC transporter, ATP-binding protein
A3XFY1	+	2.917	4.747	MED193_10156	Phosphonate ABC transporter, permease protein
A3XC77	+	5.223	4.708	MED193_03127	2',3'-cyclic nucleotide 2'-phosphodiesterase/3'-nucleotidase bifunctional periplasmic protein (EC 3.1.4.16)
A3X3L3	+	3.462	4.698	MED193_17614	Alkylphosphonate utilization protein PhnI
A3XF07	+	2.903	4.683	MED193_03045	Aminomethyl transferase family protein
A3X9N9	+	3.871	4.516	MED193_01875	3',5'-cyclic adenosine monophosphate phosphodiesterase CpdA (3',5'-cyclic AMP phosphodiesterase) (cAMP phosphodiesterase) (EC 3.1.4.53)
A3X3K9	+	3.069	4.442	MED193_17634	Alkylphosphonate utilization protein PhnL
A3X3Y5	+	3.920	4.420	MED193_17004	Transcriptional regulator, LysR family protein
A3XBP3	+	5.214	4.323	MED193_04042	Phosphate-specific transport system accessory protein PhoU
A3X5J0	+	3.734	4.234	MED193_19144	Aminomethyl transferase family protein
A3X9P3	+	2.553	4.106	MED193_01870	ABC spermidine/putrescine transporter, ATPase subunit
A3XEY3	+	2.412	4.035	MED193_12163	Uncharacterized protein
A3XD08	+	3.407	4.004	MED193_09820	Metallo-beta-lactamase family protein
A3XFN8	+	2.741	3.980	MED193_12092	Uncharacterized protein
A3XAQ4	+	2.994	3.960	MED193_04696	Methyltransferase (EC 2.1.1.-)
A3X801	+	2.739	3.955	MED193_06659	Uncharacterized protein
A3X974	+	4.042	3.851	MED193_08508	Uncharacterized protein
A3XCG1	+	1.933	3.847	MED193_10908	Uncharacterized protein
A3XC01	+	2.440	3.769	MED193_03492	Metallo-beta-lactamase family protein
A3XC83	+	3.126	3.753	MED193_11288	Phosphodiesterase
A3X8B3	+	2.782	3.589	MED193_06099	Uncharacterized protein
A3X5K9	+	2.382	3.575	MED193_19059	Uncharacterized protein
A3X8H4	+	3.612	3.520	MED193_05789	Uncharacterized protein
A3XAY5	+	2.363	3.490	MED193_04296	ExoV domain protein
A3XFR1	+	2.355	3.474	MED193_11942	Alanine dehydrogenase (EC 1.4.1.1)
A3X3R3	+	2.217	3.419	MED193_17359	Metallo-phosphoesterase
A3XA54	+	3.846	3.385	MED193_01065	Uncharacterized protein

A3X975	+	2.820	3.322	MED193_08513	Uncharacterized protein
A3X8B2	+	3.512	3.294	MED193_06094	Uncharacterized protein
A3XFV8	+	2.404	3.259	MED193_11702	Oxidoreductase, FMN-binding/pyridine nucleotide-disulfideoxidoreductase
A3XEZ2	+	2.950	3.204	MED193_03105	Uncharacterized protein
A3XC17	+	2.291	3.178	MED193_03427	Uncharacterized protein
A3XB11	+	3.483	3.147	MED193_04161	Peptidoglycan binding protein, putative
A3X9K3	+	4.018	3.105	MED193_07883	Glycerophosphoryl diester phosphodiesterase, putative
A3X7R2	+	3.790	3.105	MED193_07099	Outer membrane protein OmpW
A3X6Y4	+	2.629	3.089	MED193_14527	Uncharacterized protein
A3XFY8	+	4.069	3.054	MED193_10146	Chloramphenicol acetyltransferase, putative
A3XB16	+	3.387	3.053	MED193_04146	Beta-ketoacyl synthase family protein
A3XDF8	+	1.627	2.994	MED193_13353	Uncharacterized protein
A3XB36	+	4.043	2.962	MED193_22116	Poly(3-hydroxyalkanoate) polymerase
A3X945	+	1.176	2.905	MED193_08648	Uncharacterized protein
A3XCA6	+	1.478	2.904	MED193_11193	Iron-sulfur-binding protein, RdxA/RdxB/FixG family protein
A3XFR8	+	4.631	2.872	MED193_11927	Polyphosphate kinase, putative
A3X532	+	1.285	2.856	MED193_19939	Uncharacterized protein
A3X7B2	+	1.739	2.839	MED193_13887	Peptide methionine sulfoxide reductase MsrA (Protein-methionine-S-oxide reductase) (EC 1.8.4.11) (Peptide-methionine (S)-S-oxide reductase) (Peptide Met(O) reductase)
A3XCB2	+	2.295	2.784	MED193_11133	Glycosyl hydrolase, family 25
A3X8V3	+	5.257	2.780	MED193_09113	Formate--tetrahydrofolate ligase (EC 6.3.4.3) (Formyltetrahydrofolate synthetase) (FHS) (FTHFS)
A3X8K8	+	1.758	2.749	MED193_05624	Branched-chain amino acid ABC transporter, ATP-binding protein
A3XF89	+	1.786	2.709	MED193_21691	Uncharacterized protein
A3X889	+	2.307	2.681	MED193_06209	Thioesterase family protein
A3X687	+	2.150	2.662	MED193_15757	Creatinase
A3XAC7	+	2.725	2.643	MED193_05321	Sarcosine oxidase, beta subunit family protein
A3XAE3	+	1.444	2.641	MED193_05261	Cytokinin riboside 5'-monophosphate phosphoribohydrolase (EC 3.2.2.n1)
A3X669	+	2.204	2.627	MED193_15852	Type I secretion system ATPase
A3X960	+	3.882	2.614	MED193_08583	Glutamate dehydrogenase
A3X3C8	+	4.331	2.602	MED193_18034	Uncharacterized protein
A3XFL5	+	4.810	2.599	MED193_11419	Polyamine transport protein PotA
A3XCV8	+	1.928	2.548	MED193_09175	Uncharacterized protein
A3XC90	+	2.638	2.523	MED193_11233	Universal stress protein family protein

A3XDS4	+	2.336	2.491	MED193_12748	Glutamate synthase family protein
A3XFP8	+	3.656	2.461	MED193_12017	Pyruvate kinase (EC 2.7.1.40)
A3X531	+	2.458	2.445	MED193_19934	Uncharacterized protein
A3X4R3	+	4.528	2.426	MED193_20524	Uncharacterized protein
A3XD80	+	1.679	2.407	MED193_09440	Uncharacterized protein
A3X670	+	3.355	2.395	MED193_15857	Type I secretion membrane fusion protein, HlyD family protein
A3XDK7	+	1.827	2.380	MED193_13098	Glycosyl transferase, family 25
A3XFL3	+	2.435	2.338	MED193_11409	Probable spermidine/putrescine transport system permease, component of ATP-transporter system
A3X7K4	+	5.334	2.305	MED193_07384	Uncharacterized protein
A3XC00	+	1.728	2.294	MED193_03512	Glycerol-3-phosphate regulon repressor
A3XBU3	+	1.962	2.292	MED193_03792	L-fuculose phosphate aldolase
A3X545	+	3.671	2.257	MED193_19864	1-acyl-sn-glycerol-3-phosphate acyltransferase
A3XFA3	+	2.992	2.256	MED193_21611	Magnesium transporter MgtE
A3X7F7	+	1.754	2.238	MED193_13682	Sensor histidine kinase RegB
A3XFN1	+	2.224	2.230	MED193_12097	Mandelate racemase/muconate lactonizing enzyme family protein
A3XFN2	+	2.609	2.229	MED193_12102	D-amino acid aminotransferase, putative
A3XC27	+	2.212	2.205	MED193_03367	Hemolysin-type calcium-binding region, RTX
A3XDT6	+	3.224	2.204	MED193_00725	Chloroacetaldehyde dehydrogenase
A3X946	+	2.181	2.182	MED193_08653	Methyltransferase (EC 2.1.1.-)
A3X8T4	+	2.366	2.146	MED193_07618	Uncharacterized protein
A3X3L1	+	2.655	2.123	MED193_17624	Alpha-D-ribose 1-methylphosphonate 5-phosphate C-P lyase (PRPn C-P lyase) (EC 4.7.1.1)
A3XBX4	+	4.362	2.121	MED193_03642	Cytochrome c-type biogenesis protein CcmE (Cytochrome c maturation protein E) (Heme chaperone CcmE)
A3XAZ2	+	3.673	2.120	MED193_04251	2-isopropylmalate synthase (EC 2.3.3.13)
A3XB93	+	2.213	2.092	MED193_21831	Uncharacterized protein
A3XAH9	+	2.998	2.036	MED193_05086	OsmC-like family protein
A3XC21	+	3.696	2.017	MED193_03402	Uncharacterized protein
A3XC64	+	4.356	2.005	MED193_03182	Uncharacterized protein
A3XFN0	+	3.439	1.972	MED193_11344	Arginine decarboxylase (EC 4.1.1.19)
A3XC95	+	2.937	1.938	MED193_11213	Cbb3-type cytochrome c oxidase subunit
A3XAH6	+	3.053	1.929	MED193_05071	Uncharacterized protein
A3X8H5	+	4.475	1.864	MED193_05794	Acetolactate synthase, catabolic, putative
A3X7N9	+	3.294	1.845	MED193_07214	Uncharacterized protein

A3XEZ3	+	3.616	-1.816	MED193_03110	Trigger factor (TF) (EC 5.2.1.8) (PPIase)
A3X457	+	3.742	-1.841	MED193_16639	30S ribosomal protein S3
A3X3E4	+	2.896	-1.886	MED193_17959	Integration host factor subunit beta (IHF-beta)
A3X447	+	4.000	-1.931	MED193_16689	50S ribosomal protein L5
A3XC08	+	2.930	-2.002	MED193_03477	Enoyl-CoA hydratase/isomerase family protein
A3X771	+	3.226	-2.011	MED193_14092	Arginine biosynthesis bifunctional protein ArgJ [Cleaved into: Arginine biosynthesis bifunctional protein ArgJ beta chain; Arginine biosynthesis bifunctional protein ArgJ alpha chain] [Includes: Amino-acid acetyltransferase (EC 2.3.1.1) (N-acetylglutamate synthase) (AGSase); Glutamate N-acetyltransferase (EC 2.3.1.35) (Ornithine acetyltransferase) (OATase) (Ornithine transacetylase)]
A3X520	+	2.211	-2.056	MED193_19979	Polar amino acid uptake family ABC transporter, periplasmic substrate-binding protein
A3X583	+	3.432	-2.065	MED193_19694	Uncharacterized protein
A3X422	+	3.196	-2.075	MED193_16814	Glutamate/glutamine/aspartate/asparagine ABC transporter, permease protein
A3X423	+	2.039	-2.080	MED193_16804	Uncharacterized protein
A3X456	+	5.094	-2.087	MED193_16634	50S ribosomal protein L22
A3X738	+	2.443	-2.092	MED193_14247	Glutamate synthase, large subunit
A3X9F3	+	2.154	-2.103	MED193_08108	RNA polymerase sigma factor
A3X3F1	+	2.563	-2.120	MED193_17919	tRNA (guanine-N(7)-)-methyltransferase (EC 2.1.1.33) (tRNA (guanine(46)-N(7))-methyltransferase) (tRNA(m7G46)-methyltransferase)
A3XF90	+	1.875	-2.137	MED193_21696	DNA-binding protein, putative
A3X436	+	2.981	-2.139	MED193_16739	Adenylate kinase (AK) (EC 2.7.4.3) (ATP-AMP transphosphorylase) (ATP:AMP phosphotransferase) (Adenylate monophosphate kinase)
A3X516	+	4.159	-2.172	MED193_20009	30S ribosomal protein S4
A3X7N7	+	2.030	-2.172	MED193_07204	Peptide/nickel/opine uptake family ABC transporter, permease protein
A3X640	+	4.880	-2.175	MED193_16002	30S ribosomal protein S7
A3X7L7	+	2.816	-2.175	MED193_07319	S1 RNA binding domain protein
A3XFT8	+	1.818	-2.177	MED193_11837	2`,3`-cyclic-nucleotide 2`-phosphodiesterase, putative
A3XEU2	+	2.360	-2.184	MED193_12338	Uncharacterized protein
A3XDE0	+	1.810	-2.189	MED193_13448	Polyamine ABC transporter, permease protein
A3X420	+	2.879	-2.207	MED193_16824	Glutamate/glutamine/aspartate/asparagine ABC transporter, ATP-binding protein
A3X433	+	3.967	-2.238	MED193_16764	50S ribosomal protein L17
A3X444	+	4.362	-2.255	MED193_16709	50S ribosomal protein L18
A3XC67	+	4.942	-2.278	MED193_03172	30S ribosomal protein S6
A3X434	+	2.687	-2.279	MED193_16749	30S ribosomal protein S13
A3X6B4	+	3.254	-2.283	MED193_15612	Efflux transporter, RND family, MFP subunit

A3X8M8	+	2.442	-2.286	MED193_05514	Dihydropyrimidinase (EC 3.5.2.2)
A3X3Z2	+	2.511	-2.286	MED193_16969	Uncharacterized protein
A3X609	+	3.019	-2.309	MED193_16137	Uncharacterized protein
A3X653	+	2.887	-2.311	MED193_15922	Uncharacterized protein
A3XBR8	+	4.173	-2.316	MED193_03922	30S ribosomal protein S2
A3X424	+	3.467	-2.320	MED193_16809	Glutamate/glutamine/aspartate/asparagine ABC transporter, periplasmic substrate-binding protein
A3X9Z2	+	2.421	-2.332	MED193_01355	TRAP dicarboxylate transporter, DctP subunit, putative
A3XFS7	+	1.875	-2.337	MED193_11877	Cold shock family protein
A3X7A3	+	2.124	-2.345	MED193_13942	L-threonine dehydratase (EC 4.3.1.19) (Threonine deaminase)
A3X8N3	+	2.183	-2.351	MED193_05484	ABC transporter, periplasmic substrate-binding protein
A3X4P9	+	3.032	-2.358	MED193_20609	Uncharacterized protein
A3XCR4	+	2.382	-2.367	MED193_10378	Sugar ABC transporter, periplasmic sugar-binding protein
A3X3E3	+	4.051	-2.454	MED193_17954	30S ribosomal protein S1
A3X6B8	+	2.092	-2.459	MED193_15587	Uncharacterized protein
A3XCF3	+	1.974	-2.464	MED193_10953	Ribosomal RNA small subunit methyltransferase E (EC 2.1.1.193)
A3X473	+	2.908	-2.486	MED193_16549	ATP:cob(I)alamin adenosyltransferase, putative
A3X5W6	+	2.463	-2.489	MED193_16377	DNA-directed RNA polymerase subunit omega (RNAP omega subunit) (EC 2.7.7.6) (RNA polymerase omega subunit) (Transcriptase subunit omega)
A3X3N1	+	2.540	-2.493	MED193_17519	Uncharacterized protein
A3X446	+	4.438	-2.507	MED193_16699	30S ribosomal protein S8
A3X3H0	+	1.334	-2.515	MED193_17819	Peptidyl-prolyl cis-trans isomerase (EC 5.2.1.8)
A3XFQ6	+	4.057	-2.517	MED193_12002	50S ribosomal protein L20
A3X582	+	1.872	-2.524	MED193_19689	Uncharacterized protein
A3XBS7	+	2.417	-2.537	MED193_03877	50S ribosomal protein L27
A3X4D1	+	2.582	-2.562	MED193_21199	Uncharacterized protein
A3XAP5	+	4.233	-2.570	MED193_04741	50S ribosomal protein L13
A3XBE9	+	2.077	-2.572	MED193_22606	Uncharacterized protein
A3XCQ3	+	2.091	-2.574	MED193_10443	Uncharacterized protein
A3X5G9	+	1.614	-2.587	MED193_19259	Vitamin B12-dependent ribonucleotide reductase (EC 1.17.4.1)
A3XB89	+	1.273	-2.603	MED193_21866	Amidase (EC 3.5.1.4)
A3X3H6	+	3.045	-2.619	MED193_17789	Esterase EstC, putative
A3X7Z8	+	4.047	-2.627	MED193_06664	Translation initiation factor IF-3
A3X462	+	4.502	-2.642	MED193_16624	50S ribosomal protein L2
A3X9J5	+	2.109	-2.659	MED193_07908	Transcriptional regulator, LysR family protein

A3X464	+	4.063	-2.659	MED193_16599	30S ribosomal protein S10
A3X334	+	2.865	-2.661	MED193_18509	ABC Fe3+-siderophores transporter, periplasmic binding protein
A3X6S2	+	1.640	-2.664	MED193_14857	Uncharacterized protein
A3XAP7	+	4.711	-2.665	MED193_04726	Polyphosphate kinase 2, putative
A3X512	+	1.266	-2.675	MED193_20039	Histidinol-phosphate aminotransferase (EC 2.6.1.9) (Imidazole acetol-phosphate transaminase)
A3XBI4	+	2.058	-2.702	MED193_22426	Beta-N-acetylhexosaminidase (EC 3.2.1.52)
A3X619	+	4.693	-2.703	MED193_16092	50S ribosomal protein L19
A3XB53	+	2.099	-2.711	MED193_22036	Putative TonB protein
A3XAP4	+	3.337	-2.714	MED193_04736	30S ribosomal protein S9
A3X4M2	+	1.488	-2.727	MED193_20739	Strictosidine synthase family protein
A3X458	+	4.280	-2.730	MED193_16644	50S ribosomal protein L16
A3X445	+	4.290	-2.756	MED193_16694	30S ribosomal protein S14
A3XB45	+	1.930	-2.765	MED193_22076	FecB2
A3X649	+	3.387	-2.792	MED193_15952	50S ribosomal protein L10
A3XDH4	+	3.440	-2.798	MED193_13248	30S ribosomal protein S20
A3X8R8	+	2.012	-2.816	MED193_07698	Glycine betaine/proline ABC transporter, ATP-binding protein
A3X616	+	3.617	-2.827	MED193_16127	30S ribosomal protein S16
A3X455	+	3.754	-2.828	MED193_16629	30S ribosomal protein S19
A3X639	+	4.399	-2.840	MED193_15997	30S ribosomal protein S12
A3X648	+	3.120	-2.844	MED193_15947	50S ribosomal protein L1
A3X463	+	5.358	-2.851	MED193_16609	50S ribosomal protein L4
A3XE46	+	2.522	-2.854	MED193_00190	Putative extracellular solute-binding protein
A3X448	+	4.123	-2.887	MED193_16679	50S ribosomal protein L14
A3X647	+	4.825	-2.887	MED193_15942	50S ribosomal protein L11
A3X3D4	+	4.024	-2.894	MED193_18009	50S ribosomal protein L25 (General stress protein CTC)
A3X465	+	3.959	-2.912	MED193_16604	50S ribosomal protein L3
A3X3M9	+	2.545	-2.936	MED193_17524	Uncharacterized protein
A3XDD9	+	1.837	-2.959	MED193_13443	ABC polyamine/opine transporter, inner membrane subunit
A3X736	+	5.308	-2.997	MED193_14287	DNA-binding protein HU
A3XC66	+	3.177	-3.021	MED193_03167	30S ribosomal protein S18
A3X8N2	+	1.557	-3.023	MED193_05509	ABC transporter, ATP-binding protein
A3X7P3	+	3.092	-3.023	MED193_07184	Acetylornithine deacetylase (EC 3.5.1.-) (EC 3.5.1.16)
A3X449	+	4.664	-3.034	MED193_16684	50S ribosomal protein L24
A3X8Z9	+	4.478	-3.037	MED193_08893	Sulfate transporter family protein

A3XC71	+	5.262	-3.041	MED193_03162	50S ribosomal protein L9
A3X9G3	+	2.927	-3.062	MED193_08078	Cyclopropane-fatty-acyl-phospholipid synthase, putative
A3X7D8	+	3.193	-3.066	MED193_13777	FxsA
A3XDK9	+	3.990	-3.099	MED193_13063	30S ribosomal protein S15
A3XBS6	+	3.442	-3.120	MED193_03872	50S ribosomal protein L21
A3XFC0	+	3.653	-3.155	MED193_21546	50S ribosomal protein L33
A3X3N4	+	3.235	-3.159	MED193_17499	Hemin degrading factor
A3XDP9	+	3.276	-3.160	MED193_12863	Uncharacterized protein
A3XDP5	+	2.999	-3.167	MED193_12893	Phosphoglycerate mutase family protein
A3XC74	+	1.467	-3.170	MED193_03137	Uncharacterized protein
A3X441	+	4.578	-3.191	MED193_16714	30S ribosomal protein S5
A3X450	+	3.654	-3.216	MED193_16669	30S ribosomal protein S17
A3XAT0	+	2.283	-3.240	MED193_04576	GTPase HflX (GTP-binding protein HflX)
A3X438	+	4.265	-3.272	MED193_16729	50S ribosomal protein L15
A3X460	+	3.572	-3.283	MED193_16614	50S ribosomal protein L23
A3X435	+	3.587	-3.303	MED193_16754	30S ribosomal protein S11
A3X5F0	+	1.373	-3.323	MED193_19344	Extracellular solute-binding protein, family 5
A3X442	+	4.081	-3.409	MED193_16719	50S ribosomal protein L30
A3X8M7	+	1.614	-3.424	MED193_05534	Pyridine nucleotide-disulphide oxidoreductase family protein
A3X419	+	2.098	-3.465	MED193_16819	Glutamate/glutamine/aspartate/asparagine ABC transporter, permease protein
A3X4Q1	+	4.064	-3.472	MED193_20599	50S ribosomal protein L28
A3X8L5	+	1.796	-3.525	MED193_05574	Uncharacterized protein
A3XB35	+	2.768	-3.576	MED193_22136	Aminotransferase, DegT/DnrJ/EryC1/StrS family protein
A3X752	+	3.103	-3.598	MED193_14187	Ribosome hibernation promoting factor (HPF)
A3X443	+	3.578	-3.607	MED193_16704	50S ribosomal protein L6
A3XF76	+	3.444	-3.619	MED193_02685	Methionine synthase I (Fragment)
A3XFS4	+	4.459	-3.671	MED193_11912	30S ribosomal protein S21
A3X618	+	2.486	-3.699	MED193_16087	50S ribosomal protein L31
A3XAD4	+	3.140	-3.750	MED193_05296	Uncharacterized protein
A3X9H3	+	4.238	-3.795	MED193_08018	ABC ferric siderophore transporter, ATPase subunit
A3X4R1	+	1.061	-3.812	MED193_20539	Uncharacterized protein
A3XDR6	+	4.810	-3.851	MED193_12793	Ferric iron ABC transporter, periplasmic ferric iron-binding protein
A3X453	+	2.038	-3.887	MED193_16664	50S ribosomal protein L29
A3XFQ1	+	3.146	-4.147	MED193_12007	50S ribosomal protein L35

A3X8M6	+	1.834	-4.275	MED193_05529	Dihydropyrimidine dehydrogenase (EC 1.3.1.1)
A3X9H0	+	3.636	-4.276	MED193_08043	TonB dependent-iron siderophore receptor
A3XCY8	+	3.886	-4.309	MED193_09915	Uncharacterized protein
A3XDT0	+	1.443	-4.400	MED193_00745	Probable 1,4-butanediol diacrylate esterase
A3X744	+	3.469	-4.794	MED193_14232	Glutamate synthase, small subunit
A3XAX2	+	4.969	-4.795	MED193_04356	Uncharacterized protein
A3X3D9	+	3.600	-5.302	MED193_17984	Uncharacterized protein
A3X413	+	4.219	-5.322	MED193_16864	50S ribosomal protein L34
A3XCK6	+	2.667	-5.440	MED193_10693	Uncharacterized protein
A3XB46	+	2.988	-5.485	MED193_22061	Iron(III) dicitrate ABC transporter (ATP-binding protein)
A3X3N3	+	3.933	-5.836	MED193_17514	MotA/TolQ/ExbB proton channel family protein
A3X586	+	3.219	-5.990	MED193_19659	Uncharacterized protein
A3X3N2	+	6.289	-6.191	MED193_17509	Uncharacterized protein
A3X9G8	+	5.146	-6.559	MED193_08033	Putative ABC transporter, periplasmic Fe+3 siderophore binding protein
A3X3N7	+	3.269	-7.507	MED193_17494	Putative hemin binding periplasmic transmembrane protein
A3X9H4	+	4.369	-7.607	MED193_08013	TonB dependent iron siderophore receptor
A3X3Q9	+	3.629	-7.682	MED193_17374	Uncharacterized protein
A3X8S2	+	4.617	-9.014	MED193_07678	Uncharacterized protein
A3X587	+	4.790	-9.020	MED193_19664	Lipoprotein, putative
A3X3N5	+	5.757	-9.172	MED193_17504	Putative Hemin receptor protein HmuR
A3XB54	+	4.021	-9.776	MED193_22031	Outer membrane protein

Appendix 4.2 Significantly up- and downregulated proteins (p-value <0.01) in the exoproteome of P-deplete MED193 cultures.

Protein ID	*p-value <0.01*	*-log_{10} (p-value)*	*Log_2(fold change)*	*Locus tag*	*Uniprot annotation*
A3XC84	+	4.893	9.972	MED193_11293	Sugar ABC transporter, periplasmic sugar-binding protein
A3X9P6	+	3.293	9.971	MED193_01855	Putative periplasmic solute-binding protein
A3XFY2	+	5.268	9.209	MED193_10161	Phosphonate ABC transporter, periplasmic phosphonate-binding protein
A3XBZ9	+	3.212	8.586	MED193_03507	Iron-binding periplasmic protein
A3X815	+	4.279	7.770	MED193_06579	Glycerophosphoryl diester phosphodiesterase
A3X8H3	+	4.125	7.716	MED193_05784	Uncharacterized protein

A3X3K4	+	3.699	7.380	MED193_17649	Alkylphosphonate utilization protein PhnM
A3XBP0	+	5.487	6.725	MED193_04062	Phosphate ABC transporter, periplasmic phosphate-binding protein
A3XBP1	+	2.784	6.715	MED193_04047	Phosphate import ATP-binding protein PstB (EC 7.3.2.1) (ABC phosphate transporter) (Phosphate-transporting ATPase)
A3XAK2	+	3.129	5.886	MED193_04966	Oligopeptide/dipeptide ABC transporter, periplasmic substrate-binding protein
A3X8H4	+	6.033	5.857	MED193_05789	Uncharacterized protein
A3X384	+	2.417	5.641	MED193_18254	UshA protein
A3XC77	+	7.394	5.490	MED193_03127	2',3'-cyclic nucleotide 2'-phosphodiesterase/3'-nucleotidase bifunctional periplasmic protein (EC 3.1.4.16)
A3X8G7	+	2.802	5.266	MED193_05814	Periplasmic glucan biosynthesis protein MdoG
A3X9J4	+	5.737	5.065	MED193_07903	SN-glycerol-3-phophate ABC transporter, periplasmic SN-glycerol-3-phosphate-binding protein
A3XAA0	+	2.621	4.655	MED193_00825	Glyceraldehyde-3-phosphate dehydrogenase (EC 1.2.1.-)
A3XCG1	+	3.594	4.653	MED193_10908	Uncharacterized protein
A3X3K7	+	2.642	4.628	MED193_17644	Uncharacterized protein
A3XC90	+	4.816	4.554	MED193_11233	Universal stress protein family protein
A3XBP3	+	4.352	4.541	MED193_04042	Phosphate-specific transport system accessory protein PhoU
A3XA99	+	4.347	4.425	MED193_00820	Transcriptional regulator/arsenate reductase
A3X5K9	+	4.126	4.389	MED193_19059	Uncharacterized protein
A3XCL7	+	2.546	4.277	MED193_10618	Uncharacterized protein
A3XA72	+	1.481	4.260	MED193_00965	Uncharacterized protein
A3XE74	+	2.606	4.171	MED193_00045	TRAP dicarboxylate transporter, DctP subunit
A3XF89	+	1.388	4.150	MED193_21691	Uncharacterized protein
A3XF83	+	2.325	4.048	MED193_21716	Uncharacterized protein
A3XB36	+	2.369	3.932	MED193_22116	Poly(3-hydroxyalkanoate) polymerase
A3XAH2	+	2.481	3.918	MED193_05106	Uncharacterized protein
A3XC01	+	2.554	3.823	MED193_03492	Metallo-beta-lactamase family protein
A3XFK5	+	5.292	3.704	MED193_11424	Spermidine/putrescine ABC transporter, spermidine/putrescine-binding protein
A3XAW5	+	1.931	3.701	MED193_04391	CaiB/BaiF family protein
A3X3A1	+	1.583	3.568	MED193_18169	Uncharacterized protein
A3X7R2	+	3.202	3.441	MED193_07099	Outer membrane protein OmpW
A3XFY3	+	3.211	3.430	MED193_10166	Phosphonates import ATP-binding protein PhnC (EC 7.3.2.2)
A3XD38	+	4.935	3.400	MED193_09675	Universal stress family protein
A3X975	+	3.439	3.352	MED193_08513	Uncharacterized protein

A3X7B2	+	1.724	3.341	MED193_13887	Peptide methionine sulfoxide reductase MsrA (Protein-methionine-S-oxide reductase) (EC 1.8.4.11) (Peptide-methionine (S)-S-oxide reductase) (Peptide Met(O) reductase)
A3XD08	+	7.023	3.322	MED193_09820	Metallo-beta-lactamase family protein
A3XFL5	+	2.718	3.305	MED193_11419	Polyamine transport protein PotA
A3X6Y4	+	2.887	3.269	MED193_14527	Uncharacterized protein
A3X8T4	+	4.176	3.240	MED193_07618	Uncharacterized protein
A3XAG8	+	3.033	3.213	MED193_05121	Uncharacterized protein
A3XDT0	+	1.954	3.113	MED193_00745	Probable 1,4-butanediol diacrylate esterase
A3XD56	+	1.958	3.059	MED193_09570	Sugar ABC transporter, periplasmic sugar-binding protein
A3X8B4	+	4.727	3.038	MED193_06084	Uncharacterized protein
A3X974	+	2.955	2.902	MED193_08508	Uncharacterized protein
A3X532	+	1.348	2.879	MED193_19939	Uncharacterized protein
A3XAQ9	+	2.856	2.794	MED193_04676	Peroxiredoxin/glutaredoxin family protein
A3XBN7	+	1.401	2.773	MED193_04067	Phosphate regulon sensor histidine kinase, putative
A3XBZ8	+	2.795	2.702	MED193_03527	ErfK/YbiS/YcfS/YnhG family protein
A3XC17	+	2.312	2.617	MED193_03427	Uncharacterized protein
A3XDL5	+	3.711	2.595	MED193_13043	Uncharacterized protein
A3XC83	+	1.741	2.567	MED193_11288	Phosphodiesterase
A3X6L5	+	3.230	2.520	MED193_15112	Cytochrome c family protein
A3XCK7	+	2.050	2.496	MED193_10648	Thiol:disulfide interchange protein, putative
A3X3K6	+	1.996	2.465	MED193_17639	Ribose 1,5-bisphosphate phosphokinase PhnN (EC 2.7.4.23) (Ribose 1,5-bisphosphokinase)
A3X8I2	+	1.581	2.465	MED193_05759	Thioredoxin SoxW
A3XG05	+	4.543	2.454	MED193_10041	Bacterial extracellular solute-binding protein, family 7
A3XB37	+	2.256	2.417	MED193_22121	Phasin, PhaP
A3XAJ3	+	1.628	2.389	MED193_04996	Transglycosylase SLT domain protein
A3X9J7	+	1.899	2.345	MED193_07888	sn-glycerol-3-phosphate import ATP-binding protein UgpC (EC 3.6.3.20)
A3XF02	+	2.105	2.329	MED193_03065	Uncharacterized protein
A3X8T8	+	3.543	2.313	MED193_07608	Uncharacterized protein
A3XA73	+	2.283	2.253	MED193_00970	Uncharacterized protein
A3X7G0	+	1.802	2.239	MED193_13647	Uncharacterized protein
A3XCW5	+	2.109	2.238	MED193_09160	TonB domain protein, putative
A3X3R1	+	1.944	2.217	MED193_17364	S-adenosylmethionine-diacylglycerol 3-amino-3-carboxypropyltransferase
A3XB23	+	1.562	2.184	MED193_22181	Uncharacterized protein

A3X9N9	+	2.843	2.172	MED193_01875	3',5'-cyclic adenosine monophosphate phosphodiesterase CpdA (3',5'-cyclic AMP phosphodiesterase) (cAMP phosphodiesterase) (EC 3.1.4.53)
A3XBU1	+	1.441	2.112	MED193_03797	Methylthioribose-1-phosphate isomerase (M1Pi) (MTR-1-P isomerase) (EC 5.3.1.23) (S-methyl-5-thioribose-1-phosphate isomerase)
A3X3J2	+	2.264	2.082	MED193_17714	Oligopeptide ABC transporter, periplasmic oligopeptide-binding protein
A3X4R3	+	2.718	2.028	MED193_20524	Uncharacterized protein
A3X7S8	+	3.143	1.919	MED193_07019	Uncharacterized protein
A3X8I4	+	4.325	1.862	MED193_05734	Sulfur oxidation B protein
A3X9J0	+	3.618	1.782	MED193_07938	Oligopeptide/dipeptide ABC transporter, periplasmic substrate-binding protein
A3XC15	+	3.269	-1.704	MED193_03437	Dihydrolipoyl dehydrogenase (EC 1.8.1.4)
A3XBV5	+	4.174	-1.705	MED193_03727	Anthranilate synthase component 1 (EC 4.1.3.27)
A3XB88	+	3.314	-1.711	MED193_21861	NAD kinase (EC 2.7.1.23)
A3X7B0	+	3.327	-1.714	MED193_13877	Phosphate acetyltransferase (EC 2.3.1.8)
A3XD40	+	3.169	-1.716	MED193_09640	Cold shock family protein
A3X4L9	+	5.213	-1.721	MED193_20764	Fructose-bisphosphate aldolase (EC 4.1.2.13)
A3XDK6	+	3.087	-1.734	MED193_13093	Polyribonucleotide nucleotidyltransferase (EC 2.7.7.8) (Polynucleotide phosphorylase) (PNPase)
A3X4W5	+	3.158	-1.741	MED193_20284	Adenylyl-sulfate kinase (EC 2.7.1.25) (APS kinase) (ATP adenosine-5'-phosphosulfate 3'-phosphotransferase) (Adenosine-5'-phosphosulfate kinase)
A3XBN0	+	3.310	-1.754	MED193_04117	Branched-chain amino acid ABC transporter, ATP-binding protein
A3X577	+	2.897	-1.756	MED193_19714	Oxidoreductase, aldo/keto reductase family protein
A3XB22	+	3.738	-1.758	MED193_22201	Valine--tRNA ligase (EC 6.1.1.9) (Valyl-tRNA synthetase) (ValRS)
A3X5U1	+	3.630	-1.765	MED193_18639	Uncharacterized protein
A3XCM7	+	3.649	-1.775	MED193_10553	Succinate--CoA ligase [ADP-forming] subunit alpha (EC 6.2.1.5) (Succinyl-CoA synthetase subunit alpha) (SCS-alpha)
A3X7S7	+	4.414	-1.778	MED193_07014	NADH-quinone oxidoreductase (EC 1.6.5.11)
A3XBF4	+	4.190	-1.782	MED193_22571	MazG family protein
A3XF67	+	2.543	-1.788	MED193_02725	C4-dicarboxylate transport transcriptional regulatory protein DctD
A3X8Y2	+	3.056	-1.789	MED193_08968	TldD/PmbA family protein
A3XFN2	+	3.618	-1.805	MED193_12102	D-amino acid aminotransferase, putative
A3X655	+	3.095	-1.806	MED193_15932	Transcription termination/antitermination protein NusG
A3X7L1	+	3.859	-1.811	MED193_07359	Cobalt chelatase, CobS subunit
A3XFN8	+	2.951	-1.823	MED193_12092	Uncharacterized protein
A3XAV5	+	3.205	-1.828	MED193_04446	Metal-dependent carboxypeptidase (EC 3.4.17.19)
A3X791	+	2.295	-1.836	MED193_14007	ErfK/YbiS/YcfS/YnhG family protein/Tat domain protein

A3XA21	+	4.598	-1.856	MED193_01210	GDP-mannose 4,6-dehydratase (EC 4.2.1.47) (GDP-D-mannose dehydratase)
A3X911	+	2.831	-1.863	MED193_08833	Glycine--tRNA ligase beta subunit (EC 6.1.1.14) (Glycyl-tRNA synthetase beta subunit) (GlyRS)
A3X6W3	+	2.883	-1.865	MED193_14622	Leucine--tRNA ligase (EC 6.1.1.4) (Leucyl-tRNA synthetase) (LeuRS)
A3X468	+	2.996	-1.870	MED193_16017 MED193_16584	Elongation factor Tu (EF-Tu)
A3X907	+	3.452	-1.879	MED193_08858	Peptidoglycan binding domain protein
A3XDG1	+	2.654	-1.887	MED193_13323	Phosphoserine aminotransferase (EC 2.6.1.52)
A3X624	+	2.346	-1.890	MED193_16067	Acetyltransferase, GNAT family protein
A3XDM2	+	2.269	-1.891	MED193_13033	4-hydroxy-tetrahydrodipicolinate reductase (HTPA reductase) (EC 1.17.1.8)
A3X7L5	+	2.941	-1.910	MED193_07334	Peptidase T (EC 3.4.11.4)
A3X8S2	+	2.417	-1.911	MED193_07678	Uncharacterized protein
A3XB90	+	2.736	-1.913	MED193_21851	Serine hydroxymethyltransferase (SHMT) (Serine methylase) (EC 2.1.2.1)
A3XFS1	+	2.521	-1.923	MED193_11897	Ribonuclease T2 family protein
A3X516	+	4.153	-1.947	MED193_20009	30S ribosomal protein S4
A3X465	+	3.253	-1.949	MED193_16604	50S ribosomal protein L3
A3XAL9	+	1.882	-1.962	MED193_04866	DNA ligase (EC 6.5.1.2) (Polydeoxyribonucleotide synthase [NAD(+)])
A3XFQ2	+	2.049	-1.963	MED193_11982	Phenylalanine--tRNA ligase alpha subunit (EC 6.1.1.20) (Phenylalanyl-tRNA synthetase alpha subunit) (PheRS)
A3X651	+	3.003	-1.971	MED193_15962	DNA-directed RNA polymerase subunit beta (RNAP subunit beta) (EC 2.7.7.6) (RNA polymerase subunit beta) (Transcriptase subunit beta)
A3XFR0	+	2.846	-1.976	MED193_11977	Phenylalanine--tRNA ligase beta subunit (EC 6.1.1.20) (Phenylalanyl-tRNA synthetase beta subunit) (PheRS)
A3X429	+	1.979	-1.988	MED193_16774	Phospho-2-dehydro-3-deoxyheptonate aldolase (EC 2.5.1.54)
A3X591	+	3.755	-1.989	MED193_19639	Uncharacterized protein
A3XCZ6	+	1.689	-2.011	MED193_09850	Rod shape-determining protein MreB
A3X727	+	3.015	-2.023	MED193_14332	Carnitinyl-CoA dehydratase (EC 4.2.1.-)
A3X692	+	4.478	-2.032	MED193_15742	Succinate-semialdehyde dehydrogenase
A3X4Q9	+	3.277	-2.033	MED193_20554	Acetylornithine aminotransferase (ACOAT) (EC 2.6.1.11)
A3X4T9	+	5.269	-2.043	MED193_20409	Aspartate--tRNA(Asp/Asn) ligase (EC 6.1.1.23) (Aspartyl-tRNA synthetase) (AspRS) (Non-discriminating aspartyl-tRNA synthetase) (ND-AspRS)
A3X498	+	3.231	-2.043	MED193_16434	GTPase Era
A3XBW3	+	1.848	-2.045	MED193_03697	Cyclic pyranopterin monophosphate synthase (EC 4.6.1.17) (Molybdenum cofactor biosynthesis protein C)

A3XDH0	+	2.335	-2.045	MED193_13273	Ubiquinone/menaquinone biosynthesis C-methyltransferase UbiE (EC 2.1.1.163) (EC 2.1.1.201) (2-methoxy-6-polyprenyl-1,4-benzoquinol methylase) (Demethylmenaquinone methyltransferase)
A3X3N7	+	3.606	-2.048	MED193_17494	Putative hemin binding periplasmic transmembrane protein
A3X3L6	+	2.188	-2.054	MED193_17599	Transcriptional regulator, GntR family protein
A3XC38	+	3.627	-2.055	MED193_03322	Acetyltransferase component of pyruvate dehydrogenase complex (EC 2.3.1.12)
A3XDG4	+	1.716	-2.059	MED193_13288	DNA binding protein, putative
A3X7S4	+	2.081	-2.062	MED193_07044	NADH-quinone oxidoreductase subunit D (EC 1.6.5.11) (NADH dehydrogenase I subunit D) (NDH-1 subunit D)
A3X976	+	1.462	-2.078	MED193_08493	Riboflavin biosynthesis protein RibD [Includes: Diaminohydroxyphosphoribosylaminopyrimidine deaminase (DRAP deaminase) (EC 3.5.4.26) (Riboflavin-specific deaminase); 5-amino-6-(5-phosphoribosylamino)uracil reductase (EC 1.1.1.193) (HTP reductase)]
A3X675	+	1.501	-2.083	MED193_15832	Nitrogen regulatory protein P-II
A3X3Q2	+	2.922	-2.087	MED193_17409	Putative sulfatase
A3X5Z2	+	2.360	-2.089	MED193_16247	Aminotransferase, classes I and II
A3XBH7	+	2.073	-2.090	MED193_22466	3-oxoacyl-[acyl-carrier-protein] synthase 3 (EC 2.3.1.180) (3-oxoacyl-[acyl-carrier-protein] synthase III) (Beta-ketoacyl-ACP synthase III) (KAS III)
A3X581	+	1.727	-2.094	MED193_19684	Methionine--tRNA ligase (EC 6.1.1.10) (Methionyl-tRNA synthetase) (MetRS)
A3XC36	+	2.465	-2.094	MED193_03337	Pyruvate dehydrogenase E1 component subunit alpha (EC 1.2.4.1)
A3X619	+	3.376	-2.096	MED193_16092	50S ribosomal protein L19
A3XCZ4	+	2.317	-2.108	MED193_09890	Peptidyl-dipeptidase, putative
A3X5J5	+	2.661	-2.114	MED193_19124	2-hydroxyacid dehydrogenase (EC 1.1.1.272)
A3XAY6	+	1.411	-2.117	MED193_04301	UPF0145 protein MED193_04301
A3X3F1	+	2.584	-2.123	MED193_17919	tRNA (guanine-N(7)-)-methyltransferase (EC 2.1.1.33) (tRNA (guanine(46)-N(7))-methyltransferase) (tRNA(m7G46)-methyltransferase)
A3X736	+	4.165	-2.128	MED193_14287	DNA-binding protein HU
A3X8Q9	+	2.349	-2.139	MED193_07758	Phosphomethylpyrimidine kinase
A3XAP5	+	4.087	-2.140	MED193_04741	50S ribosomal protein L13
A3X5K3	+	3.665	-2.143	MED193_19079	Isocitrate dehydrogenase [NADP] (EC 1.1.1.42) (Oxalosuccinate decarboxylase)
A3X7N5	+	2.920	-2.143	MED193_07229	NAD(P) transhydrogenase subunit alpha (EC 7.1.1.1)
A3X649	+	1.890	-2.146	MED193_15952	50S ribosomal protein L10
A3X9B6	+	3.021	-2.150	MED193_08293	O-acetylhomoserine aminocarboxypropyltransferase
A3X3C9	+	3.066	-2.152	MED193_18039	Ribosome-binding ATPase YchF

A3XCN4	+	4.277	-2.154	MED193_10543	Succinate--CoA ligase [ADP-forming] subunit beta (EC 6.2.1.5) (Succinyl-CoA synthetase subunit beta) (SCS-beta)
A3X7H0	+	1.323	-2.161	MED193_13607	HemY domain protein
A3XAV3	+	3.907	-2.162	MED193_04456	tRNA (cytidine/uridine-2'-O-)-methyltransferase TrmJ (EC 2.1.1.200) (tRNA (cytidine(32)/uridine(32)-2'-O)-methyltransferase) (tRNA Cm32/Um32 methyltransferase)
A3X4U1	+	4.084	-2.166	MED193_20394	Carbamoyl-phosphate synthase large chain (EC 6.3.5.5) (Carbamoyl-phosphate synthetase ammonia chain)
A3XFH8	+	1.702	-2.166	MED193_11579	Soluble pyridine nucleotide transhydrogenase (EC 1.6.1.1)
A3XDZ5	+	2.083	-2.169	MED193_00440	Uncharacterized protein
A3X768	+	1.549	-2.174	MED193_14122	Chaperone protein DnaJ
A3XAJ1	+	1.368	-2.176	MED193_05026	ADP-dependent (S)-NAD(P)H-hydrate dehydratase (EC 4.2.1.136) (ADP-dependent NAD(P)HX dehydratase)
A3X6T0	+	1.464	-2.182	MED193_14802	Uncharacterized protein
A3XDN1	+	3.356	-2.182	MED193_12973	Deoxyribose-phosphate aldolase (EC 4.1.2.4)
A3X926	+	1.340	-2.182	MED193_08748	Carbamoyl-phosphate synthase small chain (EC 6.3.5.5) (Carbamoyl-phosphate synthetase glutamine chain)
A3XFA8	+	1.282	-2.186	MED193_21586	Oxidoreductase, zinc-binding dehydrogenase family protein
A3XAH0	+	2.714	-2.196	MED193_05116	Lipid A biosynthesis lauroyl acyltransferase, putative
A3X432	+	4.146	-2.202	MED193_16759	DNA-directed RNA polymerase subunit alpha (RNAP subunit alpha) (EC 2.7.7.6) (RNA polymerase subunit alpha) (Transcriptase subunit alpha)
A3X6I1	+	2.206	-2.202	MED193_15272	UDP-N-acetylglucosamine 1-carboxyvinyltransferase (EC 2.5.1.7) (Enoylpyruvate transferase) (UDP-N-acetylglucosamine enolpyruvyl transferase) (EPT)
A3X5F4	+	1.740	-2.207	MED193_19339	Transcriptional regulator
A3XAW4	+	1.500	-2.209	MED193_04396	Iron-sulfur cluster-binding protein
A3XDH4	+	2.116	-2.212	MED193_13248	30S ribosomal protein S20
A3X3D4	+	5.433	-2.216	MED193_18009	50S ribosomal protein L25 (General stress protein CTC)
A3X482	+	4.248	-2.226	MED193_16524	3-hydroxybutyryl-CoA dehydrogenase (EC 1.1.1.157)
A3XCM8	+	3.062	-2.244	MED193_10558	2-oxoglutarate dehydrogenase, E1 component
A3XAS1	+	1.425	-2.251	MED193_04611	Nitrogen regulation protein NtrC
A3XAQ2	+	3.571	-2.263	MED193_04706	GMP synthase [glutamine-hydrolyzing] (EC 6.3.5.2) (GMP synthetase) (Glutamine amidotransferase)
A3XCK0	+	1.298	-2.264	MED193_10708	Decaprenyl diphosphate synthase
A3X932	+	2.165	-2.266	MED193_08728	Cytochrome c oxidase subunit 1 (EC 1.9.3.1)

A3X7J5	+	2.029	-2.268	MED193_07429	D-alanine--D-alanine ligase (EC 6.3.2.4) (D-Ala-D-Ala ligase) (D-alanylalanine synthetase)
A3XEM5	+	3.026	-2.274	MED193_12673	Uncharacterized protein
A3XDF6	+	2.564	-2.281	MED193_13343	L-asparaginase, thermolabile family protein
A3XBC1	+	3.707	-2.281	MED193_22746	Ribonuclease D (RNase D) (EC 3.1.13.5)
A3X431	+	1.402	-2.282	MED193_16784	ATPase, AAA family protein
A3X3B0	+	1.780	-2.285	MED193_18124	Uncharacterized protein
A3XBZ5	+	1.654	-2.288	MED193_03537	Transcriptional regulator, LysR family protein
A3XEN2	+	4.327	-2.300	MED193_12663	Uncharacterized protein
A3X8J3	+	3.244	-2.307	MED193_05694	ATP-dependent Clp protease ATP-binding subunit ClpX
A3X456	+	3.347	-2.316	MED193_16634	50S ribosomal protein L22
A3X848	+	2.211	-2.320	MED193_06419	Uncharacterized protein
A3X8V1	+	3.109	-2.327	MED193_07548	Pyruvate carboxylase (EC 6.4.1.1)
A3XFY5	+	2.175	-2.328	MED193_10131	Iron-sulfur cluster carrier protein
A3X6I3	+	1.597	-2.331	MED193_15282	Histidinol dehydrogenase (HDH) (EC 1.1.1.23)
A3X5L9	+	1.997	-2.338	MED193_18999	Uncharacterized protein
A3XC35	+	3.510	-2.344	MED193_03332	Pyruvate dehydrogenase E1 component subunit beta (EC 1.2.4.1)
A3X6G6	+	2.269	-2.349	MED193_15367	Uncharacterized protein
A3X3S4	+	3.474	-2.350	MED193_17299	PaaX domain protein
A3XEX2	+	1.608	-2.364	MED193_12208	Uncharacterized protein
A3XC37	+	1.720	-2.370	MED193_03317	Serine acetyltransferase (EC 2.3.1.30)
A3XFN0	+	1.273	-2.375	MED193_11344	Arginine decarboxylase (EC 4.1.1.19)
A3X8K1	+	2.918	-2.375	MED193_05659	Biotin carboxylase (EC 6.3.4.14) (EC 6.4.1.2)
A3X7T0	+	2.211	-2.375	MED193_07029	NADH-quinone oxidoreductase subunit F (EC 1.6.5.11)
A3X6N3	+	1.887	-2.405	MED193_15047	Nicotinate phosphoribosyltransferase (NAPRTase) (EC 6.3.4.21)
A3XC71	+	3.032	-2.410	MED193_03162	50S ribosomal protein L9
A3X446	+	3.492	-2.416	MED193_16699	30S ribosomal protein S8
A3XFU2	+	4.175	-2.417	MED193_11812	Bordetella uptake gene family protein
A3XDK9	+	1.945	-2.420	MED193_13063	30S ribosomal protein S15
A3XAY3	+	3.340	-2.452	MED193_04286	FeS assembly protein SufD
A3XCR0	+	3.098	-2.452	MED193_10413	Oxidoreductase, short chain dehydrogenase/reductase family protein
A3X5Q6	+	2.834	-2.454	MED193_18819	Uncharacterized protein
A3X433	+	4.145	-2.469	MED193_16764	50S ribosomal protein L17
A3XDI1	+	2.686	-2.470	MED193_13238	Beta sliding clamp
A3XBZ2	+	2.350	-2.470	MED193_03542	CBS domain protein

A3XFB4	+	1.535	-2.471	MED193_21566	Uncharacterized protein
A3X447	+	4.961	-2.474	MED193_16689	50S ribosomal protein L5
A3X3S5	+	2.641	-2.477	MED193_17304	Phenylacetic acid degradation protein PaaZ
A3X699	+	2.248	-2.487	MED193_15722	Heat shock protein, Hsp20 family protein
A3X3V1	+	2.460	-2.498	MED193_17169	Uncharacterized protein
A3X4E0	+	2.055	-2.503	MED193_21154	DNA-binding response regulator, LuxR family protein
A3X7E3	+	3.786	-2.506	MED193_13752	ATP-dependent protease ATPase subunit HslU (Unfoldase HslU)
A3XFQ1	+	1.934	-2.511	MED193_12007	50S ribosomal protein L35
A3XBQ8	+	1.458	-2.516	MED193_03967	Uncharacterized protein
A3XC67	+	3.761	-2.518	MED193_03172	30S ribosomal protein S6
A3X4Y7	+	1.973	-2.518	MED193_20154	L-threonine aldolase, low-specificity, putative
A3X4H5	+	2.223	-2.519	MED193_20984	Acyl-CoA dehydrogenase family protein
A3X7Q2	+	1.526	-2.520	MED193_07129	Bifunctional protein GlmU [Includes: Glucosamine-1-phosphate N-acetyltransferase (EC 2.3.1.157); UDP-N-acetylglucosamine pyrophosphorylase (EC 2.7.7.23) (N-acetylglucosamine-1-phosphate uridyltransferase)]
A3X443	+	2.084	-2.524	MED193_16704	50S ribosomal protein L6
A3X583	+	2.235	-2.528	MED193_19694	Uncharacterized protein
A3X3S2	+	2.617	-2.529	MED193_17319	Phenylacetate-coenzyme A ligase (EC 6.2.1.30) (Phenylacetyl-CoA ligase)
A3XEZ3	+	3.767	-2.550	MED193_03110	Trigger factor (TF) (EC 5.2.1.8) (PPIase)
A3X7M1	+	2.942	-2.550	MED193_07299	Malate synthase G (EC 2.3.3.9)
A3XDK7	+	1.334	-2.551	MED193_13098	Glycosyl transferase, family 25
A3X4V6	+	2.054	-2.552	MED193_20319	Uncharacterized protein
A3X442	+	3.319	-2.564	MED193_16719	50S ribosomal protein L30
A3X7I3	+	3.864	-2.579	MED193_07494	UDP-N-acetylmuramoyl-tripeptide--D-alanyl-D-alanine ligase (EC 6.3.2.10) (D-alanyl-D-alanine-adding enzyme)
A3XDR2	+	2.419	-2.588	MED193_12818	Phenylacetate-CoA ligase, putative
A3X462	+	5.185	-2.591	MED193_16624	50S ribosomal protein L2
A3XAP4	+	2.396	-2.592	MED193_04736	30S ribosomal protein S9
A3XFQ6	+	3.802	-2.593	MED193_12002	50S ribosomal protein L20
A3X8R4	+	1.967	-2.596	MED193_07728	Phosphomethylpyrimidine synthase (EC 4.1.99.17) (Hydroxymethylpyrimidine phosphate synthase) (HMP-P synthase) (HMP-phosphate synthase) (HMPP synthase) (Thiamine biosynthesis protein ThiC)
A3XBS6	+	3.466	-2.598	MED193_03872	50S ribosomal protein L21
A3X9Y4	+	1.207	-2.609	MED193_01405	Uncharacterized protein
A3XBD1	+	1.845	-2.613	MED193_22681	Cytochrome P450 family protein

A3XFS4	+	1.813	-2.615	MED193_11912	30S ribosomal protein S21
A3XCM1	+	1.230	-2.616	MED193_10608	Cell division ATP-binding protein FtsE
A3X464	+	2.377	-2.625	MED193_16599	30S ribosomal protein S10
A3X6V5	+	1.622	-2.634	MED193_14682	Ubiquinone biosynthesis hydroxylase, UbiH/UbiF/VisC/COQ6 family protein
A3X427	+	1.210	-2.651	MED193_16794	Pseudouridine synthase (EC 5.4.99.-)
A3X413	+	2.417	-2.657	MED193_16864	50S ribosomal protein L34
A3X400	+	2.129	-2.660	MED193_16919	Allophanate hydrolase family protein
A3X4R0	+	2.300	-2.661	MED193_20559	Ornithine carbamoyltransferase (OTCase) (EC 2.1.3.3)
A3X4X2	+	1.254	-2.669	MED193_20244	N5-carboxyaminoimidazole ribonucleotide synthase (N5-CAIR synthase) (EC 6.3.4.18) (5-(carboxyamino)imidazole ribonucleotide synthetase)
A3XCB5	+	2.731	-2.670	MED193_11148	Methyltransferase, putative
A3X4W3	+	3.309	-2.671	MED193_20274	Phenazine biosynthesis protein, PhzF family protein
A3X3K3	+	1.206	-2.673	MED193_17659	Uncharacterized protein
A3X8Z1	+	3.681	-2.681	MED193_08933	Threonine synthase (EC 4.2.3.1)
A3X9J5	+	1.623	-2.687	MED193_07908	Transcriptional regulator, LysR family protein
A3X8K7	+	2.102	-2.690	MED193_05619	Branched-chain amino acid ABC transporter, ATP-binding protein
A3X7A0	+	4.375	-2.693	MED193_13927	Argininosuccinate synthase (EC 6.3.4.5) (Citrulline--aspartate ligase)
A3XDG0	+	3.338	-2.701	MED193_13318	D-3-phosphoglycerate dehydrogenase (EC 1.1.1.95)
A3XAY2	+	5.409	-2.711	MED193_04311	FeS assembly protein SufB
A3XFX4	+	2.818	-2.715	MED193_10211	Enoyl-CoA hydratase/isomerase/3-hydroxyacyl-CoA dehydrogenase
A3X705	+	1.536	-2.724	MED193_14407	Malonyl-CoA synthase
A3X886	+	2.974	-2.728	MED193_06239	Lipoprotein-releasing system ATP-binding protein LolD (EC 3.6.3.-)
A3X8B9	+	2.277	-2.729	MED193_06059	Uncharacterized protein
A3XFP1	+	2.892	-2.743	MED193_12062	Acetyl-coenzyme A carboxylase carboxyl transferase subunit alpha (ACCase subunit alpha) (Acetyl-CoA carboxylase carboxyltransferase subunit alpha) (EC 2.1.3.15)
A3XDI2	+	1.892	-2.744	MED193_13198	Transcriptional regulator, IclR family protein
A3XDP9	+	1.628	-2.762	MED193_12863	Uncharacterized protein
A3X5Y3	+	4.718	-2.771	MED193_16302	Aminotransferase, classes I and II
A3X7W8	+	1.744	-2.780	MED193_06824	Amidophosphoribosyltransferase (ATase) (EC 2.4.2.14) (Glutamine phosphoribosylpyrophosphate amidotransferase) (GPATase)
A3XDD3	+	1.096	-2.796	MED193_13463	Uncharacterized protein
A3XDD2	+	3.148	-2.796	MED193_13458	Spermidine/putrescine import ATP-binding protein PotA (EC 3.6.3.31)
A3X7H6	+	1.692	-2.798	MED193_07524	Iron-sulfur cluster carrier protein
A3XFX0	+	2.547	-2.799	MED193_10241	Transcriptional regulator, IclR family protein
A3X3S3	+	3.240	-2.803	MED193_17309	Enoyl-CoA hydratase (EC 4.2.1.17)

A3XBW5	+	3.683	-2.807	MED193_03687	LexA repressor (EC 3.4.21.88)
A3XF53	+	1.953	-2.824	MED193_02805	Oxidoreductase, zinc-binding dehydrogenase family protein
A3XE22	+	2.853	-2.833	MED193_00310	Replication protein a
A3X612	+	1.991	-2.834	MED193_16152	Signal recognition particle protein (Fifty-four homolog)
A3XDZ1	+	1.270	-2.840	MED193_00475	Uncharacterized protein
A3X9Q0	+	2.732	-2.843	MED193_01840	Probable oxidoreductase
A3X8S0	+	2.925	-2.854	MED193_07708	Putative adenosylmethionine-8-amino-7-oxononanoate aminotransferase
A3X4P0	+	2.431	-2.854	MED193_20659	Elongation factor 4 (EF-4) (EC 3.6.5.n1) (Ribosomal back-translocase LepA)
A3X455	+	3.095	-2.858	MED193_16629	30S ribosomal protein S19
A3XB52	+	2.476	-2.858	MED193_22056	Siderophore-interacting protein
A3XBK3	+	2.737	-2.869	MED193_22326	Uncharacterized protein
A3X5Z1	+	3.012	-2.880	MED193_16242	Pyruvate dehydrogenase complex repressor
A3X4M1	+	1.360	-2.884	MED193_20734	Aminotransferase, classes I and II
A3XCU8	+	2.766	-2.888	MED193_09235	Ribosomal protein L11 methyltransferase (L11 Mtase) (EC 2.1.1.-)
A3XCI8	+	1.201	-2.889	MED193_10758	Molybdopterin-guanine dinucleotide biosynthesis protein B
A3X777	+	0.991	-2.892	MED193_14077	Uncharacterized protein
A3XEZ6	+	1.552	-2.893	MED193_03080	3-dehydroquinate synthase (DHQS) (EC 4.2.3.4)
A3XDG6	+	4.566	-2.901	MED193_13298	2-amino-3-ketobutyrate coenzyme A ligase (AKB ligase) (EC 2.3.1.29) (Glycine acetyltransferase)
A3XDR3	+	2.454	-2.903	MED193_12823	Branched-chain amino acid ABC transporter, ATP-binding protein
A3X764	+	2.194	-2.908	MED193_14147	3-deoxy-manno-octulosonate cytidylyltransferase (EC 2.7.7.38)
A3X7K8	+	2.226	-2.965	MED193_07369	Cobalt chelatase, pCobT subunit
A3X3J9	+	1.923	-2.975	MED193_17684	Glycosyl transferase, group 1 family protein
A3X6N2	+	2.466	-2.979	MED193_15052	Aldehyde dehydrogenase family protein
A3XFC0	+	2.076	-2.983	MED193_21546	50S ribosomal protein L33
A3X7Y0	+	0.956	-2.990	MED193_06764	Replicative DNA helicase (EC 3.6.4.12)
A3XFH0	+	2.325	-2.998	MED193_11634	Acetyl-coenzyme A carboxylase carboxyl transferase subunit beta (ACCase subunit beta) (Acetyl-CoA carboxylase carboxyltransferase subunit beta) (EC 2.1.3.15)
A3XFG9	+	1.853	-3.004	MED193_11629	FolC bifunctional protein
A3X860	+	2.511	-3.005	MED193_06359	Type I site-specific deoxyribonuclease HsdM
A3X4C1	+	3.590	-3.005	MED193_21244	Transcriptional regulator
A3XB45	+	1.850	-3.011	MED193_22076	FecB2
A3XA92	+	1.280	-3.015	MED193_00870	5-carboxy-2-hydroxymuconate semialdehyde dehydrogenase
A3X648	+	2.678	-3.019	MED193_15947	50S ribosomal protein L1
A3XEX5	+	3.411	-3.026	MED193_12173	Taurine--pyruvate aminotransferase

A3X3N5	+	1.886	-3.026	MED193_17504	Putative Hemin receptor protein HmuR
A3X7G2	+	3.182	-3.031	MED193_13657	Adenosylhomocysteinase (EC 3.3.1.1) (S-adenosyl-L-homocysteine hydrolase) (AdoHcyase)
A3X618	+	3.336	-3.040	MED193_16087	50S ribosomal protein L31
A3X5V6	+	1.988	-3.052	MED193_18574	Uncharacterized protein
A3X9Y5	+	2.085	-3.061	MED193_01410	ParB-like nuclease
A3X9B0	+	2.772	-3.066	MED193_08343	Transcriptional regulator, CarD family protein
A3X6W1	+	1.014	-3.067	MED193_14662	Exodeoxyribonuclease III, putative
A3X781	+	1.540	-3.077	MED193_14052	Ubiquinone biosynthesis O-methyltransferase (2-polyprenyl-6-hydroxyphenol methylase) (EC 2.1.1.222) (3-demethylubiquinone 3-O-methyltransferase) (EC 2.1.1.64)
A3X3C7	+	1.372	-3.079	MED193_18029	Tryptophan synthase alpha chain (EC 4.2.1.20)
A3X7P9	+	4.636	-3.088	MED193_07164	Amidohydrolase family protein
A3X448	+	4.907	-3.091	MED193_16679	50S ribosomal protein L14
A3X709	+	1.838	-3.092	MED193_14382	Branched-chain-amino-acid aminotransferase (BCAT) (EC 2.6.1.42)
A3X463	+	4.157	-3.115	MED193_16609	50S ribosomal protein L4
A3X8L4	+	3.040	-3.115	MED193_05599	Transcriptional regulator, putative
A3X752	+	2.310	-3.117	MED193_14187	Ribosome hibernation promoting factor (HPF)
A3XDK1	+	2.736	-3.125	MED193_13118	Aldehyde dehydrogenase family protein
A3X626	+	2.713	-3.143	MED193_16077	Uncharacterized protein
A3XBS3	+	2.759	-3.148	MED193_03887	GTPase Obg (EC 3.6.5.-) (GTP-binding protein Obg)
A3XDZ9	+	1.865	-3.148	MED193_00410	Uncharacterized protein
A3XEY1	+	2.537	-3.169	MED193_12153	Catalase-peroxidase (CP) (EC 1.11.1.21) (Peroxidase/catalase)
A3XDF2	+	2.516	-3.171	MED193_13368	Cytokinin riboside 5'-monophosphate phosphoribohydrolase (EC 3.2.2.n1)
A3X4G2	+	2.244	-3.176	MED193_21049	Uncharacterized protein
A3X970	+	2.178	-3.183	MED193_08543	RNA polymerase sigma factor RpoD (Sigma-70)
A3X9Y1	+	2.785	-3.208	MED193_01415	ParA family ATPase
A3X434	+	2.537	-3.211	MED193_16749	30S ribosomal protein S13
A3X7N2	+	2.819	-3.240	MED193_07254	Kynureninase (EC 3.7.1.3) (L-kynurenine hydrolase)
A3X4I1	+	3.876	-3.242	MED193_20939	O-succinylhomoserine sulfhydrylase (OSH sulfhydrylase) (OSHS sulfhydrylase) (EC 2.5.1.-)
A3X825	+	1.188	-3.243	MED193_06539	Lon protease (EC 3.4.21.53) (ATP-dependent protease La)
A3XD91	+	3.484	-3.250	MED193_09400	Glyceraldehyde-3-phosphate dehydrogenase, type I
A3XC89	+	1.544	-3.267	MED193_11273	Prephenate dehydratase (EC 4.2.1.51)
A3X4Q1	+	2.685	-3.291	MED193_20599	50S ribosomal protein L28

A3XFR1	+	4.612	-3.314	MED193_11942	Alanine dehydrogenase (EC 1.4.1.1)
A3XF73	+	2.436	-3.340	MED193_02705	Phosphoribosylaminoimidazole-succinocarboxamide synthase (EC 6.3.2.6) (SAICAR synthetase)
A3XBF5	+	4.318	-3.346	MED193_22576	Amidohydrolase family protein
A3X640	+	2.521	-3.351	MED193_16002	30S ribosomal protein S7
A3X641	+	4.808	-3.351	MED193_16007	Elongation factor G (EF-G)
A3X7B1	+	2.331	-3.364	MED193_13882	Ribokinase (RK) (EC 2.7.1.15)
A3XDA1	+	2.471	-3.376	MED193_09355	2-hydroxyacid dehydrogenase
A3X423	+	3.399	-3.377	MED193_16804	Uncharacterized protein
A3XD83	+	3.609	-3.389	MED193_09455	Glycosyl transferase, WecB/TagA/CpsF family protein
A3XB89	+	2.679	-3.395	MED193_21866	Amidase (EC 3.5.1.4)
A3XD23	+	1.240	-3.402	MED193_09745	ABC transporter, ATP-binding protein
A3XBI7	+	3.564	-3.406	MED193_22416	Arginine--tRNA ligase (EC 6.1.1.19) (Arginyl-tRNA synthetase) (ArgRS)
A3X9X7	+	3.265	-3.407	MED193_01445	Regulatory protein GntR, HTH:GntR, C-terminal
A3X7K7	+	1.934	-3.410	MED193_07379	Metallopeptidase, family M24
A3X438	+	3.816	-3.432	MED193_16729	50S ribosomal protein L15
A3XEN3	+	3.706	-3.441	MED193_12668	Uncharacterized protein
A3X4H9	+	1.737	-3.489	MED193_20954	Aspartokinase (EC 2.7.2.4)
A3X4F1	+	2.374	-3.490	MED193_21099	Aminotransferase (EC 2.6.1.-)
A3X3N4	+	2.529	-3.500	MED193_17499	Hemin degrading factor
A3XFE2	+	2.457	-3.508	MED193_21406	Acyl-CoA synthase (EC 2.3.1.86)
A3XCK6	+	3.316	-3.527	MED193_10693	Uncharacterized protein
A3XA12	+	2.213	-3.534	MED193_01260	Uncharacterized protein
A3X718	+	2.986	-3.550	MED193_14377	Transcriptional regulator PetP
A3X7P4	+	1.904	-3.557	MED193_07189	Peptide/nickel/opine uptake family ABC transporter, ATP-binding protein, putative
A3XDB0	+	3.483	-3.579	MED193_09300	Isoleucine--tRNA ligase (EC 6.1.1.5) (Isoleucyl-tRNA synthetase) (IleRS)
A3XAK5	+	1.257	-3.587	MED193_04941	Isoprenyl transferase (EC 2.5.1.-)
A3XBQ2	+	2.606	-3.608	MED193_03992	Acetoacetyl-CoA synthase
A3XEM0	+	2.201	-3.642	MED193_12698	Uncharacterized protein
A3X5Y4	+	4.119	-3.644	MED193_16257	Chromosome partition protein Smc
A3XAH5	+	1.768	-3.644	MED193_05096	Adenylosuccinate lyase (ASL) (EC 4.3.2.2) (Adenylosuccinase)
A3XCV3	+	3.509	-3.646	MED193_09205	Holliday junction ATP-dependent DNA helicase RuvA (EC 3.6.4.12)
A3X3H4	+	2.541	-3.664	MED193_17804	Threonine dehydratase
A3X8N2	+	2.472	-3.668	MED193_05509	ABC transporter, ATP-binding protein
A3X586	+	2.306	-3.678	MED193_19659	Uncharacterized protein

A3X430	+	3.116	-3.704	MED193_16779	Periplasmic serine protease, DO/DeqQ family protein
A3X3F8	+	1.634	-3.710	MED193_17884	PhoH family protein
A3XBR8	+	4.040	-3.748	MED193_03922	30S ribosomal protein S2
A3X473	+	1.796	-3.761	MED193_16549	ATP:cob(I)alamin adenosyltransferase, putative
A3XC27	+	2.950	-3.786	MED193_03367	Hemolysin-type calcium-binding region, RTX
A3X6S2	+	2.535	-3.827	MED193_14857	Uncharacterized protein
A3XEN1	+	1.635	-3.842	MED193_12658	Uncharacterized protein
A3X7B6	+	2.777	-3.859	MED193_13862	Heat-inducible transcription repressor HrcA
A3X7V9	+	2.536	-3.866	MED193_06859	Uncharacterized protein
A3XDQ7	+	2.909	-3.933	MED193_12848	Branched-chain amino acid ABC transporter, ATP-binding protein
A3X738	+	3.085	-3.939	MED193_14247	Glutamate synthase, large subunit
A3X4J2	+	2.216	-3.947	MED193_20894	Phosphoribosylamine--glycine ligase (EC 6.3.4.13) (GARS) (Glycinamide ribonucleotide synthetase) (Phosphoribosylglycinamide synthetase)
A3XD97	+	2.334	-4.007	MED193_09385	Putative transcriptional regulator, IclR family protein
A3X4U0	+	2.738	-4.060	MED193_20389	Uncharacterized protein
A3XDQ9	+	2.229	-4.107	MED193_12858	AMP-binding enzyme
A3XAZ2	+	2.838	-4.117	MED193_04251	2-isopropylmalate synthase (EC 2.3.3.13)
A3X8M9	+	3.429	-4.125	MED193_05519	N-carbamoyl-L-amino acid amidohydrolase
A3X9H4	+	4.313	-4.155	MED193_08013	TonB dependent iron siderophore receptor
A3X444	+	2.820	-4.167	MED193_16709	50S ribosomal protein L18
A3X4E3	+	3.690	-4.221	MED193_21144	Acetolactate synthase small subunit (EC 2.2.1.6)
A3X8C3	+	3.891	-4.246	MED193_06054	Phosphate acetyltransferase (EC 2.3.1.8)
A3X3D9	+	2.894	-4.303	MED193_17984	Uncharacterized protein
A3X8C4	+	1.960	-4.318	MED193_06034	Phosphopentomutase (EC 5.4.2.7) (Phosphodeoxyribomutase)
A3XAX1	+	2.455	-4.344	MED193_04351	GTP-binding protein TypA
A3XCH4	+	3.226	-4.400	MED193_10823	Threonylcarbamoyl-AMP synthase (TC-AMP synthase) (EC 2.7.7.87) (L-threonylcarbamoyladenylate synthase)
A3XB54	+	1.868	-4.437	MED193_22031	Outer membrane protein
A3XD93	+	2.667	-4.458	MED193_09365	Glycine dehydrogenase (decarboxylating) (EC 1.4.4.2) (Glycine cleavage system P-protein) (Glycine decarboxylase) (Glycine dehydrogenase (aminomethyl-transferring))
A3X7Q1	+	4.080	-4.513	MED193_07174	Amidohydrolase family protein
A3XFA9	+	3.728	-4.536	MED193_21591	DNA-binding protein, putative
A3XCS0	+	3.249	-4.566	MED193_10348	Aminotransferase, class IV
A3XDG7	+	4.028	-4.831	MED193_13303	L-threonine 3-dehydrogenase (TDH) (EC 1.1.1.103)

A3X3E3	+	3.480	-4.918	MED193_17954	30S ribosomal protein S1
A3X3H8	+	3.938	-5.046	MED193_17784	3-carboxy-cis,cis-muconate cycloisomerase
A3X352	+	3.358	-5.133	MED193_18409	7-cyano-7-deazaguanine synthase (EC 6.3.4.20) (7-cyano-7-carbaguanine synthase) (PreQ(0) synthase) (Queuosine biosynthesis protein QueC)
A3X6N5	+	3.043	-5.167	MED193_15012	Glycine dehydrogenase (decarboxylating) (EC 1.4.4.2) (Glycine cleavage system P-protein) (Glycine decarboxylase) (Glycine dehydrogenase (aminomethyl-transferring))
A3X587	+	2.490	-5.274	MED193_19664	Lipoprotein, putative
A3XDH8	+	2.147	-5.391	MED193_13223	DNA gyrase subunit B (EC 5.99.1.3)
A3XBS7	+	2.992	-5.400	MED193_03877	50S ribosomal protein L27
A3XDZ8	+	2.270	-5.464	MED193_00405	Uncharacterized protein
A3X8P5	+	4.331	-5.494	MED193_05439	Acetyl-coenzyme A synthetase (AcCoA synthetase) (Acs) (EC 6.2.1.1) (Acetate--CoA ligase) (Acyl-activating enzyme)
A3X8B8	+	3.296	-5.514	MED193_06079	Threonine--tRNA ligase (EC 6.1.1.3) (Threonyl-tRNA synthetase) (ThrRS)
A3X8M7	+	4.988	-5.570	MED193_05534	Pyridine nucleotide-disulphide oxidoreductase family protein
A3XB46	+	3.300	-5.603	MED193_22061	Iron(III) dicitrate ABC transporter (ATP-binding protein)
A3XE07	+	3.238	-5.720	MED193_00395	ATPase of the AAA+ class
A3X824	+	3.676	-5.854	MED193_06534	Glutamate/leucine/phenylalanine/valine dehydrogenase family protein
A3X3Q9	+	4.939	-5.881	MED193_17374	Uncharacterized protein
A3XAV6	+	3.240	-5.977	MED193_04431	DNA gyrase subunit A (EC 5.99.1.3)
A3X8M6	+	3.217	-6.101	MED193_05529	Dihydropyrimidine dehydrogenase (EC 1.3.1.1)

Appendix 4.3 Significantly up- and downregulated proteins (p-value <0.01) in the cellular proteome of MED193 cultures supplemented with PE.

Protein ID	*p-value <0.01*	*-log$_{10}$(p-value)*	*Log$_2$ (fold change)*	*Locus tag*	*Uniprot annotation*
A3X3N5	+	1.956	4.888	MED193_17504	Putative Hemin receptor protein HmuR
A3X3N1	+	3.923	4.088	MED193_17519	Uncharacterized protein
A3X9H0	+	2.484	3.779	MED193_08043	TonB dependent iron siderophore receptor
A3X3R0	+	4.626	2.848	MED193_17379	Uncharacterized protein
A3X587	+	3.201	3.152	MED193_19664	Lipoprotein, putative
A3XG05	+	3.728	3.346	MED193_10041	Bacterial extracellular solute-binding protein, family 7
A3XG07	+	6.836	2.968	MED193_10051	Aldehyde dehydrogenase, putative

A3XFZ8	+	5.293	2.681	MED193_10056	Alcohol dehydrogenase, iron-containing
A3X7U0	+	2.291	-3.401	MED193_06959	NADH-quinone oxidoreductase subunit N (EC 1.6.5.11) (NADH dehydrogenase I subunit N) (NDH-1 subunit N)
A3X3M4	+	3.687	-3.272	MED193_17559	Quinolinate synthase A (EC 2.5.1.72)
A3XAQ9	+	1.877	-3.601	MED193_04676	Peroxiredoxin/glutaredoxin family protein
A3XFW0	+	1.473	-4.149	MED193_11712	N-methylproline demethylase, putative
A3X7Z6	+	2.435	-4.605	MED193_06674	Carbon monoxide dehydrogenase, large subunit
A3XBX7	+	2.982	-6.713	MED193_03622	Indolepyruvate ferredoxin oxidoreductase (EC 1.2.7.8)
A3X8R4	+	1.200	-4.966	MED193_07728	Phosphomethylpyrimidine synthase (EC 4.1.99.17) (Hydroxymethylpyrimidine phosphate synthase) (HMP-P synthase) (HMP-phosphate synthase) (HMPP synthase) (Thiamine biosynthesis protein ThiC)

Appendix 4.4 Significantly up- and downregulated proteins (p-value <0.01) in the exoproteome of MED193 cultures supplemented with PE.

Protein ID	*p-value <0.01*	*-log$_{10}$ (p-value)*	*Log$_2$ (fold change)*	*Locus tag*	*Uniprot annotation*
A3X3N5	+	1.835	5.880	MED193_17504	Putative Hemin receptor protein HmuR
A3X3N2	+	2.656	3.502	MED193_17509	Uncharacterized protein
A3X3N4	+	2.100	3.536	MED193_17499	Hemin degrading factor
A3XB54	+	1.565	4.653	MED193_22031	Outer membrane protein
A3X587	+	3.172	3.022	MED193_19664	Lipoprotein, putative
A3XG05	+	3.090	3.680	MED193_10041	Bacterial extracellular solute-binding protein, family 7
A3X9H0	+	2.220	3.726	MED193_08043	TonB dependent iron siderophore receptor
A3XG07	+	2.745	4.051	MED193_10051	Aldehyde dehydrogenase, putative
A3XFN9	+	2.847	3.654	MED193_12052	Transcriptional regulator, GntR family protein
A3XB18	+	2.696	-4.195	MED193_22216	Xanthine dehydrogenase family protein, large subunit
A3X6A5	+	3.125	-5.026	MED193_15662	3-isopropylmalate dehydratase small subunit (EC 4.2.1.33) (Alpha-IPM isomerase) (IPMI) (Isopropylmalate isomerase)
A3XCP6	+	1.965	-3.695	MED193_10473	Succinate dehydrogenase iron-sulfur subunit (EC 1.3.5.1)
A3X8R4	+	1.677	-4.619	MED193_07728	Phosphomethylpyrimidine synthase (EC 4.1.99.17) (Hydroxymethylpyrimidine phosphate synthase) (HMP-P synthase) (HMP-phosphate synthase) (HMPP synthase) (Thiamine biosynthesis protein ThiC)
A3XC90	+	2.731	-3.499	MED193_11233	Universal stress protein family protein
A3X7Z6	+	2.250	-4.790	MED193_06674	Carbon monoxide dehydrogenase, large subunit

Appendix 4.5 Significantly up- and downregulated proteins (p-value <0.05, ++ p-value <0.01) in the cellular proteome of MED193 cultures supplemented with PC.

Protein ID	*p-value <0.05*	*-log$_{10}$ (p-value)*	*Log$_2$ (fold change)*	*Locus tag*	*Uniprot annotation*
A3XBX7	+	++ 2.674	-5.969	MED193_03622	Indolepyruvate ferredoxin oxidoreductase (EC 1.2.7.8)
A3X3N5	+	1.797	4.513	MED193_17504	Putative Hemin receptor protein HmuR
A3X3N1	+	3.723	3.987	MED193_17519	Uncharacterized protein
A3X9H0	+	1.567	2.716	MED193_08043	TonB dependent iron siderophore receptor
A3X3R0	+	4.668	2.558	MED193_17379	Uncharacterized protein
A3X587	+	3.822	3.903	MED193_19664	Lipoprotein, putative
A3X7U0	+	1.135	-2.721	MED193_06959	NADH-quinone oxidoreductase subunit N (EC 1.6.5.11) (NADH dehydrogenase I subunit N) (NDH-1 subunit N)
A3X3M4	+	1.969	-2.211	MED193_17559	Quinolinate synthase A (EC 2.5.1.72)
A3XAQ9	+	2.157	-3.986	MED193_04676	Peroxiredoxin/glutaredoxin family protein
A3XFW0	+	1.580	-3.383	MED193_11712	N-methylproline demethylase, putative
A3X7Z6	+	1.644	-4.092	MED193_06674	Carbon monoxide dehydrogenase, large subunit
A3X8R4	+	0.709	-4.234	MED193_07728	Phosphomethylpyrimidine synthase (EC 4.1.99.17) (Hydroxymethylpyrimidine phosphate synthase) (HMP-P synthase) (HMP-phosphate synthase) (HMPP synthase) (Thiamine biosynthesis protein ThiC)
A3XB54	+	1.129	4.469	MED193_22031	Outer membrane protein
A3X3N2	+	1.068	3.506	MED193_17509	Uncharacterized protein
A3X3D9	+	1.211	3.441	MED193_17984	Uncharacterized protein
A3X3N3	+	1.262	3.489	MED193_17514	MotA/TolQ/ExbB proton channel family protein
A3X3N9	+	1.587	3.625	MED193_17484	Hemin import ATP-binding protein HmuV (EC 3.6.3.-)
A3XEY9	+	3.316	3.510	MED193_12143	Uncharacterized protein
A3X3Q7	+	1.105	3.428	MED193_17384	Putative iron ABC transport system, ATP-binding protein
A3X9H4	+	1.447	3.256	MED193_08013	TonB dependent iron siderophore receptor
A3X3N4	+	1.980	3.483	MED193_17499	Hemin degrading factor
A3X589	+	3.447	2.935	MED193_19674	Uncharacterized protein
A3X3N7	+	1.933	2.697	MED193_17494	Putative hemin binding periplasmic transmembrane protein
A3XB52	+	1.122	2.715	MED193_22056	Siderophore-interacting protein
A3X586	+	2.329	3.026	MED193_19659	Uncharacterized protein
A3X3M9	+	1.985	2.195	MED193_17524	Uncharacterized protein
A3X3Q9	+	1.195	2.662	MED193_17374	Uncharacterized protein

A3XB45	+	2.043	2.402	MED193_22076	FecB2
A3X3E6	+	3.324	1.897	MED193_17944	Uncharacterized protein
A3XBT1	+	1.878	3.034	MED193_03857	MetF protein-like
A3X6Y4	+	1.978	4.001	MED193_14527	Uncharacterized protein
A3XAQ4	+	3.746	3.102	MED193_04696	Methyltransferase (EC 2.1.1.-)
A3XF95	+	2.096	2.341	MED193_21676	Choline sulfatase
A3X5J0	+	3.479	2.805	MED193_19144	Aminomethyl transferase family protein
A3XF87	+	2.684	2.737	MED193_21681	Betaine aldehyde dehydrogenase
A3XF88	+	2.507	2.449	MED193_21686	Choline dehydrogenase (EC 1.1.99.1)
A3XF94	+	1.994	2.597	MED193_21671	Membrane protein, putative
A3X531	+	1.433	-3.284	MED193_19934	Uncharacterized protein
A3X8I5	+	1.294	-2.917	MED193_05739	SoxAX cytochrome complex subunit A (EC 2.8.5.2) (Protein SoxA) (Sulfur oxidizing protein A) (Thiosulfate-oxidizing multienzyme system protein SoxA)
A3XAQ8	+	3.211	-1.987	MED193_04671	Lipoyl synthase (EC 2.8.1.8) (Lip-syn) (LS) (Lipoate synthase) (Lipoic acid synthase) (Sulfur insertion protein LipA)
A3XD38	+	2.011	-3.579	MED193_09675	Universal stress family protein
A3X835	+	3.208	-3.384	MED193_06474	TRAP-T family transporter, DctP (Periplasmic binding) subunit
A3X7R2	+	3.657	-3.570	MED193_07099	Outer membrane protein OmpW
A3X6A5	+	1.540	-3.144	MED193_15662	3-isopropylmalate dehydratase small subunit (EC 4.2.1.33) (Alpha-IPM isomerase) (IPMI) (Isopropylmalate isomerase)
A3X5Z2	+	1.690	-2.678	MED193_16247	Aminotransferase, classes I and II
A3X6A6	+	2.460	-2.607	MED193_15667	3-isopropylmalate dehydratase large subunit (EC 4.2.1.33) (Alpha-IPM isomerase) (IPMI) (Isopropylmalate isomerase)
A3X744	+	1.768	-2.552	MED193_14232	Glutamate synthase, small subunit
A3X7Z9	+	1.643	-2.245	MED193_06669	Carbon monoxide dehydrogenase, medium subunit, putative
A3XFZ3	+	3.262	-2.833	MED193_10121	Iron-sulfur cluster-binding protein
A3X8Z9	+	1.038	-2.868	MED193_08893	Sulfate transporter family protein
A3X4F9	+	3.056	-2.924	MED193_21064	5-aminolevulinate synthase (EC 2.3.1.37) (5-aminolevulinic acid synthase) (Delta-ALA synthase) (Delta-aminolevulinate synthase)
A3X8R1	+	2.611	-3.993	MED193_07743	Thiazole synthase (EC 2.8.1.10)

Appendix 4.6 Significantly up- and downregulated proteins (p-value <0.05, ++ p-value <0.01) in the exoproteome of MED193 cultures supplemented with PC.

Protein ID	*p-value <0.05*	*-log$_{10}$ (p-value)*	*Log$_2$ (fold change)*	*Locus tag*	*Uniprot annotation*
A3X3N5	+	++ 1.821	5.764	MED193_17504	Putative Hemin receptor protein HmuR
A3XB54	+	++ 2.039	5.008	MED193_22031	Outer membrane protein
A3XFN9	+	2.866	3.726	MED193_12052	Transcriptional regulator, GntR family protein
A3XF87	+	2.643	3.830	MED193_21681	Betaine aldehyde dehydrogenase

Appendix 4.7 Significantly up- and downregulated proteins (p-value <0.05, ++ p-value <0.01) in the cellular proteome of MED193 cultures supplemented with PG.

Protein ID	*p-value <0.05*	*-log$_{10}$ (p-value)*	*Log$_2$ (fold change)*	*Locus tag*	*Uniprot annotation*
A3XBX7	+	++ 2.871	-6.022	MED193_03622	Indolepyruvate ferredoxin oxidoreductase (EC 1.2.7.8)
A3X8R4	+	++ 2.053	-6.414	MED193_07728	Phosphomethylpyrimidine synthase (EC 4.1.99.17) (Hydroxymethylpyrimidine phosphate synthase) (HMP-P synthase) (HMP-phosphate synthase) (HMPP synthase) (Thiamine biosynthesis protein ThiC)
A3X3N5	+	1.917	4.741	MED193_17504	Putative Hemin receptor protein HmuR
A3XD57	+	2.128	4.672	MED193_09575	Sugar ABC transporter, ATP-binding protein
A3XB54	+	1.186	4.669	MED193_22031	Outer membrane protein
A3X5C8	+	3.365	4.251	MED193_19449	Phosphonate-binding periplasmic protein
A3X3N1	+	3.979	4.043	MED193_17519	Uncharacterized protein
A3X3N2	+	1.224	3.993	MED193_17509	Uncharacterized protein
A3X3D9	+	1.378	3.924	MED193_17984	Uncharacterized protein
A3X3N3	+	1.356	3.737	MED193_17514	MotA/TolQ/ExbB proton channel family protein
A3X3N9	+	1.589	3.663	MED193_17484	Hemin import ATP-binding protein HmuV (EC 3.6.3.-)
A3XEY9	+	0.936	3.589	MED193_12143	Uncharacterized protein
A3X9H0	+	2.388	3.510	MED193_08043	TonB dependent iron siderophore receptor
A3X3Q7	+	1.104	3.427	MED193_17384	Putative iron ABC transport system, ATP-binding protein
A3XD58	+	1.969	3.353	MED193_09580	Sugar ABC transporter, ATP-binding protein
A3X9H4	+	1.490	3.278	MED193_08013	TonB dependent iron siderophore receptor

A3X3N4	+	1.804	3.248	MED193_17499	Hemin degrading factor
A3X5C9	+	4.412	3.240	MED193_19454	Phosphonates import ATP-binding protein PhnC (EC 7.3.2.2)
A3X589	+	3.509	3.073	MED193_19674	Uncharacterized protein
A3X7B2	+	2.450	3.015	MED193_13887	Peptide methionine sulfoxide reductase MsrA (Protein-methionine-S-oxide reductase) (EC 1.8.4.11) (Peptide-methionine (S)-S-oxide reductase) (Peptide Met(O) reductase)
A3XEY5	+	1.732	2.987	MED193_12123	Microcystin dependent protein MdpB
A3X3R0	+	4.623	2.921	MED193_17379	Uncharacterized protein
A3XD56	+	2.145	2.875	MED193_09570	Sugar ABC transporter, periplasmic sugar-binding protein
A3X3N7	+	2.013	2.843	MED193_17494	Putative hemin binding periplasmic transmembrane protein
A3X586	+	2.197	2.782	MED193_19659	Uncharacterized protein
A3X3M9	+	2.304	2.610	MED193_17524	Uncharacterized protein
A3XB45	+	2.114	2.507	MED193_22076	FecB2
A3X587	+	2.058	2.504	MED193_19664	Lipoprotein, putative
A3X805	+	2.726	2.458	MED193_06629	Uroporphyrin-III C-methyltransferase
A3XG01	+	2.268	2.177	MED193_10071	Glyceraldehyde-3-phosphate dehydrogenase (EC 1.2.1.-)
A3X5N3	+	3.431	2.045	MED193_18939	Uncharacterized protein
A3XA09	+	2.704	-2.124	MED193_01270	Probable NADH-dependent dyhydrogenase
A3X7T4	+	3.177	-2.183	MED193_07004	NADH-quinone oxidoreductase subunit H (EC 1.6.5.11) (NADH dehydrogenase I subunit H) (NDH-1 subunit H)
A3X8Q8	+	1.917	-2.292	MED193_07753	Thiamine biosynthesis protein ThiF
A3XAQ8	+	2.940	-2.378	MED193_04671	Lipoyl synthase (EC 2.8.1.8) (Lip-syn) (LS) (Lipoate synthase) (Lipoic acid synthase) (Sulfur insertion protein LipA)
A3X3M4	+	2.737	-2.435	MED193_17559	Quinolinate synthase A (EC 2.5.1.72)
A3X7R2	+	3.439	-2.597	MED193_07099	Outer membrane protein OmpW
A3X6A5	+	3.129	-2.659	MED193_15662	3-isopropylmalate dehydratase small subunit (EC 4.2.1.33) (Alpha-IPM isomerase) (IPMI) (Isopropylmalate isomerase)
A3X5Z2	+	2.003	-2.670	MED193_16247	Aminotransferase, classes I and II
A3X6A6	+	2.156	-2.738	MED193_15667	3-isopropylmalate dehydratase large subunit (EC 4.2.1.33) (Alpha-IPM isomerase) (IPMI) (Isopropylmalate isomerase)
A3X744	+	2.670	-2.912	MED193_14232	Glutamate synthase, small subunit
A3X778	+	1.211	-2.993	MED193_14037	Glutaredoxin
A3X7Z9	+	2.201	-3.009	MED193_06669	Carbon monoxide dehydrogenase, medium subunit, putative
A3XFZ7	+	3.285	-3.085	MED193_10096	Formate dehydrogenase, alpha subunit, putative
A3XFZ3	+	3.536	-3.193	MED193_10121	Iron-sulfur cluster-binding protein
A3X795	+	2.008	-3.301	MED193_13987	23S rRNA (Uracil-5-)-methyltransferase rumA

A3X8Z9	+	0.897	-3.452	MED193_08893	Sulfate transporter family protein
A3X4F9	+	2.931	-3.515	MED193_21064	5-aminolevulinate synthase (EC 2.3.1.37) (5-aminolevulinic acid synthase) (Delta-ALA synthase) (Delta-aminolevulinate synthase)
A3XAQ9	+	1.849	-3.604	MED193_04676	Peroxiredoxin/glutaredoxin family protein
A3XFW0	+	1.548	-3.751	MED193_11712	N-methylproline demethylase, putative
A3X7Z6	+	3.011	-3.982	MED193_06674	Carbon monoxide dehydrogenase, large subunit
A3X8R1	+	2.381	-4.175	MED193_07743	Thiazole synthase (EC 2.8.1.10)

Appendix 4.8 Significantly up- and downregulated proteins (p-value <0.01) in the exoproteome of MED193 cultures supplemented with PG.

Protein ID	*p-value <0.01*	*-log$_{10}$ (p-value)*	*Log$_2$ (fold change)*	*Locus tag*	*Uniprot annotation*
A3X5C8	+	2.271	6.063	MED193_19449	Phosphonate-binding periplasmic protein
A3X3N5	+	1.835	5.842	MED193_17504	Putative Hemin receptor protein HmuR
A3XB54	+	1.619	4.401	MED193_22031	Outer membrane protein
A3X3N4	+	2.144	3.997	MED193_17499	Hemin degrading factor
A3X9H0	+	2.627	3.817	MED193_08043	TonB dependent iron siderophore receptor
A3X3N2	+	2.768	3.489	MED193_17509	Uncharacterized protein
A3X6A5	+	2.136	-3.726	MED193_15662	3-isopropylmalate dehydratase small subunit (EC 4.2.1.33) (Alpha-IPM isomerase) (IPMI) (Isopropylmalate isomerase)
A3XCP6	+	2.308	-4.194	MED193_10473	Succinate dehydrogenase iron-sulfur subunit (EC 1.3.5.1)
A3X6A6	+	1.747	-4.679	MED193_15667	3-isopropylmalate dehydratase large subunit (EC 4.2.1.33) (Alpha-IPM isomerase) (IPMI) (Isopropylmalate isomerase)
A3X8R4	+	1.708	-4.778	MED193_07728	Phosphomethylpyrimidine synthase (EC 4.1.99.17) (Hydroxymethylpyrimidine phosphate synthase) (HMP-P synthase) (HMP-phosphate synthase) (HMPP synthase) (Thiamine biosynthesis protein ThiC)
A3X7Z6	+	3.264	-5.097	MED193_06674	Carbon monoxide dehydrogenase, large subunit

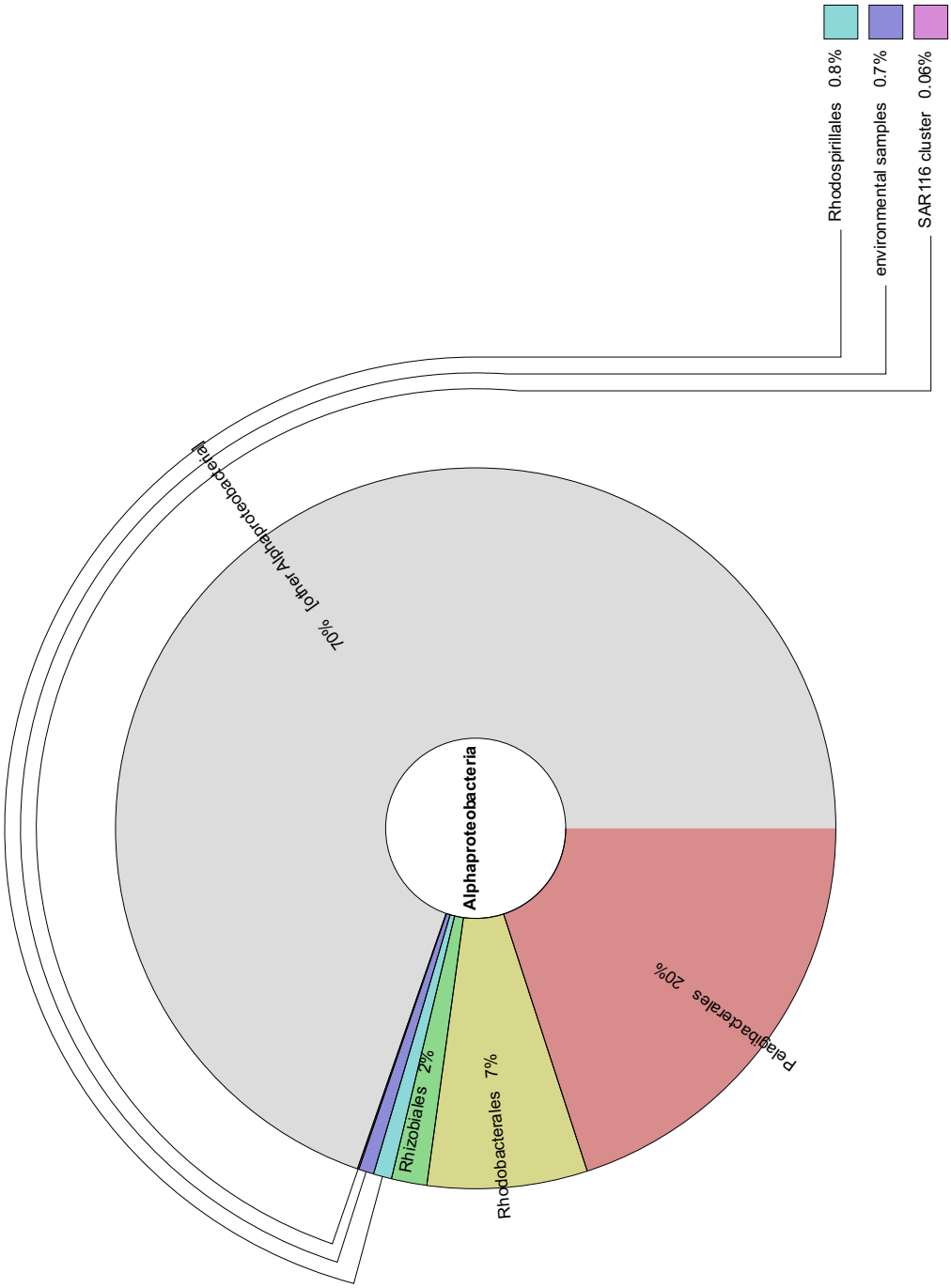

Appendix 4.9 Krona plot displays distribution of MED193 10041 homologs within Alphaproteobacteria, retrieved from OGA database.

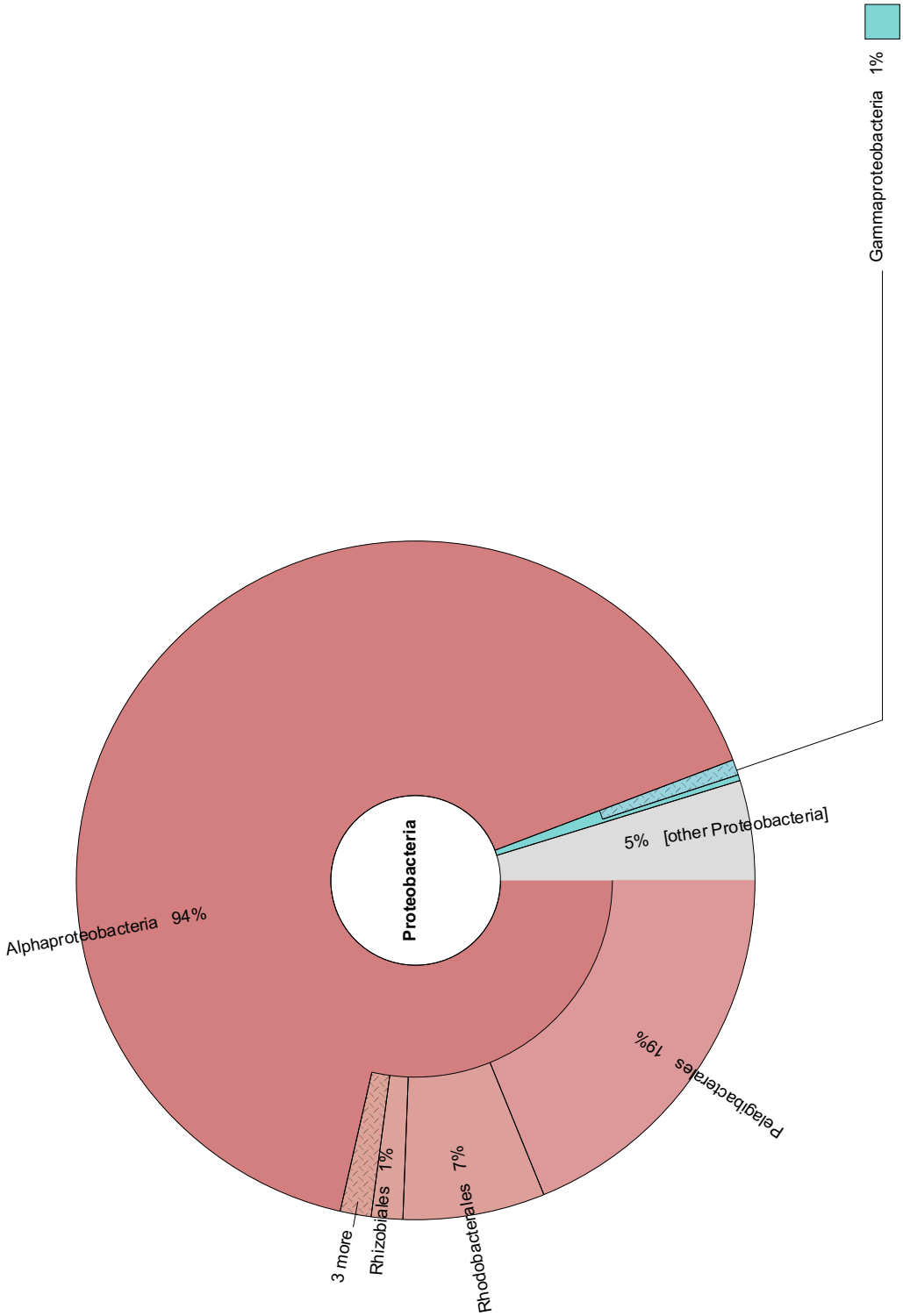

Appendix 4.10 Krona plot displays distribution of MED193_10041 homologs within proteobacteria, retrieved from OGA database.

Appendix 4.11 Colorimetric phosphatase assay using pNPP as substrate and different metal combinations. The Table (top) displays the experimental setup, the 96-well plate shows the colour change after 30 min incubation at 30°C.

	1	2	3	4	5	6	7	8	9	10	11	12
A	$CaCl_2$ negative	$ZnSO_4$ negative	$MnCl_2$ negative	$NiCl_2$ negative	$CoCl_2$ negative	Na_2MoO_4 negative	H_3BO_3 negative	Na_2SeO_3 negative	$CuCl_2$ negative	$FeCl_3$ negative	$CaCl_2$ Na_2SeO_3	$CuCl_2$ Na_2MoO_4
B	$CaCl_2$	$ZnSO_4$	$MnCl_2$	$NiCl_2$	$CoCl_2$	Na_2MoO_4	H_3BO_3	Na_2SeO_3	$CuCl_2$	$FeCl_3$	$ZnSO_4$ $CuCl_2$	$FeCl_3$ H_3BO_3
C	$CaCl_2$ $ZnSO_4$	$ZnSO_4$ $MnCl_2$	$MnCl_2$ $NiCl_2$	$NiCl_2$ $CoCl_2$	$CoCl_2$ Na_2MoO_4	Na_2MoO_4 H_3BO_3	H_3BO_3 Na_2SeO_3	Na_2SeO_3 $CuCl_2$	$CuCl_2$ $FeCl_3$	$FeCl_3$ $CaCl_2$	$MnCl_2$ $FeCl_3$	$CaCl_2$ $CuCl_2$
D	$CaCl_2$ $MnCl_2$	$ZnSO_4$ $NiCl_2$	$MnCl_2$ $CoCl_2$	$NiCl_2$ Na_2MoO_4	$CoCl_2$ H_3BO_3	Na_2MoO_4 Na_2SeO_3	H_3BO_3 $CuCl_2$	Na_2SeO_3 $FeCl_3$	$CuCl_2$ $CaCl_2$	$FeCl_3$ $ZnSO_4$	$NiCl_2$ $CaCl_2$	$ZnSO_4$ $FeCl_3$
E	$CaCl_2$ $NiCl_2$	$ZnSO_4$ $CoCl_2$	$MnCl_2$ Na_2MoO_4	$NiCl_2$ H_3BO_3	$CoCl_2$ Na_2SeO_3	Na_2MoO_4 $CuCl_2$	H_3BO_3 $FeCl_3$	Na_2SeO_3 $CaCl_2$	$CuCl_2$ $ZnSO_4$	$FeCl_3$ $MnCl_2$	$CoCl_2$ $ZnSO_4$	$MnCl_2$ $CaCl_2$
F	$CaCl_2$ $CoCl_2$	$ZnSO_4$ Na_2MoO_4	$MnCl_2$ H_3BO_3	$NiCl_2$ Na_2SeO_3	$CoCl_2$ $CuCl_2$	Na_2MoO_4 $FeCl_3$	H_3BO_3 $CaCl_2$	Na_2SeO_3 $ZnSO_4$	$CuCl_2$ $MnCl_2$	$FeCl_3$ $NiCl_2$	Na_2MoO_4 $MnCl_2$	$NiCl_2$ $ZnSO_4$
G	$CaCl_2$ Na_2MoO_4	$ZnSO_4$ H_3BO_3	$MnCl_2$ Na_2SeO_3	$NiCl_2$ $CuCl_2$	$CoCl_2$ $FeCl_3$	Na_2MoO_4 $CaCl_2$	H_3BO_3 $ZnSO_4$	Na_2SeO_3 $MnCl_2$	$CuCl_2$ $NiCl_2$	$FeCl_3$ $CoCl_2$	H_3BO_3 $NiCl_2$	$CoCl_2$ $MnCl_2$
H	$CaCl_2$ H_3BO_3	$ZnSO_4$ Na_2SeO_3	$MnCl_2$ $CuCl_2$	$NiCl_2$ $FeCl_3$	$CoCl_2$ $CaCl_2$	Na_2MoO_4 $ZnSO_4$	H_3BO_3 $MnCl_2$	Na_2SeO_3 $NiCl_2$	$CuCl_2$ $CoCl_2$	$FeCl_3$ Na_2MoO_4	Na_2SeO_3 $CoCl_2$	Na_2MoO_4 $NiCl_2$

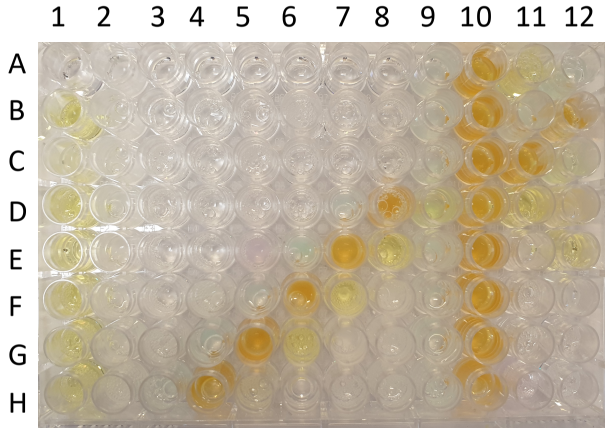

Appendix 5.1 Significantly up- and downregulated proteins (p-value <0.05) in the cellular proteome of WT MED193 G1P compared to WT MED193 +P.

Protein ID	*p-value <0.05*	*-log$_{10}$ (p-value)*	*Log$_2$ (fold change)*	*Locus tag*	*Uniprot annotation*
A3X5C8	+	3.6355	7.4876	MED193_19449	Phosphonate-binding periplasmic protein
A3X5C9	+	2.7799	6.5733	MED193_19454	Phosphonates import ATP-binding protein PhnC (EC 7.3.2.2)
A3XD56	+	2.6497	5.0190	MED193_09570	Sugar ABC transporter, periplasmic sugar-binding protein
A3X3N4	+	2.7024	4.8561	MED193_17499	Hemin degrading factor
A3X3D9	+	2.3811	4.7421	MED193_17984	Uncharacterized protein
A3XB54	+	2.1906	4.7050	MED193_22031	Outer membrane protein
A3X3N9	+	3.9758	4.6360	MED193_17484	Hemin import ATP-binding protein HmuV (EC 3.6.3.-)
A3X9H0	+	4.3725	4.3237	MED193_08043	TonB dependent-iron siderophore receptor
A3X3N3	+	2.9280	4.1783	MED193_17514	MotA/TolQ/ExbB proton channel family protein
A3X3N5	+	3.9298	4.1582	MED193_17504	Putative Hemin receptor protein HmuR
A3X9H4	+	2.7011	3.6305	MED193_08013	TonB dependent-iron siderophore receptor
A3XB52	+	2.1662	3.2479	MED193_22056	Siderophore-interacting protein
A3X587	+	1.0676	3.2417	MED193_19664	Lipoprotein, putative
A3X3Q7	+	2.7955	3.1195	MED193_17384	Putative iron ABC transport system, ATP-binding protein
A3X5D0	+	2.6234	3.1188	MED193_19459	Phosphonates ABC transporter permease protein
A3XB51	+	1.7783	3.1016	MED193_22051	MotA/TolQ/ExbB proton channel family protein
A3X589	+	1.6850	3.0926	MED193_19674	Uncharacterized protein
A3XB50	+	3.5329	3.0520	MED193_22046	Uncharacterized protein
A3X3N2	+	2.3714	2.9212	MED193_17509	Uncharacterized protein
A3X5C7	+	4.7617	2.8932	MED193_19469	Uncharacterized protein
A3X5M3	+	2.3202	2.8356	MED193_18984	Uncharacterized protein
A3X3Q9	+	2.8351	2.8319	MED193_17374	Uncharacterized protein
A3X3N7	+	2.2646	2.6677	MED193_17494	Putative hemin binding periplasmic transmembrane protein
A3XD57	+	1.4859	2.6570	MED193_09575	Sugar ABC transporter, ATP-binding protein
A3X586	+	1.5701	2.6260	MED193_19659	Uncharacterized protein
A3XFB5	+	0.9797	2.5192	MED193_21571	Membrane protein, putative
A3XG01	+	3.0259	2.4205	MED193_10071	Glyceraldehyde-3-phosphate dehydrogenase (EC 1.2.1.-)
A3X598	+	2.6260	2.3341	MED193_19624	Glycerol-3-phosphate dehydrogenase (EC 1.1.5.3)
A3XB46	+	2.4674	2.3195	MED193_22061	Iron(III) dicitrate ABC transporter (ATP-binding protein)

A3X3R0	+	3.5623	2.1808	MED193_17379	Uncharacterized protein
A3XB53	+	1.7949	2.0452	MED193_22036	Putative TonB protein
A3XB45	+	2.4938	1.8763	MED193_22076	FecB2
A3X6H4	+	2.2316	1.8369	MED193_15322	Ribonuclease, Rne/Rng family protein
A3XC04	+	2.0232	-1.9589	MED193_03482	Acyl-CoA dehydrogenase
A3XBX7	+	1.0814	-4.0088	MED193_03622	Indolepyruvate ferredoxin oxidoreductase (EC 1.2.7.8)

Appendix 5.2 Significantly up- and downregulated proteins (p-value <0.05) in the exoproteome of WT MED193 G1P compared to WT MED193 +P.

Protein ID	*p-value <0.05*	*$-\log_{10}$ (p-value)*	*$\log_2$ (fold change)*	*Locus tag*	*Uniprot annotation*
A3X5C8	+	3.362	8.030	MED193_19449	Phosphonate-binding periplasmic protein
A3X3N4	+	3.522	5.267	MED193_17499	Hemin degrading factor
A3X3N2	+	2.430	4.343	MED193_17509	Uncharacterized protein
A3XB54	+	2.035	4.299	MED193_22031	Outer membrane protein
A3X3N5	+	2.489	4.189	MED193_17504	Putative Hemin receptor protein HmuR
A3X3D9	+	3.318	3.483	MED193_17984	Uncharacterized protein
A3X413	+	1.081	3.464	MED193_16864	50S ribosomal protein L34
A3XA68	+	1.910	3.322	MED193_00995	Uncharacterized protein
A3X589	+	1.149	3.234	MED193_19674	Uncharacterized protein
A3XB52	+	2.073	3.227	MED193_22056	Siderophore-interacting protein
A3X3Q1	+	3.463	3.215	MED193_17424	Phosphogluconate dehydratase (EC 4.2.1.12)
A3XD56	+	2.149	3.200	MED193_09570	Sugar ABC transporter, periplasmic sugar-binding protein
A3X9H4	+	1.951	3.037	MED193_08013	TonB dependent-iron siderophore receptor
A3X4R3	+	1.787	2.957	MED193_20524	Uncharacterized protein
A3X587	+	2.428	2.834	MED193_19664	Lipoprotein, putative
A3X3Q9	+	2.018	2.585	MED193_17374	Uncharacterized protein
A3XG01	+	2.255	2.217	MED193_10071	Glyceraldehyde-3-phosphate dehydrogenase (EC 1.2.1.-)
A3XDT6	+	2.123	2.186	MED193_00725	Chloroacetaldehyde dehydrogenase
A3XFB8	+	2.165	-2.275	MED193_21536	Uncharacterized protein
A3XBX7	+	1.644	-2.912	MED193_03622	Indolepyruvate ferredoxin oxidoreductase (EC 1.2.7.8)

Appendix 5.3 Significantly up- and downregulated proteins (p-value <0.05) in the cellular proteome of ΔphoB G1P compared to WT MED193 +P.

Protein ID	*p-value <0.05*	*-log$_{10}$ (p-value)*	*Log$_2$ (fold change)*	*Locus tag*	*Uniprot annotation*
A3X5C8	+	3.6978	7.3127	MED193_19449	Phosphonate-binding periplasmic protein
A3X5C9	+	2.9139	7.0391	MED193_19454	Phosphonates import ATP-binding protein PhnC (EC 7.3.2.2)
A3X682	+	5.5312	6.1711	MED193_15777	EpsK domain protein
A3X3N4	+	2.7207	5.0098	MED193_17499	Hemin degrading factor
A3X3N5	+	4.1640	4.9551	MED193_17504	Putative Hemin receptor protein HmuR
A3XB54	+	2.3104	4.8866	MED193_22031	Outer membrane protein
A3X3N9	+	3.8348	4.5870	MED193_17484	Hemin import ATP-binding protein HmuV (EC 3.6.3.-)
A3X3D9	+	2.3958	4.5462	MED193_17984	Uncharacterized protein
A3X9H4	+	3.0219	4.3705	MED193_08013	TonB dependent-iron siderophore receptor
A3X3N3	+	2.9162	4.2749	MED193_17514	MotA/TolQ/ExbB proton channel family protein
A3X9H0	+	4.4463	4.1541	MED193_08043	TonB dependent-iron siderophore receptor
A3X5J0	+	3.6732	3.4129	MED193_19144	Aminomethyl transferase family protein
A3XD56	+	2.6858	3.3905	MED193_09570	Sugar ABC transporter, periplasmic sugar-binding protein
A3X5D0	+	2.8505	3.3698	MED193_19459	Phosphonates ABC transporter permease protein
A3XB50	+	3.3116	3.1059	MED193_22046	Uncharacterized protein
A3X589	+	2.2507	3.0284	MED193_19674	Uncharacterized protein
A3X587	+	3.0191	2.9763	MED193_19664	Lipoprotein, putative
A3X3N2	+	2.5152	2.9343	MED193_17509	Uncharacterized protein
A3XB51	+	1.6438	2.8392	MED193_22051	MotA/TolQ/ExbB proton channel family protein
A3X5C7	+	3.7874	2.8274	MED193_19469	Uncharacterized protein
A3XG01	+	4.7376	2.7960	MED193_10071	Glyceraldehyde-3-phosphate dehydrogenase (EC 1.2.1.-)
A3X3Q7	+	3.5289	2.7334	MED193_17384	Putative iron ABC transport system, ATP-binding protein
A3X3M9	+	3.0221	2.7092	MED193_17524	Uncharacterized protein
A3X598	+	3.3438	2.7035	MED193_19624	Glycerol-3-phosphate dehydrogenase (EC 1.1.5.3)
A3XEM0	+	1.6849	2.6802	MED193_12698	Uncharacterized protein
A3X6S9	+	3.7440	2.5524	MED193_14797	FAD dependent oxidoreductase/aminomethyl transferase
A3XB52	+	2.0384	2.4704	MED193_22056	Siderophore-interacting protein
A3X525	+	1.9378	2.3963	MED193_19954	Uncharacterized protein
A3X3Q1	+	2.8437	2.3808	MED193_17424	Phosphogluconate dehydratase (EC 4.2.1.12)

A3X3N7	+	2.6468	2.3175	MED193_17494	Putative hemin binding periplasmic transmembrane protein
A3X401	+	3.6661	2.2271	MED193_16924	Urea amidolyase-like protein
A3XCF9	+	1.0526	2.1576	MED193_10898	Glycerol-3-phosphate acyltransferase (Acyl-PO4 G3P acyltransferase) (Acyl-phosphate--glycerol-3-phosphate acyltransferase) (G3P acyltransferase) (GPAT) (EC 2.3.1.n3) (Lysophosphatidic acid synthase) (LPA synthase)
A3X9H3	+	1.1642	2.1411	MED193_08018	ABC ferric siderophore transporter, ATPase subunit
A3XB53	+	1.8353	2.0952	MED193_22036	Putative TonB protein
A3X7F3	+	1.5909	2.0033	MED193_13662	HD domain protein
A3X8K8	+	1.8746	1.9223	MED193_05624	Branched-chain amino acid ABC transporter, ATP-binding protein
A3X4I2	+	1.0811	1.9020	MED193_20944	GTP cyclohydrolase FolE2 (EC 3.5.4.16)
A3XAQ4	+	2.7736	1.9016	MED193_04696	Methyltransferase (EC 2.1.1.-)
A3X748	+	0.9751	1.8711	MED193_14212	Exonuclease, putative
A3X9G8	+	2.7372	1.8412	MED193_08033	Putative ABC transporter, periplasmic Fe+3 siderophore binding protein
A3XFW1	+	2.1377	1.8173	MED193_11717	Methyltransferase (EC 2.1.1.-)
A3XB97	+	1.9631	1.7103	MED193_21811	Membrane protein
A3X5Z4	+	1.7145	1.6135	MED193_16207	ATP synthase subunit a (ATP synthase F0 sector subunit a) (F-ATPase subunit 6)
A3XB46	+	3.3043	1.6030	MED193_22061	Iron(III) dicitrate ABC transporter (ATP-binding protein)
A3X3Q0	+	3.5754	1.5714	MED193_17419	Glucose-6-phosphate 1-dehydrogenase (G6PD) (EC 1.1.1.49)
A3X8V3	+	4.1175	1.5466	MED193_09113	Formate--tetrahydrofolate ligase (EC 6.3.4.3) (Formyltetrahydrofolate synthetase) (FHS) (FTHFS)
A3X717	+	2.0642	1.5061	MED193_14372	DNA-binding response regulator PetR
A3XC30	+	2.7050	1.4916	MED193_03362	Uncharacterized protein
A3XAD2	+	2.6250	1.4227	MED193_05311	Sarcosine oxidase, alpha subunit family protein
A3X8S2	+	3.2519	1.4003	MED193_07678	Uncharacterized protein
A3X6J8	+	3.5143	1.3821	MED193_15217	Uncharacterized protein
A3XCJ1	+	4.8869	-1.3757	MED193_10743	Transcription elongation factor GreA (Transcript cleavage factor GreA)
A3X625	+	2.7287	-1.3798	MED193_16072	Molybdenum cofactor biosynthesis domain protein
A3XDD9	+	2.8209	-1.4201	MED193_13443	ABC polyamine/opine transporter, inner membrane subunit
A3X9W0	+	2.3350	-1.4509	MED193_01525	Uncharacterized protein
A3X8C6	+	5.6420	-1.4936	MED193_06029	Uracil phosphoribosyltransferase (EC 2.4.2.9) (UMP pyrophosphorylase) (UPRTase)
A3X5U4	+	2.8862	-1.5253	MED193_18629	Probable swi/snf family helicase 2
A3XD03	+	4.2892	-1.5322	MED193_09840	2-isopropylmalate synthase (EC 2.3.3.13) (Alpha-IPM synthase) (Alpha-isopropylmalate synthase)
A3XBU2	+	3.5449	-1.5330	MED193_03802	TRAP transporter solute receptor, TAXI family protein

A3XDR5	+	1.7282	-1.5481	MED193_12788	50S ribosomal protein L36
A3XCP6	+	2.6669	-1.5505	MED193_10473	Succinate dehydrogenase iron-sulfur subunit (EC 1.3.5.1)
A3X442	+	3.9684	-1.5583	MED193_16719	50S ribosomal protein L30
A3XBX3	+	3.6054	-1.5976	MED193_03637	N-acetyl-gamma-glutamyl-phosphate reductase (AGPR) (EC 1.2.1.38) (N-acetyl-glutamate semialdehyde dehydrogenase) (NAGSA dehydrogenase)
A3XAU2	+	2.3101	-1.6000	MED193_04506	DNA-binding protein, putative
A3X6I4	+	1.9596	-1.6055	MED193_15287	UPF0262 protein MED193_15287
A3XB31	+	1.6214	-1.6154	MED193_22146	Glutamine synthetase family protein
A3X9Y4	+	1.5728	-1.6236	MED193_01405	Uncharacterized protein
A3XBC0	+	1.4022	-1.6287	MED193_22741	Phosphoribosylglycinamide formyltransferase (EC 2.1.2.2) (5'-phosphoribosylglycinamide transformylase) (GAR transformylase) (GART)
A3X7L6	+	1.3302	-1.6326	MED193_07339	Uncharacterized protein
A3XAT5	+	2.6436	-1.6398	MED193_04551	Delta-aminolevulinic acid dehydratase (EC 4.2.1.24)
A3X889	+	2.1226	-1.6418	MED193_06209	Thioesterase family protein
A3XAZ2	+	1.5289	-1.6469	MED193_04251	2-isopropylmalate synthase (EC 2.3.3.13)
A3X353	+	1.6979	-1.6746	MED193_18414	6-carboxy-5,6,7,8-tetrahydropterin synthase (EC 4.-.-.-)
A3XDL0	+	1.8420	-1.6860	MED193_13068	Uncharacterized protein
A3X8N7	+	1.3461	-1.6944	MED193_05474	Flavin reductase domain protein
A3XD83	+	1.2607	-1.6952	MED193_09455	Glycosyl transferase, WecB/TagA/CpsF family protein
A3X8B9	+	2.3931	-1.6982	MED193_06059	Uncharacterized protein
A3X4W8	+	3.1109	-1.7126	MED193_20249	N5-carboxyaminoimidazole ribonucleotide mutase (N5-CAIR mutase) (EC 5.4.99.18) (5-(carboxyamino)imidazole ribonucleotide mutase)
A3X7Y9	+	2.6873	-1.7273	MED193_06724	Uncharacterized protein
A3XFU4	+	1.1196	-1.7370	MED193_11772	Uncharacterized protein
A3XEM8	+	2.4975	-1.7490	MED193_12688	Uncharacterized protein
A3XAU9	+	2.1839	-1.7628	MED193_04461	Thiamine-phosphate pyrophosphorylase, putative
A3XCN9	+	1.9331	-1.7819	MED193_10523	Citrate lyase, beta subunit
A3X4T5	+	1.5345	-1.7919	MED193_20429	Methylmalonyl-CoA epimerase
A3XC17	+	3.1369	-1.8130	MED193_03427	Uncharacterized protein
A3XC04	+	1.8128	-1.8228	MED193_03482	Acyl-CoA dehydrogenase
A3XF74	+	1.7125	-1.8303	MED193_02710	Phosphoribosylformylglycinamidine synthase subunit PurS (FGAM synthase) (EC 6.3.5.3) (Formylglycinamide ribonucleotide amidotransferase subunit III) (FGAR amidotransferase III) (FGAR-AT III) (Phosphoribosylformylglycinamidine synthase subunit III)
A3XFS3	+	0.9855	-1.8758	MED193_11907	Uncharacterized protein

A3XDV1	+	3.8637	-1.8783	MED193_00660	Uncharacterized protein
A3XDR3	+	3.1207	-1.9007	MED193_12823	Branched-chain amino acid ABC transporter, ATP-binding protein
A3X9Q0	+	2.1454	-1.9019	MED193_01840	Probable oxidoreductase
A3XBP1	+	1.3629	-1.9396	MED193_04047	Phosphate import ATP-binding protein PstB (EC 7.3.2.1) (ABC phosphate transporter) (Phosphate-transporting ATPase)
A3X6A6	+	3.4947	-1.9565	MED193_15667	3-isopropylmalate dehydratase large subunit (EC 4.2.1.33) (Alpha-IPM isomerase) (IPMI) (Isopropylmalate isomerase)
A3XF53	+	3.1081	-1.9962	MED193_02805	Oxidoreductase, zinc-binding dehydrogenase family protein
A3XFA9	+	1.6573	-2.0113	MED193_21591	DNA-binding protein, putative
A3XFY2	+	1.3103	-2.0321	MED193_10161	Phosphonate ABC transporter, periplasmic phosphonate-binding protein
A3XE22	+	3.3206	-2.0448	MED193_00310	Replication protein a
A3X9Z5	+	2.2326	-2.0477	MED193_01340	Regulatory protein, IclR
A3X7B1	+	2.9098	-2.0523	MED193_13882	Ribokinase (RK) (EC 2.7.1.15)
A3XB64	+	3.4381	-2.0606	MED193_21976	Probable iron-containing alcohol dehydrogenase
A3XCV3	+	1.9467	-2.0707	MED193_09205	Holliday junction ATP-dependent DNA helicase RuvA (EC 3.6.4.12)
A3XBZ0	+	4.7210	-2.0719	MED193_03557	Glyceraldehyde-3-phosphate dehydrogenase, type I
A3XAW2	+	1.4927	-2.0729	MED193_04416	Glucose-6-phosphate 1-dehydrogenase (G6PD) (EC 1.1.1.49)
A3XBX4	+	1.0906	-2.0855	MED193_03642	Cytochrome c-type biogenesis protein CcmE (Cytochrome c maturation protein E) (Heme chaperone CcmE)
A3X7C9	+	2.3798	-2.0908	MED193_13792	Dephospho-CoA kinase (EC 2.7.1.24) (Dephosphocoenzyme A kinase)
A3XBW5	+	0.9286	-2.1605	MED193_03687	LexA repressor (EC 3.4.21.88)
A3X3G8	+	3.4753	-2.1650	MED193_17829	Glyoxalase family protein
A3X4R0	+	4.5400	-2.1676	MED193_20559	Ornithine carbamoyltransferase (OTCase) (EC 2.1.3.3)
A3X976	+	1.6058	-2.1709	MED193_08493	Riboflavin biosynthesis protein RibD [Includes: Diaminohydroxyphosphoribosylaminopyrimidine deaminase (DRAP deaminase) (EC 3.5.4.26) (Riboflavin-specific deaminase); 5-amino-6-(5-phosphoribosylamino)uracil reductase (EC 1.1.1.193) (HTP reductase)]
A3X621	+	1.1746	-2.1952	MED193_16102	tRNA (guanine-N(1)-)-methyltransferase (EC 2.1.1.228) (M1G-methyltransferase) (tRNA [GM37] methyltransferase)
A3XG05	+	1.7919	-2.2111	MED193_10041	Bacterial extracellular solute-binding protein, family 7
A3XC88	+	3.4966	-2.2251	MED193_11268	Cytochrome c552
A3XE23	+	3.1540	-2.2327	MED193_00315	Uncharacterized protein
A3XFG2	+	1.5722	-2.2525	MED193_11684	Uncharacterized protein
A3X4Q9	+	4.4266	-2.2621	MED193_20554	Acetylornithine aminotransferase (ACOAT) (EC 2.6.1.11)
A3X8L5	+	2.2146	-2.2624	MED193_05574	Uncharacterized protein

A3X6A0	+	1.2044	-2.2643	MED193_15682	Ribosomal silencing factor RsfS
A3X7Z6	+	1.3288	-2.2919	MED193_06674	Carbon monoxide dehydrogenase, large subunit
A3X860	+	3.1248	-2.3070	MED193_06359	Type I site-specific deoxyribonuclease HsdM
A3XDP5	+	1.8311	-2.3277	MED193_12893	Phosphoglycerate mutase family protein
A3XAQ9	+	2.4779	-2.3476	MED193_04676	Peroxiredoxin/glutaredoxin family protein
A3XAL8	+	1.6404	-2.3624	MED193_04881	tRNA-specific 2-thiouridylase MnmA (EC 2.8.1.13)
A3X701	+	2.6180	-2.3731	MED193_14432	ABC thiamine transporter, periplasmic substrate-binding protein
A3X3S2	+	4.4716	-2.3745	MED193_17319	Phenylacetate-coenzyme A ligase (EC 6.2.1.30) (Phenylacetyl-CoA ligase)
A3XDV2	+	3.7815	-2.4094	MED193_00665	Uncharacterized protein
A3X699	+	3.1196	-2.4366	MED193_15722	Heat shock protein, Hsp20 family protein
A3XD94	+	3.8917	-2.4384	MED193_09370	Glycine cleavage system H protein
A3X453	+	0.8544	-2.5048	MED193_16664	50S ribosomal protein L29
A3X7R8	+	4.1201	-2.5294	MED193_07059	NADH-quinone oxidoreductase subunit B (EC 1.6.5.11) (NADH dehydrogenase I subunit B) (NDH-1 subunit B)
A3X3M4	+	1.8048	-2.5412	MED193_17559	Quinolinate synthase A (EC 2.5.1.72)
A3X7K4	+	2.4690	-2.5510	MED193_07384	Uncharacterized protein
A3XBS8	+	2.6303	-2.5558	MED193_03882	Acetyltransferase, GNAT family protein
A3X973	+	2.7991	-2.5739	MED193_08518	Uncharacterized protein
A3X6A5	+	2.9392	-2.5889	MED193_15662	3-isopropylmalate dehydratase small subunit (EC 4.2.1.33) (Alpha-IPM isomerase) (IPMI) (Isopropylmalate isomerase)
A3XAQ8	+	1.4666	-2.6297	MED193_04671	Lipoyl synthase (EC 2.8.1.8) (Lip-syn) (LS) (Lipoate synthase) (Lipoic acid synthase) (Sulfur insertion protein LipA)
A3X6N4	+	2.4208	-2.6692	MED193_15007	Glycine cleavage system H protein
A3X744	+	2.0706	-2.6786	MED193_14232	Glutamate synthase, small subunit
A3XFQ8	+	2.0146	-2.6966	MED193_11967	Uncharacterized protein
A3XFP4	+	1.4781	-2.7088	MED193_12037	Uncharacterized protein
A3X3I3	+	1.9835	-2.7799	MED193_17759	Transcriptional regulator, ArsR family protein
A3X8A9	+	1.4474	-2.7970	MED193_06104	ArsC family protein
A3X9P6	+	4.3332	-2.9149	MED193_01855	Putative periplasmic solute-binding protein
A3X3E7	+	0.7958	-2.9601	MED193_17949	30S ribosomal protein S1
A3X9U9	+	2.3656	-3.0900	MED193_01580	Uncharacterized protein
A3XFH6	+	2.9204	-3.1630	MED193_11614	Transmembrane transporter, major facilitator family protein
A3XB17	+	3.9554	-3.1966	MED193_22211	Putative Ornithine decarboxylase
A3XBP3	+	4.0429	-3.2150	MED193_04042	Phosphate-specific transport system accessory protein PhoU

A3X795	+	5.6065	-3.2501	MED193_13987	23S rRNA (Uracil-5-)-methyltransferase rumA
A3X738	+	1.9795	-3.5365	MED193_14247	Glutamate synthase, large subunit
A3XDT6	+	3.3111	-3.5734	MED193_00725	Chloroacetaldehyde dehydrogenase
A3XA05	+	3.2018	-3.6693	MED193_01295	Na(+)-translocating NADH-quinone reductase subunit C (Na(+)-NQR subunit C) (Na(+)-translocating NQR subunit C) (EC 7.2.1.1) (NQR complex subunit C) (NQR-1 subunit C)
A3XE07	+	3.0483	-3.6957	MED193_00395	ATPase of the AAA+ class
A3X8H3	+	2.2703	-4.1225	MED193_05784	Uncharacterized protein
A3X815	+	3.9217	-4.3612	MED193_06579	Glycerophosphoryl diester phosphodiesterase
A3XA06	+	4.2865	-4.4403	MED193_01300	Na(+)-translocating NADH-quinone reductase subunit B (Na(+)-NQR subunit B) (Na(+)-translocating NQR subunit B) (EC 7.2.1.1) (NQR complex subunit B) (NQR-1 subunit B)
A3XA11	+	4.1426	-5.5219	MED193_01280	Na(+)-translocating NADH-quinone reductase subunit F (Na(+)-NQR subunit F) (Na(+)-translocating NQR subunit F) (EC 7.2.1.1) (NQR complex subunit F) (NQR-1 subunit F)
A3XBP0	+	3.5040	-5.7297	MED193_04062	Phosphate ABC transporter, periplasmic phosphate-binding protein
A3XBX7	+	3.3220	-5.8214	MED193_03622	Indolepyruvate ferredoxin oxidoreductase (EC 1.2.7.8)
A3XA04	+	6.0997	-5.9635	MED193_01305	Na(+)-translocating NADH-quinone reductase subunit A (Na(+)-NQR subunit A) (Na(+)-translocating NQR subunit A) (EC 7.2.1.1) (NQR complex subunit A) (NQR-1 subunit A)

Appendix 5.4 Significantly up- and downregulated proteins (p-value <0.05) in the exoproteome of ΔphoB G1P compared to WT MED193 +P.

Protein ID	*p-value <0.05*	*-log$_{10}$ (p-value)*	*Log$_2$ (fold change)*	*Locus tag*	*Uniprot annotation*
A3X5C8	+	3.637	8.623	MED193_19449	Phosphonate-binding periplasmic protein
A3X3N4	+	3.324	4.931	MED193_17499	Hemin degrading factor
A3X3Q1	+	2.638	4.072	MED193_17424	Phosphogluconate dehydratase (EC 4.2.1.12)
A3X3N5	+	2.029	3.903	MED193_17504	Putative Hemin receptor protein HmuR
A3X3D9	+	3.017	3.841	MED193_17984	Uncharacterized protein
A3XFE5	+	3.115	3.717	MED193_21421	Uncharacterized protein
A3X3N2	+	2.101	3.587	MED193_17509	Uncharacterized protein
A3XA68	+	2.212	3.513	MED193_00995	Uncharacterized protein

A3XB54	+	1.412	3.315	MED193_22031	Outer membrane protein
A3XD37	+	2.310	3.271	MED193_09670	Uncharacterized protein
A3XEY6	+	1.479	2.872	MED193_12128	Hypothetical microcystin dependent protein
A3X9H4	+	1.382	2.733	MED193_08013	TonB dependent-iron siderophore receptor
A3XEY7	+	2.641	2.707	MED193_12133	Microcystin dependent protein MdpB
A3XB77	+	1.507	2.657	MED193_21926	Multicopper oxidase domain protein
A3XD56	+	2.508	2.624	MED193_09570	Sugar ABC transporter, periplasmic sugar-binding protein
A3XB52	+	1.778	2.563	MED193_22056	Siderophore-interacting protein
A3XF95	+	2.431	2.292	MED193_21676	Choline sulfatase
A3XF75	+	3.949	-2.290	MED193_02715	Phosphoribosylformylglycinamidine synthase subunit PurQ (FGAM synthase) (EC 6.3.5.3) (Formylglycinamide ribonucleotide amidotransferase subunit I) (FGAR amidotransferase I) (FGAR-AT I) (Glutaminase PurQ) (EC 3.5.1.2) (Phosphoribosylformylglycinamidine synthase subunit I)
A3X6H2	+	2.235	-2.326	MED193_15352	Uncharacterized protein
A3X7K0	+	2.387	-2.392	MED193_07404	Outer membrane protein assembly factor BamD
A3XC61	+	2.361	-2.397	MED193_03202	3-oxoacyl-(Acyl-carrier-protein) reductase
A3X824	+	1.798	-2.424	MED193_06534	Glutamate/leucine/phenylalanine/valine dehydrogenase family protein
A3XD03	+	2.718	-2.455	MED193_09840	2-isopropylmalate synthase (EC 2.3.3.13) (Alpha-IPM synthase) (Alpha-isopropylmalate synthase)
A3XFB8	+	1.756	-2.522	MED193_21536	Uncharacterized protein
A3XCN4	+	1.949	-2.529	MED193_10543	Succinate--CoA ligase [ADP-forming] subunit beta (EC 6.2.1.5) (Succinyl-CoA synthetase subunit beta) (SCS-beta)
A3X650	+	1.921	-2.554	MED193_15957	50S ribosomal protein L7/L12
A3XCJ5	+	2.132	-2.597	MED193_10728	Electrotransfer ubiquinone oxidoreductase family protein
A3XBZ0	+	1.881	-2.949	MED193_03557	Glyceraldehyde-3-phosphate dehydrogenase, type I
A3X352	+	2.061	-2.970	MED193_18409	7-cyano-7-deazaguanine synthase (EC 6.3.4.20) (7-cyano-7-carbaguanine synthase) (PreQ(0) synthase) (Queuosine biosynthesis protein QueC)
A3X647	+	1.622	-3.023	MED193_15942	50S ribosomal protein L11
A3X4U1	+	1.369	-3.035	MED193_20394	Carbamoyl-phosphate synthase large chain (EC 6.3.5.5) (Carbamoyl-phosphate synthetase ammonia chain)
A3XB11	+	1.927	-3.198	MED193_04161	Peptidoglycan binding protein, putative
A3XDM7	+	1.112	-3.218	MED193_13003	Bifunctional purine biosynthesis protein PurH [Includes: Phosphoribosylaminoimidazolecarboxamide formyltransferase (EC 2.1.2.3) (AICAR transformylase); IMP cyclohydrolase (EC 3.5.4.10) (Inosinicase) (IMP synthase) (ATIC)]

A3X6A6	+	2.947	-3.315	MED193_15667	3-isopropylmalate dehydratase large subunit (EC 4.2.1.33) (Alpha-IPM isomerase) (IPMI) (Isopropylmalate isomerase)
A3XC84	+	2.535	-3.324	MED193_11293	Sugar ABC transporter, periplasmic sugar-binding protein
A3XBU5	+	2.721	-3.353	MED193_03787	Vitamin B12-dependent ribonucleotide reductase (EC 1.17.4.1)
A3XBX7	+	1.912	-3.379	MED193_03622	Indolepyruvate ferredoxin oxidoreductase (EC 1.2.7.8)
A3X738	+	1.181	-3.480	MED193_14247	Glutamate synthase, large subunit
A3X4R1	+	3.056	-3.854	MED193_20539	Uncharacterized protein
A3XFY2	+	2.696	-4.050	MED193_10161	Phosphonate ABC transporter, periplasmic phosphonate-binding protein
A3X7Z6	+	1.488	-4.078	MED193_06674	Carbon monoxide dehydrogenase, large subunit
A3X4R0	+	2.355	-4.180	MED193_20559	Ornithine carbamoyltransferase (OTCase) (EC 2.1.3.3)
A3XDH8	+	1.793	-4.340	MED193_13223	DNA gyrase subunit B (EC 5.99.1.3)
A3X6T7	+	2.366	-4.606	MED193_14742	Acetyl-CoA C-acetyltransferase
A3X4Q9	+	2.640	-4.931	MED193_20554	Acetylornithine aminotransferase (ACOAT) (EC 2.6.1.11)
A3X8H3	+	3.034	-5.202	MED193_05784	Uncharacterized protein
A3X815	+	2.763	-6.010	MED193_06579	Glycerophosphoryl diester phosphodiesterase
A3XBP0	+	3.202	-7.242	MED193_04062	Phosphate ABC transporter, periplasmic phosphate-binding protein

Appendix 5.5 Significantly up- and downregulated proteins (p-value <0.05) in the cellular proteome of WT MED193 G3P compared to WT MED193 +P.

Protein ID	*p-value <0.05*	*$-\log_{10}$ (p-value)*	*$\log_2$ (fold change)*	*Locus tag*	*Uniprot annotation*
A3X5C8	+	3.7377	7.8864	MED193_19449	Phosphonate-binding periplasmic protein
A3X5C9	+	2.8051	6.6694	MED193_19454	Phosphonates import ATP-binding protein PhnC (EC 7.3.2.2)
A3XB54	+	2.3167	4.9229	MED193_22031	Outer membrane protein
A3X3N4	+	2.5651	4.4914	MED193_17499	Hemin degrading factor
A3X587	+	3.0855	4.3752	MED193_19664	Lipoprotein, putative
A3XD56	+	3.1410	4.3403	MED193_09570	Sugar ABC transporter, periplasmic sugar-binding protein
A3X3N9	+	3.8322	4.3159	MED193_17484	Hemin import ATP-binding protein HmuV (EC 3.6.3.-)
A3X3N5	+	3.9947	4.3153	MED193_17504	Putative Hemin receptor protein HmuR
A3X3D9	+	2.2894	4.2484	MED193_17984	Uncharacterized protein
A3X3N3	+	2.9432	3.9424	MED193_17514	MotA/TolQ/ExbB proton channel family protein
A3X9H4	+	2.8767	3.8598	MED193_08013	TonB dependent-iron siderophore receptor

A3X9H0	+	4.6108	3.8558	MED193_08043	TonB dependent-iron siderophore receptor
A3XB51	+	1.8086	3.1404	MED193_22051	MotA/TolQ/ExbB proton channel family protein
A3X5D0	+	2.7335	3.1347	MED193_19459	Phosphonates ABC transporter permease protein
A3XB52	+	2.2934	2.9577	MED193_22056	Siderophore-interacting protein
A3X3N7	+	2.8817	2.9053	MED193_17494	Putative hemin binding periplasmic transmembrane protein
A3X3N2	+	2.5021	2.8744	MED193_17509	Uncharacterized protein
A3X3Q9	+	2.9334	2.8194	MED193_17374	Uncharacterized protein
A3X598	+	3.0307	2.8085	MED193_19624	Glycerol-3-phosphate dehydrogenase (EC 1.1.5.3)
A3X3Q7	+	4.1250	2.7851	MED193_17384	Putative iron ABC transport system, ATP-binding protein
A3X5C7	+	3.3970	2.6502	MED193_19469	Uncharacterized protein
A3X5M3	+	2.3152	2.6056	MED193_18984	Uncharacterized protein
A3XD57	+	1.4508	2.5900	MED193_09575	Sugar ABC transporter, ATP-binding protein
A3X589	+	1.9974	2.5737	MED193_19674	Uncharacterized protein
A3XB45	+	3.7796	2.3396	MED193_22076	FecB2
A3XFB5	+	0.9029	2.3235	MED193_21571	Membrane protein, putative
A3XEM0	+	1.4621	2.2029	MED193_12698	Uncharacterized protein
A3X9G8	+	2.7860	2.0354	MED193_08033	Putative ABC transporter, periplasmic Fe+3 siderophore binding protein
A3XB50	+	1.0209	2.0273	MED193_22046	Uncharacterized protein
A3XB46	+	3.5136	1.9767	MED193_22061	Iron(III) dicitrate ABC transporter (ATP-binding protein)
A3XA59	+	2.5497	1.9643	MED193_01035	Uncharacterized protein
A3X3R0	+	3.1170	1.9618	MED193_17379	Uncharacterized protein
A3XB53	+	1.7404	1.9581	MED193_22036	Putative TonB protein
A3XG01	+	3.2078	1.8876	MED193_10071	Glyceraldehyde-3-phosphate dehydrogenase (EC 1.2.1.-)
A3X5Z4	+	1.9103	1.8461	MED193_16207	ATP synthase subunit a (ATP synthase F0 sector subunit a) (F-ATPase subunit 6)
A3X3N6	+	1.8339	1.8435	MED193_17489	Putative hemin transport system permease transmembrane protein
A3X586	+	1.9988	1.8281	MED193_19659	Uncharacterized protein
A3X3M9	+	2.1012	1.7987	MED193_17524	Uncharacterized protein
A3X8S2	+	3.6020	1.6175	MED193_07678	Uncharacterized protein
A3XF74	+	1.4988	-1.7065	MED193_02710	Phosphoribosylformylglycinamidine synthase subunit PurS (FGAM synthase) (EC 6.3.5.3) (Formylglycinamide ribonucleotide amidotransferase subunit III) (FGAR amidotransferase III) (FGAR-AT III) (Phosphoribosylformylglycinamidine synthase subunit III)
A3XFA9	+	2.0728	-1.7999	MED193_21591	DNA-binding protein, putative
A3XDR5	+	1.7950	-1.8442	MED193_12788	50S ribosomal protein L36

A3XC88	+	1.7164	-2.0037	MED193_11268	Cytochrome c552
A3X744	+	1.9111	-2.0844	MED193_14232	Glutamate synthase, small subunit
A3X701	+	0.9365	-2.2380	MED193_14432	ABC thiamine transporter, periplasmic substrate-binding protein
A3X9Z5	+	2.1139	-2.3411	MED193_01340	Regulatory protein, IclR
A3X8R4	+	0.8598	-2.9481	MED193_07728	Phosphomethylpyrimidine synthase (EC 4.1.99.17) (Hydroxymethylpyrimidine phosphate synthase) (HMP-P synthase) (HMP-phosphate synthase) (HMPP synthase) (Thiamine biosynthesis protein ThiC)

Appendix 5.6 Significantly up- and downregulated proteins (p-value <0.05) in the exoproteome of WT MED193 G3P compared to WT MED193 +P.

Protein ID	*p-value <0.05*	*-log$_{10}$ (p-value)*	*Log$_2$ (fold change)*	*Locus tag*	*Uniprot annotation*
A3X5C8	+	3.366	7.841	MED193_19449	Phosphonate-binding periplasmic protein
A3XB54	+	2.085	4.399	MED193_22031	Outer membrane protein
A3X3N5	+	2.428	4.045	MED193_17504	Putative Hemin receptor protein HmuR
A3X3N4	+	3.050	3.656	MED193_17499	Hemin degrading factor
A3X3N2	+	2.091	3.530	MED193_17509	Uncharacterized protein
A3X9H4	+	1.980	3.072	MED193_08013	TonB dependent-iron siderophore receptor
A3X3D9	+	2.910	3.029	MED193_17984	Uncharacterized protein
A3XB52	+	1.989	2.899	MED193_22056	Siderophore-interacting protein
A3XD56	+	3.143	2.801	MED193_09570	Sugar ABC transporter, periplasmic sugar-binding protein
A3X587	+	2.318	2.394	MED193_19664	Lipoprotein, putative
A3X3Q1	+	2.146	2.262	MED193_17424	Phosphogluconate dehydratase (EC 4.2.1.12)
A3X983	+	2.706	-1.951	MED193_08468	Riboflavin synthase subunit alpha (EC 2.5.1.9)
A3XDH5	+	2.281	-1.969	MED193_13253	Enoyl-CoA hydratase
A3XFX4	+	2.400	-2.119	MED193_10211	Enoyl-CoA hydratase/isomerase/3-hydroxyacyl-CoA dehydrogenase
A3X4I0	+	3.454	-2.123	MED193_20959	Phosphoenolpyruvate-protein phosphotransferase
A3X768	+	2.262	-2.129	MED193_14122	Chaperone protein DnaJ
A3X7K0	+	1.959	-2.161	MED193_07404	Outer membrane protein assembly factor BamD
A3XAY3	+	2.099	-2.172	MED193_04286	FeS assembly protein SufD
A3XC61	+	1.630	-2.237	MED193_03202	3-oxoacyl-(Acyl-carrier-protein) reductase
A3X8X7	+	1.775	-2.254	MED193_08983	DNA topoisomerase 1 (EC 5.99.1.2) (DNA topoisomerase I)

A3XC67	+	1.513	-2.258	MED193_03172	30S ribosomal protein S6
A3XBG9	+	3.132	-2.322	MED193_22501	3-hydroxyacyl-CoA dehydrogenase, type II
A3XBX9	+	2.327	-2.359	MED193_03612	Phosphoribosylformylglycinamidine synthase subunit PurL (FGAM synthase) (EC 6.3.5.3) (Formylglycinamide ribonucleotide amidotransferase subunit II) (FGAR amidotransferase II) (FGAR-AT II) (Glutamine amidotransferase PurL) (Phosphoribosylformylglycinamidine synthase subunit II)
A3X4Z0	+	1.441	-2.389	MED193_20139	Ribose-phosphate pyrophosphokinase (RPPK) (EC 2.7.6.1) (5-phospho-D-ribosyl alpha-1-diphosphate) (Phosphoribosyl diphosphate synthase) (Phosphoribosyl pyrophosphate synthase) (P-Rib-PP synthase) (PRPP synthase) (PRPPase)
A3XBG1	+	1.346	-2.391	MED193_22536	Putative ATP-dependent RNA helicase protein
A3X926	+	1.456	-2.394	MED193_08748	Carbamoyl-phosphate synthase small chain (EC 6.3.5.5) (Carbamoyl-phosphate synthetase glutamine chain)
A3X773	+	1.752	-2.416	MED193_14102	Protein translocase subunit SecA
A3XC60	+	1.481	-2.422	MED193_03197	Malonyl CoA-acyl carrier protein transacylase (EC 2.3.1.39)
A3XC12	+	1.535	-2.442	MED193_03447	UvrABC system protein A (UvrA protein) (Excinuclease ABC subunit A)
A3X732	+	2.180	-2.485	MED193_14267	Hydantoinase/oxoprolinase family protein
A3X744	+	1.538	-2.493	MED193_14232	Glutamate synthase, small subunit
A3XBT2	+	1.816	-2.503	MED193_03862	Uncharacterized protein
A3X802	+	1.543	-2.524	MED193_06639	Sulfite reductase, putative
A3X755	+	1.332	-2.564	MED193_14152	UDP-glucose pyrophosphate
A3X7S3	+	1.472	-2.592	MED193_07039	ATP synthase subunit E (EC 3.6.3.14)
A3XCB4	+	1.292	-2.614	MED193_11143	7-alpha-hydroxysteroid dehydrogenase, putative
A3X8J3	+	1.807	-2.648	MED193_05694	ATP-dependent Clp protease ATP-binding subunit ClpX
A3X6A9	+	1.447	-2.653	MED193_15632	3-isopropylmalate dehydrogenase (EC 1.1.1.85) (3-IPM-DH) (Beta-IPM dehydrogenase) (IMDH)
A3X910	+	1.280	-2.683	MED193_08828	Pyruvate phosphate dikinase (EC 2.7.9.1)
A3XBR8	+	1.099	-2.691	MED193_03922	30S ribosomal protein S2
A3XFB8	+	2.178	-2.700	MED193_21536	Uncharacterized protein
A3X464	+	2.253	-2.759	MED193_16599	30S ribosomal protein S10
A3X8I4	+	1.535	-2.774	MED193_05734	Sulfur oxidation B protein
A3X647	+	2.168	-2.808	MED193_15942	50S ribosomal protein L11
A3X6T7	+	1.205	-2.888	MED193_14742	Acetyl-CoA C-acetyltransferase
A3XAJ4	+	1.442	-2.932	MED193_05001	Single-stranded DNA-binding protein (SSB)
A3XAY4	+	1.928	-2.935	MED193_04291	FeS assembly ATPase SufC
A3XD23	+	2.416	-2.959	MED193_09745	ABC transporter, ATP-binding protein

A3XDM5	+	3.150	-3.053	MED193_12993	Uncharacterized protein
A3XF98	+	1.251	-3.107	MED193_21641	Probable transcriptional regulatory protein MED193_21641
A3XBX7	+	1.715	-3.153	MED193_03622	Indolepyruvate ferredoxin oxidoreductase (EC 1.2.7.8)
A3XBV5	+	2.061	-3.160	MED193_03727	Anthranilate synthase component 1 (EC 4.1.3.27)
A3X9A5	+	1.525	-3.173	MED193_08358	Helicase, putative
A3X8D7	+	2.480	-3.195	MED193_05969	Fatty oxidation complex, alpha subunit
A3X655	+	2.046	-3.209	MED193_15932	Transcription termination/antitermination protein NusG
A3XFS4	+	3.073	-3.336	MED193_11912	30S ribosomal protein S21
A3XDD7	+	1.983	-3.438	MED193_13433	Ribonuclease R (RNase R) (EC 3.1.13.1)
A3X4R1	+	2.523	-3.490	MED193_20539	Uncharacterized protein
A3X6A6	+	3.141	-3.494	MED193_15667	3-isopropylmalate dehydratase large subunit (EC 4.2.1.33) (Alpha-IPM isomerase) (IPMI) (Isopropylmalate isomerase)
A3XFH8	+	1.954	-3.667	MED193_11579	Soluble pyridine nucleotide transhydrogenase (EC 1.6.1.1)
A3XFD0	+	1.282	-3.693	MED193_21496	Pseudouridine synthase (EC 5.4.99.-)
A3XDS6	+	1.539	-3.703	MED193_12758	Chaperone protein ClpB
A3X4U1	+	1.899	-3.718	MED193_20394	Carbamoyl-phosphate synthase large chain (EC 6.3.5.5) (Carbamoyl-phosphate synthetase ammonia chain)
A3X427	+	1.254	-3.760	MED193_16794	Pseudouridine synthase (EC 5.4.99.-)
A3XCJ5	+	2.773	-3.937	MED193_10728	Electrotransfer ubiquinone oxidoreductase family protein
A3X7Z8	+	1.593	-3.945	MED193_06664	Translation initiation factor IF-3
A3XC28	+	1.098	-4.060	MED193_03372	Uncharacterized protein
A3X824	+	3.092	-4.104	MED193_06534	Glutamate/leucine/phenylalanine/valine dehydrogenase family protein
A3XDH8	+	1.717	-4.222	MED193_13223	DNA gyrase subunit B (EC 5.99.1.3)
A3X825	+	2.502	-4.253	MED193_06539	Lon protease (EC 3.4.21.53) (ATP-dependent protease La)
A3X430	+	3.190	-4.334	MED193_16779	Periplasmic serine protease, DO/DeqQ family protein
A3XBE9	+	2.113	-4.387	MED193_22606	Uncharacterized protein
A3X769	+	1.905	-5.262	MED193_14082	Translation initiation factor IF-2

Appendix 5.7 Significantly up- and downregulated proteins (p-value <0.05) in the cellular proteome of ΔphoB G3P compared to WT MED193 +P.

Protein ID	*p-value <0.05*	*-log_{10} (p-value)*	*Log_2 (fold change)*	*Locus tag*	*Uniprot annotation*
A3X5C8	+	3.6103	7.0897	MED193_19449	Phosphonate-binding periplasmic protein
A3X5C9	+	2.7450	6.3570	MED193_19454	Phosphonates import ATP-binding protein PhnC (EC 7.3.2.2)
A3XB54	+	2.2119	4.7965	MED193_22031	Outer membrane protein
A3X3N4	+	2.3851	4.7661	MED193_17499	Hemin degrading factor
A3X3N5	+	3.6262	4.6599	MED193_17504	Putative Hemin receptor protein HmuR
A3X3D9	+	2.3159	4.6397	MED193_17984	Uncharacterized protein
A3X3N9	+	3.0577	4.2996	MED193_17484	Hemin import ATP-binding protein HmuV (EC 3.6.3.-)
A3X3N3	+	3.0029	4.0950	MED193_17514	MotA/TolQ/ExbB proton channel family protein
A3X9H4	+	2.9024	4.0689	MED193_08013	TonB dependent-iron siderophore receptor
A3X9H0	+	3.4534	3.9727	MED193_08043	TonB dependent-iron siderophore receptor
A3X682	+	0.8162	3.7934	MED193_15777	EpsK domain protein
A3X3N2	+	2.7129	3.3076	MED193_17509	Uncharacterized protein
A3X589	+	2.1811	3.2824	MED193_19674	Uncharacterized protein
A3XB50	+	3.5338	3.0265	MED193_22046	Uncharacterized protein
A3X525	+	2.1400	2.9797	MED193_19954	Uncharacterized protein
A3X587	+	1.9226	2.8250	MED193_19664	Lipoprotein, putative
A3X5D0	+	2.3544	2.7649	MED193_19459	Phosphonates ABC transporter permease protein
A3X3N7	+	2.1046	2.7273	MED193_17494	Putative hemin binding periplasmic transmembrane protein
A3XEM0	+	1.6615	2.6237	MED193_12698	Uncharacterized protein
A3XB45	+	3.2274	2.6082	MED193_22076	FecB2
A3XB51	+	1.4791	2.5690	MED193_22051	MotA/TolQ/ExbB proton channel family protein
A3X5J0	+	2.7205	2.5546	MED193_19144	Aminomethyl transferase family protein
A3X598	+	3.1359	2.4261	MED193_19624	Glycerol-3-phosphate dehydrogenase (EC 1.1.5.3)
A3X401	+	3.7285	2.3999	MED193_16924	Urea amidolyase-like protein
A3X9H3	+	1.4086	2.3844	MED193_08018	ABC ferric siderophore transporter, ATPase subunit
A3XB52	+	1.8432	2.3800	MED193_22056	Siderophore-interacting protein
A3X5C7	+	4.0264	2.3440	MED193_19469	Uncharacterized protein
A3X3Q7	+	2.5363	2.2120	MED193_17384	Putative iron ABC transport system, ATP-binding protein
A3XB53	+	1.8728	2.1599	MED193_22036	Putative TonB protein

A3X3M9	+	2.1825	2.1223	MED193_17524	Uncharacterized protein
A3X3Q9	+	1.7521	2.0649	MED193_17374	Uncharacterized protein
A3X6S9	+	1.4271	1.9792	MED193_14797	FAD dependent oxidoreductase/aminomethyl transferase
A3XG01	+	2.7851	1.8675	MED193_10071	Glyceraldehyde-3-phosphate dehydrogenase (EC 1.2.1.-)
A3XB46	+	2.4373	1.7138	MED193_22061	Iron(III) dicitrate ABC transporter (ATP-binding protein)
A3X9G8	+	2.1159	1.7085	MED193_08033	Putative ABC transporter, periplasmic Fe+3 siderophore binding protein
A3XA30	+	2.1440	-1.7442	MED193_01180	Uncharacterized protein
A3X5U4	+	3.2564	-1.7699	MED193_18629	Probable swi/snf family helicase 2
A3X6A6	+	3.3402	-1.7847	MED193_15667	3-isopropylmalate dehydratase large subunit (EC 4.2.1.33) (Alpha-IPM isomerase) (IPMI) (Isopropylmalate isomerase)
A3XBV7	+	1.7424	-1.7913	MED193_03717	Anthranilate synthase component II
A3X353	+	1.7052	-1.8624	MED193_18414	6-carboxy-5,6,7,8-tetrahydropterin synthase (EC 4.-.-.-)
A3XAL8	+	1.6643	-1.9035	MED193_04881	tRNA-specific 2-thiouridylase MnmA (EC 2.8.1.13)
A3XDL0	+	1.9165	-1.9548	MED193_13068	Uncharacterized protein
A3X5Z2	+	1.6763	-1.9773	MED193_16247	Aminotransferase, classes I and II
A3X9Z5	+	1.2055	-2.0130	MED193_01340	Regulatory protein, IclR
A3XFQ8	+	1.6218	-2.0295	MED193_11967	Uncharacterized protein
A3X9W0	+	3.8807	-2.0396	MED193_01525	Uncharacterized protein
A3XDR3	+	1.5896	-2.0528	MED193_12823	Branched-chain amino acid ABC transporter, ATP-binding protein
A3XFA9	+	1.9574	-2.0825	MED193_21591	DNA-binding protein, putative
A3X699	+	3.1470	-2.1740	MED193_15722	Heat shock protein, Hsp20 family protein
A3X4R0	+	1.5895	-2.1996	MED193_20559	Ornithine carbamoyltransferase (OTCase) (EC 2.1.3.3)
A3XFY2	+	2.1534	-2.2046	MED193_10161	Phosphonate ABC transporter, periplasmic phosphonate-binding protein
A3X7R8	+	1.0319	-2.2291	MED193_07059	NADH-quinone oxidoreductase subunit B (EC 1.6.5.11) (NADH dehydrogenase I subunit B) (NDH-1 subunit B)
A3X7Z6	+	3.2888	-2.2476	MED193_06674	Carbon monoxide dehydrogenase, large subunit
A3X973	+	0.9737	-2.2692	MED193_08518	Uncharacterized protein
A3XDP5	+	2.3130	-2.3430	MED193_12893	Phosphoglycerate mutase family protein
A3XDV2	+	3.3797	-2.3602	MED193_00665	Uncharacterized protein
A3XBP3	+	1.5176	-2.3996	MED193_04042	Phosphate-specific transport system accessory protein PhoU
A3XC04	+	1.9973	-2.4058	MED193_03482	Acyl-CoA dehydrogenase
A3XDV1	+	2.3422	-2.4194	MED193_00660	Uncharacterized protein
A3X6A5	+	4.1231	-2.4759	MED193_15662	3-isopropylmalate dehydratase small subunit (EC 4.2.1.33) (Alpha-IPM isomerase) (IPMI) (Isopropylmalate isomerase)

A3X738	+	1.8811	-2.5043	MED193_14247	Glutamate synthase, large subunit
A3X4Q9	+	1.5747	-2.5064	MED193_20554	Acetylornithine aminotransferase (ACOAT) (EC 2.6.1.11)
A3X3M4	+	2.3670	-2.5799	MED193_17559	Quinolinate synthase A (EC 2.5.1.72)
A3XE23	+	2.6946	-2.5852	MED193_00315	Uncharacterized protein
A3XFH6	+	1.7440	-2.5881	MED193_11614	Transmembrane transporter, major facilitator family protein
A3X9P6	+	4.3915	-2.7764	MED193_01855	Putative periplasmic solute-binding protein
A3XE22	+	2.5368	-2.7966	MED193_00310	Replication protein a
A3XBS8	+	2.1064	-3.0308	MED193_03882	Acetyltransferase, GNAT family protein
A3XAQ9	+	2.8365	-3.0362	MED193_04676	Peroxiredoxin/glutaredoxin family protein
A3X795	+	3.2221	-3.5517	MED193_13987	23S rRNA (Uracil-5-)-methyltransferase rumA
A3XDT6	+	3.7536	-3.6600	MED193_00725	Chloroacetaldehyde dehydrogenase
A3X3E7	+	0.9966	-3.7071	MED193_17949	30S ribosomal protein S1
A3XA05	+	2.2362	-3.9238	MED193_01295	Na(+)-translocating NADH-quinone reductase subunit C (Na(+)-NQR subunit C) (Na(+)-translocating NQR subunit C) (EC 7.2.1.1) (NQR complex subunit C) (NQR-1 subunit C)
A3XE07	+	3.9351	-4.3060	MED193_00395	ATPase of the AAA+ class
A3X815	+	3.1872	-4.3718	MED193_06579	Glycerophosphoryl diester phosphodiesterase
A3XA06	+	3.7443	-4.7341	MED193_01300	Na(+)-translocating NADH-quinone reductase subunit B (Na(+)-NQR subunit B) (Na(+)-translocating NQR subunit B) (EC 7.2.1.1) (NQR complex subunit B) (NQR-1 subunit B)
A3X8H3	+	4.1717	-4.7713	MED193_05784	Uncharacterized protein
A3XA11	+	4.6598	-5.2983	MED193_01280	Na(+)-translocating NADH-quinone reductase subunit F (Na(+)-NQR subunit F) (Na(+)-translocating NQR subunit F) (EC 7.2.1.1) (NQR complex subunit F) (NQR-1 subunit F)
A3XBX7	+	2.5014	-6.2592	MED193_03622	Indolepyruvate ferredoxin oxidoreductase (EC 1.2.7.8)
A3XBP0	+	4.4467	-6.3118	MED193_04062	Phosphate ABC transporter, periplasmic phosphate-binding protein
A3XA04	+	5.1529	-6.7486	MED193_01305	Na(+)-translocating NADH-quinone reductase subunit A (Na(+)-NQR subunit A) (Na(+)-translocating NQR subunit A) (EC 7.2.1.1) (NQR complex subunit A) (NQR-1 subunit A)

Appendix 5.8 Significantly up- and downregulated proteins (p-value <0.05) in the exoproteome of ΔphoB G3P compared to WT MED193 +P.

Protein ID	*p-value <0.05*	*-log$_{10}$ (p-value)*	*Log$_2$ (fold change)*	*Locus tag*	*Uniprot annotation*
A3X5C8	+	3.538	8.450	MED193_19449	Phosphonate-binding periplasmic protein
A3X3N4	+	2.923	5.075	MED193_17499	Hemin degrading factor
A3X3N2	+	2.654	4.782	MED193_17509	Uncharacterized protein
A3X3D9	+	3.041	4.417	MED193_17984	Uncharacterized protein
A3X3N5	+	2.420	4.050	MED193_17504	Putative Hemin receptor protein HmuR
A3XB52	+	2.210	3.545	MED193_22056	Siderophore-interacting protein
A3XB54	+	1.690	3.331	MED193_22031	Outer membrane protein
A3XFE5	+	1.736	3.029	MED193_21421	Uncharacterized protein
A3X4R3	+	2.917	2.951	MED193_20524	Uncharacterized protein
A3XB77	+	1.609	2.951	MED193_21926	Multicopper oxidase domain protein
A3XD37	+	2.105	2.878	MED193_09670	Uncharacterized protein
A3X9H4	+	1.852	2.822	MED193_08013	TonB dependent-iron siderophore receptor
A3XEY5	+	2.502	2.791	MED193_12123	Microcystin dependent protein MdpB
A3XEY7	+	2.419	2.785	MED193_12133	Microcystin dependent protein MdpB
A3XEY6	+	1.390	2.730	MED193_12128	Hypothetical microcystin dependent protein
A3X3Q0	+	1.976	2.710	MED193_17419	Glucose-6-phosphate 1-dehydrogenase (G6PD) (EC 1.1.1.49)
A3XBQ2	+	3.238	2.709	MED193_03992	Acetoacetyl-CoA synthase
A3X3T6	+	2.589	2.641	MED193_17244	Possible ABC transporter, periplasmic binding protein
A3X3Q1	+	2.690	2.592	MED193_17424	Phosphogluconate dehydratase (EC 4.2.1.12)
A3XAE2	+	2.762	2.246	MED193_05256	LysM domain protein
A3X445	+	2.272	-2.242	MED193_16694	30S ribosomal protein S14
A3X824	+	2.550	-2.394	MED193_06534	Glutamate/leucine/phenylalanine/valine dehydrogenase family protein
A3XDW8	+	2.148	-2.428	MED193_00545	Putative aminotransferase protein
A3X9P6	+	1.921	-2.493	MED193_01855	Putative periplasmic solute-binding protein
A3X6A6	+	2.078	-2.566	MED193_15667	3-isopropylmalate dehydratase large subunit (EC 4.2.1.33) (Alpha-IPM isomerase) (IPMI) (Isopropylmalate isomerase)
A3XC12	+	1.583	-2.573	MED193_03447	UvrABC system protein A (UvrA protein) (Excinuclease ABC subunit A)
A3XDD7	+	1.544	-2.585	MED193_13433	Ribonuclease R (RNase R) (EC 3.1.13.1)
A3XDM5	+	2.398	-2.639	MED193_12993	Uncharacterized protein

A3XFB8	+	2.852	-2.776	MED193_21536	Uncharacterized protein
A3X744	+	2.068	-2.831	MED193_14232	Glutamate synthase, small subunit
A3X441	+	2.543	-2.918	MED193_16714	30S ribosomal protein S5
A3XCJ5	+	2.248	-2.965	MED193_10728	Electrotransfer ubiquinone oxidoreductase family protein
A3X4R1	+	2.342	-2.995	MED193_20539	Uncharacterized protein
A3XBE9	+	1.455	-3.072	MED193_22606	Uncharacterized protein
A3XFS4	+	1.473	-3.135	MED193_11912	30S ribosomal protein S21
A3X8X7	+	1.712	-3.180	MED193_08983	DNA topoisomerase 1 (EC 5.99.1.2) (DNA topoisomerase I)
A3XDH8	+	1.495	-3.201	MED193_13223	DNA gyrase subunit B (EC 5.99.1.3)
A3X647	+	2.096	-3.343	MED193_15942	50S ribosomal protein L11
A3XBX7	+	1.671	-3.349	MED193_03622	Indolepyruvate ferredoxin oxidoreductase (EC 1.2.7.8)
A3X427	+	1.085	-3.545	MED193_16794	Pseudouridine synthase (EC 5.4.99.-)
A3X6T7	+	1.321	-3.549	MED193_14742	Acetyl-CoA C-acetyltransferase
A3XC84	+	2.536	-3.674	MED193_11293	Sugar ABC transporter, periplasmic sugar-binding protein
A3X4Q9	+	1.578	-3.725	MED193_20554	Acetylornithine aminotransferase (ACOAT) (EC 2.6.1.11)
A3XAF7	+	1.892	-3.969	MED193_05191	Uncharacterized protein
A3X4R0	+	1.275	-4.188	MED193_20559	Ornithine carbamoyltransferase (OTCase) (EC 2.1.3.3)
A3X7Z6	+	2.649	-4.352	MED193_06674	Carbon monoxide dehydrogenase, large subunit
A3X7Z8	+	1.894	-4.461	MED193_06664	Translation initiation factor IF-3
A3X738	+	1.711	-4.682	MED193_14247	Glutamate synthase, large subunit
A3XFY2	+	2.942	-4.961	MED193_10161	Phosphonate ABC transporter, periplasmic phosphonate-binding protein
A3X8H3	+	2.331	-5.345	MED193_05784	Uncharacterized protein
A3XBP0	+	2.765	-5.824	MED193_04062	Phosphate ABC transporter, periplasmic phosphate-binding protein
A3X815	+	3.027	-6.003	MED193_06579	Glycerophosphoryl diester phosphodiesterase

Appendix 5.9 List of proteins used to determine the phylogeny of MED193_19449, retrieved from Bisson, 2017.

Protein group and organism	*Abbreviation*	*Locus tag*	*NCBI Accession number*	*UniProt KB*
PtxB - phosphite binding protein				
Shewanella putrefaciens 200	S.putre_PtxB	Sput200_3279	ADV55672	E6XMC1
Pseudomonas stutzeri	S.stutz_PtxB	N/A	AAC71707	O69052
Klebsiella pneumoniae ATCC 700721	K.pneumo_PtxB	KPN_pKPN3p05890	ABR80269	A6TI48
Prochlorococcus marinus MIT 9301	P.9301_PtxB	P9301_12511	ABO17874	A3PDP9
Prochlorococcus marinus MIT 9303	P.9303_PtxB	P9303_11291	ABM77878	A2C8R8
Nostoc punctiforme ATCC 29133	N.puncti_PtxB	Npun_F3299	ACC81739	B2IZW8
Nostoc sp. PCC7120	N.PCC7120_PtxB	all8089	BAB77419	Q8YK29
Trichodesmium erythraeum IMS101	T.eryth_PtxB	Tery_0366	ABG49835	Q119I9
Crocosphaera subtropica ATCC 51142	C.subtr_PtxB	cce_2558	ACB51906	B1WSC0
C-P lyase, substrate-binding protein				
Pseudomonas aeruginosa ATCC 15692	P.aerug_C-P	PA3383	NP_252073	Q9HYL8
Escherichia coli K12	E.K12_C-P	b4105	NP_418529	P16682
Nostoc sp. PCC7120	N.PCC7120_C-P1	all2228	BAB73927	Q8YUV3
Nostoc sp. PCC7120	N.PCC7120_C-P2	all2229	BAB73928	Q8YUV2
Rhodopseudomonas palustris ATCC BAA-98	R.palus_C-P	RPA0699	CAE26143	Q6NBX7
Trichodesmium erythraeum IMS101	T.eryth_C-P	Tery_4993	ABG53907	Q10V17
Synechococcus sp. JA-2-3B'a(2-13)	S.JA23Ba213_C-P	CYB_0160	ABD01161	Q2JPW5
Candidatus Pelagibacter sp. HTCC7211	Can.P.HTCC7211_C-P	PB7211_926	WP_008545354	B6BPP6
Candidatus Pelagibacter ubique HTCC7217	Can.P.HTCC7217_C-P	P773DRAFT_0391	WP_029455242	N/A
Phaeobacter sp. MED193	P.MED193_C-P	MED193_10161	EAQ43272	A3XFY2
HtxB - hypophosphite binding protein				
Alcaligenes faecalis	A.faecal_HtxB	N/A	AAT12776	Q5J1M1

Pseudomonas stutzeri	P.stutz_HtxB	N/A	AAC71712	O69061
Xanthobacter flavus	X.flavu_HtxB	N/A	ABG02408	A5X3G7
Methylobacterium radioterms NDB3P7	M.radio_HtxB	Ga0132819_120142	KZB97311	N/A
Sel-P - selenophosphate binding protein				
Prochlorococcus marinus MIT 9303	P.9303_Sel-P	P9303_14311	ABM78177	A2C9L7
Prochlorococcus marinus MIT 9313	P.9313_Sel-P	PMT_0780	CAE20955	Q7V7G6
Marinobacter hydrocarbonclasticus ATCC 700491	M.hyrdo_Sel-P	Maqu_1446	WP_011784933	A1U0L2
Unknown substrate-binding protein				
Phaeobacter sp. B1627	P.B1627_SBP	FGE21_09260	TNJ43267	A0A5C4SIH9
Phaobacter sp. MED193	P.MED193_SBP	MED193_19449	EAQ47401	A3X5C8
Roseobacter sp. SK209-2-6	Rb.SK20926_SBP	RSK20926_15436	EBA15623	A4EXZ3
Silicibacter sp. TrichCH4B	S.TrichCH4B_SBP	SCH4B_0511	EEW60709	N/A
Labrenzia sp. 011	L.011_SBP	DCO57_16345	PVB60548	A0A2T7HAC0
Labrenzia sp. THAF35	L.THAF35_SBP	Ga0439824_01_5724798_5725775	WP_208984471	N/A
Roseobacter sp. NP7	Rb.NP7_SBP	Ga0266024_102016	N/A	N/A
Jannaschia helgolandensis DSM 14858	J.helgo14858_SBP	Ga0070490_2841	N/A	N/A
Roseovarius sp. THAF8	Rv.THAF8_SBP	Ga0439672_01_3909148_3910125	WP_172978929	N/A

Appendix 6.1 Conditions used for overexpression of Syn. WH8102 phosphatases in E. coli in alphabetical order. SYNW2390, pET151/D-TOPO; SYNW2391, pET151/D-TOPO (a) and pMAL c4x (b); SYNW0196, pET151/D-TOPO (c) and pMAL c4x (d); SYNW1799, pET151/D-TOPO (e) and pet22b(+) (f). Conditions that resulted in insoluble protein only are marked with an 'x', conditions that resulted in soluble protein are marked with a '+' and highlighted in green.

	SYNW2390 pET151/D-TOPO	**SYNW2391** pET151/D-TOPO (a) pMAL c4x (b)	**SYNW0196** pET151/D-TOPO (c) pMAL c4x (d)	**SYNW1799** pET151/D-TOPO (e)* pet22b(+) (f)
Formedium™, 18°C, 18h, self-inducing	x	x (a)	x (c)	
Formedium™, 23°C, 18h, self-inducing	x	x (a)	x (c)	
LB, 18°C, 18 h, 0.25 mM IPTG		x (a)		
LB, 18°C, 18 h, 0.30 mM IPTG		x (b)	x (d)	
LB, 18°C, 18 h, 0.50 mM IPTG		x (a)		
LB, 18°C, 18 h, 0.75 mM IPTG		x (a)		
LB, 18°C, 18 h, 1 mM IPTG		x (a)		
LB, 23°C, 18 h, 0.25 mM IPTG		x (a)		
LB, 23°C, 18 h, 0.30 mM IPTG		x (b)	x (d)	
LB, 23°C, 18 h, 0.50 mM IPTG		x (a)	x (c)	
LB, 23°C, 18 h, 0.75 mM IPTG		x (a)		
LB, 23°C, 18 h, 1 mM IPTG		x (a)		

LB, 30°C, 18 h, 0.6 mM IPTG	+	x (a)	x (c)	
LB, 37°C, 18 h, 0.5 mM IPTG			x (c)	
LB, 37°C, 4 h, 1 M IPTG	+			
LB, 37°C, 8 h, 1 M IPTG	+	x (a)		
LB, 37°C, 18 h, 1 M IPTG	+	x (a)		
M9, 23°C, 18 h, 0.5 mM IPTG		x (a)	x (c)	
M9, 23°C, 18 h, 0.5 mM IPTG, 1 ng/ml Thiamine		x (a)		
M9, 23°C, 18 h, 0.5 mM IPTG, 10 µM Fe^{3+}		x (a)		
M9, 23°C, 18 h, 0.5 mM IPTG, 1 ng/ml Thiamine, 10 µM Fe^{3+}		x (a)		
M9, 30°C, 18 h, 0.6 mM IPTG	+	x (a)	x (c)	
M9, 37°C, 18 h, 0.5 mM IPTG		x (a)	x (c)	
MDA-5052, 18°C, 25 h, self-inducing	+	+ (b)	+ (d)	x (e, f)
Self-inducing medium, 18°C, 18 h	x	x (a)	x (c)	
Self-inducing medium, 23°C, 18 h	x	x (a)	x (c)	
TaKaRa1, LB, 15°C, 18 h, 0.5 mg/ml arabinose, 5 ng/ml tetracycline, 0.5 mM IPTG		x (a)		
TaKaRa1, LB, 15°C, 18 h, 0.5 mg/ml arabinose, 5 ng/ml tetracycline, 1 mM IPTG		x (a)		
TaKaRa1, LB, 15°C, 18 h, 0.5 mg/ml arabinose, 5 ng/ml tetracycline, 2 mM IPTG		x (a)		

TaKaRa1, LB, 23°C, 18 h, 0.5 mg/ml arabinose, 5 ng/ml tetracycline, 0.5 mM IPTG		x (a)		
TaKaRa1, LB, 23°C, 18 h, 0.5 mg/ml arabinose, 5 ng/ml tetracycline, 0.5 mM IPTG, ASW metals		x (a)		
TaKaRa1, LB, 23°C, 18 h, 0.5 mg/ml arabinose, 5 ng/ml tetracycline, 1 mM IPTG		x (a)		
TaKaRa1, LB, 23°C, 18 h, 0.5 mg/ml arabinose, 5 ng/ml tetracycline, 2 mM IPTG		x (a)		
TaKaRa1, M9, 23°C, 18 h, 0.5 mg/ml arabinose, 5 ng/ml tetracycline, 0.5 mM IPTG		x (a)		
TaKaRa1, M9, 23°C, 18 h, 0.5 mg/ml arabinose, 5 ng/ml tetracycline, 0.5 mM IPTG, ASW metals		x (a)		
TaKaRa2, LB, 15°C, 18 h, 0.5 mg/ml arabinose, 0.5 mM IPTG		x (a)		
TaKaRa2, LB, 15°C, 18 h, 0.5 mg/ml arabinose, 1 mM IPTG		x (a)		
TaKaRa2, LB, 15°C, 18 h, 0.5 mg/ml arabinose, 2 mM IPTG		x (a)		
TaKaRa2, LB, 23°C, 18 h, 0.5 mg/ml arabinose, 0.5 mM IPTG		x (a)		
TaKaRa2, LB, 23°C, 18 h, 0.5 mg/ml arabinose, 0.5 mM IPTG, ASW metals		x (a)		

TaKaRa2, LB, 23°C, 18 h, 0.5 mg/ml arabinose, 1 mM IPTG		x (a)		
TaKaRa2, LB, 23°C, 18 h, 0.5 mg/ml arabinose, 2 mM IPTG		x (a)		
TaKaRa2, M9, 23°C, 18 h, 0.5 mg/ml arabinose, 0.5 mM IPTG		x (a)		
TaKaRa2, M9, 23°C, 18 h, 0.5 mg/ml arabinose, 0.5 mM IPTG, ASW metals		x (a)		
TaKaRa3, LB, 15°C, 18 h, 0.5 mg/ml arabinose, 0.5 mM IPTG		x (a)		
TaKaRa3, LB, 15°C, 18 h, 0.5 mg/ml arabinose, 1 mM IPTG		x (a)		
TaKaRa3, LB, 15°C, 18 h, 0.5 mg/ml arabinose, 2 mM IPTG		x (a)		
TaKaRa3, LB, 23°C, 18 h, 0.5 mg/ml arabinose, 0.5 mM IPTG		x (a)		
TaKaRa3, LB, 23°C, 18 h, 0.5 mg/ml arabinose, 1 mM IPTG		x (a)		
TaKaRa3, LB, 23°C, 18 h, 0.5 mg/ml arabinose, 2 mM IPTG		x (a)		
TaKaRa4, LB, 15°C, 18 h, 5 ng/ml tetracycline, 0.5 mM IPTG		x (a)		
TaKaRa4, LB, 15°C, 18 h, 5 ng/ml tetracycline, 1 mM IPTG		x (a)		
TaKaRa4, LB, 15°C, 18 h, 5 ng/ml tetracycline, 2 mM IPTG		x (a)		
TaKaRa4, LB, 23°C, 18 h, 5 ng/ml tetracycline, 0.5 mM IPTG		x (a)		

TaKaRa4, LB, 23°C, 18 h, 5 ng/ml tetracycline, 0.5 mM IPTG, 1 ml/l ASW metals		x (a)		
TaKaRa4, LB, 23°C, 18 h, 5 ng/ml tetracycline, 1 mM IPTG		x (a)		
TaKaRa4, LB, 23°C, 18 h, 5 ng/ml tetracycline, 2 mM IPTG		x (a)		
TaKaRa4, M9, 23°C, 18 h, 5 ng/ml tetracycline, 0.5 mM IPTG		x (a)		
TaKaRa4, M9, 23°C, 18 h, 5 ng/ml tetracycline, 0.5 mM IPTG, ASW metals		x (a)		
TaKaRa5, LB, 15°C, 18 h, 0.5 mg/ml arabinose, 0.5 mM IPTG		x (a)		
TaKaRa5, LB, 15°C, 18 h, 0.5 mg/ml arabinose, 1 mM IPTG		x (a)		
TaKaRa5, LB, 15°C, 18 h, 0.5 mg/ml arabinose, 2 mM IPTG		x (a)		
TaKaRa5, LB, 23°C, 18 h, 0.5 mg/ml arabinose, 0.5 mM IPTG		x (a)		
TaKaRa5, LB, 23°C, 18 h, 0.5 mg/ml arabinose, 1 mM IPTG		x (a)		
TaKaRa5, LB, 23°C, 18 h, 0.5 mg/ml arabinose, 2 mM IPTG		x (a)		
TB-5052, 18°C, 25 h, self-inducing	+	+ (b)	+ (d)	x (e, f)
ZYM-5052, 18°C, 25 h, self-inducing	+	+ (b)	+ (d)	x (e, f)

* various sequence combinations, pET-151/D-TOPO: with signal peptide sequence, without signal peptide sequence (2 different predictions); pet22b(+) without signal peptide sequence (2 different predictions)

Appendix 6.2 List of PhoD phosphatases and purple acid phosphatases used for multiple sequence alignment of SYNW0196.

Organism	**Protein**	**Locus tag**	**NCBI Accession**	**UniProtKB**	**PDBe**	**Publication**
Synechococcus sp. strain WH8102	*PhoD*	SYNW0196	CAE06711	Q7U9Q7		
Bacillus subtilis strain 168	*PhoD*	BSU02620	WP_009966461	P42251	2YEQ	(Rodriguez et al., 2014)
Cobetia amphilecti	*PhoD*	N/A	WP_043333989	N/A		(Noskova et al., 2019)
Cyanobium gracile strain PCC6307	*PhoD*	Cyagr_1849	WP_015109436	K9P6H2		57.19% Seq.ID, e-value 0.0
Ruegeria pomeroyi Strain DSS-3	*PhoD*	SPO0260	WP_011046022	Q5LX48		(Sebastián & Ammerman, 2011)
Sinorhizobium meliloti strain 1021	*PhoD*	SMc03243	WP_010970400	Q92LG7		(Lu et al., 2020)
Synechococcus sp. strain A18-40	*PhoD*	SynA1840_00197	WP_186574568	A0A7G8IBQ9		92.66% Seq.ID, e-value 0.0
Synechococcus sp. strain A18-46.1	*PhoD*	SynA18461_00215	WP_186482541	A0A7G8I3H7		99.73% Seq.ID, e-value 0.0
Synechococcus sp. strain BOUM118	*PhoD*	SynBOUM118_00200	WP_186592164	A0A7G8G9S8		99.47% Seq.ID, e-value 0.0
Synechococcus sp. strain WH8103	*PhoD*	SynWH8103_00217	WP_071828299	A0A0H5PNE3		99.87% Seq.ID, e-value 0.0
Synechococcus sp. strain YX04-3	*PhoD*	N/A	RNC94166	N/A		90.65% Seq.ID, e-value 0.0

Ipomoea batatas	*PAP*	PPAF1_IPOBA	AAF19821	Q9SE00	1XZW	(Schenk et al., 2005)
Phaseolus vulgaris	*PAP*	PPAF_PHAVU	CAA04644	P80366	1KBP	Klabunde et al., 1996
Triticum aestivum	*PAP*	N/A	CDM82579	F6MIW5	6GIZ	(Faba-Rodriguez et al., 2019)

Appendix 6.3 List of PhoX phosphatases used for multiple sequence alignment of SYNW1799.

Organism	**Protein**	**Locus tag**	**NCBI Accession**	**UniProtKB**	**PDBe**	**Publication**
Synechococcus sp. strain WH8102	*PhoX*	SYNW1799	CAE08314	Q7U5A8		
Pseudomonas fluorescens strain Pf0-1	*PhoX*	Pfl_5179	WP_011336247	Q3K5N8	3ZWU	(Yong et al., 2014)
Phaeobacter sp. strain MED193	*PhoX*	MED193_05784	EAQ45878	A3X8H3		This thesis, Chapter 4
Pasteurella multocida strain X73	*PhoX*	Ga0037711_01538	ABL09520	A1C3J6		(Wu et al., 2007)
Sinorhizobium meliloti strain 1021	*PhoX*	SMc02634	WP_010969036	Q92KH4		(Zaheer et al., 2009)
Synechococcus sp. strain YX04-3	*PhoX*	ED554_08490	RNC90485	N/A		99.58% Seq.ID, e-value 0.0
Synechococcus sp. strain A18-46.1	*PhoX*	SynA18461_02095	WP_186481991	A0A7G8I8T2		99.44% Seq.ID, e-value 0.0

Synechococcus sp. strain RS9915	*PhoX*	SynRS9915_02097	QNI51799	A0A7G8D410		99.72% Seq.ID, e-value 0.0
Synechococcus sp. strain WH8103	*PhoX*	SynWH8103_02053	CRY92772	A0A0H5PUI6		99.30% Seq.ID, e-value 0.0
Synechococcus sp. strain A18-40	*PhoX*	SynA1840_02000	QNJ17534	A0A7G8IGT6		99.16% Seq.ID, e-value 0.0
Synechococcus sp. strain A15-24	*PhoX*	SynA1524_01955	QNJ29647	A0A7G8JGE9		97.77% Seq.ID, e-value 0.0

Appendix 6.4 List of organisms and proteins used to generate the phylogenetic tree, including UniProt KB and accession number.

Organism and protein		**Uniprot KB**	**Accession number**
Aphanothece halophytica	AP	F5HRA5	BAK26809
Bacillus halodurans strain DSM 18197	AP	Q9KE43	BAB04734
Bos taurus	AP	P19111	AAA30571
Corynebacterium glutamicum strain DSM 20300	AP	Q8NUB6	WP_011013325
Felis catus	AP	Q29486	NP_001036028
Gallus gallus	AP	Q92058	NP_990691
Halobacterium salinarum strain ATCC 700922	AP	Q9HPW1	AAG19756
Homo sapiens	AP	P10696	NP_112603
Homo sapiens	AP	P05187	NP_001623
Lyngbya sp. strain PCC 8106	AP	A0YXL3	EAW34205
Mus musculus	AP	P09242	NP_001274101
Pandalus borealis	AP	Q9BHT8	CAC35697
Sphingobium sp. strain TCM1	AP	A0A077JBW9	WP_066861370
Vibrio sp. strain G15-21	AP	Q93P54	AAK94204

Oceanicola sp. strain S124	Atypical PhoA	N/A	WP_010139181
Ruegeria sp. strain TM1040	Atypical PhoA	Q1GDN9	WP_011539814
Synechococcus elongatus strain PCC7942	Atypical PhoA	Q31NE7	WP_011242477
Synechococcus sp. strain WH7803	Atypical PhoA	A5GHX2	CAK22537
Bacillus clausii strain KSM-K16	Multifunctional	Q5WI25	BAD63980
Ipomoea batatas	PAP	Q9SE00	AF200825_1
Phaseolus vulgaris	PAP	P80366	CAA04644
Triticum aestivum	PAP	F6MIW5	CDM82579
Alcanivorax pacificus	PhoA	A0A0B4XPE8	WP_008738497
Aphanothece halophytica	PhoA	F5HRA6	BAK26810
Calothrix sp. strain PCC 6303	PhoA	K9V1S5	WP_015198432
Candidatus Thiodiazotropha endoloripes	PhoA	A0A1E2US35	WP_069014328
Candidatus Thiodiazotropha endoloripes	PhoA	N/A	WP_069019938
Candidatus Thiodiazotropha endoloripes	PhoA	N/A	WP_069005285
Catenovulum agarivorans	PhoA	N/A	WP_016957261
Chlamydomonas reinhardtii	PhoA	A8JGF3	XP_001702318
Cyanobium sp. strain RS427	PhoA	A0A2E8TGB2	MBR76185
Desulfoglaeba alkanexedens	PhoA	A0A4P8L4H8	WP_137425169
Gayadomonas joobiniege	PhoA	N/A	WP_017445941
Haloferax sp. strain Atlit-12N	PhoA	A0A371ML28	WP_115882514
Lottia gigantea	PhoA	V4AHJ4	ESO92846
Lysobacter enzymogenes	PhoA	N/A	Q05205
Marinobacter manganoxydans	PhoA	G6YTW1	WP_008173325
Nostoc sp. strain PCC 7120	PhoA	Q8YLK7	BAB76990
Paenarthrobacter aurescens strain TC1	PhoA	A1R327	ABM07756
Paraglaciecola agarilytica	PhoA	K6Y447	WP_008304778
Pseudoalteromonas sp. strain TB64	PhoA	N/A	WP_024611285
Synechococcaceae bacterium strain WB9_4xC_028	PhoA	N/A	NDD70063

Synechococcus sp.	PhoA	Q05700	AAA27331
Synechococcus sp.	PhoA	N/A	GIR23828
Synechococcus sp. strain A15-24	PhoA	A0A7G8JI79	QNJ30277
Synechococcus sp. strain A15-24	PhoA	A0A7G8JI80	WP_186498289
Synechococcus sp. strain A15-28	PhoA	A0A7G8CFS1	QNI43660
Synechococcus sp. strain A18-40	PhoA	A0A7G8IIP8	WP_186574115
Synechococcus sp. strain A18-40	PhoA	A0A7G8IIP9	WP_186574116
Synechococcus sp. strain A18-46.1	PhoA	A0A7G8IAQ3	WP_186482339
Synechococcus sp. strain BOUM118	PhoA	A0A7G8GGN4	WP_186591901
Synechococcus sp. strain BOUM118	PhoA	A0A7G8GGN5	WP_186591902
Synechococcus sp. strain RS9902	PhoA	A0A7G8GW62	QNI98057
Synechococcus sp. strain RS9907	PhoA	A0A7G8FKF5	WP_188022096
Synechococcus sp. strain RS9915	PhoA	A0A7G8D5U1	WP_186512179
Synechococcus sp. strain RS9915	PhoA	A0A7G8D5U3	WP_186512180
Synechococcus sp. strain WH 5701	PhoA	A3YW57	EAQ75607
Synechococcus sp. strain WH8102 - 2390	PhoA	Q7U3P0	CAE08905
Synechococcus sp. strain WH8102 - 2391	PhoA	Q7U3N9	CAE08906
Synechococcus sp. strain YX04-3	PhoA	N/A	RNC94458
Synechococcus sp. strain YX04-3	PhoA	N/A	RNC94456
Synechocystis sp. strain PCC 6803	PhoA	P72939	BAA16956
Tenacibaculum sp. strain MAR_2009_124	PhoA	A0A1H4YJ99	WP_093674399
Thalassiosira pseudonana strain CCMP1335	PhoA	B5YLN5	XP_002295546
Thalassotalea euphylliae	PhoA	A0A3E0U4K6	WP_116016666
Trichormus variabilis strain ATCC 29413	PhoA	Q3MA30	ABA22156
Volvox carteri f. nagariensis	PhoA	D8UHU3	XP_002958226
Acaryochloris marina strain MBIC 11017	PhoD	B0C289	ABW28541
Acinetobacter guillouiae	PhoD	A0A077KUZ1	WP_096733442

Aphanothece halophytica	PhoD	F5HRA4	BAK26808
Bacillus subtilis strain 168	PhoD	P42251	WP_009966461
Cobetia amphilecti	PhoD	N/A	WP_043333989
Colwellia sp. strain 20A7	PhoD	N/A	WP_159820680
Cyanobium gracile strain PCC6307	PhoD	K9P6H2	WP_105109436
Nostoc punctiforme strain PCC 73102	PhoD	B2IYE6	ACC80033
Nostoc punctiforme strain PCC 73102	PhoD	B2J4U3	ACC79065
Nostoc sp. strain PCC 7120	PhoD	Q8YMF8	BAB76675
Nostoc sp. strain PCC 7120	PhoD	Q8YUU7	BAB73933
Pseudoalteromonas fuliginea	PhoD	A0A063KKL7	WP_149614914
Pseudomonas sabulinigri	PhoD	A0A1H1M3K1	WP_092283483
Pseudomonas syringae pv. syringae strain B728a	PhoD	Q4ZY42	WP_011266682
Rhodopirellula baltica strain DSM 10527	PhoD	Q7UMD8	WP_007339980
Ruegeria pomeroyi strain DSS-3	PhoD	Q5LX48	WP_011046022
Sinorhizobium meliloti strain 1021	PhoD	Q92LG7	WP_027992442
Sphingomonas wittichii strain RW1	PhoD	A5V3P3	WP_011951389
Synechococcus sp. strain A18-40	PhoD	A0A7G8IBQ9	WP_186574568
Synechococcus sp. strain A18-46.1	PhoD	A0A7G8I3H7	WP_186482541
Synechococcus sp. strain BOUM118	PhoD	A0A7G8G9S8	WP_186592164
Synechococcus sp. strain WH8102 - 0196	PhoD	Q7U9Q7	CAE06711
Synechococcus sp. strain WH8103	PhoD	A0A0H5PNE3	WP_071828299
Trichormus variabilis strain ATCC 29413	PhoD	Q3MAW6	ABA21870
Trichormus variabilis strain ATCC 29413	PhoD	Q3M6P0	ABA23346
Trichormus variabilis strain ATCC 29413	PhoD	Q3M5K7	ABA23729
Trichormus variabilis strain NIES-23	PhoD	A0A1Z4KFV2	BAY67858
Xanthomonas campestris pv. campestris	PhoD	A0A7Y8TEQ4	WP_012439582
Bacillus subtilis strain 168	PhoD-like	P19406	WP_010886458

Dokdonia sp. strain MED134	PhoD-like	N/A	EAQ39259
Flavobacterium	PhoD-like	A0A1T1CJT4	WP_024980748
Flavobacterium	PhoD-like	N/A	WP_166124931
Flavobacterium columnare	PhoD-like	A0A2N9PA05	SPE77194
Flavobacterium suaedae	PhoD-like	N/A	GGB66244
Lactobacillus johnsonii strain CNCM I-12250	PhoD-like	Q74JN1	WP_011161925
Sphingomonas sp. strain BSAR-1	PhoD-like	A1YYW7	ABL96598
Synechococcus sp. strain A15-28	PhoD-like	A0A7G8CFS0	QNI43659
Synechococcus elongatus strain PCC7942	PhoV	Q55320	CAA88739
Aliivibrio fischeri strain ES114	PhoX-I	Q5DYL9	AAW88127
Aromatoleum aromaticum strain EbN1	PhoX-I	Q5P050	CAI09314
Campylobacter coli strain RM2228	PhoX-I	A0A5T0SPG2	EAL56643
Campylobacter fetus subsp. fetus strain 82-40	PhoX-I	A0RPD8	ABK81833
Campylobacter jejuni strain RM1221	PhoX-I	A0A5T2CQM3	AAW34736
Campylobacter jejuni subsp. doylei strain 269.97	PhoX-I	A7H1M3	ABS44541
Campylobacter jejuni subsp. jejuni serotype O:2 strain NCTC 11168	PhoX-I	Q0PBZ2	CAL34316
Campylobacter jejuni subsp. jejuni serotype O:23/36 strain 81-176	PhoX-I	A0A0H3PBS6	EAQ73176
Campylobacter jejuni subsp. jejuni strain 260.94	PhoX-I	A0A7D6HKG7	EAQ58981
Campylobacter jejuni subsp. jejuni strain 81116	PhoX-I	A0A3X8T808	ABV51738
Campylobacter jejuni subsp. jejuni strain CG8486	PhoX-I	A0A3X8RRD0	EDK21812
Campylobacter jejuni subsp. jejuni strain HB93-13	PhoX-I	A0A430TPB3	EAQ60024
Campylobacter upsaliensis strain RM3195	PhoX-I	A0A381EFZ4	EAL52284
Citrobacter koseri strain ATCC BAA-895	PhoX-I	A8AF39	ABV12102
Cronobacter sakazakii strain ATCC BAA-894	PhoX-I	A7MN86	ABU78202
Jannaschia sp. strain CCS1	PhoX-I	Q28R47	ABD54815
Marinomonas sp. strain MED121	PhoX-I	A3YDS1	EAQ64690
Maritimibacter alkaliphilus strain HTCC2654	PhoX-I	A3VDZ8	EAQ13737

Methylibium petroleiphilum strain PM1	PhoX-I	A2SLP0	ABM96479
Neptuniibacter caesariensis	PhoX-I	A0A7U8C5I5	EAR61096
Nitrosospira multiformis strain ATCC 25196	PhoX-I	Q2Y5W0	ABB75861
Nodularia spumigena strain CCY9414	PhoX-I	W6FNU6	EAW44980
Nostoc sp. strain PCC 7120	PhoX-I	Q8YMY0	BAB76493
Photobacterium profundum strain 3TCK	PhoX-I	Q1Z9K7	EAS45835
Pseudomonas aeruginosa strain PA7	PhoX-I	A6V4F1	ABR83736
Pseudomonas aeruginosa strain PAO1	PhoX-I	Q9I0K3	AAG06023
Pseudomonas aeruginosa strain UCBPP-PA14	PhoX-I	A0A0H2ZC11	ABJ11858
Pseudomonas protegens strain Pf-5	PhoX-I	Q4K4S9	AAY94886
Pseudomonas savastanoi pv. phaseolicola strain 1448A	PhoX-I	Q48CR8	AAZ33688
Pseudomonas syringae pv. syringae strain B728a	PhoX-I	Q4ZMA5	AAY39717
Pseudomonas syringae pv. tomato strain DC3000	PhoX-I	Q88AA1	AAO54035
Reinekea blandensis strain MED297	PhoX-I	A4B9W1	EAR11412
Rhizobium sp. strain PDO1-076	PhoX-I	H4F0G0	EHS53818
Roseobacter denitrificans strain OCh 114	PhoX-I	Q07GN7	ABI93362
Roseobacter sp. strain CCS2	PhoX-I	A4EHV8	EBA12171
Roseovarius nubinhibens strain ISM	PhoX-I	A3SP49	EAP76239
Ruegeria pomeroyi strain DSS-3	PhoX-I	Q5LSA8	AAV95139
Ruegeria sp. strain TM1040	PhoX-I	Q1GDH9	ABF65287
Sagittula stellata strain E-37	PhoX-I	A3K4S3	EBA07972
Stappia aggregata strain IAM 12614	PhoX-I	A0P1Y3	EAV41059
Synechococcus sp. strain JA-2-3B'a(2-13)	PhoX-I	Q2JK59	ABD02936
Synechococcus sp. strain JA-3-3Ab	PhoX-I	Q2JTX7	ABC99852
Trichormus variabilis strain ATCC 29413	PhoX-I	Q3MBE9	ABA21687
Vibrio cholerae serotype O1 strain N16961	PhoX-I	Q9KND2	AAF95947
Vibrio shilonii strain AK1	PhoX-I	A6D2N1	EDL53107

Yoonia vestfoldensis strain SKA53	PhoX-I	A3V367	EAQ07798
Acaryochloris marina strain MBIC 11017	PhoX-II	B0C9Y3	ABW25423
Clavibacter michiganensis subsp. michiganensis strain NCPPB 382	PhoX-II	A5CUZ6	CAN02934
Corynebacterium jeikeium strain K411	PhoX-II	Q4JY10	CAI36297
Crocosphaera chwakensis strain CCY 0110	PhoX-II	A3INH2	EAZ91870
Dinoroseobacter shibae strain DFL 12	PhoX-II	A8LRT2	ABV94113
Escherichia coli strain K-12	PhoX-II	P00634	BAE76164
Gloeobacter violaceus strain PCC 7421	PhoX-II	Q7NN53	BAC88502
Hyphomonas neptunium strain ATCC 15444	PhoX-II	Q0C2N7	ABI78805
Kineococcus radiotolerans strain SRS30216	PhoX-II	A6WE41	ABS05080
Lentisphaera araneosa strain HTCC2155	PhoX-II	A6DKS5	EDM27973
Lyngbya sp. strain PCC 8106	PhoX-II	A0YLP7	EAW38145
Mesorhizobium japonicum strain MAFF 303099	PhoX-II	Q98M25	BAB48288
Mesorhizobium japonicum strain MAFF 303099	PhoX-II	Q98DS8	BAB51192
Mycolicibacterium gilvum strain PYR-GCK	PhoX-II	A4T4Q4	ABP43345
Nocardioides sp. strain JS614	PhoX-II	A1SHV8	ABL81393
Nostoc sp. strain PCC 7120	PhoX-II	Q8YK39	BAB77409
Ochrobactrum anthropi strain ATCC 49188	PhoX-II	A6X7E5	ABS17149
Paenarthrobacter aurescens strain TC1	PhoX-II	A1R9A2	ABM09512
Paracoccus denitrificans strain PD 1222	PhoX-II	A1B7Q1	ABL71545
Parvibaculum lavamentivorans strain DS-1	PhoX-II	A7HWF8	ABS64241
Phaeobacter sp. strain MED193	PhoX-II	A3X8H3	EAQ45878
Pseudomonas aeruginosa strain PAO1	PhoX-II	P35483	WP_003113164
Pseudomonas aeruginosa strain UCBPP-PA14	PhoX-II	Q02HI0	WP_003141140
Rhodobacter sphaeroides strain ATCC 17029	PhoX-II	A3PR92	WP_011842643
Rhodococcus jostii strain RHA1	PhoX-II	Q0SAZ9	ABG95287
Rhodospirillum rubrum strain ATCC 11170	PhoX-II	Q2RPZ4	ABC23801

Roseiflexus castenholzii strain DSM 13941	PhoX-II	A7NKR2	ABU58082
Roseiflexus sp. strain RS-1	PhoX-II	A5UU03	ABQ90106
Roseobacter denitrificans strain OCh 114	PhoX-II	Q16C45	ABG30448
Rubrobacter xylanophilus strain DSM 9941	PhoX-II	Q1AZ93	ABG03285
Saccharopolyspora erythraea strain NRRL 2338	PhoX-II	A4FR09	CAM06484
Saccharopolyspora erythraea strain NRRL 2338	PhoX-II	A4FR05	CAM06480
Sinorhizobium medicae strain WSM419	PhoX-II	A6U7C0	ABR59550
Streptomyces coelicolor strain A3(2)	PhoX-II	Q9F2J1	CAC10328
Synechococcus sp. strain RCC307	PhoX-II	A5GWP8	CAK29307
Synechococcus sp. strain RS9917	PhoX-II	A3Z5U7	EAQ69621
Synechococcus sp. strain WH 5701	PhoX-II	A3YYX3	EAQ74728
Synechococcus sp. strain WH7803	PhoX-II	A5GMS1	CAK24236
Synechocystis sp. strain PCC 6803	PhoX-II	Q6ZE62	BAD02038
Synechococcus sp. strain WH8102 - 1799	PhoX-II	Q7U5A8	CAE08314
Microbacterium oleivorans	PhoX-like	A0A031FXI0	EZP29273
Microbacterium testaceum	PhoX-like	E8NCM7	WP_013585021
Paeniglutamicibacter terrestris	PhoX-like	N/A	WP_168150638
Streptomyces griseus	PhoX-like	P09401	WP_003970245
Pseudomonas aeruginosa strain PAO1	PpgL	Q9HWH7	NP_252893
Actinobacillus pleuropneumoniae	RTX	B0BPP0	WP_012263031
Actinobacillus pleuropneumoniae	RTX	A0A1B4WRR0	WP_126395238
Escherichia coli	RTX	Q1M2T3	WP_105496270
Glaesserella	RTX	A0A328BYN9	WP_111750239
Kingella kingae	RTX	A1YKW7	WP_019388953
Mannheimia haemolytica	RTX	P0C083	WP_044427865
Mannheimia varigena	RTX	W0Q9Z2	WP_138317745
Moraxella bovis	RTX	Q93GI2	WP_078275051

Moraxella ovis	RTX	A7ISL2	WP_063514371
Morganella morganii	RTX	A0A2C5TL69	WP_061057382
Vibrio parahaemolyticus	RTX	S5J1M4	WP_140070519
Bacillus subtilis strain 168	UshA	O34313	BAA23404
Caldanaerobacter subterraneus subsp. *tengcongensis* strain DSM 15242	UshA	Q8RCR9	WP_011024797
Carboxydothermus hydrogenoformans strain DSM 6008	UshA	Q3A9A2	WP_011345355
Clostridium acetobutylicum strain ATCC 824	UshA	Q97M47	WP_010963675
Ostreococcus lucimarinus CCE9901	UshA	A4S5C3	ABO99041
Paramecium tetraurelia	UshA	A0DLX4	XP_001451438
Synechococcus sp. strain A18-46.1	UshA	A0A7G8IAQ0	WP_186482337